



Center for Volcanic & Tectonic Studies

**Department of Geoscience
University of Nevada, Las Vegas
4505 Maryland Parkway
Las Vegas
NV 89154-4010, USA**



**Department of Geoscience
University of Nevada, Las Vegas
Las Vegas, Nevada 99154-4010
(702) 895-3971
(702) 895-4064 FAX
eismith@redrock.nevada.edu (E-Mail)**

March 2, 1994

Dear Carl,

Enclosed is the annual report for the Center for Volcanic and Tectonic Studies for 1993. I left it unbound so that you can copy it. If you need additional copies, let me know.

Eugene I. Smith

A handwritten signature in cursive script that reads "Eugene".

Professor of Geology

RECEIVED

MAR 04 1994

RECEIVED WASTE PRODUCTION OFFICE

**Department of Geoscience
University of Nevada, Las Vegas
Las Vegas, Nevada 89154-4010
(702) 739-3262**

**ORGANIZATION OF THE ANNUAL REPORT OF THE
CENTER FOR VOLCANIC & TECTONIC STUDIES
(CVTS)**

(sections separated by colored paper)

INTRODUCTION

CVTS Activities

CVTS Staff

CVTS Bibliography-1993-1994

Future Directions

CONTRIBUTION OF E.I. SMITH

Paper

The role of the mantle during crustal extension: constraints from the geochemistry of volcanic rocks in the Lake Mead area: Nevada and Arizona

(Reprint from December '93 Geological Society of America Bulletin)

Abstracts of presentations

CONTRIBUTION OF T.K. BRADSHAW

Paper

Polygenetic volcanism at Crater Flat, Nevada

(Manuscript in review for publication in the Journal of Volcanology and Geothermal Research)

Further Geochemical modeling: Crater Flat.

Paper

Basaltic volcanism in the southern Basin and Range: no role for a mantle plume.

(Reprint from Earth and Planetary Sciences Letters)

Abstracts of presentations

Data tables for chemical analyses

Final thoughts

CONTRIBUTION OF G.M. YOGODZINSKI:

Summary of CVTS efforts in the Reville Range, south-central Nevada

Paper

Magmatism and tectonic development of the western Aleutians: an oceanic arc in a strike-slip setting.

(Reprint of paper published in the July '93 Journal of Geophysical Research)

Abstracts of presentations

CONTRIBUTION OF S.A. MORIKAWA

Masters of Science Thesis

The Geology of the Tuff of Bridge Spring: Southern Nevada and Northwestern Arizona."

INTRODUCTION

The annual report of the Center for Volcanic Studies (CVTS) contains a series of papers, reprints and a Master of Science thesis that review the progress made by the CVTS between October 1, 1992 and February 1, 1994. During this period CVTS staff focused on several topics that have direct relevance to volcanic hazards related to the proposed high-level nuclear waste repository at Yucca Mountain, Nevada. These topics include:

- (1) Polygenetic/polycyclic volcanism in Crater Flat, Nevada
- (2) The role of the mantle during crustal extension.
- (3) The detailed geology of Crater Flat, Nevada.
- (4) Pliocene volcanoes in the Reville Range, south-central Nevada.
- (5) Estimating the probability of disruption of the proposed repository by volcanic eruptions. This topic is being studied by Dr. C.H. Ho at UNLV.

CVTS Activities

CVTS staff presented papers at several professional meetings including:

- (a) International Association of Volcanology and Chemistry of the Earth's Interior General Assembly in Canberra Australia, September, 1993.
- (b) Geological Society of America Cordilleran/Rocky Mountain Section Meeting in Reno, Nevada: May 19-21, 1993.
- (c) Arizona/Nevada Academy of Sciences Meeting, Las Vegas, Nevada: April 17, 1993.
- (d) The Forth International Conference on Volcanism and Volcan de Colima, Colima, Mexico, January 24-28, 1994.
- (e) American Geophysical Union, Fall Meeting, San Francisco, California, December 6-10, 1993.

In addition, CVTS staff participated in several technical exchanges with NRC, State of Nevada and NAS panels. These include presentations to:

- (a) the DOE-NRC Technical Exchange on Volcanism, Las Vegas, June 9, 1993.
- (b) the National Academy of Sciences Board on Radioactive Waste Management, Las Vegas, November 9, 1993.

CVTS staff also presented several invited talks, seminars and field trips to the public about volcanism, local geology and the proposed nuclear waste repository. CVTS staff feel that part of their responsibility is to provide the public with unbiased and alternative views of the issues related to the proposed high-level nuclear waste repository at Yucca Mountain.

CVTS Staff

During the period October 1, 1993 to February 1, 1994, CVTS staff included Eugene I. Smith (PI), and Tim Bradshaw (October 1, 1992 to September 30, 1993), Jim Mills (January 1, 1993 to August 10, 1993), Shirley Morikawa (October 1, 1993 to present) and Gene Yogodzinski (October 1, 1993 to present) as research associates. During this period two graduate students, Shirley Morikawa and Alex Sanchez, were funded to do thesis research. J.D. Walker (University of Kansas) continued to do isotopic analyses in cooperation with CVTS staff. In addition, Mark Reagan and Dan Feuerbach (University of Iowa) did U-series dating of the Lathrop Wells cone, Jim Faulds (University of Iowa) completed a geologic map of the Crater Flat quadrangle, and Mark Martin (Geological Survey of Chile) completed a geological map of the Reville Quadrangle.

Future Directions

Volcanic risk studies and probability calculations require an understanding of the origin and eruption dynamics of small volume mafic volcanoes. The following list is a sampling of those studies that will have a significant impact on future probability calculations.

1. **Volatile content studies for basaltic systems:** Cinder cone eruptions are commonly characterized as strombolian (quiet, effusive), but our historical experience tells us that cinder cone-forming events can be violent, with plinian and sub-plinian eruptive phases. Based on field observations, there is evidence for explosive activity during cinder cone formation in Crater Flat and at Lathrop Wells.

The principle control of the explosivity of an eruption will generally be the volatile content of the melt. The presence of amphibole in lavas at Crater Flat indicates a relatively high pre-eruption volatile content for those magmas. We are therefore looking to the volatile content of basalts in southern Nevada for an improved understanding of eruption dynamics and cinder cone formation. Our approach will be through ion probe and FTIR (fourier transform infrared spectroscopy) studies of volatile species (mostly H₂O & CO₂) in volcanic glass and especially glass inclusions in minerals.

2. **Volcanic events and probability models:** Evaluating the probability of a future volcanic eruption is made difficult in part by the definition of the term 'volcanic event' and its use in statistical modeling. We can imagine cases where a lava flow, a cinder cone, or a chain of cinder cones might reasonably be considered a single volcanic event. In general, refinement of the 'volcanic event' definition will be limited by the information that can (practically) be obtained through geologic mapping and radiometric dating. We are investigating the practical limits of this approach in our study of the small volume, mafic volcanic field in the Reville and Pancake ranges of south-central Nevada (see contribution by G.M. Yagodinski in this report).
3. **Structural controls on volcanism and the distribution of volcanoes in a volcanic field:** Volcanic risk zones in the vicinity of Yucca Mountain are based in part on assumptions about the relative importance of structural control over the spatial distribution of cinder cone eruptions. In the vicinity of Yucca Mountain, the relative importance of NNE versus NW-trending structural control has been debated at length, but the issue remains unresolved. We have argued that analogous volcanic fields within the Great Basin (e.g., the Reville Range) show unambiguously the importance of control on NS-to-NNE-trending structures. In the future we will expand our analysis of cinder cone spatial distribution to other volcanic fields within the region.
4. **Polygenetic/polycyclic activity at small volume mafic systems.** Cinder cone are traditionally considered to have formed by eruptions lasting from 1 to 10 years. Recently, it has become apparent that Cinder Cones are complex volcanoes that erupt from more than one vent over long periods of time (up to 10,000 years). Vents can be focused in one locality or they may form volcanic chains. Our studies in Crater Flat suggest that Black and Red cones are both polycyclic and polygenetic (see the contribution by Tim Bradshaw in this report).

We propose to study cinder cones in volcanic fields that are now dormant or inactive, so that we can observe the complete eruptive and chemical history of individual cones. We will determine whether cinder cones in other areas are polycyclic and/or polygenetic. Our studies will take place in the Reveille Range, Nevada; the Fortification Hill field, Arizona and possibly the San Francisco volcanic field, Arizona and in the Trans-Mexican volcanic belt, central Mexico. Our studies will continue in Crater Flat.

Studies of this type will help us understand the origin of small volume mafic volcanoes and allow us to better define a volcanic event.

5. **Nature of the mantle in the Great Basin:** The trace element and isotopic features of basaltic rocks erupted in the vicinity of Yucca Mountain show the influence of continental lithosphere. It is widely believed that this influence is derived entirely from the lithospheric mantle, but some geochemical features suggest that there may be a significant contribution from the continental crust. The geochemical source of the magmas may hold important clues with regard to the depth of melt storage in small volume mafic systems, and the transport time between melt generation and eruption. We will continue to seek an improved understanding mantle versus crustal source contributions with the aim of improving our overall understanding of the plumbing systems that feed small volume mafic volcanic fields.

CVTS Bibliography-1993-1994

Papers

- Bradshaw, T.K., Hawkesworth, C.J., and Gallagher, K., 1993, Basaltic volcanism in the southern Basin and Range: no role for a mantle plume: *Earth and Planetary Science Letters*, v. 116, p. 45-62.
- Feuerbach, D.L., Smith, E.I., Walker, J.D. and Tangeman, J.A., 1993, The role of the mantle during crustal extension: constraints from geochemistry of volcanic rocks in the Lake Mead area, Nevada and Arizona: *Geological Society of America Bulletin*, v 105, p. 1561-1575.
- Metcalf, R.V., Smith, E.I., and Mills, J.G., 1993, Magma mixing and commingling in the northern Colorado River extensional corridor: constraints on the production of intermediate magmas: *in* Lahren, M.M., Trexler, J.H., and Spinosa, C., eds., *Crustal evolution of the Great Basin and Sierra Nevada: Cordilleran/Rocky Mountain Section*, Geological Society of America Guidebook, Department of Geological Sciences, University of Nevada, Reno, p. 35-56.
- Rowell, A.J., Rees, M.N., Duebendorfer, E.M., Wallin, E.T., Van Schmus, W.R., and Smith, E.I., 1993, An active Neoproterozoic margin: evidence from the Skelton Glacier area, Transantarctic Mountains: *Journal of the Geological Society*, London, v. 150, p. 677-682.
- Smith, E.I., , 1993, 1.76 b.y. old granites and rhyolites in the conterminous United States: *in* Reed, J.C., Bickford, M.E., Houston, R.S., Link, P.K., Rankin, D.W., Sims, P.K., and Van Schmus, W.R., *Precambrian: Conterminous U.S.*, Geological Society of America, *Decade of North America Geology (DNAG)*, v. C-2, p. 64-66.
- Yogodzinski, G.M., Rubenstone, J.L., Kay, S.M. and Kay, R.W., 1993, Magmatic and tectonic development of the western Aleutians: an oceanic arc in a strike-slip setting: *Journal of Geophysical Research*, v. 98, no. B7, p. 11,807-11, 834.

Papers and Maps in Press or in Review

Bradshaw, T.K., Smith, E.I. and Walker, J.D., 1994, Polygenetic Quaternary volcanism at Crater Flat, Nevada: *Journal of Volcanology and Geothermal Research* (in review).

Faulds, J.E., Feuerbach, D.L., Bell, J., and Ramelli, A.J., 1994, Geological map of the Crater Flat Quadrangle, Nevada: Nevada Bureau of Mines and Geology Map (in press).

Martin, M., 1994, Geological map of the Reveille Quadrangle, Nevada: Nevada Bureau of Mines and Geology Map (in press).

Mills, J.E., 1994, Geological map of the Hoover Dam Quadrangle, Nevada and Arizona: Nevada Bureau of Mines and Geology Map (in review).

Yogodzinski, G.M., Volynets, O.N., Koloskov, A.V., Seliverstov, N.I., Matvenkov, V.V., 1994, Magnesian andesites and the subduction component in a strongly calc-alkaline system at Piip Volcano, far western Aleutians, *Journal of Petrology*, v. 34, (in press).

Master of Science Thesis

Morikawa, Shirley A., 1993, The Geology of the Tuff of Bridge Spring: Southern Nevada and Northwestern Arizona: M.S. thesis, University of Nevada, Las Vegas, 165pp.

Abstracts

Bradshaw, T.R. and Smith, E.I., 1993, Quaternary basalts in S. Nevada: Melting of metasomatised lithospheric mantle: IAVCEI General Assembly, Canberra, Australia, Abstracts, p. 12.

Bradshaw, T.R., 1993, Trachyandesite magmas in the Colorado River trough: *Geological Society of America Abstracts with Programs*, v. 25, no. 5, p. 13.

Johnson, W.M., Reed, R.C., Metcalf, R.V., and Smith, E.I., 1993, Potential extrusive equivalents of the Miocene Mt. Perkins pluton, Mojave County, Arizona: (abs.) *Journal of the Arizona-Nevada Academy of Science*, v. 28, p.44.

Smith, E.I., Feuerbach, D.L., Naumann, T.R., Walker, J.D., and Tangeman, J.A., 1993, Role of the mantle during crustal extension: IAVCEI General Assembly, Canberra, Australia, Abstracts, p. 102.

- Smith, E.I., Morikawa, S.A., Martin, M.W., Gonzales, D.A. and Walker, J.D., 1993, Tuff of Bridge Spring: a mid-Miocene ash-flow tuff, northern Colorado River extensional corridor, Nevada and Arizona: Geological Society of America, Abstracts with Programs, v. 25, no. 5, p. A148.
- Smith, E.I., Bridwell, H., Schmidt, C., Switzer, T., and the UNLV 1993 Winter Field Course, 1993, Late-Miocene intermediate to felsic volcanism in the McCullough range, southern Nevada: (abs.) Journal of the Arizona-Nevada Academy of Science, v. 28, p.45.
- Smith, E.I., Bradshaw, T.K., and Walker, J.D., 1993, Polygenetic Quaternary volcanism in the western USA: an example from Crater Flat, Nevada, Abstracts for the Fourth International Meeting, Volcanology of Volcan de Colima; a decade volcano, p. 165.
- Yogodzinski, G.M., Bailey, D.G., Volynets, O.N., Braitseva, O.A., Sulerzhitsky, L.D., Melekestev, J.V., Churikova, T. and Kay, R.W., 1993, Ultramafic xenoliths and melt-peridotite interaction in a calc-alkaline igneous system: examples from Avachinsky Volcano, eastern Kamchatka: Transactions of the American Geophysical Union, v. 74, p. 679.
- Yogodzinski, G.M., Volynets, O.N., Kay, R.W., and Patoka, M.G., 1993, Alkaline magmatism in a subduction environment: late Cenozoic intraplate and arc series volcanic rocks in Kamchatka: Transactions of the American Geophysical Union, v. 73, p. 644.
- Yogodzinski, G.M., Naumann, T.R., and Smith, E.I., 1994, Temporal and geochemical features of volcanism in the Reveille Range of south-central Nevada, USA: Abstracts for the Fourth International Meeting, Volcanology of Volcan de Colima; a decade volcano, p. 187.

**CENTER FOR VOLCANIC AND TECTONIC STUDIES
1992 - 1993 ANNUAL REPORT**

Contribution by

Dr. E.I. Smith

**Reprint of the November 1993 paper from the
Bulletin of the Geological Society of America**

entitled

**The role of the mantle during crustal extension: constraints from
geochemistry of volcanic rocks in the Lake Mead area,
Nevada and Arizona**

The role of the mantle during crustal extension: Constraints from geochemistry of volcanic rocks in the Lake Mead area, Nevada and Arizona

DAN L. FEUERBACH* } *Center for Volcanic and Tectonic Studies, Department of Geoscience, University of Nevada,*
EUGENE I. SMITH } *Las Vegas, Las Vegas, Nevada 89154*
J. D. WALKER }
J. A. TANGEMAN* } *Isotope Geochemistry Laboratory, Department of Geology, University of Kansas, Lawrence, Kansas 66045*

ABSTRACT

One of the fundamental questions in areas of large-magnitude extension and magmatism is the role of the mantle in the extension process. The Lake Mead area is ideally suited for developing models that link crustal and mantle processes because it contains both mantle and crustal boundaries and it was the site of large-magnitude crustal extension and magmatism during Miocene time. In the Lake Mead area, the boundary between the amagmatic zone and the northern Colorado River extensional corridor parallels the Lake Mead fault system and is situated just to the north of Lake Mead. This boundary formed between 11 and 6 Ma during, and just following, the peak of extension and corresponds to a contact between two mantle domains. During thinning and replacement of the lithospheric mantle in the northern Colorado River extensional corridor, the lithospheric mantle in the amagmatic zone remained intact. Contrasting behavior to the north and south of this boundary may have produced the mantle domain boundary. The domain to the north of the boundary is characterized by mafic lavas with a lithospheric mantle isotopic and geochemical signature ($\epsilon_{Nd} = -3$ to -9 ; $^{87}Sr/^{86}Sr = 0.706-0.707$). To the south of the boundary in the northern Colorado River extensional corridor, lavas have an ocean island basalt (OIB)-mantle signature and appear to have only a minor lithospheric mantle component in their source ($\epsilon_{Nd} = 0$ to $+4$; $^{87}Sr/^{86}Sr = 0.703-0.705$). Mafic lavas of the northern Colorado River extensional corridor represent the melting of a com-

plex and variable mixture of asthenospheric mantle, lithospheric mantle, and crust. Pliocene alkali basalt magmas of the Fortification Hill field represent the melting of a source composed of a mixture of asthenospheric mantle, high U/Pb (HIMU)-like mantle, and lithospheric mantle. Depth of melting of alkali basalt magmas remained relatively constant from 12 to 6 Ma during, and just after, the peak of extension but probably increased between 6 and 4.3 Ma following extension. Miocene and Pliocene low ϵ_{Nd} and high $^{87}Sr/^{86}Sr$ magmas and tholeiites at Malpais Flattop were derived from a lithospheric mantle source and were contaminated as they passed through the crust. The shift in isotopic values due to crustal interaction is no more than 4 units in ϵ_{Nd} and 0.002 in $^{87}Sr/^{86}Sr$ and does not mask the character of the mantle source. The change in source of basalts from lithospheric mantle to asthenospheric mantle with time, the OIB character of the mafic lavas, and the HIMU-like mantle component in the source are compatible with the presence of rising asthenosphere, as an upwelling convective cell, or plume beneath the northern Colorado River extensional corridor during extension. The Lake Mead fault system, a major crustal shear zone, parallels the mantle domain boundary. The Lake Mead fault system may locally represent the crustal manifestation of differential thinning of the lithospheric mantle.

INTRODUCTION

In areas of large-scale extension there are fundamental questions regarding the role of the mantle in the extension process, the identification and age of mantle boundaries, and the relation between mantle and crustal boundaries. We use the Lake Mead area of southern Nevada and northwestern Arizona to address these questions. The Lake Mead

area is well suited for this purpose because it contains both mantle and crustal boundaries and it was the site of large-magnitude crustal extension and magmatism during Miocene time.

This paper focuses on Miocene and Pliocene mafic volcanoes ($SiO_2 < 55\%$) between 16.4 and 4.7 Ma in the amagmatic zone and the northern Colorado River extensional corridor. First, we present new geochemical data and infer the source of the mafic magmas. Next, we show that crustal interaction (contamination and commingling) with mafic magmas occurred, but that the isotopic values of the lavas are not shifted enough to mask the character of their mantle source. Last, we use the mafic volcanic rocks that span the boundary between the amagmatic zone and the northern Colorado River extensional corridor as "a probe" into the mantle to determine (1) isotopic differences across the boundary, (2) the age of the boundary, and (3) any link between crustal and mantle processes.

The Lake Mead area contains the boundary between the Western Great Basin and Basin-Range mantle provinces (Menzies and others, 1983; Fitton and others, 1991) and the contact between asthenospheric (OIB) and lithospheric (EM2) mantle domains (Menzies, 1989) (Fig. 1). Mafic volcanic rocks in the Basin-Range mantle province have ϵ_{Nd} between $+5$ and $+8$ and initial $^{87}Sr/^{86}Sr = 0.703$ (Perry and others, 1987; Menzies and others, 1983; Farmer and others, 1989). In contrast, the Western Great Basin province is distinguished by $^{87}Sr/^{86}Sr > 0.706$ and ϵ_{Nd} between 0 and -11 (Menzies and others, 1983; Fitton and others, 1988, 1991). Mafic volcanic rocks of the Sierra Nevada mantle province (Fig. 1) (Leeman, 1970; Menzies and others, 1983; Fitton and others, 1988) are isotopically identical to those of the Western

*Present address: Feuerbach: Department of Geology, University of Iowa, Iowa City, Iowa 52242; Tangeman: Department of Geological Sciences, University of Michigan, Ann Arbor, Michigan 48109.

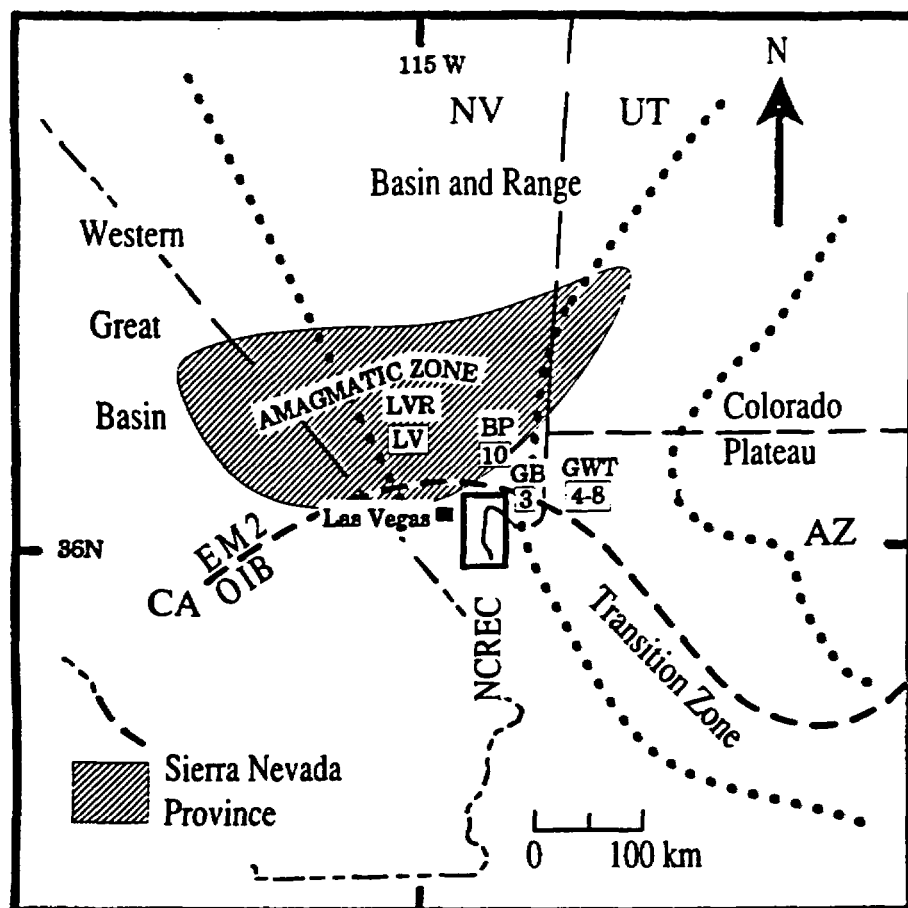


Figure 1. Major mantle and crustal provinces in the southern Basin and Range. The boundaries of the Western Great Basin province are from Fitton and others (1991). Mafic lavas in the Sierran province (Menzies and others, 1983) are identical in isotopic signature to those in the Western Great Basin province. Boundary between EM2 and OIB mantle is from Menzies (1989). Other geologic boundaries are from Fitton and others (1991). The Northern Colorado River extensional corridor (NCREC) was originally defined by Faulds and others (1990). Map also shows the location of sample stations in the Grand Wash trough (GWT), at Gold Butte (GB), Black Point (BP), and in the Las Vegas Range (LVR) (numbers or letters in boxes correspond to first two digits of sample numbers in Table 1). Rectangle indicates area represented in Figure 2.

Great Basin province. Basalts with high $^{87}\text{Sr}/^{86}\text{Sr}$ and low ϵ_{Nd} described by Farmer and others (1989) in southern Nevada lie within the Western Great Basin province.

Several important crustal structures pass through the Lake Mead area (Fig. 1). Among these are the Lake Mead fault system (Anderson, 1973; Bohannon, 1979, 1984), a northeast-trending set of left-lateral strike-slip faults, and the Las Vegas Valley shear zone, a northwest-striking set of right-lateral strike-slip faults (Longwell, 1960; Longwell and others, 1965; Duebendorfer and Wallin, 1991). Segments of the Las Vegas Valley shear zone and the Lake Mead fault system define the boundary between the amagmatic zone and the northern Colorado River exten-

sional corridor (Faulds and others, 1990) (Fig. 1). The Lake Mead fault system also separates two regions that have undergone different amounts of extension. To the south of the Lake Mead fault system, in the northern Colorado River extensional corridor, crust was extended by a factor of three to four. To the north, in the amagmatic zone, crust was extended by a factor of two (Wernicke and others, 1988).

The amagmatic zone is a region between 36° and 37° north latitude of minor igneous activity that separates the Great Basin from the Colorado River sections of the Basin and Range province. This zone corresponds to a regional southerly topographic slope and a gravity gradient with an amplitude of about

100 mgals (Eaton, 1982; Eaton and others, 1978). The zone also represents a boundary between contrasting migration directions of magmatism and extension (Glazner and Supplee, 1982; Reynolds and others, 1986; Taylor and Bartley, 1988). In addition to these structures, a major lithospheric boundary defined by Nd mapping of Proterozoic basement rocks trends north-south to the east of the Colorado River (Bennett and DePaolo, 1989). To the west of the boundary in the Lake Mead area, Proterozoic rocks are characterized by model ages of 2.0–2.3 Ga. To the east of the boundary, older basement rocks are 1.8 to 2.0 Ga.

Volcanic rocks in the amagmatic zone are limited to low-volume Pliocene basalt centers at Black Point and in the Las Vegas Range and moderate volume basaltic andesite volcanoes on Callville Mesa (Feuerbach and others, 1991) (Figs. 1 and 2). In the eastern part of the Lake Mead area at Gold Butte, and in the Grand Wash trough, are numerous late Cenozoic alkali basalt centers (Cole, 1989) (Fig. 1). Adjacent to, and within, the Lake Mead fault system is the middle to late Miocene Hamblin-Cleopatra volcano (Thompson, 1985; Barker and Thompson, 1989), the Boulder Wash volcanic section (Naumann, 1987), and flows of late Miocene basalt interbedded with Tertiary sediments near Government Wash north of Lake Mead (Fig. 2). The area south of the Lake Mead fault system contains numerous Miocene and Pliocene volcanic centers (Fig. 2). The most notable of the Miocene centers are in the River Mountains (Smith, 1982), McCullough Range (Smith and others, 1988), Eldorado Mountains (Anderson, 1971), Black Mountains (Faulds and others, 1990), Hoover Dam (Mills, 1985), at Malpais Flattop (Faulds and others, 1991), and in the White Hills (Cascaden, 1991) (Fig. 1). Pliocene centers compose the Fortification Hill volcanic field that extends discontinuously from near Willow Beach, Arizona, to Lake Mead (Fig. 2). In the Lake Mead area, for the most part, volcanism preceded block tilting related to regional extension (9 to 12 Ma; Duebendorfer and Wallin, 1991). Calc-alkaline intermediate lavas were erupted between 18.5 and ~11 Ma. Low-volume basaltic andesite (10.3 to 8.5 Ma), tholeiitic basalt (9.7 to 10.6 Ma), and alkalic basalt (4.3 to 6 Ma) mainly postdate extension (Smith and others, 1990).

ANALYTICAL TECHNIQUES

Whole-rock major-element concentrations were determined by Inductively Coupled

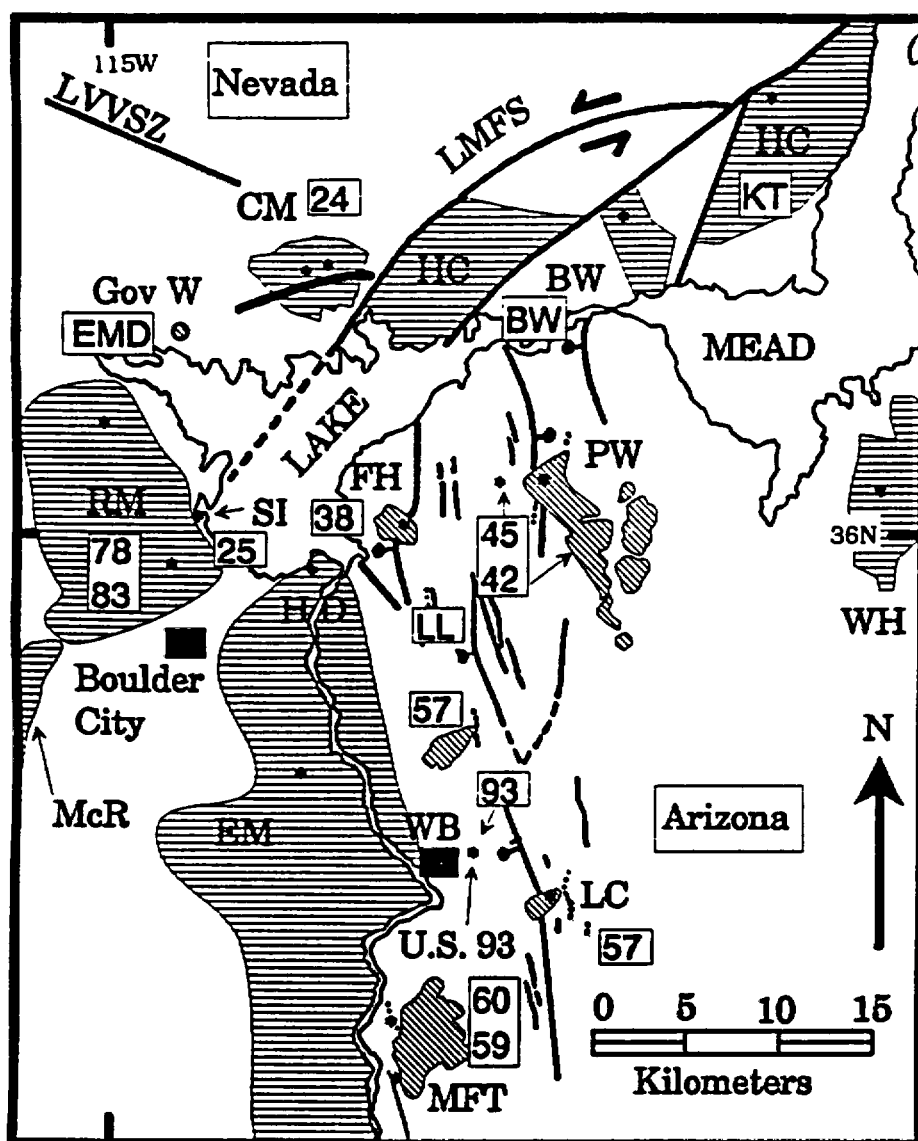


Figure 2. Detailed index map of Lake Mead area and Northern Colorado River extensional corridor showing geologic features mentioned in the text and the location of sample stations (numbers in boxes correspond to first two digits of sample numbers in Table 1). CM, Callville Mesa; BW, Boulder Wash; EM, Eldorado Mountains; HC, Hamblin-Cleopatra volcano; PW, Petroglyph Wash; FH, Fortification Hill; SI, Saddle Island; LC, Lava Cascade; HD, Hoover Dam; WB, Willow Beach; MFT, Malpais Flattop; Gov W, Government Wash; U.S. 93, exposures of alkali basalt along U.S. Route 93; LMFS, Lake Mead fault zone; LVVSZ, Las Vegas Valley shear zone; WH, White Hills; RM, River Mountains; McR, McCullough Range.

Plasma techniques (ICP) at Chemex Labs, Inc. (Sparks, Nevada). Rare-earth elements and Cr, V, Sc, Co, Ta, Hf, and Th were analyzed by Instrumental Neutron Activation Analysis (INAA) at the Phoenix Memorial Laboratory, University of Michigan. The multi-element standards G-2, GSP-1, BHVO-1, and RGM-1 were used as internal standards. Ba, Rb, Ni, and Sr were determined by atomic absorption, and Nb and Sr

were analyzed by X-ray fluorescence (XRF) at Chemex Labs, Inc. Rb and Sr were determined by isotope dilution for samples that were analyzed for Nd, Sr, and Pb isotope concentrations. Ni, Nb, Rb, Sr, Zr, Y, and Ba for Fortification Hill basalt were analyzed by XRF at the U.S. Geological Survey's analytical laboratory in Menlo Park, California. This study includes 27 new isotopic analyses from 11 volcanic sections, which represent all

major volcanic centers, and a fairly complete sample of mafic volcanic rocks in the Lake Mead area.

Samples for isotopic analysis were dissolved at about 180 °C in a sealed bomb using a HF/HNO₃ mixture. Samples were total-spiked for Rb, Sr, Nd, and Sm. Separation of Rb, Sr, and REE group elements was done using standard cation exchange techniques. The HDEHP-on-Teflon method of White and Patchet (1984) was used for separation of Sm and Nd. The HBr and HNO₃ methods were used for separation of Pb and U, respectively, on aliquots from the whole rock solution. All isotopic analyses were done on a VG Sector 54 mass spectrometer at the University of Kansas. Analyses of Sr and Nd were done in dynamic multicollector mode with ⁸⁶Sr = 4V and ¹⁴⁴Nd = 1V; Rb and Sm were analyzed in static multicollector mode with ⁸⁷Rb = 200 mV and ¹⁴⁷Sm = 500 mV. Analyses for Sr and Sm were done on single Ta filaments; Rb was run on single Re filaments. Nd was run both as NdO⁺ and Nd⁺. Analytical blanks were less than 100 pg for all elements. Strontium isotopic compositions are normalized for ⁸⁶Sr/⁸⁸Sr = 0.1194 and referenced to NBS-987 ⁸⁷Sr/⁸⁶Sr = 0.710250. Reproducibility of Sr values during these runs was better than ±0.000020 based on replicate runs of NBS-987. Neodymium isotopic compositions are normalized to ¹⁴⁶Nd/¹⁴⁴Nd = 0.7219 and referenced to LaJolla ¹⁴³Nd/¹⁴⁴Nd = 0.511850. Epsilon values for Nd at crystallization are calculated using (¹⁴³Nd/¹⁴⁴Nd)_(CHUR, 0 Ma) = 0.512638 and ¹⁴⁷Sm/¹⁴⁴Nd_(CHUR, 0 Ma) = 0.1967. Reproducibility of Nd values are about 0.25 epsilon values based on replicate analyses of LaJolla and in-house standards. Lead isotopic analyses are referenced to NBS-981 (common Pb) ²⁰⁷Pb/²⁰⁶Pb = 0.91464 and are corrected for 0.10%/amu fractionation. Fractionation uncertainty is ±0.05%/amu (for example, ±0.08 for ²⁰⁸Pb/²⁰⁴Pb, ±0.04 for ²⁰⁷Pb/²⁰⁴Pb, and ±0.04 for ²⁰⁶Pb/²⁰⁴Pb). Isotope dilution data for Sr, Rb, and Nd are reported in Table 1.

VOLCANOLOGY

Volcanic Rocks of the Northern Colorado River Extensional Corridor

Fortification Hill Field. Fortification Hill basalt crops out in a 50-km-long by 30-km-wide north-northeast elongate area that extends from Lava Cascade, Arizona, to Lake Mead (Fig. 2). We divide the Fortification Hill basalts into older and younger alkalic basalts (OAB and YAB, respectively) based on

TABLE 1. SELECTED ISOTOPIC AND GEOCHEMICAL DATA FROM THE VOLCANIC ROCKS IN THE LAKE MEAD AREA

Sample	U.S.	Petroglyph Wash			Malpais	Fortification	Lava Cascade		Petroglyph	Fortification	Black Point	
	93 YAB 93-96	YAB 45-124	YAB 42-76	YAB 25-2	Flattop TH 60-04	Hill OAB-hy 38-13	OAB 57-113	OAB 57-107	Wash OAB 42-82	Hill OAB 38-143	OAB 10-121	OAB 10-120
SiO ₂	44.05	45.50	45.00	44.90	47.28	45.79	44.15	45.35	47.52	47.97	44.58	46.32
Al ₂ O ₃	15.52	16.89	16.79	16.53	14.95	14.50	15.22	16.71	16.61	16.05	14.35	15.30
FeO	10.46	10.04	10.88	11.14	12.38	12.80	13.38	13.81	10.56	11.37	13.82	13.39
CaO	9.07	8.53	8.78	7.68	8.90	8.38	10.69	11.13	9.79	10.16	6.55	7.93
MgO	5.88	5.94	6.21	5.73	6.82	8.78	8.06	5.54	5.35	5.32	8.76	8.92
Na ₂ O	3.08	4.78	4.94	4.73	2.92	2.86	2.88	3.15	3.57	3.26	4.17	2.97
K ₂ O	2.80	2.20	3.70	1.04	1.07	0.84	1.10	1.20	2.11	1.40	0.70	0.90
TiO ₂	3.02	2.52	2.54	2.40	1.40	1.41	1.76	2.07	1.76	1.46	1.10	1.16
MnO	0.15	0.19	0.18	0.16	0.19	0.16	0.18	0.19	0.16	0.17	0.19	0.19
P ₂ O ₅	0.78	0.77	0.88	0.72	0.24	0.28	0.52	0.53	0.57	0.49	0.30	0.34
LOI	6.48	1.12	0.60	2.93	0.77	1.48	0.52	0.59	1.42	0.49	3.14	4.11
Total	101.40	98.48	100.65	98.06	96.98	97.34	98.46	100.27	99.50	98.64	97.66	101.53
Trace and rare-earth elements in ppm (instrumental neutron activation analysis [INAA], isotope dilution [ID], atomic absorption [AA], X-ray fluorescence spectrometry [XRF])												
Cr(INAA)	103		113	139	242	361	268	80	50	70	271	326
Co(INAA)	25	28	30	29	41	53	43	35	32	33	56	54
Sc(INAA)	15.2	17.4	18.6	18.0	30.0	26.5	30.2	0.0	25.0	26.3	24.5	24.7
V(INAA)		192	216	186	221	213	229	245	281	236	194	177
Hf(INAA)	7.16	6.98	7.22	6.45	3.57	3.38	3.26	4.51	4.00	4.18	1.70	2.83
Th(INAA)	6.08	12.05	12.40	8.51		2.87	3.15	3.66	5.28	3.23		1.16
Ta(INAA)	4.81	5.68	0.00	4.02		1.69	1.66	2.07	1.87	1.31	0.95	
La(INAA)	53.1	85.5	75.1	59.9	14.9	24.6	32.1	37.2	37.7	32.7	12.6	11.8
Ce(INAA)	107.0	140.9	151.0	116.3	35.7	52.4	59.2	69.7	72.3	57.5	24.3	24.7
Sm(INAA)	8.5	8.9	8.6	8.8	3.9	4.8	5.3	6.0	6.2	5.5	3.1	3.1
Eu(INAA)	2.3	2.4	2.3	2.4	1.1	1.6	1.5	1.6	1.6	1.5	0.9	1.1
Yb(INAA)	2.1	2.1	2.4	2.8	2.6	2.2	2.8	2.6	2.5	2.5	1.8	2.3
Lu(INAA)	0.3	0.4	0.2	0.3	0.3	0.3	0.3	0.4	0.4	0.4	0.3	0.2
Sr(AA)	1020	820	874	870	274	455	451	464	998	550	246	260
Rb(AA)	34	64	42	22	16	10	11	22	14	14	9	13
Ba(AA)	880	880	0	744	280	475	480	536	800	690	176	190
Ni(AA)	66	70	68	64	84	166	126	42	30	24	206	
Nb(XRF)	68	84	85	63	13	28	30	36	34	28	13	10
Zr(XRF)	285		300	260	105	116	140	160	155	138	77	90
Sr(ID)			873.59	999.69	297.25	434.24	451.23	463.93	597.57	491.11	246.12	306.35
Rb(ID)			43.4	20.24	16.69	14.31	9.68	11.09	22.13	14.86	8.98	14.45
Nd(ID)			49.48	46.29	16.72		24.77	27.26	32.26	25.45		11.09
Selected normative minerals												
Nepheline	6	12	21	7	0	0	6	5	5	3.31	7.34	1.3
Hypersthene	0	0	0	0	6	4	0	0	0	0	0	0
Isotopic analysis by mass spectrometry												
¹⁴³ Nd/ ¹⁴⁴ Nd		0.512824	0.512801	0.512211	0.512595	0.512711	0.512711	0.512603	0.512592	0.512456	0.512520	
ϵ_{Nd}		3.63	3.18	-8.33	-0.84	2.2	1.42	-0.69	-0.9	-3.55	-2.3	
(⁸⁷ Sr/ ⁸⁶ Sr) _i		0.70347	0.70433	0.70758	0.70565	0.70479	0.70479	0.70555	0.70567	0.70793	0.70753	
²⁰⁶ Pb/ ²⁰⁷ Pb		18.741	18.718	17.742	18.194	18.670	18.591	18.263	18.123	17.947	18.033	
²⁰⁷ Pb/ ²⁰⁸ Pb		15.523	15.564	15.531	15.523	15.570	15.535	15.548	15.541	15.499	15.581	
²⁰⁶ Pb/ ²⁰⁸ Pb		38.476	38.639	38.800	38.309	38.612	38.535	38.397	38.156	38.291	38.9	

Na₂O + K₂O (Fig. 3a), light rare-earth-element (REE) enrichment (Fig. 3b), and modal mineralogy. OAB are dated between 5.88 to 4.73 Ma (Feuerbach and others, 1991), and YAB range in age from 4.64 to 4.3 Ma (Anderson and others, 1972; Feuerbach and others, 1991). OAB are mildly alkalic hypersthene (OAB-hy) or nepheline-normative (OAB-ne) olivine-basalts with Ce/Yb mainly between 18 and 46 (Fig. 3b). Nepheline normative alkali basalts from Black Point have Ce/Yb between 7 and about 17 and are surrounded by a dotted line on Figure 3b. OAB lavas erupted from north-northwest-aligned cinder cones on Fortification Hill and from cinder cones at Lava Cascade and in Petroglyph Wash (Fig. 2).

YAB are xenolith-bearing nepheline-normative alkali-olivine basalts with elevated Na₂O + K₂O and Ce/Yb (37 to 68) (Fig. 3b). YAB occurs in three locations: a diatreme at Petroglyph Wash, *en echelon* dikes and a vent along U.S. highway 93, about 10 km south of Hoover Dam, and south of Saddle Island between the North Shore road and

Lake Mead (Fig. 2) (Smith, 1984). Ultramafic inclusions and megacrysts of augite and kaersutite are ubiquitous to YAB (Nielson, unpub. data; Campbell and Schenk, 1950). Except for the presence of diorite inclusions in YAB, there is no petrographic evidence of crustal contamination in Fortification Hill lavas.

River Mountains. In the River Mountains (Fig. 2), an andesite-dacite stratovolcano is surrounded by a field of dacite domes (Smith, 1982; Smith and others, 1990). Volcanism occurred in four pulses. The first three are characterized by the eruption of calc-alkaline andesite and dacite flows and the last by rhyolite and alkali basalt. The first episode is associated with the emplacement of a quartz monzonite stock (The River Mountain stock) dated at 13.4 ± 0.5 to 12.8 ± 0.5 Ma (K-Ar biotite dates; Armstrong, 1966, 1970). Anderson and others (1972) reported a K-Ar whole rock date of 12.1 ± 0.5 Ma for a basaltic andesite of the third pulse.

Boulder Wash. Boulder Wash in the northern Black Mountains (Fig. 2) contains a 700-

m-thick section of calc-alkaline dacite flows and flow breccias interbedded with flows of pyroxene-olivine andesite containing abundant xenocrysts of quartz and orthoclase (Naumann and Smith, 1987; Naumann, 1987; Smith and others, 1990). Petrographic and textural evidence of magma commingling is well developed in the volcanic section and associated plutonic rocks (Smith and others, 1990; Naumann, 1987). A dacite flow in the eastern part of the volcanic field was dated at 14.2 Ma (K-Ar whole rock date; Thompson, 1985).

Malpais Flattop. Malpais Flattop near Willow Beach, Arizona (Fig. 2) contains a 100-m-thick stack of hypersthene normative tholeiitic basalt flows that erupted from at least two centers now expressed as wide (40 m) dikes and plugs on the west side of the Malpais Flattop mesa (Faulds and others, 1991). Tholeiitic lavas have lower Na₂O + K₂O than alkali basalts with comparable SiO₂ content (Fig. 3a), have lower Ce/Yb than most OAB (Fig. 3b), and are hypersthene normative (Table 1). ⁴⁰Ar/³⁹Ar whole rock

CRUSTAL EXTENSION: LAKE MEAD AREA

TABLE 1. (Continued)

Las Vegas Range LV-104	Callville Mesa		Gold Butte 3-6	Grand Wash Trough		River Mountains				Wilson Ridge LL-66-41	Government Wash EMD-309	Hamblin-Cleopatra Volcano	
	CM 24-68	CM 24-49		4-13	5-14	78-218	78-222	78-223	83-348			KT82-15	KT82-183
42.49	55.18	55.24	46.3	47.58	48.81	47.1	59.0	67.2	72.9	54.1	51.9	56.43	55.89
10.76	15.84	15.98	14.64	14.4	14.95	14.5	16.6	14.2	12.6	16.9	15.2	16.36	16.34
12.79	8.49	8.97	12.59	14.53	11.73	10.9	6.9	3.5	2.7	8.9	9.4	6.76	7.17
9.78	6.64	6.90	7.98	8.74	8.64	11.2	5.5	2.3	0.5	7.4	8.2	6.56	5.4
13.45	4.33	4.10	9.16	8.55	7.14	6.3	2.6	0.9	0.2	4.5	3.8	3.43	3.48
2.39	3.52	3.35	3.16	3	3.22	2.8	3.9	3.6	2.2	4.2	3.7	3.98	4.1
1.00	2.54	2.33	1.59	1.55	1.57	1.8	0.9	0.4	0.2	1.5	1.8	1.31	1.39
1.69	1.07	1.13	1.19	1.25	1.54	1.2	2.3	4.9	7.5	2.1	3.2	2.47	2.72
0.16	0.10	0.14	0.18	0.19	0.16	0.1	0.1	0.1	0.1	0.1	0.2	0.1	0.11
0.67	0.30	0.25	0.27	0.26	0.43	1	0.6	0.1	0.7	1.8	1.8	0.49	0.49
1.79	2.17	0.40	1.06	0.19	1.09	2.3	1	3	0.1	0.5	1.2	1.38	2.85
96.97	100.25	99.17	98.12	100.24	99.28	99.2	99.4	100.2	98.9	100.9	100.4	99.27	99.94
Traces and rare-earth elements in ppm (instrumental neutron activation analysis [INAA], isotope dilution [ID], atomic absorption [AA], X-ray fluorescence spectrometry [XRF])													
816	134	145	253	326	256						63		47
58	28	29	46.68	50.49	39.52					30		20.65	22.76
22.2	18.2	19.6	23.73	27	23.91	29.6	11.2	3.8	1.5			14.06	14.11
234	153	171	216	242	215					198		147	145
5.22	4.29	3.86	3.63	3.14	3.24	8.1	7.3	4.8	4.9	5.1		6.76	8.15
5.20	5.46	4.89	2.72		2.78	13.2	14.9	17.6	31.2	12.4		10.46	13.53
0.71	0.96	0.97				1.5	1	1.2	15.3	2.1		2.75	2.84
46.0	34.2	34.0	23.86	9.04	19.21	107.6	81.7	52.4	55.6	123		65.23	
92.0	72.1	67.6	46.11	21.87	44.26	242.4	167.9	90.7	124.5	213		114.03	126.79
10.2	5.2	5.3				15.5	8.7	4.2	3.7	10.9		7.75	8.29
2.3	1.4	1.4	1.45	0.95	1.33	3.9	2	1.2	1	2.6		1.89	1.99
1.7	2.6	2.2	2.47	1.96	2.28	2.1	2.3	1.3	2.2	2.3		1.73	2.04
0.1	0.3	0.3	0.35	0.3	0.24	0.4	0.4	0.2	0.3	0.3			0.26
	424	970											
	51	40											
	880	840											
	60	36											
	17	23											
	145	185											
795.58	425.51	970.19	421.14	321.83	378.36		959.65	467.99	79.76	1155.78	1299.65	432.85	588.44
48.27	50.94	40.1	14.88	7.47	8.06		83.62	129.26	198.08	42.05	75.97	45.83	47.52
55.76	25.97	29.96	22.47	14.35	17.89		98.57	54.9	28.2	22.84	74.18	45.08	45.27
Selected normative minerals													
5	0	0	5.22	4.34	1.27	3.72	0	0	0	0	0	0	0
0	14	14	0	0	0	0	15.33	2.24	5.87	18.11	17.98	11.07	16.93
Isotopic analysis by mass spectrometry													
0.512269	0.512090	0.512203	0.512592	0.512295	0.512716	0.512210	0.512060	0.512055	0.512008	0.512133	0.512128	0.512390	0.512456
-7.2	-10.69	-8.49	-0.9	-0.27	1.87	-8.34	-11.28	-11.57	-12.28	-9.86	-9.94	-4.84	-3.51
0.70632	0.70792	0.70893	0.70502	0.7046	0.7044	0.708954	0.7082	0.709233	0.710015	0.70815	0.707337	0.70442	0.70562
18.963	17.173	17.332	18.130	17.821	18.127	18.299	17.922	17.885	18.156	17.887	18.16	17.971	18.096
15.642	15.453	15.496	15.527	15.550	15.509	15.605	15.537	15.553	15.578	15.537	15.56	15.515	15.538
38.845	37.314	38.01	38.068	38.050	37.895	38.699	38.791	38.982	38.906	38.725	38.939	38.344	38.549

dates of 9.7 ± 0.5 and 10.6 ± 0.5 Ma were obtained for flows near the top and at the base of the flow stack, respectively (Faulds and Gans, unpub. data).

Eldorado Mountains. A sequence of mafic to felsic volcanic rocks erupted between 18.5 and ~12 Ma in the Eldorado Mountains (Anderson, 1971; Darvall and others, 1991) (Fig. 2). The sequence is divided into a lower section of basaltic andesite (predominant) and rhyolite lavas (Patsy Mine volcanics; Anderson, 1971), and an upper section of basaltic andesite, dacite, and rhyolite (Mount Davis volcanics; Anderson, 1971). Mafic lavas lack petrographic and field textures characteristic of crustal contamination or magma commingling. A similar section of mafic lavas in the White Hills, Arizona (Fig. 1), formed by partial melting of mantle peridotite without significant crustal interaction (Cascadden and Smith, 1991; Cascadden, 1991). In the Eldorado Range, lavas and associated plutonic rocks span the period of most rapid extension. Patsy Mine and the lower parts of the Mount Davis section are tilted nearly 90° .

Younger units are rotated less in the same structural blocks (Anderson, 1971).

Hamblin-Cleopatra Volcano. The Hamblin-Cleopatra volcano (14.2–11.5 Ma) (Anderson, 1973; Thompson, 1985), which lies along the north shore of Lake Mead (Fig. 2), is a 60-km² stratovolcano composed of shoshonite, latite, trachydacite, and trachyte lava (Barker and Thompson, 1989). In addition, tephra, epiclastic sediments, intrusions, and a well-developed radial dike system form the volcano. The volcano was dismembered into three segments by left-lateral strike-slip faulting associated with the Lake Mead fault system (Anderson, 1973; Thompson, 1985; Barker and Thompson, 1989).

Volcanic Rocks at Gold Butte and in the Grand Wash Trough

The Grand Wash trough and the Gold Butte area (Fig. 2) contain flows, dikes, and plugs of olivine-phyric alkali basalt that locally contain mantle xenoliths (Cole, 1989). Basalt in the Grand Wash trough is dated at

3.99 to 6.9 Ma (K-Ar plagioclase) and is younger than alkali basalt to the west in the Gold Butte area (K-Ar plagioclase dates of 9.15 to 9.46 Ma; Cole, 1989) (Fig. 2).

Volcanic Rocks in the Amagmatic Zone

Callville Mesa. Olivine-clinopyroxene basaltic andesite erupted from compound cinder cones on Callville Mesa and in West End Wash between 10.46 and 8.49 Ma (Feuerbach and others, 1991) (Fig. 2). Basaltic andesite has similar Na₂O + K₂O and Ce/Yb to OAB but has higher SiO₂ (46.83–57.32 wt%) (Fig. 3). Basaltic andesite contains abundant quartz and alkali-feldspar xenocrysts that are rimmed by glass and acicular clinopyroxene (diopsidic-augite).

Black Point. At Black Point on the west shore of the Overton Arm of Lake Mead (Fig. 1), thin flows of nepheline-normative alkali basalts (OAB-ne) (6.02 Ma; Feuerbach and others, 1991) associated with north-striking *en echelon* dikes overlie gypsiferous sediments of the Tertiary Horse Spring

TABLE 1. (Continued)

Explanation			
YAB—Young alkali basalts of the Fortification Hill field (6–4.3 Ma).			
OAB—Older normative nepheline alkali basalts of the Fortification Hill field (6 Ma).			
OAB-hy—Older normative hypersthene alkali basalts of the Fortification Hill field (6 Ma).			
TH—Tholeiitic basalts from Malpais Flattop, Arizona (10.6–9.7 Ma).			
Locality descriptions			
Locality	Location (lat., long.)	Age* (Ma)	Description
YAB			
U.S. 93	36°00'00"N 114°45'00"W	4.64–4.3	Volcanic center with numerous dikes. Amphibole megacrysts numerous; mantle xenoliths rare.
Petroglyph Wash	36°04'37"N 114°35'44"W	4.3	Alkali basalt forms a small cylindrical vent. Amphibole megacrysts are common.
Saddle Island	36°02'30"N 114°48'00"W	Not dated	Flow interbedded with Tertiary gravel. Mantle xenoliths are rare.
TH			
Malpais Flattop	35°45'00"N 114°40'00"W	10.6–9.7 (* ⁴⁰ Ar/ ³⁹ Ar dates)	100-m-thick stack of hypersthene-normative tholeiitic basalt flows with wide dikes.
OAB			
Fortification Hill	36°03'45"N 114°40'56"W	5.89–5.42	Over 80 flows associated with cinder cones and shallow intrusions.
Lava Cascade	35°52'38"N 114°35'15"W	5.16–4.74	Flows and vent zone at summit of Black Mountains.
Petroglyph Wash	36°04'37"N 114°35'44"W	5.43–4.61	Stack of flows related to at least two vents.
Black Point	36°24'43"N 114°23'02"W	6.01	Flows and dikes. Flows interbedded with gypsiferous Tertiary sediments.
Las Vegas Range	36°30'19"N 115°02'30"W	16.4	One or two alkali basalt flows tilted about 20° east extensively covered by Quaternary sediments.
Callville Mesa	36°10'19"N 114°42'30"W	10.46 and 8.49	Olivine-clinopyroxene bearing basaltic-andesite flows erupted from compound cinder cones.
Gold Butte	36°15'00"N 114°15'00"W	9.15–9.46	Flows of alkali basalt along the Gold Butte fault.
Grand Wash trough	36°15'00"N 113°50'00"W	3.99–6.9	Flows, dikes, and plugs of olivine-phyric alkali basalt that locally contain mantle xenoliths.
River Mountains	36°05'00"N 114°50'00"W	13.4–12.1	Andesite-dacite stratovolcano surrounded by a field of dacite domes and a basalt shield.
Wilson Ridge	36°06'21"N 114°37'30"W	13.4	Basalt dikes cutting Wilson Ridge pluton.
Government Wash	36°07'00"N 114°45'00"W	12	80-m-thick section of flows and agglomerates are interbedded with the Lovell Wash member of the Tertiary Horse Spring Formation.
Hamblin-Cleopatra	36°10'00"N 114°36'00"W	14.2–11.5	60 km ² stratovolcano composed of shoshonite, latite, trachydacite, and trachyte lava. Volcano is cut by a radial dike system.
Boulder Wash	36°07'00"N 114°37'00"W	14.2	700-m-thick section of calc-alkaline dacite flows and flow breccias interbedded with flows of pyroxene-olivine andesite.
Eldorado Mountains (isotope data from Daley and DePaolo, 1992)	35°45'00"N 114°42'00"W	18.5–12 (* ⁴⁰ Ar/ ³⁹ Ar dates)	A lower section of basaltic-andesite (predominant) and rhyolite lavas and an upper section of basaltic andesite, dacite, and rhyolite. The sections are separated by a dacite ash-flow tuff (tuff of Bridge Spring).

*All dates are K-Ar except where noted.

Formation. Total outcrop area is about 12 km².

Las Vegas Range. The Las Vegas Range locality is composed of thin flows of alkali basalt in a fault-bounded basin just to the west of U.S. highway 93 (Fig. 1). Flows (2 km²) are mostly covered by Quaternary fanglomerate and alluvium, and as a result, no source area was discovered. Basalt in the Las Vegas Range is dated at 16.4 ± 0.6 Ma (K-Ar whole rock date; Smith, unpub. data).

Basalt of Government Wash. Olivine-phyric basalt crops out near Government Wash just north of Lake Mead. A 60- to 80-m-thick section of flows and agglomerates is interbedded with the Lovell Wash member of the Tertiary Horse Spring Formation (Duebendorfer, 1991, personal commun.). Basalt of

Government Wash is dated at 12.0 Ma (K-Ar plagioclase date) (Duebendorfer and others, 1991).

SOURCE OF MAFIC LAVAS

Introduction

Crustal contamination is less of a factor for alkalic than tholeiitic rocks, because the former are lower in volume and less likely to reside in upper crustal chambers where open system processes occur. Also, high Sr and light rare-earth-element concentrations of alkalic magmas tend to overwhelm any effects of crustal contamination. Furthermore, alkalic magmas commonly contain mantle xenoliths and apparently rise quickly through the

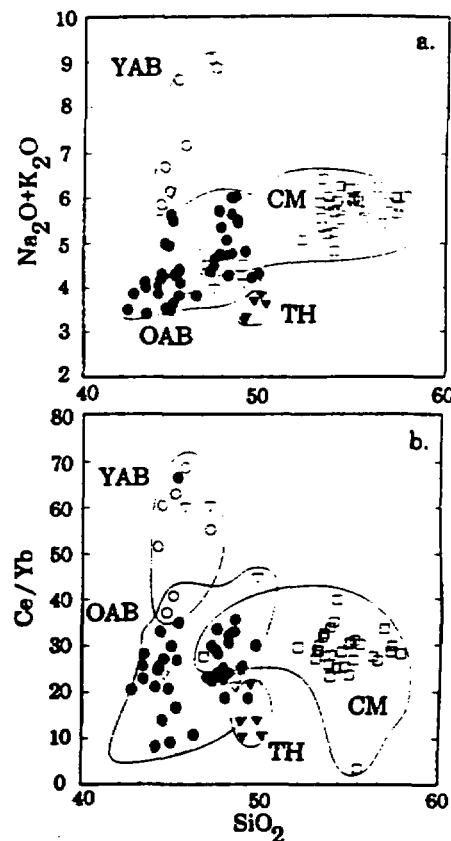


Figure 3. a. Plot of total alkalis (Na₂O + K₂O) versus SiO₂ for volcanic rocks of the Fortification Hill volcanic field, Callville Mesa, Black Point, and Malpais Flattop. Open circles, young alkali basalts (YAB) of the Fortification Hill field; filled circles, older alkali basalts (OAB) of the Fortification Hill field; open triangles, hypersthene normative alkali basalts (OAB-hy) of the Fortification Hill field; filled triangles, tholeiitic basalts (TH) from Malpais Flattop; open boxes, mafic lavas of Callville Mesa (CM).

b. Plot of Ce/Yb versus SiO₂ for volcanic rocks of the Fortification Hill volcanic field, Callville Mesa, Black Point, and Malpais Flattop. Symbols are the same as in Figure 3a. Solid circles surrounded by dotted line are mafic lavas at Black Point.

crust with little or no contamination (for example, Glazner and Farmer, 1992). Smith and others (1990) indicated that crustal contamination was an important factor in the production of intermediate lavas of the River Mountains. In this paper, we demonstrate that crustal contamination also affected the mafic lavas at Callville Mesa, hypersthene-normative alkali basalts (OAB-hy) of the Fortification Hill field, and tholeiitic basalts at Malpais Flattop. Although these magmas were con-

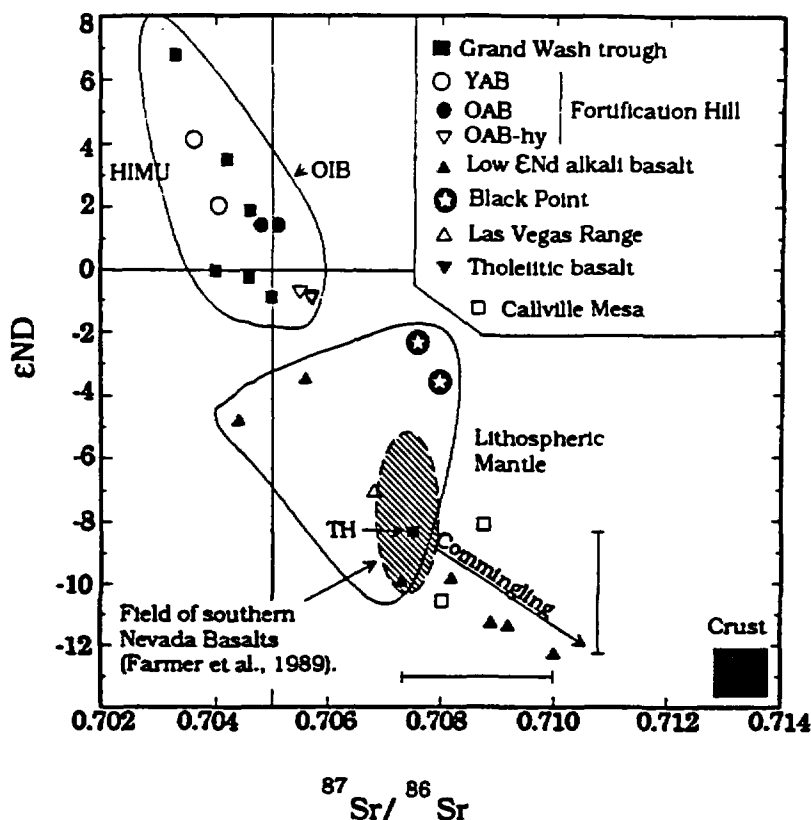


Figure 4. Post-9 Ma alkali basalts in the northern Colorado River extensional corridor are similar to ocean island basalts (OIB) in terms of ϵ_{Nd} and $^{87}Sr/^{86}Sr$. Pre-9 Ma mafic lavas region wide and post-9 Ma basalts in the amagmatic zone originated in the lithospheric mantle. Lithospheric mantle in the Lake Mead area has a wider range of isotopic compositions than lithospheric mantle reported by Farmer and others (1989) for southern Nevada basalts. In the River Mountains, magma commingling resulted in a change of ϵ_{Nd} of about 4 units and $^{87}Sr/^{86}Sr$ of about 0.002 (indicated by brackets). DM, depleted mantle (MORB); HIMU, a mantle component with high μ ($^{238}U/^{204}Pb$); OIB, ocean island basalt, TH, tholeiitic basalt.

taminated by crust, we will show that the isotopic shift due to crustal interaction is small when compared to the overall isotopic variation. Therefore, the isotopic composition of these contaminated mafic magmas is not shifted enough by crustal interaction to mask the character of their mantle source. They are still useful for the mapping of mantle domains.

Mantle Source and Crustal Contamination

OAB, YAB, and Grand Wash Trough. YAB and OAB of the Fortification Hill field and alkali basalts of Grand Wash trough have $^{87}Sr/^{86}Sr = 0.703-0.706$, $\epsilon_{Nd} = -1$ to $+6.7$, $^{206}Pb/^{204}Pb = 17.8-18.7$ and $^{208}Pb/^{204}Pb = 38-38.5$ (Table 1). These alkali basalts have Nd and Sr isotopic compositions and trace-element distributions that are similar to those of modern-day ocean island basalts (OIB) (Zindler and Hart, 1986; Fitton and others,

1991) (Fig. 4). We suggest that YAB originated from a source dominated by asthenospheric mantle, and as discussed below, OAB melted a mixed asthenospheric mantle-lithospheric mantle source dominated by asthenospheric mantle (Table 2).

When compared to typical OIB and the alkali basalts of the Grand Wash trough, OAB and YAB appear to contain an additional component. YAB and OAB plot between

lithospheric mantle and higher values of ϵ_{Nd} and $^{206}Pb/^{204}Pb$ (Fig. 5) rather than lower Pb and higher ϵ_{Nd} as do Grand Wash trough basalts. We suggest that the trend toward higher rather than lower Pb is due to the presence of HIMU-like mantle ($\epsilon_{Nd} = 3.5$, $^{206}Pb/^{204}Pb > 20$) in the source of OAB and YAB. HIMU-like mantle may reside in either the lithospheric mantle or upper asthenosphere (Zindler and Hart, 1986; Hart, 1988; Hart and others, 1992) or as detached oceanic slabs deep within the mantle (Weaver, 1991b). Weaver (1991b) and Hart and others (1992) suggest that the source of HIMU mantle is in the asthenosphere and that it is incorporated into the OIB source by rising plumes or mantle diapirs. We infer that the presence of this component in OAB and in xenolith-bearing YAB and its higher abundance in xenolith-bearing alkali basalts are more compatible with its residence in asthenospheric mantle than in lithospheric mantle.

OAB-containing normative hypersthene (OAB-hy) are the oldest mafic lavas of the Fortification Hill field and have higher $^{87}Sr/^{86}Sr$ (0.7055-0.7057) and lower ϵ_{Nd} (-0.68 to -0.9) than the nepheline normative basalts of this group (Fig. 4). Both crustal contamination and the presence of a lithospheric mantle component in the source must be considered as explanations for the lower ϵ_{Nd} and higher $^{87}Sr/^{86}Sr$ of the OAB-hy lavas. Glazner and Farmer (1992) demonstrated that xenolith-bearing alkali basalts from the Mojave Desert, California, have Sr and Nd isotopic compositions similar to typical OIB, and xenolith-free basalts have a range of compositions that trend from OIB toward values more typical of continental lithosphere. They suggest that these isotopic compositions can be explained if xenolith-bearing magmas passed through the crust quickly without interaction and xenolith-free magmas stopped in the crust long enough for xenoliths to drop or be digested and for crustal interaction to occur. In detail, alkali basalts in the Mojave Desert display a trend toward higher $^{87}Sr/^{86}Sr$ and lower ϵ_{Nd} with time (Glazner and Farmer,

TABLE 2. SOURCE OF MAFIC VOLCANIC ROCKS IN THE LAKE MEAD AREA

Magma type	YAB	OAB-ne	OAB-hy	TH	LOW ϵ_{Nd} alkali basalts
Components in source	AM + HIMU + LM	AM + HIMU + LM	AM + LM + HIMU	LM + CRUST (contamination)	LM + CRUST (commingling)

Notes: Size of text indicates relative contribution of each component. YAB, young alkali basalts of the Fortification Hill field; OAB-ne and OAB-hy, nepheline- and hypersthene-bearing alkali basalts of the Fortification Hill field; TH, tholeiitic basalts at Malpais Flattop; AM, asthenospheric mantle; LM, lithospheric mantle; HIMU, high uranium ($^{238}U/^{204}Pb$) mantle component.

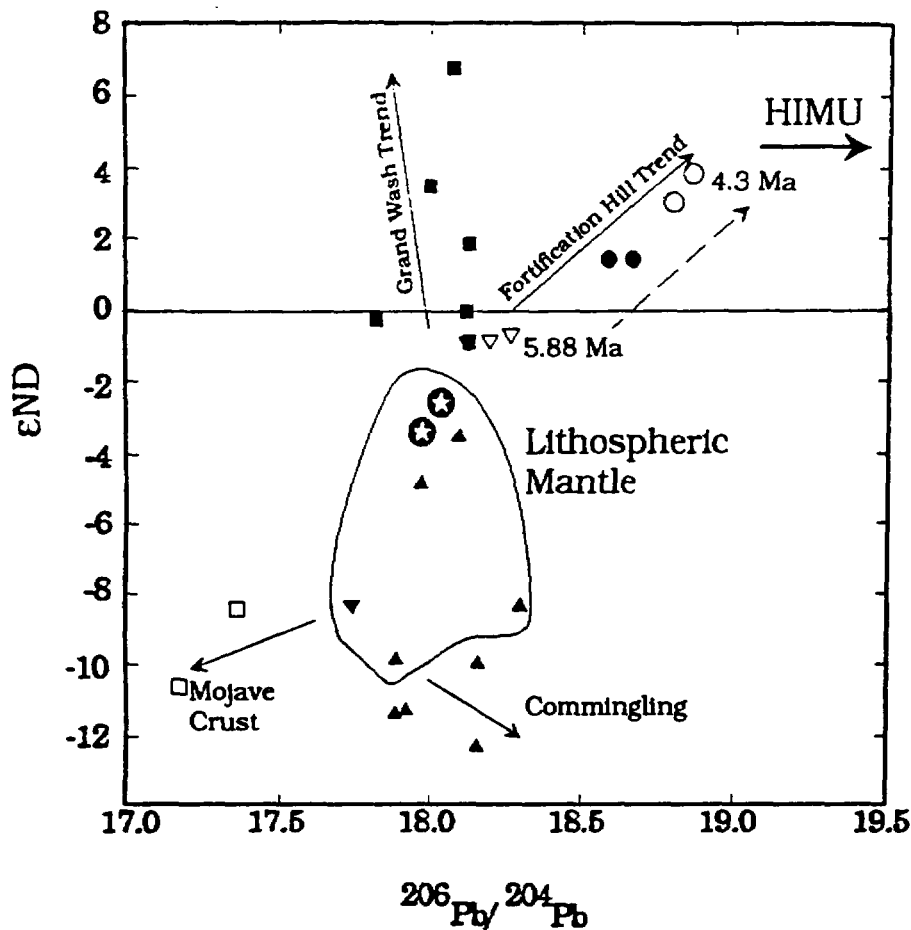


Figure 5. Mafic lavas of the Fortification Hill field appear to contain an HIMU-like component in their source. Fortification Hill basalts define a trend that extends from lithospheric mantle toward HIMU-like mantle. Mafic lavas of the Grand Wash trough lack this component and trend toward typical asthenospheric mantle. Callville Mesa lavas are low in Pb and show the effect of contamination by Mojave-type crust (lower to middle crust). Mafic volcanic rocks in the River Mountains commingling with felsic upper crust and trend toward higher $^{206}\text{Pb}/^{204}\text{Pb}$. Symbols are defined in Figure 4.

1992). They attributed this trend to the hybridization of asthenospherically derived partial melts by commingling with partial melts of Late Jurassic gabbro and Proterozoic diabase. By this mechanism, ϵ_{Nd} can be changed by as much as three units without appreciably changing major- or trace-element chemistry. Although it is possible that such a mechanism is active in this area, two observations suggest that the Glazner and Farmer (1992) model does *not* explain the isotopic composition of OAB-hy. First, in the northern Colorado River extensional corridor, a probable mafic crustal contaminant is Proterozoic (1.7 Ga) amphibolite that crops out in the footwall of the Saddle Island detachment (Duebendorfer and others, 1990). Isotopically, the amphibolite has low $^{87}\text{Sr}/^{86}\text{Sr}_{\text{T} = 6 \text{ Ma}}$ (0.7029) and high $\epsilon_{\text{NdT} = 6 \text{ Ma}}$ (3.18). There-

fore, contamination of asthenospherically derived magmas by this type of crust *will probably not* produce OAB-hy or other xenolith-free mafic lavas. Second, OAB-hy are temporally separated from other magma types in the northern Colorado River extensional corridor. This temporal distribution is circumstantial evidence that OAB-hy magmas may sample a different mixture of mantle than OAB-ne or YAB. Therefore, we suggest that OAB-hy and some OAB-ne probably represent a mixture of asthenospheric mantle and lithospheric mantle (Fig. 5) and not cryptic contamination of mafic magmas by crust.

The trend toward higher ϵ_{Nd} , lower $^{87}\text{Sr}/^{86}\text{Sr}$, and higher $^{206}\text{Pb}/^{204}\text{Pb}$ between 6 and 4 Ma (Figs. 4 and 5) suggests that if the source for OAB is a mixture of asthenospheric mantle and lithospheric mantle, then the ratio of

lithospheric mantle to asthenospheric mantle is decreasing in the source with time. This relation implies that the source of OAB was near the boundary between asthenospheric mantle and lithospheric mantle and *either* this boundary rose through the source area due to extension-related lithospheric thinning, or the depth of melting increased between 6 and 4.3 Ma. As little upper-crustal extension occurred between 6 and 4.3 Ma (Feuerbach and others, 1991), we prefer the latter model. Alkali basalts are generated from mantle peridotite at pressures between 15 and 20 kbar corresponding to a depth of about 45 to 60 km (Takahashi and Kushiro, 1983). The boundary between lithospheric mantle and asthenospheric mantle beneath the northern Colorado River extensional corridor was probably in this depth range during the Pliocene. Our depth estimate is consistent with the depth of the lithospheric mantle-depleted mantle (asthenosphere) boundary estimated by Daley and DePaolo (1992; Fig. 1) for the same time interval and geographic area.

Low ϵ_{Nd} Basalts. Low ϵ_{Nd} alkali basalts occur as pre-11 Ma lavas in the River Mountains, Eldorado Range, Boulder Wash area, Hamblin-Cleopatra volcano, and in the Las Vegas Range, and as post-11 Ma lavas at Callville Mesa and Black Point ($^{87}\text{Sr}/^{86}\text{Sr} = 0.705\text{--}0.710$ and $\epsilon_{\text{Nd}} = -4$ to -12) (Fig. 4).

Andesite and dacite in the River Mountains show abundant field and petrographic evidence of assimilation and magma commingling (Smith and others, 1990). Alkali basalt lacks evidence of contamination and was considered by Smith and others (1990) to have been generated by partial melting of mantle peridotite. Intermediate lavas in the River Mountains may represent hybrid compositions formed by the commingling of mafic and felsic end members. This interpretation is supported by a positive correlation between $^{87}\text{Sr}/^{86}\text{Sr}$ and SiO_2 and a negative correlation between ϵ_{Nd} and SiO_2 (Fig. 6). The isotopic compositions of basalt and rhyolite end members of the mixing sequence provide a quantitative estimate of the magnitude of isotopic shift due to magma commingling (Fig. 4). This shift is no more than four units in ϵ_{Nd} and 0.002 in $^{87}\text{Sr}/^{86}\text{Sr}$.

Callville Mesa lavas have $^{87}\text{Sr}/^{86}\text{Sr} = 0.708\text{--}0.709$ and $\epsilon_{\text{Nd}} = -8$ to -10 and are similar in isotopic composition and trace-element chemistry (high Ba, K, and Sr and low Nb and Ti) to mafic lavas derived from lithospheric mantle in the western United States (Fitton and others, 1991; Farmer and others, 1989). Callville Mesa lavas differ, however,

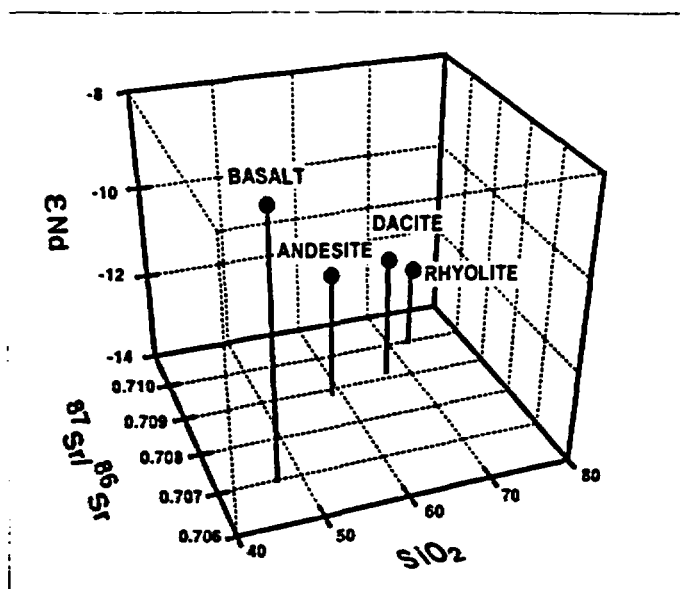


Figure 6. Three-dimensional plot of ϵ_{Nd} versus $^{87}Sr/^{86}Sr$ versus SiO_2 for volcanic rocks of the River Mountains. The positive correlation between SiO_2 and $^{87}Sr/^{86}Sr$ and the negative correlation between SiO_2 and ϵ_{Nd} suggest that rhyolite and basalt are end members of a mixing sequence. Intermediate compositions represent the mixing of the end-member compositions in various proportions.

by having lower Pb ratios ($^{207}Pb/^{204}Pb = 15.45-15.5$; $^{208}Pb/^{204}Pb = 37.7-38$; $^{206}Pb/^{204}Pb = 17.2-17.4$) than typical lithospheric-mantle-derived basalts ($^{207}Pb/^{204}Pb = 15.6$; $^{208}Pb/^{204}Pb = 38.7$; $^{206}Pb/^{204}Pb = 18.3$) (Fig. 5); having trends on Rb/Sr, Th/Nb, and La/Nb versus SiO_2 plots that project toward crustal compositions (Figs. 7a, 7b, and 7c); and by displaying ample evidence of crustal contamination. These geochemical and petrographic features suggest that Callville magmas were contaminated by the crustal material. The crustal component has $^{87}Sr/^{86}Sr > 0.710$, low Pb isotope ratios, and $\epsilon_{Nd} < -10$ (Fig. 5). We suggest that the crustal contaminant is similar in chemistry to Proterozoic rocks of the Mojave crustal province, which extends into the Lake Mead area (Wooden and Miller, 1990). Although rocks of the Mojave province display a wide range of Pb isotope values, low ratios ($^{207}Pb/^{204}Pb < 15.5$; $^{208}Pb/^{204}Pb < 38$; $^{206}Pb/^{204}Pb < 17.4$) are common. Because of the common occurrence of quartz and alkali feldspar xenocrysts in Callville Mesa lavas, the contaminant is inferred to be a felsic rock. Uncontaminated magma at Callville Mesa is similar in major- and trace-element composition to OAB. A normative nepheline-bearing alkali basalt (sample 24-100; Table 1), the oldest flow recognized from the Callville Mesa center, plots in the field of OAB in terms of $Na_2O + K_2O$

(Fig. 3a), Ce/Yb (Fig. 3b), and trace-element ratios (Fig. 7).

Tholeiitic Basalt. Tholeiitic basalts at Malpais Flattop have high Sr ($^{87}Sr/^{86}Sr = 0.7075$), low ϵ_{Nd} (-8.33), and increasing Rb/Nb, Th/Nb, and La/Nb (Figs. 7a, 7b, and 7c). These lavas may have been contaminated as they passed through the crust. It is generally accepted that tholeiitic basalts equilibrate at shallower depths in the mantle than alkali basalts (24 to 45 km; Takahashi and Kushiro, 1983). If OAB were generated near the lithospheric mantle-asthenospheric mantle boundary as suggested above, it is reasonable to conclude that the tholeiitic basalts were produced by melting of lithospheric mantle. Tholeiitic basalts in the western United States are generally assumed to have been affected by small amounts of crustal contamination as well as fractional crystallization (Dungan, 1992). The close spatial and temporal association of alkali and tholeiitic basalts, lack of mantle xenoliths, together with isotopic and chemical signatures support the contamination hypothesis (for example, Perry and others, 1987; Glazner and Farmer, 1992). To estimate the changes in isotopic composition of lithosphericly derived magmas due to crustal contamination, we compared tholeiitic basalts to alkali basalt derived in the lithospheric mantle (for example, Las Vegas Range alkali basalt to Malpais Flattop

tholeiite). Tholeiitic basalts have higher $^{87}Sr/^{86}Sr$ and lower ϵ_{Nd} than alkali basalts ($^{87}Sr/^{86}Sr = 0.0007$ higher; $\epsilon_{Nd} = 1.13$ lower). Other investigators noted similar isotopic changes due to crustal contamination. For example, Glazner and Farmer (1992) noted a shift in ϵ_{Nd} by as much as three units as the result of contamination of mafic magmas by mafic crust. Daley and DePaolo (1992) estimated that ϵ_{Nd} may be lowered by 2 to 3 units by crustal contamination. Crowley (1984) demonstrated a shift in $^{87}Sr/^{86}Sr$ by as much as 0.001 when comparing tholeiites and alkali basalts derived from the lithospheric mantle. On the basis of our data and the work of others, we conclude that the isotopic compositions of tholeiitic basalt reflect the melting of enriched mantle (lithospheric mantle) and that the changes in ϵ_{Nd} (1 to 3 units) and $^{87}Sr/^{86}Sr$ (0.001) due to crustal contamination are small when compared to overall variations of ϵ_{Nd} and $^{87}Sr/^{86}Sr$ between these rocks and the alkali basalts.

Summary

Mafic lavas of the northern Colorado River extensional corridor represent the melting of a complex and variable mixture of asthenospheric mantle, lithospheric mantle, and crust (Table 2). YAB represent the melting of a source composed mainly of a mixture of asthenospheric mantle and HIMU-like mantle. The source of OAB-hy and OAB-ne is a mixture of asthenospheric mantle and lithospheric mantle dominated by asthenospheric mantle. Low ϵ_{Nd} and high $^{87}Sr/^{86}Sr$ magmas and tholeiites were derived from a lithospheric mantle source and were contaminated as they passed through the crust. This shift in isotopic values due to crustal interaction (commingling and contamination) is no more than 4 units in ϵ_{Nd} and 0.002 in $^{87}Sr/^{86}Sr$ and does not mask the character of the mantle source.

MANTLE AND CRUSTAL BOUNDARIES

In this section, we argue that (1) the boundary between two crustal provinces, the northern Colorado River extensional corridor and the amagmatic zone, corresponds in general to a mantle boundary between asthenospheric mantle beneath the northern Colorado River extensional corridor and lithospheric mantle beneath the amagmatic zone; (2) the mantle boundary formed between about 11 and 6 Ma, during and just after the main phase of Tertiary extension in the western Lake Mead area (9 to 12 Ma),

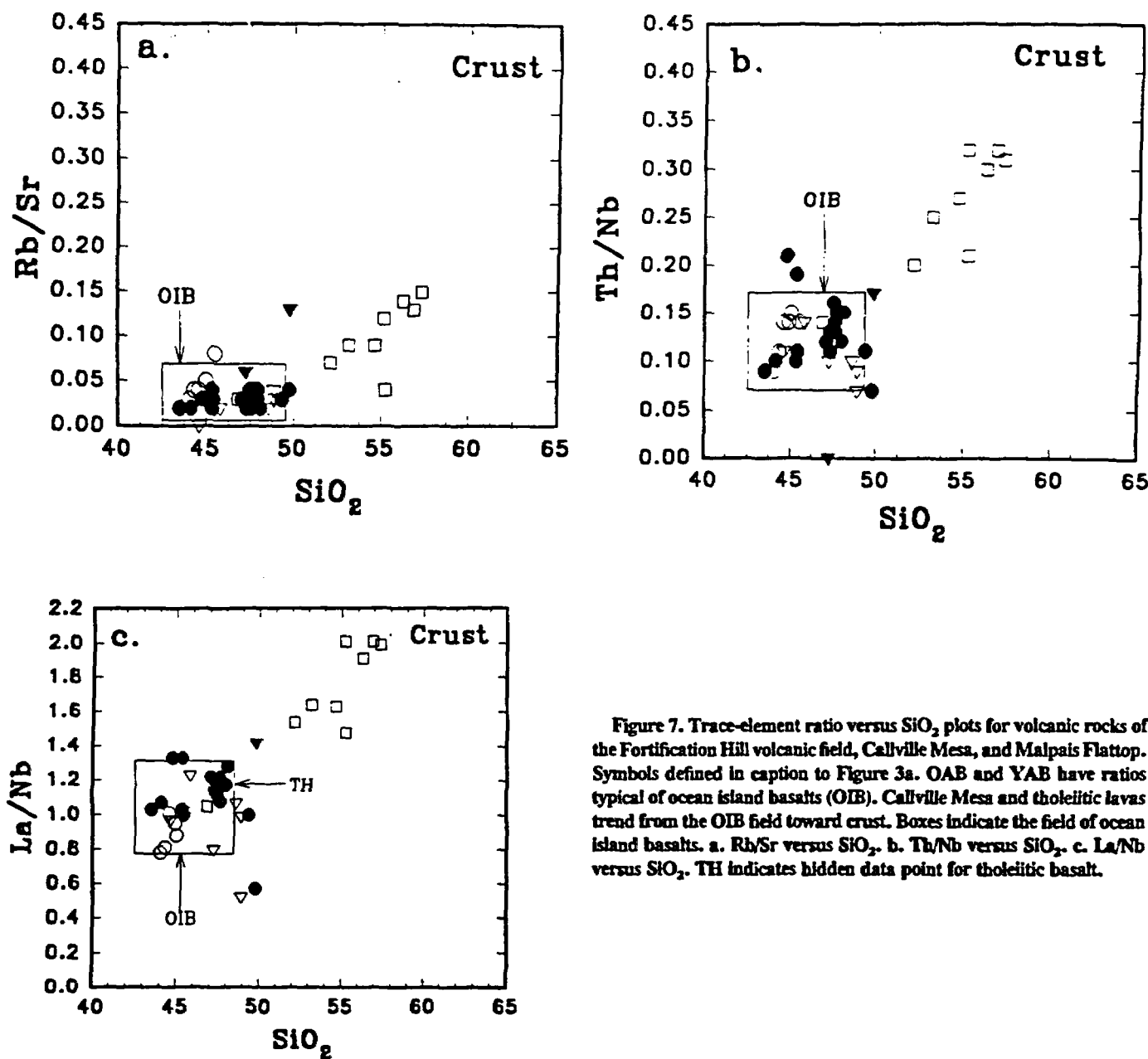


Figure 7. Trace-element ratio versus SiO_2 plots for volcanic rocks of the Fortification Hill volcanic field, Callville Mesa, and Malpais Flattop. Symbols defined in caption to Figure 3a. OAB and YAB have ratios typical of ocean island basalts (OIB). Callville Mesa and tholeiitic lavas trend from the OIB field toward crust. Boxes indicate the field of ocean island basalts. a. Rb/Sr versus SiO_2 . b. Tb/Nb versus SiO_2 . c. La/Nb versus SiO_2 . TH indicates hidden data point for tholeiitic basalt.

(3) the Lake Mead fault system may locally be the upper-crustal expression of the mantle boundary; and (4) during the peak of extension, passive rifting resulted in upwelling asthenospheric mantle beneath the northern Colorado River extensional corridor.

Our arguments below are based on the premise that depth of generation of alkali basalt magma in the study area remains relatively constant with time from 16 to 9 Ma (the period of peak extension regionally; see below). This assumption is based on the work of Takahashi and Kushiro (1983). Tholeiitic basalts are generated by partial melting of man-

tle peridotite with the mineral assemblage clinopyroxene, olivine, orthopyroxene at pressures of 8 to 15 kbar corresponding to depths of 24 to 45 km. Alkali basalts are produced from a similar source at pressures between 15 and 20 kbar corresponding to a depth of about 45 to 60 km. Crustal extension is accompanied by the rise of the geotherm to higher levels of the lithosphere. Therefore the expected relationship between extension and volcanism is the production of tholeiitic basalts during extension when isotherms are elevated, and alkali basalts late when isotherms relax. In the Lake Mead area, however, the

most compositionally primitive basalts in any given area are generally alkalic regardless of age and relation to extension. An exception is the tholeiitic basalt at Malpais Flattop. Therefore, depth of melting appears to remain relatively constant with time, and variations in chemical and isotopic compositions are due to the rise of the lithospheric mantle-asthenosphere compositional boundary rather than significant changes in the depth of melting.

In our discussion below, we divide the mafic volcanic rocks into those that erupted during and prior to the major phase of upper-crust extension and those that erupted during

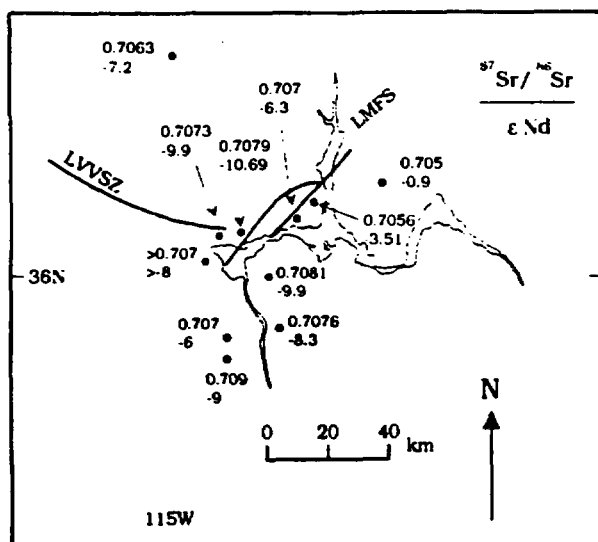


Figure 8. Map showing $^{87}\text{Sr}/^{86}\text{Sr}$ and ϵ_{Nd} for pre-9 Ma mafic lavas in the Lake Mead area. The amagmatic zone lies to the north of the Lake Mead fault system (LMFS); the Northern Colorado River extensional corridor is to the south. Prior to 9 Ma, isotopic values were relatively constant across the Lake Mead region and indicate that mafic volcanoes are tapping lithospheric mantle.

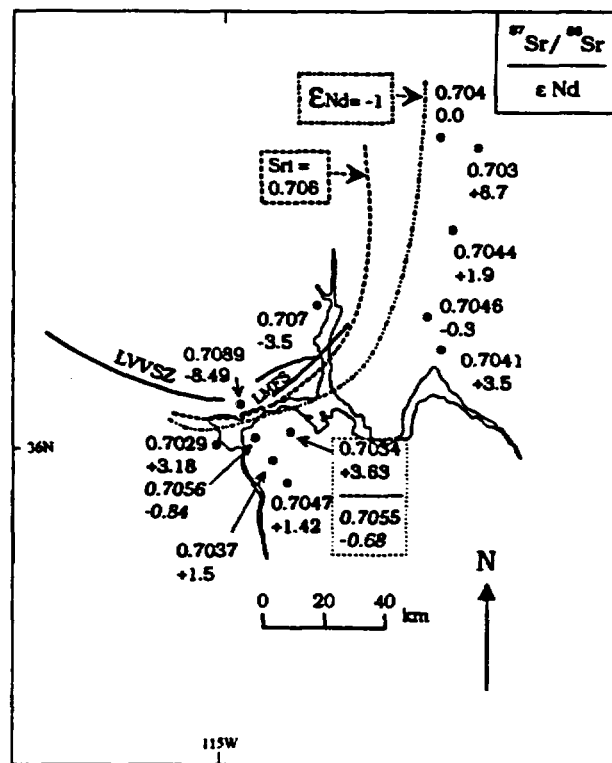
a period of reduced upper-crust extension. The time of peak upper-crustal extension varies across the region (Wernicke and others, 1988; Fitzgerald and others, 1992); however, in the Las Vegas-western Lake Mead area it occurred between 12 and 9 Ma (Duebendorfer and Wallin, 1991). To the south in the Eldorado and Black Mountains and to the east in the Gold Butte and Virgin Mountains, extension began at about 16 Ma (Anderson, 1971; Wernicke and others, 1988; Faulds and others, 1990). Wernicke estimated that in the Las Vegas region 75% of extension occurred between 16 and 10 Ma, and 25%, between 10 and 5 Ma. Structural information from the Lake Mead region suggests that 9 Ma is a more precise date for the termination of peak extension (Duebendorfer and Wallin, 1991). Therefore, we use 9 Ma to separate mafic lavas produced during the peak of extension from those that erupted during waning extension.

The Mantle Boundary

Isotopic data for post-9 Ma mafic lavas show regional differences that we infer to be a boundary in the magma's source region in the mantle. Contours ($^{87}\text{Sr}/^{86}\text{Sr} = 0.706$ and $\epsilon_{\text{Nd}} = -1$) separating lavas with a dominant lithospheric mantle component ($^{87}\text{Sr}/^{86}\text{Sr} > 0.706$, $\epsilon_{\text{Nd}} < -1$) from those with an asthenospheric mantle component ($^{87}\text{Sr}/^{86}\text{Sr} < 0.706$, $\epsilon_{\text{Nd}} > -1$) define a boundary that extends from just north of the River Mountains into the Grand Wash trough (Fig. 8). The boundary parallels the Lake Mead fault system along most of its length and is also roughly coincident with the boundary between the northern Colorado River exten-

sional corridor and the amagmatic zone. The regional extent of the boundary cannot be determined by isotopic techniques because of a lack of alkali basalt exposures of suitable age to the northeast and southwest of the Lake Mead area. The boundary in the Lake Mead area, however, may represent a short segment of a regionally continuous mantle boundary between asthenospheric and lithospheric mantle domains that passes through southern Nevada (Menzies, 1989). Post-9 Ma magmas tap mantle dominated by asthe-

Figure 9. Map showing $^{87}\text{Sr}/^{86}\text{Sr}$ and ϵ_{Nd} for post-9 Ma mafic lavas in the Lake Mead area. Contours separate areas where mafic volcanoes are tapping asthenospheric mantle ($\epsilon_{\text{Nd}} > -1$, $^{87}\text{Sr}/^{86}\text{Sr} < 0.704$) from those areas where volcanoes are tapping lithospheric mantle. Note that the Lake Mead fault system is colinear with the isotopic contours and that asthenospheric mantle is mainly present to the south in the Northern Colorado River extensional corridor. Values in italics are OAB-by.



spheric mantle to the south of the boundary and lithospheric mantle to the north. Because sample locations in some areas are separated by considerable distance, placement of these contours is somewhat arbitrary; however, they do define the general area of isotopic change. We suggest that this boundary formed during and just after the period of peak extension. Pre-9 Ma basalts throughout the region have uniform ϵ_{Nd} and $^{87}\text{Sr}/^{86}\text{Sr}$ and were derived by melting of lithospheric mantle (Fig. 9). Also, trace-element compositions of pre-9 Ma mafic lavas are similar to those basalts of the Western Great Basin province derived from lithospheric mantle (Fitton and others, 1991) (Fig. 10a). Therefore, prior to about 9 Ma, lithospheric mantle extended beneath the Lake Mead area. Post-9 Ma basalts in the northern Colorado River extensional corridor to the south of the boundary display a dramatic shift in $^{87}\text{Sr}/^{86}\text{Sr}$ and ϵ_{Nd} . $^{87}\text{Sr}/^{86}\text{Sr}$ changes from about 0.707 to 0.703-0.705, and ϵ_{Nd} changes from about -9 to higher values (-1 to +6.7) (Fig. 8). Chemically, mafic volcanic rocks acquire the signature of OIB lavas of the Transition Zone (Fig. 10b). In the amagmatic zone to the north of the boundary, post-9 Ma mafic lavas at Black Point and at Callville Mesa retain the isotopic signature of pre-9 Ma lavas (Fig. 8) and may represent the easternmost limit of the southern Nevada basalt field of Farmer and others (1989). Our

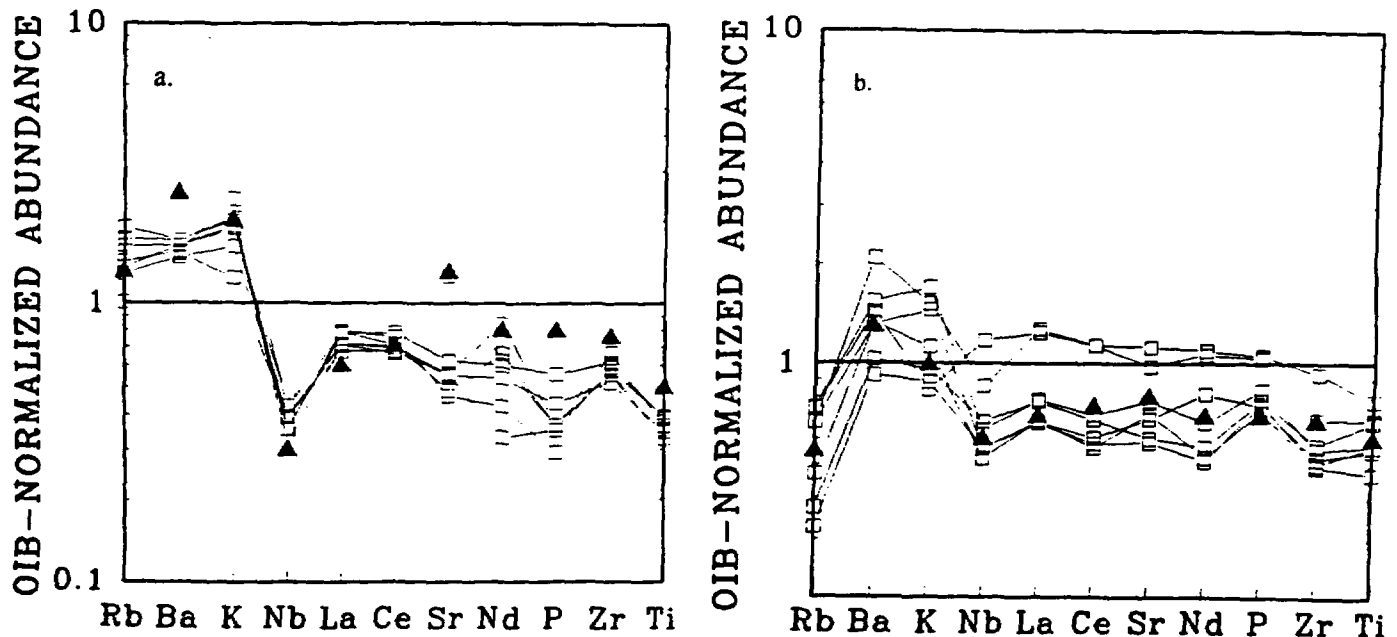


Figure 10. a. Mafic volcanic rocks in the Lake Mead area that were erupted prior to 9 Ma (open squares) are similar to lavas of the Western Great Basin province (solid triangles) produced by melting lithospheric mantle (Fitton and others, 1991). b. Spider plot of incompatible elements versus abundance normalized to OIB average of Fitton and others (1991). Post-9 Ma mafic lavas in the Northern Colorado River extensional corridor (open squares) are similar in trace-element abundance and pattern to lavas in the Colorado Plateau-Basin and Range Transition Zone derived by melting asthenospheric mantle (solid triangles) (Fitton and others, 1991).

interpretation of these data is that between 11 and about 6 Ma, the source of mafic lavas in the northern Colorado River extensional corridor changed from lithospheric mantle to asthenospheric mantle. The source of lavas in the amagmatic zone remained in the lithospheric mantle. Apparently, the lithospheric mantle was thinned or removed from beneath the northern Colorado River extensional corridor but remained intact beneath the amagmatic zone. Therefore, we infer that the mantle boundary between lithospheric mantle (north) and asthenospheric mantle (south) formed between about 11 and 6 Ma.

Mantle Plumes?

The change in source of basalts from lithospheric mantle to asthenospheric mantle with time, the OIB character of the mafic lavas, and the presence of an HIMU-type mantle component are compatible with the presence of a rising asthenospheric plume beneath the northern Colorado River extensional corridor. Mechanisms to account for lithospheric extension and OIB-type volcanism commonly call for an upwelling mantle plume (active rifting) (for example, Eaton, 1982; Fitton and others, 1991).

Unusually hot asthenosphere may not be required to induce lithospheric extension and

volcanism (Buck, 1986; Perry and others, 1987; White, 1987; White and others, 1988). Mantle upwelling may be passive and caused by stretching and thinning of the lithosphere. The mantle rises to compensate for thinning crust. Melting results from the decompression of asthenospheric mantle as it rises passively beneath the stretched and thinned lithosphere. Small increases in temperature are sufficient to generate large volumes of melt during decompression. An increase of 100 °C doubles the amount of melt; 200 °C can quadruple melt volume (White and McKenzie, 1989). During passive mantle upwelling, isotopically enriched lithosphere may be thermally but not chemically converted to asthenosphere and may convectively mix with isotopically depleted asthenospheric mantle (Perry and others, 1987). OIB basalts may result from the partial melting of this two-component mantle. Hence, a deep mantle source for OIB is not required.

Passive-rifting models imply that mantle convection is coupled to the lithosphere and OIB-type volcanism may occur for long periods of time in a restricted geographic area. Perry and others (1987, 1988) applied a passive rifting model to the Rio Grande rift in central New Mexico and suggested that volcanism in the Colorado Plateau-Basin-Range transition zone may be explained by passive

rifting. Recently, Bradshaw (1991) suggested a modified passive-rifting model. Plate tectonics, rather than deep-seated mantle plumes, may provide the ultimate driving force for extension and magmatism. According to Bradshaw, melting of lithospheric mantle in the northern Colorado River extensional corridor was initiated by heat input from warmer asthenosphere as it rose to fill a slab window left by the northward migration of the Mendocino triple junction.

Passive rifting is probably more applicable to the northern Colorado River extensional corridor than active rifting for two reasons. First, active plumes produce large volumes of mantle-derived melt (for example, Gallagher and Hawkesworth, 1992). Very low volumes of alkali basalt magma produced after 9 Ma in the Lake Mead area suggest that an active plume was not present during this time. Second, alkali basalt magmas in the northern Colorado River extensional corridor result from melting a three-component source composed of lithospheric mantle, asthenospheric mantle, and HIMU mantle. Lithospheric mantle was an important component in the source of older OAB-type and low ϵ_{Nd} alkali basalts but becomes less important with time. This geochemical pattern is compatible with the model of passive rifting and lithospheric erosion as described by

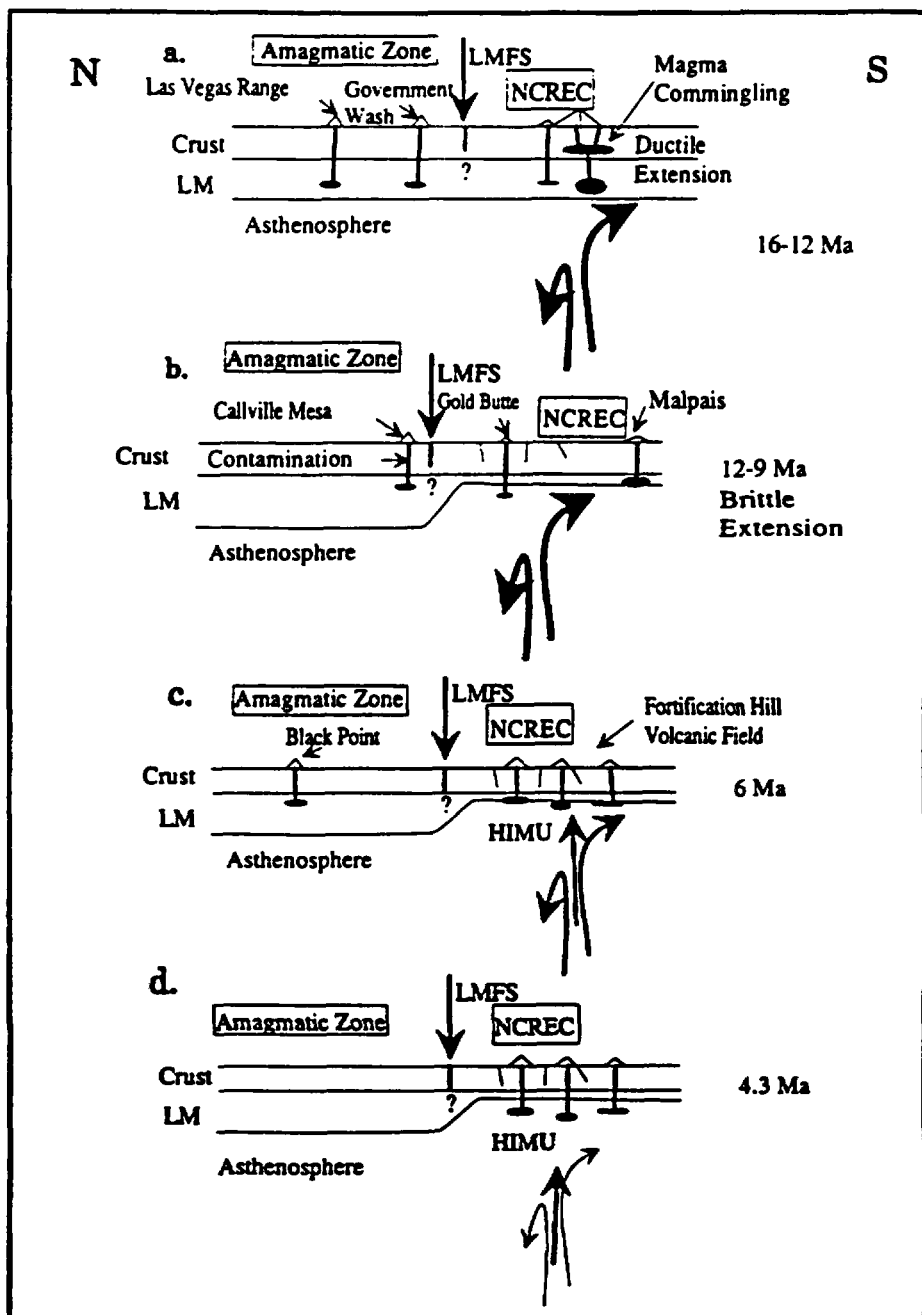
Figure 11. Summary of mantle evolution and magmatism in the Lake Mead area. Sections are diagrammatic and are roughly drawn in a north-south direction. Mantle currents and crustal extension are in an east-west direction. LMFS, Lake Mead Fault system; NCREC, northern Colorado River extensional corridor.

a. *Early Stage of Extension.* Crustal extension was initiated at about 16 Ma in the Lake Mead–Gold Butte area by either active mantle convection (Fitton and others, 1991) or the opening of a slab window (Bradshaw, 1991). Mafic magmas were generated in lithospheric mantle and locally rose to the surface without being significantly contaminated (for example, Las Vegas Range, alkali basalt in River Mountains). Mafic magma stalled in the crust at “ductile barriers” and commingled with crustal magma to form calc-intermediate volcanoes and plutons (Smith and others, 1990; Bradshaw, 1991).

b. *Peak of Extension.* Upper crustal extension occurred in the western Lake Mead portion of the northern Colorado River extensional corridor between 12 and 9 Ma but was not accompanied by significant magmatism. During extension in the northern Colorado River extensional corridor, lithospheric mantle may have been thinned and replaced by asthenosphere progressively to the west. During thinning and replacement of the lithospheric mantle in the northern Colorado River extensional corridor, the lithospheric mantle in the amagmatic zone remained intact. Contrasting behavior to the north and south of this boundary produced the mantle domain boundary. The Lake Mead fault system is spatially and temporally related to the mantle boundary. The Lake Mead fault system may be the crustal manifestation of differential thinning of the lithospheric mantle. Mantle convection between 12 and 9 Ma is probably passive and is driven by crustal thinning.

c. *After the Peak of Extension.* After the peak of extension, volcanism in the northern Colorado River extensional corridor originates in the asthenosphere near the boundary with the lithospheric mantle at a depth of 45 to 60 km. In the amagmatic zone, mafic volcanic rocks at Black Point originate in the lithospheric mantle. Isotopic compositions of alkali basalts define two mantle domains. The domain to the north is characterized by lithospheric mantle ($\epsilon_{Nd} = -3$ to -9 ; $^{87}Sr/^{86}Sr = 0.706$ – 0.707). To the south, mafic lavas have an OIB-mantle signature and appear to have only a minor lithospheric mantle component in their source ($\epsilon_{Nd} = 0$ to $+4$; $^{87}Sr/^{86}Sr = 0.703$ – 0.705). The change in source of basalts from lithospheric mantle to asthenospheric mantle with time, the OIB character of the mafic lavas, and the presence of an HIMU-like mantle component is compatible with the presence of rising asthenosphere, as an upwelling convective cell, or plume beneath the northern Colorado River extensional corridor at 6 Ma after the peak of extension.

d. *After Extension.* Low-volume xenolith-bearing alkali basalts formed in the northern Colorado River extensional corridor by melting asthenosphere mixed with an HIMU-like component. Because lithospheric thinning is unlikely at 4.3 Ma, the lower proportion of lithospheric mantle in the source of alkali basalts and the higher proportion of HIMU-like mantle suggest that the depth of melting increased between 6 and 4.3 Ma. Passive rifting may have continued as late as 4.3 Ma as evidenced by the presence of the HIMU-like mantle component in mafic lavas of this age.



Perry and others (1987) for the Rio Grande Rift.

Passive rifting may have been preceded by active rifting in the northern Colorado River extensional corridor. Faults and others (1990) suggested that upwelling was active in the northern Colorado River extensional corridor during mid-Miocene extension. Faults and others (1990) developed a kinematic model that implies that extension (spreading) occurred about discrete axes and that highly extended areas lie directly above areas of divergent flow in the asthenosphere. Alternatively, passive rifting between 11 and 6 Ma may have been a continuation of an earlier more intense passive rifting event related to the opening of a slab window left by the northward migration of the Mendocino triple junction (Bradshaw, 1991).

Links between Mantle and Crust

$^{87}\text{Sr}/^{86}\text{Sr} = 0.706$ and $\epsilon_{\text{Nd}} = -1$ contours trend east-northeast and are roughly coincident with the Lake Mead fault system (Fig. 8). The correspondence between isotopic contours and the Lake Mead fault system is especially good just north of Lake Mead where there are numerous isotopic data points and tighter control of the location of the contours (Fig. 8). The Lake Mead fault system is a set of northeast-striking left-lateral faults with 65 km of cumulative slip that occurred between 17 and 10 Ma (Anderson, 1973; Bohannon, 1979, 1984). Weber and Smith (1987) considered the Lake Mead fault system and the Saddle Island detachment (Smith, 1982; Duebendorfer and others, 1990) to be a kinematically coordinated system of faults. If the Weber and Smith (1987) model is correct, then the Lake Mead fault system is a shallow crustal structure. Recently, Smith and others (1991) suggested that the Saddle Island fault originated as a steeply dipping normal fault and that the Lake Mead fault system represents the northern boundary of the Saddle Island allochthon. In this case, the Lake Mead fault system may extend into the middle to lower crust. Faults and others (1990) considered both the Lake Mead fault system and the Las Vegas Valley shear zone as the northern boundary of the northern Colorado River extensional corridor and as corresponding to intracontinental transform faults separating *en echelon* axes of extension. We suggest that the similar trend and geographic location of the isotopic boundaries and the Lake Mead fault system argue for a genetic relationship between the two features. The Lake Mead fault system may

represent the crustal manifestation of differential thinning of the lithospheric mantle or the rejuvenation of an older lithospheric structure. Whatever the connection, it appears that the Lake Mead fault system reflects mantle processes and may be an important deeply penetrating (?) crustal structure.

SUMMARY

The formation of a mantle domain boundary is depicted on four diagrammatic north-south sections across the Lake Mead area (Fig. 11). The sections display the interaction of mantle and crust during the early stage of extension in the Lake Mead area (16–12 Ma), during the peak of extension (12–9 Ma), after the peak of extension during the eruption of Fortification Hill basalts (6 Ma), and after extension during the eruption of xenolith-bearing alkali basalts (4.3 Ma).

ACKNOWLEDGMENTS

This research was supported by a grant from the Nevada Nuclear Waste Project Office. We thank James Faults and Terry Naumann for informative discussions and for reading early versions of this paper. Ernie Duebendorfer, Scott Vetter, and John Shervais provided reviews that helped improve the quality and clarity of the paper. We thank the staff of the Phoenix Memorial Laboratory, University of Michigan, for completing the REE analyses and Dave Nealey (U.S. Geological Survey) for arranging for XRF analyses of selected samples. Partial laboratory support at the University of Kansas was provided by National Science Foundation Grant EAR-8904007 awarded to Walker. We thank Randy Van Schmus and Drew Coleman for helpful discussions concerning the collection of the isotopic data.

REFERENCES CITED

- Anderson, R. E., 1971, Thin skin distension in Tertiary rocks of southeastern Nevada: *Geological Society of America Bulletin*, v. 82, p. 42–58.
- Anderson, R. E., 1973, Large-magnitude late Tertiary strike-slip faulting north of Lake Mead, Nevada: U.S. Geological Survey Professional Paper 794, 18 p.
- Anderson, R. E., Longwell, C. R., Armstrong, R. L., and Marvin, R. F., 1972, Significance of K-Ar ages of Tertiary rocks from the Lake Mead region, Nevada-Arizona: *Geological Society of America Bulletin*, v. 83, p. 273–288.
- Armstrong, R. L., 1966, K-Ar dating using neutron activation for Ar analysis: *Geochimica et Cosmochimica Acta*, v. 30, p. 565–600.
- Armstrong, R. L., 1970, Geochronology of Tertiary igneous rocks, eastern Basin and Range province, western Utah, eastern Nevada, and vicinity, U.S.A.: *Geochimica et Cosmochimica Acta*, v. 34, p. 203–232.
- Barker, D. S., and Thompson, K. G., 1969, Hamblin-Cleopatra volcano, Nevada: Genesis of a shoshonite-lanite-trachydacite-trachyte suite, in *Continental magmatism abstracts, IAVCEI: New Mexico Institute of Mining and Geology Bulletin 131*, p. 17.
- Bennett, V. C., and DePaolo, D. J., 1987, Proterozoic crustal history of the western United States as determined by Nd isotopic mapping: *Geological Society of America Bulletin*, v. 99, p. 674–685.
- Bohannon, R. G., 1979, Strike-slip faults of the Lake Mead region of southern Nevada, in Armentrout, J. M., Cole, M. R., and Terbest, H., eds., *Cenozoic paleogeography of the western United States: Pacific Section, Society of Economic Paleontologists and Mineralogists Pacific Coast Paleogeography Symposium 3*, p. 129–139.
- Bohannon, R. G., 1984, Nonmarine sedimentary rocks of Tertiary age in the Lake Mead region: U.S. Geological Survey Professional Paper 1259, 72 p.
- Bradshaw, T. K., 1991, Tectonics and magmatism in the Basin and Range province of the western United States [Ph.D. dissert.]: Milton Keynes, Great Britain, The Open University, 247 p.
- Buck, W. R., 1986, Small-scale convection induced by passive rifting: The cause for uplift of rift shoulders: *Earth and Planetary Science Letters*, v. 77, p. 362–372.
- Campbell, I., and Schenk, E. T., 1950, *Camptonite dikes near Boulder Dam, Arizona*: *American Mineralogist*, v. 35, p. 671–692.
- Cascadden, T. E., 1991, Style of volcanism and extensional tectonics in the eastern Basin and Range province: Northern Mohave County, Arizona [M.S. thesis]: Las Vegas, Nevada, University of Nevada, 156 p.
- Cascadden, T. E., and Smith, E. L., 1991, Intermediate and mafic volcanic rocks of the northern White Hills, Arizona: Implications for the production of intermediate composition volcanic rocks during regional extension: *Geological Society of America Abstracts with Programs*, v. 23, no. 5, p. 390.
- Cole, E. D., 1989, Petrogenesis of late Cenozoic alkalic basalts near the eastern boundary of the Basin-and-Range: Upper Grand Wash trough, Arizona and Gold Butte, Nevada [M.S. thesis]: Las Vegas, Nevada, University of Nevada, 68 p.
- Cooper, J. L., and Hart, W. K., 1990, Mantle sources in the Arizona transition zone and global mantle heterogeneity: *Geology*, v. 18, p. 1146–1149.
- Crowley, J. C., 1984, Strontium isotope and rare earth element analysis of Rio Grande rift basalts: Implications for magmatism in continental rifts [Ph.D. dissert.]: Providence, Rhode Island, Brown University, 116 p.
- Daley, E. E., and DePaolo, D. J., 1992, Isotopic evidence for lithospheric thinning during extension: Southeastern Great Basin: *Geology*, v. 20, p. 104–108.
- Darvall, P., Gens, P. B., and Lister, G. S., 1991, Normal faulting in the Eldorado Mountains, southeastern Nevada: *Geological Society of America Abstracts with Programs*, v. 23, no. 2, p. 17.
- Duebendorfer, E. M., and Wallin, E. T., 1991, Basin development and syn-tectonic sedimentation associated with kinematically coupled strike-slip and detachment faulting, southeastern Nevada: *Geology*, v. 19, p. 87–90.
- Duebendorfer, E. M., Shafigullah, M., and Damon, P. E., 1991a, The Las Vegas Valley Shear Zone: A middle to late Miocene extensional transfer fault: *Geological Society of America Abstracts with Programs*, v. 23, no. 5, p. A188.
- Duebendorfer, E. M., Sewall, A. J., and Smith, E. L., 1991b, The Saddle Island Detachment fault, an evolving shear zone in the Lake Mead area of southern Nevada, in Wernicke, B., ed., *Mid-Tertiary extension at the latitude of Las Vegas: Geological Society of America Memoir 176*, p. 71–87.
- Dungan, M. A., 1992, Interpretation of elemental and isotopic signatures of extension-related basalts: Implications of Northern Rio Grande Rift volcanism [abs.]: *American Geophysical Union Transactions*, v. 73, no. 10, p. 334.
- Eaton, G. P., 1982, The Basin and Range province: Origin and tectonic significance: *Annual Review of Earth and Planetary Sciences*, v. 10, p. 409–440.
- Eaton, G. P., Wahl, R. R., Probst, H. J., Mabey, D. R., and Kleinkopf, M. D., 1978, Regional gravity and tectonic patterns: Their relation to late Cenozoic tectonics and lateral spreading in the western Cordillera, in Smith, R. B., and Eaton, G. P., eds., *Cenozoic tectonics and regional geophysics of the Western Cordillera: Geological Society of America Memoir 152*, p. 51–93.
- Farmer, G. L., Perry, F. V., Semken, S., Crowe, B., Curtis, D., and DePaolo, D. J., 1989, Isotopic evidence of the structure and origin of subcontinental lithospheric mantle in southern Nevada: *Journal of Geophysical Research*, v. 94, p. 7825–7838.
- Faults, J. E., Geissman, J. W., and Mawer, C. K., 1990, Structural development of a major extensional accommodation zone in the Basin and Range province, northwestern Arizona and southern Nevada: Implications for kinematic models of continental extension, in Wernicke, B. P., ed., *Basin and Range extensional tectonics near the latitude of Las Vegas, Nevada: Geological Society of America Memoir 176*, p. 37–76.
- Faults, J. E., Feuerbach, D. L., and Smith, E. L., 1991, New insights on structural controls and emplacement mechanisms of Pliocene/Quaternary basaltic dikes, southern Nevada and northwestern Arizona: *Geological Society of America Abstracts with Programs*, v. 23, no. 5, p. 118.
- Feuerbach, D. L., Smith, E. L., Shafigullah, M., and Damon, P. E., 1991, New K-Ar dates for late-Miocene to early Pliocene mafic volcanic rocks in the Lake Mead area, Nevada and Arizona: *Isochron West*, no. 57, p. 17–30.
- Fitton, J. G., James, D., Kempton, P. D., Ormerod, D. S., and Leeman, W. P., 1988, The role of lithospheric mantle in the generation of late Cenozoic basic magmas in the western United States: *Journal of Petrology, Special Lithosphere Issue*, p. 331–349.
- Fitton, J. G., James, D., and Leeman, W. P., 1991, Basic magma-

CRUSTAL EXTENSION: LAKE MEAD AREA

- ism associated with Late Cenozoic extension in the western United States: *Compositional variations in space and time: Journal of Geophysical Research*, v. 96, no. B8, p. 13,693-13,711.
- Fitzgerald, P. G., Fryxell, J. E., and Wernicke, B. P., 1991. Miocene crustal extension and uplift in southeastern Nevada: Constraints from fission track analysis: *Geology*, v. 19, p. 1013-1016.
- Glazner, A. F., and Farmer, G. L., 1991. Production of isotopic variability in basalts by cryptic mafic contamination: *Transactions of the American Geophysical Union*, v. 72, p. 267.
- Glazner, A. F., and Farmer, G. L., 1992. Production of isotopic variability in continental basalts as cryptic crustal contamination: *Science*, v. 255, p. 72-74.
- Glazner, A. F., and Supplee, J. A., 1982. Migration of Tertiary volcanism in the southwestern United States and subduction of the Mendocino fracture zone: *Earth and Planetary Science Letters*, v. 60, p. 429-436.
- Hart, S. R., 1988. Heterogeneous mantle domains: Signatures, genesis and mixing chronologies: *Earth and Planetary Science Letters*, v. 90, p. 273-296.
- Hart, S. R., Hauri, E. H., Oschmann, L. A., and Whitehead, J. A., 1992. Mantle plumes and entrainment: Isotopic evidence: *Science*, v. 256, p. 517-520.
- Hart, W. K., 1985. Chemical and isotopic evidence for mixing between depleted and enriched mantle, northwestern U.S.A.: *Geochimica et Cosmochimica Acta*, v. 49, p. 131-144.
- Leat, P. T., Thompson, R. N., Dicken, A. P., Morrison, M. A., and Hendry, G. L., 1989. Quaternary volcanism in northwestern Colorado: Implications for the roles of asthenosphere and lithosphere in the genesis of continental basalts: *Journal of Volcanology and Geothermal Research*, v. 37, p. 291-310.
- Leat, P. T., Thompson, R. N., Morrison, M. A., Hendry, G. L., and Dicken, A. P., 1991. Alkaline hybrid mafic magmas of the Yampa area, NW Colorado, and their relationship to the Yellowstone mantle plume and lithospheric mantle domains: *Contributions to Mineralogy and Petrology*, v. 107, p. 310-327.
- Leeman, W. P., 1970. Late Cenozoic alkali-olivine basalts of the Basin-Range province, USA: *Contributions to Mineralogy and Petrology*, v. 25, p. 1-24.
- Longwell, C. R., 1960. Possible explanation of diverse structural patterns in southern Nevada: *American Journal of Science*, v. 258-A (Bradley Volume), p. 192-203.
- Longwell, C. R., Pampayan, E. H., Bower, B., and Roberts, R. J., 1965. Geology and mineral deposits of Clark County, Nevada: Nevada Bureau of Mines and Geology Bulletin 62, 218 p.
- Mezies, M. A., 1989. Cratonic, circumcratonic and oceanic mantle domains beneath the western United States: *Journal of Geophysical Research*, v. 94, p. 7899-7915.
- Mezies, M. A., Leeman, W. P., and Hawkesworth, C. J., 1983. Isotope geochemistry of Cenozoic volcanic rocks reveals mantle heterogeneity below western U.S.A.: *Nature*, v. 303, p. 205-209.
- Mills, J. G., 1985. The geology and geochemistry of volcanic and plutonic rocks in the Hoover Dam 7.5 minute quadrangle, Clark County, Nevada and Mojave County, Arizona [M.S. thesis]: Las Vegas, Nevada: University of Nevada, 119 p.
- Naumann, T. R., 1987. Geology of the central Boulder Canyon quadrangle, Clark County, Nevada [M.S. thesis]: Las Vegas, Nevada, University of Nevada, 68 p.
- Naumann, T. R., and Smith, E. I., 1987. Evidence for magma mixing in mid-Tertiary rocks, Lake Mead region, southern Nevada: *Geological Society of America Abstracts with Programs*, v. 19, p. 435-436.
- Perry, F. V., Baldrige, W. S., and DePaolo, D. J., 1987. Role of asthenosphere and lithosphere in the genesis of late Cenozoic basaltic rocks from the Rio Grande Rift and adjacent areas of the southwestern United States: *Journal of Geophysical Research*, v. 92, p. 9193-9213.
- Reynolds, S. J., Florence, F. P., Weity, J. W., Roddy, M. S., Carnier, D. A., Anderson, B. V., and Keith, S. B., 1986. Compilation of radiometric age determinations in Arizona: Arizona Bureau of Geology and Mineral Technology Bulletin 197, 258 p.
- Smith, E. I., 1982. Geology and geochemistry of the volcanic rocks in the River Mountains, Clark County, Nevada and comparisons with volcanic rocks in nearby areas. in Frost, E. G., and Martin, D. L., eds., *Mesozoic-Cenozoic tectonic evolution of the Colorado River region, California, Arizona, and Nevada: San Diego, California, Cordilleran Publishers*, p. 41-54.
- Smith, E. I., 1984. Geological map of the Boulder Beach Quadrangle, Nevada: Nevada Bureau of Mines and Geology Map 81, scale 1:24,000.
- Smith, E. I., Schmidt, C. S., and Mills, J. G., 1988. Mid-Tertiary volcanoes of the Lake Mead area of southern Nevada and northwestern Arizona. in Weide, D. L., and Faber, M. L., eds., *This extended land, Geological journeys in the southern Basin and Range: Geological Society of America, Cordilleran Section field trip guidebook: University of Nevada, Las Vegas, Department of Geoscience Special Publication No. 2*, p. 107-122.
- Smith, E. I., Feuerbach, D. L., Naumann, T. R., and Mills, J. G., 1990. Geochemistry and evolution of mid-Miocene igneous rocks in the Lake Mead area of Nevada and Arizona. in Anderson, J. L., ed., *Cordilleran magmatism: Geological Society of America Memoir 176*, p. 169-194.
- Smith, E. I., Feuerbach, D. L., and Duebendorfer, E. M., 1991. Magmatism, extensional tectonics and sedimentation in the Lake Mead area of Nevada and Arizona: A new model: *Geological Society of America Abstracts with Programs*, v. 23, p. 63.
- Takahashi, E., and Kushiro, I., 1983. Melting of dry peridotite at high pressures and basalt magma genesis: *American Mineralogist*, v. 68, p. 859-870.
- Taylor, W. J., and Bartley, J. M., 1988. Prevolcanic extensional breakaway zone, east-central Nevada: *Geological Society of America Abstracts with Programs*, v. 19, p. 457.
- Thompson, K. G., 1985. Stratigraphy and petrology of the Hamblin-Cleopatra volcano, Clark County, Nevada [M.S. thesis]: Austin, Texas, University of Texas, 306 p.
- Walker, J. D., and Coleman, D. S., 1991. Geochemical constraints on mode of extension in the Death Valley region: *Geology*, v. 19, no. 10, p. 971-974.
- Weaver, B. L., 1991a. The origin of ocean island basalt end-member compositions: Trace element and isotopic constraints: *Earth and Planetary Science Letters*, v. 104, p. 381-397.
- Weaver, B. L., 1991b. Trace element evidence for the origin of ocean-island basalts: *Geology*, v. 19, p. 123-126.
- Weaver, B. L., Wood, D. A., Tarney, J., and Joron, J. L., 1986. Role of subducted sediment in the genesis of ocean island basalts: *Geochemical evidence from South Atlantic Ocean Islands: Geology*, v. 14, p. 275-278.
- Weber, M. E., and Smith, E. I., 1987. Structural and geochemical constraints on the reassembly of disrupted mid-Miocene volcanoes in the Lake Mead-Eldorado Valley area of southern Nevada: *Geology*, v. 15, p. 553-556.
- Wernicke, B., and Axen, G. J., 1988. On the role of isostasy in the evolution of normal fault systems: *Geology*, v. 16, p. 848-861.
- White, R. S., 1987. The earth's crust and lithosphere: *Journal of Petrology, Special Lithosphere Issue*, p. 1-10.
- White, R. S., and McKenzie, D. P., 1989. Magmatism at rift zones: The generation of volcanic continental margins and flood basalts: *Journal of Geophysical Research*, v. 94, p. 7685-7730.
- White, R. S., Spence, G. D., Fowler, S. R., McKenzie, D. P., Westbrook, G. K., and Bower, A. D., 1988. Magmatism at rifted continental margins: *Nature*, v. 330, p. 439-444.
- White, W. M., and Patchet, P. J., 1984. Hf-Nd-Sr isotopes and incompatible element abundances in island arcs: Implications for magma origins and crust-mantle evolution: *Earth and Planetary Science Letters*, v. 67, p. 167-185.
- Wooden, J. L., and Miller, D. M., 1990. Chronologic and isotopic framework for early Proterozoic crustal evolution in the eastern Mohave Desert region, SE California: *Journal of Geophysical Research*, v. 95, no. B12, p. 20,133-20,146.
- Zindler, A., and Hart, S. R., 1986. Chemical geodynamics: *Annual Review of Earth and Planetary Science Letters*, v. 14, p. 493-571.

MANUSCRIPT RECEIVED BY THE SOCIETY AUGUST 24, 1992
 REVISED MANUSCRIPT RECEIVED APRIL 5, 1993
 MANUSCRIPT ACCEPTED APRIL 15, 1993

RECENTLY PUBLISHED ABSTRACTS

BY E.I. Smith



POLYGENETIC QUATERNARY VOLCANISM IN THE WESTERN USA: AN EXAMPLE FROM CRATER FLAT, NEVADA.

Smith, E.I. and Bradshaw, T.K.1; Walker, J.D.2

1Center for Volcanic and Tectonic Studies, Department of Geoscience,
University of Nevada, Las Vegas, Nevada 89154-4010 USA

2Isotope Geochemistry Laboratory, Department of Geology, University of
Kansas, Lawrence, Kansas 66045 USA

Crater Flat lies in the Great Basin of southern Nevada and is situated approximately 140 km northwest of Las Vegas. Crater Flat is bounded on its east side by Yucca Mountain, the site of a proposed high-level nuclear waste repository. Quaternary volcanism within Crater Flat consist of five cinder cones arranged in a northeast trending chain. These are from south to north: Little Cone, Red Cone (0.95-1.01 Ma), Black Cone (1.09 Ma) and Northern Cone. Black Cone is the largest center and has a volume of about 0.067 km³ with lava flows covering about 4 km². Red Cone is slightly smaller and sits on a lava field covering about 3 km². The other centers are much smaller in size, therefore our discussion below is limited to Black Cone and Red Cone.

Alkali basalts erupted during the Quaternary at Crater Flat record a complex history of both polycyclic and polygenetic volcanism. Magmas from Black Cone and Red Cone define end-member magma types. The Black Cone type (depleted) has

lower Sr (1300), Ce (220 ppm), Ba (1700 ppm) and Th (15.5 ppm) than the Red Cone magma type (enriched) (Sr-1800 ppm), Ce (280 ppm), Ba (2000 ppm) and Th (15.5 ppm). At Red Cone, there is a complete range of compositions for these elements. The youngest samples have the most elevated values. However, there is only limited variation in the compatible trace elements (e.g., Sc and Ni). High trace element concentrations, low Nb/La and high Zr/Y ratios indicate that both end-member magma types were derived by small degrees of partial melting of the lithospheric mantle. The array of compositions at Red Cone cannot be reproduced by changes in the degree of partial melting, or by fractional crystallization. Rather, a model of magma mixing is proposed between relatively enriched and depleted end-members. The cluster of Black Cone analyses falls consistently at the least-enriched end of the Red Cone sample array, suggesting that Black Cone magma represents one of the mixing end members. Sr and Nd isotopes of basalts from Crater Flat define an unusual positive array on a plot of $^{87}\text{Sr}/^{86}\text{Sr}$ vs. ^{143}Nd with the deple-



ted Black Cone magma type having $^{87}\text{Sr}/^{86}\text{Sr} = 0.70691$ and $\bar{\text{Nd}} = 9.6$ and the enriched Red Cone Magma $^{87}\text{Sr}/^{86}\text{Sr} = 0.7071$ and $\bar{\text{Nd}} = 8.6$. The isotopic composition of the Black Cone end-member may be explained by adding up to 3% isotopically depleted lower crust to the Red Cone magma type.

This modeling may indicate that the magmatic plumbing systems of the two centers were linked, at least during the early stages of volcanism. Thus suggesting that volcanic activity was not restricted to a single center during an eruptive phase, but that a number of sites were active along the length of the magmatic feeder zone. A reconstructed sequence for the magmatic history of Crater Flat resembles the following:

1- Eruption of the Black Cone compositional type at Red Cone and at Black Cone.

2. A new magma batch with elevated trace-element concentrations erupted at Red Cone and mixing occurred with the earlier magma type. The range of compositions at Red Cone is a result of this mixing event.

3. Volcanism ceased at Red Cone while activity continued at Black Cone.

These conclusions could have significant implications for volcanic hazard assessment about the proposed high-level nuclear waste repository at Yucca Mountain, Nevada. This study raises the possibility that renewed eruption at an existing center may be accompanied by activity at other localities along the magmatic feeder zone, thus forming a volcanic chain and potentially having a direct effect on the proposed nuclear repository.

AN ALTERNATIVE TO MANTLE PLUMES

SMITH, A.D., Department of Earth Sciences, National Cheng Kung University, Tainan, Taiwan

An alternative to plumes is that rifting is accomplished by hotcell tectonics and that the ultimate source of hotspot volcanism is the continental mantle. Regions of the continental mantle proximal to ancient sutures or failed rifts are particularly prone to melting on continental rifting and to erosion into the asthenosphere. In opening basins, rifting parallel to a suture/failed rift delaminates and cycles continental mantle into the MORB source, imparting distinct inter-ocean basin isotopic signatures and Pb-Pb secondary isochron ages. Rifting at an angle to a suture/failed rift generates a hotspot track by preferential melting of metasomatized mantle as it is cycled toward the rift axis. Flood basalt provinces tend to overly anomalously heterogeneous regions such as the junctions of sutures/failed rifts in the continental mantle.

Because the asthenosphere is a weak layer, it can not transmit the Earth's entire rotation component to the lithosphere. This results in a net westward migration of the lithosphere relative to the underlying mantle such that continental mantle eroded into the asthenosphere becomes displaced to the east of the continent. The source of Pacific hotspot volcanism can be traced to continental mantle eroded from Laurasia and Gondwana by this mechanism. The association with Gondwana continental mantle gives the DUPAL signature of South Pacific hotspot volcanism and the impression that the DUPAL anomaly is global when the South Atlantic and Indian Ocean regions are considered.

A Volcanology Summer Field Course

Smith, G., Goff, F., Baldridge, S., Elston, W., Heiken, G., and Wohletz, K. Department of Earth and Planetary Sciences, University of New Mexico, Albuquerque, NM 87131-1116 and Earth and Environmental Sciences Division, Los Alamos National Laboratory, Los Alamos, NM 87545.

As part of a new volcanology program at the University of New Mexico (with adjunct professors from the Los Alamos National Laboratory), a summer volcanology field course has been established. This course fulfills an increasing student interest in volcanological field work, for which formal training has not been available. The three-week-long course is taught at Young Ranch, located in the Miocene-Quaternary Jemez volcanic field of New Mexico. A complete spectrum of volcano types and compositions, mostly eroded and well-exposed, are within an hour's drive of the Ranch.

The course consists of nine field problems, ranging from a Pleistocene pyroclastic sequence to an active hydrothermal system; mapping projects include basaltic to rhyolitic lavas and pyroclastic deposits. Attendance is limited to 15 to allow maximum interaction between students and faculty; in the first year, we had 14 students from 6 countries. Daytime field work is supplemented by evening lectures.

Volcanology is very much a multidisciplinary field. Great advances have been made in theory, modeling, technology, and laboratory studies. The basis for it all, however, is experience on the outcrop. We hope that this and perhaps other volcanological field courses at universities will maintain this much-needed expertise.

ROLE OF THE MANTLE DURING CRUSTAL EXTENSION

SMITH, E.J. Dept. Geoscience and CVTS, Univ. Nevada, Las Vegas, NV 89154 USA; FEUERBACH, D.L., Dept. Geology, Univ. Iowa, Iowa City, IA 52242 USA; NAUMANN, T.R., Dept. Geology, Univ. Idaho, Moscow, ID 83843 USA; WALKER, J.D., Dept. Geology, Univ. Kansas, Lawrence, KS 66045 USA and TANGEMAN, J.A., Dept. Geological Sciences, Univ. Michigan, Ann Arbor, MI 48109 USA

A fundamental question in areas of large-magnitude crustal extension and magmatism is whether the mantle plays an active or passive role in the extension process. Two areas in the Basin and Range, Nevada-Arizona were chosen to evaluate links between crustal and mantle processes. In the Lake Mead area, the boundary between the magmatic zone and the northern Colorado River extensional corridor (NCREC) parallels a contact between OIB and lithospheric mantle domains. Both boundaries formed between 11 and 6 Ma during and just following the peak of extension. Mafic lavas to the north of the boundary have a lithospheric mantle (LM) signature ($\epsilon_{Nd} = -3$ to -9 ; $^{87}Sr/^{86}Sr = 0.706-0.707$). South of the boundary, lavas have a source composed of OIB and HIMU-mantle ($\epsilon_{Nd} = 0$ to $+4$; $^{87}Sr/^{86}Sr = 0.703-0.705$). The source of mafic lavas in the region prior to 11 Ma was LM. The change in source with time and the HIMU-like mantle component are compatible with a plume beneath the NCREC during extension. In the Reveille-Crater Flat area, central Great Basin, there is a southward change in isotopic patterns. Between 4-2.8 Ma, mafic lavas have LM signatures. Post-2.8 Ma, mafic lavas in the Reveille Range (north) have an OIB component, however, in Crater Flat (south), coeval alkali basalt melted LM. In both areas of the Basin and Range, passive rifting is more applicable than active rifting because of very low volumes of alkali basalt, lack of a plume track, and compatibility of geochemical patterns with models of passive rifting proposed in other extensional areas worldwide.

THE LATE CENOZOIC INTRAPLATE BASALT ASSOCIATIONS IN NORTHERN NEW ZEALAND

SMITH, I.E.M., BLACK, P.M., University of Auckland, N.Z., HEGNER, E., Universität Tübingen, Germany, NAKAMURA, E., Okayama University at Misasa, Japan, and BRIGGS, R.M., University of Waikato, N.Z.

Predominantly basaltic volcanic rocks of late Cenozoic age occur in two igneous provinces in northern New Zealand. In the Northland province these are mildly alkaline, transition and tholeiitic in character and the association includes subordinate intermediate and felsic members. Eruptions began about 10Ma ago following closely on a major subduction related episode of arc-type volcanism; the intraplate volcanism has continued until Recent times. Rock types of the Auckland province are alkali basalts, basanites nephelinites and hawaiites together with some transitional and tholeiitic types. Eruptions began about 2Ma ago and have continued to the present.

Compositional and spatial patterns established in the Northland province 8-10Ma ago have persisted through the Holocene. In contrast the focus of eruptive activity in the Auckland province has migrated northward to produce a succession of regularly spaced volcano fields.

Radiogenic isotope and trace element ratios indicate that the intraplate basaltic volcanics of northern New Zealand originated in essentially similar mantle sources with the northland province showing slightly enriched ^{143}Nd (.51298-.51305) relative to the Auckland province (.51290-.51298). Contrasts in the petrography of primitive magmas and fractionation trends in each province suggest that the variations between provinces can be partly explained by differences in proportions of melting of a layered mantle source in which the upper part carries a geochemical signature inherited from an earlier subduction event. Fractionation in shallow versus deep magma chambers explains contrasting differentiation patterns in the two provinces.

Annual Report 1992/3

Center for Volcanic and Tectonic Studies

Contribution by

T. K. BRADSHAW

(September 1993)

Contents

Section 1. Introduction

Section 2. Polygenetic Quaternary Volcanism at Crater Flat, Nevada

Section 3. Further Geochemical Modelling: Crater Flat

**Section 4. EPSL Paper: Basaltic volcanism in the Southern Basin and Range-
no role for a mantle plume**

Section 5. Abstracts and Presentations

Section 6. Data Tables for 1992-1993 analyses

Section 7. Final Thoughts

Section 1

Introduction

This report summarises the work of Tim Bradshaw with the Center for Volcanic and Tectonic Studies (CVTS) from October 1992 through September 1993. The bulk of this work is presented in three main sections (Sections 2-4), covering new geochemical, petrological, and tectonic models relevant to the Yucca Mountain region.

Section 2 outlines a detailed petrologic model for magmatism at Crater Flat. This section concentrates on the two main eruptive centres in Crater Flat, Black Cone and Red Cone. Here, the merits of fractional crystallization and magma mixing are evaluated as processes that might generate the range of geochemical diversity observed at Red Cone. It is concluded that the magmatic plumbing systems for the two centres were probably linked at depth for some time during the eruptive history. In turn, this may have implications for styles of magmatic activity in the area: it is possible that the two centres were linked along a tectonic feature (NE-SW fault system), and that during eruptive cycles magmas may migrate along such features; thus generating a chain of eruptive vents with an orientation governed by local tectonics.

Section 3 advances the topic of geochemical modelling for Crater Flat, combining both trace element and isotopic analyses. This section identifies lower crustal contamination as an important contributor to geochemical variation within the suite of Black Cone samples. However, the section mainly addresses the origins of two magma types at Crater Flat (Black Cone/ early Red Cone type, and a trace element enriched later Red Cone magma). Models are proposed for how these two separate magma 'batches' might be related to each other.

Section 4 is a paper concerned with tectonics and magmatism in the southern Basin and Range. While not specifically dealing with samples collected at Crater Flat, much of the magmatism discussed is geochemically comparable. The nature of the mantle source(s), partial melting of the mantle, changes in magma composition with time, and constraints on the causes of magmatism are some of the themes covered in this paper. The latter topic investigates whether mantle plumes are the driving force behind magmatism in the western USA.

Section 5 reprints abstracts presented at geological meetings this year, and Section 6 is the definitive listing of data from Crater Flat (for Red Cone and Black Cone). Finally, Section 7 contains a brief statement on geochemical modelling and volcanism at Crater Flat.

Section 2

The paper: Polygenetic Quaternary Volcanism at Crater Flat, Nevada

The following paper was initially submitted for publication in the Journal of Geophysical Research. The paper received one reasonable and two very good reviews. However, the journal editors decided to reject the paper, on the grounds that it might prove to be too specialised and of limited appeal to its 'mass audience'. A number of useful comments and suggestions for additional material were presented by the reviewers and these were accommodated in a revised version of the manuscript. Changes included a detailed sample location map, and a more complete section on the eruptive history of Red Cone and Black Cone, to aid future researchers into volcanism in the Yucca Mountain area.

The revised manuscript is currently in review with the Journal of Volcanology and Geothermal Research. It is hoped that a publication date will be set for early in 1994.

Polygenetic Quaternary Volcanism at Crater Flat, Nevada

T.K. Bradshaw and E.I. Smith

Center for Volcanic and Tectonic Studies
Department of Geosciences
University of Nevada, Las Vegas
4505 Maryland Parkway
Las Vegas
NV 89154-4010, USA.

Abstract

Alkali basalts erupted during the Quaternary at Crater Flat, Nevada, record a complex history of polycyclic and polygenetic volcanism. Magmas from the two main centres (Black Cone and Red Cone) are petrographically and geochemically similar, although field evidence suggests a number of separate eruptive events. Elevated trace element concentrations, low Nb/La and high Zr/Y ratios indicate that the magmas were derived by small degrees of partial melting from the lithospheric mantle. At Red Cone a significant range of Sr, La, Ce, Ba and Th concentrations is observed with time (e.g., Sr range 1308-1848 ppm): the youngest samples having the more elevated values. However, there is only limited variation in the compatible trace elements (e.g., Sc and Ni). The array of compositions at Red Cone cannot be reproduced by changes in the degree of partial melting, or by fractional crystallization. Rather, a model of magma mixing is proposed between relatively enriched and depleted end-members. The cluster of Black Cone analyses falls consistently at the least-enriched end of the Red Cone sample arrays, suggesting that the Black Cone magma represents one of the mixing end-members. This modelling may indicate that the magmatic plumbing systems of the two centres were linked, at least during the early stages of volcanism. Moreover, volcanic activity may have occurred at a number of sites along the length of the magmatic feeder zone, rather than being restricted to a single centre during an eruptive phase. In turn, this could have significant implications for volcanic hazard assessment in the region around Yucca Mt. and the proposed nuclear waste repository.

Polygenetic Quaternary Volcanism at Crater Flat, Nevada

Introduction

Most cinder cones develop over relatively short periods of time (10^0 to 10^2 years) and the volcanic products of individual cones have relatively simple evolutionary histories. Magmas are typically derived from a single source and the term monogenetic is often applied. At more complex (polycyclic) centres, separate time-distinct eruptions occur over periods greater than the lifetime of a near-surface magma chamber. However, the magmas may still be derived from a single source and they are likely to be related at depth by fractional crystallization or by the degree of partial melting. The term 'polygenetic' can be used synonymously with polycyclic (Bates and Jackson, 1987), however, in this contribution we define polygenetic as a specific case where magmas erupted at one centre are derived from more than one source.

Polycyclic activity related to low-volume mafic centres appears to be rare (Basaltic Volcanism Study Project, 1981), and even fewer cases of polygenetic volcanism are on record. This is not surprising considering the inherent problems of polygenetic magmatism on a small scale. For instance, how and why magmas generated in different sources can erupt at the same site again and again, rather than form a dispersed volcanic field. Such circumstances almost certainly depend on a crustal focussing mechanism for the magmas, perhaps in terms of active structural breaks and linked magmatic pathways. Sunset Crater in Arizona is one possible polygenetic centre in the western United States (R. F. Holm and G. Larsen pers. comm.). Recently, Crowe et al. (1989b), Wells et al. (1990) and Wells et al. (1992) suggested that the Lathrop Wells cone (in southern Nevada, Figure 1) is polycyclic based on geochronology and the presence of soil horizons between flows. However, these conclusions are currently the subject of much debate (e.g., Turrin et al., 1992). Thus, in this paper we examine other sites of Quaternary volcanism at Crater Flat, near Lathrop Wells, to test this polycyclic-polygenetic hypothesis.

Crater Flat is situated approximately 140 km northwest of Las Vegas, close to U.S. Highway 95, and is bounded on its eastern side by Yucca Mountain (Figure 1). A broad overview of the Pliocene and Quaternary volcanism in this region was presented by Vaniman et al. (1982). This new contribution focuses on the nature of Quaternary volcanism in more detail. Here we compare the Crater Flat data with other suites from the western United States and attempt to model the observed geochemical variations in terms of fractional crystallization, magma mixing, and the degree of partial melting. The results of this geochemical modelling reveal a complex magmatic history at Crater Flat, with the development of both single- and multiple-sourced cinder cone centres. In addition, many of the individual centres appear to be polycyclic.

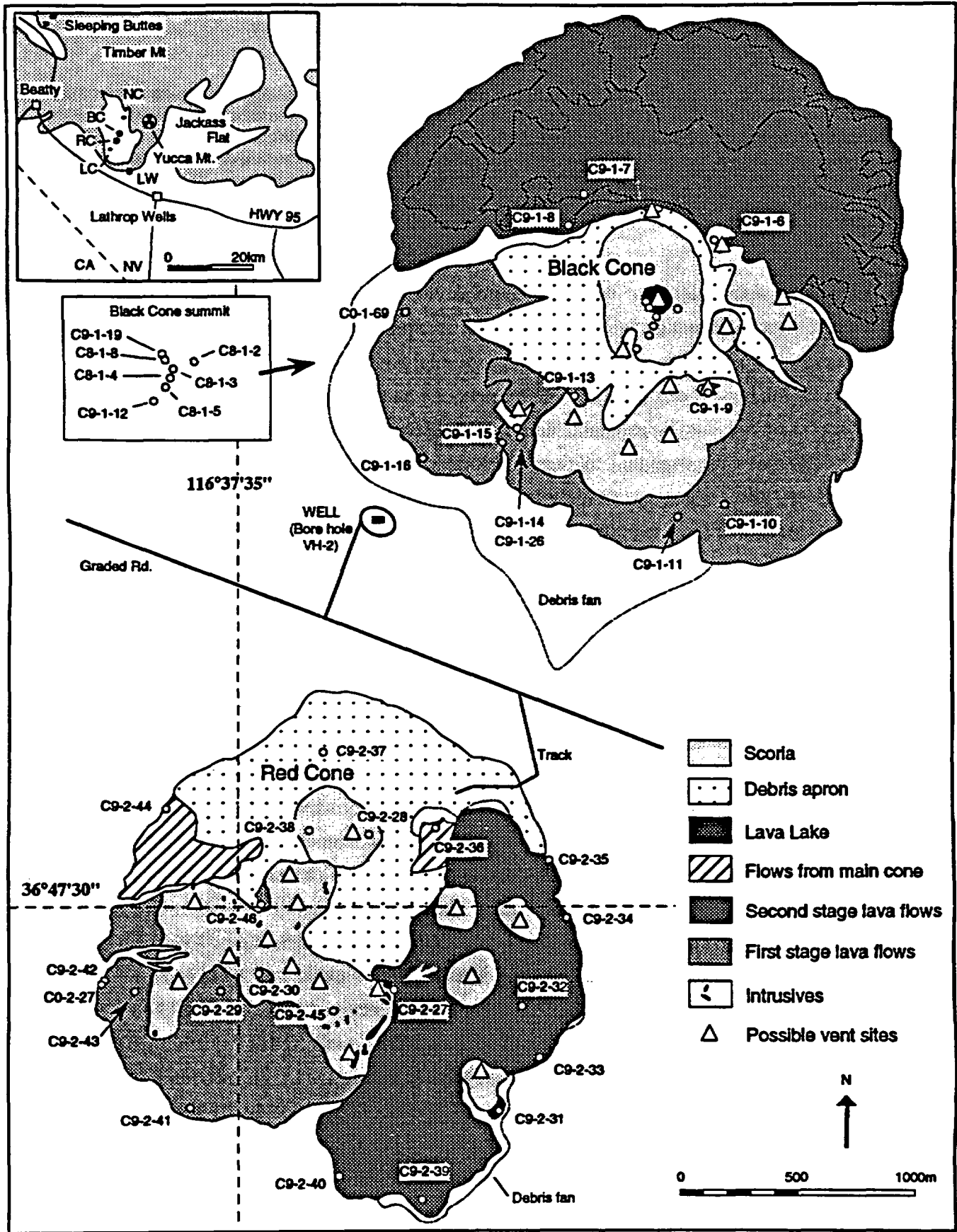
Fig. 1. FOLLOWING PAGE. Detailed geological map of the Red Cone and Black Cone centres in Crater Flat (adapted from work by D. Feuerbach, and Faulds et al., in press). Sample locations are circled and labelled. Cinder mounds representing possible vent sites are marked with open triangles. White arrow on Red Cone indicates location where a scoria mound core can be observed. Inset map displays the location of Quaternary volcanic centres in southwest Nevada. Crater Flat: LC= Little Cones, RC= Red Cone, BC= Black Cone, NC= Northern Cone. LW= Lathrop Wells centre. Proposed site of Yucca Mt. nuclear waste repository is marked with inverted triangle symbols.

Interest in volcanism in the southern Great Basin has been stimulated by the need for scientific studies to evaluate the site suitability of a proposed high-level nuclear waste repository at Yucca Mountain, Nevada. Volcanism is a potentially adverse condition that is of great concern because of the presence of multiple Quaternary-age basalt centres in the immediate vicinity of the Yucca Mountain site (Department of Energy, 1986; Crowe et al., 1989a). This study is part of an effort to assess the potential of future volcanism in the area by characterizing the nature of Quaternary mafic volcanism at these individual volcanic centres. The recognition of polygenetic volcanism in Crater Flat supports the observations of polycyclic activity at the Lathrop Wells cone and adds a further dimension to the record of Quaternary activity in this region. This work is currently in use in studies to refine volcanic risk assessments for the Yucca Mountain area.

Background geology

Crater Flat lies to the south of the Timber Mountain caldera complex, and may in itself represent a satellite caldera of lesser dimensions (Carr, 1982). The area has been a focus for volcanic activity from ~14Ma to the late Quaternary (U.S.G.S., 1984). Initially volcanism was dominated by large-volume silicic eruptions, with subordinate basaltic magmatism (e.g., Christiansen et al., 1965). This phase of activity was succeeded in the late Miocene/ early Pliocene by much smaller volume basalt-dominated volcanism. The most recent phase of volcanic activity produced a chain of five cinder cones (and associated lava flows) within Crater Flat, two cones at Sleeping Buttes, and the Lathrop Wells Cone at the southern tip of Yucca Mt., between Crater Flat and Jackass Flat. The Lathrop Wells Cone is dated at 136-141ka by $^{40}\text{Ar}/^{39}\text{Ar}$ methods (Turrin et al., 1991), although thermo-luminescence and cosmogenic ^3He studies appear to favour considerably younger ages of 4-64ka (Crowe et al., 1992a; 1992b). Evidence of erosion at Crater Flat suggests that the activity there is more ancient. Flows from Red Cone were dated at ~0.95- 1.01Ma, and flows from Black Cone at ~0.71- 1.09Ma, by the K-Ar technique on plagioclase concentrates (Smith et al., 1990b).

The location of volcanism in Crater Flat and at Lathrop Wells is apparently controlled by structure (Faulds et al., in press.), with the centres aligned along NE-SW trending zones of Quaternary faulting. In order of increasing volume, the centres of Crater Flat are: NE Little Cone,



SW Little Cone, Northern Cone (much of which is buried beneath alluvium), Red Cone and Black Cone. The volume of Black Cone is estimated to be $0.067 \pm 0.015 \text{ km}^3$ (Smith et al., 1990b), and the lava flows associated with this cone cover $\sim 4 \text{ km}^2$. Red Cone lava flows cover $\sim 3 \text{ km}^2$, a similar area to the flows associated with the Lathrop Wells Cone. The other centres of Crater Flat are considerably smaller, consisting of just one or two flow/scoria units each. Thus much of the discussion herein concerns the geochemistry of Black Cone and Red Cone, although data from the other centres will be shown for comparison.

Eruptive history of the Red Cone and Black Cone centres

The earliest activity at both Black Cone and Red Cone resulted in the eruption of a series of blocky, Aa, lava flows that spread southwards, down the topographic gradient of Crater Flat. Subsequent flows were forced northwards at Black Cone and to the east at Red Cone (Figure 1). Mounds of cinder and other pyroclastic material up to 250m across and aligned approximately NE-SW (parallel to regional structure) are observed at both centres. The internal structure of one mound is exposed on the south-side of Red Cone (Figure 1). Here, massive basaltic units and multiple dyke or plug-like intrusions occur within a mass of agglutinated scoria, splatter, and bombs up to 2 m across. Similar agglutinate-cinder mounds are reported from Sunset Crater, Arizona, where they are interpreted to be slumps of the main cone rafted away on a lava flow emerging from its base (Holm 1987). However, the cinder mounds in Crater Flat typically occur at the tail-end of individual flows and thus they may represent important vent sites (Smith et al., 1990a). Flow foliations and vesiculation in the top of one of the dyke units suggests a mushroom-like shape that might be expected as lava reaches the surface to initiate a new flow. A number of other small dykes are also observed at Red Cone and these trend both NE-SW and NW-SE. This second lineation may correspond to the orientation of a swarm of small Quaternary faults intersecting the main NE-SW structural grain in the area (Faulds et al. in press).

At both centres, the southern flows have lower relief, intense development of drainage and a generally subdued topography. The northern flows at Black Cone and the eastern flows at Red Cone have greater relief, less pronounced drainage systems, distinct margins to the flow lobes and a rugged surface topography. These differences, and an apparent truncation of earlier drainage patterns at Red Cone, suggest that there was a time interval between the major eruptions. A time gap is also recorded as an angular unconformity and a caliche layer between two of the main scoria units on the Black Cone cinder cone (Smith et al., 1990b). The older cone-forming units at Black Cone appear to represent a wide and shallow cone or saucer structure, perhaps indicating some early phreatomagmatic activity. This structure was later filled and overprinted by the prominent steep-sided cone that can be observed today. Outcrop of the earlier structure is

afforded by a partial collapse on the southwest side of the main cone. Similar evidence of multiple eruptions separated by discrete time intervals has also been recorded from the Lathrop Wells centre (Crowe et al., 1992b).

The final episode of activity produced the main cinder cones of Black Cone and Red Cone, that stand some 70 m above the surrounding lava flows. Bedded scoria deposits, and zones of agglutinated scoria and rootless flows, reflect numerous pulses of Strombolian activity fluctuating with Hawaiian-type lava fountaining (Smith et al. 1990b). Both cones display evidence of lava lake development in the summit craters. This is more pronounced on Black Cone where a sequence of massive units 2-3 m thick is exposed. On Red Cone the equivalent units are much thinner (0.2-0.8 m), but at least seven horizons can be traced around the summit, separated by scoria and spatter. Only a few small flows are thought to originate directly from the main cone sites and these occur as flow lobes high on the flanks of the cone. The trailing edges of these flows are directed back towards the main cone and are covered by its scoria.

The Black Cone edifice is well preserved in comparison to the Red Cone cinder cone, perhaps indicating that activity continued here subsequent to that at Red Cone.

General geochemistry and petrography

Samples from Black Cone, Red Cone and Northern Cone have a restricted range of major element compositions (Table 1) from 48.6-51.1 wt% SiO₂ and 4.3-5.5 wt% MgO. Samples from Lathrop Wells have slightly lower silica and higher MgO contents, and two samples collected from Little Cones have the lowest silica contents (~46 wt% SiO₂). Mg/[Mg+Fe²⁺] ratios (referred to here as Mg#, and calculated with an assumed value of 0.15 for Fe₂O₃/FeO ratio) cluster at ~52, although high total Fe contents in the two Little Cones samples results in lower values of Mg# (~48). Total alkali concentrations in the Red Cone samples are higher than those of Black Cone, and their MgO concentrations are correspondingly lower. This is the principal major element distinction between samples from Red Cone and Black Cone, although most of the older Black Cone lavas also have lower P₂O₅ contents.

Based on the total alkali vs. silica scheme of Cox et al. (1979), all of the Crater Flat samples can be classified as alkali basalts. This is a departure from the classification of 'hawaiite' assigned by Vaniman et al. (1982). However, the low alkali contents and ratios of Na₂O/K₂O < 2 are inconsistent with the modern definition of the term 'hawaiite', based on the IUGS Subcommission on the Systematics of Igneous Rocks (Le Bas et al., 1986), and thus the term 'alkali basalt' is adopted here.

Table 1. FOLLOWING THREE PAGES. Black Cone (BC) and Red Cone (RC). Sample types: F= lava flow, D= dyke, B= bomb, LL= lava lake. The final four columns provide statistical data based on the full Crater Flat data set (BC n= 18, RC n= 23). Note that the mean compositions for either suite typically lie within $1\sigma_n$ of each other. Major elements reported as wt%, trace elements as ppm. Normative mineral compositions were calculated using a CIPW Norm mineral calculation programme (D.R. Mason pers. comm). Whole rock major element concentrations were determined by Inductively Coupled Plasma techniques (ICP) at Chemex Labs. Inc. (Sparks, NV). Analytical uncertainty (relative error) for all major elements is <5%. The trace elements Co, Hf, Sc, Ta, Th, V and REE were analyzed by Instrumental Neutron Activation Analysis (INAA) at the Phoenix Memorial Laboratory, University of Michigan. The multi-element standards G-2, GSP-1, BHVO-1, and RGM-1 were used as internal standards for both ICP and INAA analyses. Other trace elements (Rb, Sr, Ba, Zr, Nb, Y, Cr, Ni) were determined with a Rigaku 3030 X-ray fluorescence spectrometer in the Rock Chemistry Laboratory at UNLV. Trace elements were analyzed on pressed powder pellets with methyl cellulose binder. Accuracy was estimated by analyzing U.S.G.S. standards AGV-1, BE-N and BHVO-1. Accuracy and relative error data is listed in Table 1a.

TABLE 1. Major and trace element analyses of representative samples from Crater Flat, NV.

Area	BC	BC	BC	BC	BC	BC	BC	BC		RC	RC	RC	RC
Type	LL	B	F	F	F	F	F	F	LL	LL	F	F	F
Sample	C8-1-2LN	C8-1-3LN	C9-1-06LN	C9-1-8LN	C9-1-9LN	C9-1-11LN	C9-1-14LN	C9-1-19LN		C9-2-28LN	C9-2-30LN	C9-2-31LN	C9-2-33LN
SiO2	49.82	49.61	49.59	48.63	48.89	49.39	49.91	51.12		49.66	49.00	49.54	49.03
TiO2	1.38	1.39	1.39	1.45	1.45	1.43	1.46	1.38		1.38	1.45	1.39	1.44
Al2O3	16.63	16.67	16.60	16.59	16.76	17.17	17.38	17.39		17.25	16.93	17.17	16.94
Fe2O3	10.73	10.84	10.64	11.03	11.22	10.45	10.97	10.51		10.22	10.44	10.24	10.61
MnO	0.17	0.17	0.17	0.17	0.18	0.17	0.17	0.17		0.19	0.18	0.20	0.17
MgO	5.11	5.12	4.92	5.11	5.19	4.91	5.19	5.28		4.78	4.75	4.60	4.83
CaO	8.34	8.34	8.45	8.87	8.39	8.80	8.44	8.62		8.56	8.50	8.57	8.43
Na2O	3.16	3.12	3.09	3.23	3.26	3.37	3.38	3.46		3.53	3.40	3.63	3.35
K2O	1.53	1.52	1.61	1.58	1.62	1.67	1.75	1.42		1.74	1.75	1.77	1.93
P2O5	1.10	1.13	0.85	0.92	0.91	0.93	0.95	0.81		1.01	1.45	1.09	1.04
LOI	0.05	0.45	0.31	0.43	0.26	0.20	0.01	0.23		0.01	0.36	0.01	0.01
Total	98.02	98.36	97.62	98.01	98.13	98.49	99.61	100.39		98.33	98.21	98.21	97.78
La	119	114	120	121	118	118	123	111		143	128	156	139
Ce	226	213	233	233	219	210	233	206		277	243	277	272
Nd	112.0		90.1		143.0		87.6				98.0	95.6	82.2
Sm	12.0	11.3	11.9	12.1	11.9	11.5	12.3	11.2		13.1	12.7	14.3	13.2
Eu	2.71	2.52	2.68	2.74	2.54	2.51	2.81	2.45		3.13	2.90	2.85	3.05
Tb	1.22		1.55		1.19	1.40	2.40	1.21		1.61		1.09	1.45
Dy										6.65	6.39	6.02	5.49
Yb	3.29	3.03	2.79	2.69	2.42	2.29	2.71	3.14		1.72	2.03	3.13	3.35
Lu	0.23	0.36	0.31	0.34	0.15	0.34	0.24	0.41		0.38			0.31
Ba	1741	1628	1721	1740	1747	1719	1726	1582		2006	1823	2030	1875
Co	26.3	24.6	28.1	27.9	25.3	23.4	26.1	24.7		23.8	24.2	23.1	15.5
Cr	114.5	134.7	106.2	110.1	135.3	97.3	115.0	80.6		48.0	82.4	95.6	68.9
Hf	7.64	7.35	7.91	8.01	7.47	7.19	8.02	7.33		7.42	7.70	6.32	7.79
Nb	33.8	35.6	36.0	36.9	35.8	34.4	36.5	32.9		35.5	37.6	35.3	35.9
Ni	36.8	44.7	40.5	44.2	46.1	36.7	44.3	43.9		39.2	40.5	45.7	40.5
Rb	23.8	20.4	20.4	20.0	20.4	19.9	20.5	19.4		19.8	18.9	19.9	20.1
Sc	18.6	17.3	19.2	19.1	17.4	16.6	18.2	17.5		17.8	17.1	16.4	17.1
Sr	1225	1204	1228	1276	1301	1282	1284	1218		1769	1462	1848	1587
Ta	1.71	1.45	1.40	1.82	1.60	1.53	1.56	1.45		1.19	1.67	1.41	1.48
Th	12.6	12.2	27.0	13.0	12.4	11.8	13.0	11.8		15.2	12.9	14.7	13.8
V	168	156	176	161	176	162	174	168		150	155	162	
Y	23.1	22.4	23.2	22.8	23.3	23.2	23.1	22.3		23.4	23.4	23.6	23.5
Zr	393	392	401	406	420	402	412	374		414	435	423	425
Mg#	52.6	52.4	51.9	51.9	51.9	52.3	52.4	53.9		52.2	51.5	51.1	51.5
Nb/Y	1.46	1.59	1.55	1.62	1.54	1.48	1.58	1.48		1.52	1.61	1.50	1.53
Or	9.3	9.3	9.9	9.7	9.9	10.1	10.5	8.5		10.6	10.7	10.8	11.8
Ab	27.6	27.2	27.1	28.3	28.5	29.3	29.0	29.5		30.7	29.7	31.6	29.3
An	27.5	27.8	27.7	27.0	27.2	27.5	27.5	27.9		26.8	26.6	26.0	26.3
Di	7.0	6.6	8.8	10.7	8.5	9.7	7.7	8.5		8.9	6.7	9.2	8.7
Hy	18.4	18.6	16.2	6.8	8.9	6.6	8.0	13.4		6.0	10.0	4.1	5.6
Ol	3.1	3.2	3.8	10.6	10.2	10.0	10.5	5.9		10.4	8.4	11.3	11.2
Mt	1.9	1.9	1.9	2.0	2.0	1.9	1.9	1.8		1.8	1.9	1.8	1.9
Il	2.7	2.7	2.7	2.9	2.8	2.8	2.8	2.6		2.7	2.8	2.7	2.8
Ap	2.7	2.8	2.1	2.3	2.2	2.3	2.3	1.9		2.5	3.5	2.7	2.5

TABLE 1 (cont.). Major and trace element analyses of representative samples from Crater Flat, NV.

Area Type	RC									Statistical Data			
	F	F	F	D	F	F	F	D	F	Black Cone		Red Cone	
	Sample	C9-2-34LN	C9-2-36LN	C9-2-37LN	C9-2-38LN	C9-2-39LN	C9-2-41LN	C9-2-44LN	C9-2-45LN	C9-2-46LN	MEAN	ST.DEV.	MEAN
SiO2	50.33	49.05	48.90	48.69	49.42	49.38	49.24	49.86	49.68	49.55	0.57	49.45	0.53
TiO2	1.48	1.47	1.50	1.35	1.37	1.53	1.51	1.48	1.4	1.43	0.03	1.45	0.06
Al2O3	17.29	17.89	17.68	17.89	17.97	17.15	17.16	17.19	17.02	16.93	0.28	17.36	0.36
Fe2O3	10.69	10.78	10.59	10.15	10.34	10.80	10.51	10.47	10.37	10.81	0.28	10.53	0.22
MnO	0.18	0.17	0.18	0.19	0.19	0.21	0.2	0.20	0.19	0.17	0.01	0.19	0.01
MgO	5.13	4.74	5.35	4.52	4.86	5.02	4.72	4.36	5.09	5.13	0.17	4.86	0.25
CaO	8.85	8.43	8.35	8.81	8.58	8.49	8.32	8.38	8.78	8.47	0.18	8.56	0.16
Na2O	3.48	3.46	3.37	3.48	3.40	3.34	3.43	3.55	3.55	3.22	0.15	3.45	0.10
K2O	1.76	1.76	1.82	1.66	1.86	2.00	1.84	1.72	1.68	1.62	0.14	1.81	0.10
P2O5	1.20	1.03	1.06	1.01	0.98	1.08	1.14	1.08	1.17	0.97	0.10	1.10	0.11
LOI	0.07	0.29	0.01	1.00	0.01	0.01	0.11	0.31	0.01	0.27	0.23	0.13	0.24
Total	100.46	99.07	98.81	98.75	98.98	99.01	98.18	98.60	98.94	98.57	0.92	98.88	1.01
La	141	136	120	157	151	122	121	137	154	119	4	138	13
Ce	268	248	214	279	276	209	212	254	295	221	8	252	26
Nd	74.7	90.4	108.0	84.0	98.7	107.0	101.0	89.1	110	100.0	23.8	94.2	9.9
Sm	13.1	12.8	11.8	13.9	13.4	11.9	11.5	13.6	14.1	11.8	0.5	13.0	0.8
Eu	2.92	2.79	2.61	2.98	3.02	2.52	2.43	3.08	3.05	2.61	0.10	2.86	0.19
Tb		1.07	1.14	1.83	1.67	1.56	0.87		1.32	1.41	0.40	1.31	0.26
Dy	6.18	6.49	5.18	5.62	4.90	6.46	7.83	6.94	5.74			6.03	0.79
Yb	2.10	2.67	2.49	3.15	2.23	2.91	3.31	3.03	2.56	2.77	0.61	2.78	0.54
Lu	0.29	0.29	0.33	0.46		0.28		0.41	0.29	0.36	0.19	0.35	0.07
Ba	1856	1781	1698	1996	1936	1738	1687	1781	1839	1716	77	1852	116
Co	24.0	24.0	25.2	24.3	23.6	23.1	21.1	26.5	25.1	25.6	1.3	23.5	2.2
Cr	73.8	70.0	128.4	88.8	79.9	109.5	59.7	65.5	76.4	109.5	19.5	81.4	18.6
Hf	7.98	7.81	7.38	7.63	7.17	7.51	6.65	8.34	8.32	7.60	0.25	7.60	0.53
Nb	36.5	35.2	36.4	35.1	32.8	33.2	35.1	35.9	33.9	35.3	1.7	35.4	1.5
Ni	35.2	32.6	48.1	46.5	42.9	46.3	42.7	47.2	36.4	42.8	3.7	41.9	4.2
Rb	19.8	19.8	22.0	19.8	22.4	20.0	19.3	19.5	17.1	20.9	1.1	20.0	1.2
Sc	16.9	16.9	17.7	17.4	17.2	16.3	14.6	18.8	17.6	17.8	0.7	17.0	0.8
Sr	1641	1496	1308	1818	1806	1363	1339	1360	1771	1257	42	1564	205
Ta	1.65	1.67	1.59	1.35	1.53	1.39	1.45	1.70	1.67	1.58	0.14	1.53	0.14
Th	13.8	12.8	11.8	15.6	15.3	11.6	10.5	13.4	15.6	13.4	3.5	13.5	1.5
V	158	176	168	155	159	171	158	264	167	165	12	170	24
Y	23.4	22.8	22.8	24.2	23.0	23.0	22.9	23.6	22.8	22.9	0.3	23.3	0.4
Zr	424	423	397	417	425	406	406	406	415	401	15	418	10
Mg#	52.8	50.6	54.1	50.9	52.3	52.0	51.1	49.3	53.4	52.52	0.89	51.77	1.10
Nb/Y	1.56	1.54	1.60	1.45	1.43	1.44	1.53	1.52	1.49	1.54	0.07	1.52	0.06
Or	10.5	10.6	11.0	10.1	10.9	12.1	11.2	10.4	10.1	9.9	0.8	11.0	0.6
Ab	29.6	29.9	29.1	30.4	30.4	28.8	29.9	30.9	30.6	28.0	1.1	29.9	0.8
An	26.5	28.7	28.3	29.2	26.2	26.4	26.8	26.6	26.1	27.7	0.5	27.1	1.1
Di	8.7	6.5	6.3	8.1	9.3	8.3	7.3	8.0	9.4	8.0	1.3	8.0	0.9
Hy	7.3	4.6	4.5	2.8	5.3	5.1	7.6	9.4	5.4	12.5	5.3	5.7	2.0
Ol	10.1	12.6	13.6	12.6	11.1	12.0	9.8	7.6	11.2	7.1	3.6	11.2	1.7
Mt	1.9	1.9	1.9	1.8	1.8	1.9	1.9	1.9	1.8	1.9	0.0	1.9	0.0
Il	2.8	2.9	2.9	2.6	2.7	3.0	3.0	2.9	2.7	2.8	0.1	2.8	0.1
Ap	2.9	2.5	2.6	2.5	2.4	2.6	2.8	2.6	2.8	2.4	0.3	2.7	0.3

TABLE 1a. Accuracy and relative error data for trace element analyses in this study.

Element	Relative error (%)	Published values for AGV-1	Mean of 10 replicate analyses of AGV-1
XRF			
Ba	10	1226	1271
Cr	5	10.1	11.0
Nb	8	15.00	14.24
Ni	3	16.00	15.91
Rb	2	67.30	65.22
Sr	2	662	657
Y	2	20.00	21.41
Zr	5	227	239
		Published values for BHVO-1	Mean of 10 replicate analyses of BHVO-1
INAA			
La	0.7		
Ce	1.5	39	38
Nd	>10	25.2	22.4
Sm	0.4	6.2	6.0
Eu	4.1	2.06	2.10
Yb	5.7	2.02	2.13
Lu	6.6		
Hf	4.3	4.38	4.68
Sc	0.6	31.8	33.4
Ta	10.3		

There is little petrographic variation in the Crater Flat samples. They typically have small phenocryst populations (<5 vol%), comprised almost entirely of fresh olivine crystals, although some phenocrysts and micro-phenocrysts of clinopyroxene and orthopyroxene are also observed. Opaque spinel inclusions are common in the olivine phenocrysts. Groundmass mineralogy is dominated by plagioclase micro-laths, often in a fine trachytic or intergranular texture with olivine, pyroxene, and opaque oxide minerals. Small percentages of fresh interstitial glass are generally present, although in a few samples patches of the interstitial material have been replaced by calcite. Fine calcite veins (<0.5 mm width) and vesicles lined with calcite also occur in many flows, but samples selected for chemistry were screened to exclude these.

Large amphibole and plagioclase crystals occur in one sample from Red Cone (C9-2-37LN), and amphibole was also recorded in a sample collected from the NE Little Cone by Vaniman et al. (1982). The amphibole crystals (up to 7 mm long) display disequilibrium textures including reaction rims and evidence of resorption. In the Red Cone sample the amphibole is associated with abundant olivine phenocrysts and olivine crystal clots up to 4mm in diameter. Such textures may indicate that the amphibole and olivine crystals are phases that fractionated during an earlier stage of magmatic evolution, and that they were subsequently remobilized from cumulus material. Another possibility is that the amphibole and plagioclase are xenocrysts. It is interesting to note that sample C9-2-37LN occurs as a massive blocky outcrop (>2 m²) on the northern flank of Red Cone, and that it appears to be a large bomb of previously erupted and solidified lava. We feel that this sample probably reflects material erupted during the earliest stage of magmatism at Red Cone.

Restricted and low MgO and Mg#s, and low concentrations of the compatible trace elements (Ni, Co, Cr, V and Sc) suggest that the basalts of Crater Flat have evolved significantly from a primary alkali basalt magma. Primary basalts typically have been defined as having Mg#s ≥ 71 (e.g., Green et al., 1974), but in the Quaternary of the western United States such basalts are rare. They do occur in the Big Pine Volcanic Field of Inyo County, California (Ormerod et al., 1991), where the average compatible element budget of the basalts is: 330 ppm Ni, 55 ppm Co, 700 ppm Cr, 200 ppm V, and 25 ppm Sc (Ormerod et al., 1991). By comparison, the average concentrations from lavas at Black Cone are 42.8, 25.5, 101, 165, and 17.8 ppm respectively. This depletion of Ni and MgO at low silica can be modelled by the fractionation of ~20-25 wt% olivine from a typical primary magma, which would be consistent with the petrographic observations (e.g., low % phenocrysts, and populations dominated by olivine). Lesser amounts of spinel, pyroxene and/or amphibole fractionation are also required to control the depletion of the other compatible trace elements. The range of Cr concentrations (48-140 ppm) within the Crater Flat suite can be accommodated by minor variations in the volume of fractionated spinel, which is

generally observed as inclusions in the olivine phenocrysts. Vaniman and Crowe (1981) reported 19 wt% Cr₂O₃ in such included phases.

Incompatible trace element variations are summarized on Figure 2, which displays the mean concentrations for Red Cone and Black Cone, standardized to typical primitive mantle values (taken from Sun and McDonough, 1989). The ordering of elements reflects increasing compatibility in mantle mineral phases from left to right. The data from both cones display a considerable amount of overlap, and only a limited range of intra-suite variation (see Table 1 for statistics on the full suites for Red Cone and Black Cone). Samples from Red Cone can only be distinguished from those of Black Cone by relatively small, but significant, enrichments in Sr, La, and Ce.

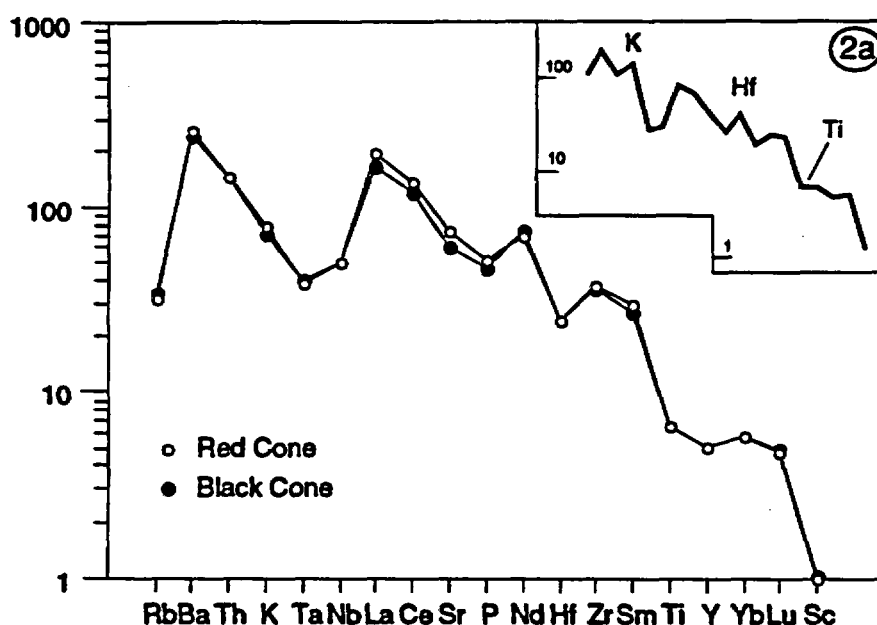


Fig. 2. Mean trace element compositions for Red Cone (n= 23) and Black Cone (n= 18) samples, normalized to primitive mantle values. See Table 1 for values of σ_n . The mean composition of syn-extensional alkali basalts (n= 22) from the Colorado River Trough (Bradshaw et al., 1993) is shown for comparison in the inset figure. Note the similarity of the patterns and the overall trace element abundances, with the exception of Rb and K₂O.

In general, the Large Ion Lithophile Elements (LILE) apart from Rb, and the Light Rare Earth Elements (LREE), are enriched relative to the High Field Strength Elements (HFSE) and the Heavy Rare Earth Elements (HREE). This produces a characteristic pattern with a Ta-Nb trough, peaks at Ba and La, and a pronounced step between elements thought to be more or less incompatible than Ti.

Trace element modelling

1. CHARACTERISTICS OF CRATER FLAT MAGMAS

The trace element abundance patterns described above are typical of those thought to be associated with melting in the sub-continental lithospheric mantle (e.g., Leat et al., 1988). The low Ta-Nb feature is modelled as a source characteristic in the western United States (Ormerod et al., 1991; Bradshaw et al., 1993) and depleted Ta-Nb concentrations relative to La appear to be a feature of lherzolite xenoliths from the lithospheric mantle (Jochum et al., 1989). The elevated LILE and LREE concentrations probably relate to lithospheric enrichment by subduction-derived fluids and melts (cf., Fraser et al., 1985; Waters and Erlank, 1988).

However, the *absolute* abundances of all the incompatible trace elements are likely to have been elevated in the order of 20-25% by olivine fractionation from the primary magmas. As the trace element distribution coefficients for these elements in olivine is uniformly low (see compilation by Henderson, 1986), this fractionation is not thought to have a significant effect on the relative abundance patterns.

The Crater Flat samples display little variation on most trace element ratio (or trace element vs. trace element) diagrams. Indeed the clustering of data on diagrams such as Zr/Y vs. Nb/La (Figure 3) suggests that the lavas within each Crater Flat centre are comagmatic. The limited range of Nb/Y, Zr/Y and concentrations of Rb, Zr, and Nb (see Table 1 and Figure 4b) also suggests that the lavas of Red Cone and Black Cone were derived by similar degrees of partial melting, and that they have subsequently undergone comparable amounts of fractional crystallization.

An unusual feature of the Crater Flat samples, compared to suites from other basaltic provinces in the vicinity (e.g., near Lake Mead, and the Colorado River Trough south of Las Vegas), is the low degree of Rb and K₂O enrichment relative to that of the LREE (see Figure 2a). There is no petrographic evidence for pervasive alteration that might be accompanied by a loss of Rb and K₂O, and neither are the concentrations of these elements unduly scattered. Thus it would appear to be a primary feature of the magmas. This might be reconciled with either a low Rb-K₂O source or with the presence of phlogopite ($D_{\text{phlog/liqK}} = 2.7$, $D_{\text{phlog/liqRb}} = 3.1$, Henderson, 1986) as a residual phase in the mantle, as suggested by Vaniman et al. (1982). Indeed, the occurrence of amphibole in the phenocryst assemblage may reflect derivation of the Crater Flat magmas from a source containing such hydrous phases.

Phlogopite is often regarded as one of the first phases to become exhausted in the source during melting of the mantle (cf., Cox et al., 1984). Thus, if phlogopite is a residual phase, very small degrees of partial melting must be inferred, probably less than 1%. High Nb/Y and Zr/Y

ratios (which should be unaffected by olivine-dominated fractionation and alteration) are also consistent with small degrees of partial melting of a garnet peridotite source (Table 1 and Figure 3), as are the relatively small volumes of magma that are present at each centre.

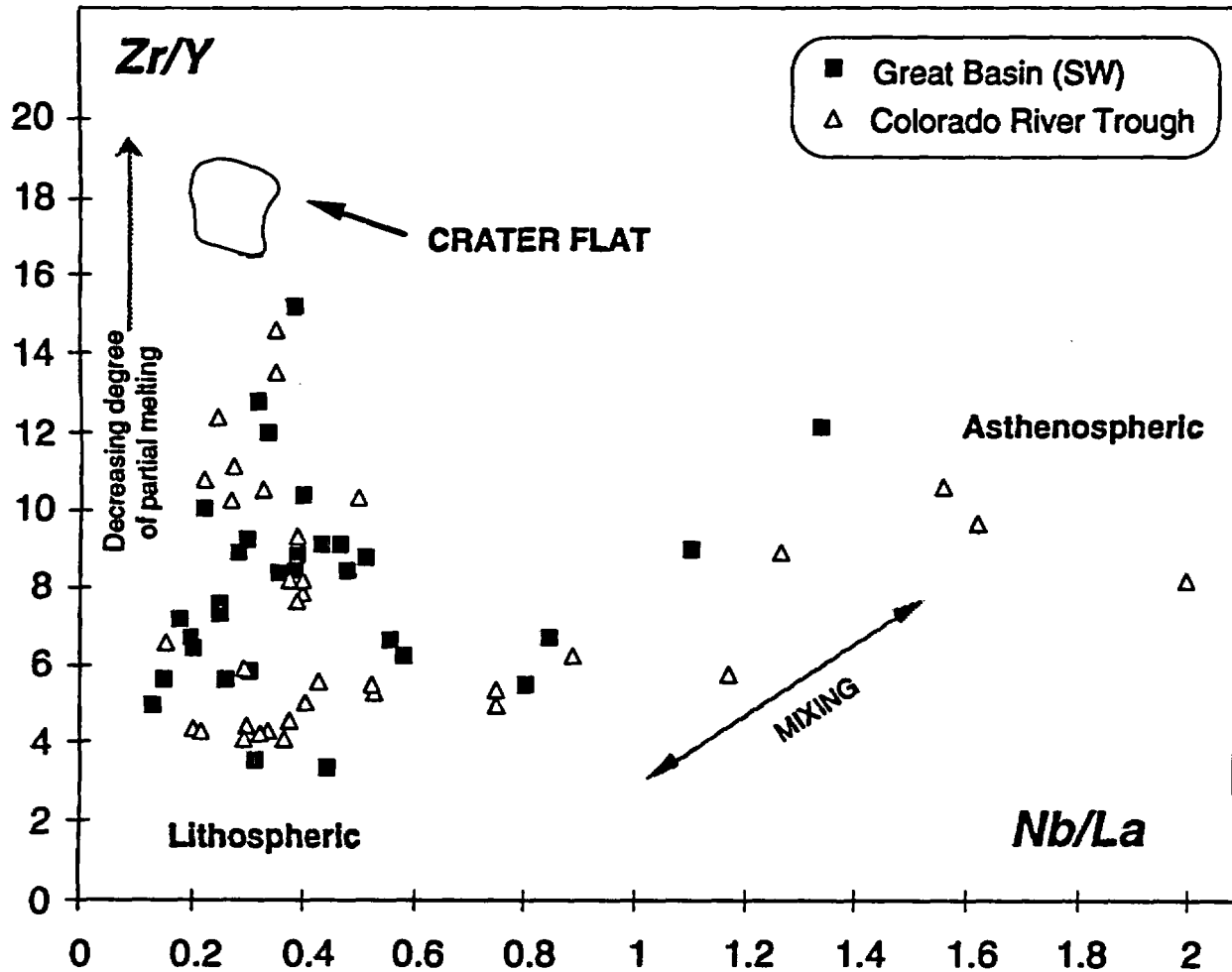


Fig. 3. Zr/Y vs. Nb/La . Crater Flat samples are compared to data from the Lake Mead area (Smith et al., 1990b) and the Colorado River Trough (C.R.T.: Bradshaw et al., 1993). The elements in each ratio are similarly incompatible and hence the ratios are unlikely to vary significantly during fractionation. Y is highly compatible in garnet, which may be present in the mantle source and behave as a residual phase at small degrees of partial melting. Increasing Zr/Y is thus modelled as a decrease in the degree of partial melting. Variation in Nb/La is primarily controlled by Nb. Typical asthenospheric basalts have high Nb/La , and basalts derived from the lithosphere have lower Nb/La reflecting the Ta-Nb 'trough' on diagrams such as Figure 2. Lake Mead and post-extensional C.R.T. basalts are thought to record mixing between lithospheric and asthenospheric end-members. The Crater Flat samples may represent small degree partial melts of a lithospheric mantle source.

2. PETROGENESIS OF RED CONE AND BLACK CONE

The Red Cone and Black Cone suites are clearly distinguished on diagrams involving La, Ce, and Sr, and to lesser extents Ba and Th (Figures 4 and 5). On such diagrams the Red Cone data spread over a large range of concentrations (and for example, La/Y ratios), whereas the Black Cone samples remain tightly clustered. Within the Red Cone suite there are reasonable positive correlations among these trace elements (Figure 4a). These correlations and the high concentration of elements such as Sr, in concert with the limited variation in fluid-mobile elements such as Rb (Figure 4b), again indicate that the observed trends are not the result of chemical alteration or weathering. Furthermore, such variations are unlikely to be the result of contamination by upper crustal material, which typically has high Rb and low Sr and LREE concentrations (Taylor and McClennan 1985). Contamination with lower crustal material to produce the Red Cone array is a possibility. However, mixing with upwards of 20-30 wt% of average lower crustal granulite (from Wendlandt et al., 1993) would be required to reproduce the variation in Ce, Sr etc. Other elements such as Nb, Zr and Hf which display little variation in the Red Cone suite would be significantly affected too, as would the major element geochemistry. In addition, there is no supporting petrographic evidence for such extreme degrees of contamination.

Trace element variations at Red Cone are apparently a function of the relative eruption age of the sample (Figure 4c). The youngest group of Red Cone lavas (from the eastern flows and associated with the final build-up of Red Cone itself) consistently have more elevated incompatible element concentrations, whereas the older lavas have values closer to or overlapping those from Black Cone. Time dependent trends of this nature could result from increasing degrees of fractionation or a systematic decrease in the degree of partial melting in the source, which would also lead to the onset of a waning phase of volcanism as magma supply rates dwindled. This sequence has been proposed for the late stages of alkali basalt magmatism at Haleakala Volcano in Hawaii (Chen et al., 1990), however it is unlikely that this can account for the magnitude of the observed variations at Red Cone. For instance, Sr concentrations at Red Cone range from approximately 1300-1850ppm (a 42% increase with time), which would necessitate approximately halving the degree of partial melting. Such a large decrease would certainly be recorded as a significant range in the concentrations of other moderately incompatible elements, such as Ta, Nb, Zr, and Hf (and the highly incompatible element Rb), but this is not observed.

Fig. 4. NEXT 2 PAGES. *See text.* The mean Black Cone composition is represented as a shaded dot on each of these diagrams and on Figure 5. Figs. 4a, b, d. Model lines are shown for fractionation of various mineral phases (with 5% intervals) from the least enriched Red Cone sample (C9-2-37LN). *See text for discussion.* Fig. 4c. Variation of Ce and La concentration with time at Red Cone. The Red Cone data is split into two main time groups and samples within these are arranged in approximate eruption sequence based on field relationships.

Figure 4a.

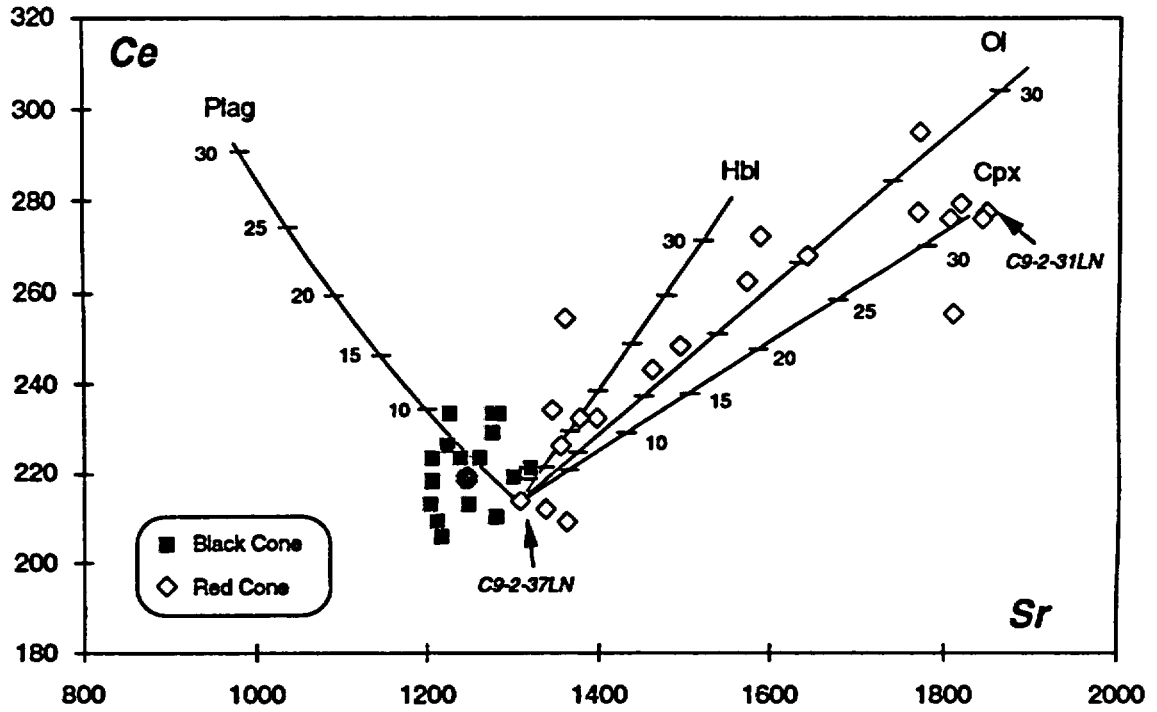


Figure 4b.

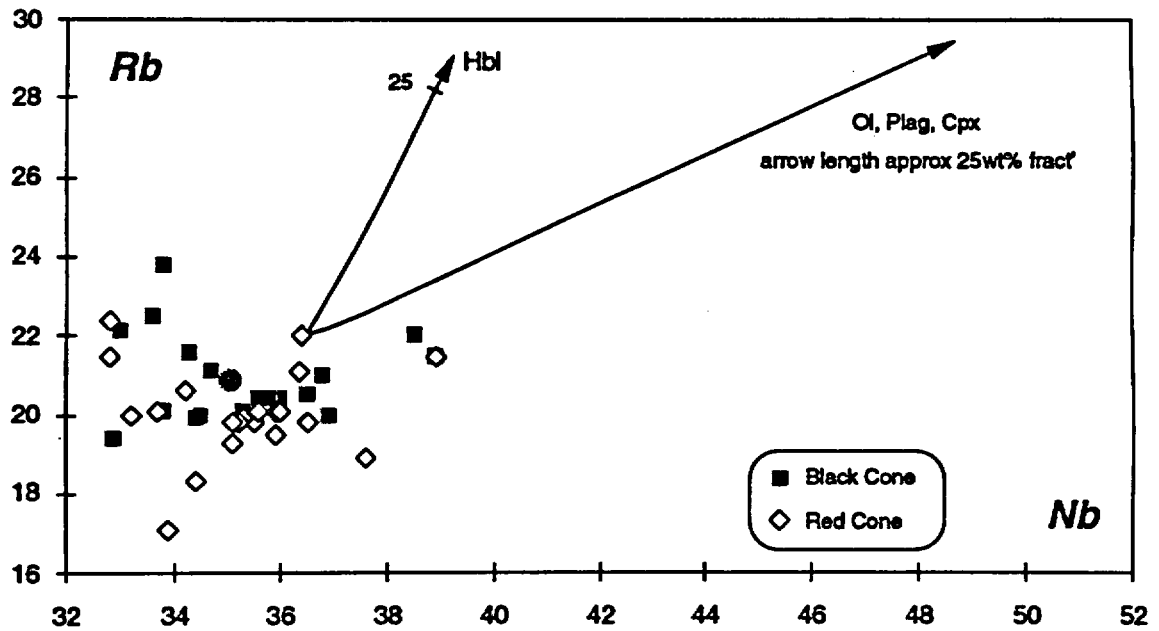


Figure 4c.

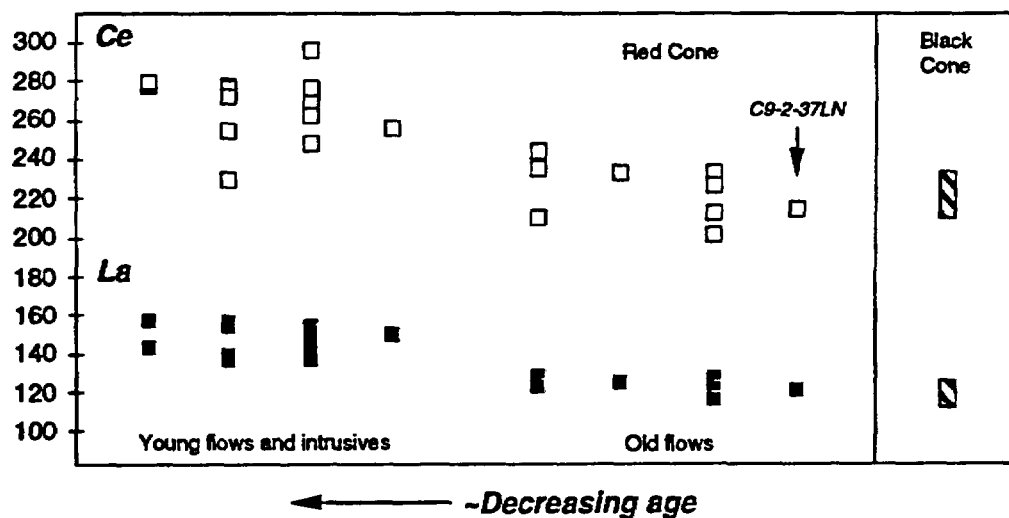
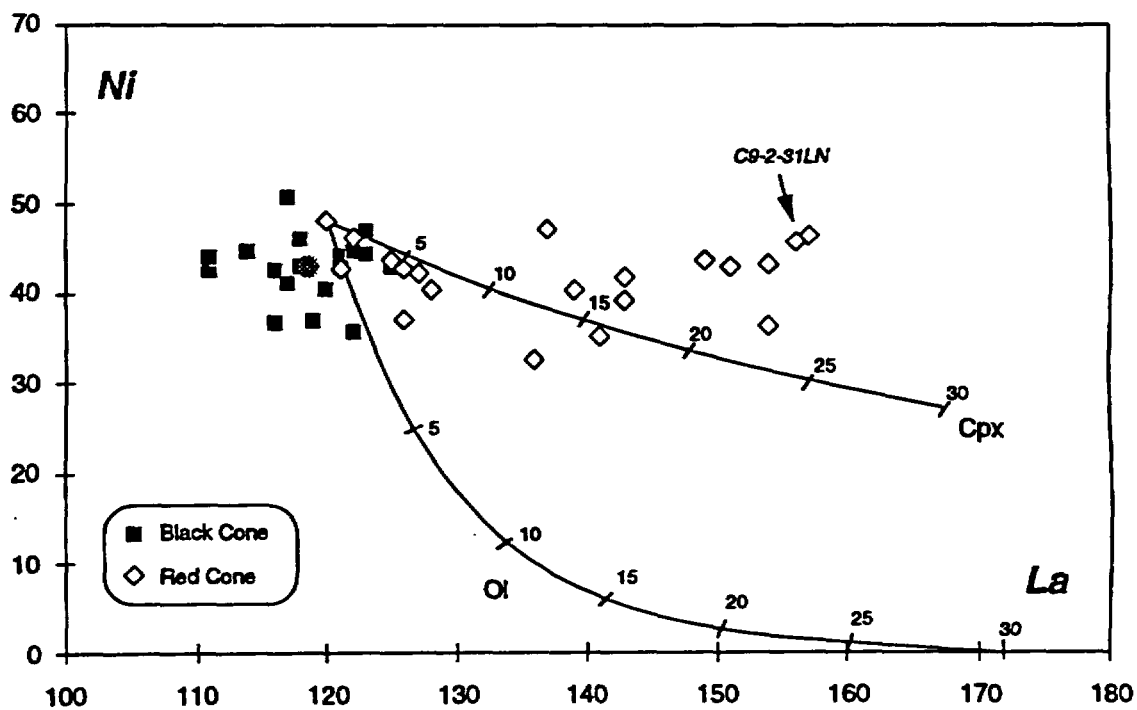


Figure 4d.



Vaniman et al. (1982) suggested that much of the major and trace element variability in a previous phase of alkali basalt volcanism in Crater Flat (3.7 Ma) can be modelled by fractionation, where olivine, amphibole, clinopyroxene and plagioclase are the principle fractionating phases. Thus, the role of fractionation is examined on Figures 4 and 5 as a possible process for generating the array of Red Cone data. In these models plagioclase is not thought to play an important role because it does not occur as a phenocryst phase, and because its fractionation would decrease both the Sr concentrations and the La/Y ratio of the residual liquid ($D_{\text{plag/liqSr}} \sim 1.8$, $D_{\text{plag/liqLa}} > D_{\text{plag/liqY}}$, Henderson, 1986).

The removal of olivine, and to a lesser extent hornblende and clinopyroxene, may reproduce the general Red Cone array on incompatible trace element diagrams, such as Ce vs. Sr (Figure 4a), with $\leq 30\%$ fractionation from the least evolved Red Cone sample (C9-2-37LN). However, olivine fractionation has little effect on the La/Y ratio of the melt and thus the fractionation of hornblende would also be required. If the fractionating proportions are 70:30 Ol:Hbl, then the fractionation vector is coincident with the Red Cone data, although the range in La/Y from 5.3-6.8 requires the extreme degree of nearly 70 wt% fractionation. Furthermore, there is no indication of a trend towards depletion in Ni, an element that is compatible in hornblende and highly compatible in olivine (Figure 4d). Hornblende or pyroxene fractionation alone can be dismissed on similar grounds because of the lack of variation in the compatible elements Sc and Ti (Figure 5).

Moreover, the Ca/Al ratio of the Red Cone samples remains a constant (at ~ 0.5) with increasing Sr, La and Ce, suggesting that fractionation of calcic phases such as amphibole and clinopyroxene has not occurred.

Thus, fractional crystallization or changes in the degree of partial melting cannot easily replicate the Red Cone data array, and an alternative model must be sought. This model must account for large variations in the concentration of certain trace elements, while inducing little or no variation in the concentration of both the most- and least-compatible elements. Little or no major element variation can be tolerated either, and the simplest model that can satisfy such strict limitations is magma mixing.

On Figures 4a and 4d mixing models can be described by straight lines between the two chosen end-members. For instance, between the Red Cone samples C9-2-37LN and C9-2-31LN, representing 'old' and 'young' end-members respectively. Mixing models on Figure 5 would also approximate to a straight line or a shallow curve, because in essence the end-members are identical except for the differences in Sr, La etc. Thus it is possible to generate the magnitude and the 'direction' of all of the observed geochemical trends. This is achieved without need of further complexity to explain the otherwise anomalous lack of variation in Ni, Sc, Nb, Zr and Rb.

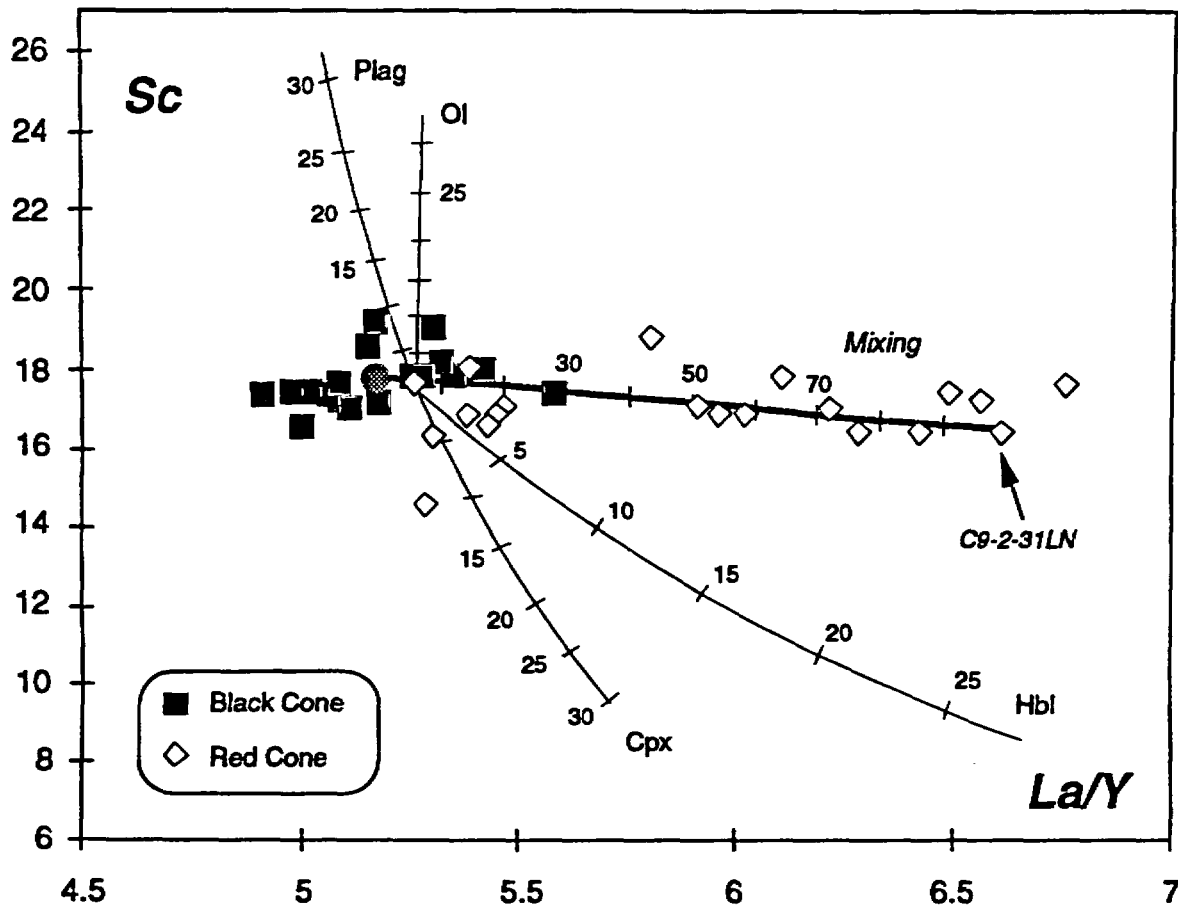


Fig. 5. Sc vs. La/Y. See text for discussion. A mixing model (with 10% intervals) is shown between the mean Black Cone composition and the Red Cone sample C9-2-31LN. Fractionation and mixing equations from Allègre and Minster (1986). Zr, Nb and Y distribution coefficients from Pearce and Norry (1979), other values from Henderson (1986).

However, it is clear that no two end-members defined from the Red Cone data set uniquely reproduce the complete Red Cone array. The scatter away from the modelled mixing lines might be attributable to small amounts of fractionation (e.g., <5 wt% olivine), or to an imperfect choice of end-member samples.

For the latter case, the Red Cone suite is comprised of two loose clusters of samples with an array between them (Figure 4). Therefore, average compositions within these small clusters would arguably represent more suitable end-member magmas. It is also apparent that the tight cluster of Black Cone data consistently falls at the less enriched ('old') end of the Red Cone array (Figures 3-5), raising the possibility that these magmas represent one end-member type. The mean composition of the Black Cone suite is indicated as shaded symbols on Figures 4-5, and on Figure 5 a mixing model has been generated between this point and the 'young' sample C9-2-31LN. This modelled line provides the closest approximation to the array, and similar model lines

would also coincide with the greatest number of sample points along the arrays in Figure 4. If the 'old' end-member is taken to lie within $\pm 2\sigma_n$ of the Black Cone mean, and a similar range is permitted for the 'young' Red Cone end-member, then mixing models can easily reproduce the entire spread of Red Cone data.

Discussion and Conclusions

The major and trace element patterns of volcanic rocks from the two largest centres in Crater Flat, Black Cone and Red Cone, are broadly similar. This suggests that they were derived from similar sources and that the magmas underwent comparable histories of differentiation before their eruption as moderately evolved alkali basalts. However, the trace element modelling presented in the previous section indicates that two different magmas were tapped at Red Cone during its development. Hence, the term polygenetic can be applied to this centre. An array of samples falling between the two Red Cone end-members indicates that magma mixing took place, and thus it must be inferred that batches of both magmas were present beneath Red Cone at the same time.

The depth at which mixing occurred, or the depth of final magmatic equilibration, can be estimated from normative mineral models based on experimental data (e.g., Presnall et al., 1978; Sack et al., 1987). On Figure 6 the normative mineral compositions of the Crater Flat samples, and comparative samples from the Lake Mead area, have been projected from normative plagioclase into the plane olivine-diopside-nepheline-hypersthene. Experimental cotectics (liquid lines of multiple saturation) have been reproduced from Sack et al. (1987). These cotectics are thought to be appropriate for the Crater Flat data as they accommodate all of the main mineral phases observed in thin section, with the exception of amphibole. Furthermore, it is thought that the low phenocryst abundances in the Crater Flat samples increases the validity of comparisons to the experimental data. Note that the one Red Cone sample with abundant amphibole phenocrysts has been excluded from the diagram because Figure 6 considers only anhydrous phases.

All of the Red Cone and most of the Black Cone analyses cluster on or around the end of the experimental Ol+Plag+Opx+Cpx high-pressure cotectic. Their distribution suggests that final equilibration occurred at 8-10 kb (e.g., deep in the crust, or in the upper mantle). There is no consistent trend within the Red Cone data to indicate a lower pressure mixing event, and thus the 8-10 kb result probably represents the depth at which the main stages of fractional crystallization occurred. Magmas subsequently reached the surface faster than the rate of reequilibration. In contrast, samples taken from the Lake Mead data set (Smith et al., 1990b) are spread between the high-pressure and 1-atmosphere cotectics, consistent with a history of polybaric evolution.

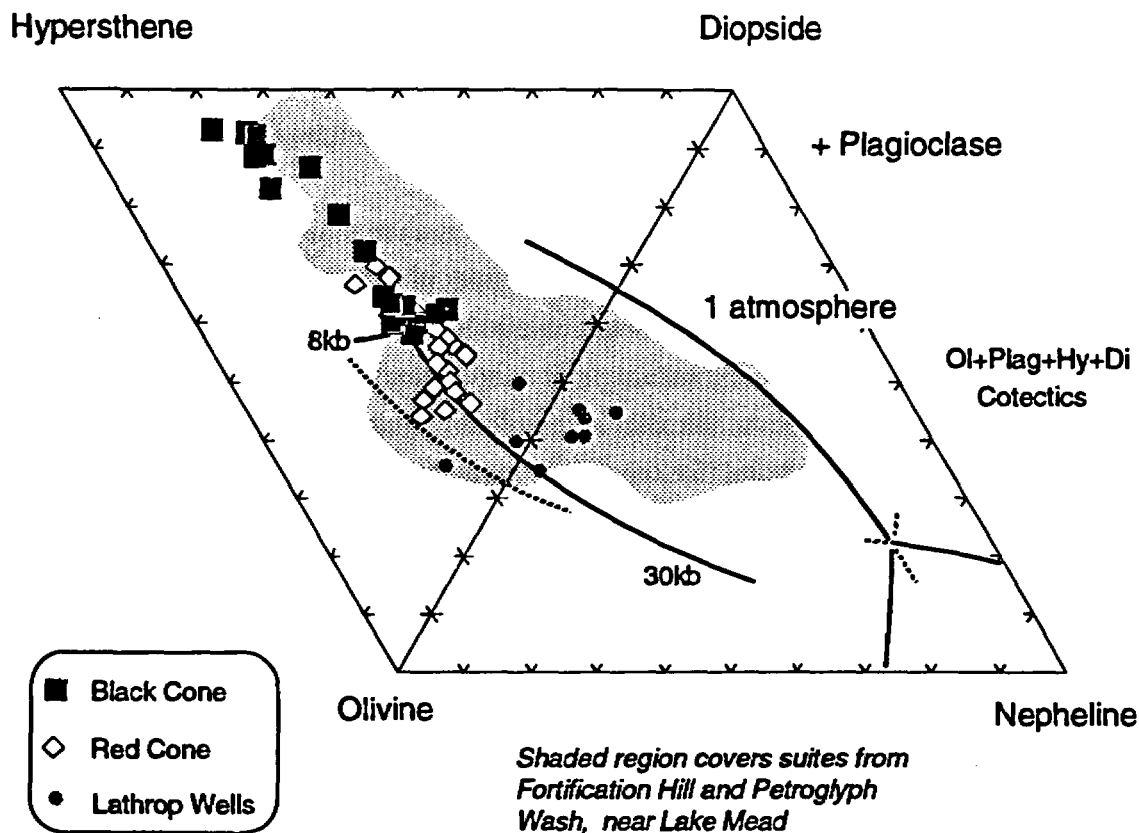


Fig. 6. Normative mineral compositions of Crater Flat and Lake Mead samples (Smith et al., 1990b) projected onto the plane Ol-Di-Ne-Hy, from normative plagioclase. Experimental cotectics (solid lines) for 1 atmosphere and 8-30kb are reproduced from Sack et al. (1987). The area between the dashed line and the 8-30 kb cotectic indicates the range of experimental Di/Ol ratios reported in that study.

The youngest samples at Black Cone, associated with the lava lake development and the northern flows, have the lowest normative olivine contents and plot farthest from the end of the high pressure cotectic on Figure 6. This is likely to indicate that the magmas last reached equilibrium at shallower crustal levels than other Black Cone and Red Cone magmas, perhaps recording a period of residency in a crustal magma chamber before eruption.

The origin of the magma batches at Crater Flat is interesting to contemplate, particularly in light of their limited volume and the compositional similarity between the Black Cone lavas and the oldest Red Cone lavas. It is compelling to suggest that magmatism at the two centres was linked, possibly via a shared sub-surface plumbing system, for at least part of their development. The position of the cones and the cinder mound vent sites is probably controlled by regional structure, and so it is easy to envisage a set of NE-SW directed feeder dykes that might have intersected either, or both, of the main vent areas. Indeed the two centres may have been active concurrently, erupting the same magma batch. This idea is proposed because of the viability in using the average Black Cone magma composition as the least enriched end-member in mixing

models at Red Cone. Thus, a reconstructed sequence for the magmatic history at Crater Flat may resemble the following:

i) Magmatism of the Black Cone/ early Red Cone compositional type commenced at Red Cone, and subsequently spread to Black Cone.

ii) A new magma batch with elevated Sr, La, Ce, etc. was then tapped at Red Cone, and mixing occurred between this magma and a diminishing supply of the earlier magma type. The structural level at which this mixing occurred was above that of any link that might have existed between the Black Cone and Red Cone plumbing systems, because the enriched magma type is not observed at Black Cone. However, the actual depth of mixing cannot be defined.

iii) Volcanic activity ceased at Red Cone while magmatism resumed or continued at Black Cone, without any noticeable change in the compositional type.

An important implication of the recognition of polycyclic-polygenetic volcanism in the southern Great Basin is that additional eruptions may occur near or at existing Quaternary-age volcanic centres. Based on this assumption and a knowledge of the size of volcanic chains and regional structural patterns in southern Nevada, Smith et al. (1990a) proposed hazard zones near Yucca Mountain. These were centred on existing volcanoes and elongated parallel to magmatic feeder zones and regional north-northeast striking faults. One hazard zone includes the Crater Flat chain and another the Lathrop Wells cone and the Yucca Mountain waste repository. Our results indicate that volcanism may occur at more than one place along the length of a magmatic feeder zone during the period of activity. Thus, it is important to consider the potential length of these feeder zones when making assessments of volcanic risk, as recognized by Smith et al. (1990a) and Ho et al. (1992). This study raises the possibility that renewed eruption at an existing cone (e.g., Lathrop Wells) may be accompanied by activity at other localities along the magmatic feeder zone, thus forming a volcanic chain and potentially having a direct effect on the proposed nuclear waste repository.

In addition, the limited but distinct trace element variations recorded between the Black Cone/ early Red Cone and later Red Cone magma types are unlikely to be preserved if the magmas had travelled any great distance laterally during ascent from their source. For example if the magmatism were in some way related to that in Death Valley. Rather, it is suggested that the magma source was in the lithospheric mantle proximal to Crater Flat and that the compositional differences may reflect small-scale mantle heterogeneities. As Sr is one of the elements that displays a large variation between the magma types, a detailed isotopic study is currently in progress to evaluate these heterogeneities.

References

- Allègre, C.J. and Minster, J.F., 1978. Quantitative models of trace element behaviour in magmatic processes. *Earth Planet. Sci. Lett.*, 38: 1-25.
- Basaltic Volcanism Study Project, 1981. *Basaltic Volcanism on the Terrestrial Planets*. Pergamon Press, New York, 1286pp.
- Bates, R.L. and Jackson, J.A., 1987. *Glossary of Geology*. Am. Geol. Institute, Alexandria, Virginia, 788pp.
- Bradshaw, T.K., Hawkesworth, C.J. and Gallagher, K., 1993. Basaltic volcanism in the southern Basin and Range: No role for a mantle plume. *Earth. Planet. Sci. Lett.*, 116: 45-62.
- Carr, W.J., 1982. Volcano-tectonic history of Crater Flat, southwestern Nevada, as suggested by new evidence from drill hole USW-VH-1 and vicinity. U.S. Geol. Surv. Open File Report 82-457: 23pp.
- Chen, C.-Y., Frey, F.A. and Garcia, M.O., 1990. Evolution of alkalic lavas at Haleakala Volcano, east Maui, Hawaii. Major, trace element and isotopic constraints. *Contrib. Mineral. Petrol.* 105: 197-218.
- Christiansen, R.L., Lipman, P.W., Orkild, P.P., Byers, F.M., Jr., 1965. Structure of the Timber Mountain Caldera, Southern Nevada, and its relation to basin-range structure. U.S. Geol. Surv. Prof. Paper, 525-B: B43-B48.
- Cox, K.G., Duncan, A.R., Bristow, J.W., Taylor, S.R. and Erlank A.J., 1984. Petrogenesis of the basic rocks of the Lebombo. *Spec. Publ. Geol. Soc. S. Africa* 13: 149-169.
- Cox, K.G., Bell, J.D. and Pankhurst, R.J., 1979. *The interpretation of igneous rocks*. George Allen and Unwin (Publishers) Ltd., London, 450pp.
- Crowe, B.M., Harrington, C., Turrin, B., Champion, D., Wells, S., Perry, F., McFadden, L. and Renault, C., 1989a. Volcanic hazard studies for the Yucca Mountain Project. *Waste Management 89*, Arizona Board of Regents, Tucson, Arizona, Vol 1: High level waste and general interest 485-491.
- Crowe, B.M., Turrin, B., Wells, S., McFadden, L., Renault, C., Perry, F., Harrington, C. and Champion D., 1989b. Polycyclic volcanism: a common eruption mechanism of small volume basaltic volcanic centers of the southwestern Great Basin, USA (IAVCEI Abstracts), New Mexico Bur. of Mines and Min. Resources Bull., 131: 63.
- Crowe, B.M., Morley, R., Wells, S., Geissman, J., McDonald, E., McFadden, L., Perry, F.V., Murrell, M., Poths, J. and Forman S., 1992a. Lathrop Wells Volcanic Centre: Status

- of field and geological studies. In Proceedings of the Third International High-Level radioactive waste Management Conference, Las Vegas, Nevada, Vol. 2: 1997-2013.
- Crowe, B.M., Valentine, G.A., Morley, R. and Perry, F.V., 1992b. Recent progress in volcanism studies: Site characterization activities for the Yucca Mountain Project. Waste management '92, Arizona Board of Regents, Tucson, Arizona, Vol. 1: 921-928.
- Department of Energy, Final environmental assessment: Yucca Mountain Site, Nevada: Research and Development, Nevada, DOE/RW-0073, Washington D.C., 1986.
- Faulds, J.E., Bell, J.W., Feuerbach, D.L. and Ramelli, A.R., 1993. Geologic map of Crater Flat, Nevada, Nevada Bur. of Mines and Geol., in press.
- Fraser, K.J., Hawkesworth, C.J., Erlank, A.J., Mitchell, R.H. and Scott-Smith, B.H., 1985. Sr, Nd and Pb isotope and minor element geochemistry of lamproites and kimberlites. *Earth Planet. Sci. Lett.*, 76: 57-70.
- Green, D.H., Edgan, H.D., Beasley, P., Kiss, E. and Ware, N.G., 1974. Upper mantle source for some hawaiites, mugearites and benmorites. *Contrib. Mineral. Petrol.*, 48: 33-43.
- Henderson, P., 1986. *Inorganic Geochemistry*, Pergamon Press, Oxford, U.K., 353pp.
- Ho, C-H., 1992. Risk assessment for the Yucca Mountain high-level nuclear waste repository site: estimation of volcanic disruption. *Math. Geol.*, 24: 347-364.
- Holm, R.F., 1987. Significance of agglutinate mounds on lava flows associated with monogenetic cones: An example at Sunset Crater, northern Arizona. *Geol. Soc. Am. Bull.* 99: 319-324.
- Jochum, K.P., McDonough, W.F., Palme, H. and Spettel, B., 1989. Compositional constraints on the continental lithospheric mantle from trace elements in spinel peridotite xenoliths. *Nature*, 340: 548-550.
- Leat, P.T., Thompson, R.N., Morrison, M.A., Hendry, G.L., and Dicken, A.P., 1988. Compositionally diverse Miocene-Recent rift-related magmatism in NW Colorado: partial melting and mixing of mafic magmas from three different lithospheric and asthenospheric mantle sources. In: *Oceanic and continental lithosphere- similarities and differences*, *J. Petrol. Spec. Vol.*, 351-378.
- Le Bas, M.J., Le Maitre, R.W., Streckeisen, A. and Zanettin, B., 1986. A chemical classification of volcanic rocks based on the total alkali-silica diagram. *J. Petrol.*, 27: 745-50.
- Ormerod, D.S., Rogers, N.W. and Hawkesworth, C.J., 1991. Melting in the lithospheric mantle: Inverse modelling of alkali-olivine basalts from the Big Pine Volcanic Field, California. *Contrib. Mineral. Petrol.*, 108: 305-317.

- Pearce, J.A. and Norry, M.J., 1979. Petrogenetic implications of Ti, Zr, Y and Nb variations in volcanic rocks. *Contrib. Mineral. Petrol.*, 69: 33-47.
- Presnall, D.C., Dixon, S.A., Dixon, J.R., O'Donnell, T.H., Brenner, N.L., Schrock, R.L. and Dycus, D.W., 1978. Liquidus phase relations on the join diopside-forsterite-anorthite from 1atm to 20kbar: Their bearing on the generation and crystallization of basaltic magma. *Contrib. Mineral. Petrol.*, 66: 203-220.
- Sack, R.O., Walker, D. and Carmichael, I.S.E., 1987. Experimental petrology of alkalic lavas: constraints on cotectics of multiple saturation in natural basic liquids. *Contrib. Mineral. Petrol.*, 96: 1-23.
- Smith, E.I., Feuerbach, D.L., Naumann, T.R. and Faulds, J.E., 1990a. The area of most recent volcanism near Yucca Mountain, Nevada: Implications for volcanic risk assessment. In: *High Level Radioactive Waste Management, Vol. 1: La Grange Park, Illinois, American Nuclear Society*, 81-90.
- Smith, E.I., Feuerbach, D.L., Naumann, T.R., Faulds, J.E. and Cascadden, T., 1990b. Annual report of the Center for Volcanic and Tectonic Studies for the period 10-1-89 to 9-30-90, Nuclear Waste Project Office, Carson City, NV. Report No. 43.
- Sun, S-s. and McDonough, W.F., 1989. Chemical and isotopic systematics of oceanic basalts: Implications for mantle composition and processes. In: *Magmatism in the Ocean Basins*, edited by A.D. Saunders and M.J. Norry, *Geol. Soc. Spec. Publ.*, 42: 313-345.
- Taylor, S.R. and McClennan, S.M., 1985. *The continental crust: its composition and evolution. Geoscience texts*, Blackwell Scientific Publications, U.K., 312pp.
- Turrin, B.D., Champion, D. and Fleck, R.J., 1991. $^{40}\text{Ar}/^{39}\text{Ar}$ age of the Lathrop Wells volcanic center, Yucca Mountain, Nevada. *Science* 253: 654-657.
- United States Department of the Interior Geological Survey, 1984. A summary of geologic studies through January 1st, 1983, of a potential high level radioactive waste site at Yucca Mountain, southern Nye county, Nevada U.S.G.S. Open File Rpt., 84-729, 103pp.
- Vaniman, D.T. and Crowe, B.M., 1981. Geology and petrology of the basalts of Crater Flat: Applications to volcanic risk assessment for the Nevada Nuclear Waste Storage Investigations. Los Alamos Nat. Lab. Rpt., LA-8845-MS.
- Vaniman, D.T., Crowe, B.M. and Gladney, E.S., 1982. Petrology and geochemistry of Hawaiite lavas from Crater Flat, Nevada. *Contrib. Mineral. Petrol.*, 80: 341-357.
- Waters, F.G. and Erlank, A.J., 1988. Assesment of the vertical extent and distribution of mantle metasomatism below Kimberly, South Africa. *J. Petrol. Spec. Lith. Issue*, 185-204.
- Wells, S.G., Crowe, B.M. and McFadden, L.D., 1992. Measuring the age of the Lathrop Wells Volcanic Center at Yucca Mountain. *Science*, 257: 555-556.

- Wells, S.G., McFadden, L.D., Renault, C.E., and Crowe, B.M., 1990. Geomorphic assessment of Late Quaternary volcanism in the Yucca Mountain area, southern Nevada: Implications for the high-level radioactive waste repository. *Geology*, 18: 549-553.
- Wendlandt, E., DePaolo, D.J. and Baldrige, W.S., 1993. Nd and Sr isotope chronostratigraphy of Colorado Plateau lithosphere: implications for magmatic and tectonic underplating of the continental crust. *Earth. Planet. Sci. Lett.*, 116: 23-43.

Section 3

Further Modelling: Crater Flat

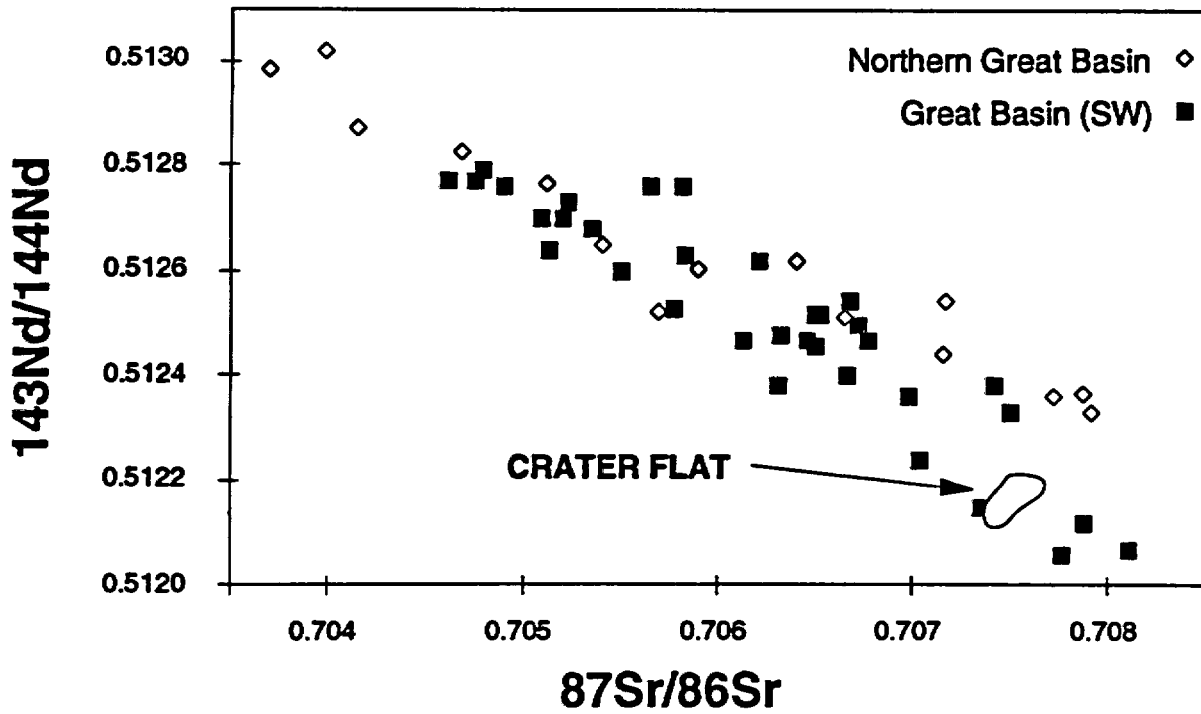
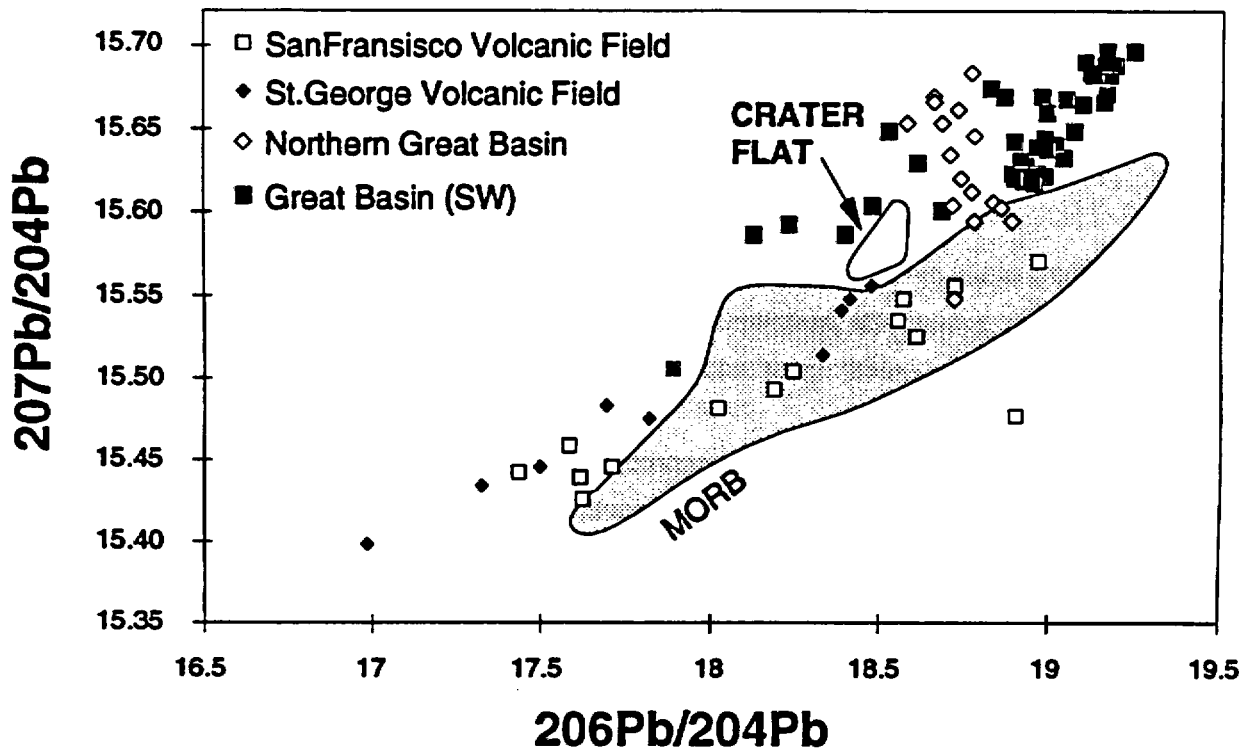
In this section an outline of additional geochemical modelling is presented for the Crater Flat region. The modelling incorporates trace element and isotope data collected during 1993. Much of this work was presented in poster format at the IAVCEI meeting in September.

The preliminary figures on the following page compare Pb, Sr and Nd isotopic analyses to samples from other regions of basaltic volcanism in the western United States. Crater Flat magmas are characterised by enriched trace element concentrations, high $87\text{Sr}/86\text{Sr}$, low $143\text{Nd}/144\text{Nd}$, and Pb isotope ratios distinct from the asthenosphere. The Crater Flat isotopic array falls within the bounds of data collected for basaltic volcanic fields along the southwestern edge of the Great Basin (data from Ormerod 1988, unpubl. PhD. thesis, The Open University, UK). Such isotopic ratios are thought to be characteristic of magmas generated predominantly from the lithospheric mantle. Only limited isotopic variation is recorded at Crater Flat. However, there is a distinct and consistent Nd-Sr isotope correlation which also corresponds to variations in certain trace element concentrations.

Summary of modelling section:

1. Trace element enrichment in the youngest magmas at Crater Flat is likely to be a result of mineralogical variations in the mantle source. We suggest that the mantle is locally heterogeneous and veined with phlogopite and amphibole. Black Cone lavas and initial magmas at Red Cone were derived from the more hydrous regions (phlog [2%] + amph [4%]). Less hydrous fractions (phlog [2%], no amphibole) melted to produce the trace element enriched Red Cone magmas.
2. Trace element and minor element variation at Black Cone, and Nd & Sr isotope differences between Black Cone and Red Cone, may be the result of small amounts of lower crustal contamination (AFC model). Least contaminated Black Cone lavas form a lava lake sequence.

ISOTOPES



A report on the state of geochemical modelling- Crater Flat volcanism (from Doc. 76)

Recent work at the CVTS has been concentrated on testing geochemical models that attempt to account for the differences between Red Cone and Black Cone magmas. More specifically, the differences between the previously identified 'enriched' and 'depleted' (Red Cone) magma batches, as these are thought to form the two endmembers in a mixing array (Bradshaw and Smith, 1993). This has required the use of both trace element and isotope modelling techniques. Identification of the two Red Cone geochemical batches is crucial to the question of polygenetic volcanism in Crater Flat, and is likely to require that estimates of volcanic hazard be revised.

For instance, earlier probability calculations (Ho et al., 1991, Bull. Volcanol.) require an estimate of E, the number of volcanic eruptions (or time-distinct events), and for the Yucca Mt. area this was set at 8 (eight) during the Quaternary: Sleeping Buttes (2 centres), Little Cones (2 centres), Red Cone, Black Cone, Northern Cone, and Lathrop Wells Cone. Individual flows and cinder mound sites at each centre were not included in E since these may not represent time-distinct events. However, this new geochemical work indicates the presence of two distinct magma batches at Red Cone. Flows corresponding to these batches also differ markedly in morphology and state of preservation, thus suggesting a significant time gap between events. If this is indeed the case, then the value of E in the Yucca Mt. area must be increased to 9 (nine), with Red Cone counted as two centres. In the calculations of Ho et al. (1991) this would increase the maximum likelihood estimate of a volcanic event from $5.9 \times 10^{-6} \text{yr}^{-1}$ to $6.7 \times 10^{-6} \text{yr}^{-1}$. This equates to approximately 1 (one) volcanic event every 150,000 yrs, although obviously an over-simplification because the occurrence of volcanic events with time is thought to follow a Poisson distribution.

A question we are currently posing is,

how might the separate magma batches be related to each other?

By answering this question we may be able to place further constraints on the origin of the Crater Flat magmas, and how the magmatism has developed with time. In turn, this may be important for volcanic hazard assessment, although it may be difficult to assign numerical 'risk factors' to such information.

Possible models under consideration are:

1. Magmas related by fractional crystallization.
2. Variable degrees of partial melting of the same source, or a partial melting continuum whereby later magmas are derived by melting of the residual material from earlier magma genesis.

3. Magmas share source trace element characteristics, but different mineralogies (e.g., the differences arise from the proportions of minerals contributing to the melt or remaining as residual phases).
4. Variable degrees of crustal assimilation (perhaps with time) leading to two distinct magma types- one original magma and one contaminated.
5. The magmas are not related by any of the models outlined above. Instead, they represent melts of very distinct source compositions, perhaps reflecting heterogeneities in the mantle resulting from non-uniform trace element enrichment processes.

Models 2-5 are examined below in some detail. Model 1 can be ruled-out on petrological grounds and on the geochemical arguments proposed in Bradshaw and Smith (1993). The reader is also directed to this paper for a general discussion of the geochemistry and petrology of samples collected in Crater Flat. However, the following table provides a summary of the main geochemical characteristics of the 'enriched' and 'depleted' end-members.

Magma type:	Depleted	Enriched
Typical sample	C9-2-37LN/ Black Cone average	C9-2-31LN
Trace elements*	Low ppm Sr (1300), La (120), Ce (220), Ba (1700), Th (12)	High ppm Sr (1800), La (155), Ce (280), Ba (2000), Th (15.5)
Major elements	No significant differences	
Sr isotopes†	$^{87}\text{Sr}/^{86}\text{Sr} = 0.70691$	$^{87}\text{Sr}/^{86}\text{Sr} = 0.7071$
Nd isotopes†	$\epsilon\text{Nd} = -9.6$	$\epsilon\text{Nd} = -8.6$
Pb isotopes†	No significant differences	

Table 1. Summary of magma type differences at Crater Flat

* Rb, K₂O, Ta, Nb, Y, Zr, Hf display little or no consistent variation between the two magma types.

† See table in section 6, this document.

Model 2- Variable degrees of partial melting

Variable degrees of partial melting of the same mantle source will produce magmas with a range of incompatible element concentrations. At small degrees of partial melting high concentrations of the incompatible elements are expected along with small volumes of magma, and this is typical of alkali basalts in general. Absolute trace element concentrations in the magmas are dependent on both the initial concentration of the element in the source and the various melting parameters (e.g., the degree of partial melting and the bulk distribution coefficients for the elements). However, the *relative* trace element concentrations are dependent only on the melting parameters, and thus will be reflected in incompatible element ratios. Elements with similar degrees of incompatibility will display little variation in ratios (relative abundances) unless the degree of partial melting is extremely small (e.g., <<1%), whereas ratios of elements with widely variable incompatibilities (e.g., Rb/Zr, Ba/Nb, Nb/Y, Zr/Y) should display considerable variation. However, none of these ratios display any notable variations within or between the Red Cone and Black Cone suites. Therefore this model appears to be unlikely.

Re-melting of a residual source from earlier melt extraction is also thought to be unlikely, again because of the lack of variation in certain trace element ratios. It is also difficult to perceive how magmas with almost identical major element concentrations could be derived from what must be a more refractory source composition after the initial melt extraction. Furthermore, one might expect the earlier magmas to be trace element enriched, and that magmas would become more depleted with time- reflecting the increasingly depleted nature of the source. Yet, the reverse is true at Red Cone (young magmas = most enriched).

Model 3- Mineralogical variations in the source

A conclusion of Bradshaw and Smith (1993) is that the basalts at Crater Flat were derived by generally small degrees of partial melting of a trace element-enriched, garnet-bearing, lithospheric mantle source.

Barring the elements Sr, La, Ce, etc. (and some isotopic differences which may be the result of crustal contamination- see model 4), there is little to distinguish between the 'enriched' and 'depleted' magma types. This suggests that the bulk source compositions for both magmas are rather similar, and that these underwent a similar extent of partial melting. Indeed, the major difference may be one of source mineralogy. For instance, at small degrees of partial melting, trace element concentrations can be influenced by the presence (or otherwise) of minor phases, that rapidly become exhausted as the degree of partial melting increases. Ilmenite, apatite, phlogopite

and amphibole are such phases. Vaniman et al. (1982) and Bradshaw & Smith (1993) suggest that phlogopite may be a residual phase in the source of Crater Flat magmas, on the evidence of very low and consistent Rb and K_2O concentrations. Amphibole may also be present if the source is hydrous, and some rare amphibole crystals in samples from Little Cone and Red Cone may be xenocrysts entrained from such a source region.

To test this hypothesis, various mantle source compositions and melting models were constructed that might reproduce the geochemical variations at Crater Flat. Initially, these models were compared empirically to limit the number of variables, and so estimates of the degree of partial melting and the trace element concentrations in the source were not required. The model results are thus dependent only on the modal mineralogy of the source and the proportions in which these minerals enter the melt (P). Standard values of P were employed along with typical distribution coefficients for trace elements in the various mineral phases (see Table 2 for details).

Thus, for a range of trace elements, the following parameters were created for each model:

D_0 (bulk distribution coefficient for each trace element in the source), and

P_0 (bulk distribution coefficient for each trace element dependent on the mineral phase proportions contributing to the melt).

This is represented graphically in Figure 1. Here, model differences in D_0 and P_0 values for enriched and depleted magmas are displayed for a series of trace elements (data from table 2). Comparative patterns are also shown for the observed difference between the enriched and depleted magmas using representative samples. In this type of modelling the actual values derived are not the primary concern because initial source concentrations and the degree of partial melting are not known for the real magmas. Rather, it is the shape of the pattern for each model that should be compared to the pattern for the real data.

The best fit to the patterns is obtained using a source containing phlogopite to generate the enriched magma, and one containing phlogopite and amphibole to generate the depleted magma. In Figure 1 it can be seen that D_0 differences closely follow the required pattern: there are comparable peaks at Th, La, Sr and Sm, a slight trough at Ce, and major troughs from K_2O to Nb and from P_2O_5 to Zr. Elements which are not modelled well are Ti, Ba and Yb. The latter may be an analytical artifact (poor data acquisition), and the problems with Ti and Ba are likely to reflect poorly constrained distribution coefficients in phlogopite and amphibole. The pattern for P_0 differences is similar to that for D_0 , although the peak at Sm is more pronounced, there is a new peak at Y, the Th peak is subdued and there is no dip at Ce.

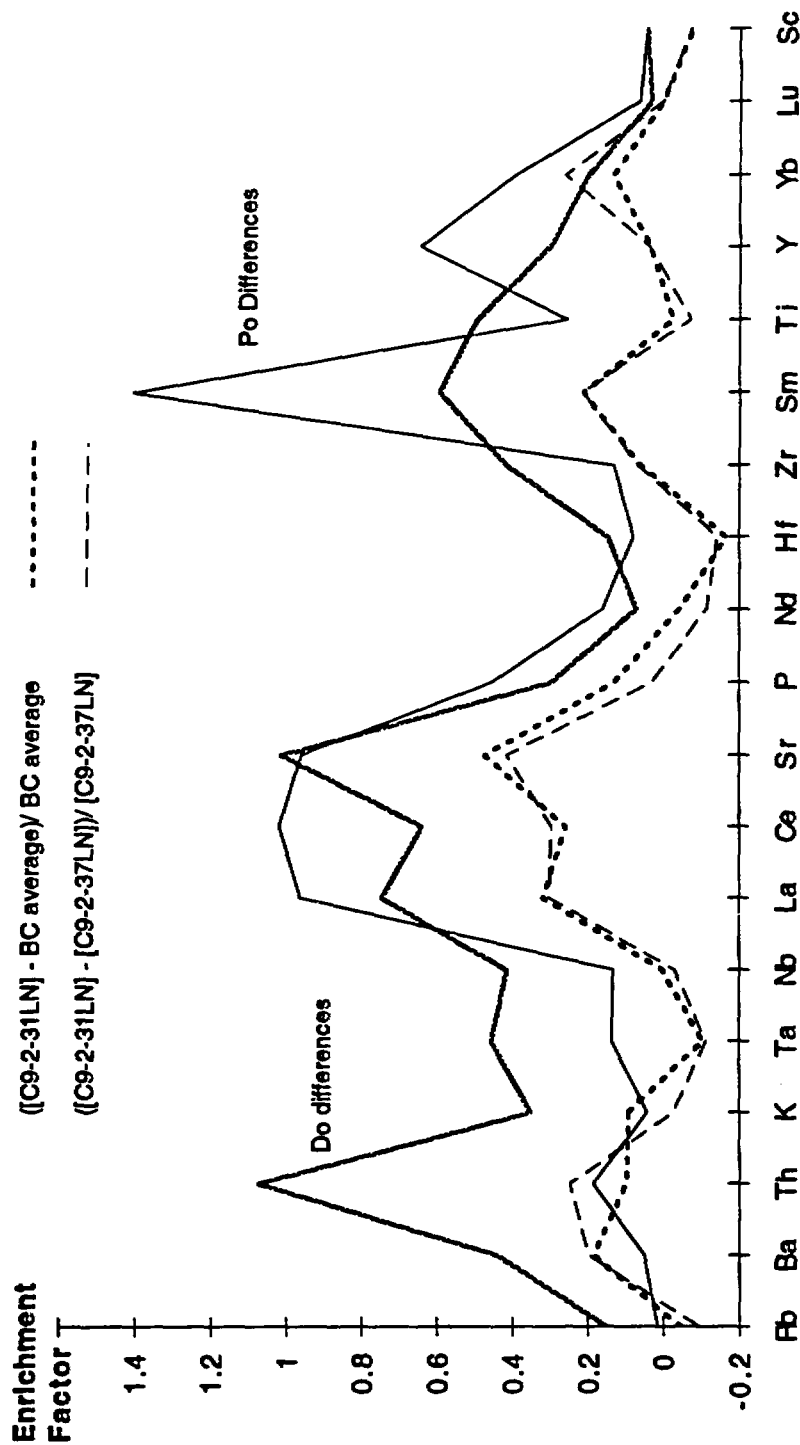


Figure 1. Samples are compared in the form: (Enriched-Depleted)/Depleted. Therefore high values represent greater enrichment factors between the two magma types (e.g., La being relatively more enriched than Hf, but not to the same extent as Sr). For ease of representation, the parameters derived from the models are compared in the format: (Depleted-Enriched)/Enriched. This is because LOWER bulk distribution coefficients will translate into higher trace element concentrations in the magma. Thus, if the data were presented in the same format as the samples the result would be a mirror image of the model lines shown. The D_o and P_o lines represent differences between a model having amphibole (4%) and phlogopite (2%) in the source, and one having only phlogopite (2%). Other details of source mineralogy and numerical results for these models are given in Table 2.

Distribution Coefficients (D-values)

	OL	OPX	CPX	GT	SP	AMPH	phlog
Rb	0.0001	0.001	0.05	0.01	0	0.25	3.1
Ba	0.0001	0.001	0.05	0.01	0	0.31	1.1
Th	0.001	0.01	0.01	0.02	0	0.3	0.31
K2O	0.007	0.015	0.03	0	0	0.6	2.7
Ta	0.001	0.15	0.07	0.1	0	0.8	1
Nb	0.001	0.15	0.1	0.1	0	0.8	1
La	0.0002	0.002	0.069	0.01	0	0.27	0.03
Ce	0.0005	0.003	0.098	0.021	0	0.34	0.03
Sr	0.001	0.01	0.1	0.01	0	0.57	0.08
P2O5	0.001	0.008	0.14	0.09	0	0.3	0.05
Nd	0.001	0.0065	0.18	0.08	0	0.19	0.03
Hf	0.001	0.04	0.31	0.3	0	0.5	0.6
Zr	0.001	0.03	0.1	0.3	0	0.5	0.6
Sm	0.0013	0.013	0.26	0.217	0	0.91	0.03
TiO2	0.02	0.1	0.3	0.3	0	1.5	0.9
Y	0.001	0.04	0.3	2	0.02	1	0.03
Yb	0.0015	0.049	0.28	4.1	0.007	0.97	0.03
Lu	0.001	0.11	0.8	10	0	0.89	0.04
Sc	0.17	1.1	2.7	4	0	3	2.5

Table 2. D-values and melting parameters used in the preparation of Figure 1.

Note:
D-values given in bold have been estimated or extrapolated

Melting Parameters

	OL	OPX	CPX	GT	SP	AMPH	phlog	
Phlogopite & amphibole	0.01	0.05	0.05	0.05	0	0.14	0.7	Proportions entering melt
('Depleted')	0.58	0.215	0.12	0.025	0	0.04	0.02	Source mineral modes

	OL	OPX	CPX	GT	SP	AMPH	phlog	
Phlogopite only	0.01	0.09	0.15	0.05	0	0	0.7	Proportions entering melt
('Enriched')	0.59	0.215	0.15	0.025	0	0	0.02	Source mineral modes

Bulk D values

	Phlogopite & amphibole		Phlogopite only		Model differences in bulk D values*		
	Do	Po	Do	Po	Do	Po	
Rb	0.0785	2.2081	0.0685	2.1781	Rb	0.14632	0.0138
Ba	0.0409	0.8165	0.0285	0.7781	Ba	0.43589	0.0493
Th	0.0226	0.261	0.0109	0.2204	Th	1.06856	0.1842
K2O	0.0889	1.9763	0.0659	1.8959	K	0.34971	0.0424
Ta	0.0957	0.828	0.0658	0.729	Ta	0.45398	0.1358
Nb	0.0993	0.8295	0.0703	0.7335	Nb	0.41214	0.1309
La	0.0205	0.0629	0.0117	0.032	La	0.74293	0.9622
Ce	0.0274	0.0747	0.0168	0.037	Ce	0.63555	1.0177
Sr	0.0394	0.1418	0.0196	0.0724	Sr	1.01021	0.9584
P2O5	0.0344	0.0889	0.0266	0.0612	P	0.2933	0.4521
Nd	0.0338	0.0609	0.0316	0.0526	Nd	0.06933	0.1586
Hf	0.0859	0.5225	0.0752	0.4851	Hf	0.14217	0.0771
Zr	0.0585	0.5115	0.0415	0.4527	Zr	0.409	0.1299
Sm	0.0772	0.1729	0.0486	0.072	Sm	0.58837	1.4005
TiO2	0.1546	0.8752	0.1038	0.6992	Ti	0.4894	0.2517
Y	0.1358	0.278	0.1048	0.1696	Y	0.29573	0.6391
Yb	0.1869	0.3783	0.1565	0.2724	Yb	0.19413	0.3885
Lu	0.4066	0.6981	0.395	0.6579	Lu	0.02934	0.0611
Sc	0.9291	2.5617	0.8918	2.4557	Sc	0.04183	0.0432

To model
'depleted' magma

To model
'enriched' magma

* (Depleted-Enriched)/Enriched

Overall, it seems that differences in D_0 values may be the strongest control on the differences observed between the enriched and depleted magma types. In terms of mineralogy this implies that amphibole in the source of the depleted magmas is the critical factor. For instance, the distribution coefficient for Sr in amphibole is 7-600 times greater than for other minerals that might be present in the mantle source. Thus even small amounts of amphibole will affect the distribution of Sr. The weaker correlation between P_0 and actual magmas may reflect the dominance of phlogopite contributions to the melt, whereas the D_0 values highlight the presence of some residual amphibole in the source during melting.

While this model may account for the trace element differences between the enriched and depleted magma types, there are problems concerning the isotope data. Such models would predict no significant differences for Pb and Nd isotopes, and at best a small difference in Sr isotope ratios. Magmas with high Sr contents would be expected to have slightly lower $^{87}\text{Sr}/^{86}\text{Sr}$ ratios as a result of the lower bulk Sr distribution coefficient for the phlogopite-only source: during melting, the magma is influenced by relatively unradiogenic Sr input from phases other than phlogopite. The observed pattern is the reverse of this (e.g., low $^{87}\text{Sr}/^{86}\text{Sr}$ ratios and low Sr ppm). However this can be rationalized if the source suffers a thermal 'event' some time before melting. Where a source contains both amphibole and phlogopite, some diffusion of in-grown (radiogenic) Sr from phlogopite to adjacent areas of amphibole may be possible. In such circumstances the resulting magmas might have lower Sr contents and lower $^{87}\text{Sr}/^{86}\text{Sr}$ than the melts from phlogopite only sources because of the residual amphibole effect. This melting scenario is outlined in Figure 2.

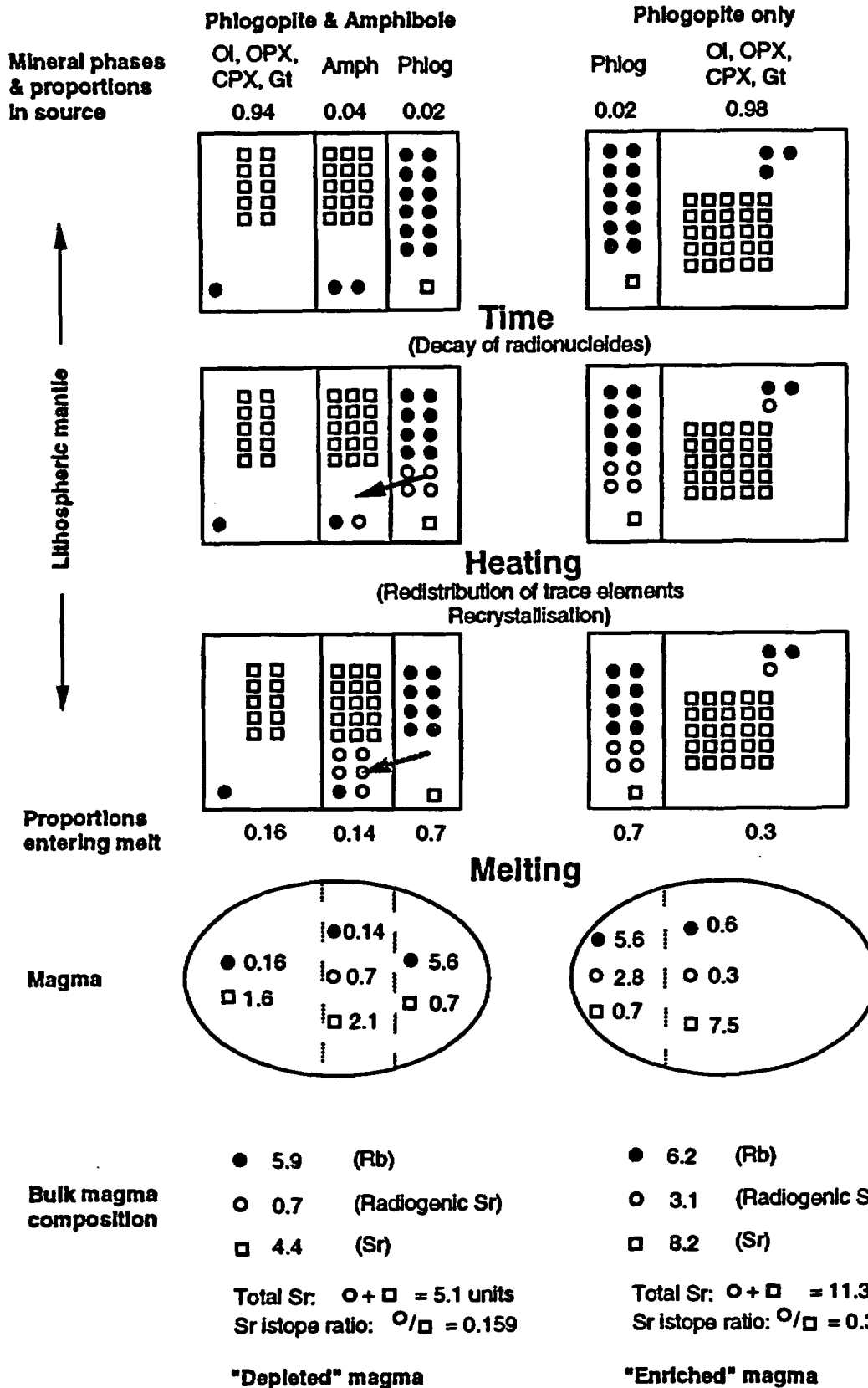
Such a thermal event could be equated with the previous episode of magmatism at 3.7Ma. However, even with this model it is impossible to account for the observed difference in ϵNd between the enriched and depleted magmas. This is because Sm and Nd distribution coefficients for phlogopite are similar and very low, and thus phlogopite would not represent a site of excess radiogenic Nd growth. An alternative model must therefore be sought to account for the isotopic differences.

Model 4- Crustal assimilation

The problem of crustal contamination was addressed briefly in Bradshaw and Smith (1993). It was thought unlikely that contamination with upper crustal material could generate the magma type differences observed at Crater Flat. Typically, upper crust has high $^{87}\text{Sr}/^{86}\text{Sr}$ and low ϵNd values combined with high Rb and very low Sr and LREE concentrations. Such compositions would not be suitable for generating the observed isotopic and trace element variations. Moreover, average

Initial trace element budget Rb ● Sr □
 Rb: 15 units Sr: 26 units Radiogenic Sr ○

Figure 2. Hypothetical model to produce trace element and Sr isotope differences between the 'enriched' and 'depleted' magmas at Crater Flat. Initial trace element budgets for each model are identical. Two model sources are compared. In addition to OL, OPX, CPX and GT: 1. has both amphibole and phlogopite, 2. has phlogopite only. Trace elements in these sources have been distributed according to standard D-values. Thus amphibole becomes a relative sink for Sr, and Rb is partitioned preferentially into phlogopite. While the lithospheric source is in a stable regime (perhaps from the Proterozoic to the early Cenozoic) radiogenic Sr is in-grown, due to the decay of ⁸⁷Rb. During a subsequent heating event, some trace elements are redistributed. This has little or no effect on the phlogopite-only source. However, if amphibole is present, radiogenic Sr in phlogopite may diffuse into adjacent areas of amphibole where it is more compatible. When small degrees of partial melting occur in the Quaternary, phlogopite is the dominant early melting phase, and some amphibole is residual, thus the sources produce two different magmas with distinctive trace element and Sr isotope characteristics. NOTE: Initial Rb/Sr ratio used here is approximately 20 times that of primitive mantle.



upper crustal material has high silica contents (60-62 wt% SiO₂), and thus some consistent variation of major element compositions in contaminated basaltic magmas would be expected.

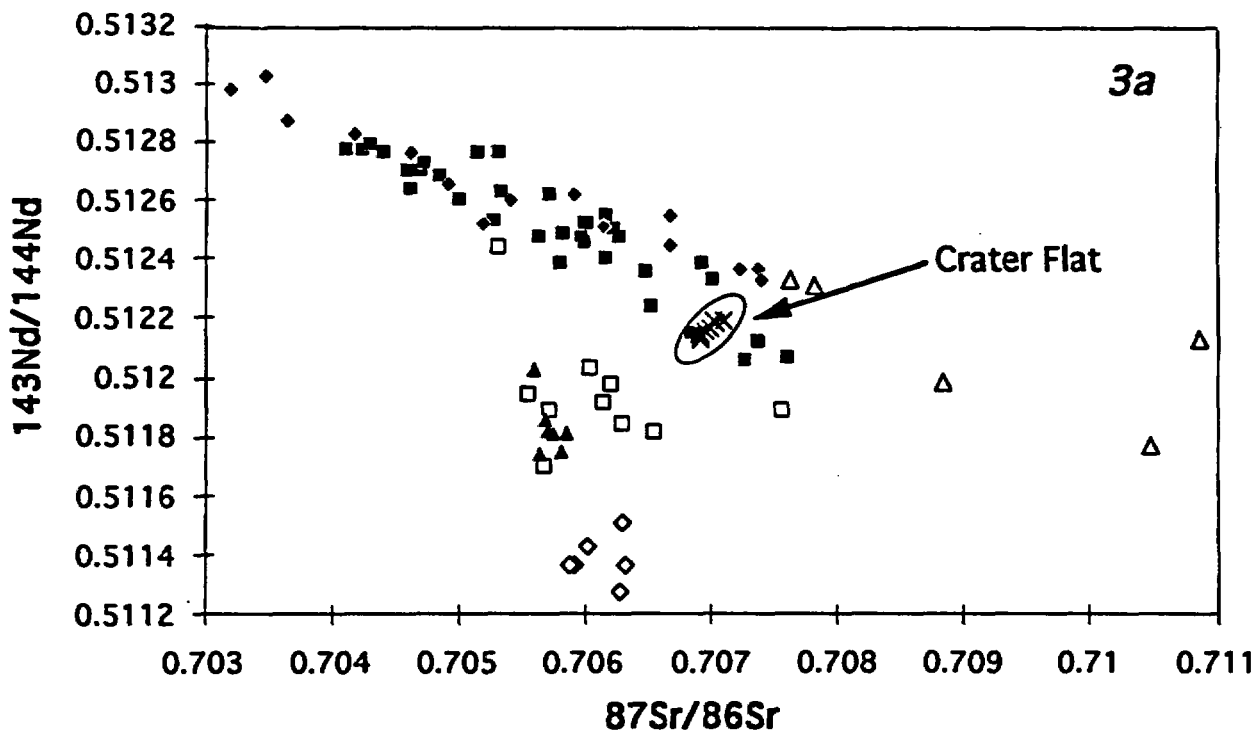
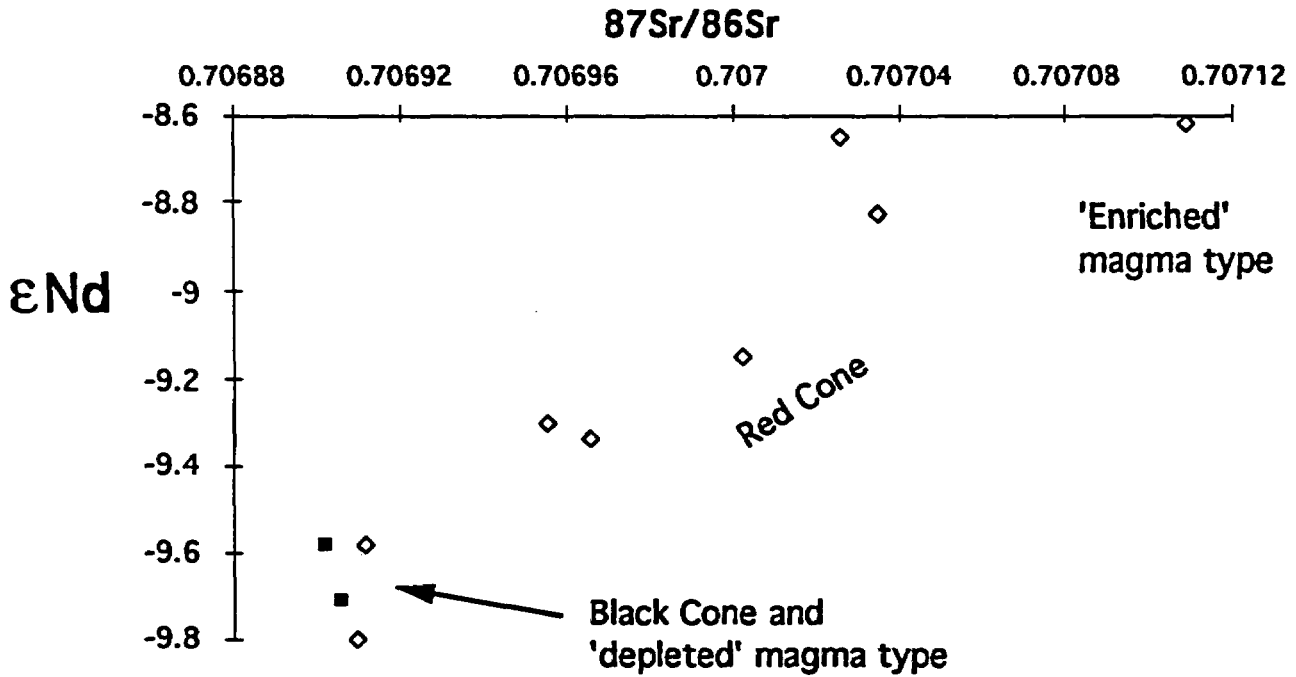
However, contamination with lower crustal material is a more likely prospect. Normative mineral modelling (Bradshaw and Smith, 1993) indicates that the magmas last equilibrated at pressures of around 8kb (~24km depth) before eruption, which would correspond to the base of the lower crust. It is probable that the magmas stalled at this crustal density barrier and fractionated olivine before attaining sufficient buoyancy to rise further. Thus it is possible that the magmas assimilated some fraction of the lower crust at the same time.

The average lower crustal composition is estimated to be around 54.4 wt% SiO₂ (Taylor and McClennan, 1985) with generally low trace element concentrations. In addition, the lower crust is expected to host a large proportion of basaltic intrusions in the form of sills, dykes and relict magma chambers. Evidence of lower crustal material of this type existing in the western USA has been indicated by studies of xenolith suites, most recently on the Colorado Plateau (Wendlandt et al., 1993). Some of these xenoliths, in particular a suite of garnet amphibolites, have moderate trace element concentrations (e.g., 600 ppm Sr, 20 ppm Nd) and both low ⁸⁷Sr/⁸⁶Sr ratios and εNd values. These xenoliths also have major element compositions (e.g., 48 wt% SiO₂, 4 wt% MgO and 11 wt% Fe₂O₃) that are rather close to that of the average Crater Flat basalt. Assimilating such material would therefore have a minimal effect on the overall basalt compositions, but might produce a significant range in some trace element abundances and isotope ratios. These effects are considered below and are illustrated in Figures 4-5.

The Sr and Nd isotope characteristics of basalts from Crater Flat are rather unusual: samples define a POSITIVE array on a plot of ⁸⁷Sr/⁸⁶Sr vs. εNd (Figure 3). The isotope systematics of Sr and Nd should lead to the generation of a negative array, and this is probably one of the first recorded cases of a positive trend. However, we are confident about the reliability of the data, and it is encouraging to note that the samples do fall within the general isotopic field for basalts in the western United States (Figure 3a). Furthermore, the isotope ratios display a consistent correlation with many of the trace elements (e.g., samples with low ⁸⁷Sr/⁸⁶Sr have low Sr, La, Ce, etc.). These correlations would be consistent with the premiss of magma mixing (Bradshaw and Smith, 1993), and the spread of data on Figure 3 is likely to represent a mixing array. However, this would imply that two isotopically distinct sources are required to generate the 'depleted' (⁸⁷Sr/⁸⁶Sr = 0.70691, εNd = -9.6) and 'enriched' (⁸⁷Sr/⁸⁶Sr = 0.7071, εNd = -8.6) magma types. An alternative possibility is that the isotope difference is the result of lower crustal contamination, and a suitable contaminant has been outlined above.

Figure 3. Sr and Nd isotope data for samples from Crater Flat.

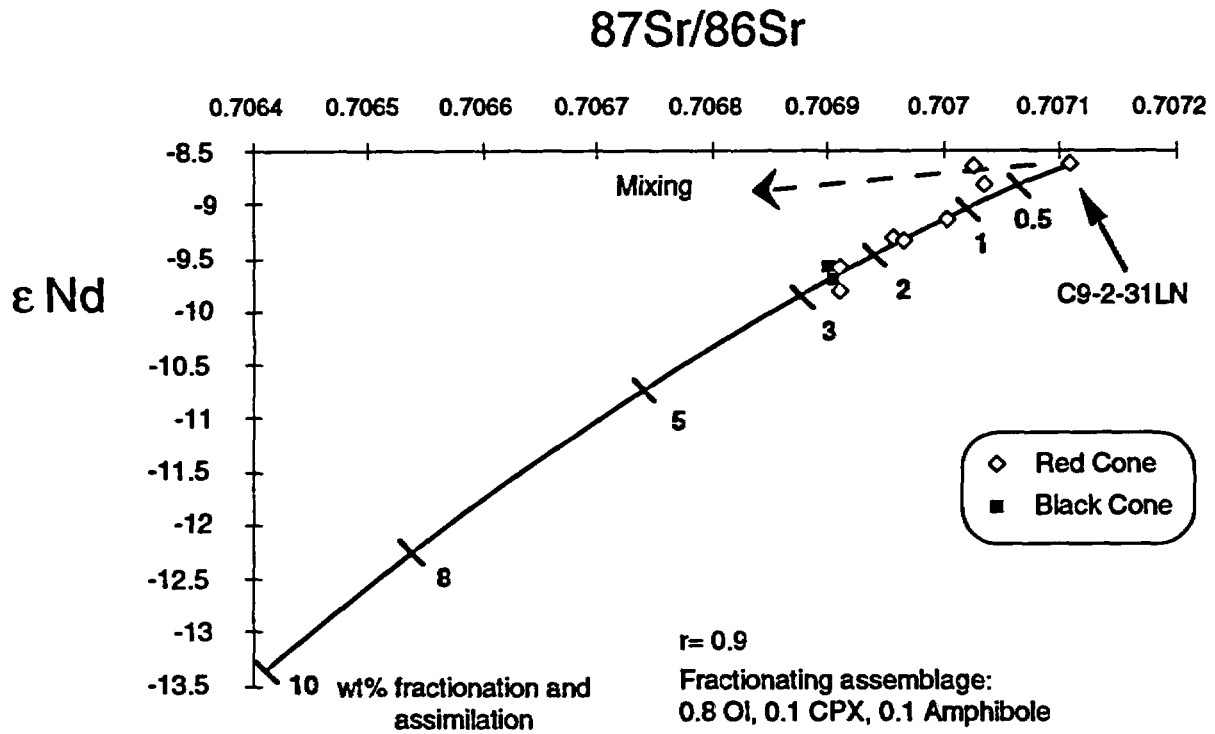
3a. Comparison of Crater Flat data to samples from other volcanic fields in the western United States. Note that the Crater Flat samples fall within the trend defined by other basalts from the southern Great Basin.



Key to Figure 3a:

- ◆ Northern Great Basin
- Crazy Mts.
- ◇ Smokey Buttes
- Southern Great Basin
- ▲ Leucite Hills
- △ Saddle Mts.

Figure 4. An AFC model to reproduce the Sr and Nd isotopic variation displayed by samples from Crater Flat



Initial basaltic magma: C9-2-31LN
Assimilant: 86MR33 gt amphibolite

C9-2-31LN: 1848 ppm Sr, 96.18 ppm Nd, $\epsilon\text{Nd} = -8.62$, $^{87}\text{Sr}/^{86}\text{Sr} = 0.707109$

86MR33: 629.6 ppm Sr, 22.17 ppm Nd, $\epsilon\text{Nd} = -9.09$, $^{87}\text{Sr}/^{86}\text{Sr} = 0.70418$

A model for lower crustal contamination is displayed in Figure 4. Simple mixing between the Crater Flat magmas and the lower crustal contaminant (garnet amphibolite 86MR33, Wendlandt et al., 1993) would produce a nearly flat trend on Figure 4, because of the similarity in Nd isotope ratios. However, a combined assimilation fractional crystallization (AFC) model is thought to be more appropriate. The compatible element budget (e.g., Cr, Ni, Sc, etc.) of the Crater Flat magmas indicates that fractionation of olivine (\pm CPX, \pm amphibole) has occurred, and thus the AFC model can be used to accommodate this stage of magma evolution. An 'r' value (ratio of mass assimilated to mass crystallized) of 0.9 is used for the model. This rather high value is considered appropriate because it is thought that the lower crust would have been at a fairly high temperature before the Quaternary magmas were intruded, as a result of previous Cenozoic activity in the area. Thus, little extra heat input would have been required to initiate melting and then assimilation. The dynamics of the AFC model make it possible to generate significantly larger isotope variations than with simple mixing and hence reproduce the the observed range of ratios. Notice that only very small amounts of lower crustal contamination are actually required (<3 wt%), and that the 'enriched' magma is used as the basaltic endmember.

Unfortunately the trace element consequences of this AFC model are quite severe because of the effect of olivine fractionation. The result is a large increase in incompatible element concentrations, projecting the model away from the 'depleted' magma composition (Figure 5). This would appear to rule-out theories of crustal contamination of the 'enriched' magma type. However, it can be observed from Figure 5 that the Black Cone ('depleted') magmas display a small range in trace element compositions that are 'orientated' in the general direction of these AFC model lines. The range of this variation is about equivalent to a 3-5% shift due to AFC processes. In fact it is possible to overlay the model lines on and through the Black Cone data, with an origin on the samples with the lowest incompatible element concentrations (samples from the crater lake). This works for virtually all the trace and minor elements. The amount of assimilation to reproduce the trace element variations is approximately equivalent to that initially calculated to account for the isotopic differences between the enriched and depleted magma types. This is very significant and suggests that the magmas from Black Cone have indeed assimilated lower crustal material.

The apparent discrepancy with the isotope vs. trace element modelling is easily reconciled if the uncontaminated 'depleted' magma has essentially the same isotopic signature as the 'enriched' magma type. Thus the isotope array on Figure 4 is a product of mixing, and it is somewhat fortuitous that it coincides with the AFC trend. On Figure 5c the uncontaminated 'depleted' magma would plot at low Sr ppm and similar ϵ Nd to the 'enriched' magma, AFC processes shift the

Figure 5. Trace element effects of the AFC model proposed to account for isotopic differences between enriched and depleted magma types. AFC model lines are generated from Red Cone sample C9-2-31LN.

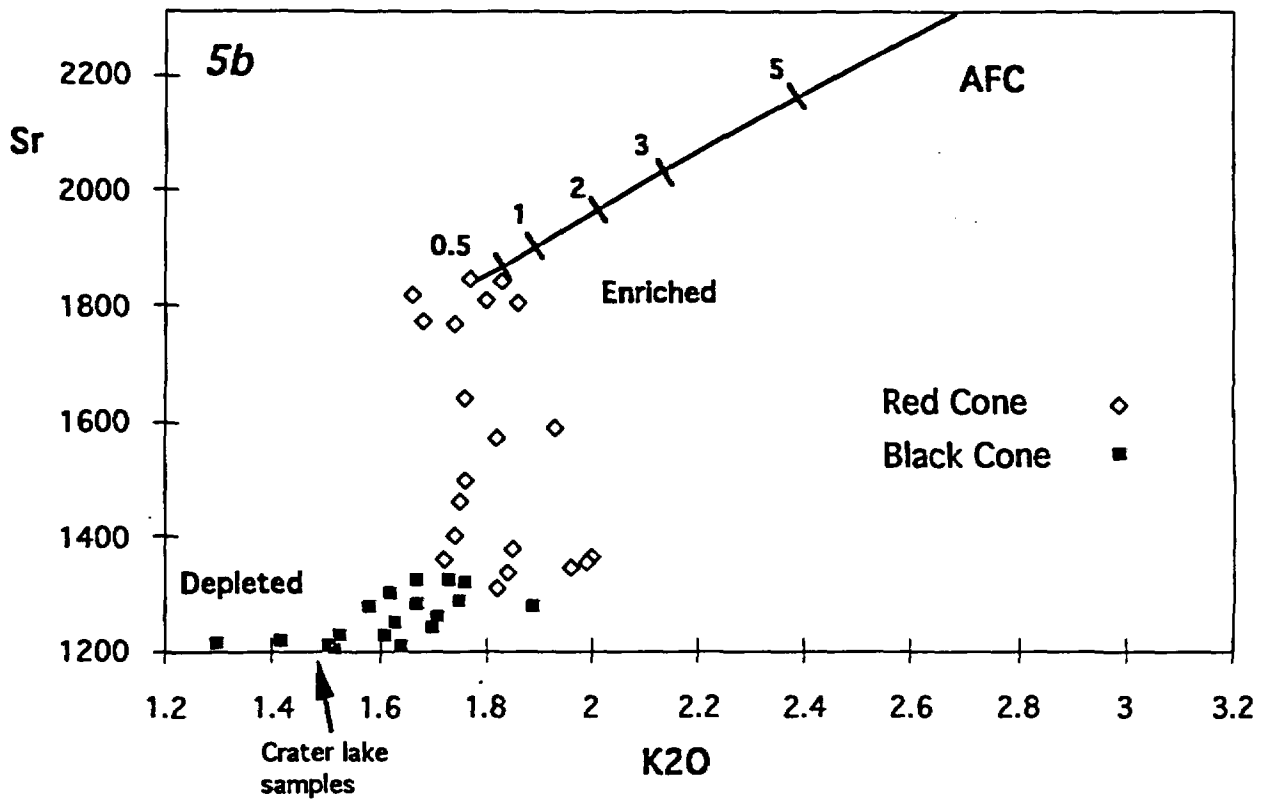
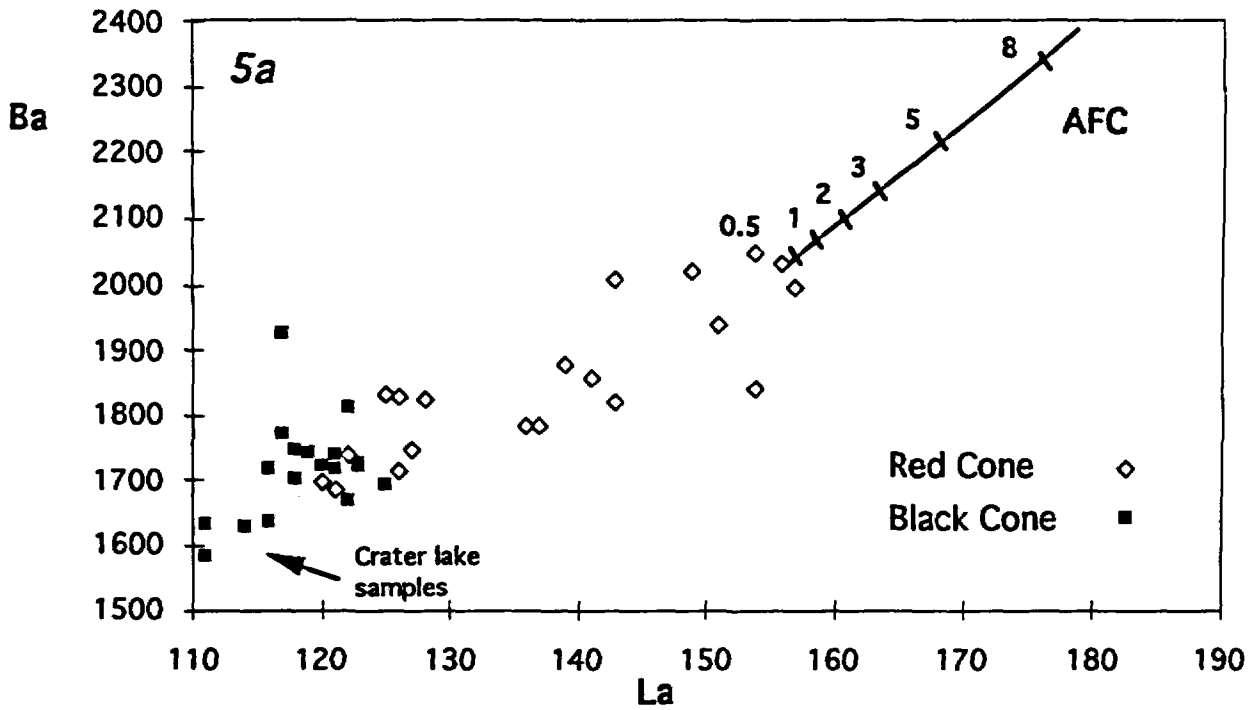
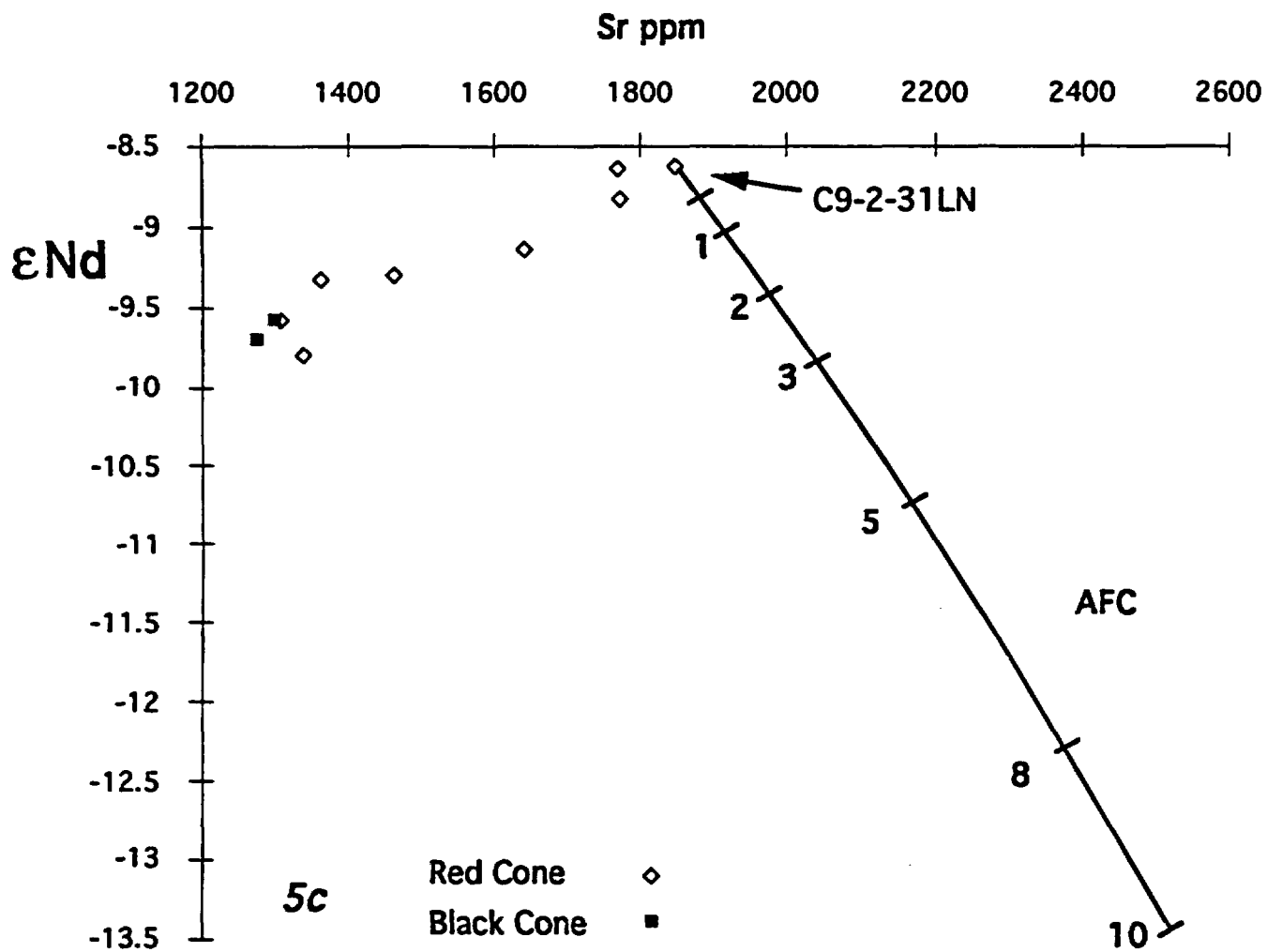


Figure 5. Continued. 5c: Trace element vs. isotope variation diagram for the AFC models depicted in previous figures. It is clear that the Black Cone (depleted) magma type can not be generated by an AFC model involving a lower crustal contaminant and the enriched magma type.



composition to that of the two Black Cone samples, and then mixing occurs with the 'enriched' magma to produce the Red Cone array.

It is interesting to note that the 'depleted' magma type is modelled to be the most contaminated magma. This magma was erupted predominantly at Black Cone and in the early stages of activity at Red Cone. Furthermore, at Black Cone, the youngest samples (all from within or around the crater lake) appear to be the least contaminated of these lavas. These observations are consistent with the crustal contamination hypothesis because it is expected that the earliest magmas would have to create conduits through the crust for continued magma transport. Thus the early magmas directly interact with the crust, whereas later magmas may pass through developed conduits and could avoid contamination enroute to the surface. Also, these depleted magmas are thought to have been derived from a source containing 6 wt% hydrous minerals (amphibole and phlogopite), it is not surprising that magmas were generated from this source earlier than the phlogopite-only source.

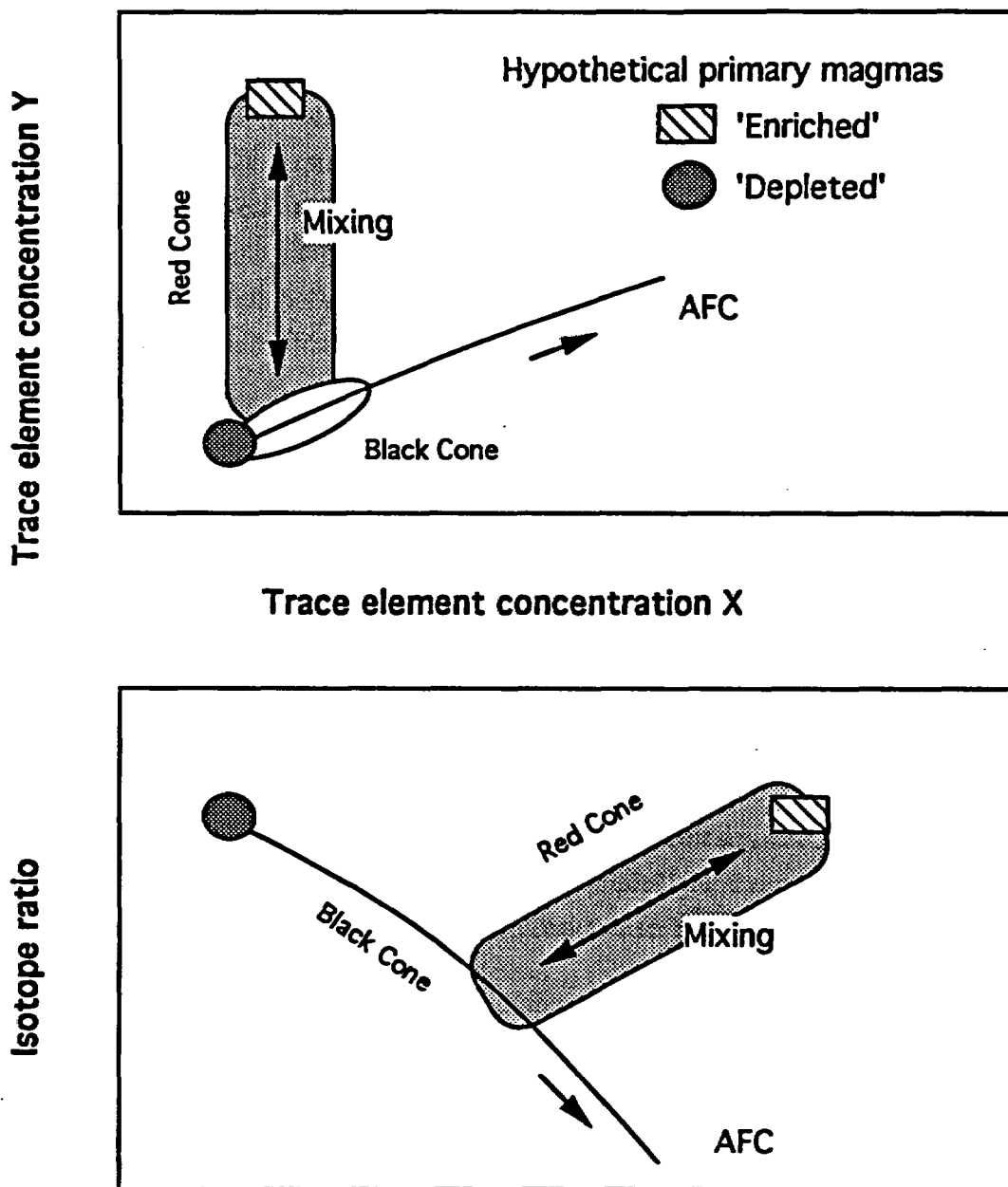
As outlined above, this model of lower crustal contamination can be used to reproduce the isotopic differences between the 'enriched' and 'depleted' magmas, and also the scatter of trace element data displayed by the latter. This model may be combined with Model 3 (mineralogical variations in the source) to produce the whole range of geochemical variation observed at Black Cone and Red Cone. Based on this hypothesis, a summary diagram depicting the trace element and isotopic variations of these magmas is presented in Figure 6. This is our favoured model for the origin of different magma types at Crater Flat, however an additional hypothesis is considered below.

Model 5- Unique source compositions

This model is still being tested. However four scenarios are under consideration: silicate melt enrichment of the source, H₂O fluid metasomatism, CO₂ metasomatism, and direct contamination of the source (perhaps by sediment derived from the subducting Farallon Plate).

Silicate melt enrichment in the source would appear to be unlikely because of the lack of HFSE and compatible element variability. Similarly, H₂O-rich fluid metasomatism would preferentially cause enrichment in the Large Ion Lithophile elements and not the REE. In addition, positive correlations between ⁸⁷Sr/⁸⁶Sr, Sr and the REE, and minimal variation in Pb isotopes argues against contamination of the source by oceanic sediment input. Instead, the pattern of enrichment is more consistent with fluxing of the source by CO₂-rich vapours. Such vapours may mobilize Sr and the light REE while having little effect on the concentration of other elements. This process will be the topic of future research, and the IAVCEI meeting in Canberra will be an excellent opportunity to discuss these models.

Figure 6. A schematic geochemical model for isotope and trace element variations observed at Crater Flat. Enriched and depleted primary magmas have similar sources in the lithospheric mantle. However, trace element compositions differ because of the effect of source mineralogy during melting. Early, depleted, magmas are contaminated with lower crustal material by an AFC process. These contaminated magmas subsequently mix with the enriched magma type (which displays little or no evidence of contamination) to produce the array of compositions observed at Red Cone.



Section 4

Publication in Earth and Planetary Science Letters

The following paper was published in the international geochemistry journal Earth and Planetary Science Letters in February 1993:

Basaltic Volcanism in the Southern Basin and Range: no role for a mantle plume.

T.K. Bradshaw, C.J. Hawkesworth, and K. Gallagher

EPSL, 116 (1993) 45-62.

This paper discusses in detail the geochemistry of Miocene to Quaternary basaltic volcanism in the Colorado River Trough (CRT) region of Nevada, Arizona and California (between Parker Dam and Las Vegas, along the Colorado River). The geochemistry of these magmas is broadly similar to those at Crater Flat. Volcanism in both areas is thought to have been dominated by melting of trace element enriched lithospheric mantle. However, magmas in the CRT apparently record greater degrees of partial melting (on average 1.5 - 5% melting, although some post-extensional magmas may be the result of up to 15% melting), whereas magmas at Crater Flat are thought to correspond to <2% partial melting of a similar source composition.

The main conclusion of this paper is that the Miocene to Recent magmatism is unlikely to have been influenced by the emplacement of a mantle plume beneath the area. Rather, lithospheric extension and/or passive replacement of asthenosphere (following the northward passage of the edge of the subducted Farallon Plate) is likely to have triggered volcanism.

Possible implications for the Yucca Mountain region:

1. The rapid waning of volcanism approximately 5-10Ma after the passage of the Farallon Plate edge in the CRT suggests that a further MAJOR episode of volcanic activity RELATED TO THE SAME TECTONIC PROCESSES is unlikely in the southern Nevada region in the near future.
2. HOWEVER: current research (e.g., this work and Smith et al. 1993) suggests that the region between the Timber Mountain Caldera (/Crater Flat) and Lake Mead is still underlain by relatively fertile lithospheric mantle. It is expected that this mantle is similarly trace element enriched to that previously beneath the CRT, and that it is hydrous (perhaps veined with phlogopite and/or amphibole). Thus, under the appropriate conditions (e.g., major extension and/or additional thermal input from the asthenosphere) this mantle could potentially constitute a significant source for further magma generation.

[UC]

Basaltic volcanism in the Southern Basin and Range: no role for a mantle plume

T.K. Bradshaw^{a,1}, C.J. Hawkesworth^a and K. Gallagher^{a,b}

^a Department of Earth Sciences, The Open University, Walton Hall, Milton Keynes, MK7 6AA, UK

^b Department of Geological Sciences, University College, Gower Street, London, WC1E 6BT, UK

Received August 24, 1992; revision accepted February 19, 1993

ABSTRACT

The Colorado River Trough (CRT), in the Southern Basin and Range, is a corridor of high extension (> 100%) associated with basaltic volcanism that took place during the Miocene. Two main geochemical groups of basalts are recognised: Group 1 has high Nb/La and Nb/Y, smooth patterns on mantle-normalised multi-element diagrams, and Sr and Pb isotope ratios similar to those in oceanic basalts. These are small volume post-extensional flows and they are thought to have been derived from the asthenospheric upper mantle. The bulk of the CRT basalts (> 95% by volume) fall into Group 2. These basalts have low Nb/La, low HREE contents, irregular minor and trace element patterns, low ¹⁴³Nd/¹⁴⁴Nd and elevated Sr and Pb isotope ratios. Such features suggest that these basalts were derived from the subcontinental lithospheric mantle and within Group 2 large variations in Ce/Yb, Nb/Y and Th/Zr can be modeled by an increase in the degree of partial melting with time as extension reaches its maximum.

Most of the basalts in the CRT were derived from the continental mantle lithosphere, although there was a change from lithosphere- to asthenosphere-derived magmatism following the main period of extension. Model calculations indicate that at 100% extension, and in the presence of small amounts of H₂O and CO₂, partial melting takes place in the mantle lithosphere without any increase in the mantle potential temperature (T_p). Moreover, the presence of elevated T_p values would result in much greater proportions of asthenosphere to lithosphere derived melts than those observed, and much greater eruption rates than those estimated for the CRT. It is concluded that the chemical changes with time in the basalts of the CRT, the eruption rates, and inferred T_p indicate that Miocene magmatism in the Southern Basin and Range was triggered by lithospheric extension, and not by the emplacement of a mantle plume.

1. Introduction

The role of mantle plumes in the generation of continental basalts, and as a possible cause of continental extension, remains highly controversial. In some models, deep-seated mantle plumes initiate partial melting and, at least in some areas, continental breakup [1]. In other models, however, the role of the plume is passive and continental magmatism is attributed to extension over areas of anomalously hot mantle [2]. The Deccan and Paraná flood basalt provinces respec-

tively may represent end-member examples of such models. At issue here are the geological and geochemical data within magmatic provinces that constrain models for the causes of magmatism, and in particular the role of mantle plumes. Geochemical data can be used to identify material from the continental mantle lithosphere and from the underlying asthenosphere. However, on geochemistry alone it is difficult to distinguish magmas generated in a mantle plume from those generated in the uppermost asthenosphere in response to continental extension [3]. Rather, the key difference between plume-related and other asthenosphere-derived magmas, for a given amount of extension, should be in the temperature of the upper mantle, and hence in the volumes of magma generated [4,5].

¹ Present address: Department of Geosciences, University of Nevada, 4505 Maryland Parkway, Las Vegas, NV 89154-4010, USA.

TABLE 1
Representative analyses from the Colorado River Trough. (For full caption, see p. 48.)

Sample:	Group 2 (Lake Havasu City)									(post extensional)	
	C-2	H-1	H-2	MH-1	MO-1	MO-2	MO-5	MO-6	MO-7	BW-4	MH-9
Longitude:	-114.3493	-114.2504	-114.2543	-114.3117	-114.3107	-114.3109	-114.3117	-114.3118	-114.3135	-114.0755	-114.2511
Latitude:	34.6137	34.4248	34.4253	34.6807	34.6833	34.683	34.6821	34.682	34.6847	34.5105	34.4857
SiO ₂	55.41	45.40	49.26	46.03	48.46	52.92	50.87	53.62	54.41	51.58	53.70
TiO ₂	1.38	1.74	1.21	1.80	1.74	1.17	1.51	1.31	1.33	1.25	1.28
Al ₂ O ₃	15.23	16.37	15.73	13.34	12.83	13.68	16.06	16.20	16.18	15.23	15.54
Fe ₂ O ₃	7.21	10.83	9.86	11.13	9.11	7.34	9.55	8.24	7.38	11.40	8.42
MnO	0.10	0.17	0.11	0.14	0.13	0.07	0.10	0.13	0.08	0.16	0.12
MgO	4.23	5.57	7.34	10.24	8.03	7.52	5.93	5.16	4.58	6.50	6.61
CaO	6.48	11.21	9.72	11.48	10.69	7.07	8.36	8.33	6.40	8.71	8.63
Na ₂ O	3.02	3.40	2.90	1.62	2.50	2.60	4.15	3.89	2.96	3.14	3.52
K ₂ O	3.70	1.49	1.06	1.14	2.79	3.81	1.64	1.72	4.66	0.93	1.73
P ₂ O ₅	0.63	1.05	0.34	0.75	0.99	0.41	0.47	0.41	0.55	0.26	0.39
Ba	1161	1114	552	959	1858	1489	899	984	1466	1009	693
Co	25.1	36.6	42.1	28.3	35.7	30.1	33.8	29.4	24.4	45.6	38
Cr	145	20	321	176	370	328	300	176	175	475	216
Hf	10.93	5.54	3.32	5.18	6.96	5.23	4.53	5.26	7.39	2.91	
Nb	37	33	8	18	28	13	19	19	24	8	16
Ni	88	45	171	79	133	214	158	67	100	105	119
Pb	32	14	13	10	21	16	7	11	23	10	14
Rb	152	37	19	33	51	124	33	28	155	11	37
Sc	16.7	20.4	29.5	19.7	28.2	19.5	23.4	21.1	19.1	25.0	
Sr	933	1250	639	823	1224	757	823	874	807	335	603
Ta	2.03	1.74	0.51	1.07	1.39	0.77	1.02	0.93	1.37	0.52	
Th	24.9	9.57	3.76	5.88	10.4	8.55	5.26	5.79	14.0	1.81	9.00
Y	35	33	24	26	30	21	27	28	31	22	25
Zr	474	258	142	242	307	227	207	230	327	121	205
La	104.9	82.3	27.3	46.4	103.3	58.6	48.8	50.8	73.2	15.3	8
Ce	195	181	57.5	97.3	202	112	89.4	96.2	134	31.3	71
Nd	85.1	94.1	33.4	46.1	102.1	52.2	40.6	43.1	60.8	16.1	40
Sm	13.41	16.05		8.30	18.18	9.18	7.58	7.75	10.63	3.80	
Eu	2.65	4.06	1.70	2.10	4.10	2.10	2.01	2.01	2.45	1.25	
Tb	1.17	1.56	0.80	0.96	1.39	0.76	0.80	0.81	1.12	0.70	
Yb	2.60	2.62	2.10	2.28	1.91	1.60	2.01	2.09	2.35	2.15	
Lu	0.43	0.39	0.35	0.33	0.34	0.28	0.35	0.35	0.36	0.32	
⁸⁷ Sr/ ⁸⁶ Sr	0.70885	0.70733	0.70777	0.70836	0.70827	0.70901	0.70781	0.70833	0.70908	0.70660	0.70796
(⁸⁷ Sr/ ⁸⁶ Sr) _i	0.70871	0.70731	0.70769	0.70833	0.70824	0.70887	0.70777	0.70831	0.70904	0.70659	0.70794
¹⁴³ Nd/ ¹⁴⁴ Nd		0.51252		0.51225	0.51233		0.51235	0.51226		0.51242	
²⁰⁶ Pb/ ²⁰⁴ Pb		18.897	18.839	18.344	18.604		18.444	18.375		17.233	18.51
²⁰⁷ Pb/ ²⁰⁴ Pb		15.623	15.636	15.561	15.595		15.6	15.581		15.471	15.586
²⁰⁸ Pb/ ²⁰⁴ Pb		39.024	39.005	38.803	38.807		38.936	38.779		37.351	39.057
Time (Ma)	21.5	21.5	20	20.5	21	20.9	20.5	20.5	21.1	10	10.6

TABLE 1 (continued)

	Group 2 (post extensional)					Group 2a (Lake Havasu City)			Group 1 (post-extensional)		
Sample:	MH-10	SL-6	D-3	BM-1	K-6	H-11	H-5	H-9	K-5	M-1	BW-6
Longitude:	-114.2511	-114.8029	-114.7649	-114.4468	-114.266	-114.304	-114.2945	-114.3059	-114.1582	-114.6051	-114.1113
Latitude:	34.4857	35.3802	34.9106	34.8541	35.4261	34.4457	34.4511	34.4447	35.7162	35.8691	34.2844
SiO ₂	53.54	55.94	55.15	51.14	55.98	46.10	46.50	46.09	50.06	45.87	48.30
TiO ₂	1.27	1.75	1.15	1.31	1.21	1.35	1.36	1.26	1.56	1.81	2.99
Al ₂ O ₃	15.32	16.49	16.17	16.73	15.49	16.50	16.28	16.31	15.49	15.33	16.56
Fe ₂ O ₃	8.36	7.96	8.82	9.62	7.22	11.76	11.28	11.40	11.40	12.09	12.07
MnO	0.13	0.10	0.14	0.15	0.11	0.19	0.18	0.17	0.16	0.18	0.19
MgO	6.44	2.18	4.79	6.80	5.03	8.20	8.46	7.94	6.53	8.40	4.06
CaO	8.33	6.34	7.69	10.00	6.95	8.74	8.73	9.44	9.29	10.93	7.59
Na ₂ O	3.06	4.53	3.34	3.42	3.55	3.31	4.28	2.81	3.35	3.11	3.97
K ₂ O	1.76	3.26	1.92	0.91	3.14	0.57	0.51	1.17	1.15	0.91	2.15
P ₂ O ₅	0.38	0.70	0.17	0.22	0.47	0.29	0.16	0.18	0.32	0.52	0.75
Ba	680	1376	443	2853	1390	272	308	181	540	417	456
Co	34.0	25	31.4	36.7	32	44.9	45.6	46.4	41.9	45	27.9
Cr	266	15	166	218	144	177	148	146	262	327	5
Hf	4.61		3.68	3.87		3.41	3.21	3.26	3.29	3.35	7.46
Nb	15	30	9	10	17	6	3	5	20	30	59
Ni	119	19	101	91	102	132	140	142	100	136	1
Pb	14	18	14	10	18	5	7	8	2	6	8
Rb	39	71	49	18	58	21	19	100	17	11	36
Sc	25.4		22.8	34.0		40.4	38.2	38.2	26.1	32.9	15.6
Sr	602	874	366	552	949	393	353	466	436	495	749
Ta	0.97		0.63	0.62		0.3	0.22	0.19	1.14	1.63	3.63
Th	5.87	11.0	5.0	3.87	14.0	1.74	1.14	1.16	2.56	3.51	4.72
Y	25	30	30	30	25	37	34	35	23	26	37
Zr	204	309	152	167	310	158	145	143	144	150	329
La	37.8	60	22.2	23.3	69	17.8	13.8	13.7	22.5	25.6	46.6
Ce	76.8	139	48	50.6	148	36.6	28.4	26.8	46.5	54.2	90.9
Nd	35.7	63	23.1	23.3	54	20.2	18.5	17.4	22.7	27.0	46.7
Sm	6.66		5.04	5.22		5	4.37	4.05	4.85	5.19	9.48
Eu	1.85		1.24	1.5		1.45	1.37	1.3	1.46	1.57	2.91
Tb	0.92		0.83	0.77		0.84	0.79	0.74	0.72	0.76	1.18
Yb	2.29		2.65	2.91		3.1	2.89	2.72	2.09	2.18	2.44
Lu	0.37		0.38	0.44		0.51	0.51	0.51	0.32	0.31	0.4
⁸⁷ Sr/ ⁸⁶ Sr	0.70766	0.70923	0.70732		0.70881	0.70980	0.70935	0.70893	0.70571	0.70487	0.70477
(⁸⁷ Sr/ ⁸⁶ Sr) _i	0.70765	0.70920	0.70727		0.70879	0.70971	0.70931	0.70889	0.70569	0.70486	0.70475
¹⁴³ Nd/ ¹⁴⁴ Nd			0.51227						0.51246	0.51273	0.51292
²⁰⁶ Pb/ ²⁰⁴ Pb	18.533	18.185	17.413	18.332	18.258	18.385	18.429	18.404		18.589	18.969
²⁰⁷ Pb/ ²⁰⁴ Pb	15.618	15.548	15.487	15.606	15.554	15.586	15.645	15.59		15.579	15.565
²⁰⁸ Pb/ ²⁰⁴ Pb	39.155	38.906	38.12	39.19	38.831	39.028	39.159	39.004		38.634	38.85
Time (Ma)	10.6	10	12.2	10		14.2	14.7	14	10	5.8	5

This contribution presents new geochemical and isotope data for igneous rocks associated with extension in the southern Basin and Range, and combines geochemical criteria for the recognition of asthenosphere- and lithosphere-derived magmas with estimates of eruption rates. With such data it is possible to evaluate likely potential temperatures in the uppermost mantle, and whether they are consistent with the presence of a mantle plume. The first step is to determine the volumes of magma generated from asthenospheric and lithospheric source regions, and the second is to evaluate the extent to which the change in source regions with time can be used to determine whether magmatism was initiated by continental extension, or the arrival of a mantle plume.

The regional controversy is whether the occurrence of late-stage basaltic magmas, with trace element and isotopic signatures similar to those of OIBs across much of the Basin and Range, should be taken as evidence for a 'southern mantle plume' beneath the western USA. Such a plume would be different from that presently beneath Yellowstone [6]; and it has been argued that it is centred beneath the Rio Grande Rift [7], and it may have been responsible for initiating magmatism and extension throughout the Basin and Range. However, this model requires two mantle plumes in the comparatively small area of the western USA. Moreover, it must be reconciled with the evidence from the southern Basin and Range that changes in magma chemistry [8], and perhaps the onset of magmatism [9], may be linked to changes in the regional tectonic setting, and in particular to the development of a slab

window at the cessation of subduction along the San Andreas transform system.

2. Local geology and general geochemistry

The Colorado River Trough (CRT) is a corridor of high extension south of Las Vegas, Nevada (Fig. 1). From approximately 22 to 9 Ma the lithosphere in this area extended in a roughly NE-SW direction by at least 100% (β factor = 2), although locally crustal extension may have reached as much as 250–450% [9–12]. The focus of both extension and magmatism was diachronous along the CRT and spread from south to north during this period. The samples considered here are alkaline or slightly subalkaline basalts, trachybasalts and basaltic andesites; they all have ≤ 56 wt% SiO_2 and for ease of presentation they are here termed simply basalts (Table 1). In the CRT as a whole, trachyandesite is volumetrically the dominant magma type. Flows are invariably vesicular and/or brecciated and some contain primary hydrous phases. Transition metal abundances (e.g. Sc, Co, Cr and Ni) and petrographic evidence indicate that all of the ≤ 56 wt% SiO_2 samples have experienced at least some olivine and/or pyroxene fractionation, although probably no significant plagioclase fractionation [11]. This obviously limits the effectiveness of some geochemical modelling, but only the least fractionated samples are used in the calculations outlined below.

Two distinct geochemical groups can be identified within the basaltic rocks of the CRT as illustrated on mantle-normalised diagrams (Figs. 2 and 3). The trace element abundances of individual basalts are highly variable, but most have

Caption to Table 1

Representative analyses of samples from the Colorado River Trough. REE, Co, Cr, Hf, Sc, Ta and Th were determined by INAA, and it is noted that Lu concentrations may be slightly high. Major elements were determined using a Link Systems Meca 10-44 Energy Dispersive XRF at The Open University. Trace element determinations were conducted on a Phillips PW-1400 Wavelength Dispersive XRF at Nottingham University by Tim Brewer. Isotope ratios quoted with $\pm 1\sigma$ errors (all samples analysed at the Open University on a Finnigan MAT261 multi-collector mass spectrometer). Raw Sr isotope analyses were corrected for mass fractionation assuming that $^{86}\text{Sr}/^{88}\text{Sr} = 0.1194$. Repeat analyses of the standard NBS 987 gave a mean of 0.710246 ± 0.000017 . Pb isotope analyses were consistently run at 1100°C , and corrected for mass fractionation using a preferred value for the NBS 981 standard of: $^{206}\text{Pb}/^{204}\text{Pb} = 16.937$, $^{207}\text{Pb}/^{204}\text{Pb} = 15.491$ and $^{208}\text{Pb}/^{204}\text{Pb} = 36.700$. Sample ages from sources listed in [11]; most of the ages quoted are estimates based on stratigraphic relationships within sections, where marker horizons (e.g. prominent tuff units) have been dated with either the K/Ar or the $^{40}\text{Ar}/^{39}\text{Ar}$ methods. A complete dataset is available from the senior author on request.

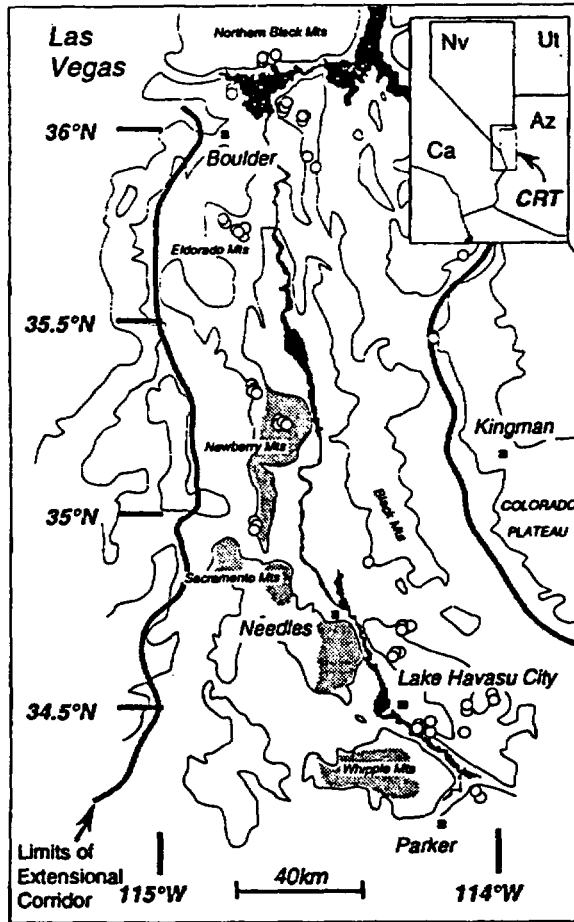


Fig. 1. The Colorado River Trough (CRT) extensional corridor, with inset showing position in the western USA. Localities for samples having $< 56\text{wt}\%$ SiO_2 are shown with circles. Most of the modelling presented in this contribution is based on samples from the vicinity of Lake Havasu City. Dark shading along the axis of the corridor represents uplifted metamorphic core complexes. The Colorado River and Lake Mead are shown in black.

high LILE contents relative to the LREE, and high LREE relative to the HREE.

Group 1 samples are all alkali basalts, including a number of the most recent post-extensional flows and a few syn-extensional samples from the Lake Mead area. Ultramafic inclusions and mantle xenocryst material are common only in CRT units within this group. The samples have fairly smooth mantle-normalised patterns that are convex upwards, and they generally have maxima at either Ta or Nb. This results in characteristic high mantle-normalised Nb/La ratios that are

generally > 0.8 (Fig. 3). The basalts also have high Nb/Y ratios, some of the highest TiO_2 contents in the CRT (up to 3 wt%), moderately high P_2O_5 , and generally low MgO contents for their low silica levels. A few of the Group 1 basalts display a spike at Ba on mantle-normalised diagrams (Fig. 2), which is recognised as a common feature in basalts from the western USA [cf. 13].

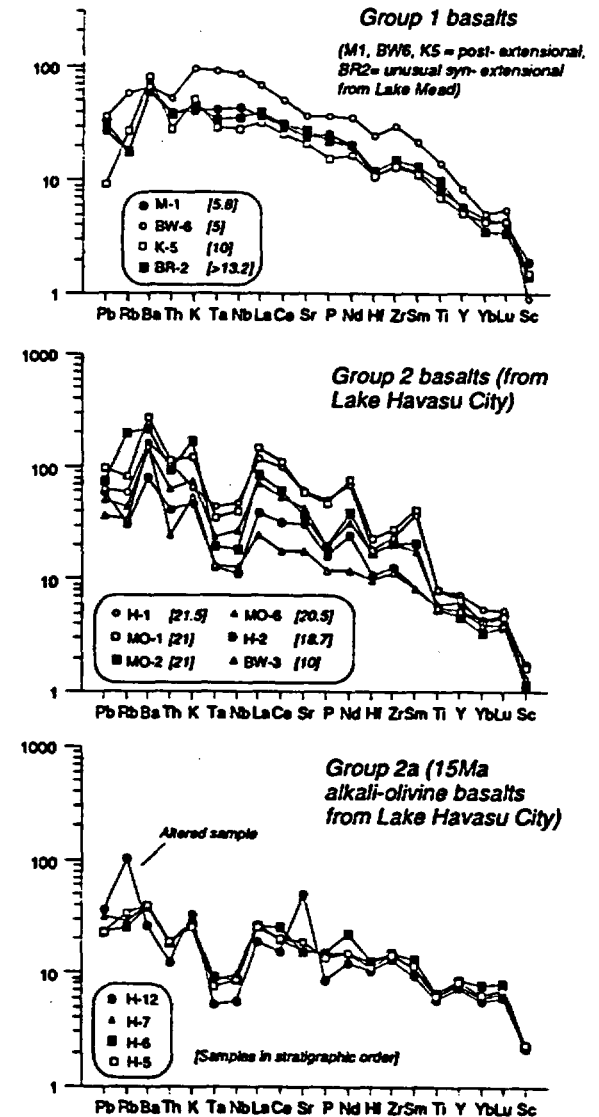


Fig. 2. Primitive mantle normalised multi-element diagrams for representative samples from the CRT (samples have been normalised to values presented in [47]). Italicised numbers in square brackets refer to sample ages in Ma; Group 2a basalts listed in stratigraphic order.

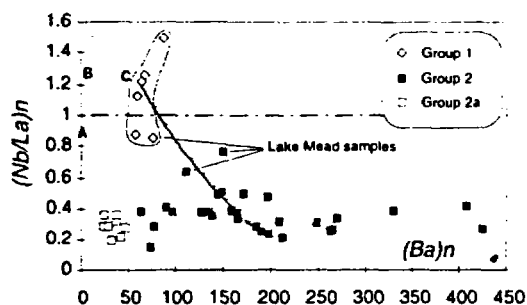


Fig. 3. Primitive mantle normalised Nb/La versus Ba. Samples above $(\text{Nb/La})_n = 1$ do not display a Ta-Nb trough in Fig. 2. A reference mixing line is drawn between these samples and the main group of data, and mixing may account for some of the range of Nb/La displayed by samples from Lake Mead. Comparative positions for typical mantle magmas are also shown: A = N-MORB; B = E-MORB; C = OIB [47].

Group 2 includes basalts from pre/syn-through post-extensional phases and covers a much broader range of geochemical and petrographic diversity. Samples in this group display an irregular mantle-normalised pattern that typically peaks at Ba. Their most striking geochemical feature is the relatively low abundance of the HFSEs with respect to the LILE and the LREE. Small troughs at P_2O_5 and Hf are common and most of the mantle-normalised diagrams also display a step between elements considered to be more or less incompatible than Ti. The greatest relative depletions occur at Ta and Nb and this produces a 'Ta-Nb trough' on mantle-normalised diagrams, such as that commonly observed in island-arc volcanics [14]. The depth of this Ta-Nb trough is fairly constant, with most of the Group 2 rocks displaying mantle-normalised Nb/La ratios of ~ 0.3 . An exception to this general feature is constituted by some of the samples from Lake Mead, which display a larger range in Nb/La (Fig. 3). Overall, Group 2 basalts display a large range of Th/Zr and Th/Nb, although Nb/Zr is rather restricted.

Within Group 2, a distinct subset of basalts is identified by their generally lower trace element concentrations (Group 2a in Fig. 2). These rocks include 15 Ma alkali olivine basalts from Lake Havasu City, representing the final stages of syn-extensional magmatism in that area. They have 45.5–47.7 wt% SiO_2 , high Al_2O_3 (≈ 16.4 wt%) and lower incompatible element contents than any other CRT basalts. However, the overall

mantle-normalised patterns are similar to those of the typical pre/syn-extensional basalts. The patterns cross at Ti, and the 15 Ma alkali olivine basalts have flatter REE profiles with higher Y, Sc and HREE contents than the other syn- and post-extensional samples (Fig. 2). Thus, the Group 2a samples represent an intriguing problem, because they are alkali basalts, which are typically regarded as the product of relatively small degrees of partial melting, and yet they have the lowest incompatible element contents of the CRT basalts.

To summarise, the following groups of basalts can be identified in the CRT based on the available geochemical data:

Group 1: high Nb/La, mostly post-extensional basalts.

Group 2: pre/syn/post-extensional basalts having a wide range of compositions, but with a marked Ta-Nb trough, and somewhat depleted Y, Sc and HREE contents.

Group 2a: HREE-enriched alkali olivine basalts that otherwise have similar trace element patterns, but at lower abundances, to the other Group 2 samples.

2.1 Isotope geochemistry

Most of the CRT samples have Nd, Sr and Pb isotope ratios that differ from those commonly observed in oceanic basalts. The mean $^{87}\text{Sr}/^{86}\text{Sr}$ ratio for all pre/syn-extensional basalts (Groups 2 and 2a) is 0.7079 ± 8 , although the post-extensional Group 2 basalts range from 0.7065 to 0.7092 with a slight tendency for the higher SiO_2 rocks to have higher $^{87}\text{Sr}/^{86}\text{Sr}$ (Table 1). $^{143}\text{Nd}/^{144}\text{Nd}$ within the Group 2 rocks range from 0.51225 to 0.51252. The lead isotope ratios for all of the Group 2 samples plot above the Northern Hemisphere Reference Line (Fig. 4), having elevated $^{207}\text{Pb}/^{204}\text{Pb}$ and $^{208}\text{Pb}/^{204}\text{Pb}$ ratios compared with typical MORB and OIB over a large range in $^{206}\text{Pb}/^{204}\text{Pb}$. Only the high Nb/La, Group 1, basalts have $^{87}\text{Sr}/^{86}\text{Sr}$ ratios which approach those of oceanic basalts (e.g. BW6 = 0.7047, BR1 = 0.7054), and these samples also have MORB-like lead isotope ratios (Fig. 4).

In general, the CRT basalts have high Sr contents (the mean Sr content of 22 basalts from Lake Havasu City is 800 ppm) and Sr displays a

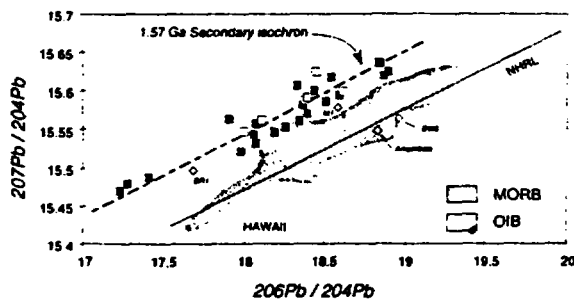


Fig. 4. Lead isotope ratios determined for CRT samples. NHRL = Northern Hemisphere Reference Line. Fields for MORB and OIB are also shown. A secondary Pb isochron can be drawn through the Group 2 and 2a samples (squares) at 1.57 Ga, consistent with published ages for a lithospheric heating event in the western United States [28]. The four highlighted samples (diamonds) are all from Group 1; the amphibole is a separate from sample M2 [24], and BR1 is an early syn-extensional sample from Lake Mead.

positive correlation with LREE concentrations. Although the average $^{87}\text{Sr}/^{86}\text{Sr}$ ratios are rather high in samples from the CRT, it is not thought that they are the result of crustal contamination. For example, to raise the $^{87}\text{Sr}/^{86}\text{Sr}$ ratio of a Group 1 sample (e.g. BW6) from 0.7047 to that of a typical Group 2 sample with a ratio of 0.7079 (e.g. MO5) would require the addition of 55 wt% of the granite NB11 (a suitable crustal end-member identified in [15]). This degree of contamination would result in a magma with 58% SiO_2 , whereas sample MO5 has only 50.9% SiO_2 .

The enriched Sr, Nd and Pb isotope ratios of the Group 2 basalts are therefore thought to have been largely inherited from their upper mantle source regions.

3. Petrogenesis

3.1. Group 2 basalts

Nb/La and Nb/Zr ratios are rather restricted in the Group 2 basalts, with the exception of those from the Lake Mead area where some mixing occurred between Group 2 and Group 1 type magmas [11]. The Lake Mead samples have therefore been excluded from the following discussion, and the interpretations presented are just for the post-extensional basalts and the basalts from the Lake Havasu City area. Within this restricted set of Group 2 basalts, the Th/Zr, Th/Nb and Ce/Yb ratios all show considerable variation, although there is no apparent correlation with isotope ratios. In Fig. 2 the trace element variations appear to be systematic in that, for example, lower REE contents are accompanied by lower LILE. Such systematic trace element variations, and the limited range in isotope ratios, is consistent with the effects of variable degrees of partial melting, and this is illustrated in Figs. 5 and 6.

The large variation in Ce/Yb observed within Group 2 (Fig. 5), relative to a smaller variation in

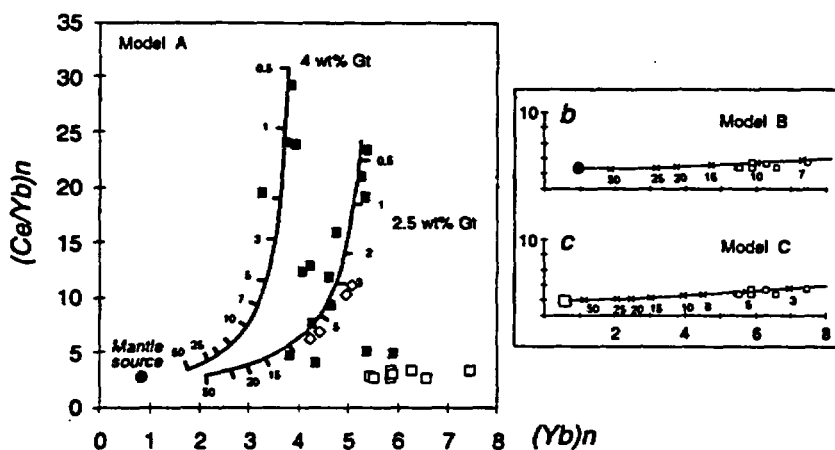


Fig. 5. Primitive mantle normalised Ce/Yb versus Yb for post-extensional samples and samples from Lake Havasu City. (a) Melting curves calculated using a batch melting equation [19] on the initial model source composition from Table 2 (Model A); percent melting is indicated along the model line. Curves are shown for 2.5 and 4.0 wt% garnet in the source. (b) Melting curve for Model B from Table 2. (c) Melting curve for Model C to reproduce the spread of Group 2a data. Symbols as in Fig. 3.

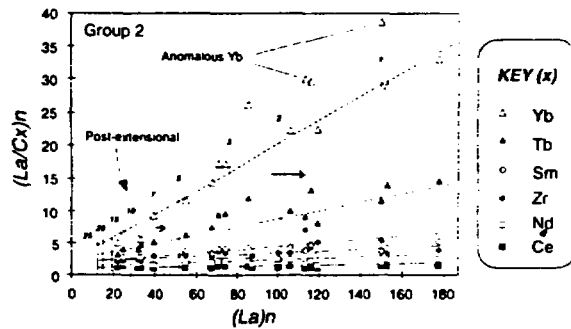


Fig. 6. Primitive mantle normalised La/Cx versus La/n for Group 2 samples, where Cx is the concentration of the elements x listed in the key [after 22]. Samples related by variable degrees of partial melting of the same source will fall on straight lines with the same slope and intercept values for each element x. The dotted lines shown in this figure are calculated by melting the initial model source composition from Table 2 (Model A). These model lines are in the same order as the elements in the key and the degree of partial melting is indicated as a percentage figure above the La/Yb melting line. There is reasonable correlation between these models and the actual data, suggesting that the initial model is close to the composition of the actual Group 2 source. Furthermore, it is suggested that the degrees of partial melting indicated might also be appropriate for the actual data. The maximum effect of 15 wt% fractionation has been indicated by small arrows, and note that this has little effect on the inferred degrees of partial melting. Four samples with anomalously low Yb concentrations (high La/Yb) fall on the 4 wt% garnet model in Fig. 5.

Yb and moderately low Yb concentrations, is also matched by a large range in Sm/Yb relative to Ce/Sm. Such features suggest that Yb was compatible during partial melting, consistent with the presence of residual garnet [16]. Thus, partial melting calculations have been undertaken using a garnet lherzolite source composition (Table 2). This initial model source is based on an average of fertile garnet lherzolite analyses from Arizona [17], and a modelled garnet-bearing source for the basic rocks in the Lebombo region of South Africa [18].

The model curves in Fig. 5 were derived from a simple batch melting equation [19] with source minerals entering the melt in the proportions given for model A in Table 2, as suggested in Beccaluva et al [20]. The data are best approximated by melting a lherzolitic mantle source containing 2.5–4.0 wt% garnet, and assuming a $Yb_{gt/melt}$ distribution coefficient of 4.1 [21].

In Fig. 6 the model has been expanded to include a number of other elements, plotted in such a way that samples related by variable degrees of partial melting will have a straight-line correlation [22,23]. Note that diagrams of this type are typically plotted with the most incompatible element available on the x-axis, and as the

TABLE 2

Model source compositions and melting parameters used in this contribution. The initial model composition is an average of garnet lherzolite samples FO77, BO82 and 105 [17], and a modelled source from Cox et al. [18]. Composition of spinel lherzolite xenolith PA-65G from Frey and Prinz [25]. Trace element distribution coefficients used in the melting models are from a compilation by Irving [48], with additional data from Irving and Frey [21], Pearce and Norry [16] and Cox et al. [18].

	Initial Model PA-65G		Distribution coefficients					Initial model	Source modes		Proportions entering melt	
			O1	Opx	Cpx	Gt	Sp		A	B	A	B
La	2.076	0.84	0.0002	0.002	0.069	0.01	0	O1	0.60	0.61	0.1	0.1
Ce	4.175	2.0	0.0005	0.003	0.098	0.021	0	Opx	0.235	0.24	0.3	0.3
Nd	2.667	1.5	0.001	0.0065	0.18	0.05	0	Cpx	0.14	0.15	0.55	0.6
Sm	0.577	0.342	0.0013	0.013	0.26	0.074	0	Gt	0.025	0.0	0.05	0.0
Eu	0.184	0.119	0.001	0.005	0.9	0.9	0					
Tb	0.104	0.06	0.0015	0.02	0.3	0.7	0.007	PA-65G	C	C		
Yb	0.405	0.27	0.0015	0.049	0.28	4.1	0.007	O1	0.6	0.1		
Lu	0.07	0.041	0.001	0.11	0.8	10		Opx	0.2	0.1		
Zr	15	na	0.001	0.03	0.1	0.3		Cpx	0.15	0.5		
								Sp	0.05	0.3		

y-axis numerator (e.g. Rb in [23]). However, in the Group 2 rocks Pb, Rb, Ba and K_2O have all undergone some degree of alteration which is difficult to quantify. It was also considered that Th distribution coefficient data are not yet sufficiently well constrained for this sort of modelling, and so La was chosen as the most incompatible element.

Most of the suites plot on sublinear arrays in Fig. 6 and the best correlations ($r^2 \geq 0.8$, $n = 17$) are observed for the HFSE and the middle to heavy REE. The ratios involving other LREE (or LILE) remain fairly constant over the whole range of La abundances, with the data arrays having only slightly positive slopes. This is an indication that such elements are incompatible, and that they behave in a similar fashion to La [23]. Some of the observed scatter may be the result of fractional crystallisation, and thus the maximum effect of 15 wt% fractionation is indicated with small arrows in Fig. 6. The shift is greater for the smaller degrees of partial melting and, typically, fractionation displaces samples horizontally, causing them to plot below the general correlation lines. However, four samples (MO1, MO2, MH8 and SL5) all have anomalously low Yb concentrations and are consequently displaced to relatively high positions in Fig. 6. This could be due either to fractionation of a phase in which Yb is highly compatible, or to an even higher D_{Yb} during partial melting (e.g. these samples fall on the modelled line for a source containing 4% garnet in Fig. 5).

Calculated partial melting lines, derived from batch melting of the model source composition, have also been added to Fig. 6. The model lines are clearly coincident with many of the data arrays (they have reasonable slope and intercept correlations), suggesting that the actual magma source may indeed have been similar to that of the initial model. Assuming that this is the case, the degrees of partial melting indicated on the model lines may also be representative of the degree of partial melting in the actual source. In both Fig. 5 and 6 the degree of partial melting of the proposed source is expressed as a percentage, calculated from just the REE data. The pre/syn-extensional basalts from Lake Havasu City can be modelled by approximately 0.5–8% partial melting of the fertile garnet lherzolite source, with

most samples corresponding to between 1.5 and 5% melting. Post-extensional basalts from Group 2 cover a larger melting interval (1.5–15%), and their sample distribution is skewed towards the higher end of this range.

3.2 Group 2a basalts

The low Ce/Yb ratios of the Group 2a basalts (Fig. 5), and the generally depleted nature of their trace element patterns (Fig. 2), might be due to greater degrees of partial melting of the proposed Group 2 source. However, this would not explain the higher Y, Sc and HREE content of these basalts, which in Fig. 5 results in their displacement away from the garnet lherzolite melting curves towards high Yb values.

One solution is to involve a two-stage process with higher degrees of melting followed by fractional crystallisation. This results in nearly flat mantle-normalised patterns, subsequently raised to higher abundances by fractional crystallisation. The distribution of the Group 2a samples in Fig. 5 would appear to support this hypothesis, with the sample trend representing part of a fractionation vector originating on the garnet lherzolite melting curves. If this trend is extrapolated back to the melting models it intersects them at ~25–30% melting, and 1.23 ppm Yb ($Yb_n = 2.5$). The nature of the fractionating assemblage is not known, but even assuming a bulk distribution coefficient for Yb of zero, the *minimum* requirement is 50 wt% fractionation to increase the Yb contents from 1.23 ppm to > 2.3 ppm observed in the rocks. However, the low silica content of the Group 2a basalts from Lake Havasu City (< 48 wt% SiO_2), and transition metal abundances consistent with just 6–8 wt% fractionation from typical primary magmatic values [11], make such large amounts of fractional crystallisation unlikely. Thus it is concluded that the Group 2a basalts were not derived by fractionation from melts of the same source as the Group 2 basalts.

The major difference between the sources could simply have been one of mineralogy, and this is considered with the garnet-absent model B, in Table 2. Garnet is the principal influence on the distribution of Yb in the upper mantle, and its absence results in more similar distribution coefficients for Yb and Ce. The new melting

model therefore defines a nearly horizontal vector on the Ce/Yb vs. Yb diagram (Fig. 5b), similar to that produced by fractional crystallisation. The least fractionated Group 2a sample (H12) can be modelled by ~13% melting of a source with no residual garnet, and the whole range of basalts by 7–13% melting.

Alternatively, the Group 2a basalts might have been derived from a source with lower incompatible element contents, by smaller degrees of partial melting. The existence of such source regions is suggested by the predominance of trace element depleted spinel lherzolite xenoliths in the Pliocene–Recent basalt fields of southern Arizona [24,25]. Model C in Table 2 is based on the most fertile, in major element terms, of these xenoliths [from 25], and typical spinel lherzolite melting modes (averaged from [20,25]). With this model the least fractionated Group 2a sample can be derived by just 6% partial melting, and the whole range of Group 2a basalts by 2–6% melting (Fig. 5c). Modelling the distribution of the other REE, in particular the low Ce/Nd ratios and restricted Tb contents, produces a similar range of results.

Thus, models B and C can both reproduce the REE geochemistry of the Group 2a basalts. However, at the high degrees of partial melting indicated in model B, subalkaline rather than alkaline compositions would be anticipated for the Group 2a basalts [4]. Indeed, all of the Group 2 post-extensional basalts which can be modelled at >10% melting are subalkaline. Thus, it is suggested that the Group 2a basalts are more likely to be derived by small degrees of partial melting of a source with relatively low trace element abundances, favouring model C in Table 2.

3.3 Group 1 basalts

These basalts apparently fall on the same garnet lherzolite melting curves in Fig. 5 as described for the Group 2 basalts, and indeed the REE profiles for the two groups are very similar (see Fig. 2). However, the high Nb/Zr and Nb/La ratios, low Th/Nb ratios, low Ba contents, low $^{87}\text{Sr}/^{86}\text{Sr}$ ratios, and lead isotope ratios close to the Northern Hemisphere Reference Line indicate that these basalts were derived from a different mantle source. This source may have been

mineralogically similar to the Group 2 source (for instance, containing residual garnet), but it had not developed the high time-integrated isotope ratios and it had a different enrichment history for trace elements more incompatible than the LREE.

3.4 A better approximation of source compositions

Using the inferred degrees of partial melting (based on REE contents) it is possible to estimate the relative source compositions of individual samples from Groups 2 and 2a. In particular, it is possible to predict the relative abundances of elements such as Ba, Sr, Ta and P, for which there are only limited data from western USA mantle xenolith analyses. The results for both groups indicate that the Ta-Nb trough and spikes at Ba and K are source-related features, and that the Group 2 source was relatively enriched in

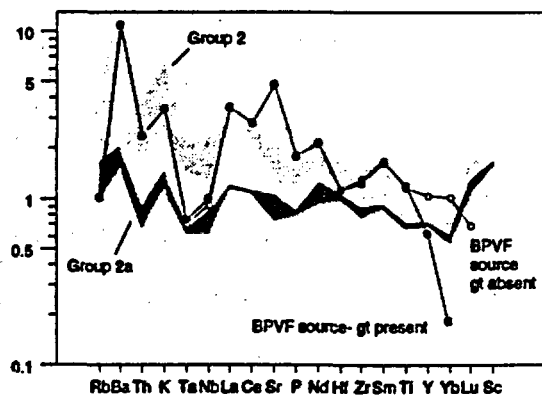


Fig. 7. Calculated source compositions (primitive mantle normalised [47]) for the Group 2 and 2a magmas. These sources have been derived by back-calculating individual samples by their inferred degrees of partial melting suggested from REE data. For instance, the REE content of sample H2 can be reproduced by 7% partial melting of the initial model source composition, using Model A in Table 2. Thus, the concentration of other trace elements in the source can be estimated if their concentrations in H2 are also back-calculated by 7% melting. The resulting shaded fields in this figure represent ± 1 standard deviation from the calculated mean source compositions, after back-calculating a number of samples for each group. Because of the dependence on La in this modelling, the source compositions for Group 2 and 2a have been standardised to the La contents of the initial model source and the xenolith PA-65G respectively. Inferred source compositions, for alkali basaltic magmatism in the Big Pine Volcanic Field (BPVF) of California, are shown for comparison [data from 23].

trace elements compared with that for Group 2a (Fig. 7). This is clearly demonstrated by the steep profile of the Group 2 source, compared with the much flatter Group 2a profile, in Fig. 7.

These calculated source profiles also have many features similar to those proposed for the alkali basalts of the Big Pine Volcanic Field of California (BPVF [23,26]). The only major departures between the BPVF source and the calculated Group 2 source occur with Ta and Nb, which are more depleted and closer to the Group 2a source abundances, and for Sr which displays a slight peak. Consequently, the Rb/Sr ratio of the BPVF source is lower than that for the calculated CRT sources, and this is reflected in lower $^{87}\text{Sr}/^{86}\text{Sr}$ ratios (mean ~ 0.7060) in the BPVF lavas [26].

4. Asthenospheric versus lithospheric sources

The available data from the CRT rocks indicate that they were derived from two distinct mantle sources, and that one of these sources was characterised by negative Ta-Nb anomalies (Figs. 2, 3 and 7) and had variable trace element abundances, as inferred for the source of the Group 2 and 2a basalts. This raises the question of how these sources were related physically, and in particular whether they were situated in the lithospheric or asthenospheric upper mantle. Moreover, changes in the magma source regions with time in the evolution of a magmatic province are important for understanding the causes of magmatism, and how this was linked to extension.

The irregular mantle-normalised trace element patterns, and trace element and isotope ratios different from those typically observed in oceanic basalts, suggests that the Group 2 and 2a basalts were derived from distinctive source regions in the continental mantle lithosphere [see also 2,7,8,13,23]. The observed Nd, Sr and Pb isotope ratios require time to develop, and so they may be used to estimate the length of time that the source has been isolated from the convecting asthenosphere. In Fig. 4, lead isotope data define a linear array that is assumed to represent a secondary isochron line reflecting the time since isolation. This yields an age of ~ 1.6 Ga, which may be significant because it effectively rules out a significant contribution from the subducted

Farallon plate, which is thought to have been < 50 My old beneath the CRT at the time of magmatism [27]. The 1.6 Ga age is instead similar to the time of Proterozoic lithosphere enrichment inferred from a number of areas across the western United States [e.g. 26,28,29], and so it is argued that the Group 2 and 2a magmas were derived from melting of the subcontinental lithospheric mantle.

Group 2a magmas are only observed along the axis of the CRT where extension is thought to have reached a maximum. Intuitively, a higher degree of partial melting in the source is therefore expected, consistent with the positive correlation between the amount of lithospheric stretching and the size of melt fraction attained in adiabatic decompression melting models [4]. However, another possibility, supported by both the major and trace element arguments outlined above, is that the Group 2a basalts represent fairly limited degrees of partial melting of a less enriched source. It is suggested that the Group 2a basalts were derived from a lithospheric source that had relatively low trace element contents and was probably spinel-bearing, whereas the predominant Group 2 basalts were derived from mantle lithosphere with garnet as a residual phase.

If the models for the Group 2a source are correct, the relationship of the Group 2 and 2a sources within the lithospheric mantle may be one of depth. The favoured model for the Group 2a source is that it is garnet-free, and probably contains spinel which is generally stable at lower pressures than garnet. Consequently, this source is inferred to have been at shallower levels in the lithosphere. A zone of spinel lherzolite overlying more enriched garnet lherzolite would also be consistent with currently accepted models for trace element enrichment in the subcontinental lithospheric mantle [30]. Moreover, similar results have been observed in other extensional provinces (e.g. in the Deccan and in the British Tertiary volcanic province [31]), where magma geochemistry is inferred to have changed from garnet residual to spinel residual with time. The spinel-garnet transition occurs at around a depth of 60–80 km, and thus the change from a steep REE profile (such as displayed by Group 2 basalts) to a shallow profile (Group 2a basalts)

may also reflect the changes in lithospheric thickness with extension.

In contrast, the Group 1 basalts have comparatively smooth mantle-normalised patterns, and trace element and isotope ratios similar to trace element enriched MORB or OIB. Thus it is argued that the Group 1 magmas were derived from the asthenospheric upper mantle. This source was most obviously tapped during the latest episode of post-extensional magmatism, although a number of samples from the Lake Mead area (e.g. BR1 and 2) indicate that melting of similar source regions occurred here during the syn-extensional phase at ~ 15 Ma. However, mixing between Group 1 and Group 2 magmas does not appear to have been a significant factor in the CRT magmatism (e.g. Fig. 3).

Basalts similar to those in Group 1 are recognised in the Pliocene–Recent volcanic fields across the Great Basin and southern Arizona (e.g. Lunar Craters [32]), and they have been termed the ‘Basin and Range magma type’ [7]. A low Th/Ta (equivalent to low Th/Nb), low $^{87}\text{Sr}/^{86}\text{Sr}$ component is also identified as the principal contributor to post-21 Ma magmatism in the Mogollon Datil Volcanic Field of New Mexico [29], and for small volumes of post-11.6 Ma magmas in the Rio Grande Rift of northwestern Colorado [33]. These authors also conclude that such basalts were derived from the asthenospheric upper mantle, and so it appears that post-extensional, asthenosphere-derived basalts were erupted at times ranging from 21 to 0 Ma in different tectonic provinces across the Western USA.

5. Constraints on the causes of magmatism in the CRT

In principle, temporal variations in the degree and depth of partial melting, during the evolution of a magmatic province, are sensitive indicators of the causes of magmatism. Moreover, when combined with estimates of magma volumes, eruption rates and amounts of extension, it should be possible to constrain the calculated potential temperature in the upper mantle, and hence any contribution from a mantle plume.

Figure 8 summarises the changes in Nb/Y and Nb/La with time in basalts from the Lake Havasu

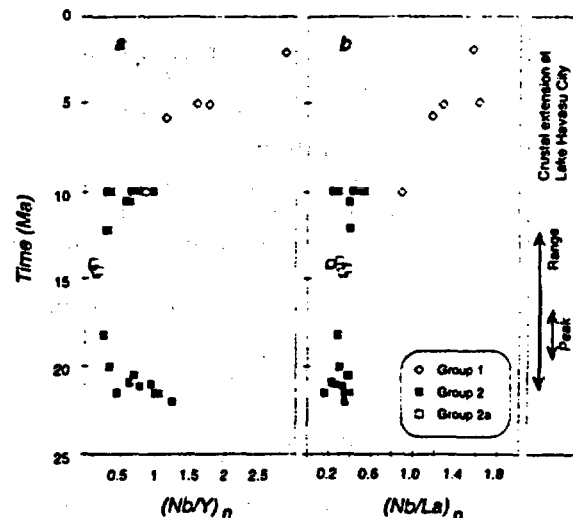


Fig. 8. Primitive mantle normalised Nb/Y and Nb/La ratios versus time, for post-extensional samples and samples from Lake Havasu City. Relationship to crustal extension is shown. (a) The initial decrease in Nb/Y with time at Lake Havasu City is thought to relate to an increase in the degree of partial melting in a trace element enriched fraction of the subcontinental lithospheric mantle (SCLM). Group 2a samples probably record small degrees of melting of a relatively trace element depleted SCLM source. (b) The switch from SCLM to asthenosphere-derived Group 1 magmas is marked by a jump in Nb/La ratios. Nb and La are similarly incompatible and thus the ratio should be unaffected by fractionation or the degree of partial melting.

City area at the centre of the CRT (Fig. 1). The variations in Nb/Y are broadly analogous to those in Ce/Yb discussed above. Nb/Y and Ce/Yb are initially high, but they decline markedly with time during the period of extension, and then increase again in the post-extensional samples. Such variations are consistent with the degree of melting initially being low, increasing to a maximum at the peak of extension, and then decreasing again in the younger basalts. Nb/La is a measure of the size of the negative Nb anomaly in mantle-normalised diagrams (Fig. 2), and in this area it remains low in the basalts erupted from 22 to 10 Ma. Low Nb/La ratios in the CRT basalts are accompanied by enriched radiogenic isotope ratios, and in the model presented here they reflect derivation from the continental mantle lithosphere. It is noticeable that the change to high Nb/La ratios, signifying less of a negative Nb anomaly, occurs several million years after the cessation of extension. Overall, however, the

site of magma generation beneath the CRT appears to have moved from being within the mantle lithosphere to within the convecting asthenosphere with time.

The average thickness of basic volcanics in the CRT is estimated to be approximately 800–1000 m. In addition, a further 500–700 m of higher silica rocks may be present in any area. Within this volcanic pile, only a few metres of lava are recognised as having an OIB signature (high Nb/La); they occur late in the sequence, and they probably represent <5% of the total volume of lavas.

Most of the CRT extension took place in the period 22–9 Ma, with the peak of activity at any location lasting from 2 to 6 My [9; P.B. Gans and E.I. Smith, pers. commun.]. Thus, it would appear that an average thickness of ~1000 m of basalt was generated across the whole region in about 5 My, with >95% being derived from the mantle lithosphere. Taking into account the observed minimum average of 100% extension [9–11] the volume of mantle-derived magma in the CRT can be estimated at $40 \times 290 \times 1 \text{ km}^3$. This excludes non-erupted magma volumes, since seismic velocity variations across the CRT [34] indicate that underplating of mafic magmas was not a significant process during extension. Thus, if the calculated volume of magma was generated in ~5 My, an eruption rate of $\sim 0.0023 \text{ km}^3 \text{ yr}^{-1}$ is implied. Obviously this is only a first-order estimate, but such a rate is low when compared with $0.16 \text{ km}^3 \text{ yr}^{-1}$ for Hawaii [35], $8 \text{ km}^3 \text{ yr}^{-1}$ for the Deccan [36], and possibly up to $22 \text{ km}^3 \text{ yr}^{-1}$ for the Ontong Java Plateau [37]. In each of these cases, the geochemistry of the lavas, and the rates and volumes of magma production, indicate that they were derived from asthenospheric upper mantle in which the potential temperature may have been typically 200°C greater than that under normal mid-ocean ridges, thus providing strong evidence for the influence of a mantle plume in magma generation. In contrast, the estimated eruption rates for the CRT would appear to argue against a high mantle potential temperature, and thus not to require the presence of a mantle plume.

This hypothesis can be tested independently by considering melting thermodynamics, and by evaluating the likelihood of asthenospheric or

lithospheric melting based on physical parameters appropriate for the western United States. Melting thermodynamics are largely controlled by three variables: temperature, pressure and volatile content. A major contribution to the thermal influence comes from the upwelling of hot mantle plumes, but significant partial melting does not generally occur without some lithospheric extension. The approach used by McKenzie and Bickle [4] and Arndt and Christensen [38] concentrated on the roles of temperature and pressure in melting anhydrous peridotite. McKenzie and Bickle [4] showed how the volume of melt generated increases with both the amount of extension (causing decompression melting) and mantle potential temperature. The significant conclusions were that nearly all, and certainly the initial, melt generation occurs in mantle beneath the mechanical boundary layer (which can effectively be equated with the lithosphere), and that any enriched isotope signatures therefore had to have been picked up as the asthenosphere-derived melts rose through the lithosphere. Partial melting at the dry solidus in the mantle lithosphere only occurs after a significant amount of melting has already taken place in the sublithospheric mantle [4, fig. 21]. Such conclusions appear to be in conflict with the geochemical interpretation of dominantly lithospheric signatures in certain continental flood basalt suites [e.g. 2,39,40], and in most of the CRT basalts described here.

Gallagher and Hawkesworth [41] considered the fact that the presence of volatiles can reduce the solidus temperature of peridotite by 300–500°C at pressures between 2 and 5 GPa. They developed a model which incorporated a dry peridotite solidus [4] in the asthenosphere, and a fluid-absent, CO₂- and H₂O-bearing peridotite solidus [42] in the lithosphere. They proposed that if the lithosphere contained small amounts of volatiles, while the underlying convective mantle was effectively dry, then significant amounts of melt could be generated in the lithosphere [41]. This would occur before melting was initiated in the underlying asthenosphere, and result from even modest increases in temperature in the lower lithosphere. However, once lithospheric extension occurs, the amount of melting within the lithosphere does not change significantly, but the relative amount of asthenospheric melt increases

rapidly as extension proceeds, and pressure is reduced. Here this model is developed further to assess the relationship between mantle potential temperature and extension, and melting in lithospheric (i.e. at the fluid-absent peridotite solidus) and asthenospheric (i.e. dry) source regions.

Steady-state horizontally averaged convective geotherms were calculated according to the parameterisation of McKenzie and Bickle [4], and the significant variables of interest are: (i) the mantle potential temperature (T_p), (ii) the thickness of the mechanical boundary layer (MBL), which we equate with the lithospheric source region thickness, and (iii) the amount of extension, as measured by β , the ratio of the pre-extension and final thicknesses of the crust (assuming that no underplating has contributed to the final crustal thickness). The purpose of the calculations was to determine the value of β required to initiate melting (i.e. when the solidus temperature is intersected by the geotherm) in both the lithosphere and the asthenosphere regions for given values of the MBL thickness and T_p . In the following discussion we consider only steady-state geotherms. If thermal equilibrium is not fully achieved, this approach will tend to overestimate the amount of melting in the MBL. However, it is always the lowermost part of the MBL and the uppermost thermal boundary layer in the asthenosphere that melt, and consequently the de-

duction and final thicknesses of the crust (assuming that no underplating has contributed to the final crustal thickness). The purpose of the calculations was to determine the value of β required to initiate melting (i.e. when the solidus temperature is intersected by the geotherm) in both the lithosphere and the asthenosphere regions for given values of the MBL thickness and T_p . In the following discussion we consider only steady-state geotherms. If thermal equilibrium is not fully achieved, this approach will tend to overestimate the amount of melting in the MBL. However, it is always the lowermost part of the MBL and the uppermost thermal boundary layer in the asthenosphere that melt, and consequently the de-

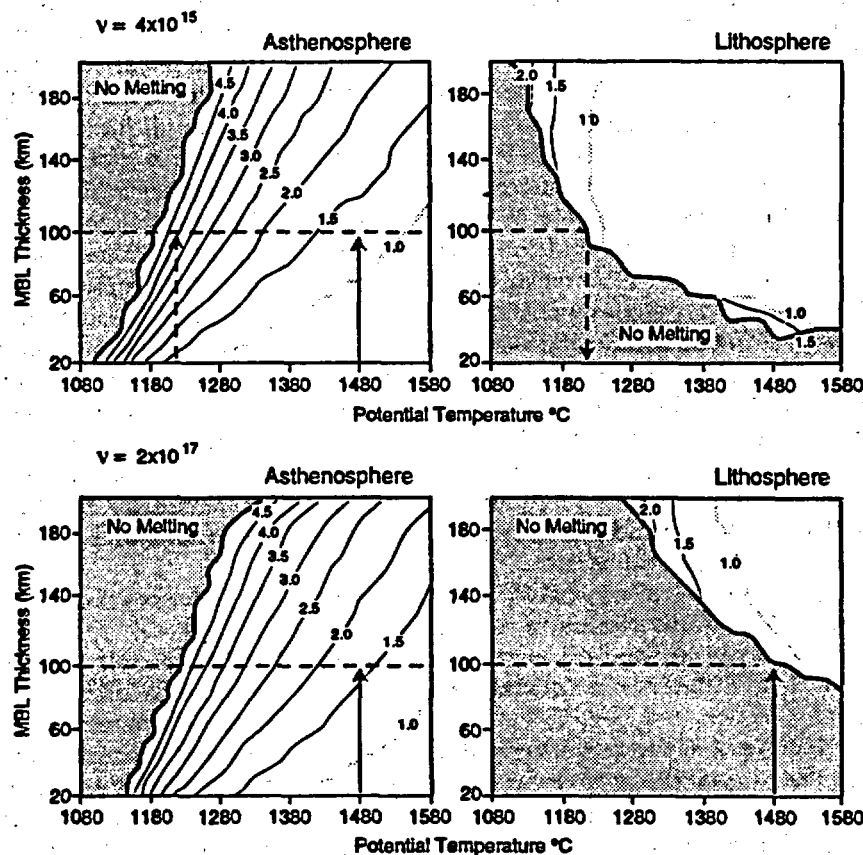


Fig. 9. Results of model calculations for the initiation of melting in the asthenosphere and lithosphere for two values of the mantle viscosity (ν). The contours are for the minimum value of β required to initiate melting as a function of mantle potential temperature (T_p) and initial mechanical boundary layer thickness (MBL). Thus, the shaded regions represent conditions where melting will not occur. The top two figures indicate that for conditions applicable to the CRT melting will occur in the lower part of the lithosphere at $T_p = 1230^\circ\text{C}$, and that there will be no contribution from the asthenosphere. In contrast, at high T_p values (equivalent to a mantle plume) melting in the asthenosphere is rapidly initiated after only limited degrees of extension. Note that the initiation of melting in the lithosphere is more sensitive to the assumed mantle viscosity, because of its influence on the calculated geotherm. See text for details.

gree of thermal equilibrium in both of these regions should be similar, and the interpretation of the model calculations unaffected.

The results are illustrated for two values of the kinematic viscosity (ν), 4×10^{15} and 2×10^{17} $\text{m}^2 \text{s}^{-1}$, because this parameter is not particularly well constrained and yet it has a significant influence on the calculated geotherms in the lithosphere (Fig. 9). Higher values of ν lead to less vigorous mantle convection, a thicker thermal boundary layer and a shallower geotherm (lower temperatures) in the lithosphere. As discussed by McKenzie and Bickle [4], the lower value is probably appropriate for the viscosity in the thermal boundary layer just below the MBL, while the viscosity of the bulk of the upper mantle is probably two orders of magnitude greater, consistent with the higher value adopted here. The results of these calculations are presented in Fig. 9 and the role of the kinematic viscosity, through its influence on the geotherm, is clearly shown by the reduction in the size of the parameter space (MBL, T_p) where melting is predicted in the lithosphere for the higher value of ν , while calculated conditions for the onset of melting in the asthenosphere are relatively unaffected. The important features of the diagrams are these:

(1) Melting can occur in both the asthenosphere and lithosphere in the absence of extension, provided T_p is large enough.

(2) Partial melting in the lithosphere in the absence of extension is favoured by the presence of a thicker MBL, while the opposite is true for melting in the asthenosphere.

(3) At least for $\nu = 4 \times 10^{15}$ $\text{m}^2 \text{s}^{-1}$, lower values of T_p favour melting in the lithosphere only, with no asthenosphere contribution (with normal MBL thicknesses and limited or no extension).

(4) Melting of the asthenosphere with no melting in the lithosphere may occur if the MBL is thin enough, or if ν is high.

(5) In the region where partial melting occurs in both the asthenosphere and the lithosphere, the lithosphere nearly always melts at lower β values (i.e. before the asthenosphere is predicted to melt).

(6) At lower values of T_p , higher β values are required to initiate melting in both the asthenosphere and lithosphere.

To relate these models to the western United States, estimates of MBL thickness, β and asthenospheric potential temperature are required. An initial MBL thickness of 90–100 km is inferred as reasonable for lithosphere of Proterozoic age, consistent with lithospheric thicknesses measured for the unextended Colorado Plateau [43], and structural observations in the CRT suggest values of $\beta \geq 2$ [9,10]. For a mechanical boundary layer thickness of 100 km and $\nu = 4 \times 10^{15}$ $\text{m}^2 \text{s}^{-1}$, the lower portion of the lithosphere will begin to melt at potential temperatures of only 1230°C, even under minor amounts of extension, while the underlying asthenosphere does not begin to melt until extreme degrees of extension are achieved. Thus it might be predicted that initial magmatism would have a lithospheric signature under such conditions, although this magmatism would be of limited volume as a consequence of the relatively cool geotherm. Asthenospheric magmas would only be observed after considerable thinning of the MBL, probably after the main episode of extension. In contrast, at higher T_p values, the magmas become dominated by asthenospheric melting, and greater thicknesses of basaltic magma (ca. 5–7 km, at $T_p = 1480^\circ\text{C}$ [4]) are generated. Clearly, this is inconsistent with the CRT observations which display a similar pattern of magmatism to that suggested for the low T_p model. Thus, the implication is again that a mantle plume (i.e. at elevated mantle temperatures) is not required beneath the southwestern United States.

6. Summary and model for CRT magmatism

Two distinct geochemical groups of basalt have been identified in the CRT. Group 1 alkali basalts have isotope ratios similar to MORB or OIB and smooth mantle-normalised trace element patterns. The abundant Group 2 basalts have enriched isotope ratios and more irregular mantle-normalised patterns with a Ta-Nb trough. Basalts within Group 2 are thought to be related by variable degrees of partial melting from a trace element enriched lherzolitic source. Melting calculations indicate that it contained 2.5–4% garnet, and its composition was similar to that invoked for Cenozoic basalts in southern Nevada [e.g. 44,45]. Alkali olivine basalts erupted in the

final stages of extension (Group 2a) are thought to have been derived from a similar, but less trace element enriched, source in which garnet was absent. The trace element and isotope signatures of both sets of Group 2 basalts are consistent with the melting of a non-convecting mantle capable of sustaining geochemical heterogeneities developed during the Proterozoic, i.e. the continental mantle lithosphere.

The youngest post-extensional basalts (Group 1) are similar to the typical 'Basin and Range magma type' [7], and their isotopic and trace element signatures are consistent with their derivation from the asthenospheric upper mantle. Basalts from this source constitute a very small percent of the overall magma volume (< 5%) in the CRT. The degree of partial melting of this source is difficult to evaluate, although the small volumes of magma observed suggest only limited amounts of melting. Furthermore, asthenospheric source regions are anticipated to have lower Nb/Y ratios than old trace element enriched lithosphere, and thus the high Nb/Y ratios of Group 1 basalts (Fig. 8) are also consistent with smaller degrees of partial melting than those inferred for most of the Group 2 basalts.

The chemical variations within the Group 2 magmas indicate that the degree of partial melting within the mantle lithosphere increased with time in the period 22–18 Ma, the time of maximum extension (Fig. 8). The picture is complicated by the Group 2a magmas which are erupted along the central axis of the CRT, and which appear to have been derived from a shallower (and hence garnet-free) less enriched lithospheric source. In terms of eruptive volumes, the peak of magmatic activity occurred during the main pre/syn-extensional phase, and particularly after ~ 13 Ma the volumes of magma decreased significantly.

The key conclusions are therefore that most basalts in the CRT were derived from the continental mantle lithosphere, that there were systematic changes in the composition of the basalts with time, and that the youngest basalts were derived from the asthenospheric upper mantle. It is inferred that the degree of partial melting increased with time in the period of maximum extension, and that there was a progression to melting at shallower levels along the axis of maxi-

um extension. In a more restricted study of basalts just from the Lake Mead area, Daley and DePaolo [46] also suggested an initial decrease in the depth of magma generation with time, and that relaxation of the geotherm following extension subsequently forced the melting zone back to greater depths.

It is argued that the progression from lithosphere- to asthenosphere-derived basalts with time indicates that extension was a significant factor in their generation. Most of the basalts appear to have been generated by partial melting in the lithosphere, by inference in the presence of small amounts of CO₂ and H₂O [41]. In detail the amounts and proportions of H₂O and CO₂ and are not well constrained, although the alkali nature of the CRT basalts is consistent with higher CO₂/H₂O ratios than may be present in the generation of continental tholeiites. The small volumes of asthenosphere-derived basalts further constrain the potential temperature at the time of magmatism. Elevated T_p values would result in much greater proportions of asthenosphere- to lithosphere-derived melts than those observed, and much greater eruption rates than those estimated for the CRT. It is concluded that the mantle beneath the CRT was not characterised by anomalously high temperatures, and thus there is little evidence for a deep-seated mantle plume beneath the southern Basin and Range in the period 22–0 Ma.

Acknowledgements

We thank Gail Mahood and Phil Gans for encouraging our interest in the extension-related magmatism of the western United States, and for their help and support in the field. Early drafts of the manuscript were greatly improved by discussions with Peter Hooper, Nick Rogers and Gene Smith, and we thank Nick Arndt, Rob Ellam and Godfrey Fitton for their constructive and thorough reviews. This research was funded by grants from the NERC.

References

- 1 I.H. Campbell and R.W. Griffiths, Implications of mantle plume structure for the evolution of flood basalts, *Earth Planet. Sci. Lett.* 99, 79–93, 1990.

- 2 D.W. Peate, C.J. Hawkesworth, M.S.M. Mantovani and W. Shukowsky, Mantle plumes and flood basalt stratigraphy in the Paraná, South America. *Geology* 18, 1223-1226, 1990.
- 3 M.J. Hole, G. Rogers, A.D. Saunders and M. Storey, Relation between alkalic volcanism and slab-window formation. *Geology* 19, 657-660, 1991.
- 4 D.P. McKenzie and M.J. Bickle, The volume and composition of melt generated by extension of the lithosphere. *J. Petrol.* 29, 625-679, 1988.
- 5 D. Latin and N. White, Generating melt during lithospheric extension: pure shear vs. simple shear. *Geology* 18, 327-331, 1990.
- 6 W.P. Leeman, Development of the Snake River Plain-Yellowstone Plateau, Idaho and Wyoming: an overview and petrologic model, in: *Cenozoic Geology of Idaho*. B. Bonnicksen and R.M. Breckenridge, eds.. *Bull. Idaho Bur. Mines Geol.* 26, 155-177, 1990.
- 7 J.G. Fitton, D. James and W.P. Leeman, Basic magmatism associated with late Cenozoic extension in the western United States: compositional variations in space and time. *J. Geophys. Res.* 96, 13693-13711, 1991.
- 8 D.S. Ormerod, C.J. Hawkesworth, N.W. Rogers, W.P. Leeman and M.A. Menzies, Tectonic and magmatic transitions in the Western Great Basin, USA. *Nature* 333, 349-353, 1988.
- 9 P.B. Gans, G.A. Mahood and E. Schermer, Synextensional magmatism in the Basin and Range Province: A case study from the Eastern Great Basin. *Geol. Soc. Am. Spec. Pap.* 233, 54 pp., 1989.
- 10 G.A. Davis and G.S. Lister, Detachment faulting in continental extension; perspectives from the southwestern U.S. Cordillera. *Geol. Soc. Am. Spec. Pap.* 218, 133-160, 1988.
- 11 T.K. Bradshaw, Tectonics and magmatism in the Basin and Range Province of the western United States, 248 pp., Ph.D. Thesis, Open University, Milton Keynes, 1991.
- 12 E.M. Duebendorfer and E.T. Wallin, Basin development and syntectonic sedimentation associated with kinematically coupled strike-slip and detachment faulting, southern Nevada. *Geology* 19, 87-90, 1991.
- 13 J.G. Fitton, D. James, P.D. Kempton, D.S. Ormerod and W.P. Leeman, The role of lithospheric mantle in the generation of late Cenozoic basic magmas in the Western United States. *J. Petrol. Spec. Lithosphere Issue*, pp. 331-349, 1988.
- 14 J.B. Gill, *Orogenic Andesites and Plate Tectonics*, 385 pp., Springer, Berlin, 1981.
- 15 T.K. Bradshaw, The adaptation of Pearce element ratio diagrams to complex high silica systems. *Contrib. Mineral. Petrol.* 109, 450-458, 1992.
- 16 J.A. Pearce and M.J. Norry, Petrogenetic implications of Ti, Zr, Y and Nb variations in volcanic rocks. *Contrib. Mineral. Petrol.* 69, 33-47, 1979.
- 17 S.N. Ehrenberg, Rare earth element geochemistry of garnet lherzolite and megacrystalline nodules from minette of the Colorado Plateau province. *Earth Planet. Sci. Lett.* 57, 191-210, 1982.
- 18 K.G. Cox, A.R. Duncan, J.W. Bristow, S.R. Taylor and A.J. Erlank, Petrogenesis of the basic rocks of the Lebombo. *Spec. Publ. Geol. Soc. S. Afr.* 13, 149-169, 1984.
- 19 C.J. Allègre and J.F. Minster, Quantitative models of trace element behaviour in magmatic processes. *Earth Planet. Sci. Lett.* 38, 1-25, 1978.
- 20 L. Beccaluva, G. Gabbionelli, F. Lucchini, P.L. Rossi and C. Savelli, Petrology and K/Ar ages of volcanics dredged from the Eolian seamounts: implications for geodynamic evolution of the southern Tyrrhenian basin. *Earth Planet. Sci. Lett.* 74, 187-208, 1985.
- 21 A.J. Irving and F.A. Frey, Distribution of trace elements between garnet megacrysts and host volcanic liquids of kimberlitic to rhyolitic composition. *Geochim. Cosmochim. Acta* 42, 771-787, 1978.
- 22 A.W. Hofmann and M.D. Feigenson, Case studies on the origin of basalt: I. Theory and reassessment of Grenada basalts. *Contrib. Mineral. Petrol.* 88, 382-389, 1983.
- 23 D.S. Ormerod, N.W. Rogers and C.J. Hawkesworth, Melting in the lithospheric mantle: Inverse modelling of alkali-olivine basalts from the Big Pine Volcanic Field, California. *Contrib. Mineral. Petrol.* 108, 305-317, 1991.
- 24 H.G. Wilshire, C.E. Meyer, J.K. Nakata, L.C. Calk, J.W. Shervais, J.E. Nielson and E.C. Schwarzman, Mafic and ultramafic rocks of the western United States. *USGS Open File Rep.* 85, 1985.
- 25 F.A. Frey and M. Prinz, Ultramafic inclusions from San Carlos, Arizona: Petrologic and geochemical data bearing on their petrogenesis. *Earth Planet. Sci. Lett.* 38, 129-176, 1978.
- 26 D.S. Ormerod, Late- to post-subduction magmatic transitions in the Western Great Basin, USA, 313 pp., Ph.D. Thesis, Open University, Milton Keynes, 1988.
- 27 D.C. Engebretson, A. Cox and R.G. Gordon, Relative motions between oceanic and continental plates in the Pacific Basin. *Geol. Soc. Am. Spec. Pap.* 206, 59 pp., 1985.
- 28 F.O. Dudas, R.W. Carlson and D.H. Eggler, Regional middle Proterozoic enrichment of the subcontinental mantle source of igneous rocks from central Montana. *Geology* 15, 22-25, 1987.
- 29 J.M. Davis, The geochemical evolution of basic and intermediate mid- to late Tertiary volcanism of the Mogollon-Datil volcanic field, southwestern New Mexico, USA, 270 pp., Ph.D. Thesis, Open University, Milton Keynes, 1991.
- 30 F.G. Waters and A.J. Erlank, Assessment of the vertical extent and distribution of mantle metasomatism below Kimberley, South Africa. *J. Petrol. Spec. Lithosphere Issue*, pp. 185-204, 1988.
- 31 R.M. Ellam, Lithospheric thickness as a control on basalt geochemistry. *Geology* 20, 153-156, 1992.
- 32 C.C.L. Lum, W.P. Leeman, K.A. Foland, J.A. Kargel and J.G. Fitton, Isotopic variations in continental basaltic lavas as indicators of mantle heterogeneity: examples from the western U.S. Cordillera. *J. Geophys. Res.* 94, 7871-7884, 1989.
- 33 P.T. Leat, R.N. Thompson, M.A. Morrison, G.L. Hendry and A.P. Dickin, Compositionally diverse Miocene-Recent rift related magmatism in NW Colorado: partial melting, and mixing of mafic magmas from three different asthenospheric and lithospheric mantle sources. *J. Petrol. Spec. Lithosphere Issue*, pp. 351-378, 1988.
- 34 J. McCarthy, A.S.P. Larkin, G.S. Fuis, R.W. Simpson and A. Howard, Anatomy of a metamorphic core complex: seismic reflection/wide-angle reflection profiling in south-

- eastern California and western Arizona. *J. Geophys. Res.* 96, 12259-12291, 1991.
- 35 S. Watson and D. McKenzie, Melt generation by plumes: A study of Hawaiian volcanism, *J. Petrol.* 32, 501-537.
- 36 M.A. Richards, A.R. Duncan and V.E. Courtillot, Flood basalts and hot spot tracks: plume heads and tails, *Science* 246, 103-107, 1989.
- 37 J.A. Tarduno, W.V. Sliter, L. Kroenke, M. Leckie, H. Mayer, J.J. Mahoney, R. Musgrave, M. Storey and E.L. Winterer, Rapid formation of Ontong Java Plateau by Aptian mantle plume volcanism, *Science* 254, 399-403, 1991.
- 38 N.T. Arndt and U. Christensen, The role of lithospheric mantle in continental flood volcanism: thermal and geochemical constraints, *J. Petrol.* 97, 10967-10981, 1992.
- 39 J.M. Hergt, D.W. Peate and C.J. Hawkesworth, The petrogenesis of Mesozoic Gondwana low-Ti flood basalts, *Earth Planet. Sci. Lett.* 105, 134-148, 1991.
- 40 P.R. Hooper and C.J. Hawkesworth, The origin and evolution of the Columbia River Basalt, *Earth Planet. Sci. Lett.*, in press.
- 41 K. Gallagher and C.J. Hawkesworth, Dehydration melting and the generation of continental flood basalts, *Nature* 358, 57-59, 1992.
- 42 M. Olafsson and D.H. Eggler, Phase relations of amphibole, amphibole-carbonate, and phlogopite-carbonate peridotite: petrologic constraints on the asthenosphere, *Earth Planet. Sci. Lett.* 64, 305-315, 1983.
- 43 L.C. Pakiser, Geophysics of the intermontane system, in: *Geophysical Framework of the Continental United States*, L.C. Pakiser and W.D. Mooney, eds., *Geol. Soc. Am. Mem.* 172, 235-247, 1989.
- 44 G. van Kooten, Mineralogy, petrology and geochemistry of an ultrapotassic basaltic suite, central Sierra Nevada, California, USA, *J. Petrol.* 21, 651-684, 1980.
- 45 M.A. Menzies, W.P. Leeman and C.J. Hawkesworth, Isotope geochemistry of Cenozoic volcanic rocks reveals mantle heterogeneity below the western USA, *Nature* 303, 205-209, 1983.
- 46 E.E. Daley and D.J. DePaolo, Isotopic evidence for lithospheric thinning during extension: Southeastern Great Basin, *Geology* 20, 104-108, 1992.
- 47 S.-S. Sun and W.F. McDonough, Chemical and isotopic systematics of oceanic basalts: implications for mantle composition and processes, in: *Magmatism in the Ocean Basins*, *Geol. Soc. Am. Spec. Publ.* 42, 313-345, 1989.
- 48 A.J. Irving, A review of experimental studies of crystal/liquid trace element partitioning, *Geochim. Cosmochim. Acta* 42, 743-770, 1978.

Section 5

Abstracts and Presentations

The following section contains abstracts presented by Tim Bradshaw during 1992-1993:
GSA Conference, May 1993,
LAVCEI Conference, September 1993.

In addition:

A presentation was given to the Nuclear Regulatory Commission and the Department of Energy concerning the document- "Status of Volcanic Hazard Studies for the Yucca Mountain Site Characterisation Project. Preliminary Draft" by B.M. Crowe, F.V. Perry, and G.A. Valentine.

Tim gave further presentations to the the UNLV faculty and students, including four lectures on igneous petrology and geochemistry, and a summary of work on the Crater Flat project.

Tim was third author on two more abstracts (presented by Prof. C.J. Hawkesworth, The Open University, UK), concerning the causes of continental magmatism. Talks presented at EUG in Strasbourg, and the VSG meeting at Milton Keynes (UK).

QUATERNARY BASALTS IN S. NEVADA, USA: MELTING OF METASOMATISED LITHOSPHERIC MANTLE

BRADSHAW, T.K., SMITH, E.I., Center for Volcanic and Tectonic Studies, Dept. of Geoscience, Univ. of Nevada, Las Vegas, NV 89154, USA; **WALKER, J.D.,** Dept. of Geology, Univ. of Kansas, Lawrence, KS 66045, USA

Magmas erupted during the Quaternary at Crater Flat, Nevada, suggest derivation from a source that has undergone localized metasomatism by trace element-rich CO₂ vapours.

The alkali basalts are geochemically similar in respect to major elements, High Field Strength elements (HFSE), and the heavy REE. Elevated trace element concentrations, low Nb/La, high Zr/Y, and ⁸⁷Sr/⁸⁶Sr ratios of 0.7069 - 0.7071 indicate that the magmas were derived from the lithospheric mantle by small degrees of partial melting. At one centre (Red Cone) a significant range of moderately incompatible trace element concentrations is observed with time: the youngest samples having the more elevated values and also higher ⁸⁷Sr/⁸⁶Sr and ²⁰⁶Pb/²⁰⁴Pb ratios. However, there is only limited variation in the compatible trace elements (e.g., Sc and Ni) and the highly incompatible elements (e.g., Rb and K₂O). This array of compositions is thought to be the result of mixing between relatively enriched and depleted end-member magmas with the enrichments reflecting variable source compositions.

The magnitude of trace element enrichment increases in the order Ba, Sm, Th, Ce, La, Sr. The Sr concentration in the youngest magma batch is nearly 50% higher than in the earliest magmas. Silicate melt enrichment in the source is unlikely because of the lack of HFSE and compatible element variability, H₂O-rich fluids would preferentially cause enrichment in the Large Ion Lithophile elements and not the REE, and positive correlations between ⁸⁷Sr/⁸⁶Sr, Sr and the REE argues against contamination of the source by oceanic sediment input. Instead, the pattern of enrichment is consistent with fluxing by CO₂-rich vapours. Such vapours may mobilize Sr and the light REE while having little effect on the concentration of other elements in the source.

**IAVCEI Conference: September 25th- October 1st 1993
Australian National University, Canberra, Australia.**

TRACHYANDESITE MAGMAS IN THE COLORADO RIVER TROUGH
BRADSHAW, T.K., Center for Volcanic and Tectonic Studies, Dept. of
Geosciences, University of Nevada- Las Vegas, 4505 Maryland Parkway,
Las Vegas, NV 89154-4010.

Extension related magmatism along the Colorado River Trough (CRT) is typified by trachyandesitic suites with a limited compositional range (58-66wt% SiO₂, 6.5-8wt% Na₂O+K₂O). Although, bimodal basalt-rhyolite/dacite suites are predominant in the vicinity of Lake Mead, and along the CRT axis.

The trachyandesites are highly porphyritic, having abundant plagioclase phenocrysts plus clinopyroxene, hornblende and minor occurrences of olivine. Olivine crystals show resorption, and plagioclase and clinopyroxene phenocrysts display complex twinning, zoning and reaction textures indicative of a complex crystallization history.

Trachyandesite trace element patterns have many of the characteristics of basalts derived from the lithospheric mantle in the CRT. However, relative depletions of the high field strength elements (Ta, Nb, P, Ti) are more pronounced, and Pb, Rb and Th contents are higher relative to Ba in the basalts. Sr isotope ratios are also rather elevated. Trace element modelling suggests that the trachyandesites are not related to typical CRT basalt compositions by crystal fractionation, even if hornblende is modelled as principal fractionating phase. Rather, simple mixing between basaltic and silicic end-member melts is favoured, and fractionation and/or AFC processes only play a minor role. Isotopic evidence indicates that crustal material, possibly Mesozoic granite, is a suitable silicic end-member.

The relatively narrow range of observed major element compositions may indicate highly efficient mixing processes or that magma chambers were long-lived and often reached equilibrium before being tapped.

GSA Conference: Reno Hilton, Nevada, USA. May 1993
GSA Abstr. Prog. 25, No. 5, pg. 13.

Section 6

Data Tables for 1992-1993 analyses

DATA

Red Cone and Black Cone data set.

Tables include INAA data, new XRF trace element data and new isotopic analyses.

New Norm calculations based on the Mac programme CIPWNorm 3.1.

Th and Cr data from XRF, and Sm and Nd data from isotope dilution techniques are listed separately. A compilation of isotope data is given at the end of this section.

"R"-labelled samples from Red Cone have been excluded until adequate progress has been made with the XRF machine. Currently the data fall outside the expected bounds based on other XRF analyses of Red Cone samples.

XRF

Major elements,

Trace elements: Ba, Nb, Ni, Rb, Sr, Y, Zr

INAA

Trace elements: La, Ce, Nd, Sm, Eu, Gd, Tb, Dy, Yb, Lu, Co, Cr, Hf, Sc, Ta, Th, U, V.

Area Type (AGE)	BC LL	BC LL	BC B	BC B	BC B	BC F	BC F	BC F	BC F	BC F	BC F
Sample	C8-1-1-LN	C8-1-2-LN	C8-1-3-LN	C8-1-4-LN	C8-1-5-LN	C8-1-06-LN	C8-1-07-LN	C8-1-08	C8-1-09	C8-1-10-LN	C8-1-11-LN
SiO2	49.49	49.82	49.61	49	49.3	49.59	49.89	48.83	48.89	49.88	49.39
TiO2	1.36	1.38	1.39	1.43	1.42	1.39	1.45	1.45	1.45	1.46	1.43
Al2O3	16.63	16.63	16.67	16.71	16.65	16.6	16.93	16.59	16.76	17.09	17.17
Fe2O3	10.51	10.79	10.84	10.53	10.6	10.64	10.99	11.03	11.22	11.03	10.45
MnO	0.16	0.17	0.17	0.16	0.17	0.17	0.17	0.17	0.18	0.18	0.17
MgO	5.08	5.11	5.12	4.73	5.39	4.92	5.05	5.11	5.19	5.16	4.91
CaO	8.44	8.34	8.34	8.36	8.23	8.45	8.47	8.87	8.39	8.39	8.8
Na2O	3.19	3.18	3.12	3.08	2.87	3.09	3.32	3.23	3.26	3.32	3.37
K2O	1.3	1.53	1.52	1.51	1.84	1.81	1.83	1.58	1.62	1.71	1.87
P2O5	1.1	1.1	1.13	1.1	1.15	0.85	0.91	0.92	0.91	0.9	0.93
LOI	0.71	0.05	0.45	0.79	0.38	0.31	0.01	0.43	0.26	0.27	0.2
Total	97.97	98.02	98.36	97.38	97.80	97.62	98.82	98.01	98.13	99.19	98.49
Mg#	52.98	52.61	52.40	51.15	54.24	51.87	51.71	51.92	51.88	52.16	52.27
INAA/ XRF											
La	111	119	114	125	116	120	118	121	118	122	116
Ce	209	226	213	218	223	233	213	233	219	223	210
Nd		112				90.1	94		143		
Sm	11	12	11.3	12.7	11.6	11.9	11.7	12.1	11.9	12.2	11.5
Eu	2.54	2.71	2.52	2.68	2.62	2.68	2.41	2.74	2.54	2.65	2.51
Gd						24.3				21.2	
Tb		1.22			1.78	1.55			1.19	1.62	1.4
Dy											
Yb	1.57	3.29	3.03	3.26	3.33	2.79	1.54	2.69	2.42	3.09	2.29
Lu	0.55	0.23	0.36	0.41	0.25	0.31	0.23	0.34	0.15	1.01	0.34
Ba	1633	1741	1628	1692	1635	1721	1702	1740	1747	1670	1719
Co	24.3	26.3	24.8	23.8	24.7	28.1	25.8	27.9	25.3	27.2	23.4
Cr	97.8	103	100	88.2	102	117	100	119	106	104	79.7
Hi	7.43	7.64	7.35	7.38	7.69	7.91	7.24	8.01	7.47	7.62	7.19
Nb	34.5	33.8	35.6	34.3	33.8	36	34.7	36.9	35.8	33	34.4
Ni	42.5	36.8	44.7	42.9	42.4	40.5	42.9	44.2	46.1	35.7	36.7
Pb	20	23.8	20.4	21.6	20.1	20.4	21.1	20	20.4	22.1	19.9
Sc	17.4	18.6	17.9	17.4	17.1	19.2	17.2	19.1	17.4	17.9	16.8
Sr	1211	1225	1204	1208	1206	1228	1249	1276	1301	1261	1282
Ta	1.81	1.71	1.45	1.43	1.79	1.4	1.66	1.82	1.6	1.72	1.53
Th	11.8	12.6	12.2	12.2	12.2	27	15.6	13	12.4	13.3	11.8
U			6.03			6.32					
V	152	168	156	148	147	176	158	161	176	168	162
Y	22.6	23.1	22.4	22.4	22.7	23.2	22.8	22.8	23.3	23.2	23.2
Zr	378	393	392	391	386	401	394	406	420	402	402
NORM											
Or	C8-1-1-LN	C8-1-2-LN	C8-1-3-LN	C8-1-4-LN	C8-1-5-LN	C8-1-06-LN	C8-1-07-LN	C8-1-08LN	C8-1-09LN	C8-1-10-LN	C8-1-11-LN
Ab	7.98	9.32	9.27	9.33	10.05	9.87	9.85	9.67	9.88	10.32	10.14
An	28.02	27.56	27.23	27.07	25.17	27.13	28.71	28.29	28.47	28.68	29.29
Ne	28.26	27.49	27.84	28.64	28.72	27.68	27.06	27.02	27.16	27.24	27.52
Na	0.00	0.00	0.00	0.00	0.00	0.00	0.00	0.00	0.00	0.00	0.00
Di	7.02	7.02	6.60	6.59	5.44	6.81	6.62	10.70	8.51	8.15	9.68
Hy	19.49	18.42	18.63	19.13	21.38	16.18	11.30	6.78	8.88	9.25	6.64
Ol	2.18	3.10	3.24	2.00	1.96	3.76	7.67	10.64	10.20	9.58	10.01
Mt	1.88	1.91	1.93	1.90	1.89	1.90	1.94	1.97	2.00	1.94	1.85
Il	2.68	2.70	2.72	2.84	2.80	2.74	2.81	2.85	2.84	2.83	2.79
Ap	2.70	2.69	2.76	2.72	2.82	2.09	2.20	2.26	2.22	2.18	2.26
XRF											
Th	7.9	8.8	11.7	7.9	7.5	7.7	6.9	9.5	8.2	5.9	8.5
Cr	122.2	114.5	134.7	87.8	102.7	106.2	87.4	110.1	135.3	86.1	97.3
ISO											
206/204								18.474	18.487		
207/204								15.576	15.577		
208/204								38.429	38.43		
87/86								0.706908	0.706902		
143/144								0.51214	0.512147		
Nd								74.9989	78.3341		
ENd now								-9.71	-9.58		
ISO DIL											
Sm								11.3283	11.7411		
Nd								74.9989	78.3341		

Area Type (AGE)	BC B	BC F	BC F	BC F	BC F	BC LL	BC F	FC D	FC LL
Sample	Co-1-12-LN	Co-1-13-LN	Co-1-14-LN	Co-1-15-LN	Co-1-16-LN	Co-1-16-LN	Co-1-16-LN	Co-2-27-LN	Co-2-28-LN
SiO2	49.77	49.35	49.91	48.96	50.24	51.12	49.32	49.26	49.66
TiO2	1.44	1.45	1.45	1.44	1.46	1.38	1.48	1.54	1.38
Al2O3	16.93	17.22	17.38	16.97	17.31	17.39	17.03	17.29	17.25
Fe2O3	10.63	11.01	10.97	10.76	11.47	10.51	10.64	10.69	10.22
MnO	0.17	0.17	0.17	0.17	0.18	0.17	0.19	0.18	0.19
MgO	5.45	5.14	5.19	5.17	5.32	5.28	5.03	5.07	4.78
CaO	8.19	8.55	8.44	8.39	8.64	8.62	8.52	8.57	8.56
Na2O	3.03	3.29	3.38	3.28	3.35	3.45	3.24	3.51	3.59
K2O	1.7	1.67	1.75	1.76	1.73	1.42	1.89	1.74	1.74
P2O5	0.93	0.92	0.95	0.92	0.88	0.81	1	1.11	1.01
LOI	0.33	0.24	0.01	0.01	0.12	0.23	0.01	0.01	0.01
Total	98.57	99.01	99.61	97.83	100.70	100.39	98.35	98.97	98.39
Mgf	54.44	52.11	52.44	52.83	51.95	53.94	52.42	52.50	52.16
INAA/ XR									
La	121	117	123	117	122	111	123	125	143
Ce	223	220	233	220	221	206	229	232	277
Nd			87.6	78.2	122		72.9		
Sm	12.2	11.9	12.3	11.3	12.3	11.2	12	12.8	13.1
Eu	2.66	2.54	2.81	2.65	2.7	2.45	2.6	2.95	3.13
Gd	20.6							18.5	
Tb	0.95		2.4	1.2	1.36	1.21	1	1.04	1.61
Dy							4.9	5.61	6.65
Yb	3.23	2.87	2.71	3.4	1.8	3.14	3.41	2	1.72
Lu	0.39	0.31	0.24	0.21	0.38	0.41	0.295	0.34	0.38
Ba	1716	1772	1726	1924	1813	1582	1721	1830	2006
Co	25.7	25.5	26.1	25.1	26.3	24.7	25.4	25.7	23.8
Cr	95.4	97.4	109	104	115	91	87.3	97.9	77.8
Hf	7.55	7.74	8.02	7.68	7.88	7.33	7.61	7.97	7.42
Nb	33.6	36.8	36.5	38.9	38.5	32.9	35.3	34.4	35.5
Ni	42.9	50.6	44.3	41.2	44.7	43.9	47	43.7	39.2
Rb	22.5	21	20.5	21.5	22	19.4	20.1	18.3	19.8
Sc	17.9	17.7	18.2	17.5	17.9	17.5	18	18.1	17.8
Sr	1239	1322	1284	1317	1322	1218	1276	1399	1769
Ta	1.58	1.66	1.56	1.33	1.44	1.45	1.66	1.49	1.19
Th	12.7	12.8	13	12	12.8	11.8	12.4	12.8	15.2
U									
V	191	161	174	169	163	168	181	167	150
Y	22.6	23	23.1	23.3	23.1	22.3	22.7	23.2	23.4
Zr	395	420	412	423	422	374	407	402	414
NORM									
Cr	10.33	10.09	10.49	10.74	10.27	8.46	11.47	10.49	10.56
Ab	26.35	28.47	29.00	28.65	28.47	29.51	28.15	30.30	30.66
An	28.34	27.90	27.46	27.24	27.20	27.94	27.05	26.82	26.78
Ne	0.00	0.00	0.00	0.00	0.00	0.00	0.00	0.00	0.00
Di	6.43	8.22	7.72	8.39	8.82	8.55	8.53	8.19	8.87
Hy	17.01	8.24	8.02	7.24	7.47	13.38	7.95	4.26	5.96
Ol	4.76	10.27	10.49	10.93	11.07	5.92	9.85	12.61	10.41
Ml	1.88	1.94	1.92	1.92	1.99	1.83	1.88	1.88	1.81
Il	2.81	2.82	2.81	2.82	2.78	2.64	2.89	2.98	2.69
Ap	2.26	2.23	2.28	2.25	2.09	1.93	2.43	2.68	2.48
XRF									
Th	6.8	11	8.9	12.5	6.9	6.2	6.9	7.9	13.6
Cr	90	132.9	115	135	135.7	80.6	98.1	87.7	48
ISO									
206/204									
207/204									
208/204									
87/86								0.707026	
143/144								0.512195	
Nd								89.9771	
ENd now								-8.65	
ISO DIL									
Sm								13.0837	
Nd								89.9771	

Area Type (AGE)	FC F	FC D	FC F									
Sample	C9-2-29-LN	C9-2-30-LN	C9-2-31-LN	C9-2-32-LN	C9-2-33-LN	C9-2-34-LN	C9-2-35-LN	C9-2-36-LN	C9-2-37-LN	C9-2-38-LN	C9-2-40-LN	
SiO2	49.22	49	49.54	50.54	49.03	50.33	48.9	49.05	48.9	48.69	49.48	
TiO2	1.48	1.45	1.39	1.45	1.44	1.48	1.42	1.47	1.5	1.35	1.38	
Al2O3	17.04	16.93	17.17	17.53	16.94	17.29	17.98	17.89	17.68	17.89	17.04	
Fe2O3	10.64	10.44	10.24	10.84	10.81	10.69	10.53	10.78	10.59	10.15	10.33	
MnO	0.21	0.18	0.2	0.21	0.17	0.18	0.18	0.17	0.18	0.19	0.2	
MgO	4.85	4.75	4.6	5.25	4.83	5.13	4.67	4.74	5.35	4.52	4.88	
CaO	8.38	8.5	8.57	8.86	8.43	8.85	8.6	8.43	8.35	8.81	8.52	
Na2O	3.9	3.4	3.63	3.55	3.35	3.48	3.41	3.46	3.37	3.48	3.49	
K2O	1.96	1.75	1.77	1.83	1.93	1.76	1.82	1.76	1.82	1.66	1.8	
P2O5	1.06	1.45	1.09	1.2	1.04	1.2	1.05	1.03	1.06	1.01	1	
LOI	0.01	0.36	0.01	0.01	0.01	0.07	0.01	0.29	0.01	1	0.01	
Total	98.15	98.21	98.21	101.27	97.78	100.46	98.55	99.07	98.81	98.75	98.13	
Mg#	51.51	51.47	51.15	53.03	51.48	52.80	50.83	50.61	54.07	50.93	52.40	
INAA/ XR												
La	128	128	156	154	139	141	143	136	120	157	149	
Ce	234	243	277	276	272	268	262	248	214	279	255	
Nd		98	95.6	94.6	82.2	74.7	80.5	90.4	108	84	95.6	
Sm	12.5	12.7	14.3	13.9	13.2	13.1	13.6	12.8	11.8	13.9	13.6	
Eu	2.7	2.9	2.85	2.84	3.05	2.92	2.92	2.79	2.61	2.98	2.87	
Gd	17.6	16.6		20.5	21.3	20.3			19.4			
Tb	1.13		1.09	1.42	1.45		1.16	1.07	1.14	1.83	1.35	
Dy	5.97	6.39	6.02	6.65	5.49	6.18	5.6	6.49	5.18	5.62	4.18	
Yb	2.57	2.03	3.13	3.2	3.35	2.1	2.97	2.67	2.49	3.15	3.2	
Lu				0.31	0.31	0.29	0.36	0.29	0.33	0.46		
Ba	1829	1823	2030	2045	1875	1856	1819	1781	1698	1996	2018	
Co	24.3	24.2	23.1	23.2	15.5	24	24	24	25.2	24.3	22.2	
Cr	78			71.7	74.3	72.5	69.5	75.4	108	77.9	74	
Hf	7.73	7.7	6.32	6.94	7.79	7.98	8.28	7.81	7.38	7.63	7.36	
Nb	33.7	37.6	35.3	35.6	35.9	36.5	36	35.2	36.4	35.1	34.2	
Ni	42.8	40.5	45.7	43.3	40.5	35.2	41.8	32.6	48.1	46.5	43.7	
Pb	20.1	18.9	19.9	20.1	20.1	19.8	20.1	19.8	22	19.8	20.6	
Sc	18.9	17.1	18.4	18.4	17.1	18.9	17	18.9	17.7	17.4	18.4	
Sr	1346	1462	1848	1842	1587	1641	1571	1496	1308	1818	1811	
Ta	1.7	1.67	1.41	1.42	1.48	1.65	1.65	1.67	1.59	1.35	1.65	
Th	12	12.9	14.7	14.8	13.8	13.8	13.8	12.8	11.8	15.6	14.5	
U				5.57				4.34	4.28	5.35	5.46	
V	162	155	162	172		158	174	176	168	155	164	
Y	23.4	23.4	23.6	23.97	23.5	23.4	23	22.8	22.8	24.2	23.7	
Zr	412	435	423	430	425	424	423	423	397	417	418	
NORM												
Or	11.92	10.67	10.75	10.78	11.78	10.46	11.02	10.63	10.99	10.13	10.94	
Ab	29.79	29.68	31.57	29.95	29.27	29.61	29.56	29.93	29.14	30.40	30.38	
An	26.64	26.58	26.03	26.41	26.32	26.51	29.02	28.71	28.35	29.21	26.25	
Ne	0.00	0.00	0.00	0.00	0.00	0.00	0.00	0.00	0.00	0.00	0.00	
Di	8.05	6.73	9.18	8.57	8.74	8.72	6.93	6.51	6.28	8.11	9.25	
Hy	7.19	9.97	4.15	4.76	5.59	7.30	3.66	4.60	4.47	2.84	5.26	
Ol	10.32	8.40	11.35	12.30	11.24	10.09	12.83	12.57	13.63	12.58	11.14	
Mt	1.89	1.86	1.81	1.86	1.89	1.85	1.86	1.90	1.87	1.81	1.83	
Il	2.89	2.84	2.71	2.75	2.82	2.83	2.76	2.85	2.91	2.65	2.70	
Ap	2.58	3.54	2.65	2.83	2.54	2.86	2.55	2.49	2.57	2.47	2.44	
XRF												
Th	10.4	10	10.7	13	10	13.2	12.9	8.5	13.1	13.3	11	
Cr	106.3	82.4	95.6	76	68.9	73.8	84.1	70	128.4	88.8	60.5	
ISO												
208/204			18.552			18.554		18.439				
207/204			15.582			15.598		15.566				
208/204			38.473			38.519		38.39				
87/86		0.706956	0.707109			0.707003		0.706912				
143/144		0.512161	0.512196			0.512169		0.512147				
Nd		83.1758	96.1805			90.9783		78.3777				
ENd now		-9.3	-8.62			-9.15		-9.58				
ISO DIL												
Sm		12.3381	13.8477			13.2382		11.8751				
Nd		83.1758	96.1805			90.9783		78.3777				

Area Type (AGE)	FC F	FC F	FC F	FC F	FC D	FC F	FC B				
Sample	1.6	2	2	2	1.2	1.6	1.3	2	1.2	OLD?	
	C9-2-41-LN	C9-2-42-LN	C9-2-43-LN	C9-2-44-LN	C9-2-45-LN	C9-2-46-LN	C9-2-39-LN	C0-2-72-LN	CO-2-73-LN	C2-R-35-LN	
SiO2	49.38	49.21	50.51	49.24	49.86	49.68	49.42				
TiO2	1.53	1.48	1.54	1.51	1.48	1.4	1.37				
Al2O3	17.15	17	17.71	17.16	17.19	17.02	17.97				
Fe2O3	10.8	10.45	10.98	10.51	10.47	10.37	10.34				
MnO	0.21	0.19	0.21	0.2	0.2	0.19	0.19				
MgO	5.02	4.69	4.96	4.72	4.36	5.09	4.86				
CaO	8.49	8.5	8.68	8.32	8.38	8.78	8.58				
Na2O	3.34	3.28	3.56	3.43	3.55	3.55	3.4				
K2O	2	1.85	1.99	1.84	1.72	1.68	1.86				
P2O5	1.08	1.05	1.16	1.14	1.08	1.17	0.98				
LOI	0.01	0.27	0.01	0.11	0.31	0.01	0.01				
Total	99.01	97.97	101.31	98.18	98.60	98.94	98.98				
Mg#	52.00	51.12	51.29	51.14	49.25	53.36	52.28	52.28			
INAA/ XR											
La	122	127	126	121	137	154	151	116	136		
Ce	209	232	226	212	254	295	276	201	229		
Nd	107	94.6	97.9	101	89.1	110	98.7	75.8	103		
Sm	11.9	12.8	12.3	11.5	13.6	14.1	13.4	10.5	11.5		
Eu	2.52	2.62	2.78	2.43	3.08	3.05	3.02	2.79			
Gd			16		24.4	17.3					
Tb	1.56	1.36	1.23	0.87		1.32	1.67		1.04		
Dy	6.46	6.36	6.38	7.83	6.94	5.74	4.9	4.66	4.74		
Yb	2.91	3.68	3.2	3.31	3.03	2.56	2.23	2.07	2.55		
Lu	0.28	0.37	0.53		0.41	0.29		0.293	0.34		
Ba	1738	1746	1713	1687	1781	1839	1936				1727
Co	23.1	23.8	22.8	21.1	26.5	25.1	23.6	26.2	24.5		
Cr	79.5	73.5	72.4	59.7	86.6	76.4	73.2	283	160		
Hf	7.51	7.57	8.06	6.65	8.34	8.32	7.17	7.17	7.12		
Nb	33.2	38.9	36.35	35.1	35.9	33.9	32.8				32.8
Ni	46.3	42.3	37.1	42.7	47.2	36.4	42.872				62.8
Rb	20	21.5	21.1	19.3	19.5	17.1	22.4				21.5
Sc	16.3	16.9	16.6	14.6	18.8	17.6	17.2	16.1	15.4		
Sr	1363	1378	1355	1339	1360	1771	1806				1336
Ta	1.39	1.47	1.48	1.45	1.7	1.67	1.53	1.42	1.38		
Th	11.6	12.7	12.5	10.5	13.4	15.6	15.3	11.1	12.7		
U						5.65		3.33	3.8		
V	171	173	166	158	264	167	159	148	138		
Y	23	23.3	23.2	22.9	23.6	22.8	23				23.2
Zr	406	429	422	406	408	415	425				412
NORM											
Cr	12.06	11.30	11.72	11.19	10.44	10.13	11.21				
Ab	28.83	28.68	30.03	29.88	30.85	30.65	29.34				
An	26.41	27.07	26.38	26.76	26.59	26.06	28.84				
Ne	0.00	0.00	0.00	0.00	0.00	0.00	0.00				
Di	8.33	8.38	8.07	7.32	7.96	9.38	7.19				
Hy	5.10	9.07	8.73	7.64	9.44	5.42	4.49				
Cl	12.01	8.36	12.75	9.83	7.55	11.21	12.27				
Mt	1.90	1.86	1.89	1.87	1.85	1.82	1.82				
I	2.95	2.90	2.92	2.95	2.89	2.71	2.65				
Ap	2.61	2.57	2.74	2.78	2.63	2.83	2.37				
XRF											
Th	4.2	11.8	8	8	9.1	9.3	10.1				9.83
Cr	109.5	63.8	69.8	80.4	65.5	87.6	79.9				145
ISO											
206/204	18.471			18.484		18.549					
207/204	15.569			15.577		15.574					
208/204	38.42			38.464		38.465					
87/86	0.706966			0.70691		0.707035					
143/144	0.512159			0.512135		0.512185					
Nd	81.9148			82.5413		94.0918					
ENd now	-9.34			-9.8		-8.83					
ISO DIL											
Sm	12.1879			12.3191		13.5494					
Nd	81.9148			82.5413		94.0918					

New Isotopic analyses on samples from Crater Flat, Nevada.

(Sm and Nd isotope dilution data)

Sample	206Pb/204Pb	207Pb/204Pb	208Pb/204Pb	87Sr/86Sr	143Nd/144Nd	ENd now	Sm (ppm)	Nd (ppm)
Black Cone								
C9-1-08LN	18.474	15.576	38.429	0.706906	0.51214	-9.71	11.33	75.00
C9-1-09LN	18.487	15.577	38.43	0.706902	0.512147	-9.58	11.74	78.33
Red Cone								
C9-2-28-LN				0.707026	0.512195	-8.65	13.08	89.98
C9-2-30-LN				0.706956	0.512161	-9.3	12.34	83.18
C9-2-31-LN	18.552	15.582	38.473	0.707109	0.512196	-8.62	13.85	96.18
C9-2-34-LN	18.554	15.598	38.519	0.707003	0.512169	-9.15	13.24	90.98
C9-2-37-LN	18.439	15.566	38.39	0.706912	0.512147	-9.58	11.88	78.38
C9-2-41-LN	18.471	15.569	38.42	0.706966	0.512159	-9.34	12.19	81.91
C9-2-44-LN	18.484	15.577	38.464	0.70691	0.512135	-9.8	12.32	82.54
C9-2-46-LN	18.549	15.574	38.465	0.707035	0.512185	-8.83	13.55	94.09

Samples analysed at the Isotope Geoscience Lab, University of Kansas, Lawrence, Kansas.

Section 7

Final Thoughts on Volcanism and Crater Flat

The previous sections discussed a number of possible petrogenetic models for volcanism at Crater Flat, and in the Basin and Range province of the western USA in general. We suggest that most of the magmas were derived from melting of the lithospheric mantle throughout this region during the Cenozoic. The spread of volcanism with time in the Great Basin and in the Colorado River Trough appears to be consistent with plate tectonic models, and with the passive rise of asthenospheric mantle to replace and/or displace areas previously underlain by the subducted Farallon Plate.

However, some problems are still not fully resolved. One of the key questions concerns the nature and origin of the 'amagmatic corridor' developed between Las Vegas and the Yucca Mountain/Lathrop Wells area. It is observed that regions to the north of this corridor (e.g., Timber Mountain caldera complex) and to the south (Lake Mead region), were sites of some of the most intense and prolonged volcanic activity during the late Cenozoic. Whereas no volcanic centres developed within the corridor itself.

The southern boundary of the corridor is particularly sharp and it has been suggested (Smith et al. [1992] *CVTS Annual Report*) that this represents a major (lithosphere cutting?) structure. In turn, this structure may have acted as a crustal focussing mechanism for magmas. Thus, accounting for the localised magmatic intensity. In light of this possibility, the northern margin of the corridor (which is within a few km of the Yucca Mountain site) also deserves further study. In particular, to evaluate what risks might be involved in such an inherently active feature.

Another problem concerns the nature of the lithospheric mantle beneath the amagmatic corridor. Work presented in this document suggests significant similarities between the lithospheric mantle beneath Crater Flat, the western edge of the Great Basin (e.g., Big Pine Volcanic Field) and the Colorado River Trough. The lithosphere in each of these areas is of Proterozoic age and has undergone a similar history of tectonic and geochemical evolution. Thus, there is no reason to suggest that the lithospheric mantle beneath the amagmatic corridor is of any different composition to that of the surrounding areas. In which case this would represent a major fertile lithospheric source for future magmatism, and thus the conditions under which this source might become 'active' also warrant further study.

Furthermore, the association of volcanism with structural lineaments cannot be understated. If the northern margin of the anagmatic corridor does correspond to a major structural feature, then it is important to note that the intense volcanic activity of the Timber Mountain- Crater Flat region is localised at the intersection of this feature and NNE-SSW structures that continue to the Reveille Range and Lunar Craters Volcanic Field. Any future volcanic episode is also likely to be influenced by such structures.

It is easy to forget or sideline the possible volcanic hazards in southern Nevada when there have been no eruptions in historical times. However, the region as a whole has seen significant volcanic activity over the last 20Ma, and, while we may be at present in a 'quiet phase', there is no reason to believe that volcanism has ceased on a permanent basis. Indeed, there is potential for future volcanic activity.

CENTER FOR VOLCANIC AND TECTONIC STUDIES
1992 - 1993 ANNUAL REPORT

Contribution by

Dr. G.M. Yogodzinski

<u>Contents</u>	<u>Page</u>
Section 1: INTRODUCTION TO YOGODZINSKI'S CONTRIBUTION_____	GMY2
Section 2: CVTS EFFORTS IN THE REVELLE RANGE, SOUTH-CENTRAL NEVADA_____	GMY2
<i>Introduction</i>	GMY2
<i>Volcanic Stratigraphy in the Reville Range</i>	GMY4
<i>Geochemistry of the Reville Range Volcanic System</i>	GMY4
<i>Crustal Contamination & Eruptive Cycles in the Reville Range System</i>	GMY6
<i>Discussion - Conclusions</i>	GMY11
<i>Future Work</i>	GMY11
<i>References</i>	GMY12
Section 3: JOURNAL OF GEOPHYSICAL RESEARCH PAPER (title page)_____	GMY13
Section 4: ABSTRACTS (title page)_____	GMY14

Section 1

INTRODUCTION TO YOGODZINSKI'S CONTRIBUTION

This report summarizes the work of Gene M. Yogodzinski with the Center for Volcanic and Tectonic Studies (CVTS) for the period October through December, 1993. The bulk of this report is contained in Section 2, which is a summary of Yogodzinski's contribution to the ongoing CVTS project in the Reveille Range of south-central Nevada (see also contributions by Naumann in previous CVTS annual reports). Section 3 of this report is a copy of a paper published by Yogodzinski in the *Journal of Geophysical Research* (7/93). This paper is part of Yogodzinski's dissertation research at Cornell University. As such, it does not deal directly with volcanic hazard assessment at Yucca Mountain, but it does illustrate the kinds of geochemical studies that are essential to our understanding of volcanic systems in general. Section 4 of this report is a compilation of abstracts presented by Yogodzinski at professional meetings over approximately the past 14 months.

Section 2

CVTS EFFORTS IN THE REVELLE RANGE

Introduction

The Reveille Range of south-central Nevada, and the adjacent Pancake Range - Lunar Crater Volcanic Field, constitute the largest Pliocene-to-Recent field of mafic volcanism within the central Great Basin of the western United States. This field is located within the NNE-trending zone of mafic volcanism that stretches from Death Valley to Lunar Crater (Figure 1). The proposed high level nuclear waste repository at Yucca Mountain, Nevada, lies within the southern part of this zone. Thus, studies of Pliocene Volcanism in the Reveille Range will provide insight into the plumbing systems, eruptive dynamics and petrogenesis of volcanic centers near Yucca Mountain.

In the Reveille Range study, our aim is to understand how the volcanic field developed from its inception to demise, and to use that information in evaluating volcanic risk in the geologically similar environment at Yucca Mountain. Our approach has been to combine geochemical studies with detailed mapping and radiometric dating. With this information, we can define the spatial and chronological boundaries of the Reveille Range volcanic system, identify eruptive cycles and spatial eruptive patterns within that system, and determine recurrence rates for eruptions throughout the lifetime of the system.

PLIOCENE - RECENT BASALTIC VOLCANISM

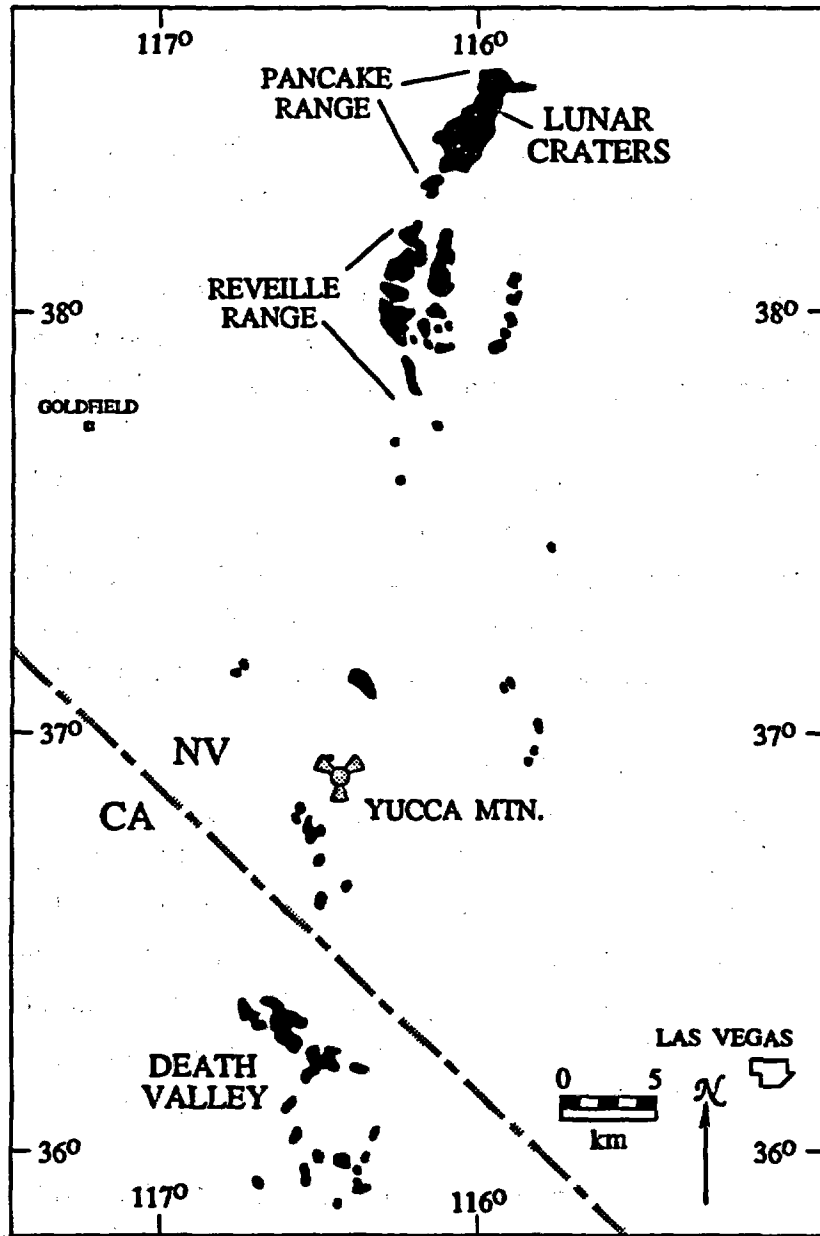


Figure 1: Generalized geologic map showing the distribution of Pliocene-to-Recent mafic volcanism in southern Nevada and southeastern California. Location of proposed high-level nuclear waste repository at Yucca Mountain is within the zone of mafic volcanism that stretches from Death Valley to Lunar Crater.

Ultimately this information will be used to evaluate the probability of future eruptions in the Reveille Range and adjacent Pancake Range - Lunar Crater Volcanic Field. We recognize that a future eruption in this area may not be regarded as a threat to the repository at Yucca Mountain. This area will however, serve as an excellent analog (a test case), that will help evaluate the viability of statistical models that have been applied to the Yucca Mountain area.

Volcanic Stratigraphy in the Reveille Range

Two episodes of mafic volcanism spanning approximately 3 Ma were identified by geologic mapping and K-Ar dating in the Reveille Range (see Naumann *et al.*, 1991 and previous CVTS reports). Basalts of episode-1 are approximately 5.1 to 5.9 m.y. old. They comprise a minimum volume ¹ of approximately 8 km³, and were erupted from 52 vents throughout the Reveille Range (Figure 2). Basalts of episode-2 are approximately 3.0 to 4.6 m.y. old. These comprise a minimum volume of 1 km³, and were erupted from 14 vents located only along the eastern margin of the range (Figure 2).

A relatively small volume of trachytic magma (~0.3 km³ total) was erupted in the northeastern Reveille Range 4.3 m.y. ago, at approximately the time-stratigraphic transition from episode-1 to episode-2 (Figure 2). It is an important point that the trachytic eruptions were explosive, and that they produced not only lava, but also pyroclastic surge deposits that occur between episode 1 and episode 2 basalts in the northeastern part of the range (Figure 2; see also Naumann *et al.*, 1990).

Geochemistry of the Reveille Range Volcanic System

Pliocene basalts of the Reveille Range are mildly alkaline, ranging from 43-49% SiO₂ with 0.9-2.4% K₂O and total alkalis of 4-6% (K₂O+Na₂O). Some episode 1 basalts range to subalkaline compositions (up to 5% normative hypersthene), but most basalts in the Reveille Range contain 0-9% normative nepheline. They include alkali basalts, basanites, and hawaiites (Figure 3). On average, basalts of episode 1 are slightly less alkaline than basalts of episode 2 (Figures 4). Intermediate composition rocks in the Reveille Range (55-62% SiO₂) include phonolites, trachy-andesites and trachytes (Figure 2). These will be referred to collectively as the trachytic rocks or trachytic series.

Incompatible trace element characteristics of episode 1 and episode 2 basalts are similar to each other and to average ocean island basalt (OIB). Extended plots of normalized incompatible element concentrations produce smoothly varying patterns with high concentrations of K, Th, Ba, Ta and

¹ volume estimates are not corrected for erosion.

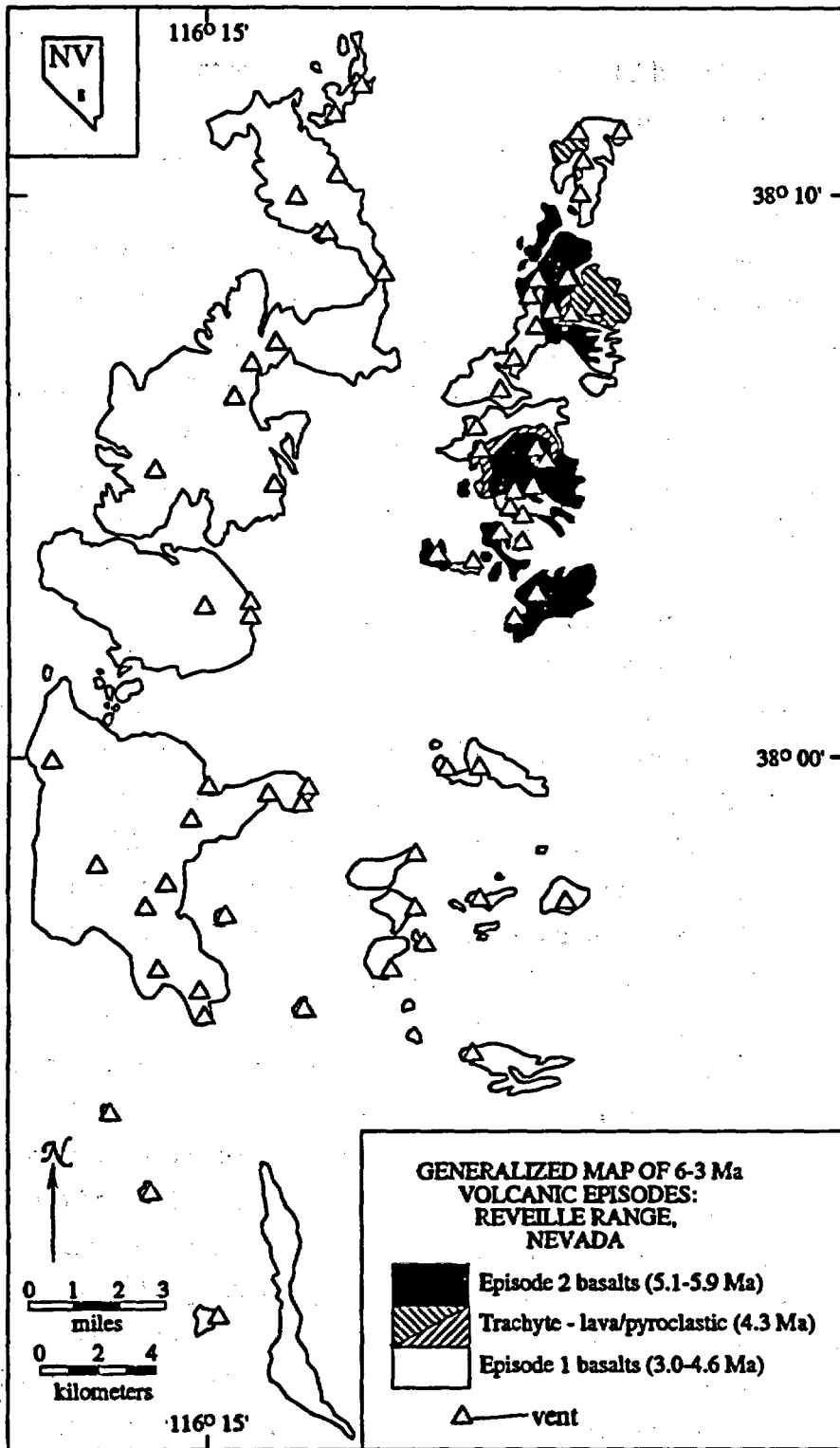


Figure 2: General geologic map of Pliocene basalts in the Reveille Range (mapping by Naumann, see 1990 CVTS annual report)

La relative to Sr, Sm, Hf, Ti and Yb (Figure 5). Interelement ratios and overall abundances are nearly the same for average episode 1 and episode 2 compositions, and for average OIB.

Despite their broadly homogeneous major and trace element characteristics, the isotopic compositions of episode 1 and episode 2 basalts are quite varied. Episode 1 basalts show a wide range in $^{87}\text{Sr}/^{86}\text{Sr}$ (0.7043 - 0.7061) whereas the range in episode 2 is more restricted (0.7035 - 0.7037). Neodymium isotopes are also more variable in basalts of episode 1 than episode 2, though the differences are not as great as for Sr (Figure 6). A similar pattern can be seen in the Pb isotope data. Episode 2 basalts form a linear trend immediately above the mantle reference line at high $^{206}\text{Pb}/^{204}\text{Pb}$ (~19.2), whereas the episode 1 basalts scatter away from the mantle trend toward high $^{207}\text{Pb}/^{204}\text{Pb}$ (Figure 7). The trachytic rocks in the Reveille Range also extend to high $^{87}\text{Sr}/^{86}\text{Sr}$ and $^{207}\text{Pb}/^{204}\text{Pb}$, and in this way are they are isotopically akin to basalts of episode 1.

Crustal Contamination and Eruptive Cycles

Within the Reveille Range System

The major and trace element features of episode 1 and episode 2 basalts indicate that they were produced by melting of an asthenospheric mantle source, similar to that which is commonly sampled by plume-related magmatism in oceanic basins (i.e., OIB). Broad similarity in normative compositions, incompatible element abundances, and interelement ratios, indicate that the nature of the melting process in the Reveille Range was not substantially changed between episode 1 and episode 2 time; that is, the smaller volume of basalt erupted during episode 2 does not reflect a lower percentage mantle melting than during episode 1.

The isotopic results indicate that the episode 1 basalts and the trachytic rocks were contaminated by continental crust, whereas the episode 2 rocks were not. In particular the large variation in $^{87}\text{Sr}/^{86}\text{Sr}$ with little variation in ϵNd in episode 1 and trachytic data (Figure 6) are unlike the well correlated trends that generally are produced in largely mantle-derived volcanic systems (e.g., Figure 6 'Great Basin basalts'). Foland et al. (1991) and Foland and Bergman (1992) showed that Sr and Nd isotopes in basalts of the Reveille Range and Pancake Range - Lunar Crater Volcanic Field are strongly correlated with oxygen isotopes ($\delta^{18}\text{O}$), and they too argue for crustal contamination in the older (Pliocene-age) rocks throughout the region.

The isotopic contrasts between basalts of episode 1 and episode 2, and the isotopic similarities between episode 1 basalts and the trachytic rocks, provide evidence for two eruptive cycles within the Pliocene-age rocks of the Reveille Range. Episode 1 basalts comprise the largest volume of basalt in the Reveille Range, they are dominated by a low pressure phenocryst assemblage (olivine + plagioclase), and were contaminated by crustal material. These observations indicate that there was a well developed, shallow magma chamber during episode 1 time. The explosive eruption of

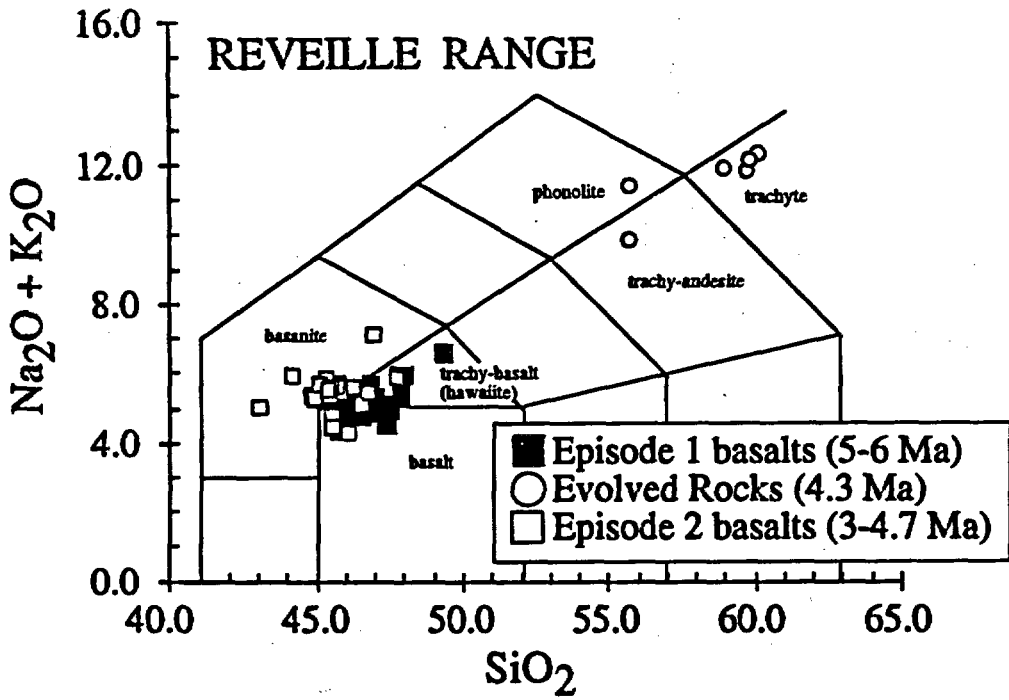


Figure 3: Alkali - Silica diagram with classification grid after Le Maitre (1989). Reveille Range basalts fall into the fields of alkali basalt, basanite, and hawaiite. Intermediate composition rocks fall in the fields trachy-andesite, phonolite and trachyte.

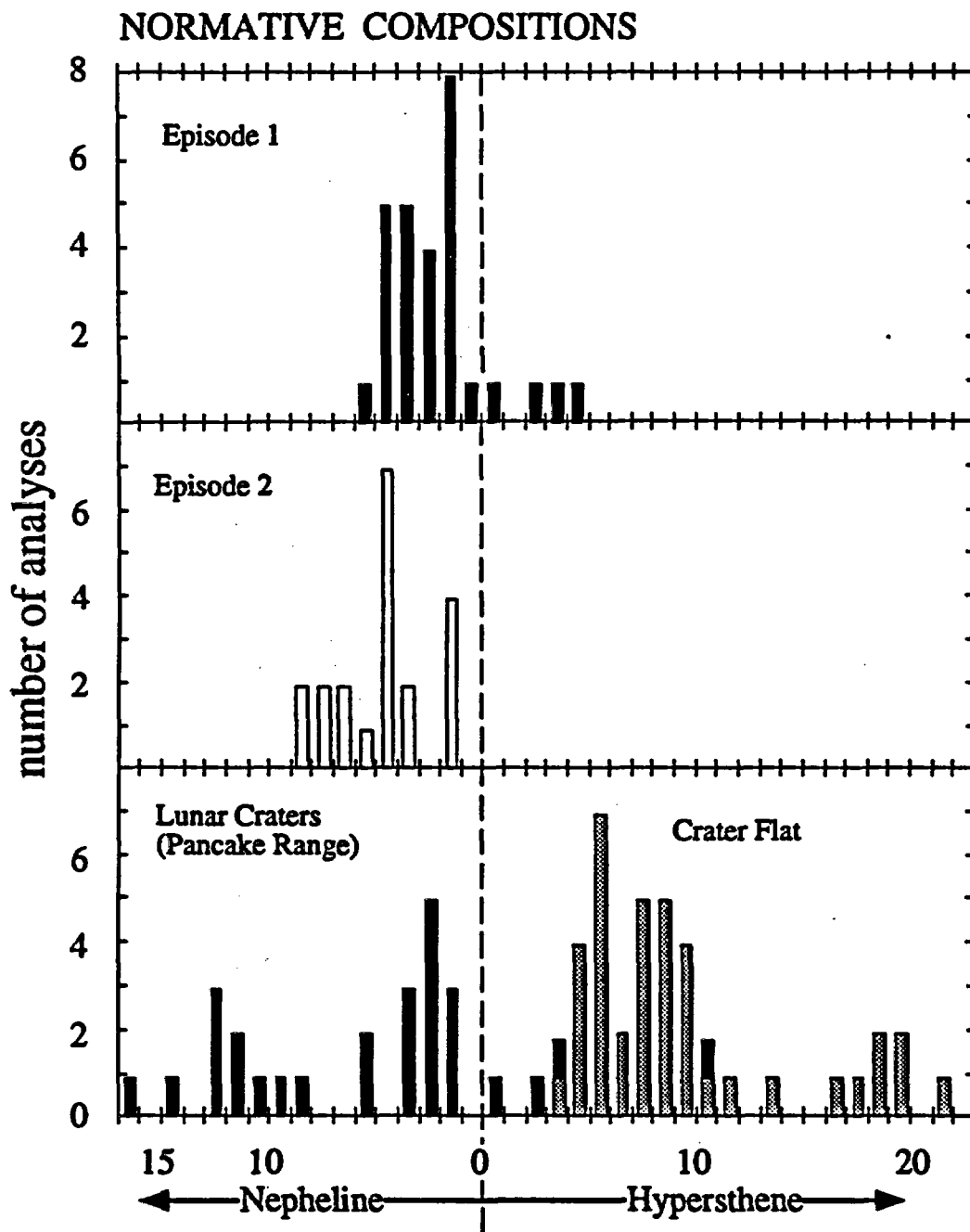


Figure 4: Histogram of normative compositions of Reville Range basalts compared to basalts of the Lunar Craters Volcanic Field (Pancake Range) and Crater Flat. Norms were calculated with assumption that $Fe_2O_3/FeO^* = 0.20$.

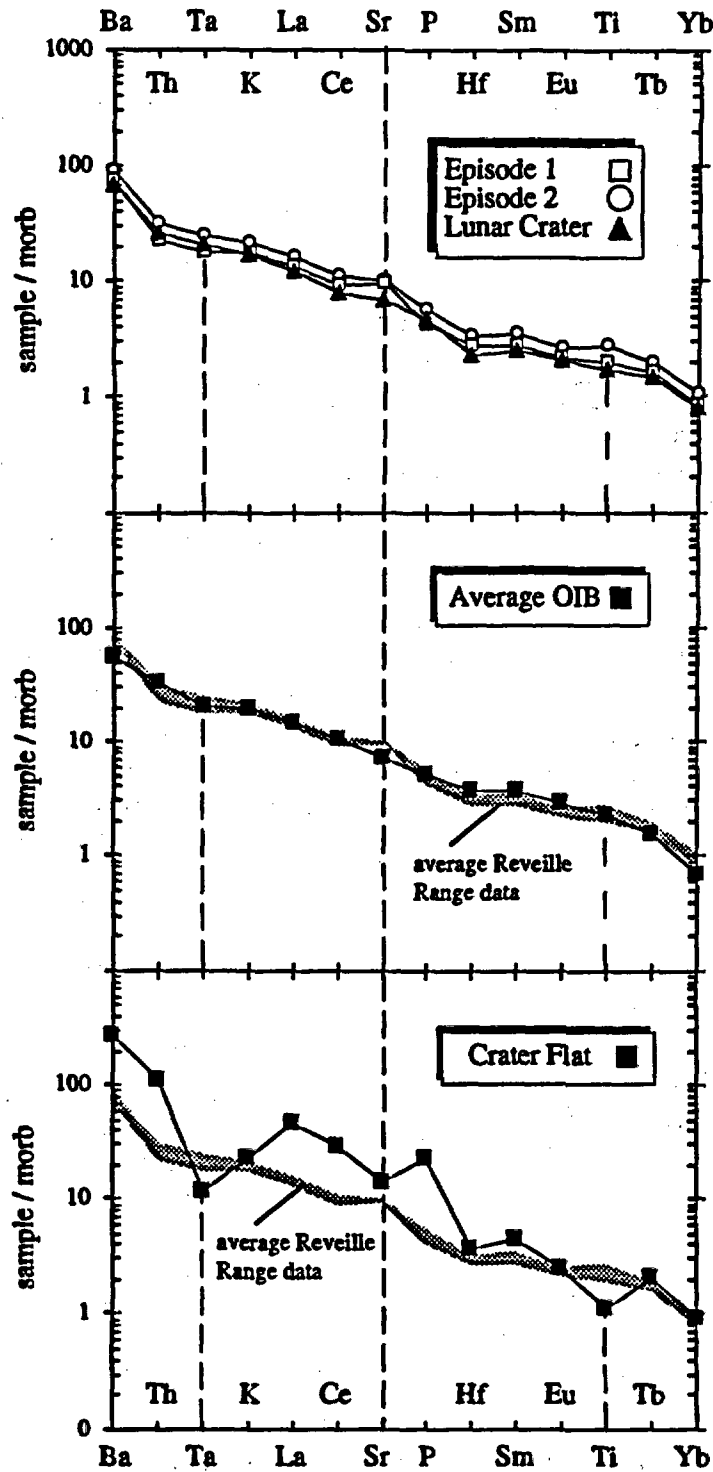


Figure 5: Normalized incompatible element concentrations of average episode 1 and episode 2 basalts compared with average ocean island basalt (OIB) and with the average Black Cone analysis from Crater Flat. Similarity of Reville Range data to average OIB suggests an asthenospheric mantle source. Average Black Cone analysis has low relative concentrations of Ta and Ti, which indicates a lithospheric source (Bradshaw et al., in press). OIB and MORB values are from Sun & McDonough (1989).

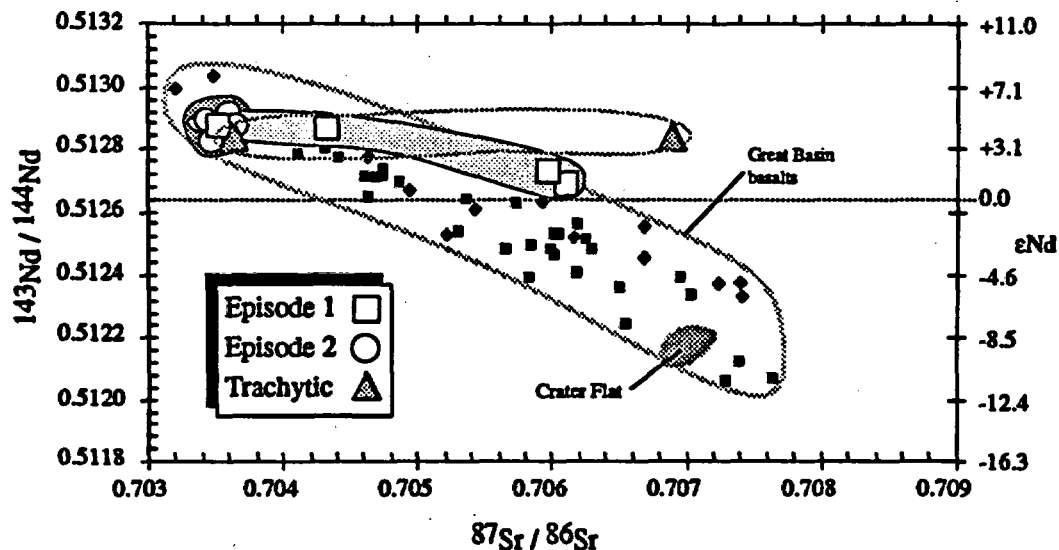


Figure 6: Sr and Nd isotopes for Reville Range rocks compared with field of Basin & Range basalts and samples from Crater Flat. The wide range in $^{87}\text{Sr}/^{86}\text{Sr}$ relative to $^{143}\text{Nd}/^{144}\text{Nd}$ in basalts of episode 1 and in the trachytic rocks is interpreted as the result of crustal assimilation. Narrow range in isotopic values for episode 2 basalts is consistent with the asthenospheric-type mantle source which is implied by the incompatible trace element data (see Figure 5). Filled diamonds are published data from the Northern Great Basin, filled squares are from the Southern Great Basin. Crater Flat data are from Bradshaw et al., (in press).

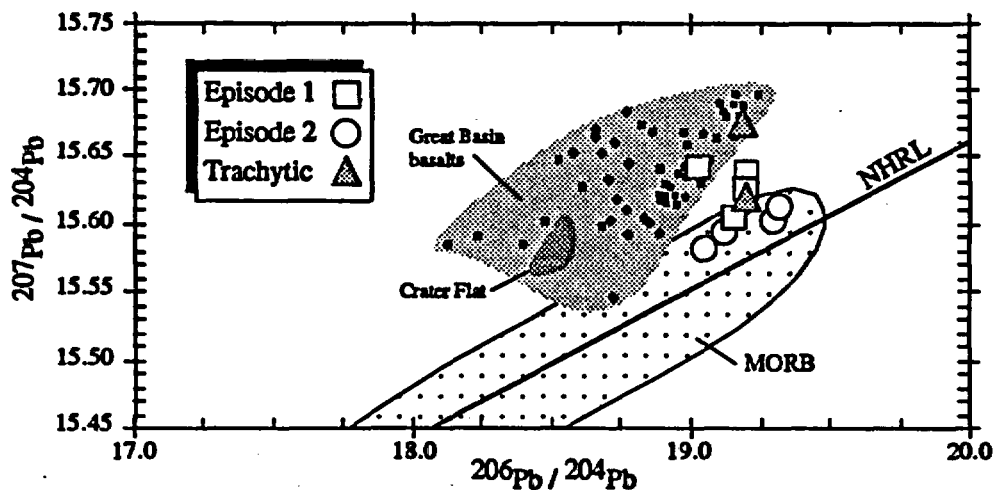


Figure 7: Pb isotope data for Reville Range rocks compared with field of Basin & Range basalts and samples from Crater Flat. Straight trend of the episode 2 data parallel to the mantle reference line (NHRL = northern hemisphere reference line, Hart, 1984) contrasts the episode 1 data and the trachytes which range to high $^{207}\text{Pb}/^{204}\text{Pb}$ relative to $^{206}\text{Pb}/^{204}\text{Pb}$. Lead isotope data for episode 2 basalts are consistent with an asthenospheric source (OIB-type mantle) that has not been contaminated by crust (see also Figures 5 & 6). Great Basin basalt and Crater Flat data as in Figure 6.

a small volume of trachytic melt (isotopically akin to episode 1 basalts) probably marked the death of this high-level magmatic system. It is unlikely that episode 2 basalts could have re-occupied the shallow episode 1 storage system without also showing isotopic evidence of crustal contamination. We assume therefore, that episode 2 eruptions were fed from a separate storage location. The widespread occurrence of clinopyroxene phenocrysts and megacrysts in episode 2 basalts, indicates that this storage location was deeper than during episode 1 time. This is confirmed at least in part, by the presence of mantle-derived xenoliths (dunites, harzburgites) and amphibole megacrysts in the youngest episode 2 flows in the Reville Range. These xenoliths provide good evidence that their host basalts were stored near the crust-mantle boundary, and were erupted rapidly without a significant period of storage within the shallow crust.

Discussion - Conclusions

Broad geochemical similarities among basalts of the Reville and Pancake ranges contrast those at Crater Flat and in other Pliocene and Pleistocene-age systems in the vicinity of Yucca Mountain (Figures 4-7). It is clear from the geochemical and spatial-temporal patterns outlined above, that the Reville Range and Pancake Range - Lunar Crater Volcanic Field are parts of a single volcanic system which became active approximately 6 m.y. ago, and was last active approximately 300,000 years ago (see also Foland & Bergman, 1992).

The geological and geochemical data suggest that as the Reville Range volcanic field grew older, there was a decrease in both the volume of magma produced and in the length of time that magma was stored in the crust. Episode 1 basalts were produced in the largest volume and were contaminated during storage in crustal magma systems. Episode 2 basalts were produced in much smaller volumes, they were not contaminated by lengthy storage in the crust, and in some cases they were erupted rapidly enough to carry mantle xenoliths and high pressure megacrysts (amphibole) to the surface.

Foland et al. (1987; 1988; 1991) and Foland and Bergman (1992) reached similar conclusions in their studies which have focused mostly on Pleistocene-age basalts in the Pancake Range - Lunar Crater Volcanic Field. In particular, they show that the youngest rocks in the Pancake Range (~300,000 years old) were produced in very small volumes, they were derived from an asthenospheric source uncontaminated by continental crust, and they frequently contain large quantities of mantle-derived and other high pressure xenoliths.

Future Work

From the standpoint of understanding small volume mafic volcanic systems in the Great Basin, detailed mapping and geochemical sampling similar to our studies in the Reville Range (e.g., Figure 2) will have to be done in the Pancake Range where there is a thick, poorly known

section of Pliocene-age volcanic rock. Our immediate goal is to outline the spatial-temporal development of the entire volcanic field within narrowly defined time-stratigraphic windows. To do this we require new $^{40}\text{Ar}/^{39}\text{Ar}$ ages to supplement our mapping and geochemical studies. The $^{40}\text{Ar}/^{39}\text{Ar}$ technique is the most accurate dating method that can be practically applied to basaltic rocks of Pliocene and Pleistocene age.

Ultimately our goal is to characterize the number and kind of volcanic events that have occurred during specific time periods (defined as narrowly as possible) throughout the 5-6 Ma development of the Reveille - Pancake system. This information will be most useful in evaluating the accuracy and viability of statistical models that have been applied to the problem of risk assessment in the vicinity of Yucca Mountain.

References

- Foland, K. A. & Bergman, S. C., 1992, Temporal and spatial distribution of basaltic volcanism in the Pancake and Reveille ranges north of Yucca Mountain, *Third International Conference on High Level Radioactive Waste Management*, LaGrange Park, IL, 2366-2371.
- Foland, K. A., Kargel, J. S., Lum, C. L. & Bergman, S. C., 1987, Time-spatial-composition relationships among alkali basalts in the vicinity of the Lunar Crater, south-central Nevada, *Geological Society of America Abstracts with Programs* 19, 666.
- Foland, K. A., Kargel, J. S., Schucker, D. E., Hubacker, F. A. & Bergman, S. C., 1988, Sources for Cenozoic alkalic basalts in the vicinity of the Lunar Crater volcanic field, south-central Nevada, *Transactions of the American Geophysical Union* 69, 519.
- Foland, K. A., Schucker, D. E., Smith, B. M., Todt, W. & Bergman, S. C., 1991, Isotope geochemistry of Cenozoic alkali basalts in the vicinity of the Lunar Crater volcanic field, south-central Nevada: O and Pb evidence for crustal components, *Geological Society of America Abstracts with Programs* 23, 45.
- Naumann, T. R., Smith, E. I. & Shafiqullah, M., 1990, Post-6 Ma intermediate (trachytic) volcanism in the Reveille Range, Central Great Basin, Nevada, *Geological Society of America Abstracts with Programs* 22, 72.
- Naumann, T. R., Smith, E. I., Shafiqullah, M. & Damon, P. E., 1991, New K-Ar ages for Pliocene mafic to intermediate volcanic rocks in the Reveille Range, Nevada, *Isochron West* 57, 12-16.

Section 3

**JOURNAL OF GEOPHYSICAL RESEARCH PAPER PUBLISHED BY
G.M. YOGODZINSKI, JULY 1993**

**Magmatic and Tectonic Development of the Western Aleutians:
An Oceanic Arc in a Strike - Slip Setting**

Magmatic and Tectonic Development of the Western Aleutians: An Oceanic Arc in a Strike-Slip Setting

G.M. YOGODZINSKI¹

Institute for the Study of the Continents and Department of Geological Sciences, Cornell University, Ithaca, New York

J.L. RUBENSTONE

Lamont-Doherty Earth Observatory of Columbia University, Palisades, New York

S.M. KAY, AND R.W. KAY

Institute for the Study of the Continents and Department of Geological Sciences, Cornell University, Ithaca, New York

The Paleogene Basement Series on Attu Island in the Western Aleutians is dominated by tholeiitic basalts chemically similar to mid-ocean ridge basalts (MORB; $La/Yb - 2$, $\epsilon Nd > +10.0$, $^{206}Pb/^{204}Pb < 18.4$). These basalts evolved in "open" magma systems. Contemporaneous rhyolites and albite granites are chemically analogous to silicic volcanic rocks of modern ocean ridges (e.g., Iceland, Galapagos Spreading Center). The occurrence of chemically arc-type tholeiitic basalts, with high Th/La and La/Ta relative to MORB, suggests that a depleted MORB-like mantle source was variably modified by a subduction component. The Attu Basement Series is not allochthonous. Geological and tectonic constraints imply formation in arc-adjacent, transtensional rifts that developed in a strike-slip regime that was established ~43 m.y. ago. Rifting of this kind may have produced much of the Western Aleutian crust between ~43 and 15 Ma. Subsequently, small volumes of crystal-rich andesite and dacite were erupted on Attu Island as well as throughout the Western Aleutians. These strongly calcalkaline rocks ($FeO^*/MgO \sim 1.1$, $CaO/Al_2O_3 \sim 0.35$ at 65% SiO_2) are chemically akin to magnesian andesites of Piip Volcano, a hydrothermally active seamount that overlies small dilational structures within the broadly transpressional regime of the modern western arc. This transpressional setting is inferred to have been established throughout the Western Aleutians approximately 15 m.y. ago. The switch from tholeiitic magmatism in a transtensional regime to strongly calcalkaline magmatism in a transpressional regime may have resulted from clogging of the Aleutian-Kamchatka junction with buoyant, subduction-related terranes. These terranes probably originated to the east and were transported by strike-slip motion along the western arc.

INTRODUCTION

An outstanding feature of the modern Aleutian subduction system is the regular decrease in the angle of Pacific-North America convergence that occurs between southern Alaska, where convergence is nearly orthogonal to the trench, and the westernmost arc, where relative Pacific-North America motion is approximately arc-parallel and convergence rates are consequently low (Figure 1). This geometry has produced a well-defined magmatic front and Wadati-Benioff Zone in the Central and Eastern Aleutians, but in the western arc there is no deep or intermediate-depth seismicity, and Pleistocene to Recent magmatism has been volumetrically minor [Scholl *et al.*, 1976; Borusk and Tsvetkov, 1982; Newberry *et al.*, 1986;

Boyd and Creager, 1991; Tsvetkov, 1991; Baranov *et al.*, 1991; Romick *et al.*, 1993; Yogodzinski *et al.*, 1993].

The general decrease in orthogonal convergence from east to west along the arc correlates with magma production rates over the past several million years [Marsh, 1982]. The relative motions of the Pacific, Eurasian, and North American plates in the North Pacific region have, however, been approximately constant since ~43 Ma [Engebretson *et al.*, 1985]. For this reason, Vallier *et al.* [1993] have suggested that the early magmatic rocks of the Western Aleutian Ridge formed largely prior to 43 Ma when convergence was at a higher angle. This view implies that Western Aleutian arc growth paralleled the earlier stages in the Central and Eastern Aleutians where voluminous magmatism between ~55 and ~37 Ma resulted in rapid growth of the arc crust to nearly its present thickness [Scholl *et al.*, 1970, 1987; Marlow *et al.*, 1973; Hein and McLean, 1980].

Contrasting early Tertiary magmatic histories imply, however, that the Western Aleutians has experienced a tectonic evolution unlike that of the central and eastern arc. Early and Middle Tertiary magmatic rocks of the Central and Eastern Aleutians have arc-type geochemical signatures [Kay and Kay, 1993], indicating a long-term history of subduction for this part of the arc [Kay *et al.*, 1983; Rubenstone, 1984; McLean

¹Now at Department of Geology, Hamilton College, Clinton, NY 13323

Copyright 1993 by the American Geophysical Union.

Paper number 93JB00714.
0148-0227/93/93JB-00714\$05.00

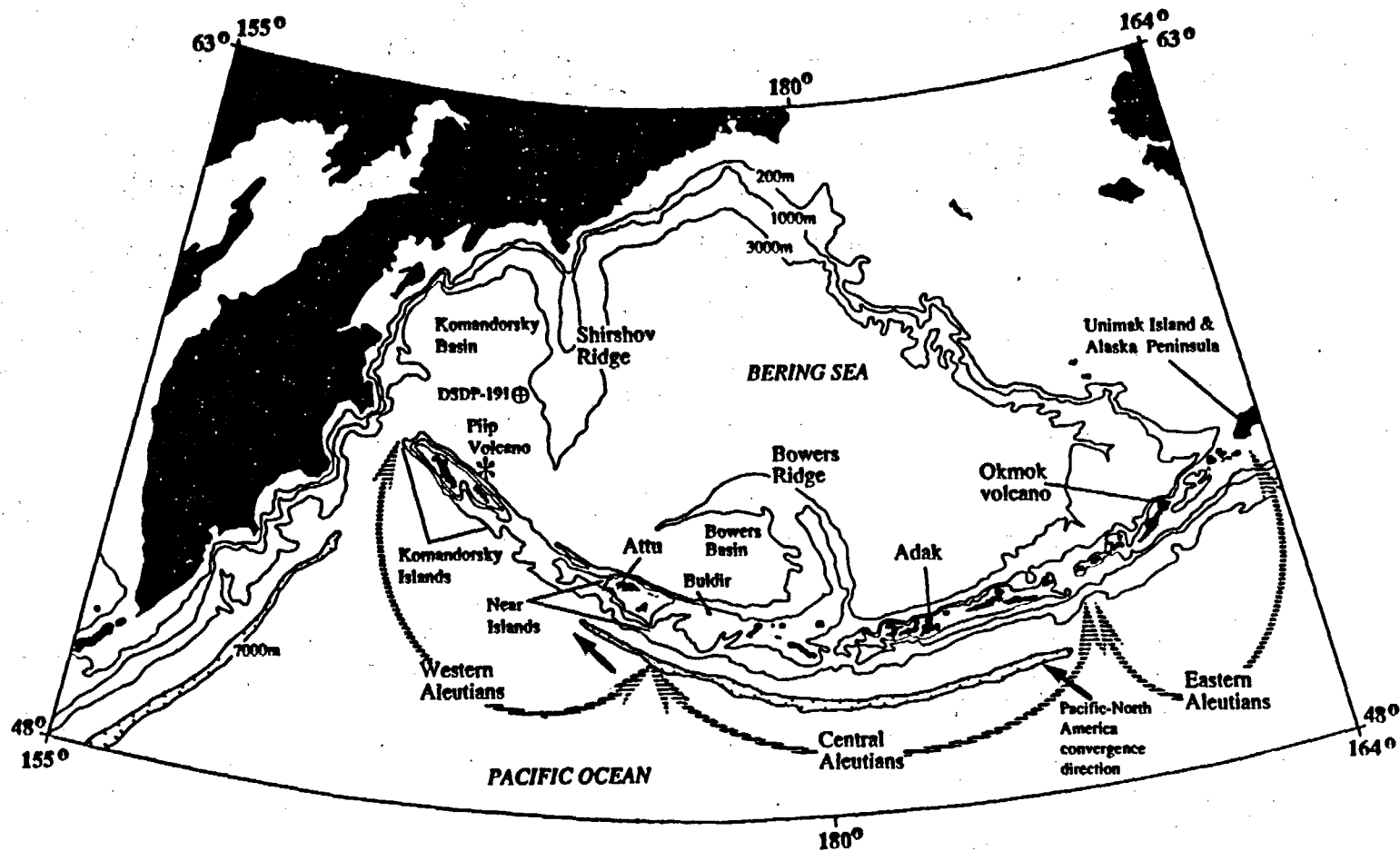


Fig. 1. Insular Aleutian arc and surrounding region. Bathymetry is from Scholl *et al.* [1986]. Modern Pacific-North America convergence in the western and central Aleutians (N49°W, 92 mm/yr and N42°W, 87 mm/yr, respectively) are from Engebretson *et al.* [1985, Table 5]. Piip Volcano in the far western arc is a hydrothermally active seamount [see Seliverstov *et al.*, 1990a, b; Baranov *et al.*, 1991; Romick *et al.*, 1993; Yogodzinski *et al.*, 1993].

and Hein, 1984; Hein and McLean, 1980; Kay et al., 1990; Kay and Kay, 1993]. This interpretation is consistent with past plate motions [e.g., Engebretson et al., 1985; Lonsdale, 1988] and with the chronology of magmatism in the Alaska-Bering Sea region [e.g., Scholl et al., 1987; Davis et al., 1989]. In contrast, magmatism in the Western Aleutians has undergone dramatic changes from mid-ocean ridge basalt (MORB)-like, to calcalkaline, boninitic, and alkaline compositions [Borusk and Tsvetkov, 1982; Rubenstone, 1984; Kay et al., 1986; Shelton, 1986; Tsvetkov, 1991; Volynets et al., 1992; Romick et al., 1993; Yogodzinski et al., 1993]. We infer that the diverse magmatic history of the western arc reflects the diverse tectonic history of the Western Aleutian-Bering Sea region, whereas the geochemical monotony of magmatism in the Central and Eastern Aleutians reflects the relatively simple tectonics of that region.

Exposures of the Western Aleutian Ridge occur on two bathymetrically distinct crustal blocks, the Russian Komandorsky Block in the west and the American Near Islands Block in the east (Figure 1). Here, we use the geochemistry of Eocene through Mio-Pliocene tholeiitic and calcalkaline magmatic successions on Attu Island in the Near Islands as a guide to the changing magmatic sources and evolving tectonics of the Western Aleutian region.

GEOLOGY OF ATTU AND THE NEAR ISLANDS

Attu Island is the largest, most accessible, and best exposed of the Western Aleutian Near Islands. Figure 2 summarizes the geology of Attu after Gates et al. [1971, Plate 80]. Five map units composed largely or entirely of volcanic and plutonic rocks were distinguished by Gates et al. [1971]. Our results indicate that these units may be combined into two broadly distinctive magmatic series. These are termed the Attu Basement Series and Attu Calcalkaline Series (Figure 2).

The Attu Basement Series

Map units of Gates et al. [1971] included within the Attu Basement Series are the earliest Attu rock units (mostly pillow lavas and volcanoclastics), the diabase-gabbro intrusions, and the albite granite-quartz keratophyre intrusions (Figure 2). The age of the Attu Basement Series is poorly constrained, but K-Ar and fossil evidence suggest a formation age between the late Eocene and late Oligocene [Vallier et al., 1993] (also see discussion below).

The oldest and volumetrically most important units in the Attu Basement Series are pillow lavas, volcanic breccias, and volcanoclastic rocks, with interbedded marine sedimentary

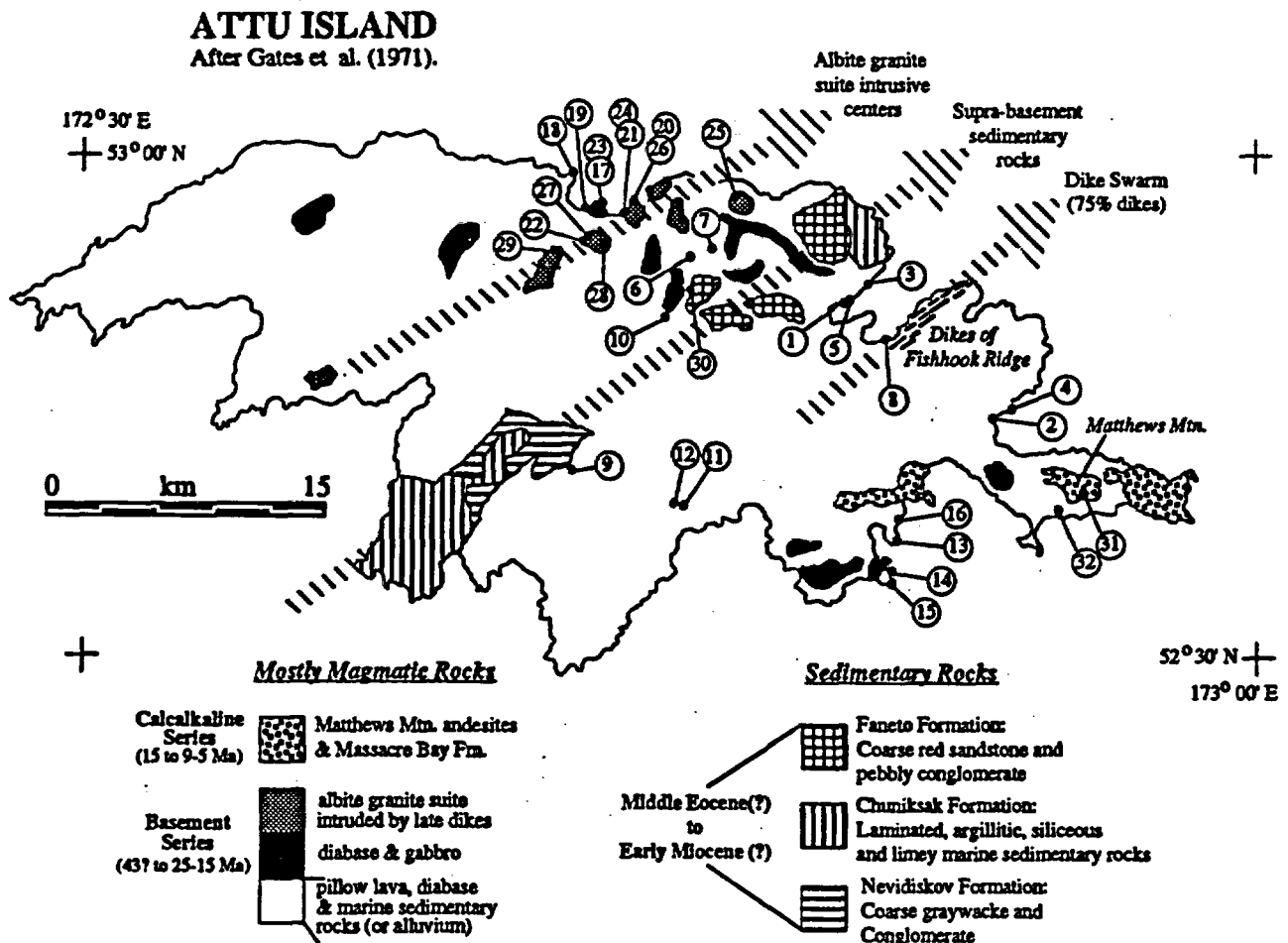


Fig. 2. Geologic sketch map of Attu Island. The Basement Series consists of the oldest map units from Gates et al. [1971]: pillow lavas, diabase-gabbro, albite granite, and quartz keratophyre. The Calcalkaline Series includes the Matthews Mountain andesites and volcanoclastics of the Massacre Bay Formation. Intrusive rocks of the Attu Basement Series that crosscut the Faneto Formation imply an older age for the Faneto Formation than assigned by Vallier et al. [1993]. See text for discussion of other age assignments. Large, dashed arrows highlight northeast trending belts thought to reflect the structural and magmatic alignment during formation of the Attu Basement Series. Sample locations are keyed to Tables 1a and 1b; see also Table 2.

rocks that include graywacke and conglomerate, widespread thinly bedded cherts, cherty argillites, and cherty shales [Gates et al., 1971; Marlow et al., 1973; Rubenstone, 1984]. Volcanic rocks within the Basement Series are dominantly mafic with phenocrysts (<10%) of plagioclase, olivine (now replaced by secondary minerals), and clinopyroxene in a generally ophitic to subophitic groundmass. Pervasive hydrothermal metamorphism in these rocks is usually subgreenschist facies but locally reaches amphibolite grade [Gates et al., 1971; Rubenstone et al., 1982; Vallier et al., 1993].

The volcanic and volcanoclastic units are intruded by a series of diabasic sills and dikes and by small plutons of medium-grained isotropic gabbro (diabase-gabbro intrusions of Gates et al. [1971]). Figure 2 shows only the largest gabbroic bodies [e.g., Shelton, 1986] and the well-developed dike swarm at Fishhook Ridge (75% dikes). These rocks range from ophitic diabase to hypidiomorphic gabbro. Mineralogically, they are dominated by plagioclase and clinopyroxene, with some olivine replaced by alteration minerals. There is a subgreenschist metamorphic overprint. Petrographically, the diabasic sills and dikes are broadly akin to the lavas they intrude.

Silicic volcanic and subvolcanic intrusive rocks of the Attu Basement Series occur in small intrusive centers (1-5 km² exposures) that form a NE trending belt across Attu Island (Figure 2). These silicic bodies are dominated by albite granite and rhyolite, with only a small amount of intermediate composition plutonic rock. We refer to these rocks collectively as the albite granite suite (Figure 2). The albite granites are medium grained (1-5 mm), generally nonfoliated, compositionally homogeneous, and free of mafic enclaves. They are mineralogically dominated by plagioclase and quartz (> 90 modal % of the rock) with minor clinopyroxene, Fe-Ti oxides, and occasional amphibole (total ~4-10 modal %). Biotite occurs in the mesostasis of the most quartz-rich samples. The rhyolites (including quartz keratophyre of Gates et al. [1971]) are generally crystal poor, with phenocrysts of plagioclase, Fe-Ti oxides, clinopyroxene, and occasional amphibole. When present, amphibole phenocrysts are euhedral, nonfibrous, and in some cases zoned, with brown cores and pleochroic blue-green rims. The most silicic rhyolites also contain phenocrysts(?) of rounded and embayed quartz. Intermediate composition rocks of the albite granite suite occur only as small, irregularly shaped plutonic bodies along the (lithologically) heterogeneous margins of the intrusions. These rocks are also mineralogically dominated by plagioclase, but they contain more clinopyroxene and amphibole and less quartz than the albite granites. Chlorite, epidote, and calcite are common alteration minerals, and apatite and zircon are common accessory minerals throughout the albite granite suite. It is an important point that the albite granite suite is volumetrically minor compared to the main mass of mafic rocks that makes up the Attu Basement Series (Figure 2).

The youngest rocks of the Attu Basement Series are a series of dikes, 1-2 m wide, that intrude the rocks of the albite granite suite. We refer to these as the late dikes (Figure 2). They are petrographically similar to the older volcanic rocks and the sills and dikes of the diabase-gabbro intrusive complex, although some (e.g., sample AT21) contain sparse phenocrysts of amphibole and Fe-Ti oxides.

In summary, intrusive rocks of the Attu Basement Series (the diabase-gabbro complex, the albite granite suite, and the late dikes) are thought to be only slightly younger than the volcanic rocks they intrude [Gates et al., 1971]. Analyses presented below indicate that these volcanic and plutonic rocks are related and represent aspects in the development of a single type of magmatic system that characterized early magmatism in the Near Islands.

The Attu Calcalkaline Series

Map units of Gates et al. [1971] included within the Attu Calcalkaline Series are the andesitic rocks of Matthews Mountain and the volcanoclastics of the Massacre Bay Formation (Figure 2). These rocks were deposited subaerially on an erosional surface formed on the Basement Series. Radiometric dating of lavas brackets the age of the Attu Calcalkaline Series at 15 to 5 Ma [DeLong and McDowell, 1975; Vallier et al., 1993].

Andesitic lavas, dikes, and subvolcanic intrusions at Matthews Mountain (Figure 2) are rich in plagioclase and contain primary hornblende. On neighboring Near Islands (unlabeled in Figure 1), the Attu Calcalkaline Series includes crystal-rich dacite porphyries that contain quartz, plagioclase, amphibole, and biotite [Gates et al., 1971]. These rocks are petrographically and geochemically similar to calcalkaline volcanic rocks of the modern Aleutian arc and thus are readily distinguished from older, mostly mafic rocks of the Attu Basement Series.

GEOCHEMISTRY

Most of the igneous rocks on Attu Island have undergone subgreenschist grade metamorphism. Our interpretation of the Attu data is therefore based largely on elements which are thought to be immobile. These are principally the rare earth elements (REE), Th, and the high field strength elements (HFSE). The consistency of the data presented here provides strong evidence that the magmatic features of the Attu rocks are preserved in these elements. For recent and thorough discussion of element mobility during alteration, the reader is referred to Dunning et al. [1991].

Geochemistry of the Mafic Volcanic Rocks

Basalts ($\text{SiO}_2 < 53\%$) and basaltic andesites ($\text{SiO}_2 = 53-56\%$) of the Attu Basement Series have been altered by exchange with seawater during hydrothermal metamorphism; they are Na_2O -enriched (up to 6-7%) and CaO-depleted (down to 6%) with highly variable K_2O (0.20-1.27% ; see Table 1), but their high FeO^* contents (up to 12.86%), high FeO^*/MgO (up to 2.5), and variably high TiO_2 contents (up to 1.98%) distinguish them as tholeiitic (Figure 3; Table 1; petrographic descriptions of analyzed samples in Table 2). These rocks are mineralogically and texturally uniform but can be grouped into two types, MORB-like and arc-like, on the basis of their trace element characteristics.

The MORB-like tholeiites are relatively depleted in light REE (LREE) and Th, with incompatible trace element characteristics similar to normal MORB (NMORB, Figures 4-6). A few LREE-enriched samples similar to enriched MORB are also included in this group (e.g., HO962A in Figure 5). Concentrations of the heavy REE (HREE; e.g., Yb) relative to compatible elements (Ni and Cr) in these basalts are also generally similar to those in MORB (Figure 7), but some samples have low compatible element concentrations, a characteristic that is commonly seen in arc basalts (Cr less than 30 ppm; see Figure 7). These low-Cr examples nonetheless retain the LREE-depleted signature of MORB and do not show the low HFSE character that is typical of arc volcanic rocks (Figures 5a and 6). In general, MORB-like Attu rocks differ consistently from NMORB only in their HREE patterns (note Tb/Yb in Figure 5). The Tb/Yb values of the Attu MORB-like tholeiites average ~ 0.30, which is substantially higher than NMORB $\text{Tb/Yb} = 0.220$ of Sun and McDonough [1989]. Note, however, that Juan de Fuca MORB also have Tb/Yb greater than Sun and McDonough's NMORB (e.g., Juan de Fuca $\text{Tb/Yb} \sim 0.255$ approximated from Kay et al. [1970] and Wakeman [1978]). Note also that the REE

TABLE 1a. Attu Island Whole Rock Major and Trace Element Analyses

	Map site/Specimen															
	MORB-like												Arc-like			
	1-P/ HO925B	2-P*/ SB1A	3-P*/ HO914B	4-P*/ SB5A	5-P*/ HO922	6-P/ AT61	7-P/ AT73	8-P/ HO962A	9-M/ AT114	10-M/ AT144	11-M/ AT101	12-P/ AT100	13-P*/ CP98	14-P*/ MP2	15-P*/ MP10	16-P/ CP916C
SiO ₂	49.37	49.70	49.04	51.40	49.79	48.50	50.58	49.47	53.28	51.52	52.77	55.55	53.59	53.46	52.85	56.53
TiO ₂	0.96	1.46	1.53	1.64	1.83	1.74	1.98	1.64	1.08	1.91	1.40	1.23	0.87	0.96	0.99	0.90
Al ₂ O ₃	18.67	15.49	18.45	15.31	15.47	16.25	16.75	18.00	15.72	16.35	15.61	15.52	16.06	16.17	16.79	16.65
FeO*	8.84	8.94	8.60	9.03	10.03	9.29	9.47	7.48	11.61	11.70	12.45	11.15	11.33	12.01	12.86	10.15
MnO	0.13	0.12	0.18	0.21	0.16	0.16	0.15	0.14	0.17	0.19	0.20	0.16	0.22	0.18	0.26	0.17
MgO	9.96	8.52	8.24	8.79	8.79	7.02	7.11	5.48	5.12	4.96	4.53	3.94	5.44	5.70	4.79	4.33
CaO	6.81	11.47	10.30	8.17	8.04	11.27	9.42	13.34	9.00	7.94	8.38	5.12	5.76	4.73	6.61	7.03
Na ₂ O	3.78	3.82	3.38	3.37	3.84	3.60	4.66	3.08	2.90	4.84	3.45	6.59	4.70	4.70	5.95	3.27
K ₂ O	0.80	0.23	0.20	0.76	1.27	0.46	0.28	0.79	1.12	0.32	0.38	0.28	1.12	2.83	0.11	0.25
Total	99.32	99.75	99.92	98.68	99.22	98.29	100.40	99.42	100.00	99.73	99.17	99.54	99.16	100.88	101.38	99.28
La	2.33	3.90	6.26	6.91	6.10	5.22	7.36	9.64	2.40	3.98	3.09	3.07	4.51	4.89	6.53	6.36
Ce	6.73	12.7	18.4	20.3	18.8	15.8	19.6	22.1	6.36	11.2	8.75	8.54	11.3	12.9	16.3	15.3
Nd	4.5	10.1	13.4	14.5	14.9	12.4	15.6	15.0	6.3	9.5		8.1				
Sm	2.08	3.22	3.75	4.37	4.51	4.16	5.10	4.25	2.22	3.43	3.04	3.02	2.75	2.99	3.26	3.47
Eu	0.80	1.19	1.36	1.54	1.57	1.41	1.78	1.30	0.75	1.41	1.09	0.99	0.93	0.95	1.27	1.09
Tb	0.50	0.81	0.94	1.09	1.04	0.95	1.11	0.81	0.58	0.87	0.80	0.79	0.57	0.63	0.64	0.79
Yb	1.69	2.47	2.73	3.30	3.23	3.20	4.28	2.75	2.37	2.98	2.87	3.03	2.00	2.26	2.22	2.69
Lu	0.253	0.385	0.422	0.518	0.487	0.430	0.680	0.410	0.358	0.420	0.422	0.439	0.297	0.332	0.308	0.359
Sr	313	183	229	206	267	414	355		172	286	231	111	255	494	235	269
Ba	104	40	35	65	204	125	38	87	167	55	84	31	392	1526	16	42
Cs	0.18	0.19	0.28	0.36	0.30	0.86	0.14	0.14	0.13	0.18	0.12	0.05	0.06	0.30		0.07
U		0.12	0.31	0.07	0.77	0.09	0.30	0.43	0.10		0.05	0.06	0.15	0.11	0.23	0.06
Th	0.10	0.22	0.38	0.44	0.30	0.23	0.16	0.90	0.24	0.14	0.19	0.16	0.11	0.49	0.44	0.18
Hf	1.41	2.47	3.00	3.54	3.41	3.21	4.00	3.34	1.60	2.22	2.06	2.16	1.58	1.83	1.61	1.62
Ta	0.12	0.18	0.37	0.30	0.26	0.31	0.46	1.20	0.11	0.30	0.27	0.13	0.05	0.07	0.06	0.04
Sc	35	36	36	3	37	38	42	32	42	36	36	29	40	43	43	39
Cr	269	408	363	407	342	348	263	328	26	18	13	13	18	15	32	24
Ni	103	185	187	153	168	171	127	206	14	7	13	10	9	14	17	16
Co	43	44	41	38	44	45	44	40	37	28	40	29	36	38	43	32

Map is keyed to Figure 2; letter refers to rock-type or occurrence (P is pillow basalt, M is massive diabase). Major element analyses are by electron microprobe, trace element analyses are by instrumental neutron activation analysis. Technique descriptions and standard analyses are given by *Kay and Kay* [1988] and *Kay et al.* [1987]. Analytical precision on trace elements is given by *Romick et al.* [1992].

*Analysis from *Rubenstein* [1984].

TABLE 1b. Attu Whole Rock Major and Trace Element Analyses

	Map Site / Specimen															
	Late Dikes						Albite Granite-Suite						Calcalkaline			
	17-D/ AT11	18-D/ AT50	19-D/ AT16	20-D/ AT27	21-D/ AT22	22-D/ AT21	23-G/ AT6	24-IC/ AT23	25-R/ AT65	26-R/ AT29	27-R/ AT19	28-AG/ AT3	29-AG/ AT56	30-R/ AT143	31-A*/ AT8032	32-A/ AT83
SiO ₂	49.90	50.63	48.70	49.75	53.17	58.35	47.48	60.92	72.30	72.99	73.79	74.51	76.72	76.99	58.20	56.94
TiO ₂	2.16	2.29	2.95	3.00	1.85	2.04	4.44	1.34	0.30	0.43	0.29	0.46	0.22	0.25	0.65	0.61
Al ₂ O ₃	15.50	15.48	15.58	14.64	16.60	16.24	15.35	17.21	13.80	14.45	13.79	12.93	12.65	12.65	18.66	18.03
FeO*	10.42	10.68	11.78	13.02	9.75	8.51	13.30	6.17	2.37	1.84	2.71	2.12	1.16	1.41	5.72	6.13
MnO	0.17	0.18	0.21	0.22	0.17	0.12	0.25	0.10	0.04	0.03	0.04	0.03	0.02	0.02	0.15	0.12
MgO	6.57	6.41	7.50	4.38	5.31	3.67	4.91	1.77	0.14	0.39	0.24	0.30	0.22	0.16	4.44	4.59
CaO	8.60	8.60	7.33	7.72	5.87	3.94	10.21	3.87	0.45	0.79	0.39	0.38	0.71	0.49	6.83	6.67
Na ₂ O	3.84	3.95	4.32	4.93	5.80	6.12	3.35	7.53	5.89	7.15	6.84	6.43	4.80	5.54	4.03	3.47
K ₂ O	1.57	1.18	0.53	0.71	1.01	1.87	0.54	0.83	3.31	1.59	1.61	2.64	3.14	2.19	1.12	1.56
Total	98.73	99.40	98.90	98.37	99.53	100.86	99.83	99.74	98.60	99.66	99.70	99.80	99.64	99.70	99.80	98.12
La	8.66	9.30	11.90	11.4	13.7	23.2	5.11	16.4	32.7	26.8	28.0	36.5	20.4	24.6	8.80	6.85
Ce	24.5	25.1	33.9	32.0	34.6	50.9	14.0	41.0	79.8	69.1	59.5	93.2	53.0	54.0	20.1	15.8
Nd		18.2	24.7	22.3	23.2			32.6	39.1	41.8		58.9	24.8	26.4	12.7	10.8
Sm	5.33	5.52	7.69	6.83	6.11	9.41	4.03	9.42	9.63	9.87	10.4	15.4	5.84	5.34	2.72	2.52
Eu	1.87	1.78	2.37	2.24	1.98	2.86	1.82	5.56	1.54	2.36	2.31	3.23	0.80	0.69	0.78	0.74
Tb	1.11	1.22	1.67	1.37	1.20	1.80	0.87	1.67	1.85	1.80	1.93	2.84	1.22	0.87	0.40	0.37
Yb	3.46	3.93	5.32	4.35	3.83	6.64	2.04	3.60	8.65	8.20	9.15	12.60	6.37	5.05	1.56	1.50
Lu	0.480	0.550	0.750	0.600	0.540	0.990	0.280	0.490	1.28	1.19	1.42	1.92	0.900	0.700	0.210	0.215
Sr	531	399	229	158				468								
Ba	597	246	82	97	212	308	91	317	349	276	236	279	304	335	375	412
Cs	0.15	0.23	0.13	0.02	0.36	0.03	0.15	0.05	0.17	0.02	0.06	0.15	0.15	0.02	0.10	0.17
U	0.09	0.18	0.23	0.23	0.49	0.91		0.11	1.83	1.28	1.36	2.37	1.88	2.13	0.71	0.53
Th	0.43	0.45	0.74	0.57	1.17	1.71	0.18	0.57	4.25	2.47	3.10	5.19	5.02	5.23	1.14	0.83
Hf	3.79	4.17	6.28	4.61	5.17	7.86	1.82	2.10	14.19	11.80	13.70	16.20	5.94	5.18	2.69	2.43
Ta	0.54	0.52	0.87	0.61	0.65	0.99	0.56	0.87	2.81	1.82	2.33	3.01	2.43	1.61	0.20	0.12
Sc	45	41	37	38	30	26	49	20	7	6	12	9	2	2	19	19
Cr	137	124	119	8	38	34	5	3	2	5	13	8	5	13	105	111
Ni	34	46	69	14	37	12	1	12	1	4	6	7	2	2	40	51
Co	40	40	43	38	36	24	34	22	20	21	10	9	4	6	21	22

Map is keyed to Figure 2; letter refers to rock type or occurrence (D is dike, G is gabbro/diorite, IC is intermediate composition plutonic rock, AG is albite granite, R is rhyolite, A is hornblende andesite). Major element analyses are by electron microprobe; trace element analyses are by instrumental neutron activation analysis. Technique descriptions and standard analyses are given by Kay and Kay (1988) and Kay et al. (1987). Analytical precision on trace elements is given by Romick et al. (1992).

*Analysis from Rubenstone (1984).

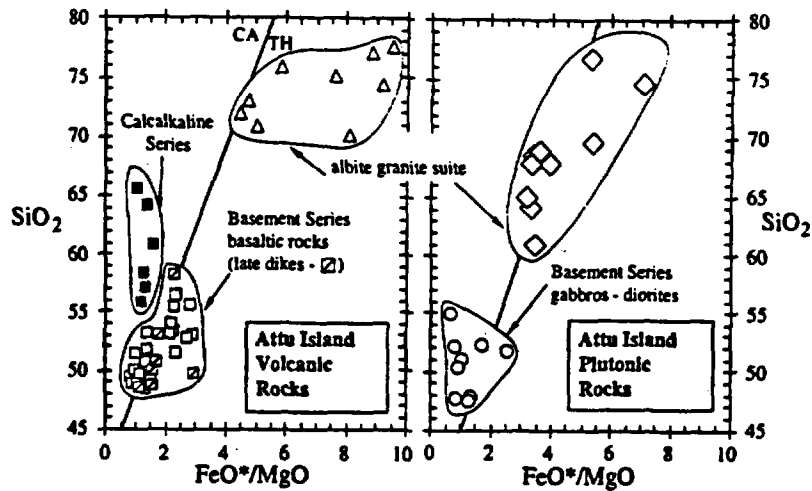


Fig. 3. SiO_2 versus FeO^*/MgO for magmatic rocks of Attu Island. Note that the Basement Series rocks are bimodal with a compositional gap between 60 and 70% SiO_2 . Basement Series gabbros and diorites include samples from the dominantly silicic intrusive centers of the albite granite suite (e.g., sample AT6, Table 1b; also see text). Data from Aggatu Island (large, unlabeled Near Island in Figure 1) are included in the Attu Calcalkaline Series. Calcalkaline - tholeiitic line from Miyashiro [1974]. Data from Table 1 here, Gates et al. [1971], Shelton [1986], and unpublished Cornell data.

pattern of the Komandorsky Basin basalt is like that of the Attu MORB-like tholeiites suggesting that this is a regional mantle characteristic (Figure 4).

The arc-like tholeiites, the second type of Attu basalt, have all of the trace element characteristics expected in subduction-related volcanic rocks. They have relatively low concentrations of HREE (e.g., low Yb relative to Cr; see Figure 7), and they are flat to slightly enriched in the LREE with high relative Th compared to the MORB-like samples (Figures 4 and 5). Most characteristically, the Attu arc-like tholeiites have low relative concentrations of the HFSE (Figures 4b, 5c, and 6).

Isotopic characteristics of the Attu MORB-like and arc-like tholeiites are broadly consistent with their trace element and petrological affinities. All of the Attu tholeiites have ϵNd within the range of North Pacific MORB (Figure 8), but on average, the MORB-like samples are more radiogenic (+10 to +12) than the arc-like samples (+9 to +10). High $^{87}\text{Sr}/^{86}\text{Sr}$ in the Attu rocks (> 0.7030 ; see Figure 8) relative to NMORB are thought to reflect postmagmatic alteration [Rubenstone et al., 1982]. In contrast, Pb isotope ratios cluster in the nonradiogenic region of the North Pacific MORB field (Figure 9) and are consistent with geochemical parameters that are resistant to hydrothermal exchange (e.g., high $^{207}\text{Pb}/^{204}\text{Pb}$ and Th/Ta with low $^{143}\text{Nd}/^{144}\text{Nd}$ in the arc-like rocks). The linear trend of the Attu basalts on Pb-Pb diagrams (e.g., Figure 10) suggests that disruption of $^{238}\text{U}/^{204}\text{Pb}$ by alteration has been relatively minor because 30-40 m.y. of radioactive decay have not produced highly variable $^{206}\text{Pb}/^{204}\text{Pb}$ [e.g., Hamelin et al., 1984]. The Pb isotope ratios of the MORB-like and arc-like tholeiites thus appear to be magmatic values.

Geochemistry of the Albite Granite Suite

Albite granites ($\text{SiO}_2=67-77\%$) and compositionally equivalent rhyolites have high Na_2O (4.3-7.2%), low CaO (0.2-1.3%), and variable K_2O (1.8-3.3%) which generally increases with increasing SiO_2 . These rocks have high incompatible trace element concentrations (La up to $\sim 100\text{X}$ chondrites), they are slightly Th and LREE-enriched (chondrite-normalized La/Sm $\sim 2.0-2.5$), and have flat HREE

patterns (normalized Tb/Yb ~ 1.0 , Figure 11). Large negative Eu anomalies in the albite granites and rhyolites increase with increasing SiO_2 and REE abundance (up to $\text{SiO}_2=75\%$, $\text{Eu}/\text{Eu}^*=0.60$, and La= 97X chondrites). At higher SiO_2 (up to 77%), Eu anomalies continue to increase (to $\text{Eu}/\text{Eu}^*=0.40$), whereas REE and Hf concentrations drop sharply and the most incompatible elements (Th, U, etc.) continue to increase or remain unchanged (Figure 11 and Table 1b).

The rhyolites and albite granites have Nd and Sr isotopic compositions that are broadly similar to the MORB-like tholeiites. They have ϵNd (8.6-9.6) that is on average slightly less radiogenic than North Pacific MORB, and $^{87}\text{Sr}/^{86}\text{Sr}$ that are high relative to ϵNd (Figure 8). As in the basaltic rocks, high $^{87}\text{Sr}/^{86}\text{Sr}$ in the rhyolites and albite granites was probably produced by exchange with seawater Sr. The Pb isotopic compositions of the silicic rocks are distinctly more radiogenic than the MORB-like basalts; $^{207}\text{Pb}/^{204}\text{Pb}$ and $^{208}\text{Pb}/^{204}\text{Pb}$ in the rhyolites and albite granites overlap the most radiogenic of the MORB-like and arc-like tholeiites, while $^{206}\text{Pb}/^{204}\text{Pb}$ in the silicic rocks extends to much higher values (Figure 10 and Table 3).

Intermediate composition rocks (SiO_2 58-66%) have extremely high Na_2O (6.3-8.1%), relatively low CaO (1.3-1.4%), and highly variable K_2O (0.16-2.0%). Most of the intermediate composition plutonic rocks have either no Eu anomaly, a small positive Eu anomaly ($\text{Eu}/\text{Eu}^*=1.1-1.2$), or in one case a large positive Eu anomaly ($\text{Eu}/\text{Eu}^*=1.8$; Figure 12). Isotopic analyses are not available for the intermediate composition plutonic rocks. On the basis of their mineralogy, texture, and geochemistry, the intermediate composition plutonic rocks appear to be crystal cumulates.

Geochemistry of the Late Dikes

The late dikes are also tholeiitic (high FeO^* , FeO^*/MgO), and they fall along approximately the same fractionation trends as most of the Basement Series MORB-like tholeiites (e.g., Figure 7). The late dikes are however, more evolved, ranging to ferrobasalt (TiO_2 up to 3.0%, FeO^* up to 13%, FeO^*/MgO up to 2.8), and andesitic compositions (sample AT21, Table 1) with higher incompatible element abundances

TABLE 2. Sample Locations and Petrography

Sample	Structure	Rock Type	Phenocrysts	Latitude	Longitude	Elevation m (feet)
HO925B	pillow lava	basalt	pl	52°56.14'N	173°07.88'E	0
SB1A	pillow lava	basalt	ol	52°52.96'N	173°16.10'E	0
HO914B	pillow lava	basalt	aphyric	52°56.14'N	173°07.88'E	0
SB5A	pillow lava	basalt	ol	52°52.91'N	173°16.21'E	0
H922	pillow lava	basalt	pl-ol-cpx	52°56.22'N	173°08.40'E	0
AT61	pillow lava	basalt	aphyric with cpx megacrysts	52°57.95'N	173°00.10'E	671 (2200)
AT73	pillow lava	basalt	pl	52°58.32'N	173°01.75'E	701 (2300)
H962A	pillow lava,	basalt	aphyric	52° 55.04'N	173°10.05'E	0
AT114	massive diabase	basaltic andesite	pl-cpx	52°51.20'N	172°55.30'E	640 (2100)
AT144	massive diabase	basalt	aphyric	52°55.45'N	172°59.75'E	335 (1100)
AT101	massive diabase	basalt	aphyric	52°50.10'N	173°00.45'E	533 (1750)
AT100	massive diabase	basaltic andesite	aphyric	52°50.10'N	173°00.35'E	457 (1500)
CP98	pillow lava	basalt	pl-cpx-olv	52°49.08'N	173°10.83'E	0
MP2	pillow lava	basalt	pl-ol	52°48.40'N	173°10.44'E	0
MP10	pillow lava	basalt	pl-ol	52°47.82'N	173°08.67'E	0
CP916C	pillow lava	basalt	pl-cpx	52°49.59'N	173°10.91'E	0
AT11	dike	basalt	pl-cpx	52°58.60'N	172°56.00'E	0
AT50	dike	basalt	pl-cpx-olv	52°59.65'N	172°54.60'E	0
AT16	dike	basalt	pl-cpx	52°58.62'N	172°55.40'E	0
AT27	dike	basalt	aphyric	52°58.80'N	172°57.60'E	0
AT22	dike	basaltic andesite	pl-cpx-olv	52°58.55'N	172°57.45'E	0
AT21	dike	andesite	aphyric with trace amph-ox.	52°57.60'N	172°54.70'E	472 (1550)
AT6	stock	gabbro	pl-cpx-ox-amph	52°58.52'N	172°56.35'E	0
AT23	stock	plutonic rock	pl-ox-amph-qtz	52°58.55'N	172°57.45'E	0
AT65	dike	rhyolite	pl-ox	52°59.40'N	173°01.10'E	76 (250)
AT29	lava	rhyolite	pl-amph-ox	52°58.80'N	172°57.60'E	0
AT19	lava	rhyolite	pl-ox	52°57.85'N	172°55.00'E	457 (1500)
AT3	stock	albite granite	pl-qtz-cpx-ox	52°57.60'N	172°56.25'E	472 (1550)
AT56	stock	albite granite	pl-qtz-ox-biot- amph	52°56.65'N	172°53.00'E	76 (250)
AT143	sill intruding Faneto Formation	rhyolite	pl-qtz.	52°56.15'N	173°01.30'E	640 (2100)
AT8032	stock	andesite	pl-amph-rich	52°51.04'N	173°18.5'E	vicinity of Alexai Pass
AT83	dike	andesite	pl-amph-rich	52°49.80'N	172°17.50'E	0

Mineral abbreviations are cpx (clinopyroxene), olv (olivine), pl (plagioclase), ox (Fe-Ti oxides), and amph (amphibole). Phenocryst phases in volcanic rocks and minerals in plutonic rocks are listed in order of decreasing abundance. The former presence of olivine is inferred from alteration products.

(e.g., La = 20-40X chondrites) and lower compatible element abundances. The late dikes have, on average, higher La/Sm, $^{207}\text{Pb}/^{204}\text{Pb}$, and lower average ϵNd than the older MORB-like tholeiites (Figures 4-10). None of the late dikes have the HFSE-depleted trace element signature of the arc-like basement tholeiites.

Geochemistry of the Matthews Mountain Andesites and Other Western Aleutian Calcalkaline Rocks

The Calcalkaline Series rocks are distinguished from those of the Basement Series by their silicic-to-intermediate composition ($\text{SiO}_2=55-65\%$) and low FeO^*/MgO (1.0-1.5,

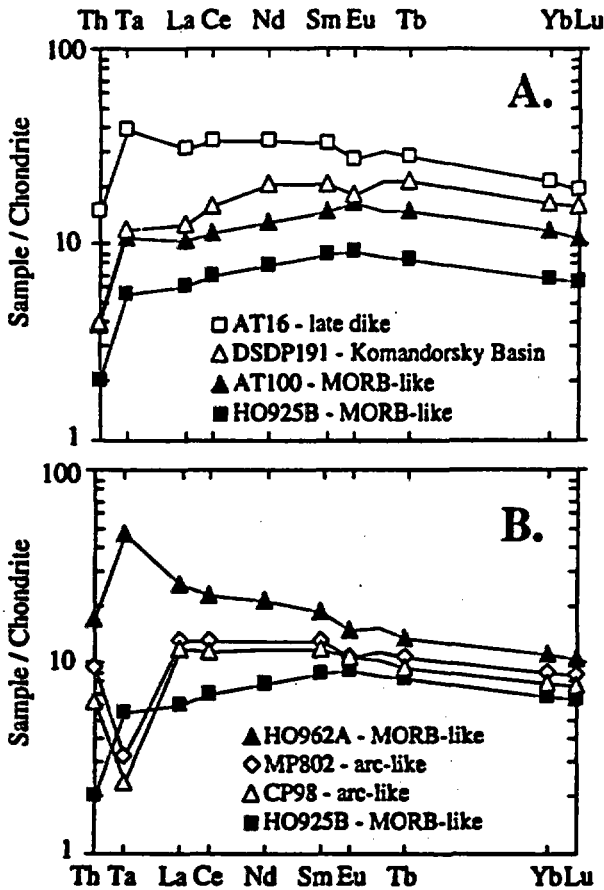


Fig. 4. Chondrite-normalized rare earth elements (REE), Th, and Ta in mafic volcanic rocks of the Attu Basement Series and in Komandorsky Basin basalt (DSDP-191; analysis from Rubenstone [1984]). In Figure 4a, note that mid-ocean ridge basalt (MORB)-like samples are light REE-depleted, similar to the Komandorsky Basin basalt, whereas the late dike sample has slightly higher La/Sm. Figure 4b includes a light REE-enriched MORB-like sample similar to enriched MORB (see also Figure 5). Note also that arc-like samples have high Th and low Ta but cannot be distinguished by their REE patterns alone. Normalizing values are Leedy Chondrite: Th (0.050), Ta (0.022), La (0.378), Ce (0.976), Nd (0.716), Sm (0.230), Eu (0.0866), Tb (0.0589), Yb (0.249), and Lu (0.0387).

Figure 3). As noted above, the Near Islands Calcalkaline Series is petrographically diverse. The discussion here focuses principally on the Matthews Mountain andesites which are located on Attu (Tables 3 and 4). These rocks appear to be broadly representative of middle Miocene magmatic rocks throughout the Near Islands and on the Komandorsky Islands of the westernmost arc (also see discussion below).

The Matthews Mountain andesites have geochemical characteristics similar to calcalkaline rocks of the modern Central and Eastern Aleutian arc. They are relatively rich in large ion lithophile and LREE (La/Yb-5, Ba/La-40-60) and have low relative HFSE abundances (Figures 6 and 13). The Matthews Mountain andesites are, however, distinct from the Central and Eastern Aleutian suite in two important ways. First, incompatible element abundances (especially Th and HREE) are frequently lower than in calcalkaline samples of equivalent SiO₂ content from the central and eastern arc (Figure 14); second, the Matthews Mountain andesites are isotopically more similar to MORB. The MORB-like isotopic character is seen most clearly in Pb-Pb plots where the Matthews

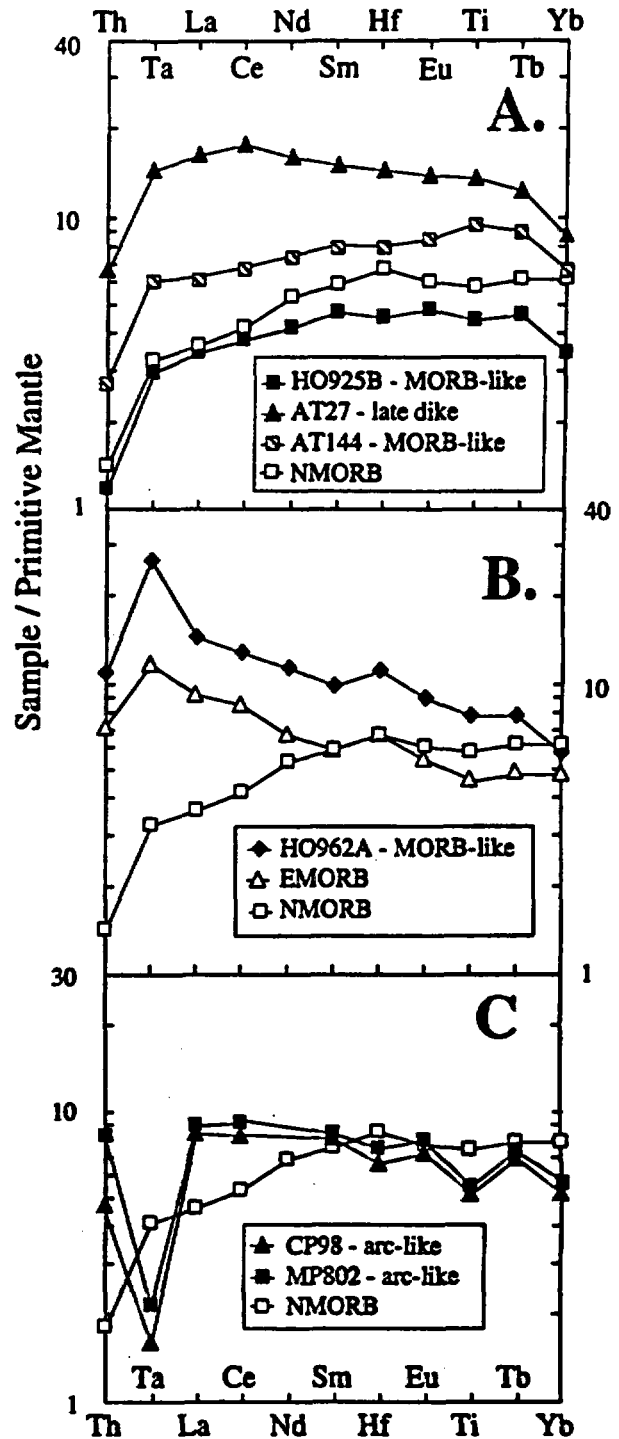


Fig. 5. Immobile-incompatible elements in Attu Basement Series basalts normalized to primitive mantle. In Figure 5a, note the broad similarity of the late dikes to the mid-ocean ridge basalt (MORB)-like samples and to normal MORB. Note also that sample AT144, which has some characteristics of the arc-like samples (Cr-20, Yb-3 ppm; see Figure 7 and Table 1a) is MORB-like with respect to its incompatible trace element characteristics. In Figure 5b, note the similarity of pillow lava HO962A and enriched MORB. In Figure 5c, note the low relative concentrations of Ti, Hf, and Ta and the high relative concentrations Th in the arc-like Attu basalts. MORB and normalizing values are from Sun and McDonough [1989]. Eu value is interpolated between Sm and Tb from REE patterns for Attu samples with small negative Eu anomalies.

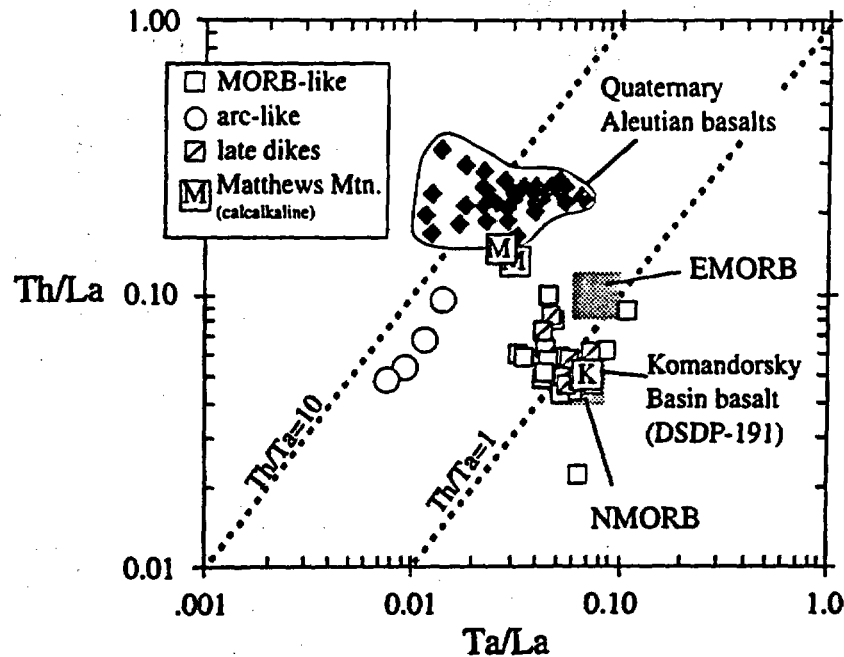


Fig. 6. Th/La versus Ta/La for Attu rocks compared to mid-ocean ridge basalts (MORB) and Quaternary basalts of the Central and Eastern Aleutians. Note similarity of Attu MORB-like tholeiites and late dikes to the Komandorsky Basin basalt and to MORB. Note also similarity of Matthews Mountain andesites to Aleutian basalts. Attu arc-like basalts have Ta/La ratios like Quaternary Aleutian suite but lower relative Th concentrations. MORB values from Sun and McDonough [1989]. Data are from Table 1, and Kay and Kay [1993].

Mountain andesites are indistinguishable from North Pacific MORB (Figure 10). Similarly, ϵNd in the Matthews Mountain andesites overlap with the most radiogenic of the modern Aleutian suite and with the least radiogenic of North Pacific MORB (Figure 8).

MORB-like isotopic characteristics and low relative Th contents are not typical of calcalkaline magmatic rocks of the modern Central and Eastern Aleutian arc. These characteristics are, however, seen in Miocene volcanic and subvolcanic rocks of the far Western Aleutian Komandorsky Islands [Borusk and Tsvetkov, 1982; Tsvetkov, 1991] and in Recent volcanic rocks of Piip Volcano [Yogodzinski et al., 1993; Romick et al., 1993] (locations in Figure 1). Post middle Miocene Western Aleutian magmatic rocks (Near Islands, Komandorsky Islands, and Piip Volcano) have lower FeO^*/MgO and $\text{CaO}/\text{Al}_2\text{O}_3$ than most calcalkaline rocks of the modern Central and Eastern Aleutian arc, and in this respect the Western Aleutian rocks form a more strongly calcalkaline series (Figure 15).

DISCUSSION AND GEOCHEMICAL MODELING

Evidence for a Rift Tectonic Setting

Small geochemical differences notwithstanding, source characteristics of the Attu Basement Series rocks are unmistakably those of NMORB. It is thus an important first-order conclusion that during middle Eocene through late Oligocene time the mantle beneath the Western Aleutians was a depleted peridotite similar to the source of modern MORB.

Beyond similarities in source chemistry, the Attu Basement Series rocks appear to have formed by processes physically similar those that operate at modern oceanic or back-arc spreading centers. The magmatic sequence on Attu began with the eruption of voluminous, chemically MORB-like tholeiitic

basalts, progressed to the formation of highly evolved silicic differentiates (albite granites), and ended with the intrusion ferrobasic and andesitic dikes (late dikes). This sequence is similar to that observed at propagating oceanic rifts [Christie and Sinton, 1981] and is reasonable within the context of physical-chemical models of ocean ridge magma chambers [Sinton and Detrick, 1992].

A rift tectonic setting is also implied by the style of metamorphism on Attu. Most of the Basement Series rocks are subgreenschist in grade, but Rubenstone [1984] and Rubenstone et al. [1982] noted that metamorphic gradients are locally high, reaching amphibolite facies at the Fishhook Ridge dike swarm. This metamorphic style contrasts with that in basement assemblages of the Central and Eastern Aleutians (e.g., Adak), where metamorphism resulted from fracture-controlled hydrothermal circulation of meteoric water (low $\delta^{18}\text{O}$) driven by heat from the younger plutonic bodies [Perfit and Lawrence, 1979; Rubenstone et al., 1982; Kay, 1983]. The style of metamorphism on Adak is like that expected in an emergent island arc. The style on Attu is similar to that produced by dynamic hydrothermal metamorphism beneath oceanic rift valleys [Bonatti et al., 1975], and is common in ophiolites. Indeed, the abundance of pillow basalts and laminated marine sedimentary rock in the Near Islands prompted Wilcox [1956] to comment that except for the absence of serpentinized peridotite, the Attu Basement Series was similar to an ophiolite. Such characteristically oceanic assemblages are not found in early and middle Tertiary sequences of the Central and Eastern Aleutians.

If the Attu crust formed by a processes broadly analogous to seafloor spreading or back-arc rifting, then crystal-liquid fractionation in the Attu tholeiites may also follow the characteristic evolutionary behavior of modern ocean-ridge systems. A plot of incompatible element enrichment (relative to the most primitive sample) versus FeO^*/MgO shows that

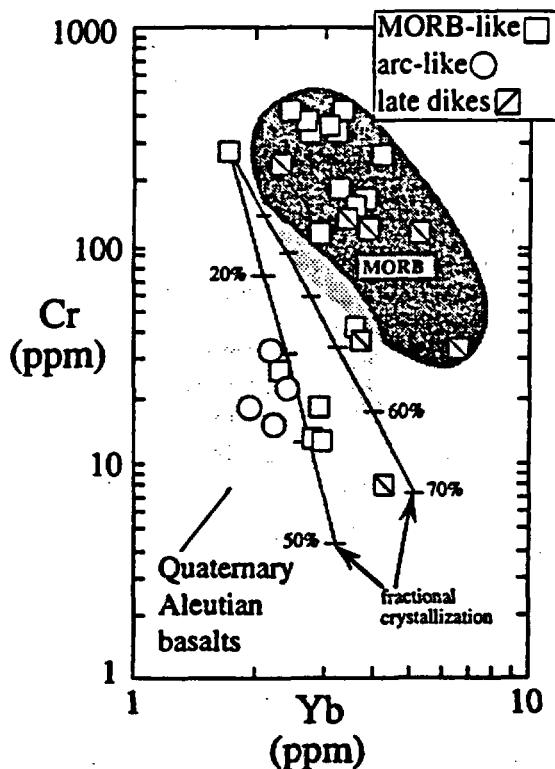


Fig. 7. Cr versus Yb in Attu basalts. Low-Cr mid-ocean ridge basalt (MORB)-like samples (<30 ppm) have isotopic and incompatible trace element characteristics like MORB (e.g., sample AT144 in Figure 5a). The arc-like basalts have the lowest Yb relative to Cr among the Attu basalts. Closed-system Rayleigh fractionation lines calculated for bulk solid/liquid distribution coefficients (D) $D_{Yb}=0.1$, $D_{Cr}=7$ (lower curve), and $D_{Cr}=4$ (upper curve). Aleutian basalt field from Kay and Kay [1993] and references therein. MORB field is approximated from published and unpublished analyses from the Mid-Atlantic Ridge, East Pacific Rise, and Juan de Fuca and Gorda ridges.

most of the MORB-like tholeiites and late dikes do not follow closed system, fractional crystallization paths (Figure 16). In general, the Attu trend is one of rapidly increasing incompatible element concentration relative to FeO^*/MgO . The compatible and incompatible elements in the Attu MORB-like tholeiites and late dikes are thus decoupled. This kind of behavior is common in MORB [e.g., Walker et al., 1979], and is frequently attributed to evolution in an open or periodically recharged magma chamber [O'Hara, 1977]. Similar trends may be produced by in situ crystallization, where magmas evolve by liquid exchange between the hot, convecting part of the chamber and its cooler, partly crystalline margins [e.g., Langmuir 1989]. The actual fractionation mechanism is less important than the observation that incompatible elements are strongly enriched relative to FeO^*/MgO in the Attu rocks. This pattern is not typical of tholeiitic volcanoes of the modern Aleutian arc (see Okmok caldera sequence in Figure 16). Only the low-Cr MORB-like Attu basalts ($Cr < 40$ ppm; see Figure 7) have the relatively low enrichment factors expected from simple closed system evolution (Figure 16).

Origin of the Albite Granites

Within the context of an oceanic or back-arc rift analogue for the Attu Basement Series, the origin of the albite granite suite remains unexplained. Examples of silicic rocks in

oceanic rift settings include the rhyolites and rhyodacites from the Galapagos Spreading Center [Clague et al., 1981], quartz diorites and trondhjemites from the Mid-Atlantic Ridge [Aldiss, 1981], and Icelandic rhyolites [O'Nions and Gronvold, 1973; Wood, 1978; Shimokawa and Masuda, 1972]. Moreover, bimodal associations are a common feature of back-arc spreading centers in the Western Pacific [see Lonsdale and Hawkins, 1985; Ishizuka et al., 1990; Hochstaedter et al., 1990; Fryer et al., 1990]. Silicic end-members in all of these settings are similar to the Attu rhyolites in that they have high incompatible element abundances, large negative Eu anomalies, and relatively unfractionated REE patterns. Similar REE characteristics are also seen in subduction-related tholeiitic systems (e.g., dacitic rocks from Okmok Volcano, Eastern Aleutians), but the isotopic characteristics of the Attu rocks are more akin to MORB than to normal arc volcanic rocks.

The origin of rhyolites in oceanic bimodal assemblages remains a matter of debate [e.g., Sigmarsson et al., 1991; MacDonald et al., 1990], but many authors favor extreme fractional crystallization of basaltic parents. In this regard, the Attu late dikes are of interest, because they include Fe-Ti rich compositions, similar to those associated with silicic volcanism at oceanic rifts (e.g., Iceland and Galapagos Spreading Center). The late dikes range from normal tholeiitic basalts ($FeO^*=10.5\%$, $TiO_2=1.6\%$), to ferrobasalts (up to $FeO^*=13\%$, $TiO_2=3.0\%$) and tholeiitic andesites or icelandites ($SiO_2=58\%$, $TiO_2=2.0\%$, $FeO^*/MgO=2.32$).

Two other lines of evidence support the importance of fractional crystallization in the origin of the Attu silicic rocks. First, gabbros and intermediate composition plutonic rocks of the albite granite suite commonly have concave-downward REE patterns with positive Eu anomalies suggesting that they are complementary crystal cumulates to the evolved silicic rocks (Figure 12). Second, gabbroic rocks of the albite granite suite are also Fe and Ti-enriched ($FeO^*=13.3\%$, $TiO_2=4.5\%$; see sample AT6) and in this way are similar to cumulates that are required by extreme fractionation of tholeiitic basalts [e.g., Stern, 1979; Hunter and Sparks, 1987]. Note also that the decreased REE and Hf abundances in the most evolved albite granites and rhyolites ($SiO_2=77\%$, Figure 11) suggest that these elements have been removed by fractionation of accessory mineral phases, probably apatite and possibly a small amount of zircon. These minerals are common in rocks of the albite granite suite. While accessory phase saturation is uncommon in modern ocean ridge magmas, it is predicted on experimental grounds and is frequently observed in ophiolites [DeLong and Chatelain, 1990].

The isotopic characteristics of the Attu rhyolites suggest that in the course of crystallization they have assimilated some crust. If we assume, on the basis of their REE pattern, that the late dikes are similar to the parental magmas, then low ϵNd in the silicic differentiates ($\epsilon Nd=8.6-9.7$) relative to the late dikes ($\epsilon Nd=9.5-11.5$) is consistent with the assimilation of crust (probably marine sediment) during fractionation and emplacement. High $^{207}Pb/^{204}Pb$ and $^{208}Pb/^{204}Pb$ in some of the silicic rocks (e.g., AT143) also suggest interaction with marine sediments. Post-emplacement growth may account for some of the high $^{206}Pb/^{204}Pb$ signature if the albite granites have undergone U addition or Pb loss to produce high $^{238}U/^{204}Pb$ either during magma genesis or by hydrothermal alteration [e.g., Hamelin et al., 1984].

Evidence for a Near-Arc Setting and Origin of the Subduction Component

Three geochemical lines of evidence suggest that the Attu sub-arc mantle was variably modified by a subduction

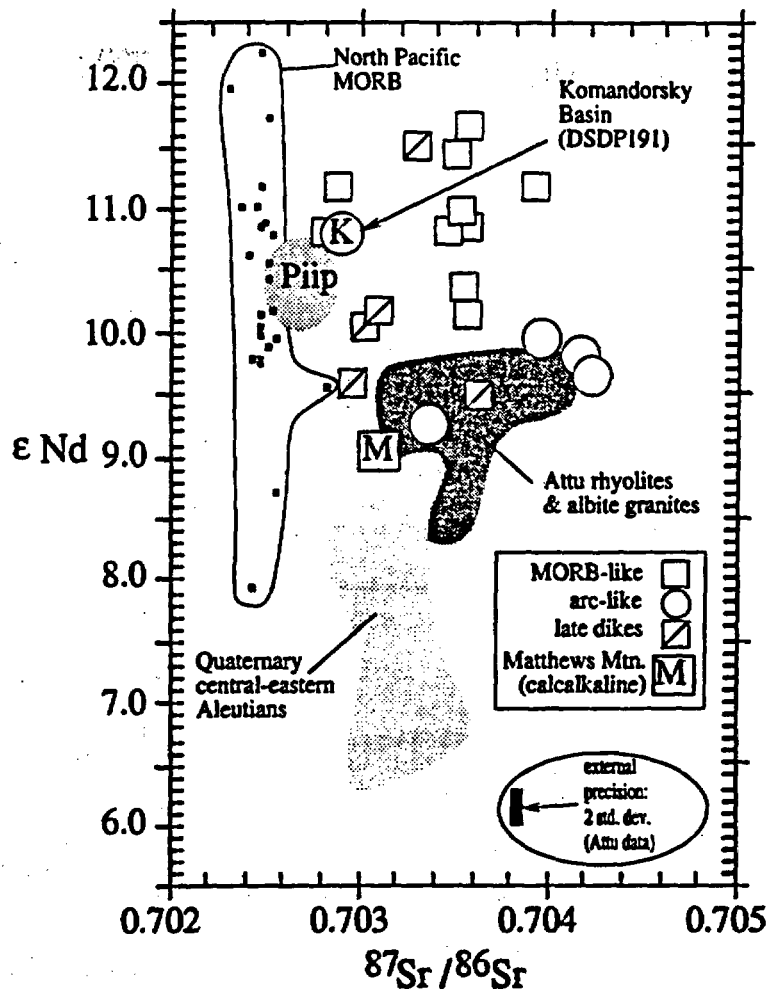


Fig. 8. ϵ_{Nd} versus $^{87}Sr/^{86}Sr$. The ϵ_{Nd} in the mid-ocean ridge basalt (MORB)-like samples and late dikes overlap (ϵ_{Nd} up to ~ 11.5), but late dikes range to lower values ($\epsilon_{Nd} < 10.0$). Arc-like basalts have low ϵ_{Nd} (< 10.0) relative to the MORB-like samples. Rhyolites and albite granites (darkly shaded field) have the lowest ϵ_{Nd} ($\sim 8.6-9.6$). Komandorsky Basin basalt and Piip Volcano samples have ϵ_{Nd} similar to Attu basement rocks and North Pacific MORB. Attu calcaline Matthews Mountain andesite has ϵ_{Nd} that straddles the Aleutian and MORB fields. High $^{87}Sr/^{86}Sr$ relative to ϵ_{Nd} in the Attu rocks reflects Sr exchange during seawater alteration. Attu data are from Table 3. External precision is based on repeated analyses of standard solutions (see Table 3). North Pacific MORB data (Juan de Fuca and Gorda ridges) are from *White et al.* [1987] and *Hegner and Tatsumoto*, [1987]. Quaternary Central and Eastern Aleutian data are referenced in *Kay and Kay* [1993]. Piip Volcano data are from *Romick et al.* [1993] and *Yogodzinski et al.* [in press]. Komandorsky Basin analysis is from *Kay et al.* [1986].

component. First, relatively high Th/La and La/Ta in the Attu arc-like tholeiites (Figures 5c and 6) are broadly similar to those of subduction-related magmas worldwide [e.g., *Pearce*, 1982]. Second, Pb isotope compositions in mafic rocks of the Attu Basement Series form a trend at a high angle to the mantle reference line (Figures 9 and 10), with the highest $^{207}Pb/^{204}Pb$ values occurring in the arc-like samples (i.e., those with high Th/Ta, La/Ta). Third, concentrations of HREE are low relative to compatible elements in the arc-like tholeiites compared to MORB (e.g., Cr-Yb relationship in Figure 7), resulting in a depleted signature that is most common in island arc basalts and most strongly developed in boninites [e.g., *Pearce*, 1982; *Duncan and Green*, 1987].

The chemistry of Attu Basement Series is broadly akin to MORB, but source heterogeneity in the sub-arc mantle is characteristic of subduction-related settings. The arc-like rocks have been found only in southeastern Attu (Figure 2), but there is no geologic basis for separating them from the

MORB-like rocks which volumetrically dominate the island; the arc-like and MORB-like tholeiites both occur as pillow lavas and diabase associated with marine sedimentary rocks. The late dikes, which postdate the albite granite suite, are geochemically similar to the MORB-like basalts which dominated the main pulse of mafic magmatism on Attu. Within the Basement Series there was apparently not a succession from MORB-like to arc-like compositions with time. The MORB-like and arc-like magma types appear to have been largely contemporaneous.

Because their source characteristics are chemically akin to those of MORB, the Attu arc-like basalts may provide additional insights into our understanding of the subduction geochemical signature in arc magmas (i.e., the subduction component). Note in particular that ratios among Hf, Ti, and HREE in the Attu arc-type tholeiites are similar to those of MORB but that Ta appears to be depleted relative to other HFSE and HREE (compare sample AT27 and CP98 in Figure 5).

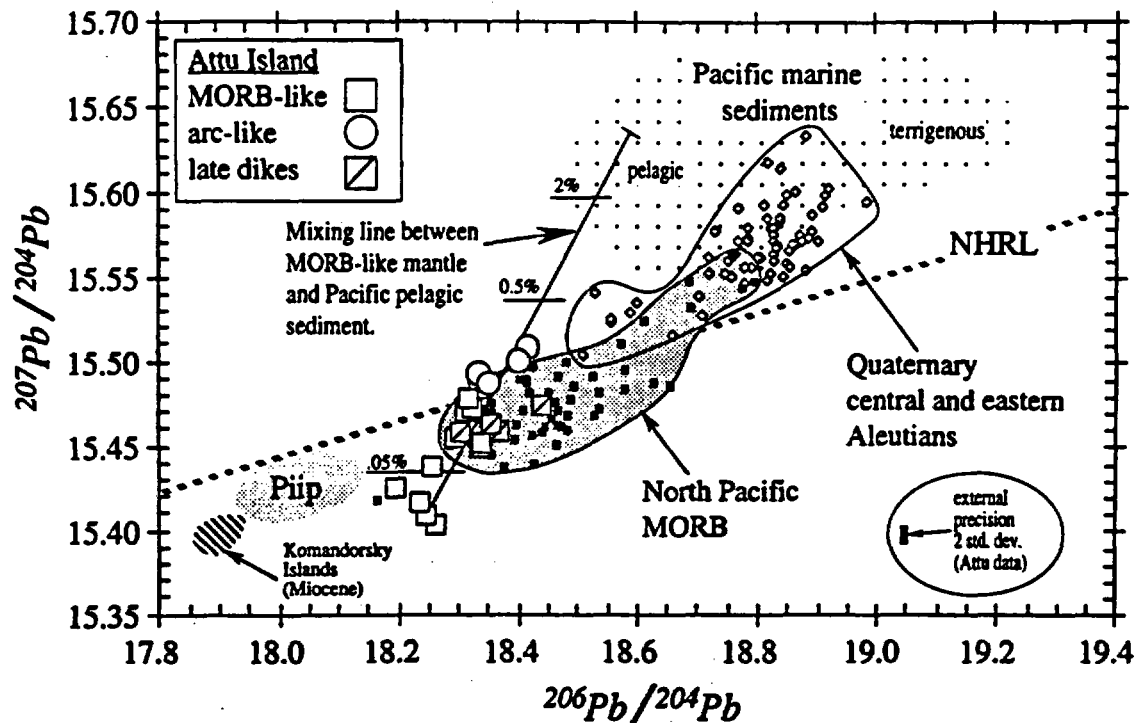


Fig. 9. Pb isotopes. Attu basalts have lower $^{206}\text{Pb}/^{204}\text{Pb}$ than most North Pacific mid-ocean ridge basalts (MORB) and all Quaternary age volcanic rocks from the central and eastern Aleutians. The mixing line parallel to steep Attu trend is between Pacific pelagic sediment (21.5 ppm Pb, $^{207}\text{Pb}/^{204}\text{Pb}=15.63$, $^{206}\text{Pb}/^{204}\text{Pb}=18.59$) and MORB-type Attu mantle (0.08 ppm Pb, $^{207}\text{Pb}/^{204}\text{Pb}=15.41$, $^{206}\text{Pb}/^{204}\text{Pb}=18.25$). Piip Volcano Pb values are similar to the least radiogenic Attu basalts. Miocene age calcalkaline rocks of the Komandorsky Islands are the least radiogenic in the Aleutian arc. External precision is based on replicate analyses of standard solutions (see Table 3). Northern hemisphere reference line (NHRL) is from Hart [1984]. Field of marine sediments includes ~60 analyses from Ben Othman et al. [1989] and Kay et al. [1978 and references therein]; North Pacific MORB data are from Church and Tatsumoto [1975] and references in Figure 8, Quaternary Aleutian data is referenced by Kay and Kay [1993], Piip data are from Yogodzinski et al. [1993]. Komandorsky data are from Housh et al. [1989], and unpublished Cornell data.

This seems to require that a HFSE-bearing phase has been stabilized in the source of the arc-like magmas. Low Ti contents indicate however, that these magmas are not saturated in such phases [Ryerson and Watson, 1987; Green and Pearson, 1987]. If residual Ti-rich minerals are to explain the Ta anomalies in these and other arc magmas, then a two-stage process is required wherein fluids or felsic melts, saturated in a Ti-rich mineral (probably rutile), are removed from the subducting slab to contaminate the overlying mantle wedge [e.g., Ryerson and Watson, 1987]. Yogodzinski et al. [1993] argue that on a regional scale, sources enrichment by slab melting is the most reasonable explanation for the arc trace element signature in isotopically MORB-like Western Aleutian volcanic rocks.

The steep trend formed by the Attu data on Pb-Pb plots is also a feature of the subduction component. This trend can be explained by mixing Pb-rich, high $^{207}\text{Pb}/^{204}\text{Pb}$ marine sediment or sedimentary rock with Pb-poor, low $^{207}\text{Pb}/^{204}\text{Pb}$ mantle or mantle-derived magma [Armstrong, 1971; Kay et al., 1978; Ben Othman et al., 1989]. Such mixing might occur by crust-mantle recycling via subduction, crustal assimilation, or by postmagmatic alteration. Alteration is not an adequate explanation because the Pb isotopic composition of the Attu rocks is correlated with parameters that are largely immune to such processes (e.g., Th/Ta, La/Ta). Crustal assimilation may account for high $^{207}\text{Pb}/^{204}\text{Pb}$ in some MORB-like samples (evolved, low-Cr MORB-like samples have slightly elevated $^{207}\text{Pb}/^{204}\text{Pb}$, Tables 1 and 3), but the occurrence of low Ta

concentrations (<0.10 ppm) with high $^{207}\text{Pb}/^{204}\text{Pb}$ in the arc-like tholeiites cannot be produced by assimilation alone. We interpret the Pb isotope signature of the Attu Basement Series rocks as a product of recycling of upper crust into the sub-arc mantle via subduction [Kay, 1980]. A simple mixing model between pelagic sediment and depleted peridotite (Figures 9 and 10) shows that a small quantity of Pb from sediment mixed into a Pb-poor MORB-like upper mantle can account for the trend of the Attu Pb data.

Origin of the Matthews Mountain Andesite and the Western Aleutian Calcalkaline Trend

Because calcalkaline volcanic rocks are petrologically complex, simple geochemical models do not in general reproduce their major and trace element characteristics well. Many aspects of modern Central and Eastern Aleutian calcalkaline magmas are nonetheless consistent with an origin by crystal fractionation and magma mixing beginning with parental Mg-rich basalts [Kay et al., 1982; Kay and Kay, 1985; Conrad and Kay, 1984; Brophy, 1990]. These primitive basalts show a range of geochemical characteristics and are known from several locations in the Central and Eastern Aleutian arc [Kay and Kay, 1993, Table 1 and Figure 4].

Miocene to Recent calcalkaline rocks from Attu and throughout the Western Aleutians cannot, however, be derived from parental basalts or basaltic andesites like those from the Central and Eastern Aleutians. This is because the Western

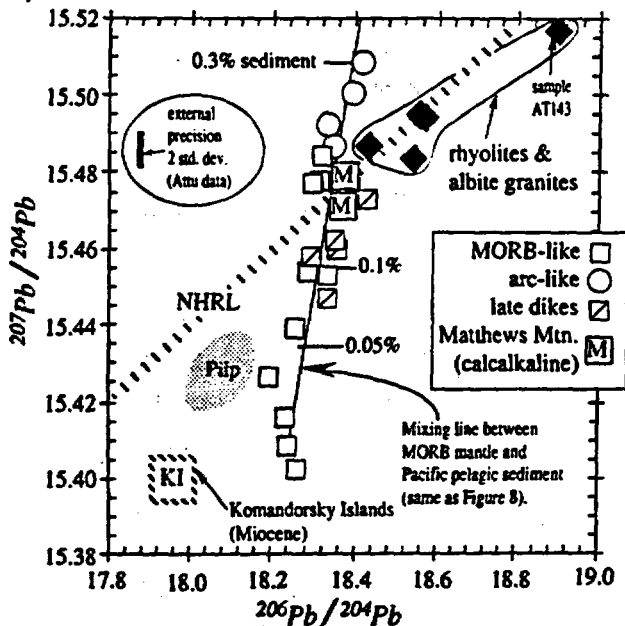


Fig. 10. Pb isotopes in blow-up of Figure 9. Mixing line is as in Figure 9. Note that Mathews Mountain andesites, which have arc-like major and trace element characteristics (e.g., Figures 3 and 6), have Pb isotopes like Attu mid-ocean ridge basalt (MORB)-like rocks. Middle Miocene rocks of the Komandorsky Islands and Piip Volcano have similar characteristics. High $^{206}\text{Pb}/^{204}\text{Pb}$ in the Attu rhyolites and albite granites may in part reflect in situ radioactive decay if $^{238}\text{U}/^{204}\text{Pb}$ in these rocks is high relative to the basalts (see text). External precision is based on replicate analyses of standard solutions (see Table 3). Komandorsky Islands values of $^{206}\text{Pb}/^{204}\text{Pb}$ —17.88, $^{207}\text{Pb}/^{204}\text{Pb}$ —15.40 are from Housh *et al.* [1989], and unpublished Cornell data.

Aleutians rocks have generally lower incompatible element concentrations (Figures 13 and 14) and are more strongly calcalkaline (Figure 15) than most Central and Eastern Aleutian volcanic rocks. Model 1 illustrates this point (Figure 17). The parental basaltic andesite in this model was chosen because it has major elements that are relatively close to the daughter (thereby minimizing the amount of fractionation required), and because the shape of its REE pattern is similar to that of the daughter (Figure 17). Closed system fractionation (49%) of an anhydrous mineral assemblage reproduces the major element features of the daughter Mathews Mountain andesite well (Σ residuals² = 0.03), but the calculated REE concentrations are too high by more than a factor of 2 (Figure 17). Amphibole fractionation may lower the calculated heavy and middle REE abundances slightly [e.g., Romick *et al.*, 1992], but it is difficult to produce the low $\text{CaO}/\text{Al}_2\text{O}_3$ of the Western Aleutian rocks without substantial clinopyroxene fractionation (Figures 15 and 17). This is because removal of amphibole ($\text{CaO}/\text{Al}_2\text{O}_3$ -0.6 to -1.5) and/or calcic plagioclase (An_{85} $\text{CaO}/\text{Al}_2\text{O}_3$ -0.55) has little effect on $\text{CaO}/\text{Al}_2\text{O}_3$ in a primitive basalt (0.60-0.80). Low REE concentrations in the Western Aleutian rocks therefore cannot be the result of extensive amphibole fractionation but must be a characteristic of the parental magma.

The failure of model 1 is not surprising in light of the abundant evidence that Aleutian calcalkaline rocks show for magma mixing [Kay *et al.*, 1982; Conrad and Kay, 1984; Kay and Kay, 1985; Romick *et al.*, 1992]. A simple mixture between a primitive Aleutian basalt and an Aleutian dacite is illustrated in model 2 (Figure 17). This kind of mixture

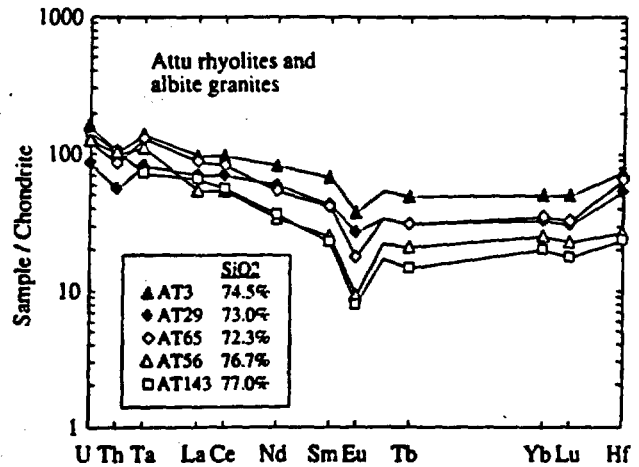


Fig. 11. Chondrite-normalized incompatible elements in Attu rhyolites and albite granites. Note the generally flat rare earth element (REE) patterns and large negative Eu anomalies. Low REE and Hf concentrations in Attu samples AT56 and AT143 (largest Eu anomalies; highest SiO_2) probably result from REE compatibility in accessory mineral phases (e.g., apatite). Note constant Th/U in all samples. Normalizing values are U (0.015), Th (0.050), Ta (0.022), and Hf (0.22). REE normalizing values are as in Figure 4.

reproduces the LREE features of the Mathews Mountain andesite relatively well, but it does not reproduce the HREE features or the low $\text{CaO}/\text{Al}_2\text{O}_3$ and FeO^*/MgO values which characterize the Mathews Mountain andesites and all other Western Aleutian calcalkaline rocks. Choice of different mixing end-members from the Central or Eastern Aleutians will not substantially change this result. We conclude from models 1 and 2 that middle Miocene to Recent calcalkaline rocks of the Western Aleutians cannot be related to Central and Eastern Aleutian basalts or basaltic andesites by reasonable combinations of fractionation and magma mixing.

Model 3 is a fractionation model that begins with a parental magnesian andesite from Piip Volcano (far Western Aleutians, Figure 1). These primitive andesites have low incompatible element abundances (Yb -5-6 times chondrites) and major element compositions (SiO_2 , $\text{CaO}/\text{Al}_2\text{O}_3$, FeO^*/MgO) similar to those of the Mathews Mountain andesites (Figure 17; see also Yogodzinski *et al.* [1993] and Volynets *et al.* [1992]). Model 3 requires only 11% crystallization, and because REE in the parental rock are similar to those in the daughter, the calculated REE also match the observed reasonably well. Model 3 shows that magnesian andesites from Piip Volcano have the general features that are required of parental magmas in the Western Aleutians (low $\text{CaO}/\text{Al}_2\text{O}_3$, FeO^*/MgO , and REE concentrations). This implies that the strongly calcalkaline magmatic rocks from throughout the Western Aleutians (i.e., Figure 15), are more akin to magnesian andesites than to basalts like those of the modern Central and Eastern Aleutian arc. Relatively large major element residuals in model 3 (Σ residuals² = 0.38) suggest however, that there is significant variation among Western Aleutian magnesian andesites.

It is important to note that magnesian andesites parental to the Western Aleutian suite are chemically unlike Aleutian "adakites" [Defant and Drummond, 1990] which have high Sr (>1500 ppm), high La/Yb (~30), and appear to have originated by melting of the subducting oceanic crust [Kay, 1978]. The modeling presented here indicates that Piip Volcano-type magnesian andesites (Sr-380 ppm, La/Yb-4.2) are a reasonable parental composition to the strongly calcalkaline

TABLE 3. Isotopic Analyses of Attu and Related Rocks

	$^{206}\text{Pb}/^{204}\text{Pb}$	$^{207}\text{Pb}/^{204}\text{Pb}$	$^{208}\text{Pb}/^{204}\text{Pb}$	$^{143}\text{Nd}/^{144}\text{Nd}$	ϵNd	$^{87}\text{Sr}/^{86}\text{Sr}$
ORB-like						
HO962A	18.263	15.402	37.601	0.513165	11.1	0.70291
AT73	18.245	15.408	37.573	0.513150	10.9	0.70360
HO922	18.235	15.416	37.609			
SB1A	18.196	15.426	37.624		11.0*	0.70357*
HO914B*†	18.255†	15.438†	37.624†		10.7*	0.70281*
HO925B*					11.1*	0.70369*
HO925B	18.337	15.452	37.738	0.513179	11.4	0.70353
AT144	18.296	15.454	37.760	0.513191	11.7	0.70359
AT114	18.317	15.478	37.851	0.513112	10.1	0.70359
AT114 (duplicate)	18.309	15.471	37.823	0.513118	10.2	
AT114 (duplicate)	18.322	15.472	37.835	0.513125	10.4	0.70357
AT100	18.330	15.484	37.893	0.513165	11.1	0.70395
AT101	18.313	15.478	37.839	0.513147	10.8	0.70348
Arc-like						
MP8010	18.353	15.486	37.901	0.513104	10.0	0.70397
MP802	18.416	15.508	37.971	0.513089	9.7	0.70424
CP98	18.403	15.500	37.952	0.513097	9.8	0.70418
CP916C	18.336	15.492	37.922	0.513069	9.3	0.70339
Late dikes						
AT27	18.337	15.448	37.810	0.513107	10.0	0.70305
AT16	18.300	15.458	37.756	0.513183	11.5	0.70331
AT50	18.364	15.460	37.861	0.513079	9.5	0.70365
AT22	18.354	15.462	37.834	0.513085	9.6	0.70299
AT21	18.423	15.473	37.904	0.513116	10.2	0.70313
Albite granite suite						
AT3	18.538	15.483	37.958	0.513046	8.8	
AT29	18.582	15.494	38.012	0.513087	9.6	0.70324
AT56	18.571	15.495	37.968	0.513036	8.6	0.70349
AT143	18.901	15.517	38.072	0.513086	9.6	0.70378
AT65	18.435	15.487	37.889	0.513089	9.7	0.70401
Calkaline						
AT83	18.379	15.471	37.858			
AT8032	18.372	15.479	37.854		9.3*	0.70306*
Komandorsky Basin						
DSDP-191 basalt*					11.2*	0.70289*

All isotope analyses are by thermal ionization mass spectrometry at Cornell University. Mean standard values and analytical precision (\pm two standard deviations) reported below are based on analyses performed between August and November 1990. Analytical technique for Pb is after *White et al.* [1990]. Measured values for NBS SRM-981 Pb standard were $^{206}\text{Pb}/^{204}\text{Pb}=16.907$, $^{207}\text{Pb}/^{204}\text{Pb}=15.435$, $^{208}\text{Pb}/^{204}\text{Pb}=36.496$. Each ratio was corrected for mass fractionation independently assuming standard values of $^{206}\text{Pb}/^{204}\text{Pb}=16.937$, $^{207}\text{Pb}/^{204}\text{Pb}=15.493$, $^{208}\text{Pb}/^{204}\text{Pb}=36.705$. Analytical precision of ± 0.008 ($^{206}\text{Pb}/^{204}\text{Pb}$), ± 0.007 ($^{207}\text{Pb}/^{204}\text{Pb}$), and ± 0.024 ($^{208}\text{Pb}/^{204}\text{Pb}$) is based on 13 analyses of NBS SRM-981. Nd isotopes by single filament technique after *Walker et al.* [1989]. Ratios were corrected for mass fractionation assuming $^{146}\text{Nd}/^{144}\text{Nd}=0.7219$. Measured values for LaJolla Nd standard were $^{143}\text{Nd}/^{144}\text{Nd}=0.511817 \pm 0.000012$ and $^{143}\text{Nd}/^{144}\text{Nd}=0.348412 \pm 0.000013$ based on 15 analyses. Epsilon Nd (ϵNd) are deviations in 10^4 from present-day chondritic $^{143}\text{Nd}/^{144}\text{Nd}$ assuming LaJolla $\epsilon\text{Nd}=-15.15$ [*Lugmair and Carlson, 1978; Wasserburg et al., 1981*]. Sr analyses were done on W single filaments by quadruple collector dynamic procedure. Ratios were corrected for mass fractionation assuming $^{86}\text{Sr}/^{88}\text{Sr}=0.11940$. Average measured value for NBS SRM-987 Sr standard was $^{87}\text{Sr}/^{86}\text{Sr}=0.710228$ with analytical precision of ± 0.000042 based on 28 analyses.

*Analysis from *Kay et al.* [1986]; epsilon recalculated assuming ϵNd for BRC1= $+0.20$

†Analyzed at Lamont Doherty by J. L. Rubenstone.

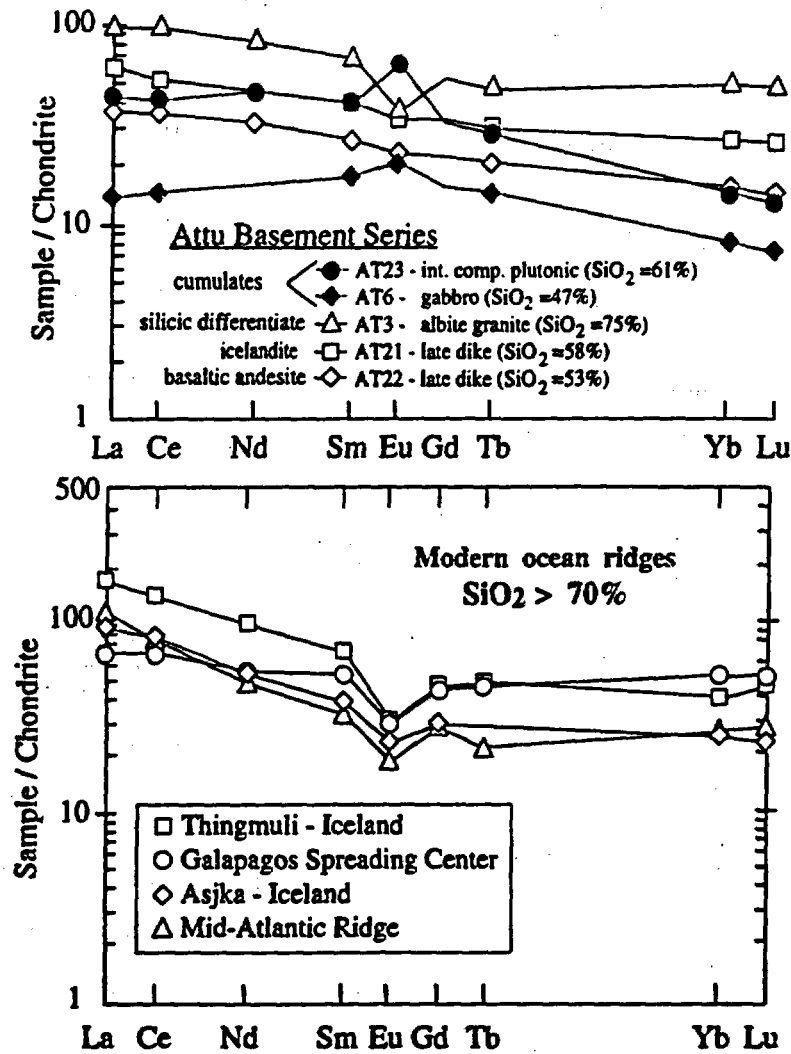


Fig. 12. Comparison of rare earth elements (REE) in cumulate rocks of albite granite suite with late dikes, albite granite, and modern ocean ridge rhyolites. Note the REE patterns in the cumulates are the mirror image of the albite granite (compare La/Sm, Eu/Sm, and Tb/Yb in AT23 and AT3). Note also the broad similarity of silicic from modern ocean ridges to the Attu albite granite (see also Figure 11). Thingmuli data are from Wood [1978], Askja data are from Shimokawa and Masuda [1972], Galapagos Spreading Center data are from Clague *et al.* [1981], Mid-Atlantic Ridge data are from Aldiss [1981].

Western Aleutian assemblage (i.e., Figure 15 and model 3 in Figure 17). Magnesian andesites of this type are commonly viewed as low-pressure melts of hydrous peridotite [see Tatsumi, 1982]. Yogodzinski *et al.* [1993] argue, however, that magnesian andesites of this type may also form through melt-peridotite interaction in the uppermost mantle, immediately beneath calcalkaline volcanoes. This is consistent with the idea that Aleutian calcalkaline volcanism is produced by relatively low temperature fractionation near the base of the arc crust [Kay *et al.*, 1982; Kay and Kay, 1985; Conrad and Kay, 1984; Kay and Kay, 1993; Brophy, 1990], and with the observation that Aleutian calcalkaline volcanoes form by relatively small volume eruptions in zones of tectonic compression where magma ascent through the arc crust appears to have been structurally inhibited [Kay *et al.*, 1982; Geist *et al.*, 1988; Singer and Meyers, 1992; Romick *et al.*, 1992]. Results from the Western Aleutians imply that fractionation of calcalkaline magmas may begin not within the crust but within the uppermost mantle where the assimilation of relatively hot peridotite is likely [i.e., Kelemen, 1986, 1990].

WESTERN ALEUTIAN TECTONICS AND THE ORIGIN OF ATTU AND THE NEAR ISLANDS

Geochemical source variation among the Attu basalts indicates that the Basement Series rocks originated in a near-arc setting. Attu therefore cannot be a tectonically captured slice of Kula or Pacific oceanic crust. The regional trend of decreasing Pb isotope ratios in volcanic rocks from east to west along the Aleutian arc provides direct evidence that the Attu Basement Series rocks formed in situ. In general, $^{206}\text{Pb}/^{204}\text{Pb}$ values in Miocene to Recent volcanic rocks in the Central and Eastern Aleutians are high (18.5-18.9); in the Western Aleutian Near Islands (Attu) they are low (18.2-18.4); and in the far Western Aleutian Komandorsky region they are very low (17.8-18.2; see Figure 9). Interestingly, this east-west trend is also seen in Pacific ocean ridge and back-arc basin basalts [e.g., White *et al.*, 1987; Hickey-Vargas, 1991; Tatsumoto and Nakamura, 1991]. Regional source variation of this kind in the Aleutians would be fortuitous indeed, if the volcanic rocks of Attu and the Near Islands were part of an allochthonous terrane.

TABLE 4a. Modeling Parameters: Mineral Compositions

	cpx1*	cpx2†	An66††	hbl‡	tmtg™	Fo89‡‡
SiO ₂	51.99	51.27	51.68	49.47	0.15	41.43
TiO	0.49	0.40	0.00	0.91	8.51	0.00
Al ₂ O ₃	1.64	3.31	30.40	5.44	6.68	0.00
FeO*	11.04	4.66	0.48	12.18	75.16	10.52
MgO	15.15	16.18	0.00	16.02	3.73	48.14
CaO	18.85	23.09	13.21	10.57	0.00	0.49
Na ₂ O	0.36	0.20	3.67	1.02	0.00	0.00
K ₂ O	0.00	0.00	0.11	0.15	0.00	0.00

*Clinopyroxene (SIT5B, [Kay and Kay, 1985])

†Clinopyroxene (BUL6B, [Kay and Kay, 1985])

††Plagioclase feldspar (75A-113, [Romick et al., 1992])

‡Hornblende (75A-110, [Romick et al., 1992])

™Titanomagnetite (75A-21, [Romick et al., 1992])

‡‡Olivine (4b, [Conrad and Kay, 1984])

TABLE 4b. Modeling Parameters: Distribution coefficients

	Mineral					Whole-rock	
	hbl‡	plag†	cpx††	tmtg™	olv™	SIT-RK5‡	OK4**
La	0.54	0.24	0.10	0.03	0.01	14.61	4.29
Ce	0.84	0.20	0.15	0.03	0.01	32.3	11.03
Nd	1.34	0.14	0.31	0.03	0.01	18.3	6.40
Sm	1.80	0.11	0.50	0.03	0.01	4.68	2.00
Eu	1.56	0.73	0.51	0.03	0.01	1.09	0.70
Tb	2.02	0.06	0.64	0.05	0.01	0.76	0.374
Yb	1.64	0.03	0.62	0.10	0.01	3.42	1.29
Lu	1.56	0.03	0.56	0.12	0.01	0.500	0.199

Some distribution coefficients were determined by interpolation or extrapolation. Whole rock values are given in parts per million. Abbreviations are hbl‡, hornblende; plag†, plagioclase; cpx, clinopyroxene; tmtg™, titanomagnetite; and olv, olivine.

*Fujimaki et al. [1984] average of calcalkaline andesites.

†Schnetler and Philpotts [1970] andesite GFC271.

††Arth and Hanson [1975] average for augite in basaltic-to-andesitic rocks.

‡Smith and Lecman [1987].

™Values for olivine assumed to be arbitrarily low.

‡Dacite mixing end-member in model 3 [Romick et al., 1992].

**Basalt mixing end-member in model 3 [Kay and Kay, 1993].

Vallier et al. [1993] have argued that Western Aleutian islands were formed by arc-type magmatism largely prior to 43 Ma when underthrusting was at a higher angle to the strike of the arc. This implies that growth of the western arc paralleled the early stages in the Central and Eastern Aleutians where voluminous magmatism between 55 and 37 Ma resulted in rapid crustal thickening [Scholl et al., 1970, 1987; Marlow et al., 1973; Hein and McLean, 1980]. This view is not, however, consistent with the magmatic development of Attu, because the bimodal, dominantly MORB-like chemistry of the Attu Basement Series rocks is more characteristic of a back-arc basin than an island arc [Rubenstone et al., 1982; Rubenstone, 1984; Kay et al., 1986].

Ultimately, the age of the Attu Basement Series will be critical to our understanding of its tectonic origin. Because the

magmatic rocks were subjected to seawater metamorphism, and the sedimentary rocks are largely devoid of age-diagnostic fossils, the age of the Attu Basement Series remains poorly constrained. Attempts to date Basement Series basalts by ⁴⁰Ar/³⁹Ar were unsuccessful [Rubenstone, 1984]. Metamorphic ages are between 28 and 38 Ma (K-Ar method [e.g., DeLong and McDowell, 1975], but if magmatism and metamorphism were largely contemporaneous (see section on evidence for a rift tectonic setting), then some of these dates might approximate emplacement ages. The oldest and most reliable date on a Basement Series rock is 41.5 ± 2 Ma, obtained on an amphibole separate from a mafic amphibolite [Vallier et al., 1993]. If we assume that tholeiitic magmatism on Attu ended before the beginning of calcalkaline magmatism at ~15 Ma [DeLong and McDowell, 1975; Borusk and Tsvetkov, 1982;

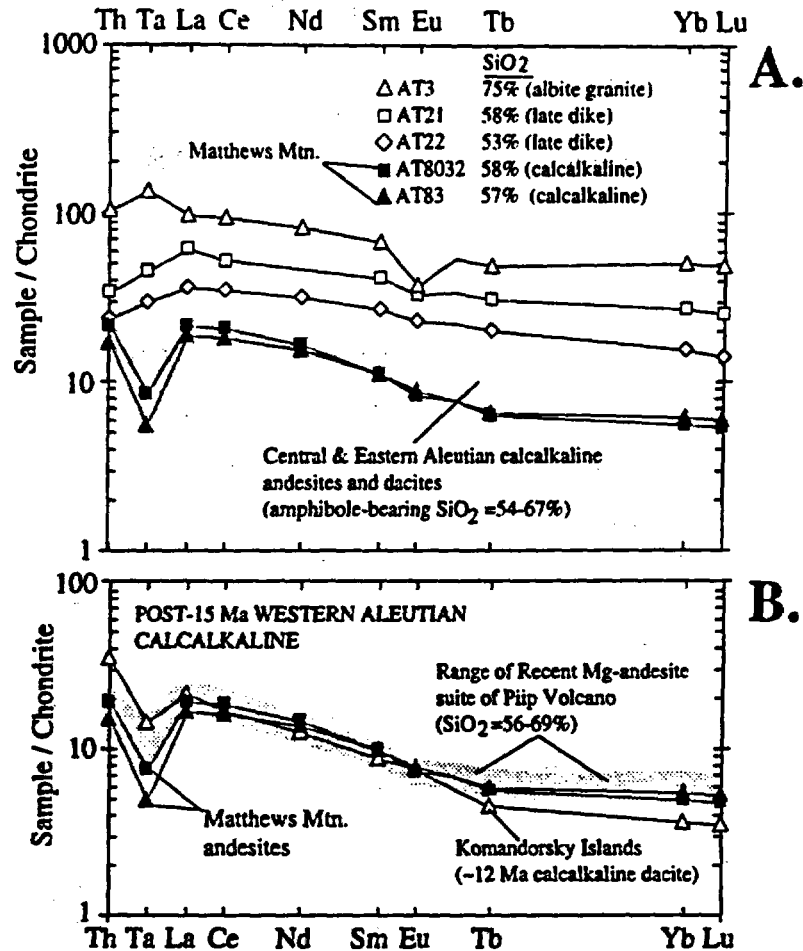


Fig. 13. Chondrite-normalized trace elements of the Attu calcalkaline Matthews Mountain andesites compared to the late dikes and albite granites. In Figure 13a, note the low Ta and low overall incompatible trace element concentrations of the Matthews Mountain andesites relative to Basement Series rocks with equivalent SiO₂ (compare AT8032 and AT21). In Figure 13b, note the similarity of the Matthews Mountain andesites to the Miocene age calcalkaline dacite of the Komandorsky Islands and magnesian andesite suite from Piip Volcano. Data are from Tables 1 and 2, *Yogodzinski et al.* [1993], and *DeLisio* [1984].

Tsvetkov, 1991], then the Basement Series (including the albite granite suite and late dikes) must be middle Eocene to late Oligocene or early Miocene in age (43? Ma to 25 or 15 Ma). Fossil ages from marine sedimentary rocks of the Near Islands [*Vallier et al.*, 1993] are in accord with this estimate.

A simple tectonic model for the development of the Western Aleutian-Bering Sea region is presented in Figure 18. Rifting and tholeiitic magmatism in the Attu region (Figure 18a) are associated with stretching of the overriding plate in response to the switch from oblique to highly oblique convergence following plate reorganization at 43 Ma [*Engebretson et al.*, 1985]. We envision a transtensional regime, broadly analogous to those found in some modern arc systems (e.g., the Philippine Marinduque Basin [*Sarwitz and Lewis*, 1991]). The inferred NE-SW orientation of the rift axis through Attu is consistent with the trend of the Fishhook Ridge dike swarm, the alignment of the silicic intrusive centers (rhyolites, albite granites), and the NE trending belt of well-preserved marine and nonmarine sedimentary rocks that overlie the volcanic-dominated basement (Nevidiskov, Chuniksak, and Faneto formations, Figure 2). These sedimentary rocks were probably deposited within a rift depression prior to and during uplift of the Attu Basement Series. Local amphibolite grade metamorphism and occurrence of a 400-m-thick sill complex

in the central part of the island [*Vallier et al.*, 1993] are consistent with a rift interpretation. We assume that clockwise rotation of Attu in dextral Western Aleutian shear zones has been relatively minor; this is consistent with the findings of *Geist et al.* [1988] which suggest that only 3° of rotation of the Near Island block has occurred in late Cenozoic time. Paleomagnetic data from Attu are inconsistent and do not provide a reasonable constraint on rotation of the Near Island crustal block (W. Harbert, personal communication, 1992).

Note that the NE-SW orientation of the rift axis and the presence of EW-oriented (not NS-oriented) magnetic lineations in the Bowers Basin immediately north of the Near Islands [*Cooper et al.*, 1992, Figure 3] argue against formation of the Attu Basement Series by simple back-arc spreading behind the Bowers island arc. We assume that the Bowers subduction system largely predates 43 Ma (Figure 18a). Subduction beneath the Bowers Ridge and spreading in the Bowers Basin may however, have continued through the Middle Tertiary [*Cooper et al.*, 1992, figure 7]. If so, then the Attu Basement Series may simply be an extension of Bowers Basin crust onto the Western Aleutian Ridge crest [e.g., *Kay et al.*, 1986, Figure 3b]. Figure 18a is based on the general idea that after plate reorganization at 43 Ma [*Engebretson et al.*, 1985], the

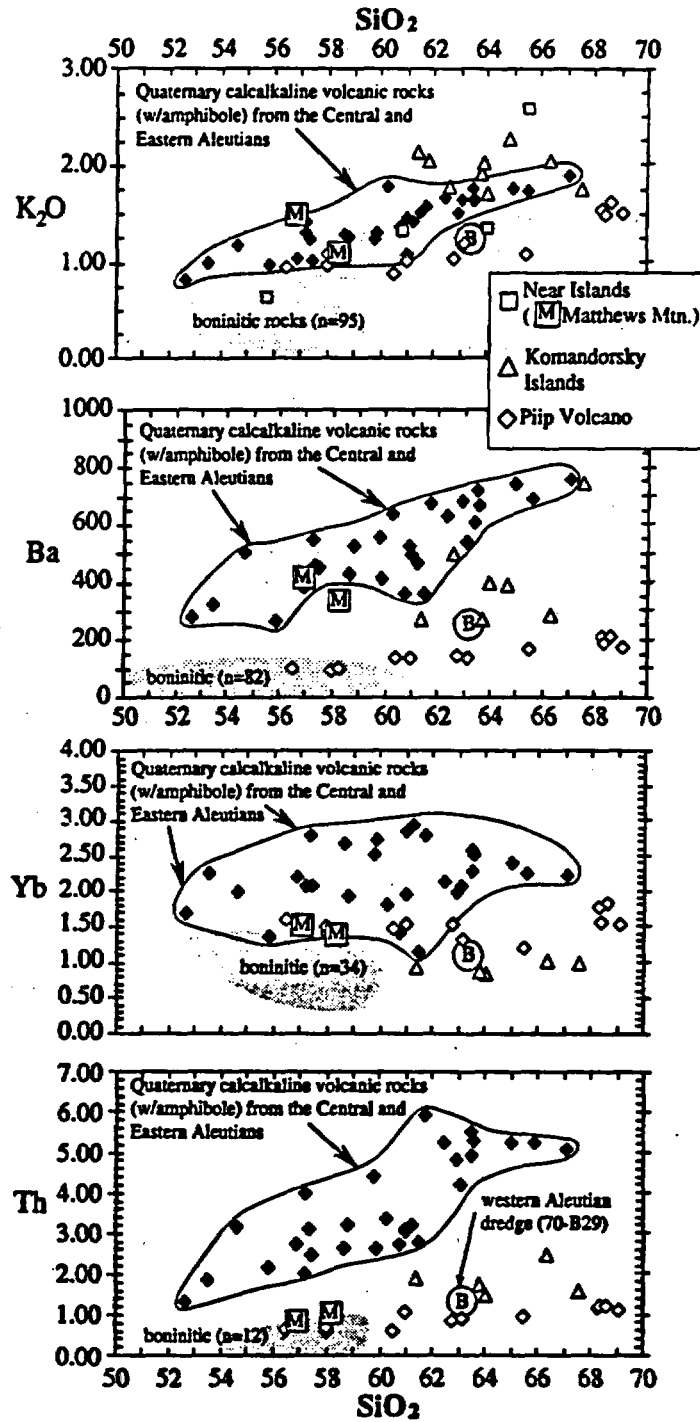


Fig. 14. Silica variation diagrams for post-15 Ma Western Aleutian calcalkaline rocks compared with central and eastern Aleutian calcalkaline rocks (solid symbols) and with boninites and related rocks (gray fields). Note that Ba, Yb, and Th contents in the western arc are lower than those in the Aleutian reference suite, but that K_2O contents broadly overlap. Boninite fields provide comparison with arc-related magmas with low abundances of incompatible elements. Western Aleutian dredge sample labeled "B" (Quaternary age) was collected between Attu and Buldir islands [Scholl *et al.*, 1976] (complete analysis by Kay and Kay [1993]). Western Aleutian data sources are the same as in Figure 15.

tectonics of the Western Aleutian Ridge proper must have been dominated by strike-slip faulting (see also Cooper *et al.* [1992, Figure 7D]).

Baranov *et al.* [1991] have shown that the trenchward (western) margin of the Shirshov arc was rifted to the west

during the Neogene opening of the Komandorsky Basin, while the eastern margin of the Shirshov arc remained approximately stationary. This is shown in Figure 18b as a simple arc-splitting [Karig, 1971], and in this respect it differs from the transform-style rifting mechanism of Baranov *et al.* [1991].

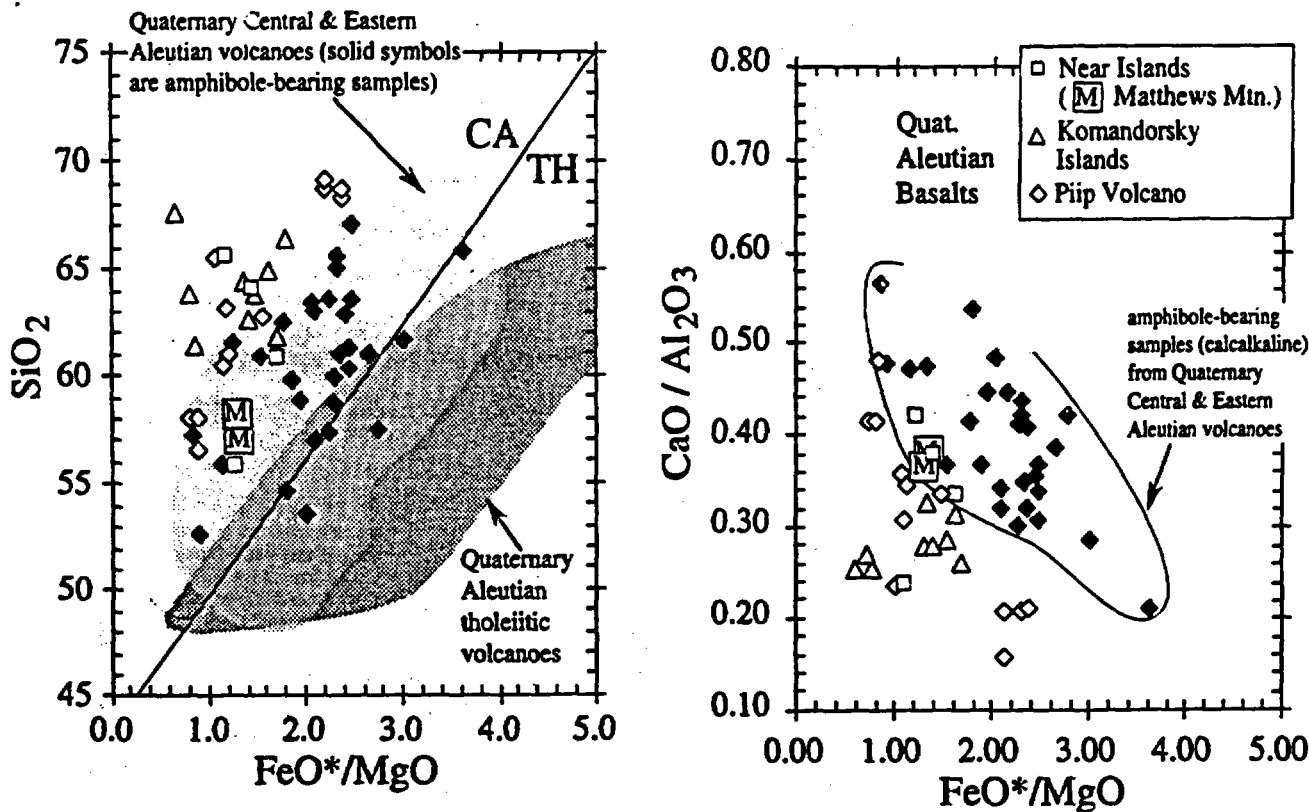


Fig. 15. Post-15 Ma Western Aleutian calcalkaline rocks compared to central and eastern Aleutian basalts and calcalkaline suite. Note low FeO^*/MgO relative to SiO_2 , and low $\text{CaO}/\text{Al}_2\text{O}_3$ relative to FeO^*/MgO in the Western Aleutian suite making them more strongly calcalkaline than the central and eastern Aleutian assemblage. Data are from Gates *et al.* [1971], Borusk and Tsvetkov [1982], DeLisio [1984], Kay and Kay [1993], and Yogodzinski *et al.* 1993].

In any case, active rifting was presumably accompanied by voluminous tholeiitic magmatism which formed the Neogene oceanic-type basement that underlies the Komandorsky Basin [Cooper *et al.*, 1987].

The eruption of calcalkaline volcanic rocks in the Near and Komandorsky islands beginning 15 m.y. ago, marks a profound change in the tectonic style of the Western Aleutian arc at that time. Chemically, the calcalkaline rocks of the Near and Komandorsky islands are analogous to late Pleistocene rocks of Piip Volcano. Piip Volcano is centered on small dilational structures within the broadly transpressional tectonic regime of the modern Western Aleutian arc [Baranov *et al.*, 1991; Seliverstov *et al.*, 1990a, b; Geist *et al.*, 1988]. We therefore infer that the onset of calcalkaline magmatism 15 m.y. ago, marks the switch from transtensional to transpressional tectonics in the western arc. This is consistent with the observation that calcalkaline, subduction-related magmatism did not become active along the full length of the modern Aleutian arc until approximately middle Miocene time [Kay *et al.*, 1990].

The model in Figure 18 does not account for the topographically elevated Komandorsky Islands in the westernmost Aleutians (the "Komandor block" of Seliverstov *et al.* [1984]). The crust of the Komandorsky Islands was probably thickened by an Early to Middle Tertiary episode of subduction-related magmatism [e.g., Borusk and Tsvetkov, 1982; Tsvetkov, 1991], but such an episode is difficult to reconcile with contemporaneous rift-related magmatism in the Near Islands. One possibility is that the Komandorsky block is largely allochthonous, having been moved by strike-slip motion along the Western Aleutian Ridge to its present

location in the westernmost arc [Scholl *et al.*, 1987; Geist *et al.*, 1991; Cooper *et al.*, 1992]. Westward motion of the Komandorsky block may have occurred in conjunction with the opening of the Komandorsky Basin and rifting of the (former) Shirshov arc (e.g., Figure 18b). This kind of model allows for the distinctly different early magmatic histories (>30 Ma) of the Komandorsky and Near Island groups, and it suggests that the alkaline, arc-type magmatism in the Komandorsky Islands at 20-25 Ma [Borusk and Tsvetkov, 1982; DeLisio, 1984; Housh *et al.*, 1989; Tsvetkov, 1991] may be associated with unusual tectonic conditions at the Shirshov-Aleutian junction immediately prior to or during arc splitting and westward transport of the Komandorsky block (see Figure 18b).

The onset of calcalkaline magmatism in the Western Aleutians may have resulted from the clogging of the Aleutian-Kamchatka junction by the collision of the westward drifting Komandorsky block at ~15 Ma (Figure 18c, see also Scholl *et al.* [1987] and Geist *et al.* [1991]). In this interpretation, the Komandorsky Islands would have arrived at their present location prior to the youngest Komandorsky magmatic episode (middle to late Miocene [Borusk and Tsvetkov, 1982; Tsvetkov, 1991]). There are no Pleistocene or Recent magmatic rocks on any of the Western Aleutian Islands, but seafloor imaging (GLORIA images, A. Stevenson, personal communication, 1990) has shown that there is a zone of active magmatism along the northern margin of much of the Western Aleutian Ridge. Piip Volcano, which is located not on the Aleutian Ridge proper but on back-arc crust of the southernmost Komandorsky Basin (Figure 1), is probably the westernmost extent of this active zone of Western Aleutian

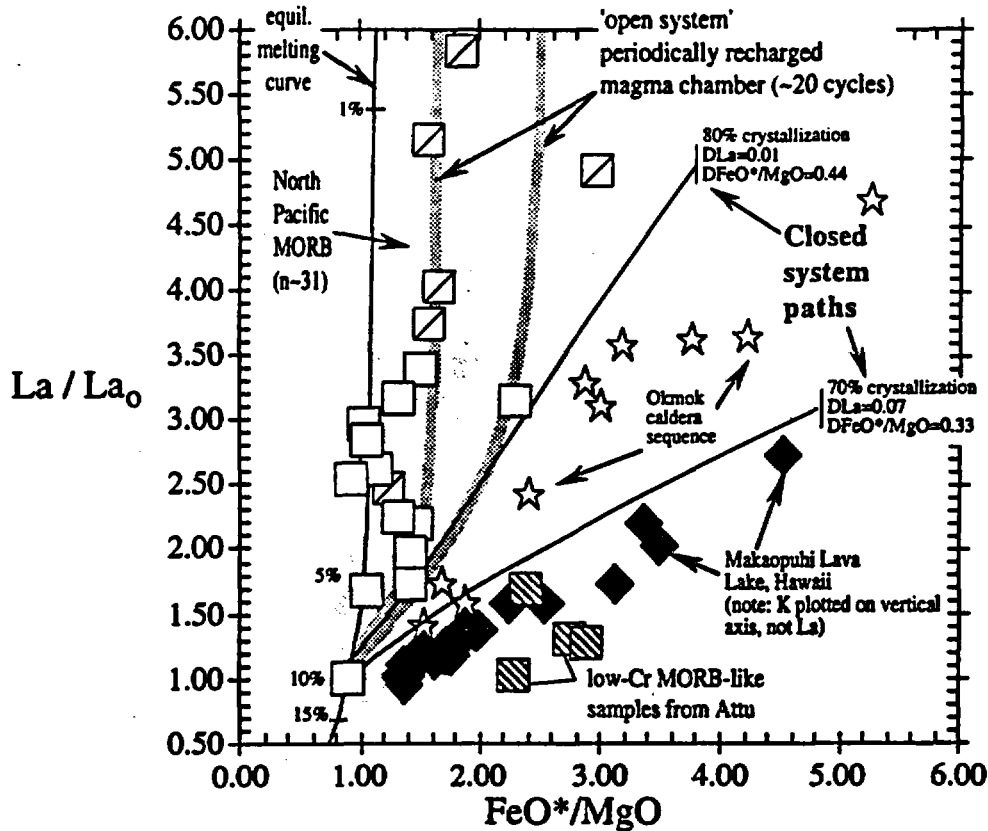


Fig. 16. Attu basalts compared to modeled crystallization and melting trends. Parental composition in crystallization models is the least evolved Attu Basement Series basalt (sample HO925B, Table 1a - $La=2.33$, $FeO^*/MgO=0.89$). La/La_0 (enrichment factor) is La concentration in the residual melt divided by the La concentration in the parental magma. Closed system models are simple Rayleigh fractionation. Steep trend of most Attu data requires low DLa and high $DFeO^*/MgO$ (D =mineral/melt bulk distribution coefficient). Open system model ("periodically recharged magma chamber," [O'Hara, 1977]) assumes a constant magma volume with parameters chosen to maximize the steepness of the trend (38% crystallization, 2% eruption, 40% recharge, $DLa=0.01$, $DFeO^*/MgO=0.44$). High FeO^*/MgO line in the open system model are expected values prior to recharge and mixing; low FeO^*/MgO line is the residual magma after recharge and mixing. Data fitting this "open system" model would fall between these lines. Note that the Attu data fall between the open system model and the equilibrium melting line. Equilibrium batch melting model [Shaw, 1970, equation 11] is adjusted to pass through the parental Attu basalt at approximately 10% melting ($DLa=0.01$, $DFeO^*/MgO=0.27$). Makaopuhi lava lake data from Wright and Okamura [1977] show the trend of closed system fractionation in a natural system. Data from Eastern Aleutian Okmok caldera (location in Figure 1) are from Kay and Kay [1993 and references therein]. North Pacific MORB data are from Wakeman [1978]. Figure is modified from Kay et al. [1982].

magmatism. The northward shift of the Western Aleutian magmatic front between late Miocene and Pleistocene time probably came at 5 Ma with the 5° northward shift of Pacific plate motion relative to North America [Cox and Engebretson 1985].

Alternatives to the tectonic model in Figure 18 are many. All models, however, will remain speculative until the ages of regionally important structures (e.g., Bowers and Shirshov ridges) become more clearly known (see also Cooper et al. [1992]). We emphasize primarily that the early tectonic events in the Western Aleutians (43-20 Ma) as more closely allied to contemporaneous activity in the Western Bering Sea than to the development of the central and eastern arc; the chemistry of the Attu Basement Series rocks seem to require this. We believe further that the transition to calcalkaline magmatism on Attu and throughout the Western Aleutian islands in the middle Miocene marks a change to a compressional tectonic regime at that time. The predominance of calcalkaline magmatism in compressional regimes and

tholeiitic magmatism in extensional regimes has been noted previously in the Aleutians [e.g., Kay et al., 1982; Singer and Myers, 1992]. We emphasize that these associations are particularly well developed in the history of Attu and western part of the arc (see also Yogodzinski et al. [1993]).

CONCLUSIONS

The Attu Basement Series is most similar to back-arc basin crust, but the age and structure of the Attu Basement Series and its position on the crest of the modern Aleutian Ridge do not readily provide for its formation within the framework of arc-parallel rifting (e.g., the Mariana system). Figure 18 provides a model for another style of arc-adjacent, oceanic rift, wherein the lithosphere of the overriding plate is stretched in response to tectonic adjustments resulting from a switch from convergence to strike-slip-dominated tectonics. On Attu, magmatism in this setting produced oceanic-type crust with the geologic, metamorphic, and geochemical signature of a

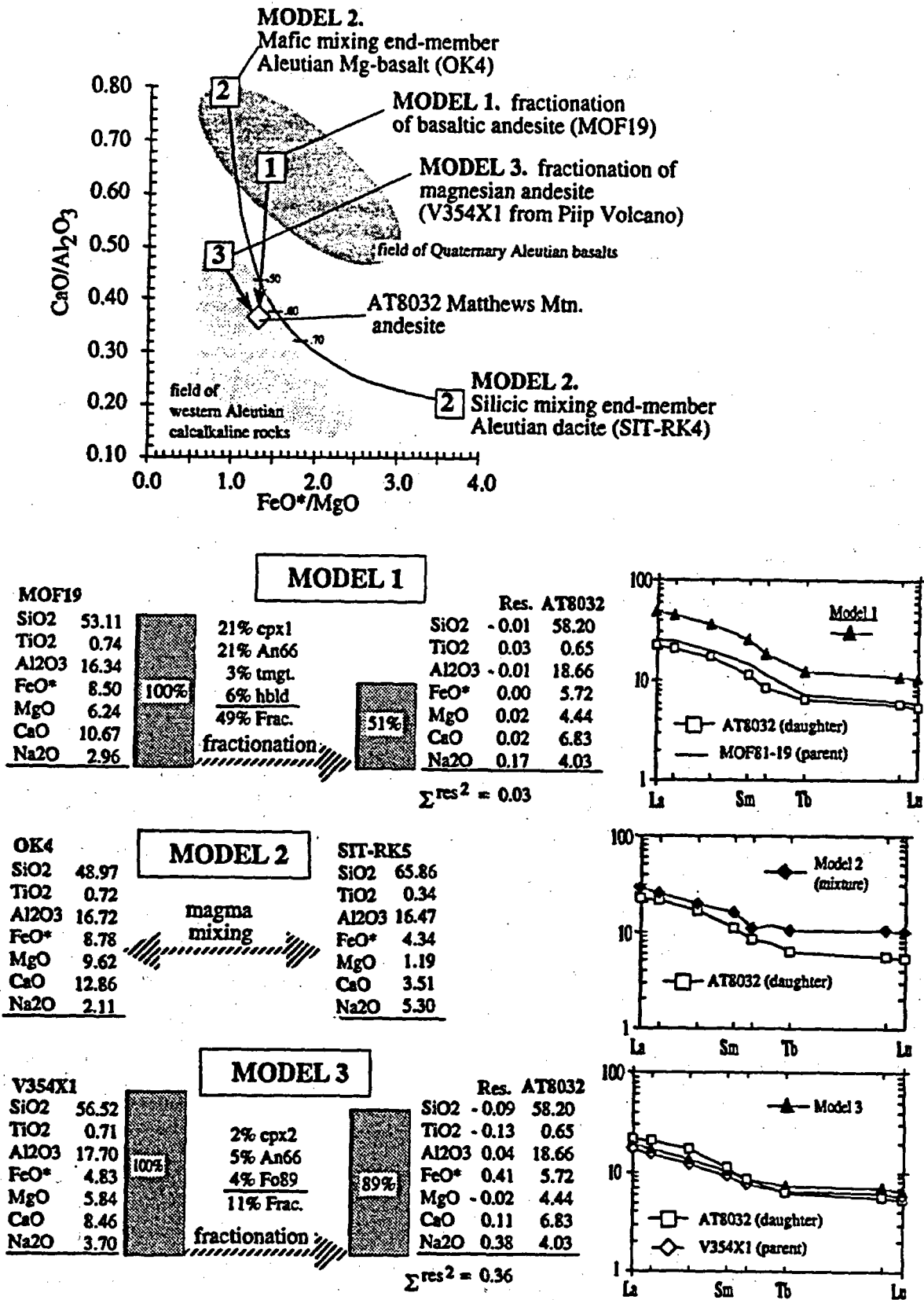


Fig. 17. Simple crystal fractionation and magma mixing models for the origin of the calcalkaline Matthews Mountain andesite (AT8032) demonstrate the distinction between calcalkaline rocks of the Western versus Central and Eastern Aleutian arc. In model 1, major elements are modeled by least squares to obtain mineral percentages removed in Rayleigh fractionation models for the rare earth elements (REE). Good fit to the major elements in model 1 requires 49% crystallization, but this produces calculated REE concentrations that are too high (compare REE in AT8032 and model 1). Note that removal of amphibole with the aim of dampening REE

subduction-related ophiolite (e.g., suprasubduction zone ophiolite of *Pearce et al.* [1984]). The Attu Basement Series is, however, not allochthonous. Rather, it formed in situ by rift-related magmatism within the broadly transtensional tectonic setting that was established in the Western Aleutians after plate reorganization at ~43 Ma. The back-arc type crust of the Attu Basement Series was eventually uplifted, more or less in place, in the transpressional regime of the Late Tertiary Western Aleutian Ridge [e.g., *Kay et al.*, 1986, Figure 3b].

Diffuse generation of oceanic crust and the association of rift tectonics with major strike-slip boundaries provide a mechanism for the in situ formation and emplacement of suprasubduction zone ophiolites [*Sarewitz and Lewis*, 1991]. The Andaman Sea, Cayman Trough, Gulf of California, and the Philippine Marinduque Basin provide actualistic models for the formation of the Western Aleutian arc crust. While the scales and the tectonic geometries associated with these examples vary widely, they illustrate the kinds of processes that may have operated in the formation and preservation of the Attu Basement Series. These kinds of processes are increasingly recognized in the geologic record. Examples may include the Troodos or other Tethyan ophiolites [e.g., *Moores et al.*, 1984], the Rocas Verdes ophiolite of southern Chile [*Dalziel*, 1981], and the Andaman ophiolite of northern Sumatra [*Ray et al.*, 1988].

The Attu Basement Series also has important consequences for arc magma formation in the modern Aleutian system. The history of oblique subduction and rift-related magmatism in the Western Aleutian arc has provided an opportunity to sample Aleutian sub-arc mantle that was relatively unmodified by subducted components. The geochemistry of the tholeiitic basalts of the Attu Basement Series requires that in Early to Middle Tertiary time, the Aleutian sub-arc mantle at ~176°E was like that of MORB. This is important, because in the more conventional tectonic geometry of the Central and Eastern Aleutian arc, recycling, mixing, and melting are complete to the extent that even in the most primitive magmas, it is difficult to know whether the unmodified mantle source was more similar to MORB or OIB [e.g., *Kay*, 1980; *Morris and Hart*, 1983; *Perfit and Kay*, 1986]. The Attu Basement Series tholeiites presumably escaped contamination by recycled upper crust because recycling was minimized by oblique subduction, and because eruption rates in the rift environment were relatively high (see also *Yogodzinski et al.* [1993]).

The eruption of a strongly calcalkaline series throughout the Western Aleutians beginning approximately 15 m.y. ago, heralded the end of transtensional tectonics and the beginning of Western Aleutian style transpressional tectonics and associated magmatism. Late Pleistocene activity at Piip Volcano is a continuation of this magmatic episode. At Piip Volcano, hydrous (and oxidized?), amphibole-bearing melts of intermediate-to-silicic composition (mostly 60-68% SiO₂) have leaked to the surface along a small zone of tectonic

dilation within the broadly transpressional Western Aleutian Ridge [see *Seliverstov et al.*, 1990a, b; *Baranov et al.*, 1991; *Romick et al.*, 1993; *Yogodzinski et al.*, 1993]. We infer from geochemistry and regional magmatic history that the modern transpressional tectonic style of the Western Aleutian arc [*Geist et al.*, 1988; 1991] was established approximately 15 m.y. ago.

Miocene to Recent magmas that have erupted in the Western Aleutians cannot be produced by crystal fractionation of basalts or basaltic andesites like those found in the central and eastern arc. The Western Aleutian calcalkaline trend is produced by the removal of amphibole and Fe-Ti oxides from primitive magnesian andesites [see *Yogodzinski et al.*, 1993]. This implies that calcalkaline magmatism is tied not only to specific crystallization conditions within the arc crust [e.g., *Kay and Kay*, 1985], but also to distinctive conditions within the sub-arc mantle conducive to the formation of primitive andesites. These may include shallow and hydrous melting conditions [e.g., *Tatsumi*, 1982], small percentage melting, and/or an extended melt-peridotite reaction history (i.e., mantle assimilation [*Kelemen*, 1986, 1990]).

The role of magnesian andesites in the Central and Eastern Aleutians remains unclear. Primitive mafic xenocrysts (Mg number >88) in andesites and dacites of some of the most strongly calcalkaline Aleutian centers (e.g., Buldir Volcano [*Kay and Kay*, 1985]) has been taken as good evidence that primitive basalts [*Kay et al.*, 1982; *Nye and Reid*, 1986] are parental to the calcalkaline trend in the Central Aleutians. The recognition of magnesian andesites at Piip Volcano provides another possible source for primitive xenocrysts in calcalkaline lavas.

Acknowledgments. This paper constitutes a portion of Gene Yogodzinski's Ph.D. dissertation at Cornell University. Support for this research was provided by National Science Foundation (grants EAR-8707577 and EAR-9104964), a Geological Society of America Harold T. Stearns research award, and an American Association of Petroleum Geologists Grant-in-Aid. Assistance was also provided by the Meyer Bender Memorial Fund of the Department of Geological Sciences at Cornell. Valuable assistance in the field was provided by the U.S. Coast Guard on Attu and Kodiak Islands, by the U.S. Naval Air Station on Adak Island, and by the U.S. Fish and Wildlife Service. The assistance of Kurt Dodd, Dee Gardner, Janice Lee, Jeff Reynolds, and Jay Romick are gratefully acknowledged. Thanks also to Dan Karig, Dan Sarewitz, Dave Scholl, Tracy Vallier, Oleg Volynets, Alexander Koloskov and Nikolai Seliverstov for valuable scientific discussion, to Michael Cheatham for his efforts in the clean lab-mass spectrometer facilities, and to Howard Aderhold and the crew at the Cornell TRIGA reactor. This paper benefited from helpful reviews by Jim Myers, Chris Nye and an anonymous reviewer.

increases during fractionation [e.g. *Romick et al.*, 1992], will produce large major element residuals, because amphibole removal from basalts or basaltic andesites cannot produce the low CaO/Al₂O₃ values seen in the Western Aleutian rocks (see text). Model 2 is a mixing model between primitive Aleutian Mg-basalt (OK4) and a dacite from the Central Aleutians (SIT-RK4). Note that high Al₂O₃ in the Matthews Mountain andesite cannot be explained by mixing the end-members in model 2. Similarly, the low CaO/Al₂O₃ relative to FeO*/MgO of the Western Aleutian suite cannot be explained by such a mixing line or by any other mixing line using end-members selected from the central or eastern Aleutian arc. Most importantly, no combination of fractionation and mixing of magmas from the central and eastern Aleutians (models 1 and 2) can explain the Western Aleutian data (compare with Figure 15). In model 3, simple fractionation of a Piip Volcano magnesian andesite reproduces the major elements reasonably well with only 11% crystallization. This small degree of crystallization also results in a relatively good match for the REE. Modeling parameters are given in Table 3.

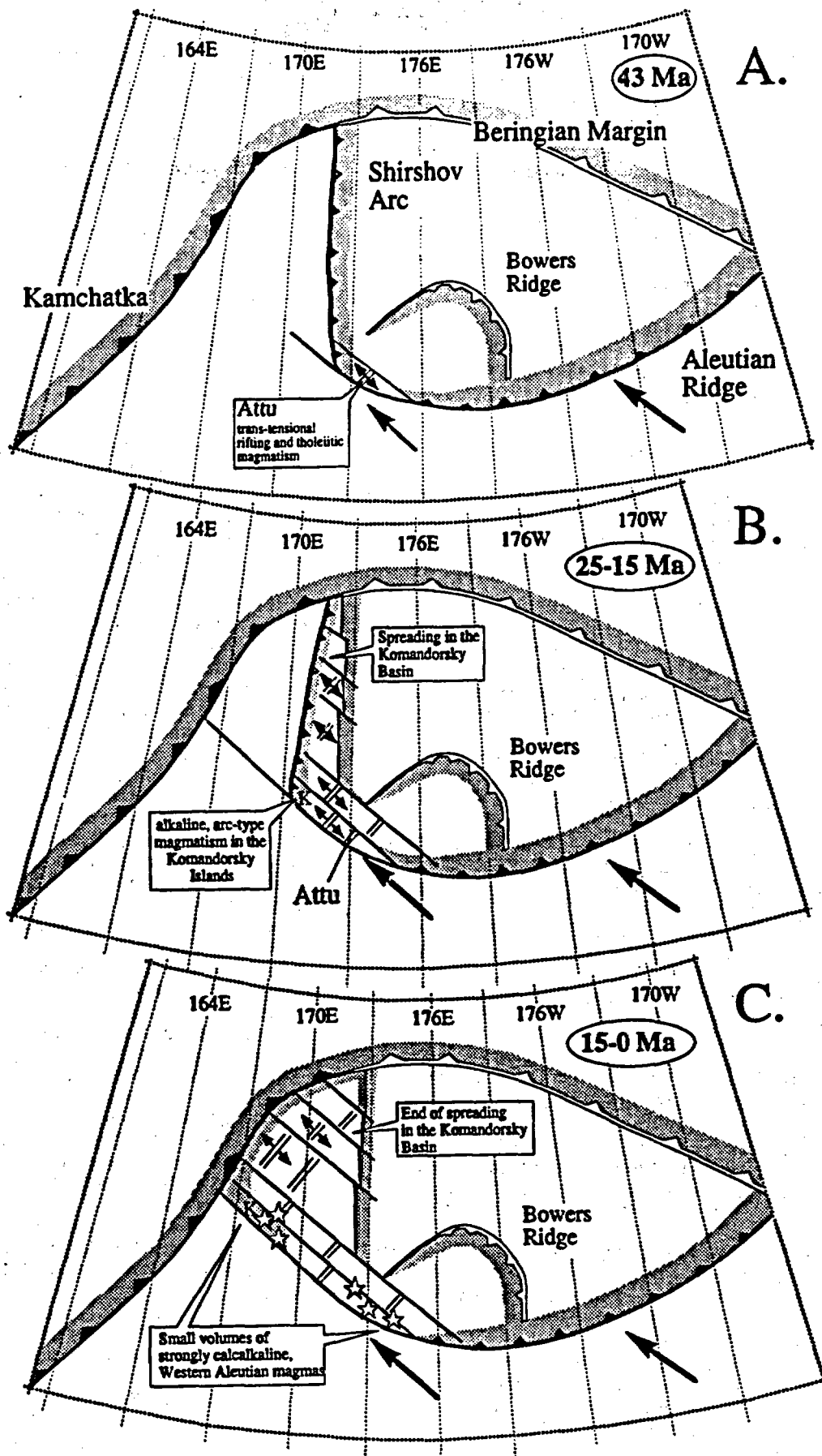


Fig. 18. Tectonic cartoon for the origin of the Near Islands and the Western Aleutian-Bering Sea region. (a) At -43 Ma, change to highly oblique convergence in the Western Aleutians results in trans-tensional rifting and tholeiitic magmatism at the Aleutian-Shirshov junction to form the Attu Basement Series. The aseismic Shirshov Ridge (Figure 1) is shown as the northwestern extension of the pre-43 Ma Aleutian island arc [Scholl

et al., 1989; Baranov *et al.*, 1991; Cooper *et al.*, 1992]. This tectonic geometry was probably accommodated by convergence across the Bering Sea [Scholl *et al.*, 1989; Cooper *et al.*, 1992]. The Bowers Ridge is assumed here to have become inactive by ~43 Ma. This is a simplifying assumption as the Bowers arc may have been active into the middle Tertiary (see discussion in text and Cooper *et al.* [1992]). (b) At approximately 25 Ma, breakup of the Shirshov island arc and westward opening of the Komandorsky Basin occur in conjunction with the westward migration of arc-related crustal blocks (terranes) that will eventually become accreted to the Kamchatka margin and possibly form portions of the Komandorsky Islands in the westernmost Aleutians (Figure 1). Komandorsky alkaline volcanic rocks with arc-type geochemical signatures are approximately 20-25 m.y. old [Borusk and Tsvetkov, 1982; Tsvetkov, 1991]. (c) Collision of arc-related terranes with the Kamchatka trench changes the tectonic regime of the Western Aleutians from transtensional to transpressional (see also Watson and Fujita [1985], and Geist *et al.* [1991]). This results in the observed shift from voluminous tholeiitic magmatism to volumetrically minor, strongly calcalkaline magmatism in the Near Islands (Matthews Mountain andesites) and in the Komandorsky Islands beginning ~15 m.y. ago. This kind of magmatism continues along the northern margin of the Western Aleutian Ridge today (e.g., Piip Volcano). Stars are locations of post-15 Ma calcalkaline magmatism along the Western Aleutian Ridge.

REFERENCES

- Aldiss, D.T., Plagiogranites from the ocean crust and ophiolites, *Nature*, 289, 577-578, 1981.
- Armstrong, R.L., Isotopic and chemical constraints on models of magma genesis in volcanic arcs, *Earth Planet. Sci. Lett.*, 12, 137-142, 1971.
- Arth, J.G., and G.N. Hanson, Geochemistry and origin of the early Precambrian crust of northeastern Minnesota, *Geochim. Cosmochim. Acta*, 30, 325-362, 1975.
- Baranov, B.C., N.I. Seliverstov, A.V. Murav'ev, and E.L. Muzurov, The Komandorsky Basin as a product of spreading behind a transform plate boundary, *Tectonophysics*, 199, 237-269, 1991.
- Ben Othman, D., W.M. White, and J. Patchett, The geochemistry of marine sediments, island arc magma genesis, and crust-mantle recycling, *Earth Planet. Sci. Lett.*, 94, 1-21, 1989.
- Bonatti, E., J. Honnorez, P. Kirst, and F. Radicati, Metagabbros from the Mid-Atlantic Ridge at 6° N: contact-hydrothermal-dynamic metamorphism beneath the axial valley, *J. Geol.*, 83, 61-78, 1975.
- Borusk, A.M., and A.A. Tsvetkov, Magmatic associations of the western part of the Aleutian Island arc, *Int. Geol. Rev.*, 24, 317-329, 1982.
- Boyd, T.M., and K.C. Creager, The geometry of Aleutian subduction: Three-dimensional seismic imaging, *J. Geophys. Res.*, 96, 2267-2291, 1991.
- Brophy, J.G., Andesites from northeastern Kanaga Island, Aleutians, *Contrib. Mineral. Petrol.*, 104, 568-581, 1990.
- Christie, D.M., and J.M. Sinton, Evolution of abyssal lavas along propagating segments of the Galapagos Spreading Center, *Earth Planet. Sci. Lett.*, 56, 321-355, 1981.
- Church, S.E., and M. Tatsumoto, Lead isotope relations in oceanic ridge basalts from the Juan de Fuca-Gorda Ridge area, N.E. Pacific Ocean, *Contrib. Mineral. Petrol.*, 53, 253-279, 1975.
- Clague, D.A., F.A. Frey, G. Thompson, and S. Rindge, Minor and trace element geochemistry of volcanic rocks dredged from the Galapagos Spreading Center: Role of crystal fractionation and mantle heterogeneity, *J. Geophys. Res.*, 86, 9469-9482, 1981.
- Conrad, W.K., and R.W. Kay, Ultramafic and mafic inclusions from Adak Island: crystallization history, and implications for the nature of primary magmas and crustal evolution in the Aleutian arc, *J. Petrol.*, 25, 88-125, 1984.
- Cooper, A.K., M.S. Marlow, and D.W. Scholl, Geologic framework of the Bering Sea crust, in *Geology and Resource Potential of the Continental Margin of Western North America and Adjacent Ocean Basins--Beaufort Sea to Baja California*, edited by D.W. Scholl, A. Grantz, and J.G. Vedder, pp. 73-102, Circum-Pacific Council for Energy and Mineral Resources, Houston, Tex., 1987.
- Cooper, A.K., M.S. Marlow, A.J. Stevenson, and D.W. Scholl, Evidence for Cenozoic crustal extension in the Bering Sea region, *Tectonics*, 11, 719-731, 1992.
- Cox, A., and D. Engebretson, Change in motion of Pacific plate at 5 Myr BP, *Nature*, 313, 472-474, 1985.
- Dalziel, I.W.D., Back-arc extension in the southern Andes: a review and critical appraisal, *Philos. Trans. R. Soc. of London, Ser. A*, 300, 319-335, 1981.
- Davis, A.S., L.B.G. Pickthorn, T.L. Vallier, and M.S. Marlow, Petrology and age of volcanic-arc rocks from the continental margin of the Bering Sea: implications for Early Eocene relocation of plate boundaries, *Can. J. Earth Sci.*, 26, 1474-1490, 1989.
- Defant, M.J., and M.S. Drummond, Derivation of some modern arc magmas by melting of young subducted lithosphere, *Nature*, 347, 662-665, 1990.
- DeLisio, G.P., Petrology and geochemistry of the Komandorski Islands, Aleutians and Simushir Island, Kuriles, Bachelors thesis, 46 pp., Cornell Univ., Ithaca, N.Y., 1984.
- DeLong, S.E., and C. Chatelain, Trace-element constraints on accessory-phase saturation in evolved MORB magma, *Earth Planet. Sci. Lett.*, 101, 206-215, 1990.
- DeLong, S.E., and F.W. McDowell, K-Ar ages from the Near Islands, Western Aleutian Islands, Alaska: indication of a mid-Oligocene thermal event, *Geology*, 3, 691-694, 1975.
- Duncan, R.A., and D.H. Green, The genesis of refractory melts in the formation of oceanic crust, *Contrib. Mineral. Petrol.*, 96, 326-342, 1987.
- Dunning, G.R., H.S. Swinden, B.F. Kean, D.T.W. Evans, and G.A. Jenner, A Cambrian island arc in Iapetus: geochronology and geochemistry of the Lake Ambrose volcanic belt, Newfoundland Appalachians, *Geol. Mag.*, 128, 1-17, 1991.
- Engebretson, D.C., A. Cox, and R.G. Gordon, Relative Motion Between Oceanic and Continental Plates in the Pacific Basin, *Spec. Pap. Geol. Soc. Am.*, 206, 59 pp., 1985.
- Fryer, P., B. Taylor, C.H. Langmuir, and A.G. Hochstaedter, Petrology and geochemistry of lavas from the Sumisu and Torishima backarc rifts, *Earth Planet. Sci. Lett.*, 100, 161-178, 1990.
- Fujimaki, H., M. Tatsumoto, and K. Aoki, Partition coefficients of Hf, Zr, and REE between phenocrysts and groundmasses, *Proc. Lunar Planet. Sci. Conf.*, 14th, Part 2, *J. Geophys. Res.*, 89 suppl., B662-B672, 1984.
- Gates, O., H.A. Powers, and R.E. Wilcox, Geology of the Near Islands, Alaska, *U.S. Geol. Surv. Bull.*, 1028-U, 709-822, 1971.

- Geist, E.L., J.R. Childs, and D.W. Scholl, The origin of summit basins of the Aleutian Ridge: Implications for block rotation of an arc massif, *Tectonics*, 7, 327-341, 1988.
- Geist, E.L., D.W. Scholl, and T.L. Vällier, Collision of the Aleutian Island Arc with Kamchatka (abstract), *Eos Trans. AGU*, 72, Fall Meeting Suppl., 440, 1991.
- Green, T.H., and N.J. Pearson, An experimental study of Nb and Ta partitioning between Ti-rich minerals and silicate liquids at high pressure and temperature, *Contrib. Mineral. Petrol.*, 91, 24-36, 1987.
- Hamelin, B., B. Dupre, and C.J. Allegre, The lead isotope systematics of ophiolite complexes, *Earth Planet. Sci. Lett.*, 67, 351-366, 1984.
- Hart, S.R., A large-scale isotope anomaly in the Southern Hemisphere mantle, *Nature*, 309, 753-757, 1984.
- Hegner, E., and M. Tatsumoto, Pb, Sr, and Nd isotopes in basalts and sulfides from the Juan de Fuca Ridge, *J. Geophys. Res.*, 92, 11380-11386, 1987.
- Hein, J.R., and H. McLean, Paleogene sedimentary and volcanogenic rocks from Adak Island, Central Aleutian islands, Alaska, *U.S. Geol. Surv. Prof. Pap.*, 1126-E, 16 pp., 1980.
- Hickey-Vargas, R., Isotope characteristics of submarine lavas from the Philippine Sea: implications for the origin of arc and basin magmas of the Philippine tectonic plate, *Earth Planet. Sci. Lett.*, 107, 290-304, 1991.
- Hochstaedter, A.G., J.B. Gill, M. Kusakabe, S. Newman, M. Pringle, B. Taylor, and P. Fryer, Volcanism in the Sumisu Rift, I. Major element, volatile, and stable isotope geochemistry, *Earth Planet. Sci. Lett.*, 100, 179-194, 1990.
- Housh, T., S.A. Bowring, and A.A. Tsvetkov, Pb isotopic compositions of Oligocene-Miocene basalts from the Komandorsky Islands, Western Aleutian island arc, *Geol. Soc. Am. Abstr. Programs*, 21, A56, 1989.
- Hunter, R.H., and R.S.J. Sparks, The differentiation of the Skaergaard intrusion, *Contrib. Mineral. Petrol.*, 95, 451-461, 1987.
- Ishizuka, H., Y. Kawanobe, and H. Sakai, Petrology and geochemistry of volcanic rocks dredged from the Okinawa Trough, an active back-arc basin, *Geochem. J.*, 24, 75-92, 1990.
- Karig, D.E., Origin and development of marginal basins in the western Pacific, *J. Geophys. Res.*, 76, 2542-2560, 1971.
- Kay, R.W., Aleutian magnesian andesites: melts from subducted ocean crust, *J. Volcanol. Geotherm. Res.*, 4, 117-132, 1978.
- Kay, R.W., Volcanic arc magma genesis: implications for element recycling in the crust-upper mantle system, *J. Geol.*, 88, 497-522, 1980.
- Kay, R.W., and S.M. Kay, Crustal recycling and the Aleutian arc, *Geochim. Cosmochim. Acta*, 52, 1351-1359, 1988.
- Kay, R.W., N.J. Hubbard, and P.W. Gast, Chemical characteristics and origin of oceanic ridge volcanic rocks, *J. Geophys. Res.*, 75, 1585-1613, 1970.
- Kay, R.W., S.S. Sun, and C.N. Lee-Hu, Pb and Sr isotopes in volcanic rocks from the Aleutian Islands and Pribilof Islands, Alaska, *Geochim. Cosmochim. Acta*, 42, 263-273, 1978.
- Kay, R.W., J.L. Rubenstone, and S.M. Kay, Aleutian terranes from Nd isotopes, *Nature*, 322, 605-609, 1986.
- Kay, S.M., Metamorphism in the Aleutian arc: the Finger Bay Pluton, Adak, Alaska, *Can. Mineral.*, 21, 665-681, 1983.
- Kay, S.M., R.W. Kay, Aleutian tholeiitic and calc-alkaline magma series I: the mafic phenocrysts, *Contrib. Mineral. Petrol.*, 90, 276-290, 1985.
- Kay, S.M., and R.W. Kay, Aleutian magmas in space and time, in *Decade of North American Geology, Geology of Alaska, GNA-G1*, edited by G. Plafker and D.L. Jones, Geological Society of America, Boulder, Colorado, in press, 1993.
- Kay, S.M., R.W. Kay, and G.P. Citron, Tectonic controls on tholeiitic and calc-alkaline magmatism in the Aleutian arc, *J. Geophys. Res.*, 87, 4051-4072, 1982.
- Kay, S.M., R.W. Kay, H.K. Brueckner, and J.L. Rubenstone, Tholeiitic Aleutian Arc plutonism: the Finger Bay Pluton, Adak, Alaska, *Contrib. Mineral. Petrol.*, 82, 99-116, 1983.
- Kay, S.M., Maksiyev, R. Moscoso, C. Mpodozis, and C. Nasi, Probing the evolving Andean lithosphere: mid-late Tertiary magmatism in Chile (29° -30° 30'S) over the modern zone of subhorizontal subduction, *J. Geophys. Res.*, 92, 6173-6189, 1987.
- Kay, S.M., R.W. Kay, G.P. Citron, and M.R. Perfit, Calc-alkaline plutonism in the intra-oceanic Aleutian arc, Alaska, in *Plutonism from Antarctica to Alaska*, edited by S.M. Kay and C.W. Rapela, *Spec. Pap. Geol. Soc. Am.*, 241, 233-255, 1990.
- Kelemen, P.B., Assimilation of ultramafic rock in subduction-related magmatic arcs, *J. Geol.*, 94, 829-843, 1986.
- Kelemen, P.B., Reaction between ultramafic rock and fractionating basaltic magma, I, Phase relations, the origin of calc-alkaline magma series, and the formation of discordant dunite, *J. Petrol.*, 31, 51-98, 1990.
- Langmuir, C.H., Geochemical consequences of in situ crystallization, *Nature*, 340, 199-205, 1989.
- Lonsdale, P.J., Paleogene history of the Kula plate: Offshore evidence and onshore implications, *Geol. Soc. Am. Bull.*, 100, 733-754, 1988.
- Lonsdale, P.J., and J. Hawkins, Silicic volcanism at an off-axis geothermal field in the Mariana Trough back-arc basin, *Geol. Soc. Am. Bull.*, 96, 940-951, 1985.
- Lugmair, G.W., and R.W. Carlson, The Sm-Nd history of KREEP, *Proc. Lunar Planet. Sci. Conf.*, 9th, 689-704, 1978.
- MacDonald, R., D.W. McGarvie, H. Pinkerton, R.L. Smith, and Z.A. Palacz, Petrogenetic evolution of the Torfajokull volcanic complex, Iceland, I, Relationship between the magma types, *J. Petrol.*, 31, 429-459, 1990.
- Marlow, M.S., D.W. Scholl, E.C. Buffington, and T.R. Alpha, Tectonic history of the Central Aleutian arc, *Geol. Soc. Am. Bull.*, 84, 1555-1574, 1973.
- Marsh, B.D., The Aleutians, in *Orogenic Andesites and Related Rocks*, edited by R.A. Thorpe, pp. 99-114, John Wiley & Sons, N.Y., 1982.
- McLean, H., and J.R. Hein, Paleogene geology and chronology of southwestern Umnak Island, Aleutian Islands, Alaska, *Can. J. Earth Sci.*, 21, 171-180, 1984.
- Miyashiro, A., Volcanic rock series in island arcs and active continental margins, *Am. J. Sci.*, 274, 321-355, 1974.
- Moore, E.M., P.T. Robinson, J. Malpas, and C. Xenophonotos, Model for the origin of the Troodos massif, Cyprus, and other mid-east ophiolites, *Geology*, 12, 500-503, 1984.
- Morris, J.D., and S.R. Hart, Isotopic and incompatible element constraints on the genesis of island arc volcanics from Cold Bay and Amak Island, Aleutians, and implications for mantle structure, *Geochim. Cosmochim. Acta*, 47, 2015-2030, 1983.
- Newberry, J.T., D.L. Laclair, and K. Fujita, Seismicity and tectonics of the far Western Aleutian Islands, *J. Geodyn.*, 6, 13-32, 1986.
- Nye, C.J., and M.R. Reid, Geochemistry of primary and least fractionated lavas from Okmok Volcano, Central Aleutians: Implications for arc magmagenesis, *J. Geophys. Res.*, 91, 10271-10287, 1986.
- O'Hara, M., Geochemical evolution during fractional crystallization of a periodically refilled magma chamber, *Nature*, 266, 503-507, 1977.
- O'Nions, R.K., and K. Gronvold, Petrogenetic relationships of acid and basic rocks in Iceland: Sr-isotopes and rare-earth elements in late and postglacial volcanics, *Earth Planet. Sci. Lett.*, 19, 397-409, 1973.

- Pearce, J.A., Trace element characteristics of lavas from destructive plate boundaries, in *Orogenic Andesites and Related Rocks*, edited by R.A. Thorpe, pp. 525-548, John Wiley & Sons, N.Y., 1982.
- Pearce, J.A., S.J. Lippard, and S. Roberts, Characteristics and tectonic significance of supra-subduction zone ophiolites, in *Marginal Basin Geology: Volcanic and Associated Sedimentary and Tectonic Processes in Modern and Ancient Marginal Basins*, edited by B.P. Kokelaar and M.F. Howells, pp. 77-94, Blackwell Scientific, Boston, Massachusetts, 1984.
- Perfit, M.R., and R.W. Kay, Comment on "Isotopic and incompatible element constraints on the genesis of island arc volcanics from Cold Bay and Amak Island, Aleutians, and implications for mantle structure" by J.D. Morris and S.R. Hart, *Geochim. Cosmochim. Acta*, 50, 477-481, 1986.
- Perfit, M.R., and J.R. Lawrence, Oxygen isotopic evidence for meteoric water interaction with the Captains Bay Pluton, Aleutian Islands, *Earth Planet. Sci. Lett.*, 45, 16-22, 1979.
- Ray, K.K., S. Sengupta, and H.J. Van Den Hul, Chemical characters of volcanic rocks from Andaman ophiolite, India, *J. Geol. Soc. London*, 145, 393-400, 1988.
- Romick, J.D., S. M. Kay, and R.W. Kay, The influence of amphibole fractionation on the evolution of calc-alkaline andesite and dacite tephra from the Central Aleutians, Alaska, *Contrib. Mineral. Petrol.*, 112, 101-118, 1992.
- Romick, J.D., A.A. Tsvetkov, and N.I. Seliverstov, Silicic volcanism in the Komandorski Basin: Evidence for storage of a slab component in the backarc mantle, *J. Geophys. Res.*, in press, 1993.
- Rubenstein, J.L., Geology and geochemistry of early Tertiary submarine volcanic rocks of the Aleutian Islands, and their bearing on the development of the Aleutian Island Arc, Cornell Univ. Ph.D. thesis, 313 pp., Ithaca, N.Y., 1984.
- Rubenstein, J.L., T.F. O'Brien, and G.P. Citron, Low-grade metamorphism controlled by eruptive setting in Aleutian Paleogene volcanic rocks, *Geol. Soc. Am. Abstr. Programs*, 14, 604, 1982.
- Ryerson, F.J., and E.B. Watson, Rutile saturation in magmas: implications for Ti-Nb-Ta depletion in island-arc basalts, *Earth Planet. Sci. Lett.*, 86, 225-239, 1987.
- Sarewitz, D.R., and S.D. Lewis, The Marinduque intra-arc basin, Philippines: Basin generation and in situ ophiolite development in a strike-slip setting, *Geol. Soc. Am. Bull.*, 103, 597-614, 1991.
- Schnetzler, C.C., and J.A. Philpotts, Partition coefficients of rare-earth elements between igneous matrix material and rock-forming mineral phenocrysts, II, *Geochim. Cosmochim. Acta*, 34, 331-340, 1970.
- Scholl, D.W., H.G. Greene, and M.S. Marlow, Eocene age of the Adak Paleozoic (?) rocks, Aleutian Islands, Alaska, *Geol. Soc. Am. Bull.*, 81, 3583-3592, 1970.
- Scholl, D.W., M.S. Marlow, N.S. MacLeod, and E.C. Buffington, Episodic Aleutian Ridge igneous activity: implications of Miocene and younger submarine volcanism west of Buldir Island, *Geol. Soc. Am. Bull.*, 87, 547-554, 1976.
- Scholl, D.W., T.L. Vallier, and A.J. Stevenson, Terrane accretion, production, and continental growth: A perspective based on the origin and tectonic fate of the Aleutian-Bering Sea region, *Geology*, 14, 43-47, 1986.
- Scholl, D.W., T.L. Vallier, and A.J. Stevenson, Geologic evolution and petroleum geology of the Aleutian ridge, in *Geology and Resource Potential of the Continental Margin of Western North America and Adjacent Ocean Basins--Beaufort Sea to Baja California*, edited by D.W. Scholl, A. Grantz, and J.G. Vedder, pp. 103-122, Circum-Pacific council for Energy and Mineral Resources, Houston, Texas, 1987.
- Scholl, D.W., A.J. Stevenson, T.L. Vallier, H.F. Ryan, and E.L. Geist, Aleutian arc-trench system: perspective of ocean margin evolution controlled by regional changes in plate-boundary conditions, *Proc. Int. Geol. Congr.*, 28th (3), 52-53, 1989.
- Seliverstov, N.I., Structure of the junction zone between the Kuril-Kamchatka and Aleutian Island arcs from continuous seismic profiling, *Volcanol. Seismol.*, 5, 175-190, 1984.
- Seliverstov, N.I., G.P. Avdieko, A.N. Ivanenko, V.A. Shkira, and S.A. Khubunaya, A new submarine volcano in the west of the Aleutian Island arc, *Volcanol. Seismol.*, 8, 473-495, 1990a.
- Seliverstov, N.I., B.V. Baranov, Y.O. Egorov, and V.A. Shkira, New data on the structure of the southern Komandorsky Basin provided by cruise 26 of R/V VULKANOLOG, *Volcanol. Seismol.*, 10, 499-524, 1990b.
- Shaw, D.M., Trace element fractionation during anatexis, *Geochim. Cosmochim. Acta*, 34, 237-243, 1970.
- Shelton, D.H., The geochemistry and petrogenesis of gabbroic rocks from Attu Island, Aleutian islands, Alaska, M.S. theses, 178 pp., Cornell Univ., Ithaca, N.Y., 1986.
- Shimokawa, T., and A. Masuda, Rare-earths in Icelandic neovolcanic rocks, *Contrib. Mineral. Petrol.*, 37, 39-46, 1972.
- Sigmarrsson, O., C. Hemond, M. Condomines, S. Fourcade, and N. Oskarsson, Origin of silicic magma in Iceland revealed by Th isotopes, *Geology*, 19, 621-624, 1991.
- Singer, B.F., and J.D. Myers, Intra-arc extension and magmatic evolution in the Central Aleutian arc, Alaska, *Geology*, 18, pp. 1050-1053, 1992.
- Sinton, J.M., and R.S. Detrick, Mid-ocean ridge magma chambers, *J. Geophys. Res.*, 97, 197-216, 1992.
- Smith, D.R., and W.P. Leeman, Petrogenesis of Mount St. Helens dacitic magmas, *J. Geophys. Res.*, 92, 10313-10334, 1987.
- Stern, C., Open and closed system igneous fractionation within two Chilean ophiolites and the tectonic implication, *Contrib. Mineral. Petrol.*, 68, 243-258, 1979.
- Sun, S.S., and W.F. McDonough, Chemical and isotopic systematics of oceanic basalts: implications for mantle composition and processes, in *Magmatism in the Ocean Basins*, edited by A.D. Saunders and M.J. Norry, *Geol. Soc. Spec. Pub.* 42, 313-345, 1989.
- Tatsumi, Y., Origin of high-magnesian andesites in the Setouchi volcanic belt, southwest Japan, II. Melting phase relations at high pressures, *Earth Planet. Sci. Lett.*, 60, 305-317, 1982.
- Tatsumoto, M., and Y. Nakamura, DUPAL anomaly in the Sea of Japan: Pb, Nd, and Sr isotopic variations in the Eastern Eurasian continental margin, *Geochim. Cosmochim. Acta*, 55, 3697-3709, 1991.
- Tsvetkov, A.A., Magmatism of the westernmost (Komandorsky) segment of the Aleutian Island Arc, *Tectonophysics*, 199, 289-317, 1991.
- Vallier, T.L., D.W. Scholl, M.A. Fisher, R. von Huene, T.R. Bruns, and A.J. Stevenson, Geologic framework of the Aleutian Arc, in *Decade of North American Geology, Geology of Alaska, GNA-GI* edited by G. Plafker and D.L. Jones, Geological Society of America, Boulder, Colo., in press, 1993.
- Volynets, O.N., A.V., Koloskov, G.M., Yogodzinski, N.I., Seliverstov, V.O., Igorov, V.A., Shkira, V.V., Matvenkov, Boninitic tendencies in lavas of the submarine Piip Volcano and surrounding area (far Western Aleutians): Geology, petrochemistry, and mineralogy (in Russian), *Volcanol. Seismol.*, no. 1, 3-19, 1992.
- Wakeman, S.E., Petrochemical patterns in young pillow basalts dredged from Juan de Fuca and Gorda ridges, M.S. thesis, 95 pp., Oreg. State Univ., Corvallis, 1978.
- Walker, D., T. Shibata, and S.E. DeLong, Abyssal tholeiites

- from the Oceanographer Fracture Zone, *Contrib. Mineral. Petrol.*, **70**, 111-125, 1979.
- Walker, R.J., R.W. Carlson, S.B. Shirey, and F.R. Boyd, Os, Sr, Nd, and Pb isotope systematics of southern African peridotite xenoliths: implications for the chemical evolution of subcontinental mantle, *Geochim. Cosmochim. Acta*, **53**, 1583-1595, 1989.
- Wasserburg, G.J., S.B. Jacobsen, D.J. DePaolo, M.T. McCulloch, and T. Wen, Precise determination of Sm/Nd ratios, Sm and Nd isotopic abundances in standard solutions, *Geochim. Cosmochim. Acta*, **45**, 2311-2323, 1981.
- Watson, B.F., and K. Fujita, Tectonic evolution of Kamchatka and the Sea of Okhotsk and implications for the Pacific Basin, in *Tectonostratigraphic Terranes of the Circum-Pacific Region*, edited by D.G. Howell, pp. 333-348, Circum-Pacific Council for Energy and Mineral Resources, Houston, Tex., 1985.
- White, W.M., M.M. Cheatham, and R.A. Duncan, Isotope geochemistry of leg 115 basalts and inferences on the history of the Reunion mantle plume, in *Proc. Ocean Drill. Program Sci. Results*, **115**, 53-61, 1990.
- White, W.M., A.W. Hofmann, and H. Puchelt, Isotope geochemistry of Pacific mid-ocean ridge basalt, *J. Geophys. Res.*, **92**, no. B6, 4881-4893, 1987.
- Wilcox, R.E., Igneous rocks of the Near Islands, Aleutian Islands, Alaska, *Proc. Int. Geol. Cong.*, **20th**, 365-378, 1956.
- Wood, D.A., Major and trace element variations in the Tertiary lavas of Eastern Iceland with respect to the Iceland geochemical anomaly, *J. Petrol.*, **19**, 393-436, 1978.
- Wright, T.L., and R.T. Okamura, Cooling and crystallization of tholeiitic basalts, 1965 Makaopuhi Lava Lake, Hawaii, *U.S. Geol. Surv. Prof. Pap.*, **1004**, 78 pp., 1977.
- Yogodzinski, G.M., O.N. Volynets, A.V. Koloskov, and N.I. Seliverstov, Magnesian andesites and the subduction component in a strongly calcalkaline series at Piip Volcano in the far Western Aleutian arc, *J. Petrol.*, in press, 1993.
-
- R.W. Kay, S.M. Kay, and G.M. Yogodzinski, Department of Geological Sciences, Snee Hall, Cornell University, Ithaca, NY 14853-1504.
- J.L. Rubenstone, Lamont-Doherty Earth Observatory of Columbia University, Palisades, NY 10964.

(Received November 4, 1991;
revised February 8, 1993;
accepted March 11, 1993.)

Section 4

**RECENTLY PUBLISHED ABSTRACTS
BY G.M. YOGODZINSKI**

MPIC. Biotite isopleths have been documented for several stratigraphic units, namely, the Wymen meta-argillites, Deep Spring and Andrews Mountain metagranites, and Montenegro phyllites. Metamorphic grade west of the range crest is chlorite zone of the greenschist facies (~300°C) but rises abruptly on the extreme north adjacent to the Barrois Granodiorite, and gradually increases eastward towards the Beer Creek / Cottonwood pluton. Pressures attending thermally-induced recrystallization are poorly constrained but were on the order of 2-1 kbar. Most of the mid- to late Mesozoic intrusive igneous bodies in the White Mountains crosscut the regional fold pattern in the country rocks. The anclinorium is manifested in strata ranging from latest Precambrian to at least as young as mid-Paleozoic in age. Background low-grade regional diagenetic metamorphism could have been produced synkinematic with deformation, and therefore might be substantially older than the mid- to late Mesozoic time of calc-alkaline arc intrusion. In any case, the progressive metamorphic mineral parageneses reported here do not represent a synchronous thermal event, but instead constitute a composite of more local recrystallization episodes attending granitoid emplacement, perhaps overprinting a pervasive but feeble, chloritic metamorphism which was produced during earlier folding.

V518-7 0830h POSTER
Ca, U, Th and Sr Depleted High-Pressure Granulites of the Bohemian Massif, Lower Austria. Geochemical Evidence for Depletion by Dehydration.

C. Vellmer (USGS, 345 Middlefield Road, Menlo Park, CA 94025) (Sponsor: Sieger van der Laan)

High-pressure granulites which represent the highest structural level of the Gföhl Nappe Unit in the Moldanubian Zone of Lower Austria are relicts of an original extensive nappe complex. Although high temperature mylonites, they partly preserve high-grade mineralogies which indicate a derivation from deep crustal levels (1.5 GPa/930°C). Available U-Pb zircon ages of 345 Ma support an early Variscan high-pressure metamorphism.

These granulites are dominantly felsic (73%), but intermediate (15%) and mafic (10%) granulites also occur. Major and trace element chemistry for 39 samples characterizes the protoliths of the granulites as dioritic to granitic rocks. A comparison with non-metamorphic equivalents shows that Ca, Th and U are highly depleted in the studied granulites, but it appears that no Rb depletion (except for samples with K concentrations below 1%) has occurred. The latter is demonstrated by K/Rb ratios of about 250 which resemble those of common igneous rock types. Comparatively low Sr concentrations (<130 ppm) and high Ca/Sr ratios up to 1200 of the dioritic, tonalitic and granodioritic granulites additionally indicate Sr loss relative to Ca.

The depletion of Ca, U, Th and Sr is not correlated with a depletion in K and Ba and therefore cannot be explained by melt extraction. The observed trace element characteristics may be related to metamorphic mineral reactions with fluid release (e.g., break down of biotite and quartz under high a_{CO_2} to enstatite, sanidine and fluid). Replacement reactions of accessory phases and solution of anorthite and albite components in garnet and clinopyroxene, respectively, might have enhanced the mobility of Th, U and Sr during rock metamorphism.

V518-8 0830h POSTER
Kinematic, Thermal and Petrological model of the Central Alps: Lepontine Metamorphism in the Upper Crust and Eclogitization of the Lower Crust.

B. Goffé, X. Le Fichon, C. Chopin, R. Bousquet and P. Henry (Laboratoire de Géologie, ENS, 24 rue Lhomond, 75231 Paris Cedex 05, France)

From seismic profiles, seismic velocity analysis and gravimetric models show that a slab of European lower crust is currently underthrust below the Apulian crust. Thus we assume a kinematic model in which the lower and upper crust are decoupled along a décollement. The upper crust deforms by pure shear with an horizontal compression axis. Different distributions of erosion are used. In all cases the total erosional flux is adjusted to balance upper crust input so that the belt keeps the same geometry. The lower crust goes into the subduction without deformation. The computed temperature field is in steady-state if the kinematic model applies during a minimum time of 40 My for a convergence rate of 8 mm/y. Equilibrium mineral assemblages and densities are determined from the computed P,T conditions for a granodioritic chemical composition of the upper crust and an andesitic composition of the lower crust. Assuming local isostasy, the density model fits the average topographic profile across the Central Alps. The PT paths obtained for the part of the upper crust initially at depths 10 to 16 km are compatible with the medium pressure oligocene metamorphism in the leponetine dome. The peak temperature of calculated path for the deepest rocks is reached at 600°C for a pressure of 0.8 GPa, near the lower limit of high pressure amphibolites. We conclude that the leponetine metamorphism corresponds to the thermal regime of a belt at steady-state. However, faster erosion rates in the internal part of the belt or tectonic denudation is required for exhumation of the deeper parts. The computed temperature fields imply eclogitization of the lower crust at a depth of 55 to 60 km. We conclude that the moto below the deepest part of the root may correspond to the limit of eclogitization. Lower crust eclogites have a density comparable or higher than that of the mantle depending on their chemical composition (3.37 g/cm³ for andesitic eclogites, 3.56 g/cm³ for gabbroic eclogites) and thus can stay below the root or continue into subduction.

V518-9 0830h POSTER
Retrograded evolution of coesite-bearing eclogite in the Dabie mountains, central China

Ruxuan Zhang and J. G. Liou (Dept. of Geol. & Environm. Sci., Stanford Univ., CA 94305); **Bolin Cong and Ming-Guo Zhai** (Institute of Geol., Academia Sinica, Beijing 100029, China)

Coesite-bearing eclogites in Shounghe of the Dabie collision zone exhibit distinct layers of various composition and extent of retrogression. In a single outcrop about 10 m thick, thin eclogite layers range from less retrograded coesite eclogite containing abundant coesite relics, through amphibolite with partially preserved eclogitic texture. These eclogites are interbedded with garnet-jadeite quartzite, marble with eclogite blocks, and quartzofeldspathic hornblende gneiss. The coesite eclogites contain a primary assemblage of Grt (Alm₄₁-64 Prp₁₃-27 Grs₄-39) + omphacite (Id₄₃ to 61) + coesite/quartz + rutile ± phengite (Si = 3.5) ± kyanite ± magnesite (Mg/Fe:Ca = 72:25:03) ± zoisite ± amphibole. Coesite relics and/or quartz pseudomorphs after coesite occur as abundant inclusions in Grt, Omp and Id. Retrogressive recrystallization is divided into three stages: in stage 1, Grt and Omp show incipient alteration at their margins and magnesite is replaced by a thin dolomite rim. In stage 2, all omphacites are replaced by a symplectite of Ca-pr, Amp, Pl and biotite; Garnet is partially altered to Amp and Pl, and Rt to ilmenite and/or titanite. Kyanite shows a corona of Ca, phlogopite, Pl and mica including muscovite and margarite [Ca(Ca-Na) = 0.79-0.83]. In stage 3, garnet is replaced by Pl, Am and Ep with rare garnet relics, and zoisite is replaced by a thin rim of plagioclase. The most retrograded domains, similar to country rock Hbl gneiss, contain Omp, Pl and minor Bt and opaxites which preserve a coarse-grained granuloblastic texture of the eclogites. For garnet-jadeite quartzite, jadeites (Jdgs) are successively rimmed by coronas of fibrous oligoclase (inner rim) and albite (outer rim) + minor Ca-pr, garnet is replaced by Amp, opaxite, Ab and seignite rimward. Garnet of these eclogite layers increases in Grt component from Gr25 in the less retrograded to Gr39 in the most retrograded eclogite layers. Prp component decreases from 27 to 13, while Alm is nearly constant (41-49). A well-constrained retrograde path was determined by a combination of observed textures and mineral parageneses, and P-T estimates of various stages. The peak metamorphic P-T condition is 450-680°C and P = 26 kb; formation of Zo at the expense of Ky took place at about 22-24 kb and 500-550°C, and Ab after Jd(85) formed at 14-16 kb, margarite and hornblende formed at P < 10 kb. Selective fluid infiltration may be responsible for different extents of retrogression of eclogite layers in a single outcrop.

V518-10 0830h POSTER
Siliceous Dolomitic Marbles from the Shandong Area, Eastern China—A Preliminary Report on the Country Rocks of Ultrahigh-Pressure Eclogites

Yoshihide Ogasawara, J. G. Liou and Ruyuan Zhang (Dept. of Geol. & Environm. Sci., Stanford Univ., Stanford, CA 94305); **Soichi Onuma and Sadahide Morita** (Institute of Earth Sci., Waseda Univ., Tokyo 169-80, Japan)

Marbles are interbedded with biotite-hornblende gneiss in the Se-La ultrahigh-P metamorphic terrane, Eastern China. Both marbles and gneisses include ultrahigh-P eclogite layers and boudins that contain coesite-pseudomorph inclusions in garnet and/or omphacite. Several siliceous dolomitic marbles were selected for preliminary investigation of mineral parageneses and chemistry in order to determine the P-T-X_{CO₂} conditions of ultrahigh-P and subsequent retrograde metamorphism.

The siliceous dolomitic marbles show typical granuloblastic texture and have the following mineral assemblages: a) Mg-calcite+dolomite+forsterite, b) Mg-calcite+dolomite+diopside+forsterite, c) Mg-calcite+dolomite+diopside (omphacite, phlogopite), d) Mg-calcite+dolomite+clinohumite, e) Mg-calcite+clinohumite+diopside (omphacite, phlogopite), f) Mg-calcite+dolomite+clinohumite+diopside+forsterite (omphacite), Dolomite, diopside, and forsterite are nearly pure in composition. Clinohumites of assemblages d and e contain 3 to 4 wt% TiO₂, but those in assemblage f have less than 3 wt%. Amphiboles of assemblages c and f are actinolite-pargasite hornblende to tremolite.

Calcic-dolomite intergrowths are common in their assemblages. No clear relationship was detected between bulk compositions of calcic-dolomite intergrowths and mineral assemblages. The maximum bulk X_{CaCO₃} of the intergrowth (assemblage b) is 0.025 and the estimated solvus temperature is 640 °C. Inclusions of Mg-calcite were found in clinohumite of assemblage d with well developed radial fractures around inclusions. The maximum X_{CaCO₃} value of 0.111 yields solvus temperature at 700 °C.

Mineralogical evidence showing ultrahigh-P metamorphism was not apparent in the siliceous dolomitic marbles. Similar to other country gneisses, the lack of index ultrahigh-P minerals may be due to the extensive regional amphibolite facies recrystallization during exhumation of the ultrahigh-P terrane.

V518-11 0830h POSTER
Proterozoic Ghanaian Metakimberlites

R.A. McKitterick and D I Norman (both at: Dept. of Geoscience, New Mexico Inst. of Mining and Technology, Socorro, NM 87801; 505-835-5634)
H Appiah (Dept. of Geology and Survey, UST School of Mines, Tarkwa, Ghana, West Africa)

The Birim (Akwatia) Diamondfield of Ghana has produced in excess of 100 million cts. of diamonds from alluvial and residual deposits. To date, no kimberlitic rocks have been recognized in Ghana. Field mapping and geochemical analysis have shown the presence of highly altered, metamorphosed ultramafic rocks within the diamondfield. These rocks, which are now actinolite schists, outcrop SE of the town of Akwatia, in a NE-SW trending

zone which extends at least 2 km along strike within Proterozoic Birimian metasediments. They have a fabric parallel to that of the metasediments and have been hydrothermally altered with the introduction of silica and carbonate. No kimberlite/lamproite indicator minerals have been identified. However, major and trace element compositions of these rocks corresponds well with those published for kimberlite. Particularly distinctive is the extreme LREE enrichment, with La to 1800 X chondrite, and La/Lu ratios in excess of 30. Also indicative that the protolith was kimberlite is the presence of diamonds.

V51C CA: Brooks Fri 0830h
Subduction-Related Dehydration, Fluids, and Melting Posters
Presiding: M C Johnson, Lamont-Doherty Earth Observatory

V51C-1 0830h POSTER
Ultramafic Xenoliths and Melt-Peridotite Interaction in a Calc-alkaline Igneous System: Examples From Avachinsky Volcano, Eastern Kamchatka.

G. M. Yezhovskiy, D.G. Bailey (Both at: Department of Geology, Hamilton College, Clinton, NY 13323); **O. N. Volynets, O. A. Bratsva, I. D. Sakeratsky, I. V. Melnikova, T. Chirikova** (All at: Institute of Volcanic Geology and Geochemistry, Petropavlovsk, Kamchatka 683005 Russia); **R. W. Kay** (Dept. of Geological Sciences and INSTOC, Cornell University, Ithaca, NY 14853).

Abundant ultramafic xenoliths occur in four Holocene age (1150, 3200, 4000, and 5000 14C-years) pyroclastic deposits at Avachinsky Volcano. The most common of the xenoliths are eclogized harzburgites cut by cm-scale veins of websterite. Olivine and orthopyroxene in the harzburgites are Mg-rich (Mg/Mg+Fe = 85-94), and spinel is Cr-rich (Cr/(Cr+Al) = 30-75). Clinopyroxene, occurring primarily in the grain-size-reduced portions of the xenoliths, is also Mg-rich and refractory (low Ti, Al, Na). Trace amphibole in the harzburgites is Cr-rich (1.5-2.5% Cr₂O₃), largely actinolite hornblende. Pyroxene and trace amphibole in the websterite veins are similar to those in the harzburgites. Xenoliths of olivine clinopyroxene also occur in these deposits. These are less deformed, and their mineral compositions are more Fe-rich (Mg/Mg+Fe = 74-81), than the harzburgites.

The host pyroclastic deposits include gray basaltic andesite pumice (~34% SiO₂) and white andesite pumice (~59% SiO₂). The xenoliths which occur only in the gray pumice, show extensive reaction zones with the host melt. Pargasitic amphibole + clinopyroxene crystallized in the reaction zones, and Mg-rich olivine and pyroxene was resorbed and/or reacted to iron-rich compositions. Xenoliths of hornblende appear to be the end-product of the melt-peridotite interaction. The hornblende contains euhedral pargasitic amphibole (Mg/Mg+Fe = 84-70), clinopyroxene (Mg/Mg+Fe = 74-87), resorbed/reacted olivine and orthopyroxene (Mg/Mg+Fe = 74-81), and minor interstitial glass and anorthitic plagioclase (An₅₁₋₆₅).

The Avachinsky xenoliths are likely to be lithospheric fragments from the vicinity of the crust-mantle boundary. This lithosphere was probably accreted in a Tertiary collisional event. The chemical history of the xenoliths prior to incorporation in the host deposits was apparently like that of "group one" xenoliths (Frey & Prinz, 1972, 1981, 1974). Reaction of these xenoliths with the host melt produces an amphibole-rich cumulate that entrains residual melt along a calc-silicate igneous trend (decreasing FeO/MgO, CaO/Al₂O₃, & TiO₂). This suggests that reaction-assimilation processes within the uppermost mantle may be important in calc-alkaline magmatism.

V51C-2 0830h POSTER
Preliminary Results on the Stability of Phengitic Muscovite in Deep Subduction Zones

Kenneth J. Domanik¹ and John S. Holloway^{1,2}
¹Department of Geology and ²Department of Chemistry, Arizona State University, Tempe, AZ 85287)

The possible stability of muscovite in subducting slabs has important implications for trace element recycling in subduction zones and for metamorphism of the overlying mantle wedge. Experiments to determine the stability and composition of muscovite in the model system K₂O-CaO-MgO-Al₂O₃-SiO₂-H₂O under H₂O saturated conditions have been performed in a multianvil apparatus from 3.5 to 7.0 GPa and 550 to 800°C. Natural muscovite, phlogopite, kyanite, quartz, and Ca-Mg garnet were used as starting materials, with a total of about 6 wt% H₂O. Run duration was 48 hrs and significant reaction progress was observed in all runs at temperatures of 700 °C and above. Run products were examined using optical, electron microprobe, FTIR, and XRD analysis. Preliminary results indicate that phengitic muscovite and pyrope-rich garnet is stable throughout the P-T range examined whereas phlogopite and coesite were not observed in the run products of these experiments. At 3.5 GPa and 800 °C the phase assemblage consists of approximately 30% phengitic mica (3.6 Si per 11 oxygens), 43% garnet (X_{py}=0.7), 25% kyanite, and 5% quartz phases. Similar results are observed at higher pressures although a second, unidentified hydrous phase is present in

EOS, V73, p644

have cores of here underlying by more calcic ...

around Khabarovsk, the volcanoes of the CKD are very active and have produced an unusually large volume of material.

Data from CKD volcanic rocks fall into two groups: an enriched group that contains incompatible element concentrations about a factor of two greater than a more depleted group, which itself contains smaller, or slightly greater, incompatible element contents in those of the volcanic front.

Volcanic on (20°-22°S), and Space (6-9180)

lar de Uyuni in across-strike s. In particular, the Peru-Chile Pb, Nb, Th, and ...

V42A-2 1330h POSTER

The Association of High-Nb Basalts and Adakites with the Subduction of Young Crust in Kamchatka, Russia: A Possible Origin

Margi J. Defant¹, Pavel K. Kozhevnikov², Mark S. Drummond³ and Alfred G. Hockstaedter²

- 1. Department of Geology, University of South Florida, Tampa, Florida 33620, USA, 813-974-2233
2. Institute of the Lithosphere, Russian Academy of Sciences, Moscow 109180, Russia
3. Department of Geology, University of Alabama at Birmingham, Alabama 35294, USA

Westward subduction of young oceanic crust generated within the Komandorsky Basin has produced the northern segment of the Kamchatka arc. The volcanism probably terminated about 1.5 Ma although the arc has been active since the late Eocene and is typical of that associated with other regions where young crust is being subducted.

and (0.51250-ant component nination cannot ge geochemical y trace element y Ca/Sr ratios about 650 to 250 sies (-0.51245) reation of these nds is that they lect an across- e decrease in proportion of a E-rich, slab-ived component d) added to the nile source for rocks, with :one-mittant rease in the re of mantle melting, ough all of imination, we s effects and x of this result tain evidence th the central where in spots crupt because tal crust is so

The Al- and Nb-rich silicious rocks appear to be adakitic rocks derived from the subduction of young and therefore relatively hot subducted crust. We believe that the high-Nb basalts are generated from magmas that have been metasomatized by adakite melts. The xenoliths and megacrysts found in these basalts substantiate this claim.

V42A-3 1330h POSTER

Alkaline Magmatism in a Subduction Environment: Late Cenozoic Intraplates and Arc Series Volcanic Rocks in Kamchatka

Gene M. Yordanzinski (Department of Geology, Hamilton College, Clinton, NY 13323), Oleg N. Volynets (Institute of Volcanic Geology and Geochemistry, Petropavlovsk, Kamchatka 683006), Robert W. Kay (Department of Geological Sciences and INSTOC, Cornell University, Ithaca, NY, 14853), Mikhail G. Prutko (Kamchatka Branch of the Russian Geological Survey, Petropavlovsk, Kamchatka, 683006)

From Late Miocene to Late Pleistocene time, there was a gradual magmatic shift in Eastern Kamchatka from small volumes of intraplate series (IPS) to large volumes of arc series volcanic rocks. Late Miocene IPS basalts (up to 12.8% MgO) are nepheline normative (44-48% SiO2), high in TiO2 (1.5-2.6%), and have total alkalis up to 7% (Na2O+K2O). Phenocrysts are olivine +/- high-Ca pyroxene. Trace elements are similar to those in ocean island basalts (La/Yb=13-33, Sr 600-1700 ppm, Ba/La=5-15, normalized Ta/La and Ta/Th >1). IPS basalts make up a small part of the volcanism, largely Plio-

Pleistocene plateau basalts (~1-3 Ma, ages uncertain) which predate the Late Pleistocene volcanism. Most of the plateau basalts are mildly alkaline or subalkaline, ranging to compositions typical of arc volcanic rocks (low Ti-Ta, Ba/La >20).

IPS volcanic rocks of Sredinney Ridge (Central Kamchatka) range from Pliocene(?) to Holocene in age. Holocene IPS basalts erupted from cinder cones associated with volcanoes composed of chemically arc-type rocks. IPS basalts in this setting have higher Na2O (>3.5%), TiO2 (>1.5%), and P2O5 (~0.5%) and lower CaO (<9.5%) than associated arc basalts. Relative concentrations of all high field strength elements (esp. Ta-Nb) are higher in IPS basalts than in the arc-type basalts, while La/Yb ratios in IPS basalts (~8-12) are only slightly higher than in the arc basalts. Abundances of incompatible elements are generally lower in the arc-type basalts. The second style of IPS volcanism on Sredinney Ridge is the basalt-trachyte-trachyrhyolite series, which occurs in dissected volcanoes of Pliocene(?) and Early Pleistocene age (Nulkande, Belogolovski, Bolshoi). Basalts of this series have incompatible element characteristics similar to other Sredinney Ridge IPS basalts. Evolved members of the trachyte series have incompatible element characteristics consistent with an origin by fractionation of an amphibole and spatio-bearing mineral assemblage from IPS basalts or basaltic andesites.

V42A-4 1330h POSTER

Geologic Relations of the Yunaska Volcanic Complex, Central Aleutian Arc

Kirsten E. Nicolayson and James D. Myers (Both at: Department of Geology and Geophysics, University of Wyoming, Laramie, WY 82071), Scott R. Linneman (Lewis-Clark State College, Lewiston, ID 83503), Drew Lamb (Department of Geology, Colorado College, Colorado Springs, CO 80903)

The active volcanic complex of Yunaska Island stretches 22.9 km from southeast to northwest, with a width of 8.9 km. Aerial photographs, radar images, and reconnaissance mapping and sampling reveal multiple volcanic vents, expressed variously as caldera, stratocone, and cinder cones. These have erupted primarily mafic flows intercalated with pyroclastic deposits.

The eastern half of the island consists of a large shield volcano (17 km diameter) topped by a nested caldera complex. The remnants of the older, everted caldera (C-I) partially encircle the inner Coats (C-II) Caldera (3.5 km diameter). The C-I caldera, with a diameter of approximately 13 km, approaches the breadth of Okmok Caldera, establishing C-I as the largest in the central and western Aleutians (Lamb et al., 1992).

Four stratocones have coalesced into a linear ridge (915 m) that dominates the topography of the western half of Yunaska. The ridge has deeply dissected lower flanks which expose plagioclase-porphyrphyrite flows. Erosion has also exposed the upper ramparts, however, those of the summit's parasitic cinder craters remain intact. A second zone of cinder cones extends from the west end of the stratocone complex. A fissure oriented SW-NE splits these of these cones. Two other fissure flows, oriented SW-NE and SE-NW, suggest tectonically-modified eruption sites. This may also account for the unusually elongate morphology of the western ridge, which is unique in the central and western Aleutians.

In the center of Yunaska stands the prominent Middle Mountain cinder cone (~300 m) associated with an olivine-plagioclase basalt and an aphyritic mafic flow. The topography and orientation of flows in the sea-cliffs suggest three older, eroded centers at the north, south, and western edges of the island. Of these, the southern Laha Complex appears much more silicious than the more recent volcanism of the caldera or of the western ridge complex. These older lavas are blue-grey, intermediate-composition flows. Several mafic, aphyritic dikes outcrop in this complex, including the 3 m thick "Finger" dike which extends almost 2 km inland.

Although most of the Yunaska flows contain plagioclase, olivine, and rare clinopyroxene, these phenocrysts are surprisingly small in size and abundance compared to other young Aleutian rocks. Other deposits included scoriaeous pyroclastic flow and air fall sequences up to 100 m thick (Lamb et al., 1992).

V42A-5 1330h POSTER

Caldera Formation on Yunaska Island, Central Aleutian Arc

Drew Lamb (Geology Department, Colorado College, Colorado Springs 80903), Scott R. Linneman (Lewis-Clark State College, Lewiston, ID 83503), James D. Myers and Kirsten E. Nicolayson (Department of Geology and Geophysics, University of Wyoming, Laramie, WY 82071)

Yunaska Island covers approximately 180 km2, representing several different local volcanism (Nicolayson et al., 1992). A large shield volcano topped by two caldera forms the NE part of the island. The younger caldera (Coats Caldera, C-II) lies within the older one (C-I), and is much more morphologically distinct.

Caldera I has a diameter of ~10 km and is defined only by its northern wall. Discontinuous flows up to 8 m thick compose the northern rampart of C-I. Six stratigraphic samples contain a plagioclase phenocryst assemblage. In contrast, Coats Caldera (C-II) has a diameter of approximately 3 km with caldera walls that rise 50-150 m from the caldera floor to the rim. The younger caldera wall exposes a continuous section of basalt characteristic of a shield volcano. These flows reach thicknesses of 5 m and contain plagioclase. Occasionally radiating dikes up to 3 m thick crosscut the flows. We collected a north-south section of twenty-four flows. Within the younger caldera (C-II), is a cinder cone about 640 m high containing two summit craters. The floor of the caldera is covered with younger lava flows which have a minimum thickness of 10 m. One of these flows breaches the southwestern rim of C-II and extends 1.6 km to the south. Additional young, post-caldera flows originated from outside the caldera at the base of the northeastern flank. The top unit on the rim of the caldera wall is composed of tephra deposits probably related to those erupted at the time of the caldera's formation. This same unit

can be topographically linked to tephra deposits located in the cliffs at the south-central portion of the island (South Anchorage cinder cone field of approximately eight individual vents extending northwesterly from the NW flank of Coats Caldera).

The South Anchorage beach cliffs (~75 m) expose 4 d. pyroclastic units of roughly equal thickness. Each unit consists of flows and air-fall deposits that can be traced 2-3 km along the beach. Distinguishing characteristics include grain size, abundance of volcanic bombs, welding characteristics, and color. In addition to their topographic relationship, the top caldera unit a pyroclastic flows are almost identical in their appearances, compositions, and similar lithic fragments. These units presumably were formed during the formation of caldera II. The character pyroclastics suggests that the caldera formation occurred in a few discrete eruptions.

V42A-6 1330h POSTER

Geology and Geochemistry of Mt. Douglas Volcano, Eastern Aleutian Arc, Alaska

Clive L. JE Began¹, RJ Moryk², PW Layer^{2,3} (Alaska Volc. Observatory at Alaska Div Geol Geophys Surv, 794 Univ. Ave., Fairbanks, AK 99709, 907-474-7430, 3Geophys Inst, Univ Alaska, Fairbanks, AK 99775, 3Dept Geol Geophys, Univ Alaska, AK 99775, 4Alaska Div Geol Geophys Surv, 400 Willoughby Ave., Juneau, AK 99801)

Mt Douglas is a 2135 m high ice-covered stratocone in lower Cook Inlet. It is located at one of the most pronounced segment breaks in the Aleutian arc, between the N20E-trending Cook Inlet volcanoes and the N50E-trending Kamai volcanoes. It is 80 km above the Benioff zone, in contrast to neighboring Augustine volcano which is 100 km above the Benioff zone. Lava flows are exposed discontinuously around the mountain. Non-volcanic bedrock is exposed as high as 1630 m, but some flows reach nearly to sea-level. Exposed lavas are, with rare exceptions, 2-pyroxene andesite flow with 57-63% SiO2. There are no exposed dikes, despite the fact that Douglas lavas are as silicious and crystal-rich as those which form domes at neighboring volcanoes. Rare pumice with 66% SiO2 is exposed low in the section. The oldest lavas exposed are Mt. Pleistocene (40Ar/39Ar age of 427±23 ka). Geomorphically youngest flows are 116±29 ka and 91±50 ka. Holocene deposits as lahars, block-and-ash flows, or lava flows, are conspicuously absent. There are coarse late-Pleistocene tephra, but Holocene are also conspicuously absent. The lack of Holocene deposits is remarkable in view of the geomorphic youth of the summit crater, which is filled with a 200 m diameter 21°C lake with pH of 1.1. Summit fumaroles are moderately pressurized, superheated (110°C) and have chemical characteristics of magmatic influence, such as CO2, 16% SO2, 10% HCl, and 9% N2 (dry-gas basis). 8180 in condensates are 1.7 and -4.8, respectively. 3He/4He is 1.8 x atmospheric.

Douglas lavas are medium-K calcalkaline andesites. They are thought to those of neighboring Augustine volcano in their low Na, Al, and Ba. They are diamural to Benioff zone beneath Douglas) HREE are the lesser depth to the Benioff zone beneath Douglas) HREE increase with increasing Si, which distinguishes Douglas from Cook Inlet volcanoes, as do very low Nb and Ta, and thus high and Hf/Ta. Douglas lavas also have high Mg, V, Sr, Cr, and Ni.

V42A-7 1330h POSTER

Post-caldera Eruptive History of Aniakchak Caldera, Alaska

CA-Maall¹, RG McInnes¹, O Bralstova², TP Miller³, JC Riebelberger³, C Mye^{3,4} (1USG 780-1420 Univ. of Anchorage, AK 99522, 2USG 784-7455, 3Inst. of Volcanic Geol. and Geochim., Petropavlovsk-Kamchatka; 3Geol. Inst., AVO, UAF, Fairbanks, AK 99775, 4A. B.V. of Geol. and Geophys. Surveys, AVO, Univ. Ave, Fairbanks, AK 99775)

Aniakchak Crater is a young (14C age 2433-18-hm-wide, ice-free caldera located on the Alaska Peninsula 678 km southwest of Anchorage. Tephra deposits record more than 20, centuries of dacitic, post-caldera eruptions.

A generalized stratigraphy is as follows: oldest identified post-caldera deposit is massive, frothy pumice, possibly the source of a lava dome on the north shore of Surge Lake. Younger scoriaeous deposits occur with two tuff cones west of the current margin are, in turn, overlain by a sequence of tephra and lava flows from the main, apparently long-lived vent: (1) Vent Mountain, a 400 m high spatter and scoria zone in the southern central part of the caldera and (2) Main composite vent, now well exposed in cross-section at the north edge of the caldera. One is the likely source of the most recent eruption (up to ~1 km3) and explosive post-caldera eruptions, including a widespread pumice fall, 14C age ~900 BP. In general, recent eruptive activity appears to have progressed from east to west across the caldera.

The most recent eruption, in May, 1992, was from a series of vents that transected the mountain and continue along the west margin of the caldera. This eruption produced a pumice-rich tephra that fell up to 600 m away from the south caldera wall. Post-caldera youngest (1932?) flows from Vent Mountain

University Dept. and CI Keyan, ME7 ...



TEMPORAL AND GEOCHEMICAL FEATURES OF VOLCANISM IN THE REVELLIE RANGE OF SOUTH- CENTRAL NEVADA, USA.

Gene M. Yogodzinski¹; Terry R. Naumann²; Eugene I. Smith¹.

The Revellie Range of south-central Nevada, and the adjacent Pancake Range-Lunar Craters Volcanic Field, constitute the largest Pliocene-to Recent field of mafic volcanism within the central Great Basin of the Western United States. This field lies along the northeast-trending zone of volcanism that extends from Death Valley to Lunar Crater. The proposed high level nuclear waste repository at Yucca Mountain, NV, lies within the southern part of this zone. Thus, studies of Pliocene Volcanism in the Revellie Range will provide insight into the plumbing systems, eruptive dynamics and petrogenesis of volcanic centers near Yucca Mountain.

Two episodes of basaltic volcanism spanning approximately 3 Ma were identified by geologic mapping and K-Ar dating in the Revellie Range. Basalts of episode-1 (5-6 Ma old) comprise a volume of ~8 km³, and were erupted from 52 vents throughout the Revellie Range. Basalts of episode-2 (3-4.5 Ma old) comprise a much smaller volume (~1 km³), and were erupted from 14 vents located

only along the eastern margin of the range. Trachytic volcanism produced two small domes (~0.3 km³ total) in the northeastern Revellie Range 4.3 m.y. ago, at approximately the transition between the eruption of episode-1 and episode-2 basalts.

Basalts of episodes 1 and 2 closely resemble average ocean island basalt. Most samples are mildly alkalic, with 1-7% normative nepheline, 43-47% SiO₂, and total alkalis of 4-7% (Na₂O+K₂O). They have steep rare-earth element patterns (La/Yb~13), and are moderately enriched in large ion lithophile elements (e.g., Ba/La~15) with high relative concentrations of Ta and Nb (e.g., La/Ta~13).

The dominant source for Revellie Range basalts was apparently asthenospheric mantle, but there are important chemical differences between episode-1 and episode-2, which indicate that there was a systematic change in source composition with time. Episode-1 basalts for example, range up to 6% normative hypersthene, and are thus slightly less alkaline than episode-2 basalts which are generally nepheline normative. Episode-2 basalts have



higher average concentrations of incompatible trace elements (K, Ba, Th, La), even though both episodes have apparently undergone similar amounts of crystal fractionation (e.g., FeO^*/MgO , $\text{CaO}/\text{Al}_2\text{O}_3$ are the same). Episode-2 basalts also range to higher La/Yb (up to 24) and higher Sr concentrations (up to 1700 ppm). The largest chemical differences are in Sr isotopes, which are less radio-

genic and less variable in the episode-2 basalts ($^{87}\text{Sr}/^{86}\text{Sr} \sim 0.7034$ to 0.7040) compared to episode-1 ($^{87}\text{Sr}/^{86}\text{Sr} \sim 0.7035$ to 0.7062). Similar differences are seen in Nd isotopes ($\epsilon_{\text{Nd}} = +3.6$ to $+4.5$ in episode-2). Pb isotopes cluster near the mantle reference line at high $^{206}\text{Pb}/^{204}\text{Pb}$ (~ 19.25), but are not substantially different between episode-1 and episode-2.

**CENTER FOR VOLCANIC AND TECTONIC STUDIES
1992 - 1993 ANNUAL REPORT**

Contribution by

S.A. Morikawa

**1993 Masters of Sciences Thesis
Department of Geosciences
University of Nevada, Las Vegas**

entitled

**The Geology of the Tuff of Bridge Spring: Southern Nevada and
Northwestern Arizona**

**The Geology of the Tuff of Bridge Spring:
Southern Nevada and Northwestern Arizona**

by

Shirley Ann Morikawa

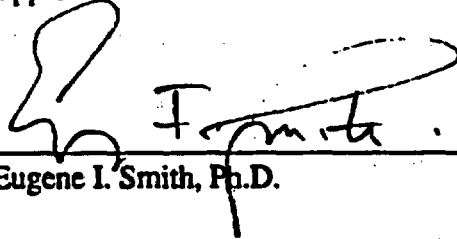
**A thesis submitted in partial fulfillment
of the requirements for the degree of**

**Master of Science
in
Geology**

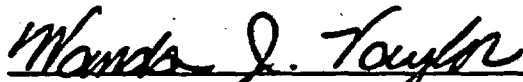
**Geoscience Department
University of Nevada, Las Vegas
December, 1993**

© 1994 Shirley Ann Morikawa
All Rights Reserved

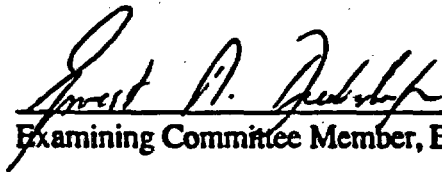
The thesis of Shirley Ann Morikawa for the degree of Master of Science in Geology is approved.



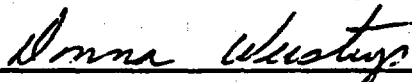
Chairperson, Eugene I. Smith, Ph.D.



Examining Committee Member, Wanda J. Taylor, Ph.D.



Examining Committee Member, Ernest M. Duebendorfer, Ph.D.



Graduate Faculty Representative, Donna E. Weistrop, Ph.D.

Dean of the Graduate College, Ronald W. Smith, Ph.D.

University of Nevada, Las Vegas
December, 1993

Abstract

The Tuff of Bridge Spring (TBS) is a regionally-widespread, andesite to rhyolite (59.50 to 74.91 wt. %) ash-flow tuff of mid-Miocene age (ca. 15.2 Ma) that is exposed in the northern Colorado River extensional corridor of southern Nevada and northwestern Arizona. Determination of the areal distribution, geochronology, lithology, geochemistry, and internal stratigraphy of the TBS is important for its establishment as a reliable stratigraphic reference horizon for tectonic reconstructions of the extensional corridor during the middle Miocene. Based on reoccurring patterns of major and trace element variation, the TBS is divided into constant Cr/variable SiO₂ and variable Cr/variable SiO₂ chemical members. Reconciliation of chemical member assignments and regional stratigraphic relationships allows the division of the TBS into three stratigraphic members. The regionally-extensive nature of a Zr/Ti vs. Ba chemical horizon in the TBS suggests that its chemical signature is magmatic in origin.

The presence of linear isotopic arrays of Nd/Rb/Pb plots, regionally-consistent geochemical trends, and disequilibrium textures in feldspars in the TBS suggests it was formed by magma mixing processes which involved the injection of mafic magma into a normally-zoned felsic magma chamber. The Nd/Rb/Pb isotopic signature of the Tuff of Bridge Spring suggests that the TBS may be cogenetic with either the Aztec Wash pluton, Nevada or the Mt. Perkins pluton, Arizona. Comparison of the isotopic signatures of the TBS with tuffs collected from Salt Spring Wash, Arizona, and the Lucy Gray Range, Nevada suggests that these tuffs are not cogenetic with the TBS. Incremental release ⁴⁰Ar/³⁹Ar analysis of the tuff of Dolan Springs (16.09 ± 0.15 Ma) suggests it was derived from a different source than the TBS.

Contents

Abstract	iii
Figures	vi
Tables.....	viii
Acknowledgments.....	ix
Introduction.....	1
The Tuff of Bridge Spring: A Brief Description.....	3
Regional Setting: The Northern Colorado River Extensional Corridor.....	5
History of Extension.....	5
Regional Volcanic/Plutonic Stratigraphy.....	6
Instrumental Techniques	12
Analytical Techniques	12
Whole Rock Vs. Pumice Sampling	14
Analytical Data.....	20
Major and Trace Element Geochemistry.....	20
Tuff of Bridge Spring Geochemistry.....	21
Other Ash-flow Tuffs.....	24
Petrologic Descriptions.....	25
Regional Correlation	61
Isotopic Correlation of the Tuff of Bridge Spring.....	61
Interstate-15.....	63
Other Ash-flow Tuffs.....	64
Salt Spring Wash and Lucy Gray Range.....	64
Dolan Springs.....	64
Origin of the Tuff of Bridge Spring Data Array.....	65
Lithic Contamination.....	66
Patsy Mine Volcanics	66
Alkali Olivine Basalts.....	68
Precambrian Basement.....	69
Mixing Trend.....	70
The Role of Contaminants in the Genesis of the Salt Spring Wash and Lucy Gray Range Tuffs.....	70

Internal Stratigraphy	80
Introduction	80
Eruptive Units.....	82
Chemical Criteria.....	82
Field Evidence	83
Chemical Members of the Tuff of Bridge Spring.....	86
Regional Members of the Tuff of Bridge Spring	88
Fine Scale Chemical Variation.....	89
Magma Chamber Processes.....	91
Location of Source.....	109
Introduction	109
Radiogenic Isotopes.....	111
Geochronology	112
Discrepancies in Tuff of Bridge Spring Geochronology.....	113
Comparative Geochronology	114
Geochemistry	114
Chemical path correlation	115
Field and Petrologic Studies	117
Field Indicators.....	118
Location of Pluton.....	119
Magmatic Mixing Textures.....	119
The Dolan Springs Volcanic Section	120
Summary and Conclusion	121
Summary and Conclusion	127
Future Work	131
References Cited.....	132
Appendix A: Major and Trace Element Analyses	139
Appendix B: Thin Section Point Counts	145
Part I: Whole Rock Modal Analyses.....	145
Part II: Phenocryst Modal Analyses.....	152
Appendix C: Stratigraphic Section Descriptions.....	156

Figures

Figure 1. Map showing locations of mountain ranges of the northern Colorado River extensional corridor referred to in the text.	8
Figure 2. Map showing known exposures (in black) of the Tuff of Bridge Spring.....	9
Figure 3. Generalized geologic map of the northern Colorado River extensional corridor and adjacent regions (from Faulds, 1989).....	10
Figure 4. Location map of plutons and volcanic complexes of the northern Colorado River extensional corridor.....	11
Figure 5. Plot of xenolith abundance vs. element concentration for the Eldorado Mountains section.....	19
Figure 6. Map showing locations of sections sampled for geochemistry and petrology.	28
Figure 7. Plot of Na ₂ O vs. K ₂ O. The field of unmetasomatized rocks shown from Carmichael et al. (1974).....	29
Figure 8. Harker variation plots of Tuff of Bridge Spring sections: major element oxides and trace elements vs. SiO ₂	31
Figure 9. Plots of relative stratigraphic position vs. element concentration of Tuff of Bridge Spring sections.	40
Figure 10. Harker variation plots of Tuff of Bridge Spring sections and three non-correlative tuffs: major element oxides and trace elements vs. SiO ₂	56
Figure 11: Plot of Nd vs. ⁸⁷ Sr/ ⁸⁶ Sr of the Tuff of Bridge Spring and three non-correlative tuffs. Sample numbers shown.....	73
Figure 12. Plot of ⁸⁷ Sr/ ⁸⁶ Sr vs. SiO ₂ of the Tuff of Bridge Spring and three non-correlative tuffs shown with sample numbers.....	74
Figure 13. ⁴⁰ Ar/ ³⁹ Ar incremental release age analysis (biotite) of the Dolan Springs Tuff.....	75
Figure 14. Generation of a hypothetical isotope array by xenolith contamination. See text for explanation.....	76
Figure 15. Plot of Nd vs. ⁸⁷ Sr/ ⁸⁶ Sr for the Tuff of Bridge Spring, Patsy Mine Volcanics, and Petroglyph Wash Basalt.....	77

Figure 16. Approximate geographic distribution of Early Proterozoic Nd and Pb provinces in the southwestern United States shown with the distribution area of the Tuff of Bridge Spring.	78
Figure 17. Pb isotope plots of a representative Tuff of Bridge Spring sample with samples of Mojave and Arizona Early Proterozoic crustal provinces rocks.	79
Figure 18. Diagram showing different types of chemical breaks.....	94
Figure 19. Plot of relative position vs. element concentration for the Eldorado Mountains section showing chemical breaks.....	95
Figure 20. Division of Tuff of Bridge Spring stratigraphic sections into eruptive units.....	100
Figure 21. Plot of Cr vs. SiO ₂ showing division of the Tuff of Bridge Spring into constant Cr and variable Cr members.	101
Figure 22. Plots of Cr vs. Sr, and Y vs. Zr, and Ti/Sr vs. FeO.	102
Figure 23. Plot of Ti/Sr vs FeO.....	103
Figure 24. Plot of Zr/Ti vs. Ba showing division of the Tuff of Bridge Spring into variable Zr/Ti, constant Ba group (constant Cr member), and variable Zr/Ti, variable Ba group (variable Cr member).....	104
Figure 25. Regional members of the Tuff of Bridge Spring. See text for explanation.	105
Figure 26. Distribution of the regional members of the Tuff of Bridge Spring.....	106
Figure 27. Compilation of plots of sections with variable Zr/Ti, constant Ba showing chemical paths and inflection points.....	107
Figure 28. Harker variation plots of the Eldorado Mountains section showing cyclical variation.	108
Figure 29. Plot of Nd vs. ⁸⁷ Sr/ ⁸⁶ Sr for the Tuff of Bridge Spring and selected plutons and volcanic suites of the northern Colorado River extensional corridor.	123
Figure 30. Plot of ⁸⁷ Sr/ ⁸⁶ Sr vs. ²⁰⁶ Pb/ ²⁰⁴ Pb for the Tuff of Bridge Spring and selected volcanic complexes and plutons of the northern Colorado River extensional corridor.	124
Figure 31. Hypothetical Zr/Ti vs. Ba chemical path diagram.....	126

Tables

Table 1: Calibration standards for the Rigaku X-Ray Fluorescence Spectrometer, University of Nevada, Las Vegas.....	16
Table 2: Precision for the Rigaku 3030 X-Ray Fluorescence Spectrometer, University of Nevada, Las Vegas.	17
Table 3: Accuracy for the Rigaku 3030 X-Ray Fluorescence Spectrometer, University of Nevada, Las Vegas.	18
Table 4: Regional major and trace element variation of the Tuff of Bridge Spring.....	30
Table 5: Major and trace element variation of sections compared to a base composition averaged from Highland Spring, Eldorado Mountains, Sheep Mountain, and Interstate 15 sections.....	50
Table 6: Nd, Rb, and Pb isotope analyses.....	72
Table 7: Geochronology of the Tuff of Bridge Spring.	125

Acknowledgments

Financial support for this thesis was provided by the Center for Volcanic and Tectonic Studies (CVTS) at UNLV, and by research grants from the Geological Society of America and the Graduate Student Association of UNLV.

I would like to thank the members of my graduate committee: Dr. Gene Smith (a most patient and generous advisor), Dr. Wanda Taylor, Dr. Ernie Duebendorfer, and Dr. Donna Weistrop for their guidance and support. I would like to acknowledge the following individuals for contributions of data that were incorporated into this thesis: Dr. Jim Faulds (University of Iowa) for Tuff of Bridge Spring $^{40}\text{Ar}/^{39}\text{Ar}$ geochronology, Hayden Bridwell (UNLV) for Interstate 15 thin sections, Dr. Jim Mills (CVTS) for Tuff of Hoover Dam isotope data, Dr. Rod Metcalf (UNLV) for Mt. Perkins pluton isotope data, and Claudia Falkner and Dr. Calvin Miller (Vanderbilt University) for Aztec Wash pluton isotope data and geochronology. Isotope analyses were completed by Dr. Doug Walker (University of Kansas), Dr. Tim Bradshaw (CVTS), and Dr. Mark Martin (CVTS). Dr. Dan Lux (University of Maine) ran the tuff of Dolan Springs $^{40}\text{Ar}/^{39}\text{Ar}$ analysis.

For logistical support, my thanks goes to the UNLV geoscience staff: Margaret Kaufman, Vicki DeWitt, Daryl Depry, and Sarah Crooks, and to Gina Jaramillo (Motor Pool), Barbara Hogue (UNLV Graduate College), Yagang Wang (CVTS), and Kathy Morgan (UNLV Operations and Maintenance).

I would especially like to express my gratitude to my parents- Don and Harlene Morikawa, my sister Sandy, and brother Steve for their support and interest in my studies.

And finally, my personal thanks to all the good people- students, faculty, and

staff- I've come to know during my stay at UNLV, especially: Joe Blaylock (for encouragement and much appreciated reality adjustments), Jan Lamb, Clint Christensen, John Schmeltzer, and Gary Gin.

Introduction

The Tuff of Bridge Spring is a regionally-extensive, andesitic to rhyolitic ash-flow tuff (57 to 75 wt. % SiO₂) that crops out in the Lake Mead region of the southern Basin and Range province, Clark County, Nevada and Mohave County, Arizona (Fig. 1). Eruption of the Tuff of Bridge Spring was coeval with intense crustal extension in the structurally-complex northern Colorado River extensional corridor of southern Nevada and northwestern Arizona. The timing of the emplacement of the Tuff of Bridge Spring, its widespread distribution, and distinctive lithology makes it a key stratigraphic reference horizon on which correlations of Miocene-aged stratigraphic units and tectonic reconstructions in the northern Colorado River extensional corridor are based (Anderson, 1971; Anderson et al., 1972; Smith, 1982; Davis, 1984; Schmidt, 1987; Faulds, 1989; Cascadden, 1991; and Bridwell, 1991). The complex nature of these stratigraphic correlations and tectonic reconstructions require that correlation and identification of the Tuff of Bridge Spring are based on reliable parameters. It is the purpose of this study to determine the areal distribution, geochronology, lithology, geochemistry, internal stratigraphy, and locate the source of the Tuff of Bridge Spring in order to establish the unit as a reliable stratigraphic marker.

This thesis utilizes Nd, Sr, and Pb isotopes as the primary criteria on which regional correlation of sections is based. Major and trace element geochemistry, field studies, and ⁴⁰Ar/³⁹Ar geochronology was used to confirm isotope-based correlations. This body of evidence suggests that stratigraphic sections in the Eldorado Mountains, McCullough Range, Highland Spring Range, Interstate 15 (near Sloan, Nevada), and Sheep Mountain in Nevada, and the Black Mountains, Temple Bar, White Hills in Arizona are correlative to the Tuff of Bridge Spring (Fig. 1).

The Tuff of Bridge Spring is divided into two chemical members on the basis of the occurrence of two distinct patterns of major and trace element variation. The presence of these two regionally-persistent chemical groups directly reflects chemical processes and zonations within the source chamber at the time of eruption of the Tuff of Bridge Spring. The chemical group concept not only forms the foundation for further division of the Tuff into three regional stratigraphic members, but also has important implications for the petrogenesis of the Tuff of Bridge Spring.

Lastly, this thesis compares the isotopic signature of the Tuff of Bridge Spring with available isotopic analyses of several plutons of the northern Colorado River extensional corridor to tentatively suggest that the source of the Tuff of Bridge Spring is either the Aztec Wash pluton, Nevada, or the Mt. Perkins pluton, Arizona.

Although not directly related to the Tuff of Bridge Spring, an important finding in this thesis is the identification of proximal-type pyroclastic deposits in the volcanic complex at Dolan Springs, Arizona. The occurrence of these deposits are suggestive of the presence of a caldera somewhere in the immediate area. Similarities of isotopic signature of the Dolan Springs tuff and the Tuff of Bridge Spring, and the overlap in ages of the Dolan Springs tuff and the Mt. Perkins pluton has interesting implications for the existence of regionally-extensive magmatic systems and the possible correlation of the Dolan Springs tuff to the Mt. Perkins pluton.

Organization of this thesis is built around three main topics: (1) regional correlation; (2) determination of internal stratigraphy; and (3) location of the source of the Tuff of Bridge Spring. For each topic, only those aspects of isotopic, major/trace geochemistry, field studies, petrologic studies, geochronology, and introductory material (e.g., previous work) which can be utilized to synthesize an interpretation and conclusion are presented. This requires that introductory material, geochemistry, descriptive volcanology, and interpretation are spread throughout the thesis, unlike the

format of a more "traditional" thesis in which such information is usually presented in separate/isolated sections. Repetition of data or discussion is avoided wherever possible by the use of cross references. Most of the supporting data and section descriptions are included in appendices. Summary figures and tables are included at the end of each section to clarify discussions.

The Tuff of Bridge Spring: A Brief Description

The first description of the Tuff of Bridge Spring was made by Longwell (1963) in a study of the regional geology of the Lake Mead/Davis Dam area of Nevada and Arizona. Ash-flow tuffs exposed in this area were originally correlated to the Golden Door Volcanics of Arizona, but were later given the informal name Tuff of Bridge Spring when Anderson (1971) demonstrated that the type section of the Golden Door Volcanics correlated with the Middle Member of the regionally-extensive Patsy Mine Volcanics. The designation Golden Door Volcanics was formally abandoned in 1971 (Anderson, 1971).

The type section of the Tuff of Bridge Spring is Bridge Spring (Anderson, 1971), which is located approximately 2.5 km north-northeast of Nelson, Nevada, in the Eldorado Mountains. The name Bridge Spring refers to a small spring that occurs near a natural rock arch that formed in variably welded exposures of the Tuff of Bridge Spring.

Based upon the occurrence of stratigraphic sections examined in this study, the Tuff of Bridge Spring extends discontinuously over an area of approximately 4300 km² from latitude 36° 00' N (Temple Bar) to latitude 35° 35' N (Highland Spring Range), and from longitude 115° 15' W (Interstate 15 section) to longitude 114° 22' W (Temple

Bar). The present overall distribution pattern of the Tuff of Bridge Spring is elongated east to west (Fig. 2).

The Tuff of Bridge Spring is mid-Miocene in age and is one of two regionally extensive lithostratigraphic units that crop out in this region; the other unit is the 18.5 Ma Peach Springs Tuff (Young and Brennan, 1989). Other ash-flow tuffs of similar age are exposed in the northern Colorado River extensional corridor (e.g., the tuff of Hoover Dam) (Mills, 1985), but have limited distributions. While the absolute age of the Tuff of Bridge Spring has not been unequivocally resolved by radiometric analysis (see later discussion of geochronology), a date of 15.23 ± 0.14 Ma ($^{40}\text{Ar}/^{39}\text{Ar}$ on sanidine, Bridwell, 1991) is accepted in this study as being representative of the true age of the Tuff of Bridge Spring.

The topographic expression of the Tuff of Bridge Spring varies with the degree of welding. Densely-welded outcrops form prominent ledges or ridges, and moderately- to poorly- welded intervals form slopes. Tuff affected by vapor phase mineralization has a characteristic pale lilac-gray weathered color that is associated with low, rounded outcrops that are platy to cavernous. Color of the weathered Tuff of Bridge Spring varies from black, dark brown, to reddish brown in densely welded intervals. Poorly welded intervals are light colored. The Tuff of Bridge Spring contains between 7.8 (Black Mountains) and 46.4 (Temple Bar) modal percent phenocrysts of sanidine, plagioclase, biotite, clinopyroxene, sphene, opaque iron oxide (undifferentiated), \pm zircon, \pm apatite, and \pm hornblende (rare). The Tuff of Bridge Spring also contains pumice (usually in the form of fiamme), and lithic clasts of mafic composition (basalt to basaltic andesite).

Regional Setting: The Northern Colorado River Extensional Corridor

History of Extension

The northern Colorado River extensional corridor of the southern Basin and Range province is a 50 to 100 km wide structural terrane that was subjected to severe extensional tectonism during the mid-Tertiary (approximately 18–4.7 Ma) (Anderson et al., 1972; Duebendorfer and Smith, 1991; Faulds et al., 1992;) (Fig. 3). The extensional corridor is bounded to the north by the Lake Mead fault zone (Lake Mead shear zone) and the Las Vegas Valley shear zone, to the east by the stable Colorado Plateau, and to the west by the Spring Range. The rocks of the northern Colorado extensional corridor consist of Tertiary volcanic and sedimentary rocks that were deposited directly upon Proterozoic crystalline basement. Thick accumulations of Paleozoic and Mesozoic rocks lie to north, east, and west of the extensional corridor, but are absent in the corridor itself (Anderson et al., 1972). Bisecting the northern Colorado River extensional corridor in the southern Eldorado Mountains, Nevada and the central Black Mountains, Arizona, is an east-west trending, five to ten kilometer wide, 40 km long accommodation zone which separates a northern extensional domain of east-tilted fault blocks from a southern domain of west-tilted fault blocks (Faulds, 1989).

The intense nature of mid-Miocene extensional deformation in the northern Colorado River extensional corridor is reflected by estimates of 300 to 400% total extension of the Las Vegas region during the Neogene (Wernicke et al., 1988), 100% extension of the Eldorado Mountains (Anderson, 1971), and up to 65 km of west-directed, strike-slip fault displacement of the Frenchman Mountain block (Anderson, 1973; Rowland et al., 1990). Anderson (1971) was the first to suggest that large

magnitude extension was accommodated by low-angle detachment faults. Later work in the Lake Mead area suggested that synchronous movement on regional detachment structures (the Saddle Island detachment fault) and strike-slip structures (the Lake Mead fault zone and the Las Vegas Valley Shear Zone) accommodated extension from 13 to 9 Ma. (Smith, 1982; Choukroune and Smith, 1985; Duebendorfer and Wallin, 1991). From 9 to 4.7 Ma, extension was accommodated by high angle normal faulting.

Regional Volcanic/Plutonic Stratigraphy

The Miocene volcanic stratigraphy of the Lake Mead area consists of (in order of decreasing age): (1) the 18.5 Ma Peach Springs Tuff- a regionally extensive, rhyolitic ash-flow tuff (Young and Brennan, 1989); (2) andesites, basalts, basaltic andesites, and rhyolites of the Patsy Mine Volcanics (18.3 to 15.2 Ma) (Anderson, 1971; Anderson et al., 1972); (3) the ca. 15.2 Ma Tuff of Bridge Spring (Bridwell, 1991); and (4) rhyolite, andesites, and basalts of the approximately 15 to 12 Ma Mt. Davis Volcanics (Anderson, 1971; Anderson et al., 1972; Darval, 1991).

A number of localized Neogene volcanic complexes occur in the Lake Mead region. These include the Eldorado Mountains stratovolcano, Nevada (Anderson, 1971); the Hoover Dam volcanic center, Nevada and Arizona (Mills, 1985); the River Mountains volcanic complex, Nevada which is the coeval volcanic cover of the Wilson Ridge pluton of Arizona (Smith et al., 1982; Weber and Smith, 1987); the McCullough Pass caldera (Schmidt, 1987), Sloan Sag (Bridwell, 1991), and the Henderson volcanic complex, Nevada (Tuma-Switzer and Smith, 1993); and the Dolan Springs volcanic complex, Arizona (this study) (Fig. 4).

Miocene-aged plutons exposed in the northern Colorado River extensional corridor include the Nelson/Aztec Wash pluton (15.12 ± 0.6 Ma) (Calvin Miller,

personal communication to Smith, 1993) which crops out in the Eldorado Mountains, Nevada, the 15.96 ± 0.04 Ma Mt. Perkins pluton and the Wilson Ridge pluton (13.5 ± 0.4 Ma) in the Black Mountains, Arizona (Faulds, personal communication to Smith, 1993; and Larsen and Smith, 1990), and the Boulder City pluton, Arizona (13.8 ± 0.6 Ma) (Anderson et al., 1972) (Fig. 4).

The topographic surface upon which the Tuff of Bridge Spring was erupted consisted of paleohills formed by a series of stratovolcanoes and associated dome fields, and paleovalleys containing regionally-extensive mafic flows (Anderson, 1971). In the McCullough Range, a structural buttress of Precambrian basement rock formed a major topographic barrier to the flow of the Tuff of Bridge Spring (Schmidt, 1987).

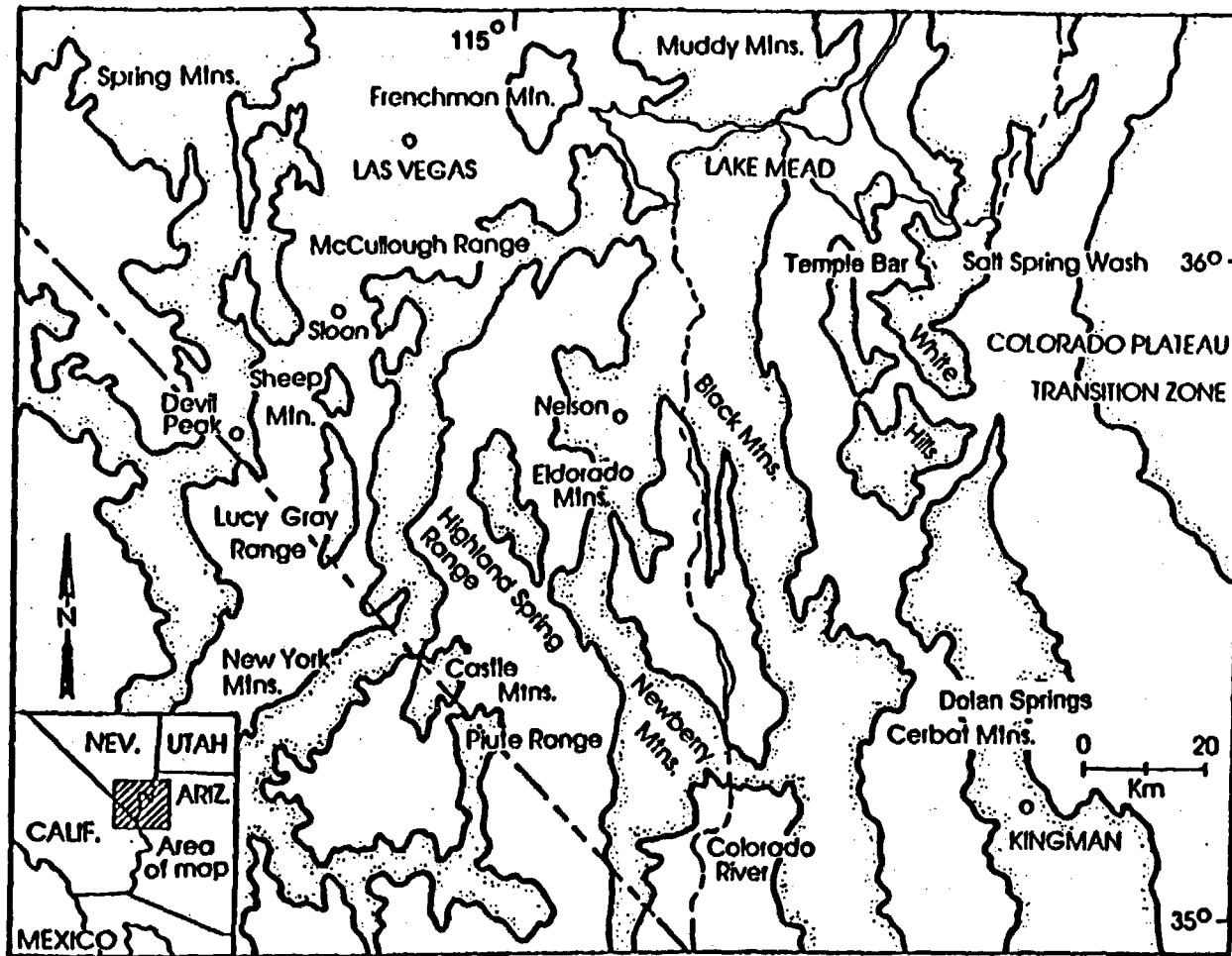


Figure 1. Map showing locations of mountain ranges of the northern Colorado River extensional corridor referred to in the text.

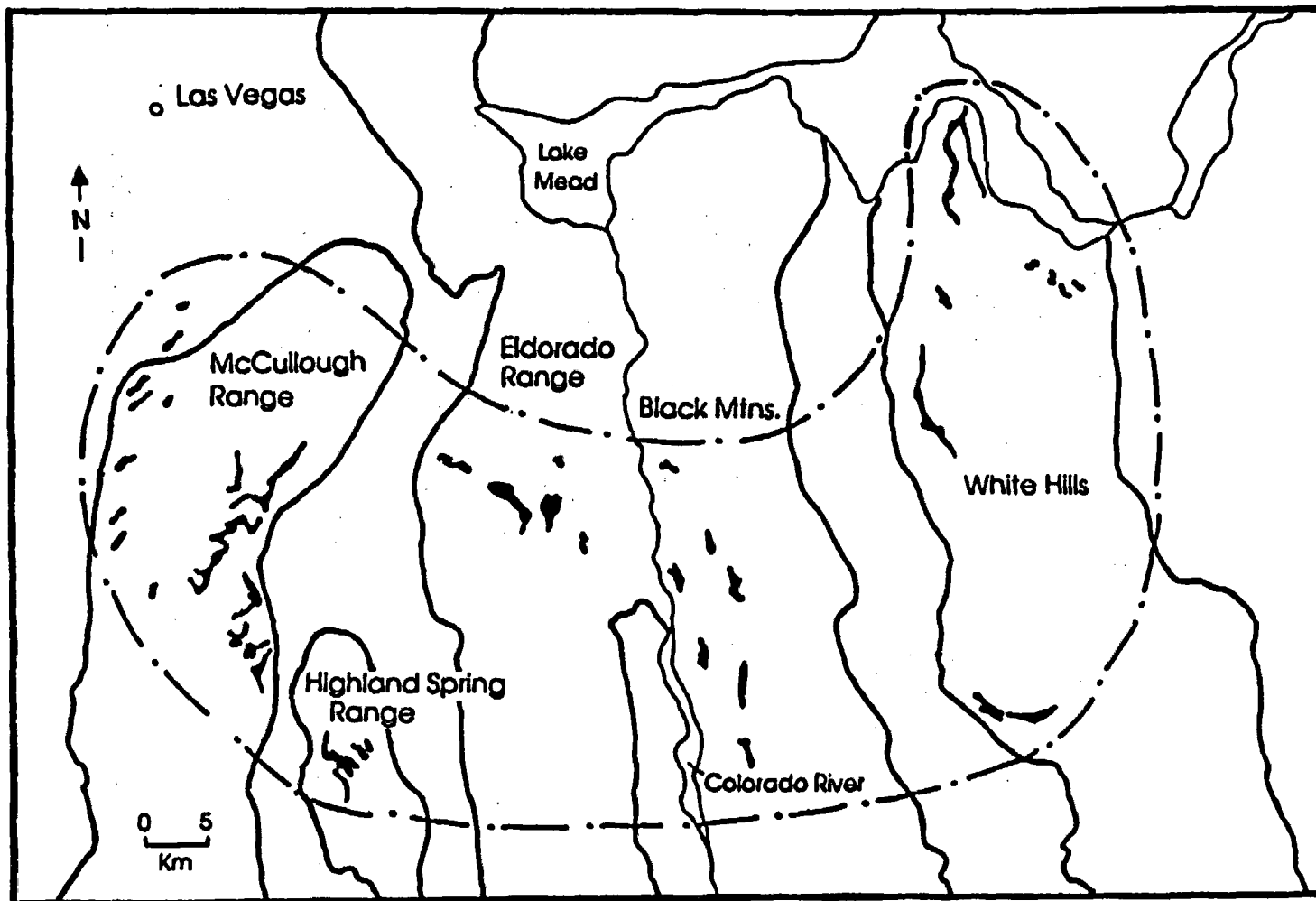


Figure 2. Map showing known exposures (in black) of the Tuff of Bridge Spring. Area of distribution is enclosed by dashed/dotted line. Modified from Cascadden (1991).

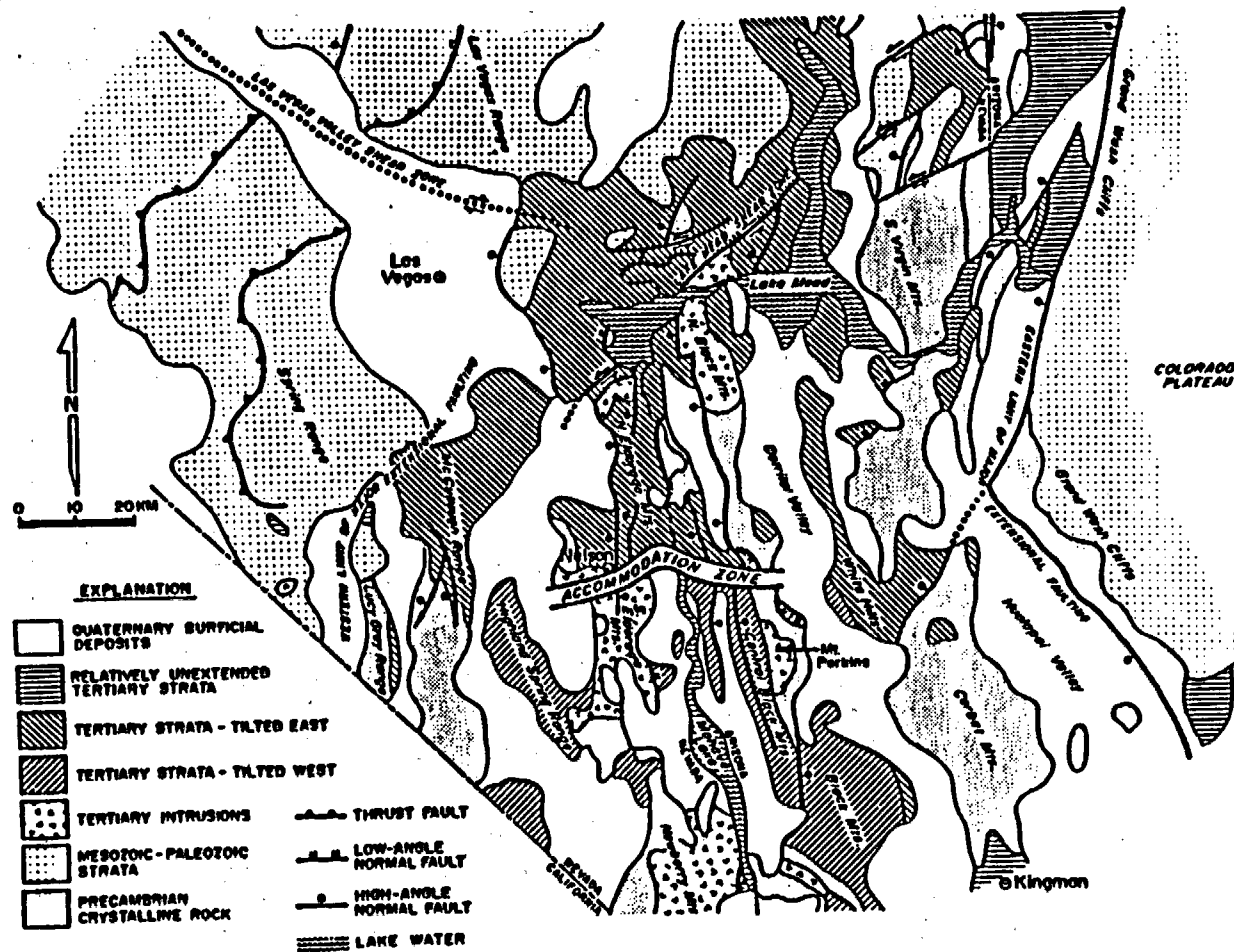


Figure 3. Generalized geologic map of the northern Colorado River extensional corridor and adjacent regions (from Faults, 1989).

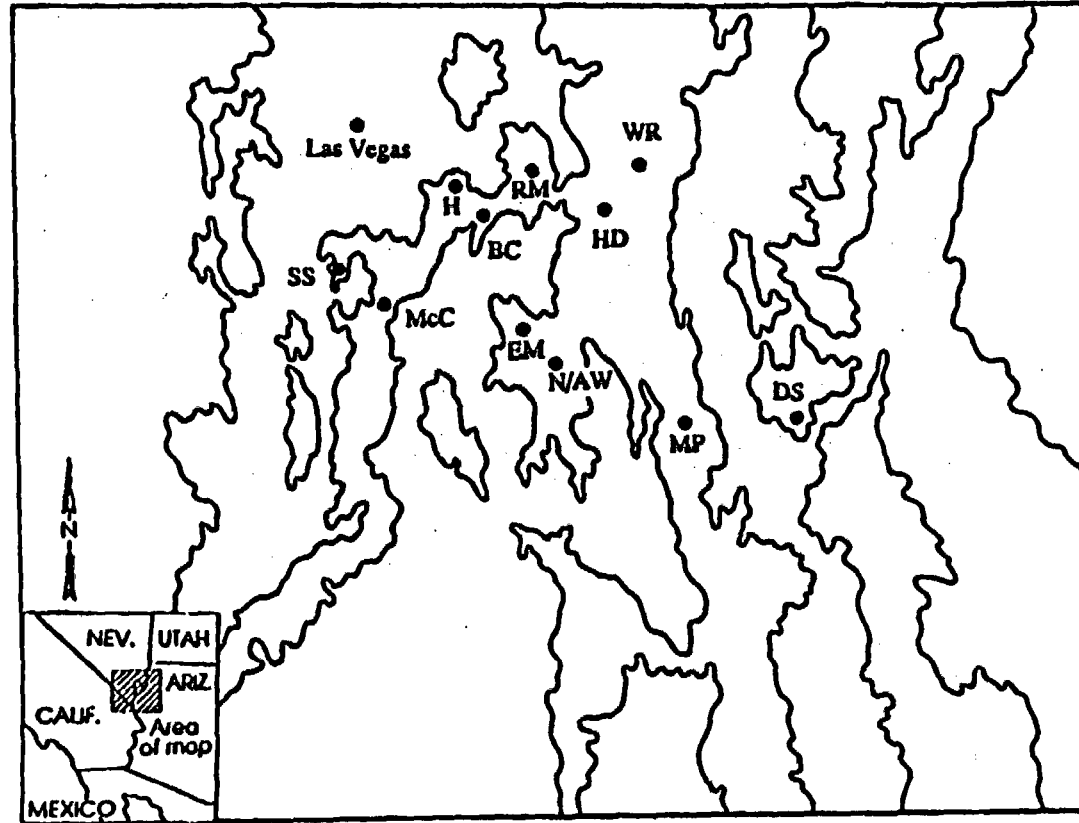


Figure 4. Location map of plutons and volcanic complexes of the northern Colorado River extensional corridor. EM = Eldorado Mountains stratovolcano; HD = Hoover Dam volcanic center; RM = River Mountains volcanic complex; McC = McCullough Pass caldera; SS = Sloan Sag volcanic center; H = Henderson volcanic complex; DS = Dolan Springs volcanic complex. N/AW = Nelson/Aztec Wash pluton; MP = Mt. Perkins pluton; BC = Boulder City pluton; WR = Wilson Ridge pluton.

Instrumental Techniques

Analytical Techniques

Fifty-seven samples were collected and analyzed for major and trace elements. Radiogenic isotope analyses (Sm/Nd, Rb/Sr, and Pb systems) were completed on fourteen samples. Geochemistry was completed almost exclusively on whole rock samples. Samples were selected on the basis of distinctive changes in tuff lithology. Approximately 1-1.5 kg of fresh, unweathered sample were collected for each analysis. Xenoliths larger than 0.7 cm were removed by hand from samples prior to pulverizing. Samples were initially pulverized to <100 mesh in a Dyna Mill Supercollider air suspended impact attrition mill. A geochemical split (approximately 300 ml in volume) was separated from each pulverized sample and powdered to <200 mesh using a Pulverisette automated agate mortar and pestle. The standard practice of leaching powdered rock samples in dilute HCl solution to remove carbonate contaminants was found to significantly affect retention of major and trace elements. For this reason, dilute HCl leaching was not employed in this study for preparation of samples for major and trace element analysis (unpublished study, Morikawa, 1992). Radiogenic isotope compositions of rock samples are presumably not affected by dilute acid leaching. Consequently, this method was used to treat samples submitted for isotope analyses.

Samples were processed into fused glass disks for major element analysis by heating 1.0 g sample, 9.0 g lithium tetraborate, and 0.16 g ammonium nitrate at 1100°C in gold-platinum crucibles and pouring the resultant melt into heated Au-Pt molds (Noorish and Hutton, 1969; Mills, 1991). Samples for trace element analysis were prepared by mixing 2.5 g sample with 0.5 g methyl cellulose, enclosing this mixture with a rim and backing of additional methyl cellulose, and compressing to 10,000 psi in

a Buehler specimen mount press to form a disk (Hutchison, 1974). All samples and reagents were weighed to ± 0.0005 g. All prepared samples were stored in dessicators prior to analysis.

X-ray fluorescence analysis of major and trace elements were completed using the Rigaku 3030 X-ray Spectrometer at the University of Nevada, Las Vegas.

Calibration of this spectrometer was based on the internal standards listed in Table 1. The analytical uncertainty and accuracy for major and trace elements are given in Tables 2 and 3. Comparison of the average of several analyses of a commercially prepared analytical standard (AGV-1) to the published values is given in Table 3.

Loss on Ignition (LOI) was determined for two samples from each location sampled for this study (Appendix A). Each sample (approximately 2 to 4 g) was initially weighed, heated in ceramic crucibles to 1000°C for 2 hours, cooled in the oven gradually to 300°C , and cooled completely to room temperature under dessication. Comparison of heated sample weight to initial (wet) weight was used to calculate % weight loss (LOI).

Isotopes were analyzed using the VG Sector 54 mass spectrometer at the University of Kansas, Lawrence. A thorough discussion of isotope analytical methods is presented by Feuerbach et al., (in press).

An incremental release $^{40}\text{Ar}/^{39}\text{Ar}$ analysis of sanidine and biotite separated from pumice collected from an ash-flow tuff that crops out in Dolan Spring, Arizona was completed at the University of Maine, Orono. Approximately 8 pounds of pumice were collected, trimmed of any weathered rind, crushed in the attrition mill described previously, and sieved into five fractions (600, 250, 180, 125, and $90\ \mu\text{m}$) using a Rotap automated shaker. Initial separation of biotite ($180\ \mu\text{m}$ fraction) and feldspar was done using the Frantz magnetic separator. Final separation of biotite was done by hand using the paper shaking technique (Taylor, personal communication, 1993), and

hand-picking under a binocular microscope. Final separation of feldspar (125 μm fraction) was done using heavy liquids (sodium metatungstate and bromoform), and hand picking.

Whole Rock Vs. Pumice Sampling

The primary magmatic compositions of ash-flow tuffs can be modified by eruptive and/or flow-induced mechanical fractionation processes as well as by entrainment of xenolithic/xenocrystic contaminants during emplacement (Hildreth and Mahood, 1985) (Valentine et al., 1992). Because of these factors, the original magmatic chemical signatures of ash-flow tuffs are more likely to be preserved by cognate pumice than by whole rock ash-flow tuffs. Pumice represents essentially a magmatic "grab-sample" unaltered by syn- and post-eruptive fractionation processes. Therefore, pumice is the material of choice for regional correlation of ash-flow tuffs that are based specifically upon geochemical signatures.

Pumice in the Tuff of Bridge Spring generally occurs as fiamme that cannot be easily separated from rock matrix and is rarely suitable for collection for geochemical analysis. The Tuff of Bridge Spring does, however, exhibit several characteristics that allow sampling of whole rock in lieu of pumice to obtain meaningful chemical analyses. (1) The Tuff of Bridge Spring contains low modal abundances of xenoliths (average= 6.1%). Xenoliths are consistently mafic (basaltic to basaltic andesite) in composition. (2) Thin section studies indicate that the majority of phenocrysts present in the Tuff of Bridge Spring are primary (i.e., are not xenocrystic). (3) Geochemical data (see internal stratigraphy section) demonstrate the presence of relatively simple magmatic zonation, the regional preservation of extremely fine-scale chemical partitioning in the Tuff of Bridge Spring, and a non-correspondence of modal lithic abundances to the

concentration of those elements normally present in mafic rocks (e.g., Cr, Mg, etc.) (Fig. 5). These regionally-distributed chemical patterns indicate that syn- and/or post-eruption chemical fractionation/contamination did not significantly alter the original magmatic composition of the Tuff of Bridge Spring. The presence of regionally-distributed chemical patterns suggests that xenoliths did not significantly skew the geochemical signature of the Tuff of Bridge Spring other than by imparting a minimal and constant background "static" that is persistent over its entire range of composition. These observations support the use of whole rock samples for determination of the geochemistry of the Tuff of Bridge Spring.

Table 1: Calibration standards for the Rigaku 3030 X-ray Fluorescence Spectrometer, University of Nevada, Las Vegas. All standards are United States Geological Standards unless otherwise noted.

Trace Elements	Major Elements
G-2	SCO-1
W-2	STM-1
BIR-1	GSP-1
RGM-1	GSP-1
QLO-1	DNC-1
BHVO-1	RGM-1
PCC-1	BHVO-1
GSP-1	PCC-1
AGV-1	AGV-1
DNC-1	QLO-1
	AL-1*

* French Standard

Table 2: Precision for the Rigaku 3030 X-ray Fluorescence Spectrometer, University of Nevada, Las Vegas using U.S.G.S. Standard AGV-1 as reference.

Element	Mean Relative Error (%)	Element	Mean Relative Error (%)
SiO ₂	3.00	Nb	10.00
Al ₂ O ₃	7.00	Ni	>20
TiO ₂	2.00	Rb	2.00
FeO (total)	3.00	Sr	2.00
CaO	2.00	Th	12.00
K ₂ O	2.00	Y	2.00
MnO	10.0	Zr	5.00
P ₂ O ₅	10.00	Ba	10.00
Na ₂ O	6.00		
MgO	2.00		

Table 3: Accuracy for the Rigaku 3030 X-Ray Fluorescence Spectrometer, University of Nevada, Las Vegas. Accuracy determined by analyzing U.S.G.S. standards AGV-1, BIR-1, and BHVO-1. Results for 10 replicate analyses of AGV-1 are given below.

Element	Published concentration of AGV-1	Mean of 10 replicate analyses of AGV-1
Cr	10.1	11.0
Ni	16	15.91
Rb	67.3	65.22
Sr	662	657
Th	6.5	6.1
Y	20	21.41
Zr	227	239
Ba	1226	1271
Nb	15	14.24

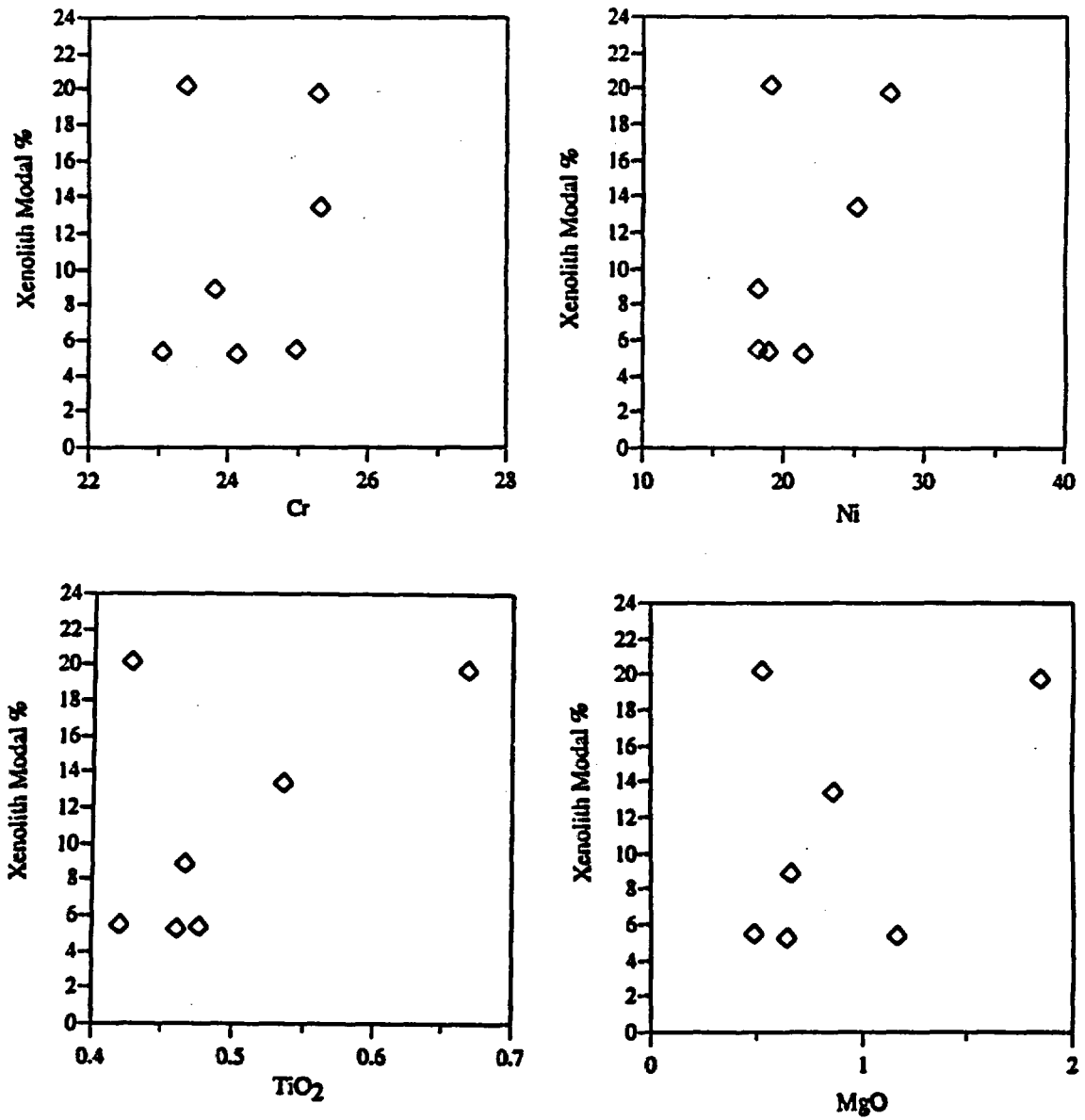


Figure 5. Plot of xenolith abundance vs. element concentration for the Eldorado Mountains section. Oxides in wt. % and trace elements in ppm in this and all subsequent plots.

Analytical Data

Presented below are summaries of major/trace element geochemical data and thin section petrology for the Tuff of Bridge Spring. Major and trace element analyses are given in Appendix A. Major element oxide values used in plots presented in the text have been normalized to 100 wt. %. LOI values were excluded from these calculations. Major element concentrations are reported in wt. % and trace element concentrations are reported in ppm. Thin section point counts (whole rock) and normalized phenocryst modes are given in Appendix B. 500 points were counted in each thin section. Presentation of isotopic analyses is deferred to the discussion of regional correlation. Detailed stratigraphic section descriptions are given in Appendix C.

Major and Trace Element Geochemistry

Fifty-seven samples for major and trace element analysis were collected from eleven sections scattered across the northern Colorado River extensional corridor (Fig. 6: location map of samples). Major and trace element analyses of these samples are given in Appendix A.

K-metasomatism of volcanic rocks is common in many locations in the extensional corridor (Smith et al., 1990). In order to determine whether metasomatism has significantly affected Tuff of Bridge Spring samples, Tuff of Bridge Spring data are plotted on a Na_2O versus K_2O plot from Smith et al., (1990) which includes the field of unmetasomatized intermediate and felsic rocks as defined by Carmichael et al. (1974) (Fig. 7). This plot indicates that 47 % of the analyses have not been metasomatized. With the exception of the analyses of the Temple Bar ash-flow tuff,

the remaining data points fall very close to the field of unmetasomatized rocks. Also, 70 % of the LOI values determined for twenty Tuff of Bridge Spring samples have values under 2 %, which suggests that they have not been altered. Since most incompatible trace element concentrations are not appreciably affected by metasomatism (Smith et al., 1990), and since negative correlation of K and Na concentrations in some northern Colorado River extensional corridor rocks (Wilson Ridge pluton) suggests the presence of closed system/equilibrium conditions (Smith et al., 1990), it is assumed that metasomatism did not significantly affect the chemistry of samples collected for this study and, consequently, that the analyses are representative of ash-flow tuff compositions present at the time of their eruption.

Tuff of Bridge Spring Geochemistry

The following description of geochemistry focuses on those stratigraphic sections that are isotopically equivalent to the Tuff of Bridge Spring (see regional correlation section). Discussion of the geochemistry of those sections that are isotopically different from the Tuff of Bridge Spring (Lucy Gray and Salt Spring Wash) or are not equivalent in age to the Tuff of Bridge Spring (Dolan Springs) will be deferred to the end of this discussion. Interpretation of geochemistry will be presented in later sections.

The Tuff of Bridge Spring continuously ranges in composition from andesite (White Hills: 59.50 % SiO_2) to rhyolite (Black Mountains: $\text{SiO}_2 = 74.91$ % SiO_2), and has an average composition of dacite (67 % SiO_2) (Table 4). There is a rough trend of decreasing silica in a northeastward direction across the distribution area of the Tuff of Bridge Spring. In the southwest portion of the Tuff of Bridge Spring distribution area, the Black Mountains, Highland Spring Range, and Sheep Mountain are rhyolitic in

composition. Sections in the middle of the distribution area, which includes the Eldorado Mountains, McCullough Range, and Interstate 15 sections, range in composition from dacite to rhyolite. The Temple Bar section is dacitic in composition, and the White Hills section in the northeastern corner of the Tuff of Bridge Spring distribution area ranges from andesite to dacite. The greatest variation of SiO_2 within a single section is found in the McCullough Range (8.6 wt. % SiO_2). The smallest variation is found in the Sheep Mountain section (0.46 wt. % SiO_2).

Harker variation plots (Fig. 8) show a general trend of decreasing Al, Ti, Fe, Mg, Ba, Zr, and Sr with increasing silica, and increasing Th and Nb with increasing silica. Other general observations of Tuff of Bridge Spring chemistry include (1) unusually high concentrations of Cr (approximately 150 ppm in the Sheep Mountain section); (2) very low K (5.7 wt. % in the basal Sheep Mountain section); and (3) anomalously large ranges of Rb (40 to 300 ppm), Ba (100 to >1500 ppm), Sr (50 to >1500 ppm), and Na (0.2 to 4 wt. %).

Since the large variation of silica in each Tuff of Bridge Spring section tends to obscure distinct element groupings in conventional Harker variation plots, comparisons of general patterns of geochemical trends and detection of any departures from these patterns were found to be more clearly discerned by the use of relative stratigraphic position vs. elemental oxide plots (Fig. 9). These plots use the convention in which larger numerical values are assigned to stratigraphic intervals which occur higher in the section and smaller numerical values are assigned to intervals lying in lower positions in the section. (N.B.- correlation of intervals having the same relative stratigraphic position value is not inferred between different sections; e.g., position 5.5 in one section is not equivalent to position 5.5 in another section).

Relative stratigraphic position vs. elemental oxide plots (Fig. 9) show that the chemistry of the Tuff of Bridge Spring (1) varies widely over its range; (2) can vary

considerably within each stratigraphic section; and (3) the geochemical trends of the Eldorado Mountains, Highland Spring Range, Interstate 15, and Sheep Mountain sections are relatively invariable for most major and trace elements (with the exceptions of Ca, Cr, Ni, and Th) and form a chemical group that can be used to create a baseline reference against which any deviations exhibited by the other Tuff of Bridge Spring sections can be compared with and quantified (Table 5).

The following is a short summary of deviations from the invariable Tuff of Bridge Spring group described above. Important variations from the baseline reference chemistry include (Fig. 9 and Table 5):

(1) The lower part of the Temple Bar section (intervals 4-8) is enriched in K by approximately 4.4 wt. %.

(2) The Temple Bar and Black Mountains sections have slightly lower Mn concentrations (0.02 wt. % Mn).

(3) The Interstate 15, Temple Bar, and Sheep Mountain sections show highly variable (a minimum of 23 ppm) enrichment of Cr.

(4) The lower Temple Bar section (intervals 5-8) is significantly enriched in Rb (100 ppm).

(5) The McCullough Range and White Hills sections are enriched in Sr (a minimum of 170 ppm).

(6) Intervals 6-7.5 of the McCullough Range section are significantly enriched in Zr (210 ppm).

(7) The McCullough Range is enriched in Ba by a minimum of 320 ppm and contains a Ba spike at stratigraphic intervals 6-7.5. This spike corresponds to the peak observed for Zr at the same stratigraphic positions. The Temple Bar and White Hills sections also show enrichment in Ba (870 ppm).

(8) The McCullough Range, White Hills, and Black Mountains sections show much greater variability of Y than the rest of the sections.

(9) The basal interval of the McCullough Range section consistently shows significant variation for Si, Al, K, Mg, Na, Rb, Zr, and Sr as compared to the upper part of the section. In the Eldorado Mountains, large variation of Ca, Na, Rb, Y, Na and Mg occurs in the three stratigraphically lowest-lying intervals. In the Temple Bar section, deviation of Ti, Ca, K, Mg, Rb, Y, Fe, and Mn occurs in the stratigraphically uppermost interval.

(10) The McCullough Range section shows a significant enrichment in Fe, Si, Al, Ti, Ca, Zr, Ba, Y, and Nb at position 8.

Other Ash-flow Tuffs

Based on isotopic analyses (see regional correlation section), the Salt Spring Wash, Lucy Gray, and Dolan Springs sections are not equivalent to the Tuff of Bridge Spring. These tuffs are rhyolitic in composition (Tuff of Dolan Springs: 73.7-75.6 wt. % SiO₂; Salt Spring Wash: 70.1-73.9 wt. % SiO₂; and Lucy Gray Range: 72.4-72.9 wt. % SiO₂) (Appendix A). The maximum SiO₂ value of Tuff of Dolan Springs exceeds that of the highest value of the Tuff of Bridge Spring (Black Mountains section: 74.91 %). Harker variation plots for these sections compared with the Tuff of Bridge Spring (Fig. 10) show:

(1) The Dolan Springs section is noticeably depleted in Al, Ti, Fe, and Mn, and is significantly depleted in Nb (5.3 ppm), Th (8.5 ppm), Y (2.2 ppm), and Zr (139.7 ppm) with respect to the Tuff of Bridge Spring.

(2) The Lucy Gray Range section exhibits depletion in Fe, Ca, Ba, Mg, Ti, and Sr, and is enriched in Y with respect to the Tuff of Bridge Spring.

(3) The lowest value of the Salt Spring Wash section for Zr, Y, Th Ca, Nb, and Al falls below the lowest value for these elements for the Tuff of Bridge Spring.

Petrologic Descriptions

The Tuff of Bridge Spring contains from 7.8 % to 46.4 % phenocrysts (Black Mountains and Temple Bar sections, respectively) and from 0 % to 25.4 % lithic fragments (maximum from the Black Mountains section) (Appendix B). The matrix of the Tuff of Bridge Spring is moderately devitrified, which is reflected by the presence of fine- to coarse-grained crystallization textures. Another common matrix texture is an axiolitically-devitrified matrix in which the faint outlines of glass shards in the matrix are still discernable. Unaltered glass shards are rare in the Tuff of Bridge Spring with the exceptions of the Sheep Mountain and Interstate 15 sections. Spherulitic devitrification is also rare in the Tuff of Bridge Spring. Spherulites in the Highland Spring Range section are anomalously large (< 7 cm in diameter).

Pumice is rare in the Tuff of Bridge Spring and generally occurs as moderately-compressed, subangular fragments that are less than one millimeter wide. Preservation of larger pumice fragments is rare, and is limited to occurrences in the basal intervals of the Sheep Mountain and Interstate 15 sections. Pumice from these sections range in size from <3 mm to 8 cm.

Eutaxitic textures are common in the Tuff of Bridge Spring. Fiamme vary from <1.0 cm to over 9 cm (Eldorado Mountains section). Banded fiamme can sometimes be observed in the Eldorado Mountains section.

The majority of Tuff of Bridge Spring sections are either unaltered or are weakly-altered by secondary carbonate. Temple Bar samples are heavily contaminated with secondary carbonate. Alteration of feldspar phenocrysts in Temple Bar samples

makes the discrimination of sanidine from plagioclase difficult, requiring the use of the "undifferentiated feldspar" nomenclature used in the Appendix B.

Lithic fragments in the Tuff of Bridge Spring consist of basalt to basaltic andesite. Basalts commonly contain plagioclase phenocrysts. Basaltic andesite lithic fragments contain phenocrysts of plagioclase, clinopyroxene, and opaque iron oxide (undifferentiated).

Phenocrysts in the Tuff of Bridge Spring include, in decreasing order of abundance: sanidine, plagioclase, biotite, clinopyroxene, opaque iron oxide (undifferentiated), sphene, \pm zircon, and \pm apatite (Appendix B). Primary quartz is not present in the Tuff of Bridge Spring. Trace amounts of hornblende, which is rare and possibly xenocrystic, is present in the McCullough Range and White Hills sections. Plagioclase ranges from An₁₁ (Black Mountains section) to An₃₆ (Eldorado Mountains section) (Table 6). Feldspar phenocrysts commonly display disequilibrium textures which include resorbed margins in sanidine phenocrysts, sieve textures in plagioclase and sanidine, and mantling of plagioclase phenocrysts by sanidine.

Glomerocrysts are ubiquitous in the Tuff of Bridge Spring, and occur as: (1) monomineralic clusters of plagioclase, sanidine, or sphene, and (2) polymineralic clusters that commonly occur in the following combinations: (i) clinopyroxene + sphene + Fe-oxide opaque \pm plagioclase \pm biotite \pm zircon \pm apatite; (ii) sphene + Fe-oxide opaque + zircon \pm apatite \pm biotite; and (iii) plagioclase + biotite + sphene \pm zircon \pm sanidine. Glomerocrysts generally occur as aggregations of five or fewer crystals, and are < 0.8 mm in width.

Two small (< 0.3 mm in length) mafic enclaves were observed in thin sections of the Tuff of Bridge Spring. These consist of the following samples. (1) Sample 92-E3-10 (Eldorado Mountains section): this oblate-shaped enclave (length $\cong 2$ mm) consists of a core of blebby biotite, opaque iron oxide, and plagioclase feldspar which is

enclosed in a microcrystalline matrix of unknown composition. This core is enclosed within a rim of subhedral to anhedral plagioclase feldspar. (2) Sample Mc 69 (Interstate 15 section): this enclave, found in a thin section that was previously described by Bridwell (1991), is approximately 3 mm long and consists of an irregularly fractured core of orange, microcrystalline unknown mineral that is enclosed in successive, concentric rims of (i) anhedral, opaque iron oxide enclosed in black, microcrystalline matrix, (ii) anhedral clinopyroxene, and (iii) euhedral to subhedral biotite (listed in order of occurrence from enclave core to rim).

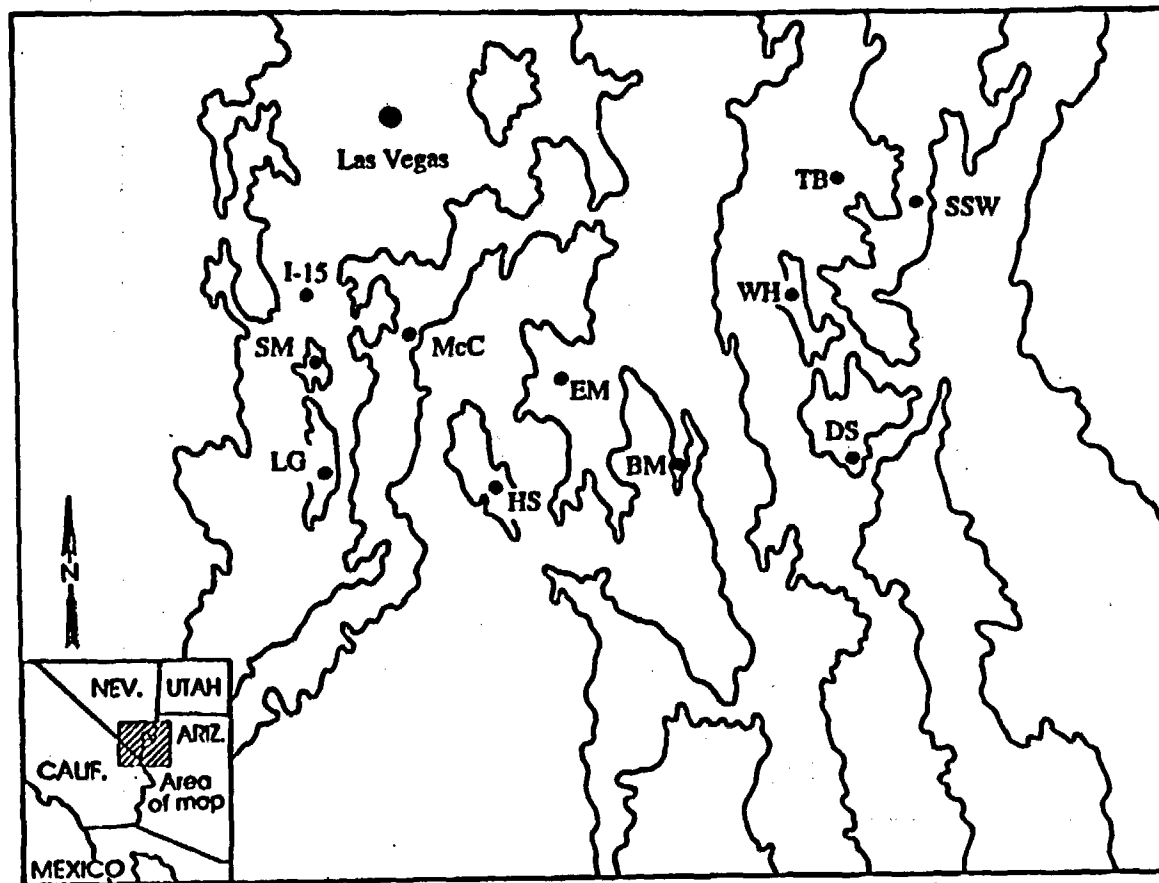


Figure 6. Map showing locations of sections sampled for geochemistry and petrology. LG = Lucy Gray Range; SM = Sheep Mountain; I-15 = Interstate 15; EM = Eldorado Mountains; McC = McCullough Range; HS = Highland Spring Range; BM = Black Mountains; TB = Temple Bar; WH = White Hills; DS = Dolan Springs; SSW = Salt Spring Wash.

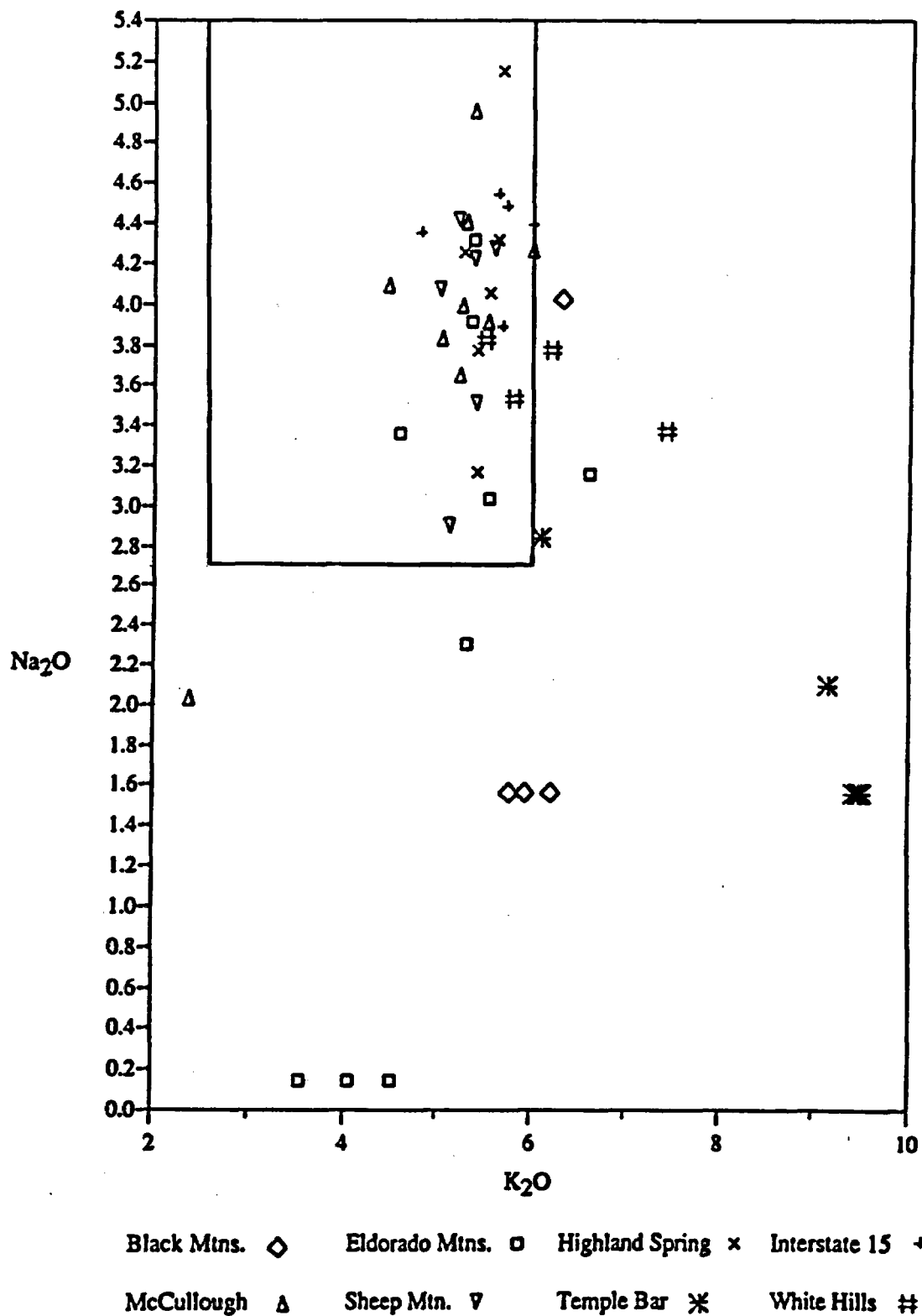
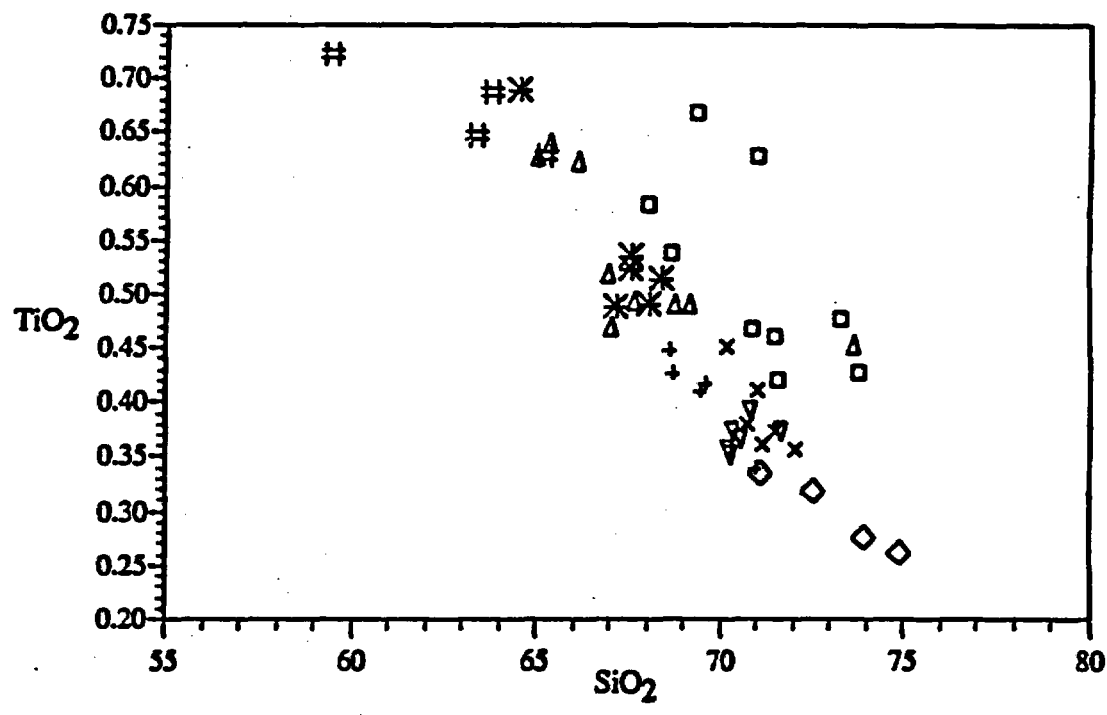
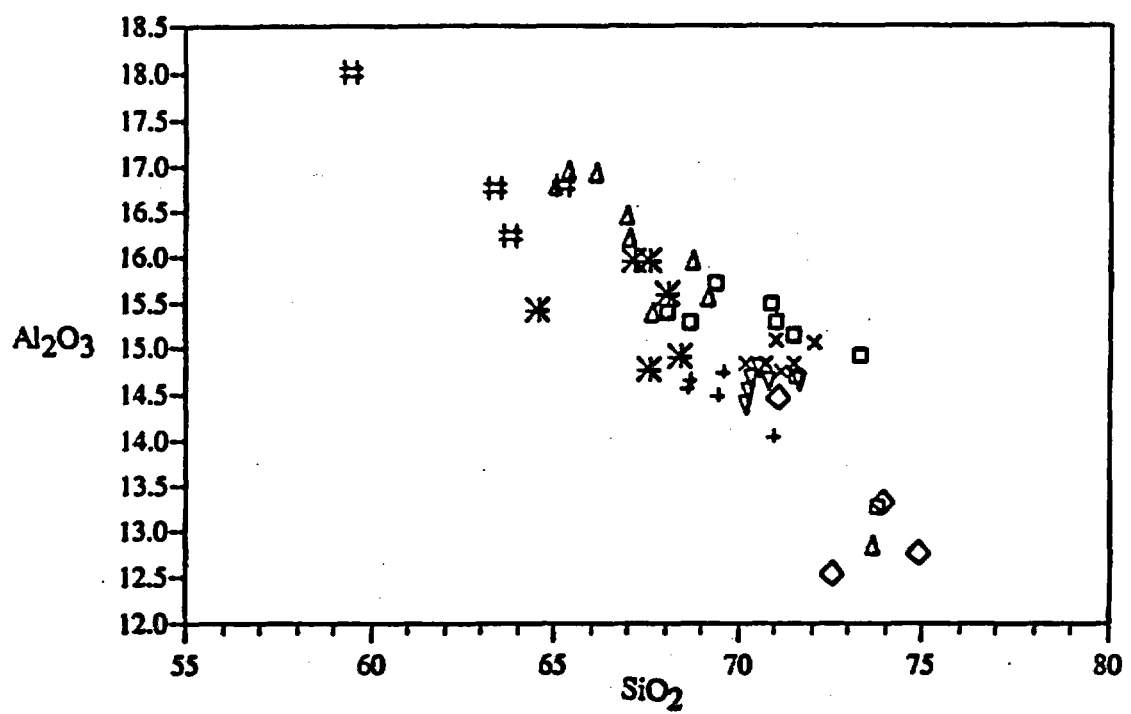


Figure 7. Plot of Na₂O vs. K₂O. The field of unmetasomatized rocks from Carmichael et al. (1974). Samples falling within the field are interpreted to be either unaffected or marginally affected by metasomatization.

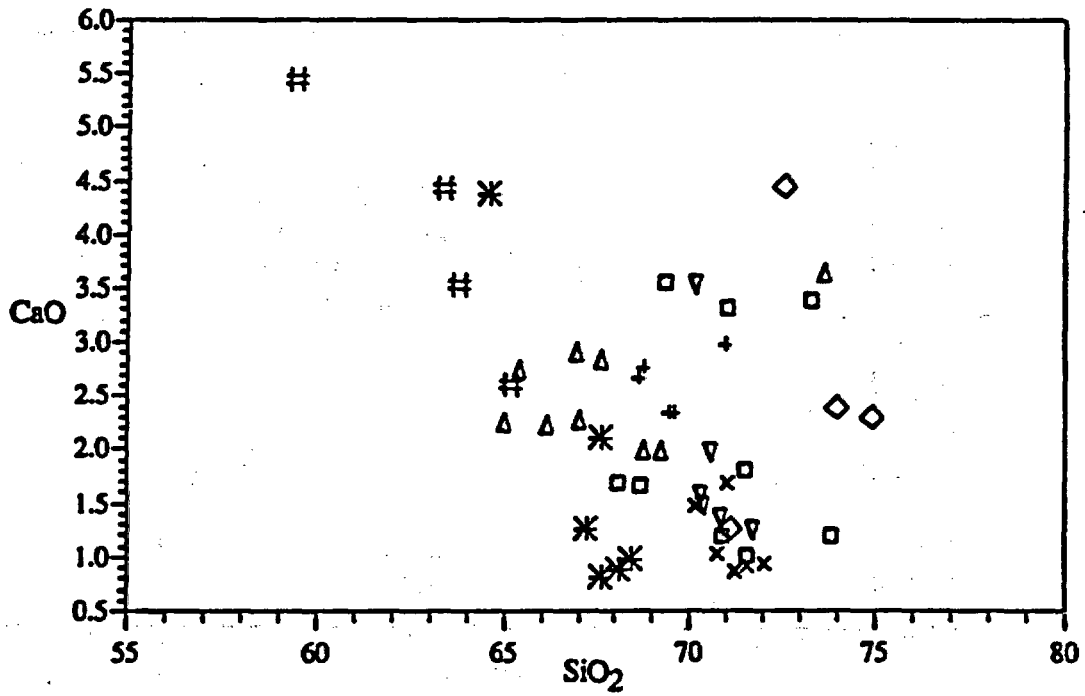
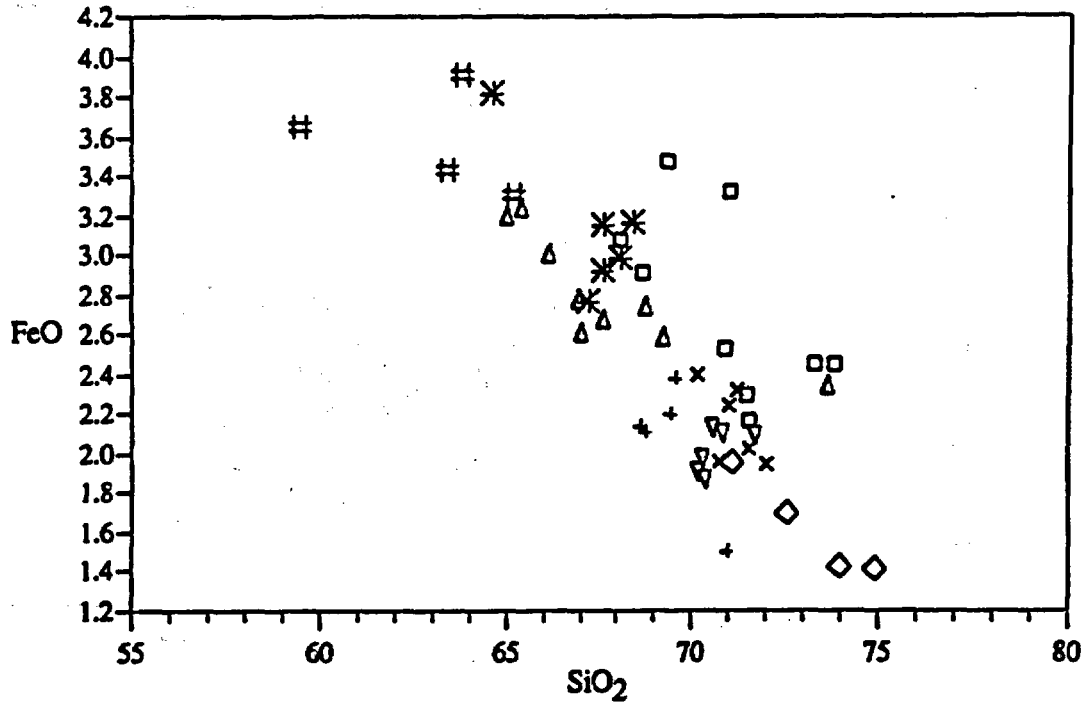
Table 4: Regional Major and Trace Element Variation: Tuff of Bridge Spring.
Major element oxides in wt.% and trace elements in ppm.

	Minimum	Maximum	Range	Section Containing Minimum Value	Section Containing Maximum Value	Section Containing Least Variation	Range of Variation	Section Containing Greatest Variation	Range of Variation
SiO ₂	57.47	74.91	17.44	White Hills	Black Mountains	Highland Spring	1.88	McCullough Range	8.6
Al ₂ O ₃	12.52	17.38	4.86	Black Mountain	White Hills	Highland Spring	0.32	McCullough Range	4.12
TiO ₂	0.28	0.70	0.43	Black Mountain	White Hills	Sheep Mountain	0.05	Eldorado Mountains	0.25
Fe ₂ O ₃	1.69	3.65	2.46	Black Mountain	White Hills	Sheep Mountain	0.26	Eldorado Mountains	1.31
CaO	0.79	5.25	4.45	Temple Bar	White Hills	I-15	0.64	Black Mountains	3.19
K ₂ O	2.62	9.88	7.26	Temple Bar	Temple Bar	Black Mountains	0.26	McCullough Range	3.64
MnO	0.03	0.10	0.07	Temple Bar	White Hills	Highland Spring	0	Temple Bar	0.04
P ₂ O ₅	0.00	0.25	0.25	Sheep Mtn./Highland Spring	White Hills	I-15	0.05	White Hills	0.15
Na ₂ O	0.14	5.00	4.85	Eldorado Mtns.	Highland Spring	White Hills	0.04	Eldorado Mountains	4.25
MgO	0.14	2.13	1.99	Black Mountains	McCullough Range	Black Mountains	0.19	Eldorado Mountains	1.34
Cr	2.2	111.6	109.5	Black Mountains	Sheep Mountain	Eldorado Mountains	3.7	Sheep Mountain	92.9
Nb	24.0	51.9	27.9	McCullough Range	Highland Spring	Sheep Mountain	2.6	Highland Spring	15.4
Ni	8.2	30.4	22.2	Black Mountains	Eldorado Mountains	White Hills	2.1	Sheep Mountain	15.1
Rb	36	314	278	McCullough Range	Temple Bar	Sheep Mountain	19	McCullough Range	144
Sr	49	1063	1034	Black Mountains	McCullough Range	Sheep Mountain	39	McCullough Range	753
Th	16.7	44.8	27.9	White Hills	Highland Spring	Sheep Mountain	5.5	Highland Spring	15.4
Y	22.9	31.0	8.1	McCullough Range	Eldorado Mountains	Sheep Mountain	1	McCullough Range	5.1
Zr	261	638	377	Black Mountains	McCullough Range	White Hills	15	McCullough Range	337
Ba	63	1753	1690	Sheep Mountain	McCullough Range	Sheep Mountain	20	McCullough Range	1223



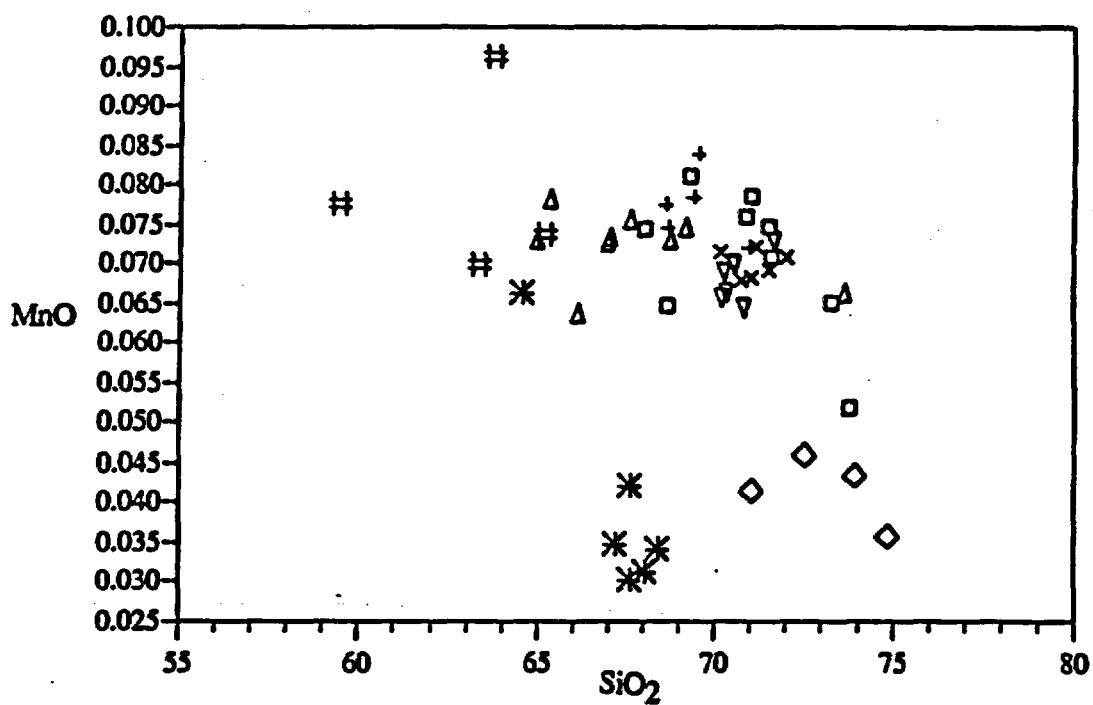
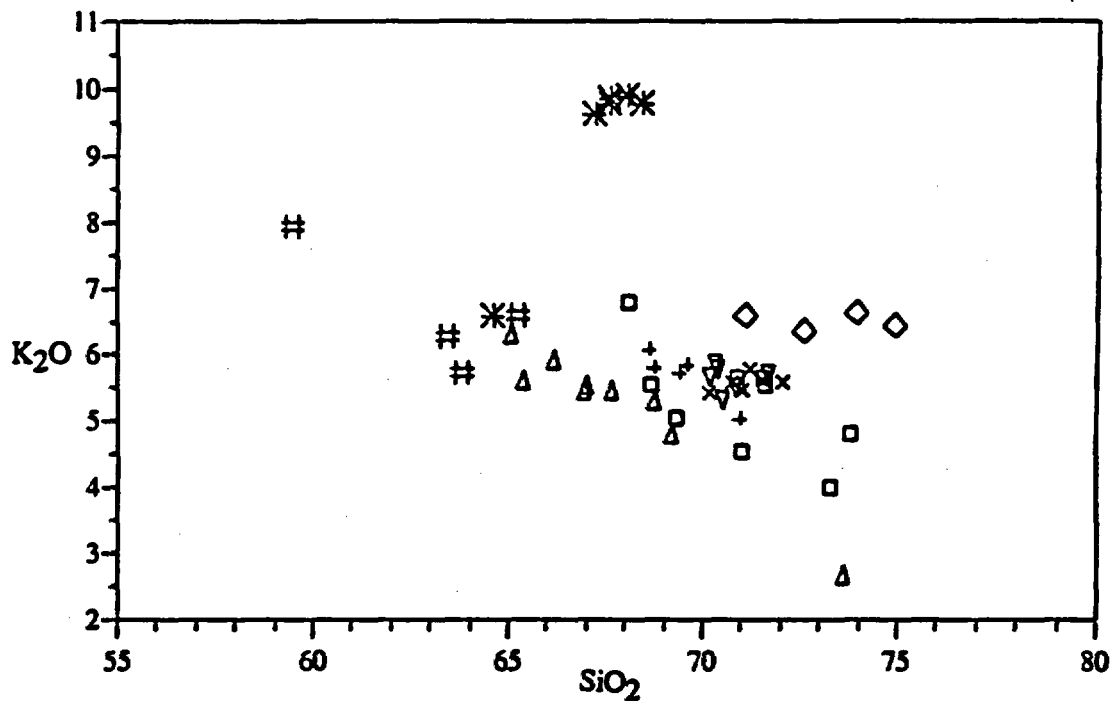
Black Mtns. ◊ Eldorado Mtns. ◻ Highland Spring × Interstate 15 +
 McCullough Δ Sheep Mtn. ▽ Temple Bar ✱ White Hills #

Figure 8. Harker variation plots of Tuff of Bridge Spring sections: major element oxides and trace elements vs. SiO₂.



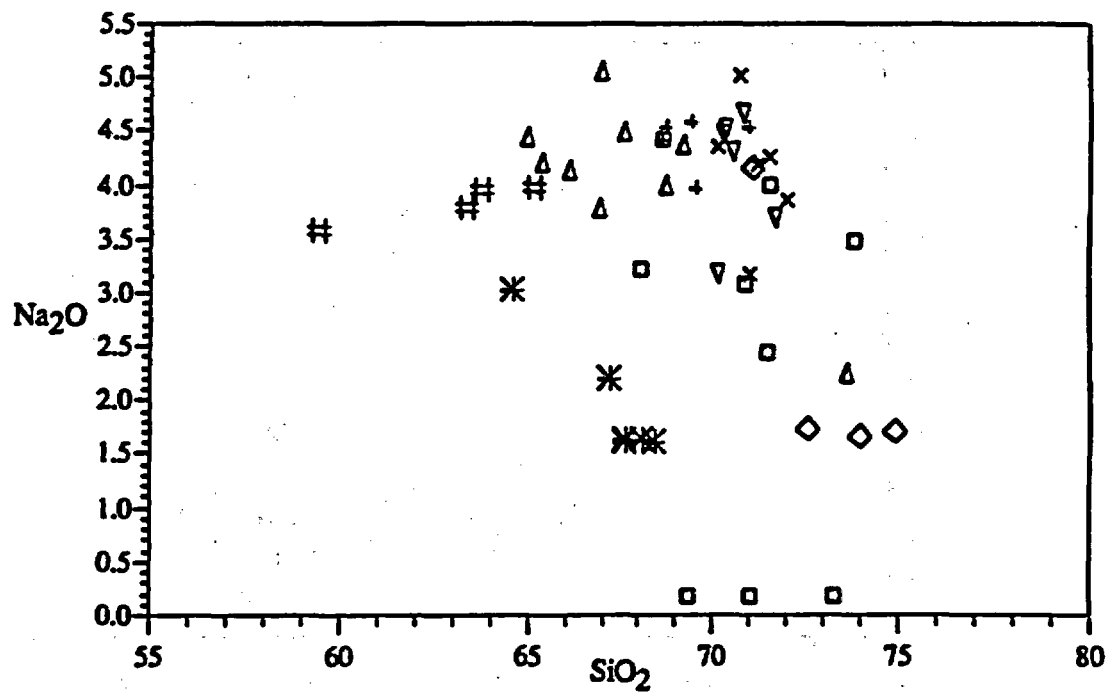
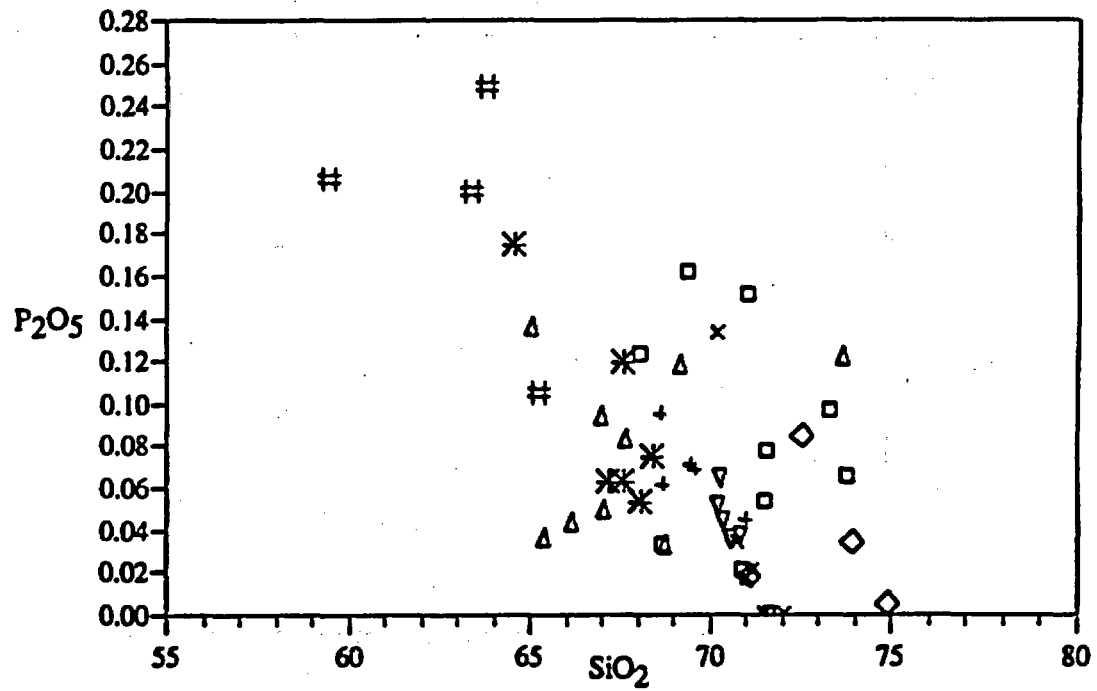
Black Mtns. ◊ Eldorado Mtns. □ Highland Spring × Interstate 15 +
 McCullough Δ Sheep Mtn. ▽ Temple Bar ✱ White Hills #

Figure 8, continued.



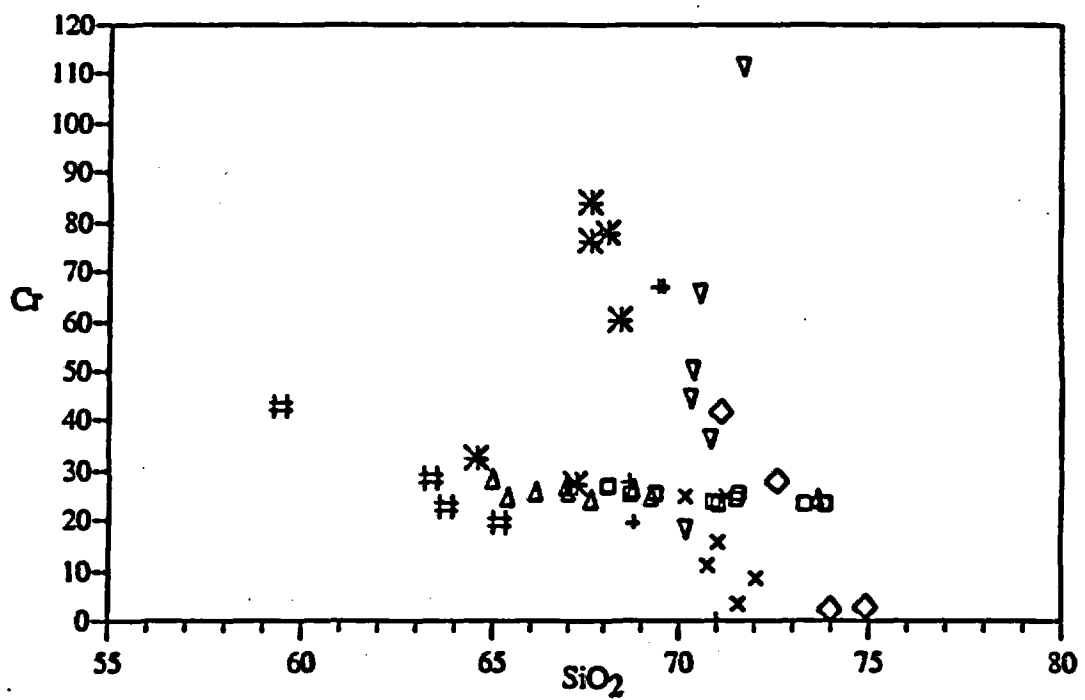
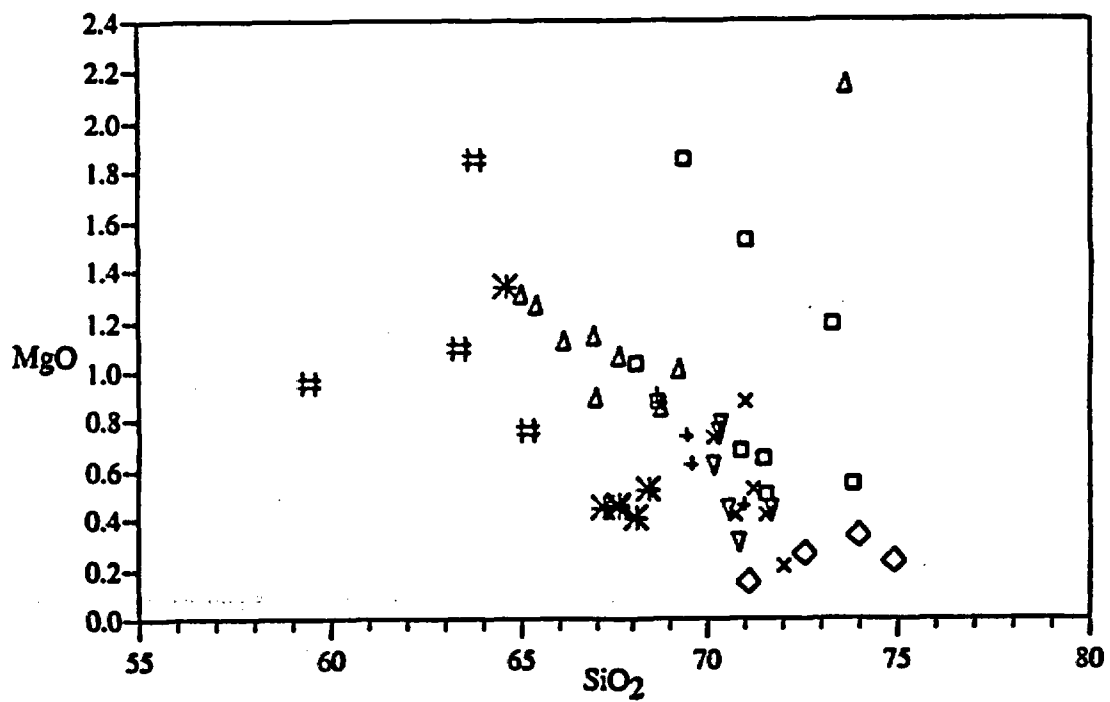
Black Mtns. ◇ Eldorado Mtns. □ Highland Spring × Interstate 15 +
 McCullough Δ Sheep Mtn. ▽ Temple Bar * White Hills #

Figure 8, continued.



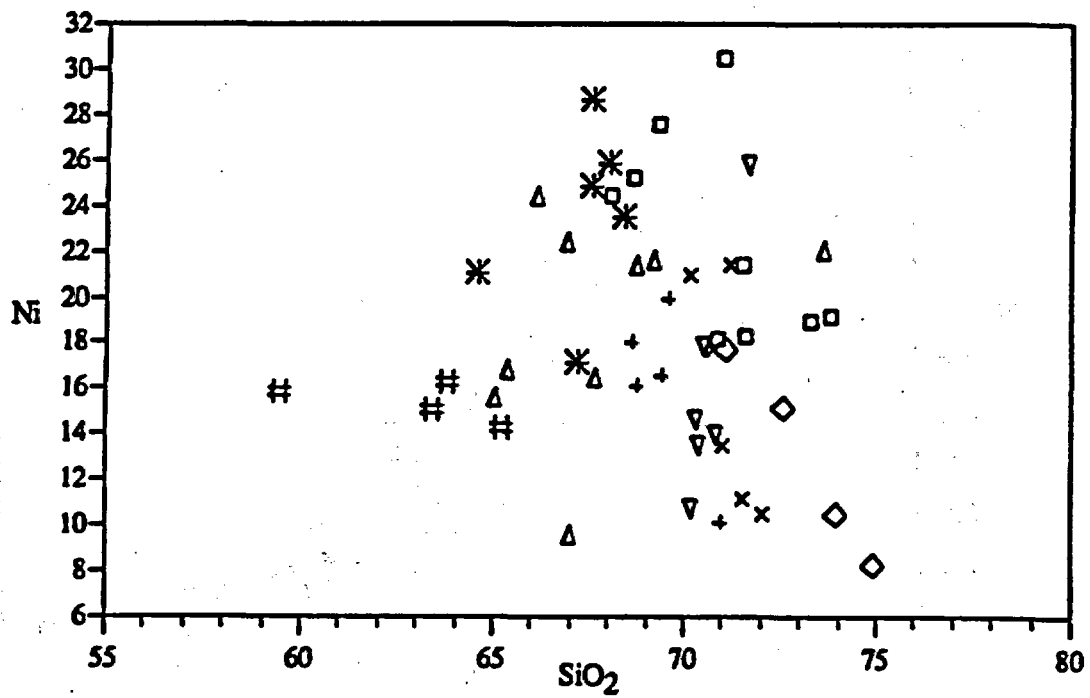
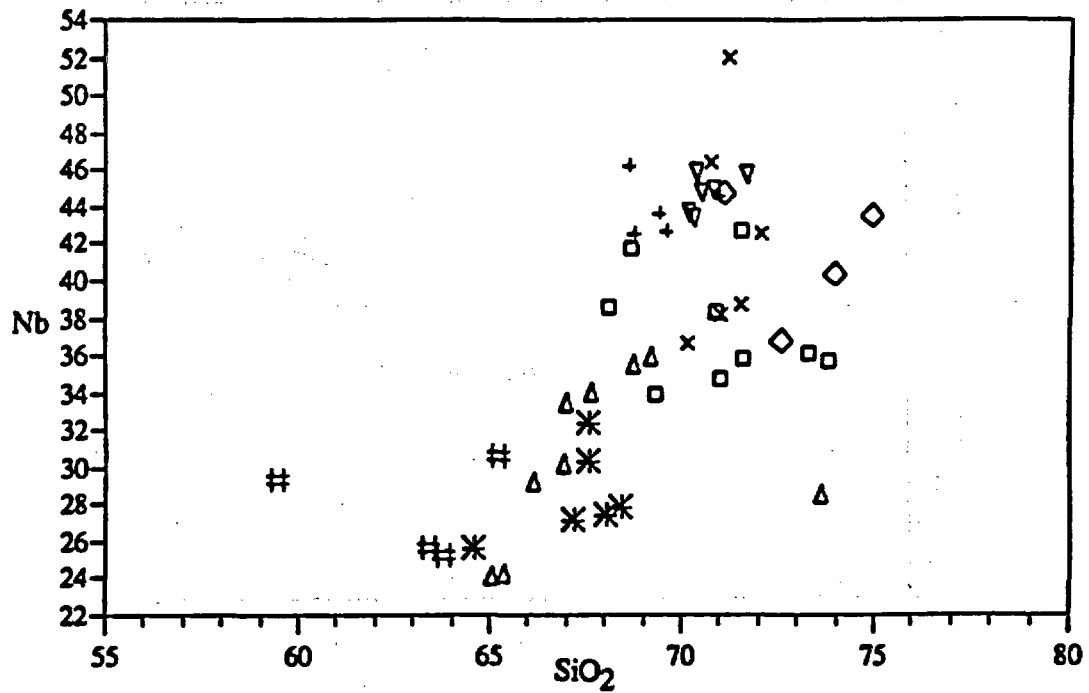
Black Mtns. \diamond Eldorado Mtns. \square Highland Spring \times Interstate 15 $+$
 McCullough Δ Sheep Mtn. ∇ Temple Bar $*$ White Hills $\#$

Figure 8, continued.



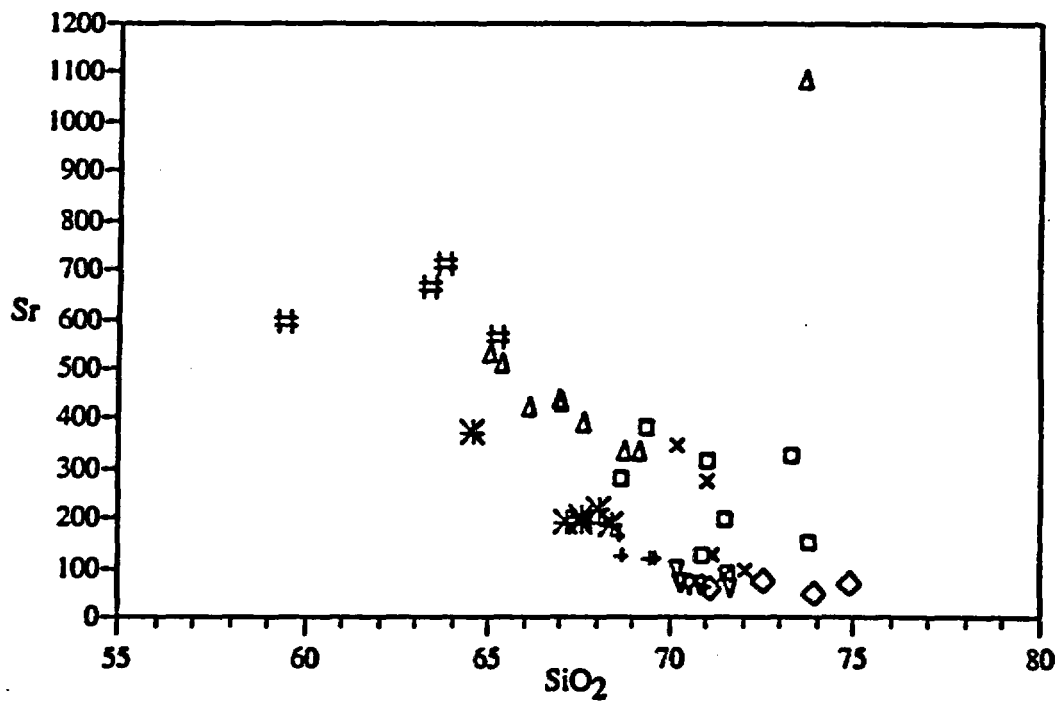
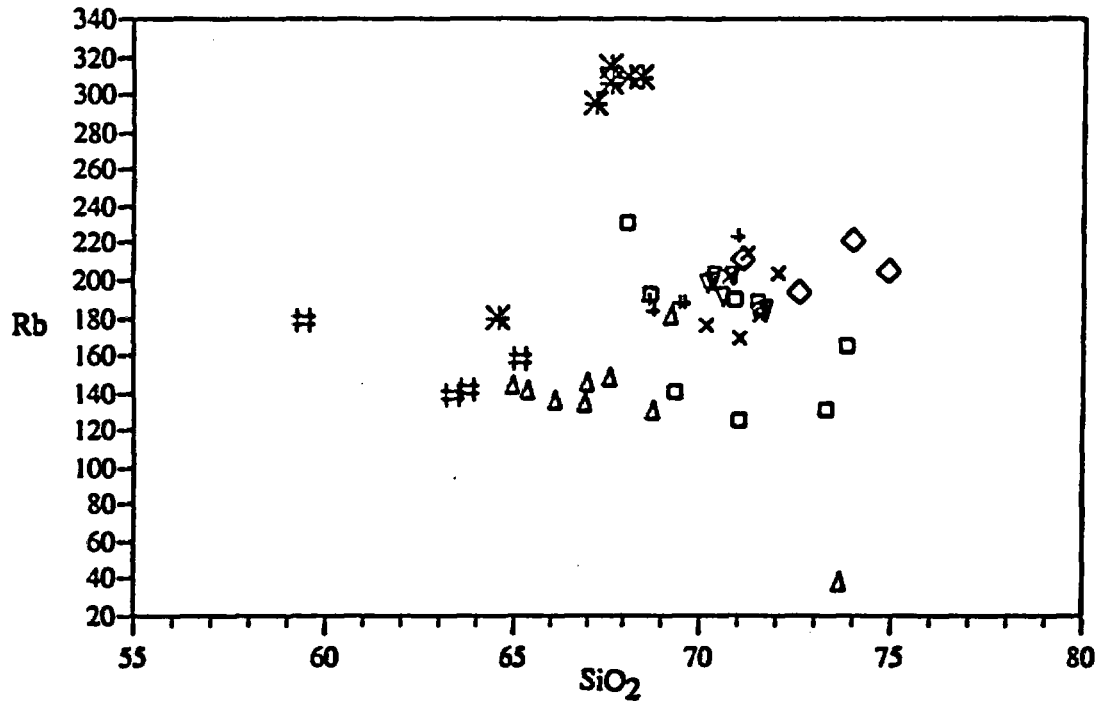
Black Mtns. ◇ Eldorado Mtns. □ Highland Spring × Interstate 15 +
 McCullough Δ Sheep Mtn. ▽ Temple Bar * White Hills #

Figure 8, continued.



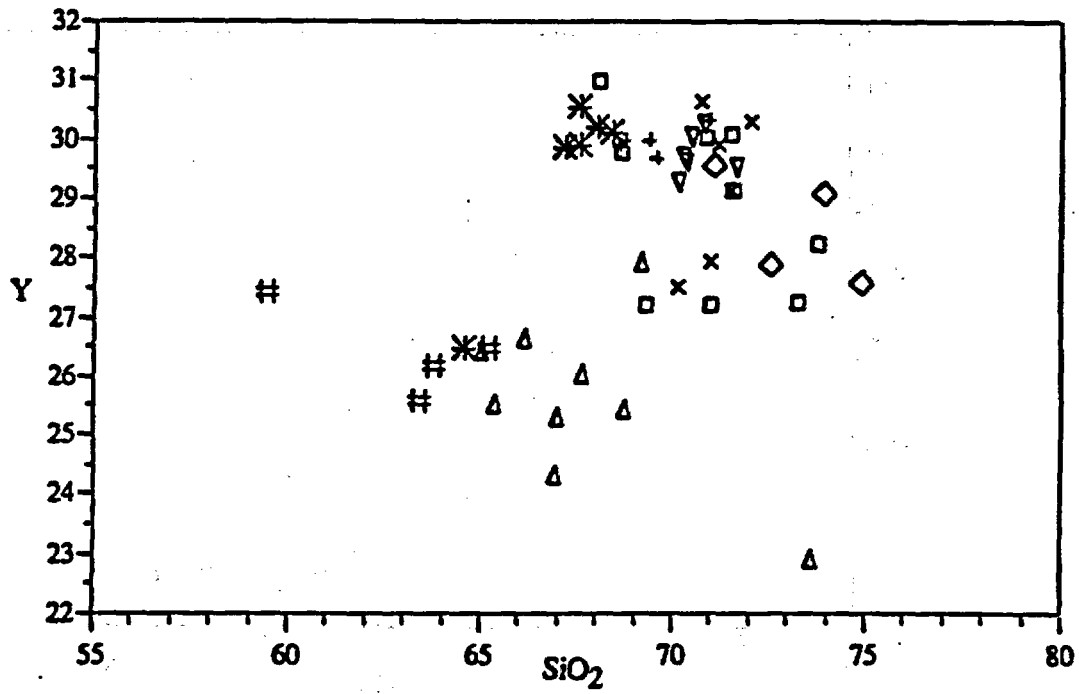
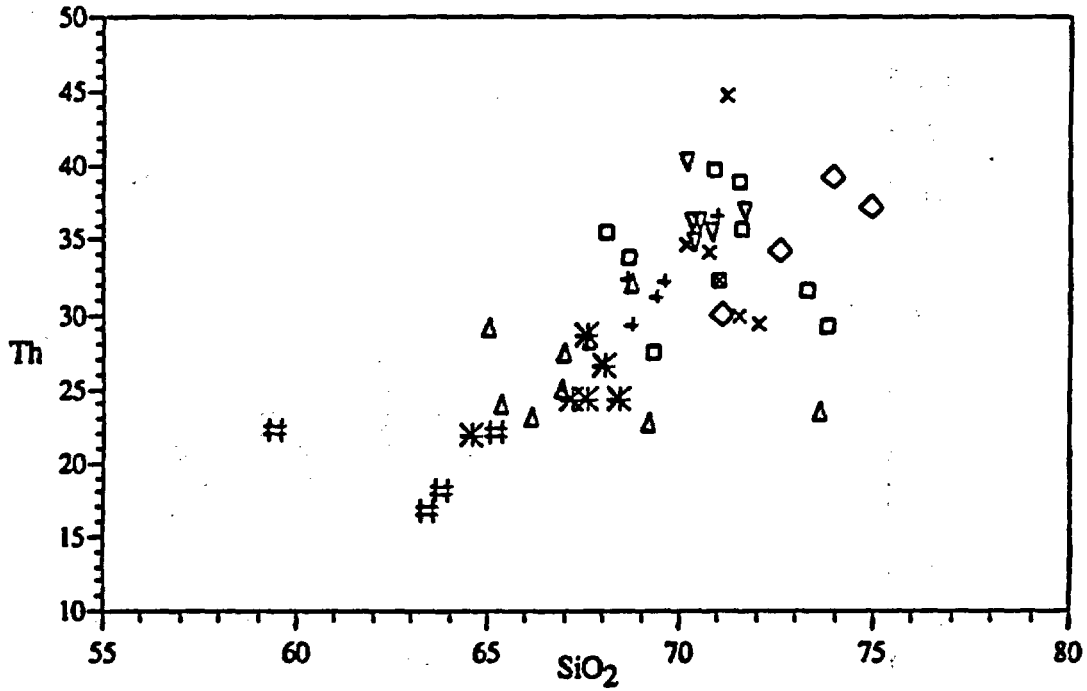
Black Mtns. \diamond Eldorado Mtns. \square Highland Spring \times Interstate 15 $+$
 McCullough Δ Sheep Mtn. ∇ Temple Bar $*$ White Hills $\#$

Figure 8, continued.



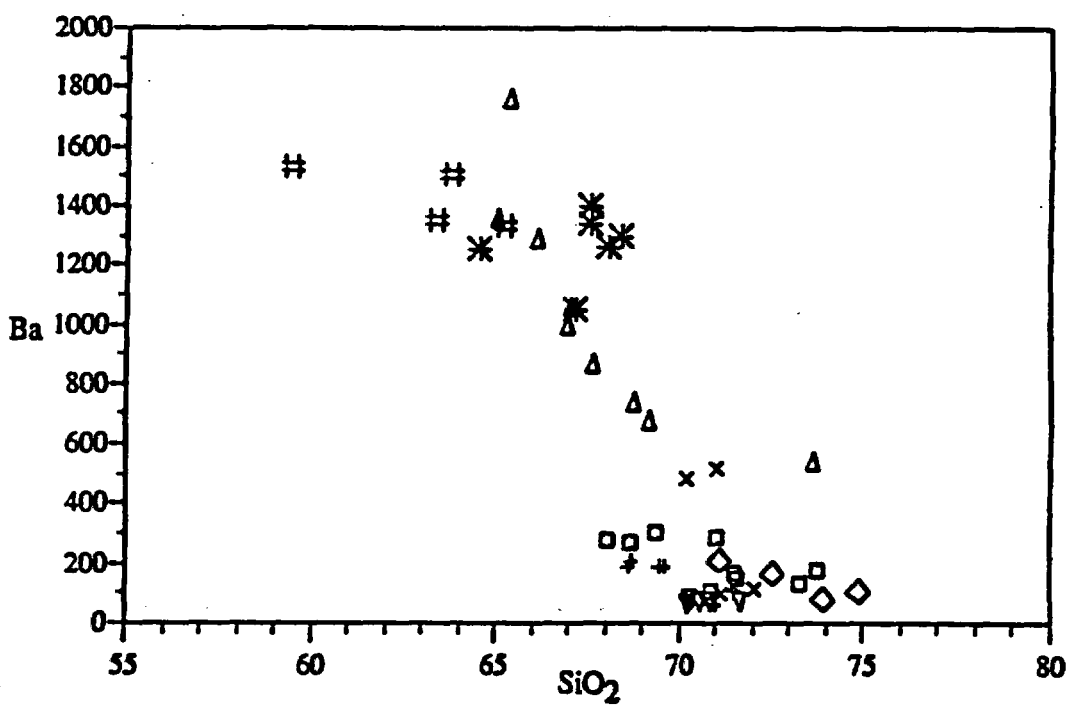
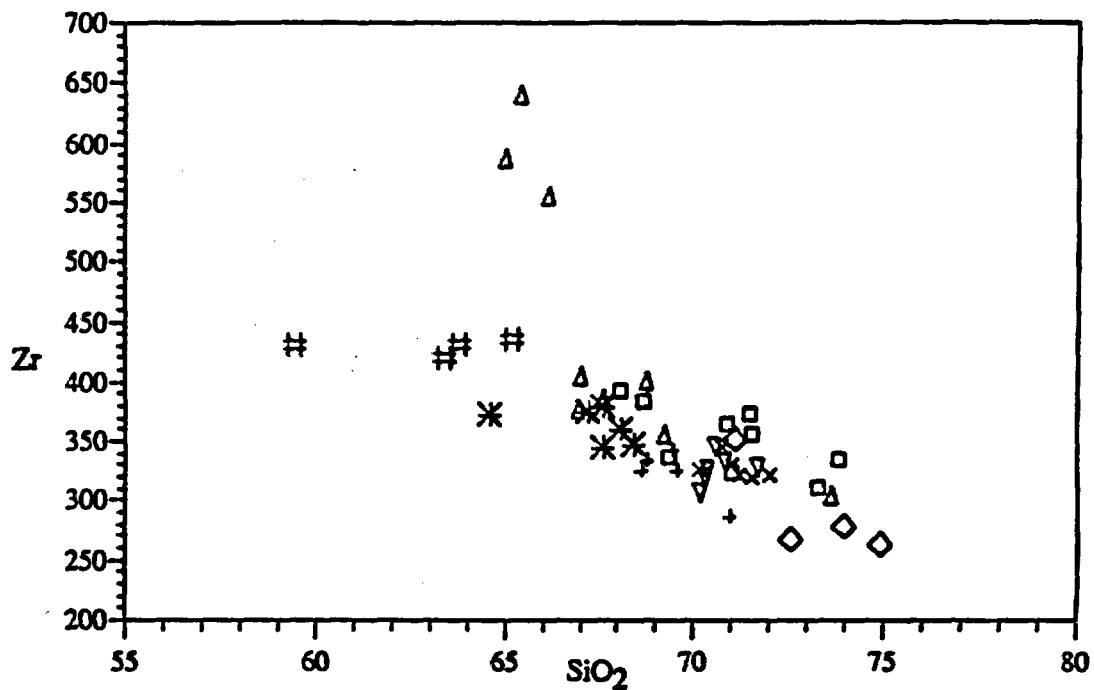
Black Mtns. ◇ Eldorado Mtns. □ Highland Spring × Interstate 15 +
 McCullough Δ Sheep Mtn. ▽ Temple Bar * White Hills #

Figure 8, continued.



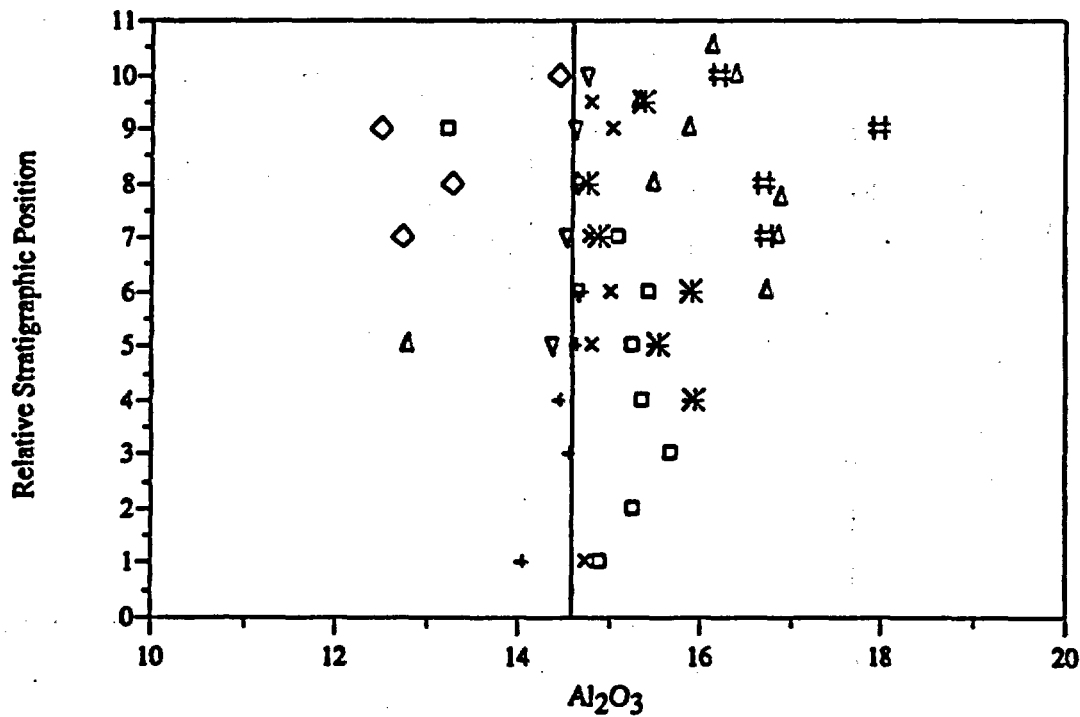
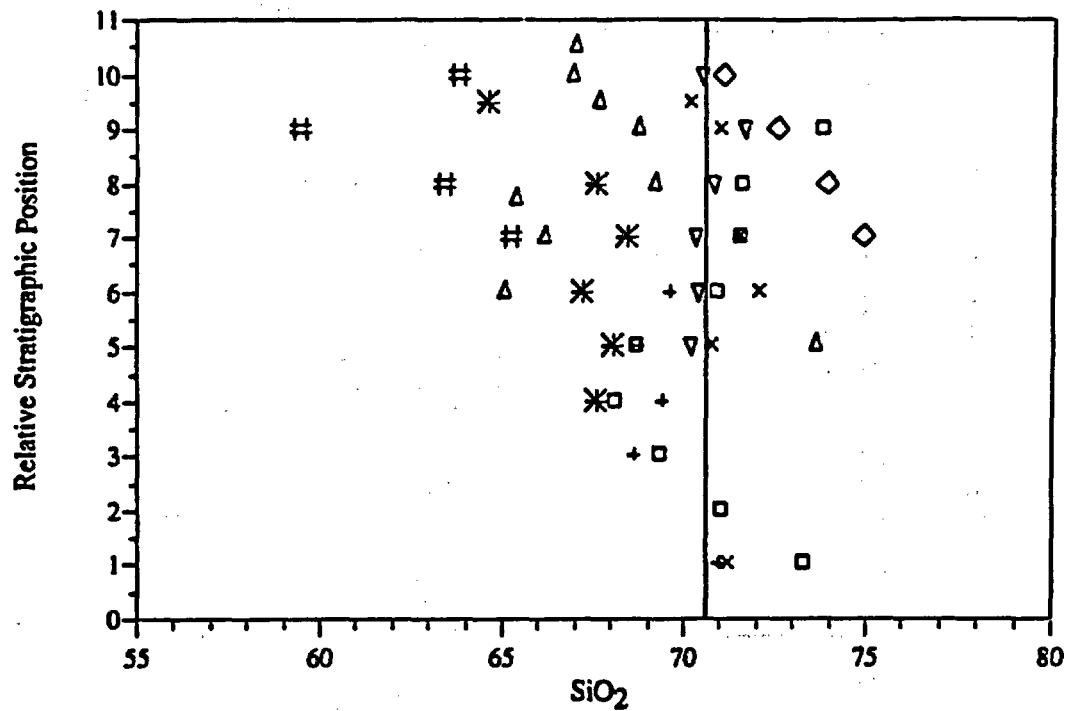
Black Mtns. \diamond Eldorado Mtns. \square Highland Spring \times Interstate 15 $+$
 McCullough \triangle Sheep Mtn. ∇ Temple Bar \ast White Hills $\#$

Figure 8, continued.



Black Mtns. ◇ Eldorado Mtns. □ Highland Spring × Interstate 15 +
 McCullough Δ Sheep Mtn. ∇ Temple Bar * White Hills #

Figure 8, continued.



Black Mtns. ◊ Eldorado Mtns. □ Highland Spring × Interstate 15 +
 McCullough Δ Sheep Mtn. ▽ Temple Bar ✱ White Hills #

Figure 9. Plots of relative stratigraphic position vs. element concentration of Tuff of Bridge Spring sections. Average concentration value for each element indicated by vertical line.

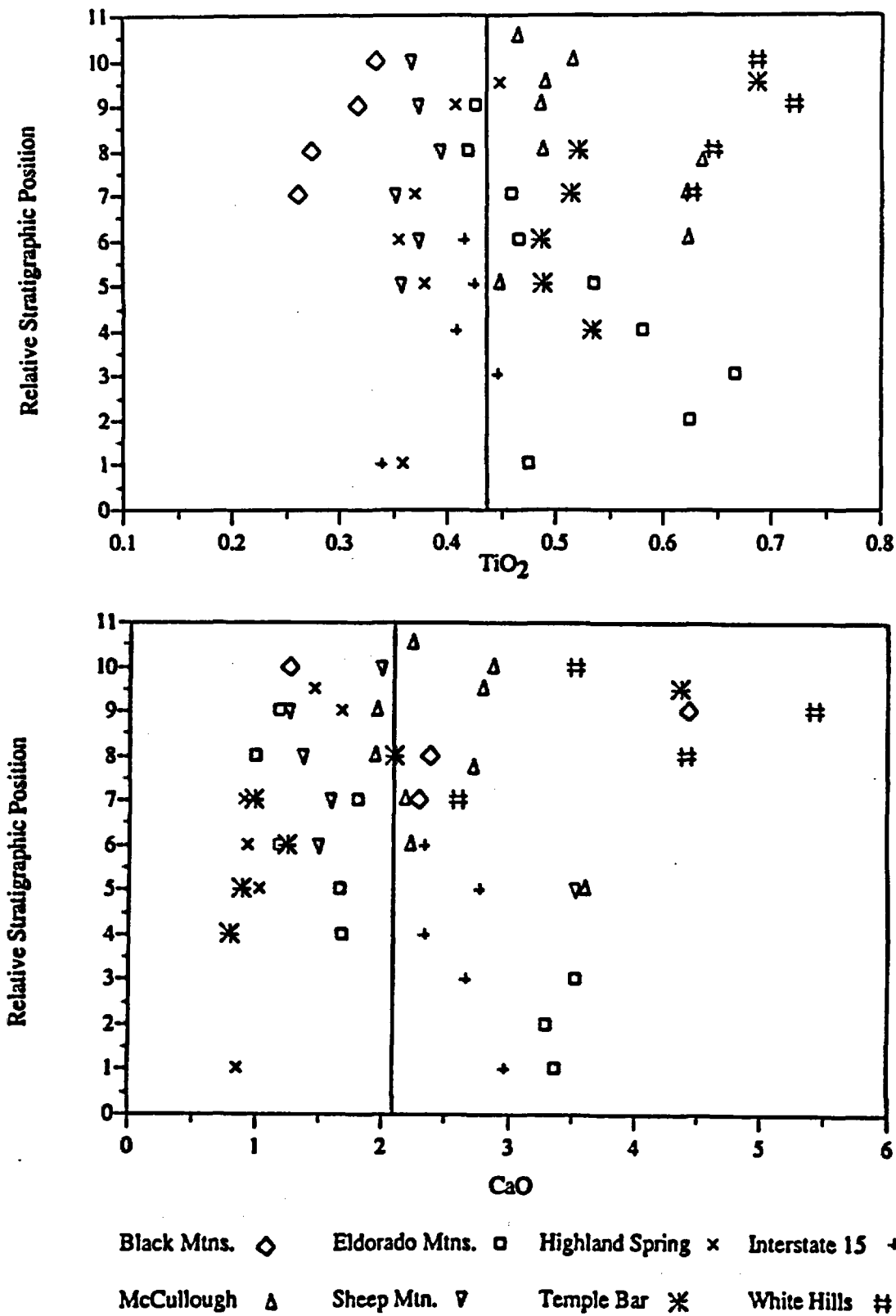
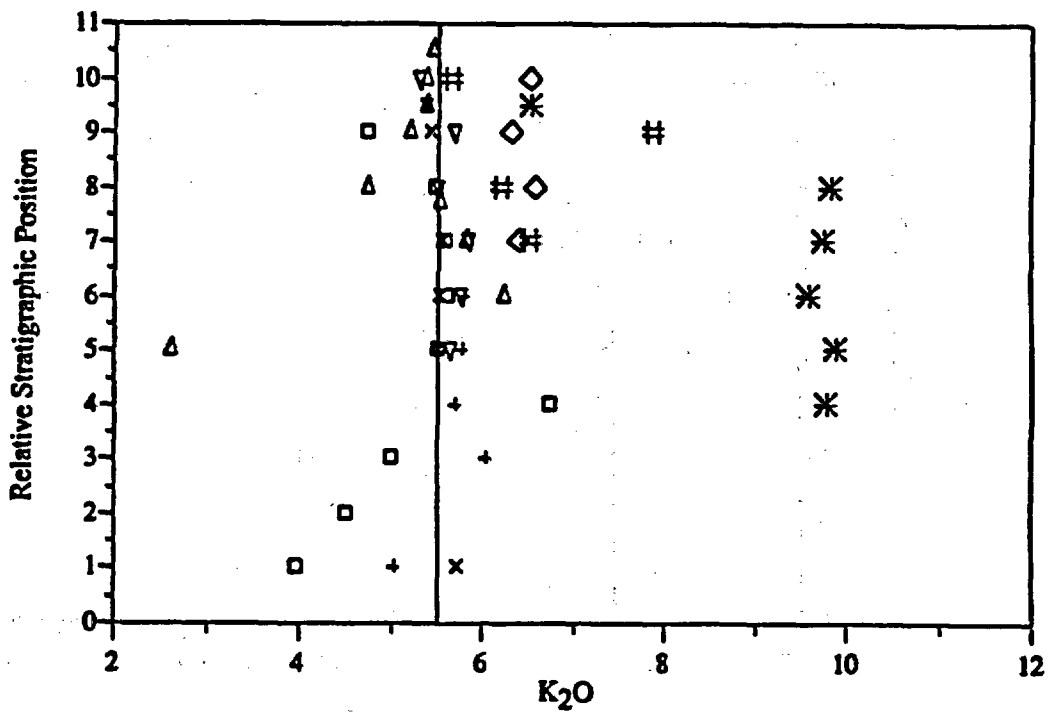
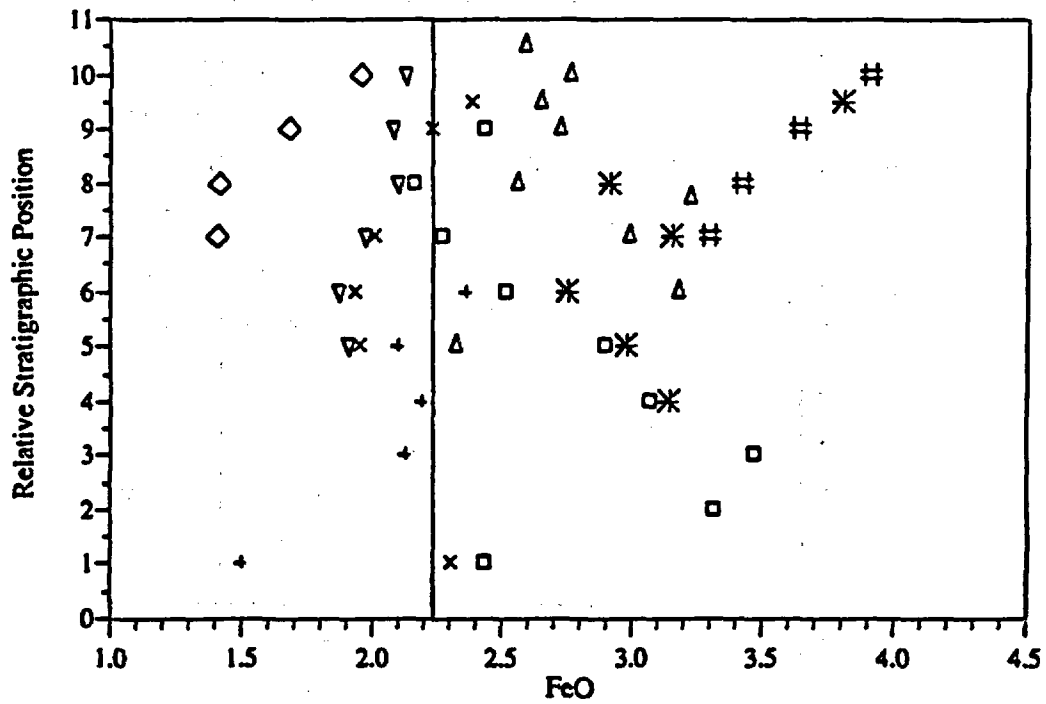
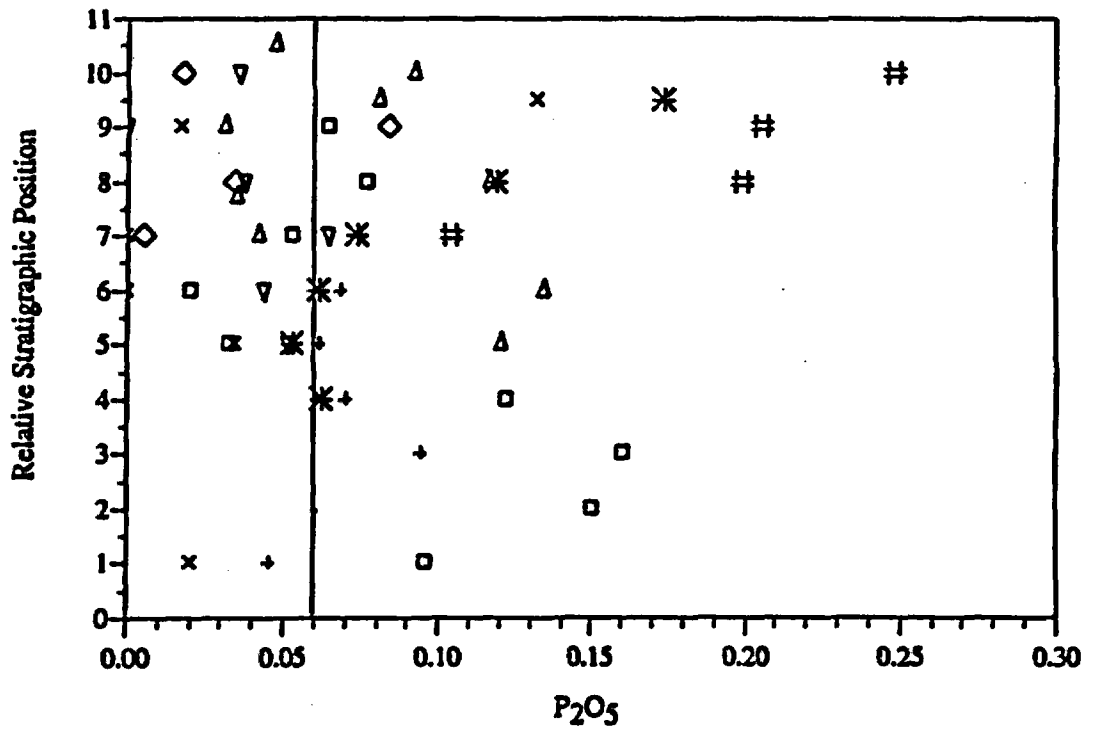
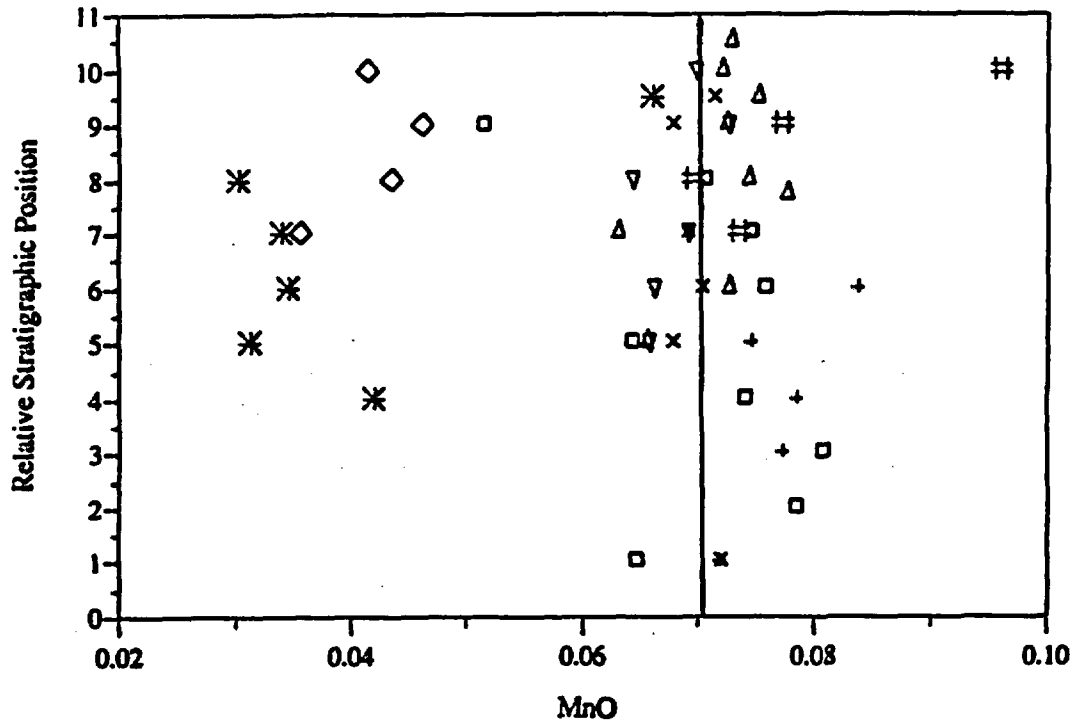


Figure 9, continued.



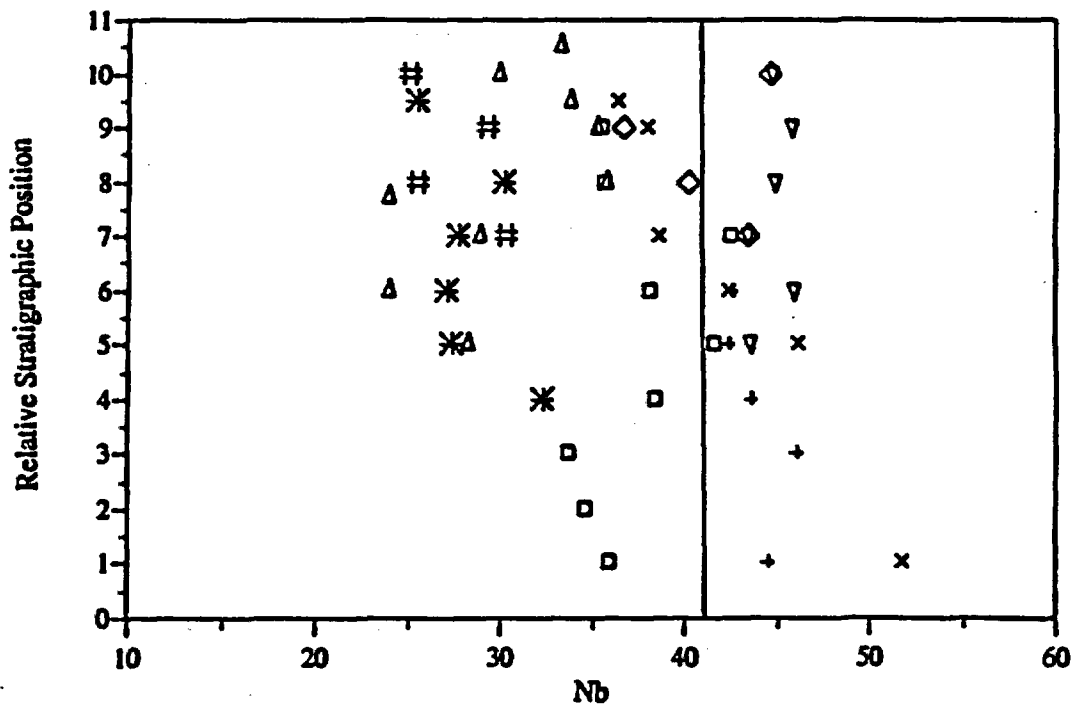
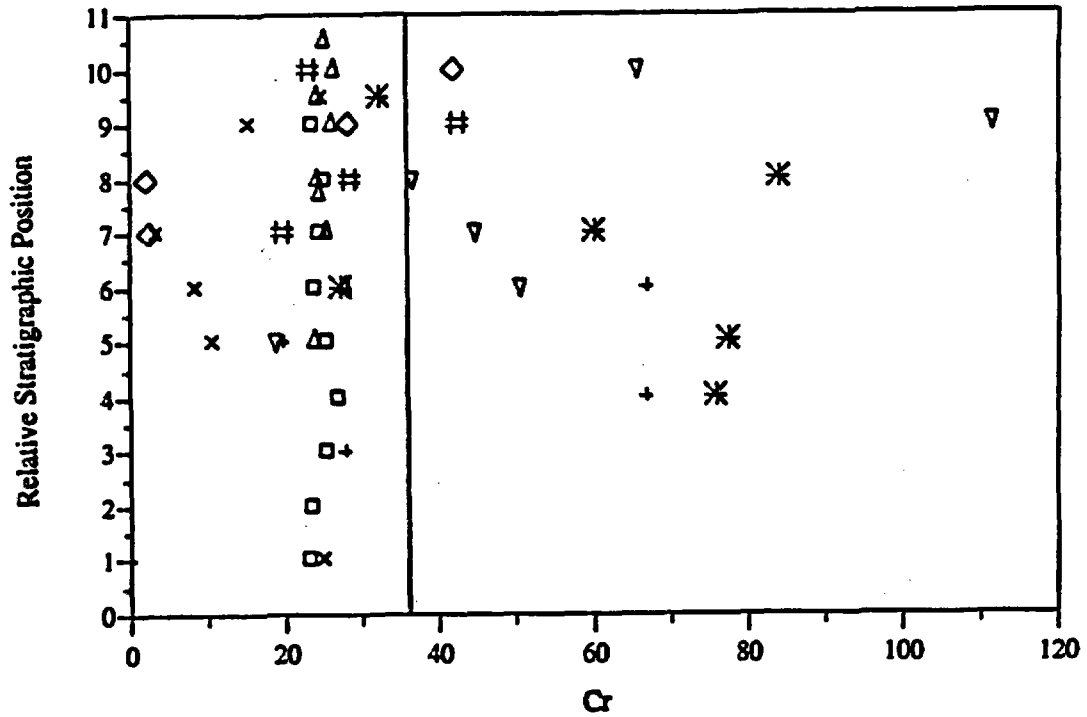
Black Mtns. ◊ Eldorado Mtns. ◻ Highland Spring × Interstate 15 +
 McCullough Δ Sheep Mtn. ▽ Temple Bar * White Hills #

Figure 9, continued.



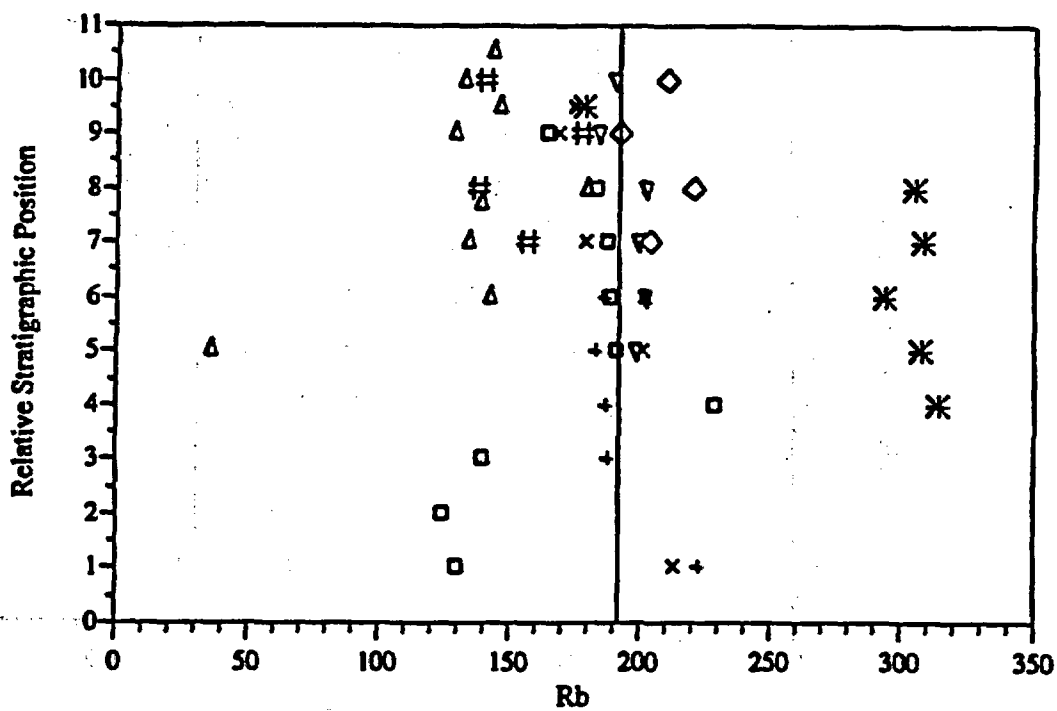
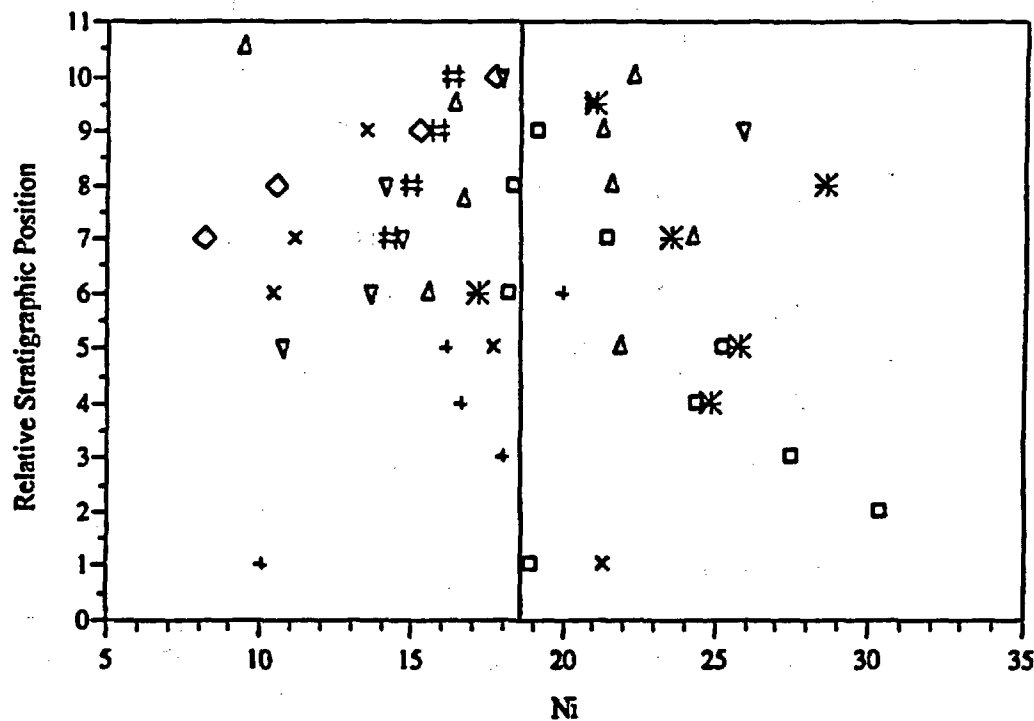
Black Mtns. ◇ Eldorado Mtns. □ Highland Spring × Interstate 15 +
 McCullough Δ Sheep Mtn. ▽ Temple Bar * White Hills #

Figure 9, continued.



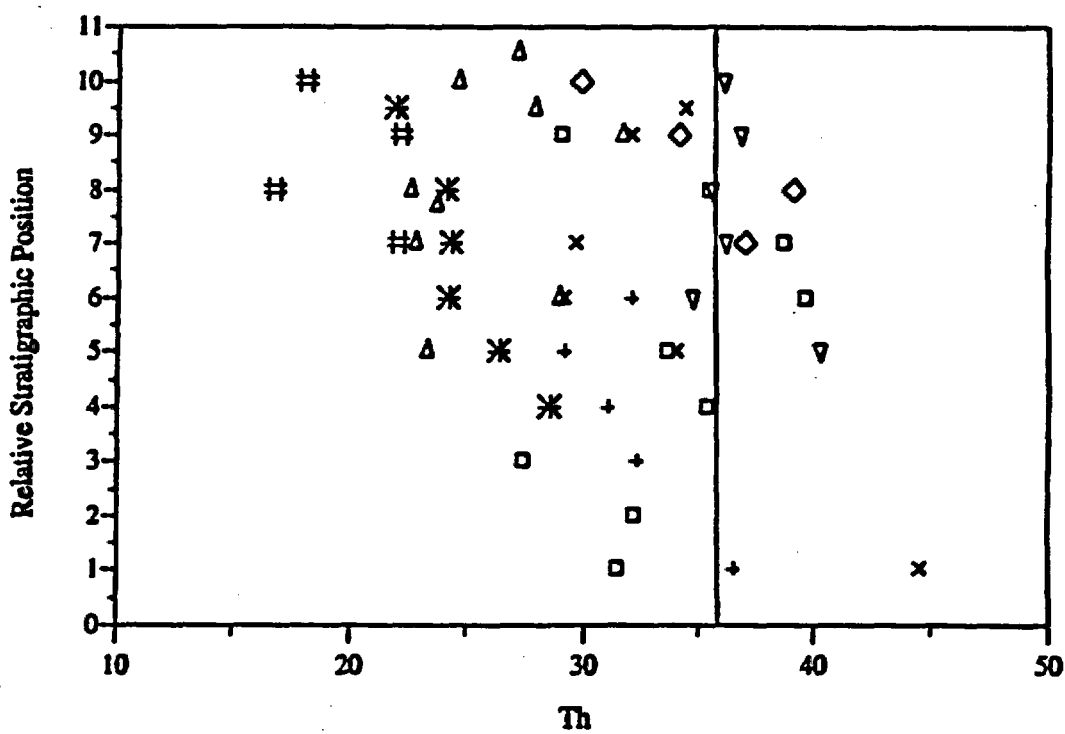
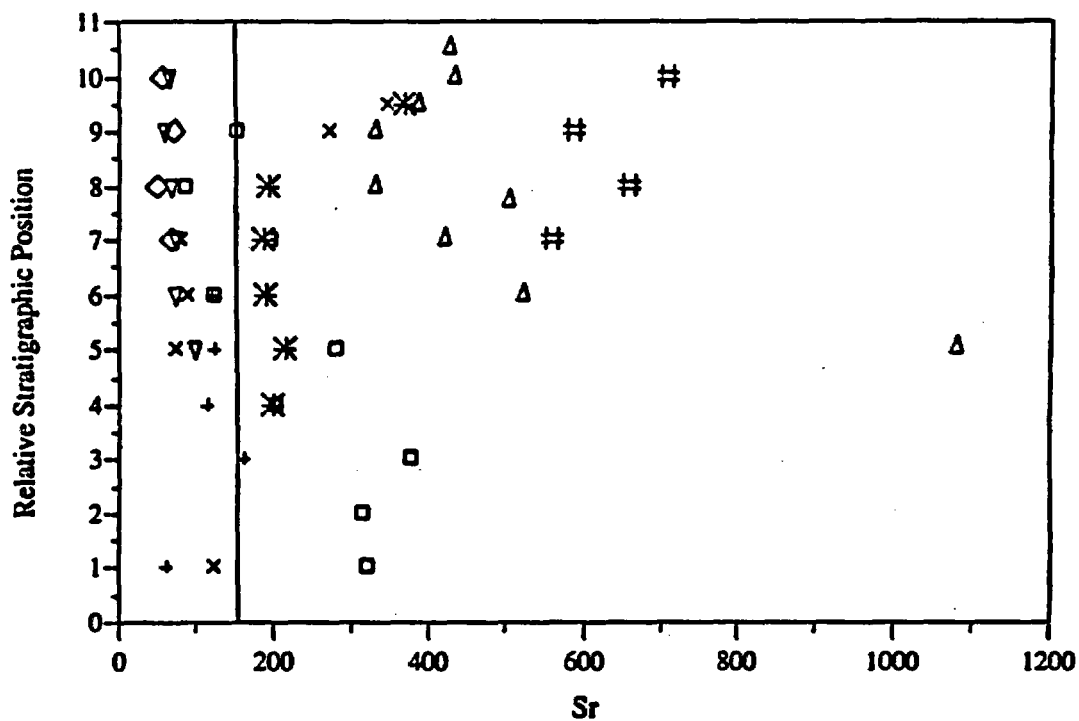
Black Mtns. ◊ Eldorado Mtns. ◻ Highland Spring × Interstate 15 +
 McCullough Δ Sheep Mtn. ▽ Temple Bar * White Hills #

Figure 9, continued.



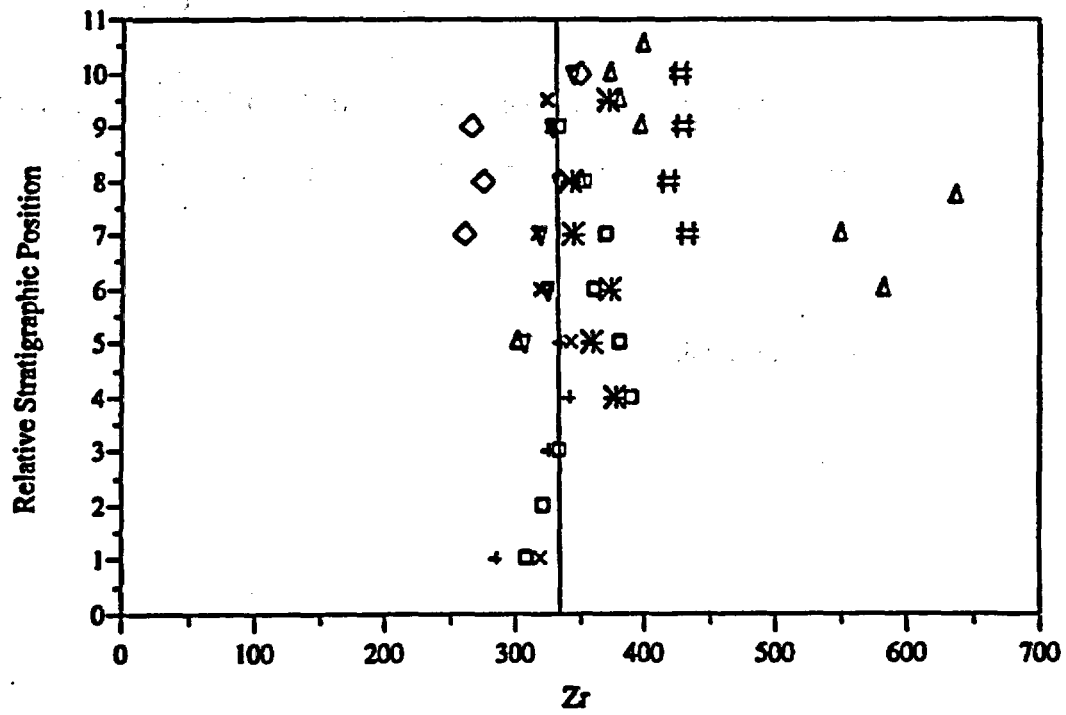
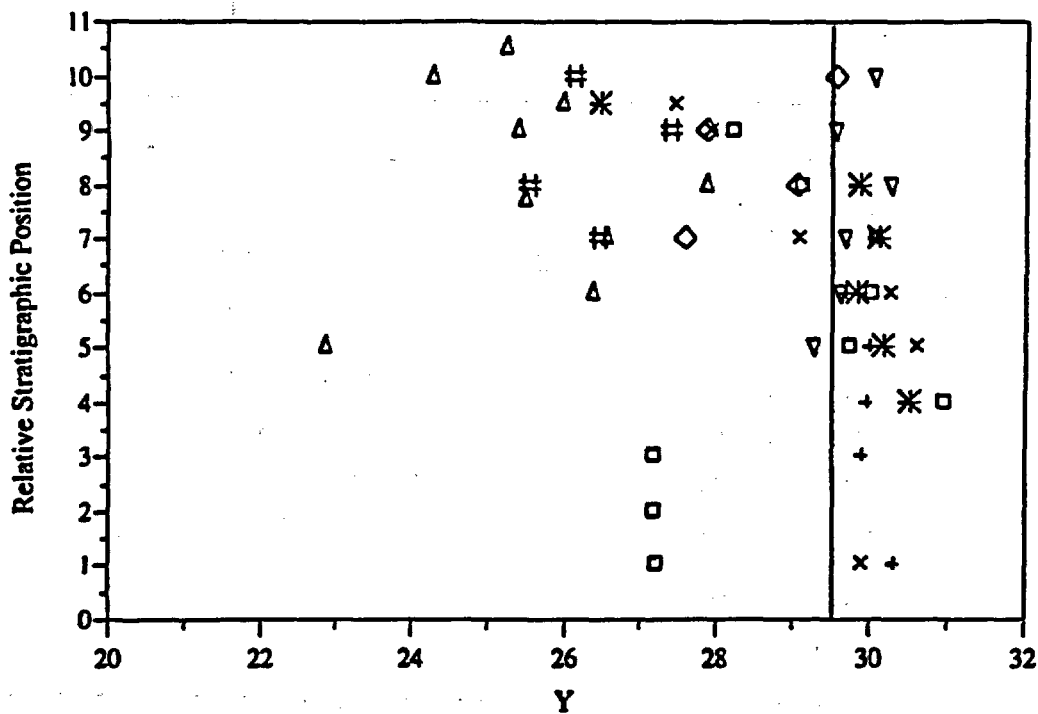
Black Mtns. ◊ Eldorado Mtns. ◻ Highland Spring × Interstate 15 +
 McCullough Δ Sheep Mtn. ▽ Temple Bar * White Hills #

Figure 9, continued.



Black Mtns. \diamond Eldorado Mtns. \square Highland Spring \times Interstate 15 $+$
 McCullough Δ Sheep Mtn. ∇ Temple Bar $*$ White Hills $\#$

Figure 9, continued.



- Black Mtns. ◇
- Eldorado Mtns. □
- Highland Spring ×
- Interstate 15 +
- McCullough ▲
- Sheep Mtn. ▼
- Temple Bar ※
- White Hills #

Figure 9, continued.

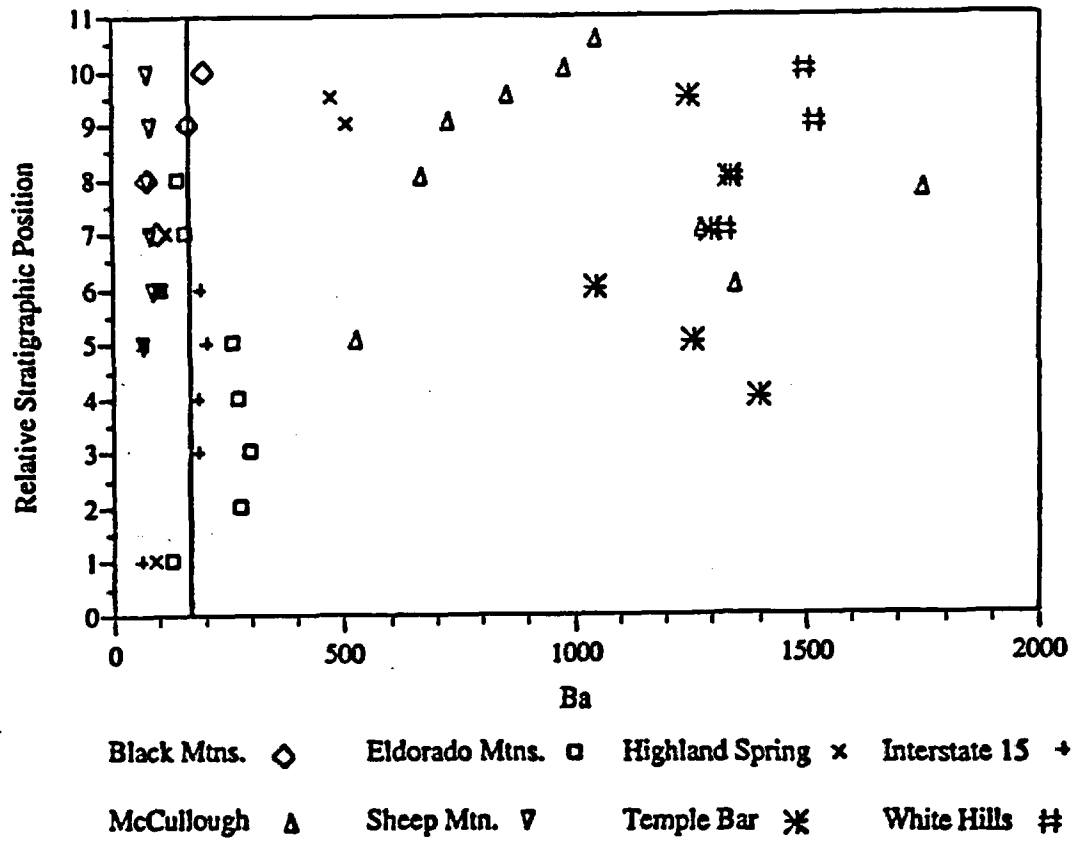


Figure 9, continued.

Table 5: Major and Trace Element Variation. Deviation is based on comparison of averaged section value to the base composition of each element. Base compositions are calculated by averaging analyses from Highland Spring, Eldorado Mtns., Sheep Mtn., and Interstate 15 sections. Major element oxides in wt.% and trace elements in ppm.

Section	Black Mountains					Dolan Springs				
	Minimum	Maximum	Range	Average	Deviation	Minimum	Maximum	Range	Average	Deviation
SiO ₂	71.08	74.91	3.83	72.995	2.28	73.69	75.59	1.90	74.64	3.92
Al ₂ O ₃	14.00	12.76	1.24	13.38	-1.21	12.60	13.06	0.46	12.83	-1.76
TiO ₂	0.26	0.34	0.08	0.3	-0.13	0.28	0.24	0.04	0.26	-0.17
FeO	1.95	1.41	0.54	1.68	-0.55	1.22	1.66	0.44	1.44	-0.79
CaO	1.26	4.45	3.19	2.855	0.71	2.57	1.08	1.49	1.825	-0.32
K ₂ O	6.34	6.60	0.26	6.47	0.95	4.65	5.43	0.78	5.04	-0.48
MnO	0.04	0.05	0.01	0.045	-0.02	0.04	0.06	0.02	0.05	-0.02
P ₂ O ₅	0.00	0.08	0.08	0.04	-0.02	0.07	0.12	0.05	0.095	0.03
Na ₂ O	1.66	4.15	2.49	2.905	-0.74	2.89	3.26	0.37	3.075	-0.57
MgO	0.14	0.33	0.19	0.235	-0.50	0.48	0.77	0.29	0.625	-0.11
Cr	2.2	41.9	39.7	22.05	-14.81	25.8	47.3	21.5	36.55	-0.31
Nb	36.7	44.6	7.9	40.65	-2.20	17.1	18.7	1.6	17.9	-24.95
Ni	8.2	17.7	9.5	12.95	-25.93	10.4	16.7	6.3	13.55	-25.33
Rb	193	221	28	207	15.75	108	143	35	125.5	-65.75
Sr	49	71	22	60	-98.88	125	196	71	160.5	1.63
Th	29.6	39.2	9.6	34.4	-0.82	13.2	15.9	2.7	14.55	-20.67
Y	27.6	29.6	2.0	28.6	-0.89	20.6	22.1	1.5	21.35	-8.14
Zr	261	350	89	305.5	-24.63	101	121	20	111	-219.13
Ba	75	205	130	140	-36.75	240	356	116	298	121.25

Table 5, continued.

Section	Eldorado Mountains					Highland Spring				
	Minimum	Maximum	Range	Average	Deviation	Minimum	Maximum	Range	Average	Deviation
SiO ₂	68.10	73.82	5.72	70.96	0.24	70.19	72.07	1.88	71.13	0.41
Al ₂ O ₃	13.26	15.69	2.43	14.475	-0.11	14.74	15.06	0.32	14.9	0.31
TiO ₂	0.42	0.67	0.25	0.545	0.12	0.36	0.45	0.09	0.405	-0.03
FeO	2.16	3.47	1.31	2.815	0.59	1.93	2.39	0.46	2.16	-0.07
CaO	1.00	3.54	2.54	2.27	0.12	0.86	1.68	0.82	1.27	-0.88
K ₂ O	3.98	6.76	2.78	5.37	-0.15	5.40	5.74	0.34	5.57	0.05
MnO	0.05	0.08	0.03	0.065	-0.00	0.07	0.07	0.00	0.07	0.00
P ₂ O ₅	0.02	0.16	0.14	0.09	0.03	0.00	0.13	0.13	0.065	0.00
Na ₂ O	0.16	4.41	4.25	2.285	-1.36	3.16	5.00	1.84	4.08	0.44
MgO	0.50	1.84	1.34	1.17	0.44	0.21	0.87	0.66	0.54	-0.19
										0.00
Cr	23.1	26.8	3.7	24.95	-11.91	3.3	25.0	21.7	14.15	-22.71
Nb	33.8	42.6	8.8	38.2	-4.65	36.5	51.9	15.4	44.2	1.35
Ni	18.2	30.4	12.2	24.3	5.90	10.5	21.4	10.9	15.95	-2.45
Rb	124	230	106	177	-14.25	169	213	44	191	-0.25
Sr	87	379	292	233	74.13	74	345	271	209.5	50.63
Th	27.4	39.7	12.3	33.55	-1.67	29.2	44.6	15.4	36.9	1.68
Y	27.2	31.0	3.8	29.1	-0.39	27.5	30.6	3.1	29.05	-0.44
Zr	309	390	81	349.5	19.38	319	344	25	331.5	1.38
Ba	106	300	194	203	26.25	69	511	442	290	113.25

Table 5, continued.

Section	Interstate-15					Lucy Gray Range				
	Minimum	Maximum	Range	Average	Deviation	Minimum	Maximum	Range	Average	Deviation
SiO ₂	68.66	71.00	2.34	69.83	-0.89	72.88	72.42	0.46	72.65	1.93
Al ₂ O ₃	14.05	14.72	0.67	14.385	-0.20	14.21	14.31	0.10	14.26	-0.33
TiO ₂	0.34	0.45	0.11	0.395	-0.04	0.28	0.30	0.02	0.29	-0.14
FeO	1.50	2.37	0.87	1.935	-0.29	1.75	1.79	0.04	1.77	-0.46
CaO	2.33	2.97	0.64	2.65	0.50	0.71	0.87	0.16	0.79	-1.36
K ₂ O	5.03	6.04	1.01	5.535	0.01	5.30	5.90	0.60	5.6	0.08
MnO	0.07	0.08	0.01	0.075	0.01	0.06	0.06	0.00	0.06	-0.01
P ₂ O ₅	0.04	0.09	0.05	0.065	0.00	0.05	0.05	0.00	0.05	-0.01
Na ₂ O	3.97	4.58	0.61	4.275	0.63	4.11	4.38	0.27	4.245	0.60
MgO	0.46	0.90	0.44	0.68	-0.05	0.21	0.34	0.13	0.275	-0.46
Cr	19.5	66.9	47.4	43.2	6.34	23.9	24.2	0.3	24.05	-12.81
Nb	42.5	46.1	3.6	44.3	1.45	30.6	32.1	1.5	31.35	-11.50
Ni	10.1	19.9	9.8	15	-23.88	19.1	19.8	0.7	19.45	-19.43
Rb	184	223	39	203.5	12.25	190	214	24	202	10.75
Sr	62	163	101	112.5	-46.38	35	43	8	39	-119.88
Th	29.2	36.6	7.4	32.9	-2.32	24.6	25.0	0.4	24.8	-10.42
Y	29.7	30.3	0.6	30	0.51	30.4	30.8	0.4	30.6	1.11
Zr	285	342	57	313.5	-16.63	258	261	3	259.5	-70.63
Ba	63	207	144	135	-41.75	28	102	74	65	-111.75

Table 5, continued.

Section	McCullough Range					Sheep Mountain				
	Minimum	Maximum	Range	Average	Deviation	Minimum	Maximum	Range	Average	Deviation
SiO ₂	65.05	73.65	8.60	69.35	-1.37	70.20	71.69	1.49	70.945	0.23
Al ₂ O ₃	12.80	16.92	4.12	14.86	0.27	14.40	14.78	0.38	14.59	0.00
TiO ₂	0.45	0.64	0.19	0.545	0.12	0.35	0.40	0.05	0.375	-0.06
FeO	2.32	3.22	0.90	2.77	0.54	1.87	2.13	0.26	2	-0.23
CaO	1.95	3.62	1.67	2.785	0.64	1.26	3.54	2.28	2.4	0.25
K ₂ O	2.62	6.26	3.64	4.44	-1.08	5.33	5.88	0.55	5.605	0.08
MnO	0.06	0.08	0.02	0.0715	0.00	0.06	0.07	0.01	0.065	-0.00
P ₂ O ₅	0.03	0.14	0.11	0.0855	0.02	0.00	0.06	0.06	0.03	-0.03
Na ₂ O	2.22	5.02	2.80	3.62	-0.02	3.19	4.68	1.49	3.935	0.29
MgO	0.84	2.13	1.29	1.485	0.75	0.31	0.78	0.47	0.545	-0.19
Cr	23.7	27.8	4.1	25.75	-11.11	18.7	111.6	92.9	65.15	28.29
Nb	24.0	35.8	11.8	29.9	-12.95	43.4	46.0	2.6	44.7	1.85
Ni	9.4	24.3	14.9	16.85	-22.03	10.8	25.9	15.1	18.35	-20.53
Rb	36	180	144	108	-83.25	184	203	19	193.5	2.25
Sr	330	1083	753	706.5	547.63	61	100	39	80.5	-78.38
Th	22.5	31.7	9.2	27.1	-8.12	34.8	40.3	5.5	37.55	2.33
Y	22.8	27.9	5.1	25.35	-4.14	29.3	30.3	1.0	29.8	0.31
Zr	301	638	337	469.5	139.38	306	346	40	326	-4.13
Ba	530	1753	1223	1141.5	964.75	69	89	20	79	-97.75

Table 5, continued.

Section	Salt Spring Wash					Temple Bar				
	Minimum	Maximum	Range	Average	Deviation	Minimum	Maximum	Range	Average	Deviation
SiO ₂	70.08	73.88	3.80	71.98	1.26	64.60	68.44	3.84	66.52	-4.20
Al ₂ O ₃	11.58	15.15	3.57	13.365	-1.22	14.77	15.94	1.17	15.355	0.77
TiO ₂	0.37	0.50	0.13	0.435	0.00	0.49	0.69	0.20	0.59	0.16
FeO	2.12	2.66	0.54	2.39	0.16	2.75	3.81	1.06	3.28	1.05
CaO	0.50	2.99	2.49	1.745	-0.40	0.80	4.38	3.58	2.59	0.44
K ₂ O	6.51	9.01	2.50	7.76	2.24	6.54	9.88	3.34	8.21	2.69
MnO	0.03	0.04	0.01	0.035	-0.03	0.03	0.07	0.04	0.05	-0.02
P ₂ O ₅	0.02	0.11	0.09	0.065	0.00	0.05	0.17	0.12	0.11	0.05
Na ₂ O	1.63	1.65	0.02	1.64	-2.00	1.61	3.02	1.41	2.315	-1.33
MgO	0.40	0.76	0.36	0.58	-0.15	0.40	1.33	0.93	0.865	0.13
Cr	13.5	23.0	9.5	18.25	-18.61	27.1	84.0	56.9	55.55	18.69
Nb	23.5	32.2	8.7	27.85	-15.00	25.6	32.3	6.7	28.95	-13.90
Ni	12.9	14.2	1.3	13.55	-25.33	17.2	28.6	11.4	22.9	-15.98
Rb	130	196	66	163	-28.25	179	314	135	246.5	55.25
Sr	56	112	56	84	-74.88	186	368	182	277	118.13
Th	18.1	23.8	5.7	20.95	-14.27	21.9	28.6	6.7	25.25	-9.97
Y	23.2	27.6	4.4	25.4	-4.09	26.5	30.5	4.0	28.5	-0.99
Zr	226	340	114	283	-47.13	344	378	34	361	30.88
Ba	388	392	4	390	213.25	1048	1400	352	1224	1047.25

Table 5, continued.

Section White Hills

	Minimum	Maximum	Range	Average	Deviation	Base Composition
SiO ₂	59.50	65.26	5.76	62.38	-8.34	70.72
Al ₂ O ₃	16.22	18.00	1.78	17.11	2.52	14.59
TiO ₂	0.63	0.72	0.09	0.675	0.25	0.43
FeO	3.30	3.91	0.61	3.605	1.38	2.23
CaO	2.61	5.44	2.83	4.025	1.88	2.15
K ₂ O	5.70	7.90	2.20	6.8	1.28	5.52
MnO	0.07	0.10	0.03	0.085	0.02	0.07
P ₂ O ₅	0.10	0.25	0.15	0.177	0.11	0.06
Na ₂ O	3.56	3.96	0.40	3.76	0.12	3.64
MgO	0.76	1.84	1.08	1.3	0.57	0.73
Cr	19.5	42.5	23.0	31	-5.86	36.86
Nb	25.2	30.4	5.2	27.8	-15.05	42.85
Ni	14.2	16.3	2.1	15.25	-3.15	18.40
Rb	138	178	40	158	-33.25	191.25
Sr	560	712	152	636	477.13	158.88
Th	16.7	22.2	5.5	19.45	-15.77	35.23
Y	25.5	27.4	1.9	26.45	-3.04	29.49
Zr	419	434	15	426.5	96.38	330.13
Ba	1330	1524	194	1427	1250.25	176.75

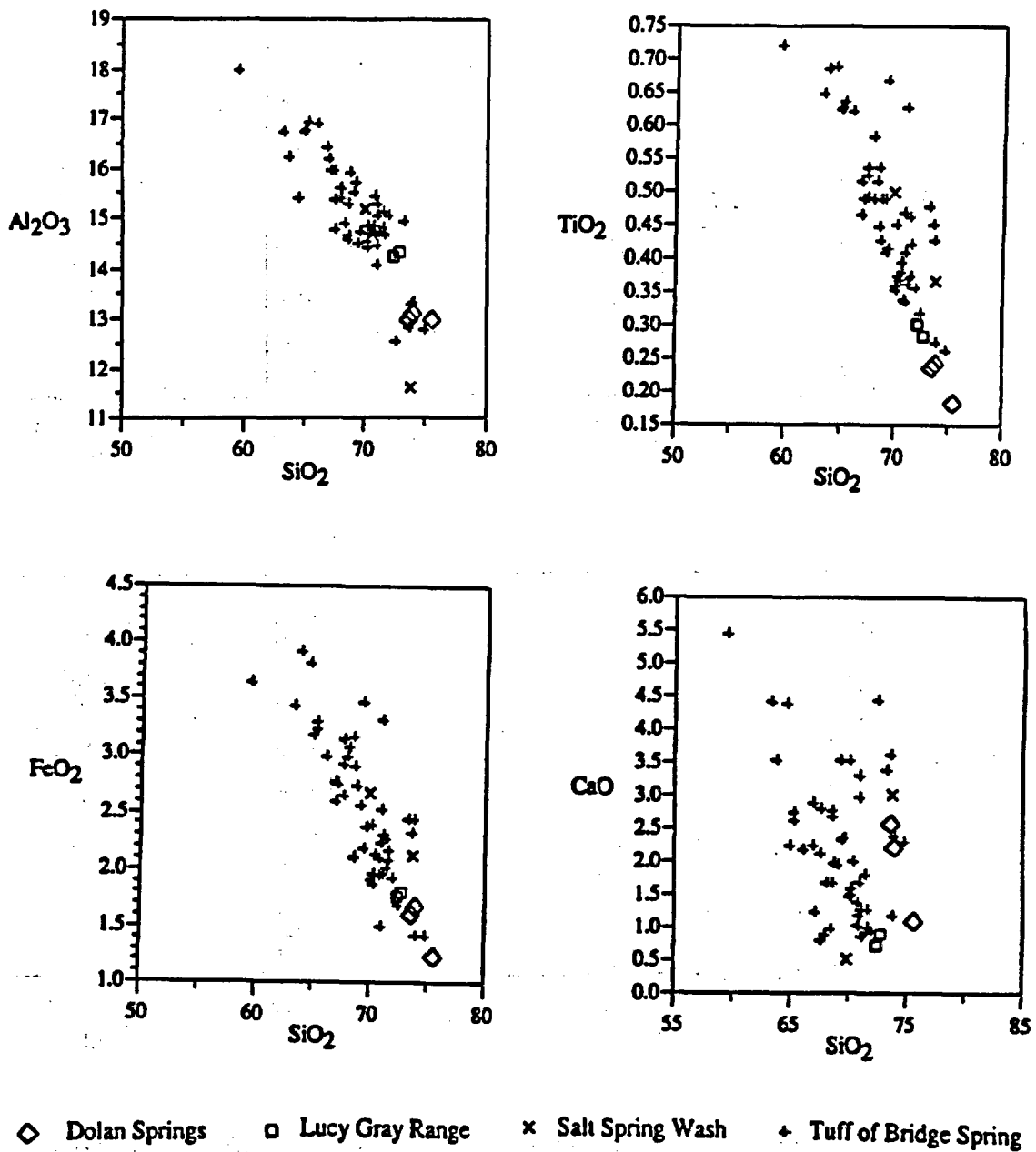


Figure 10. Harker variation plots of Tuff of Bridge Spring sections and three non-correlative tuffs: major element oxides and trace elements vs. SiO₂.

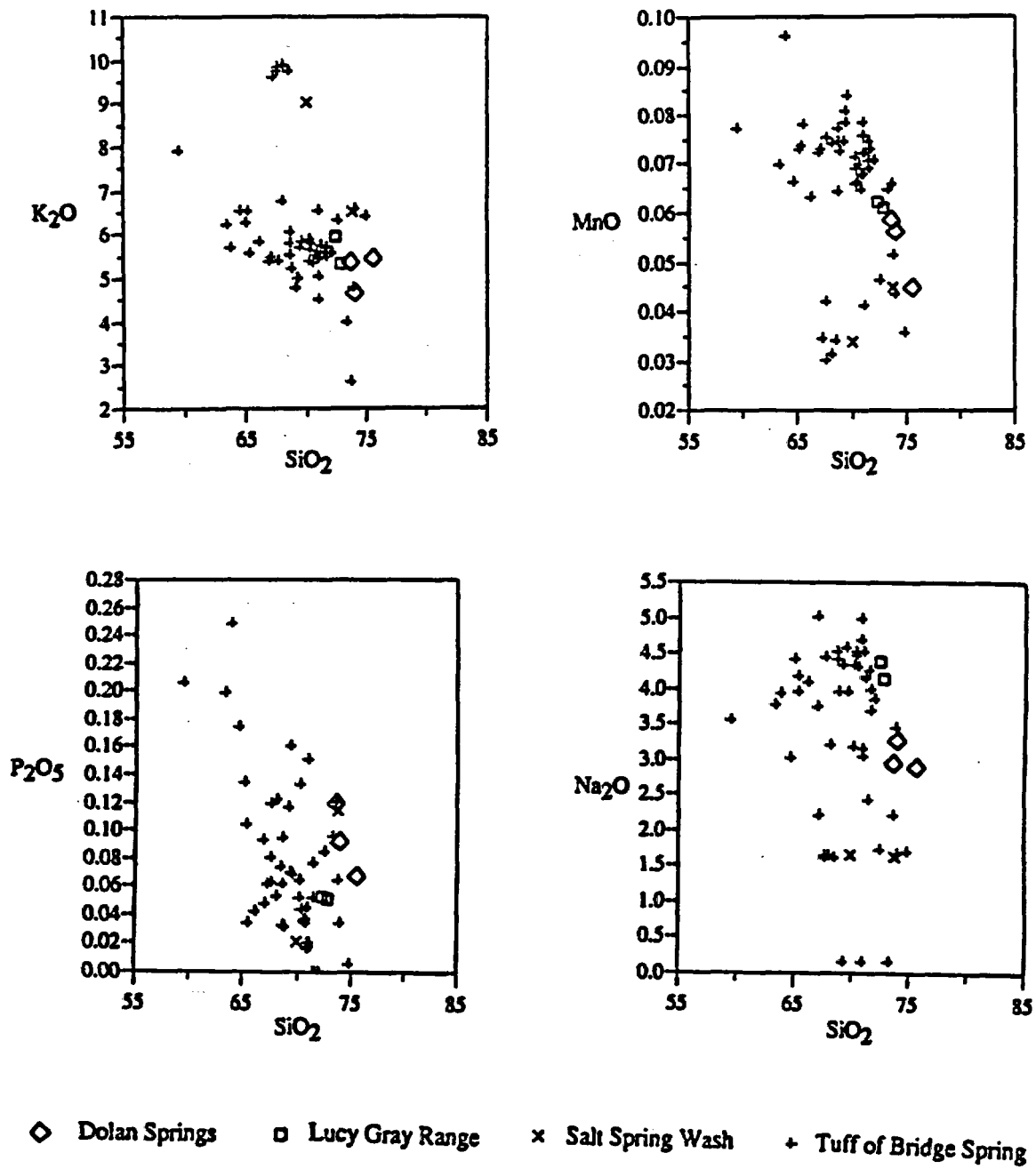


Figure 10, continued.

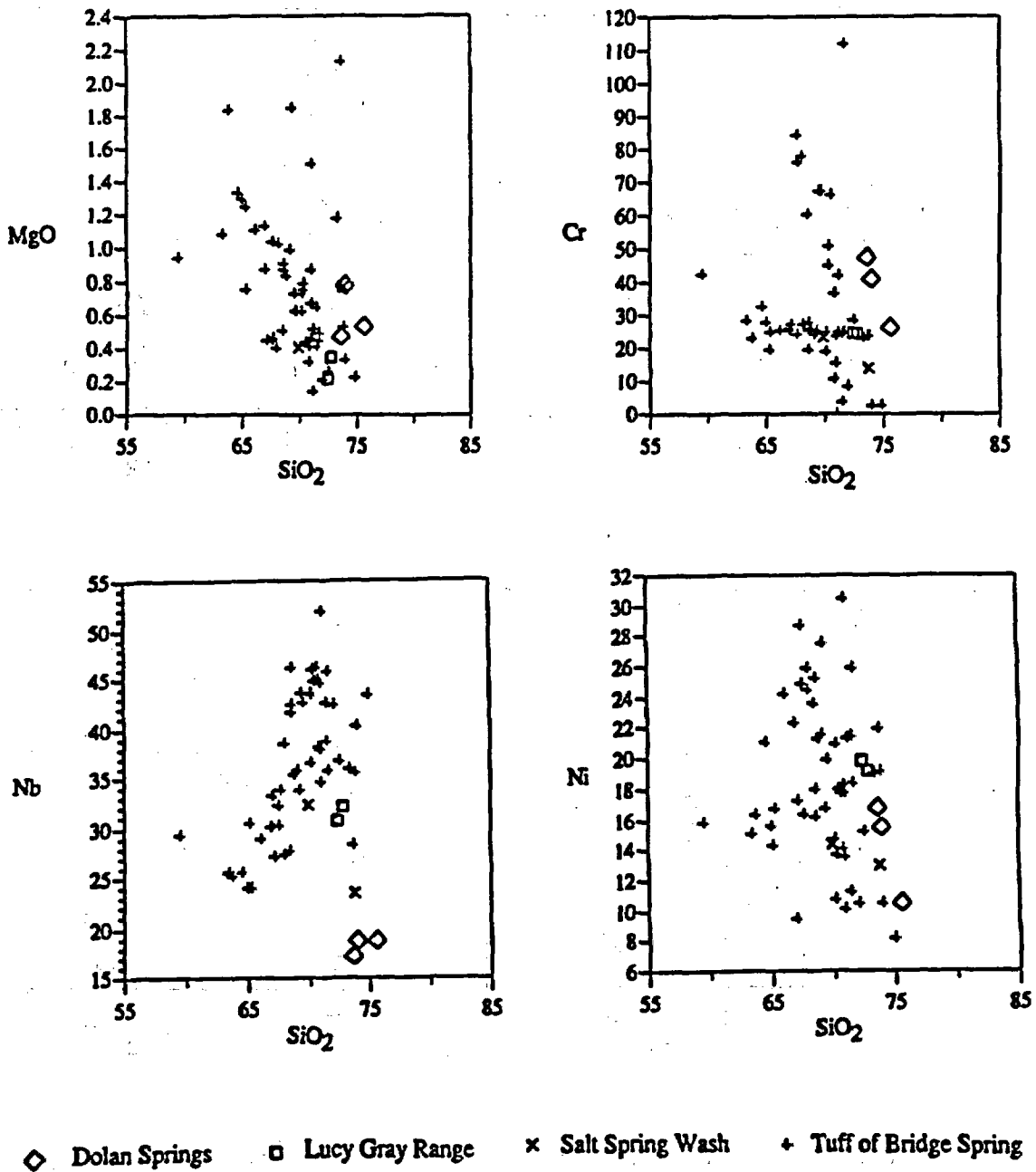
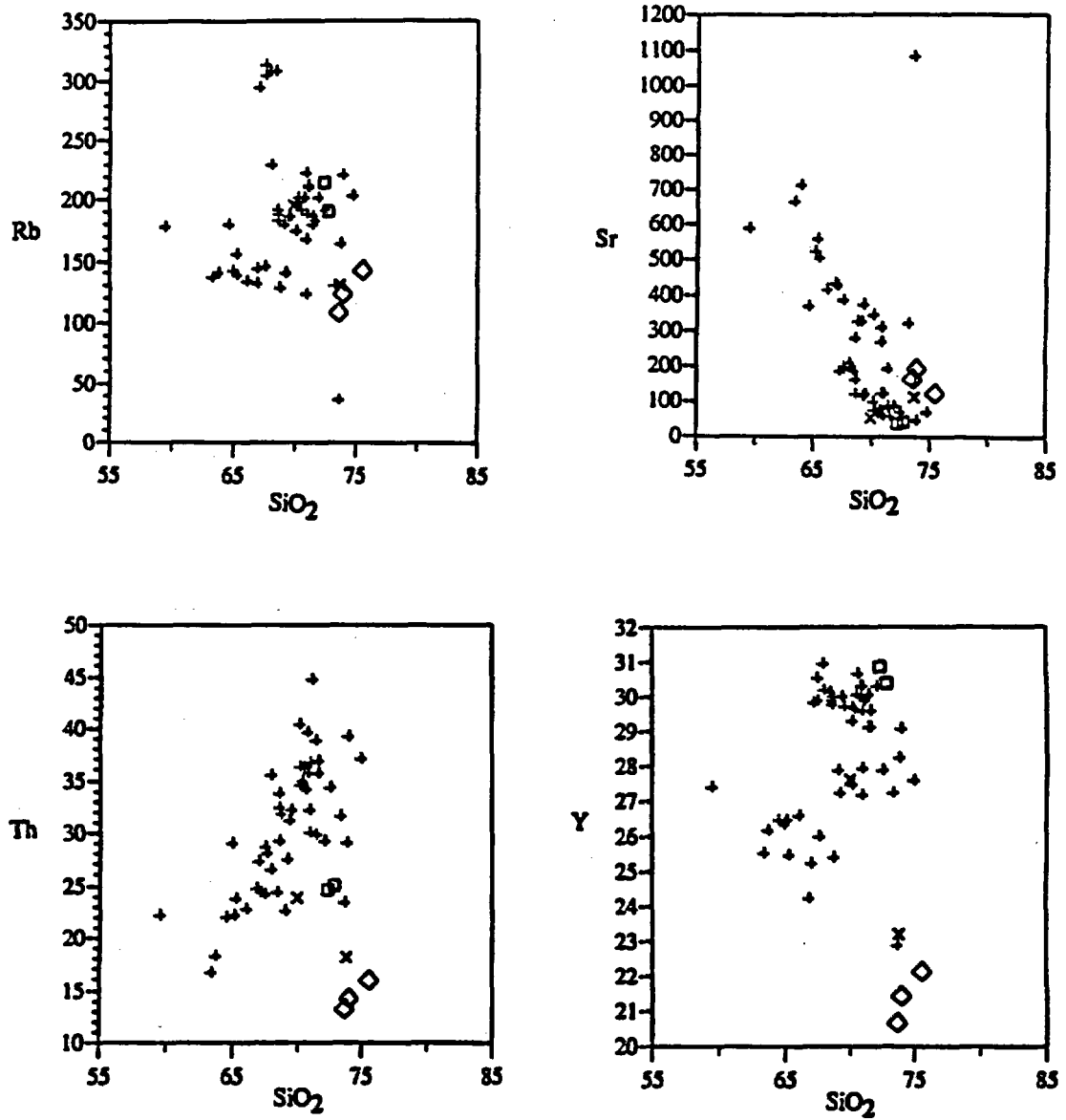
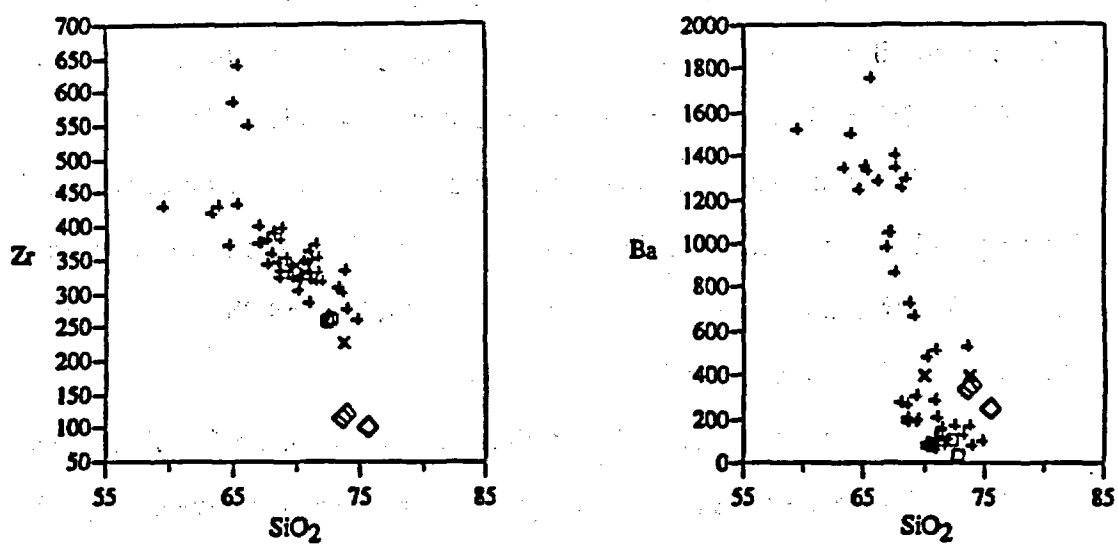


Figure 10, continued.



◇ Dolan Springs □ Lucy Gray Range × Salt Spring Wash + Tuff of Bridge Spring

Figure 10, continued.



◇ Dolan Springs □ Lucy Gray Range × Salt Spring Wash + Tuff of Bridge Spring

Figure 10, continued.

Regional Correlation

Isotopic Correlation of the Tuff of Bridge Spring

Previous regional correlations of the Tuff of Bridge Spring were based upon its modal mineralogy, distinctive lithology, and relative position in the Miocene volcanic section (Anderson, 1971; Anderson et al., 1972; Davis, 1985; Schmidt, 1987; Faulds, 1989; Bridwell, 1991; Cascadden, 1991). In this study, identification and correlation of the Tuff of Bridge Spring was established by determining its isotopic signature.

Isotopic ratios are not altered by magmatic, eruptive, or weathering processes and consequently can be used as sensitive indicators to discriminate cogenetic magmatic suites. For this reason, isotopic ratios of H, O, Ar, Sr, Nd, and Pb are commonly used to correlate ash-flow tuffs (Hildreth and Mahood, 1985).

Eleven locations in the northern Colorado River extensional corridor in which the Tuff of Bridge Spring is either known or suspected to crop out were sampled and analyzed for Nd, Sr, and Pb isotopes (Fig. 6; Table 6). A plot of ϵ_{Nd} vs. $^{87}Sr/^{86}Sr$ for the Tuff of Bridge Spring (Fig. 11) shows that the majority of samples define a linear trend that varies from $^{87}Sr/^{86}Sr = 0.708653$ to 0.71036 and $\epsilon_{Nd} = -8.070$ to -10.070 .

Because cogenetic isotopic suites characteristically plot in tight clusters on ϵ_{Nd} vs. $^{87}Sr/^{86}Sr$ diagrams, the presence of a linear array suggests that the magmatic system evolved either as the result of open system magmatic processes, or developed under closed system conditions but was subsequently contaminated with isotopically-exotic xenoliths and/or xenocrysts. As will be discussed below, the linear isotopic array shown in Fig. 11 is interpreted to represent a cogenetic sequence that formed as the result of open system magmatic processes, and stratigraphic sections that preserve these isotopic values are interpreted to comprise the Tuff of Bridge Spring. These

sections include the McCullough Range, Eldorado Mountains, Highland Spring Range, and Sheep Mountain in Nevada, and the White Hills, Temple Bar, and Black Mountains in Arizona. Also, for reasons discussed below, the Interstate 15, Nevada section will also be correlated with the Tuff of Bridge Spring.

It is important to note that correlation of sections to the Tuff of Bridge Spring cannot be established by isotopic signature alone, but must be confirmed by additional criteria such as geochemistry, mineralogy, lithology, and available geochronology. Isotope-based correlations of the sections listed above to the Tuff of Bridge Spring are strongly supported by geochemical studies (see discussion of internal stratigraphy) which indicate the presence of distinct geochemical trends in the Tuff of Bridge Spring which can be correlated across its entire area of distribution.

There are, however, two examples of isotope-based correlations in which isotopic signatures are contradicted by other correlation criteria. In the first example, the isotope values of the Interstate 15 sample suggest it is not correlative to the Tuff of Bridge Spring, but the phenocryst mineralogy, lithology, and geochemistry of the section strongly suggest it is correlative to the Tuff of Bridge Spring (see discussion below). In the second example, the isotopic signature of the Dolan Springs section falls within the Tuff of Bridge Spring isotope array, but $^{40}\text{Ar}/^{39}\text{Ar}$ dating (see following discussion of other ash-flow tuffs) shows that the tuff is significantly older than the Tuff of Bridge Spring. In addition, it has a different phenocryst mineralogy.

In summary, based on evidence provided by non-isotopic correlation criteria, and contrary to isotopic evidence, the Interstate 15 section will be included in the Tuff of Bridge Spring. Using the same criteria, the tuff of Dolan Springs will be excluded from the Tuff of Bridge Spring.

Interstate 15

The Interstate 15 tuff plots outside of the Tuff of Bridge Spring isotopic array on ϵ_{Nd} vs. $^{87}Sr/^{86}Sr$ and $^{87}Sr/^{86}Sr$ vs. SiO_2 plots (Fig. 11 and Fig. 12, respectively) which indicates it is not cogenetic with the Tuff of Bridge Spring. However, the mineralogy, geochemistry and lithology of this section is similar to that of the Sheep Mountain section whose isotopic signature falls within the Tuff of Bridge Spring isotopic array (Fig. 11).

There are three possible explanations for the contradictions of the isotope and secondary correlation criteria data of the Interstate 15 section. First, the isotope analysis of the basal interval of Interstate 15 is spurious. Second, the basal interval of Interstate 15 is a locally-derived flow that is isotopically unrelated to the Tuff of Bridge Spring, but the unsampled interval of welded tuff overlying it is the Tuff of Bridge Spring. Third, the Interstate 15 section is entirely of local derivation (i.e., not correlative to the Tuff of Bridge Spring as indicated by the isotope analysis).

Re-analysis of the Interstate 15 basal pumiceous tuff and analysis of a densely-welded, uppermost interval from the Interstate 15 section will be conducted to determine the isotopic affinities of these units. Until these analyses are completed, the Interstate 15 section will be tentatively correlated with the Tuff of Bridge Spring.

Other Ash-flow Tuffs

Salt Spring Wash and Lucy Gray Range

The ϵ_{Nd} vs. $^{87}Sr/^{86}Sr$ plot (Fig. 11) of the Lucy Gray Range tuff implies it may be a felsic endmember to the Tuff of Bridge Spring mixing array, but this is contradicted by $^{87}Sr/^{86}Sr$ vs. SiO_2 plots (Fig. 12) which show that the Lucy Gray Range tuff plots away from the Tuff of Bridge Spring isotopic trend. The Salt Spring Wash isotope sample plots away from the Tuff of Bridge Spring array on both ϵ_{Nd} vs. $^{87}Sr/^{86}Sr$ and $^{87}Sr/^{86}Sr$ vs. SiO_2 diagrams (Figs. 11 and 12). Isotope plots indicate that both the Salt Spring Wash and Lucy Gray Range tuffs were derived from sources that are not cogenetic with the Tuff of Bridge Spring. This conclusion is supported by modeling of possible contaminants (see discussion of lithic contaminants below) which indicate these tuffs are not Tuff of Bridge Spring samples that have acquired hybridized isotopic signatures as the result of xenolith contamination.

Dolan Springs

Isotope-based correlation of the Dolan Springs volcanic complex to the Tuff of Bridge Spring is contradicted by an $^{40}Ar/^{39}Ar$ date of 16.09 ± 0.15 Ma (incremental release, biotite; this study) (Fig. 13). This date falls outside the uncertainty of the 15.23 ± 0.14 Ma date by Bridwell (1991) for the McCullough Range Tuff of Bridge Spring, and effectively eliminates the possibility that the Dolan Springs section is cogenetic with the Tuff of Bridge Spring. The exclusion of this section from the Tuff of Bridge Spring is also supported by significant differences of geochemistry and modal

mineralogy. The tuff of Dolan Springs, unlike the Tuff of Bridge Spring, contains abundant quartz phenocrysts.

Even though the tuff of Dolan Springs does not correlate with the Tuff of Bridge Spring, it is still of interest to this study. The similarity of isotopic compositions of the tuff of Dolan Springs and the Tuff of Bridge Springs suggests that the source of the tuff of Dolan Springs is isotopically similar to the Tuff of Bridge Spring. If the Tuff of Bridge Spring correlates with the Aztec Wash pluton in Nevada, this suggests that the source of the tuff of Dolan Springs and the Aztec Wash pluton were both derived from a regionally-extensive/isotopically similar crustal/mantle source. A date of 16.09 Ma for the Dolan Springs section also implies correlation with the 15.96 ± 0.04 Ma Mt. Perkins pluton (laser fusion $^{40}\text{Ar}/^{39}\text{Ar}$, sanidine) (Faulds, personal communication to E.I. Smith, 1993) (see later discussion of source).

Origin of the Tuff of Bridge Spring Data Array

Because rocks produced by closed system magma processes characteristically plot in tight clusters on ϵ_{Nd} vs. $^{87}\text{Sr}/^{86}\text{Sr}$ diagrams, the linearity of the Tuff of Bridge Spring data array indicates that the Tuff of Bridge Spring magma chamber evolved under open system conditions (see discussion of mixing trend below). Isotopic variability in the Tuff of Bridge Spring occurs not only on the regional scale (i.e., between different sections widely separated across the distribution area of the tuff), but also within individual sections (e.g., Sheep Mountain and Eldorado Mountain sections) (Table 6).

Variability of Nd/Sr, $^{87}\text{Sr}/^{86}\text{Sr}$, and SiO_2 values of the Tuff of Bridge Spring (Fig. 11 and Fig. 12) may result from either the incomplete mixing of an isotopically-homogeneous, compositionally-zoned felsic magma body with a volumetrically smaller,

end member fraction of isotopically-dissimilar mafic magma, or the incorporation of xenoliths and/or xenocrysts during eruption and deposition of an isotopically homogeneous ash-flow tuff. The following discussion eliminates lithic contamination as a possible mechanism for variability of isotopes in the Tuff of Bridge Spring, and suggests that the process of magma-mixing produced the linear Tuff of Bridge Spring isotopic array. The following discussion also demonstrates that the isotopic signatures of the Salt Spring Wash and Lucy Gray Range tuffs were not produced by contamination of Tuff of Bridge Spring with mafic and/or felsic lithic fragments.

Lithic Contamination

Possible sources of lithic contamination of the Tuff of Bridge Spring include Patsy Mine Volcanics, Precambrian crystalline basement, and alkali-olivine basalts that were derived from the melting of asthenospheric mantle.

Patsy Mine Volcanics

Xenoliths in the Tuff of Bridge Spring are predominantly mafic in composition (basaltic to basaltic andesite) and contain plagioclase, clinopyroxene, and Fe-oxide phenocrysts. A possible source of these xenoliths is the upper member of the Patsy Mine Volcanics. In the Eldorado Mountains, the Patsy Mine Volcanics consists of thick flows (457 ± 91 m) of plagioclase-, pyroxene-, olivine-, and magnetite-bearing basaltic andesite (Anderson, 1971). Coeval and lithologically equivalent units crop out in the McCullough Range (Schmidt, 1987), Highland Spring Range (Davis, 1985), Black Mountains (Faulds, 1989) and in the White Hills (Cascadden, 1991). Recent $^{40}\text{Ar}/^{39}\text{Ar}$ geochronology of lavas and tuffs in the northern Eldorado Mountains by

Faulds (personal communication to Smith, 1993) show that basaltic andesite flows located in the middle of the Upper Patsy Mine Member are 15.18 ± 0.07 m.y. old (laser fusion $^{40}\text{Ar}/^{39}\text{Ar}$ on plagioclase) which closely brackets the eruption of the Tuff of Bridge Spring at 15.12 ± 0.03 Ma (laser fusion $^{40}\text{Ar}/^{39}\text{Ar}$, sanidine).

Generation of the Tuff of Bridge Spring data array by lithic contamination requires that the contaminant have an isotopic composition that is sufficiently removed from the Tuff of Bridge Spring trend such that reasonably small amounts of contaminant can be assimilated to produce the trend. An example of this is shown in Fig. 14, which shows a hypothetical data array with two different contaminants. Generation of the data array by incorporation of a contaminant is calculated by adding successive amounts of pure contaminant to pure end member host rock. In these models, the composition of the contaminant represents 100 % assimilation and the composition of the uncontaminated tuff represents 0 % assimilation. When modeling the incorporation of a contaminant into a host rock to produce a succession of intermediate isotopic values, it is important to note that in order to produce the data trend, large amounts of contaminant must be assimilated when the composition of the contaminant is similar to that of the host rock. In Fig. 14, the isotope composition of Contaminant A requires that, in order to produce the data array, 100 % contaminant must be added to the pure end member host rock. Assimilation of Contaminant B, however, requires only 10 % contamination to produce the data array.

ϵ_{Nd} vs. $^{87}\text{Sr}/^{86}\text{Sr}$ values of clinopyroxene separated from two samples of Patsy Mine Volcanics (Upper and Lower Members) by Daley (1992) indicate that the isotope values of the Patsy Mine Volcanics are coincident with the lower portion of the Tuff of Bridge Spring field (Fig. 15). This similarity suggests that generation of the Tuff of Bridge Spring array by the incorporation of Patsy Mine Volcanics would require assimilation of very large quantities of Patsy Mine Volcanics (nearly 100 modal

percent). Incorporation of this much material is both unrealistic and not supported by modal analyses of the Tuff of Bridge Spring. The Tuff of Bridge Spring contains an average of 5.7 % lithic fragments (standard deviation = 6.6 %). Using this modal value, it is theoretically possible to generate the Tuff of Bridge Spring data array by incorporating a hypothetical mafic contaminant of lithospheric mantle derivation that has a calculated value of $\epsilon_{Nd} = -55.070$ and $^{87}Sr/^{86}Sr = 0.7419$. Rocks with this isotopic value are not known in the northern Colorado River extensional corridor, which effectively precludes the incorporation of Patsy-Mine type xenoliths as a possible mechanism for producing the Tuff of Bridge Spring data array.

Alkali Olivine Basalts

A second possible source of lithic contamination is asthenosphere-derived basalts. An example of a typical alkali olivine basalt in the northern Colorado River extensional corridor is the nepheline-normative Petroglyph Wash Basalt of the Fortification Hill volcanic field in Arizona (Feuerbach et al., in press). This rock, which has the values $\epsilon_{Nd} = 3.63$, and $^{87}Sr/^{86}Sr = 0.0.70347$ (Fig. 15), has isotopic affinities to contemporary oceanic island basalts (OIB). The ϵ_{Nd} and $^{87}Sr/^{86}Sr$ values of the Petroglyph Wash sample are significantly removed from the general trend of the Tuff of Bridge Spring array. This suggests the possibility that the array was generated as the result of contamination by xenoliths having OIB-type isotopic signatures. However, xenoliths of olivine-bearing alkali basalt are not present in the Tuff of Bridge Spring. This eliminates the incorporation of alkali basalt xenoliths as a controlling factor in producing the Tuff of Bridge Spring isotope array.

Precambrian Basement

Typical Early Proterozoic crystalline basement in the northern Colorado River extensional corridor consists of 1.7 Ga granitic and garnet-bearing gneisses, schists, and granite pegmatites (Anderson, 1971). These rocks belong to the Mojave crustal province (Wooden and Miller, 1990; Bennett and DePaolo, 1987), which is defined in terms of regional Pb and Nd isotopic signatures (Fig. 16). Wooden and Miller (1990) estimate average initial Pb values of the Mojave crustal province as $^{206}\text{Pb}/^{204}\text{Pb} = 16.1$, $^{207}\text{Pb}/^{204}\text{Pb} = 15.38$, and $^{208}\text{Pb}/^{204}\text{Pb} = 35.65$.

Pb isotope ratios of the Tuff of Bridge Spring range in value from $^{206}\text{Pb}/^{204}\text{Pb} = 18.030$ to 18.240 , $^{207}\text{Pb}/^{204}\text{Pb} = 15.557$ to 15.586 , and $^{208}\text{Pb}/^{204}\text{Pb} = 38.890$ to 39.025 (Table 6). Superimposing plots of Tuff of Bridge Spring Pb values on $^{207}\text{Pb}/^{204}\text{Pb}$ vs. $^{206}\text{Pb}/^{204}\text{Pb}$ and $^{208}\text{Pb}/^{204}\text{Pb}$ vs. $^{206}\text{Pb}/^{204}\text{Pb}$ plots of early Proterozoic rocks of the Mojave and Arizona crustal provinces (Wooden and Miller, 1990) shows that the Tuff of Bridge Spring array is coincident with the Mojave province trend (Fig. 17). This similarity indicates that production of the Tuff of Bridge Spring by assimilation with Mojave Province-type crust is unlikely because a considerable amount of Mojave-type crust (nearly 100 %) would have to be added to the Tuff of Bridge Spring in order to produce the required changes in isotope values. This conclusion is supported by thin section and field studies which indicate that crystalline lithic fragments are not present in the Tuff of Bridge Spring.

Assimilation of Mojave-type crust is also contradicted by Rb and Sm geochemistry. Generation of the Tuff of Bridge Spring by assimilation of 10 % lithic fragments of Mojave-type crust would require a xenolith having a composition of $\epsilon_{\text{Nd}} = -30$ and $^{87}\text{Sr}/^{86}\text{Sr} = 0.7294$. Smaller amounts of contamination would force ϵ_{Nd}

values lower and $^{87}\text{Sr}/^{86}\text{Sr}$ values higher. Again, such isotopic values are not found in Mojave Province rocks.

Mixing Trend

Because the evidence presented above eliminates lithic contamination as a plausible mechanism for the origin of the Tuff of Bridge Spring isotope array, isotopic variation is interpreted to result from open system conditions in the Tuff of Bridge Spring magma chamber.

Open system magmatic processes include country rock assimilation and/or magma mixing. There is abundant evidence of magma mixing and assimilation in plutonic rocks of the northern Colorado River extensional corridor (e.g., Wilson Ridge, Mt. Perkins pluton, and the Aztec Wash pluton) (Larsen, 1990; Metcalf et al., 1992; Falkner et al., 1993). These features support the assumption that open system conditions were common in plutons that developed in this region during the Miocene, and implies similar mechanisms of origin for volcanic rocks of the region.

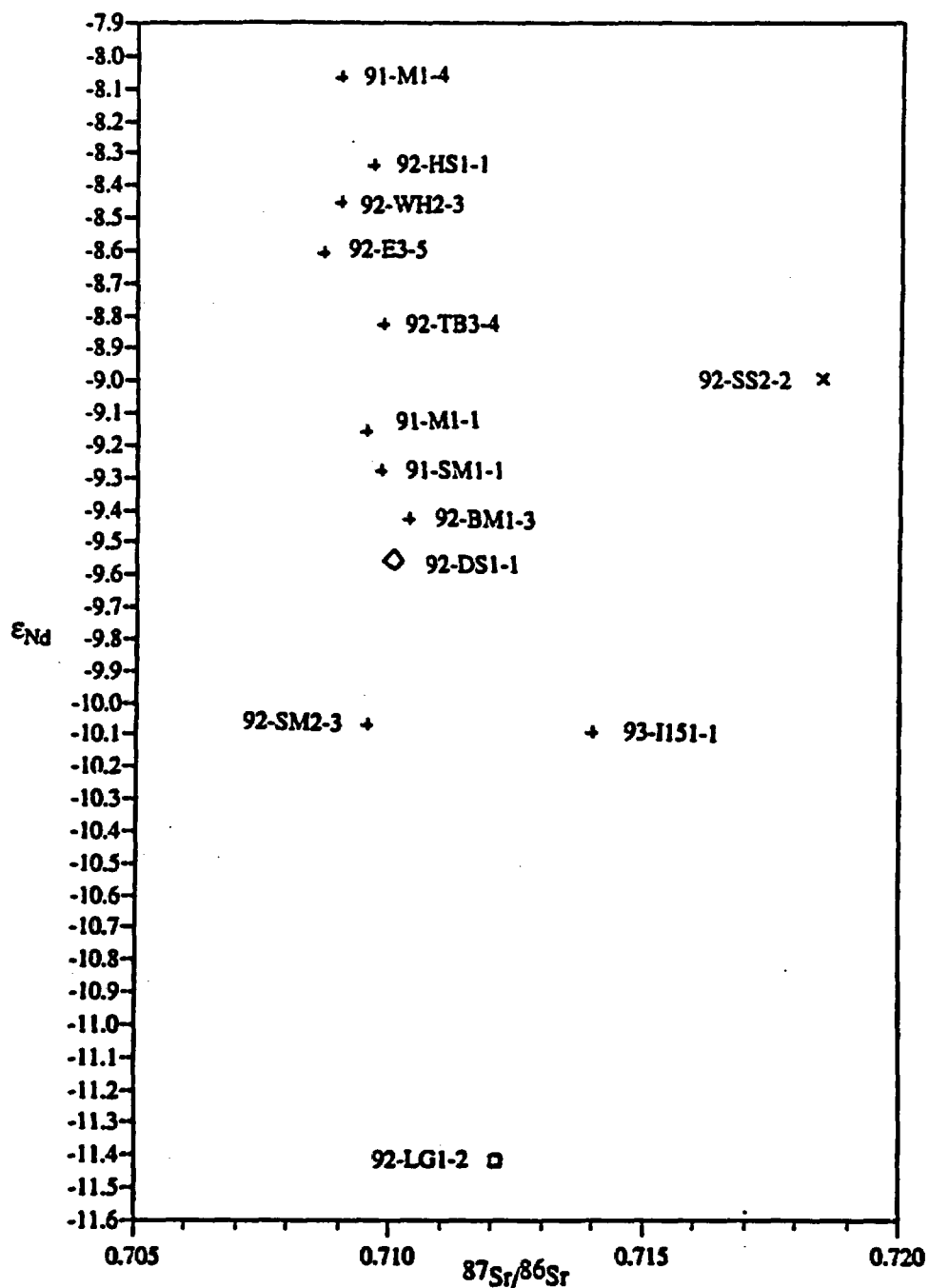
The Role of Contaminants in the Genesis of the Salt Spring Wash and Lucy Gray Range Tuffs

Contaminant modeling of both the tuff of the Lucy Gray Range tuff and the tuff of Salt Spring Wash indicate they were not generated as the result of contamination of the Tuff of Bridge Spring with xenoliths that have isotopic signatures typical of Patsy Mine Volcanics mafic rocks, OIB basalts, or Mojave-province Precambrian crystalline basement. Fig. 15 shows the plot of ϵ_{Nd} vs. $^{87}\text{Sr}/^{86}\text{Sr}$ of the Lucy Gray and Salt Springs Wash tuffs and the Tuff of Bridge Spring array. Assimilation of reasonable

volumes of xenoliths by the Tuff of Bridge Spring to produce the tuff of Salt Spring Wash requires contamination by a source that has values of $^{87}\text{Sr}/^{86}\text{Sr}$ that are not found in the extensional corridor. Likewise, generation of the tuff of the Lucy Gray Range by xenolith contamination requires assimilation of a source that has values of ϵ_{Nd} that are unrealistic for rocks of this area. These observations suggest that the isotopic signatures of these tuffs reflect derivation from different magmatic sources. Therefore, the Salt Spring Wash and Lucy Gray Range tuffs are not cogenetic with the Tuff of Bridge Spring.

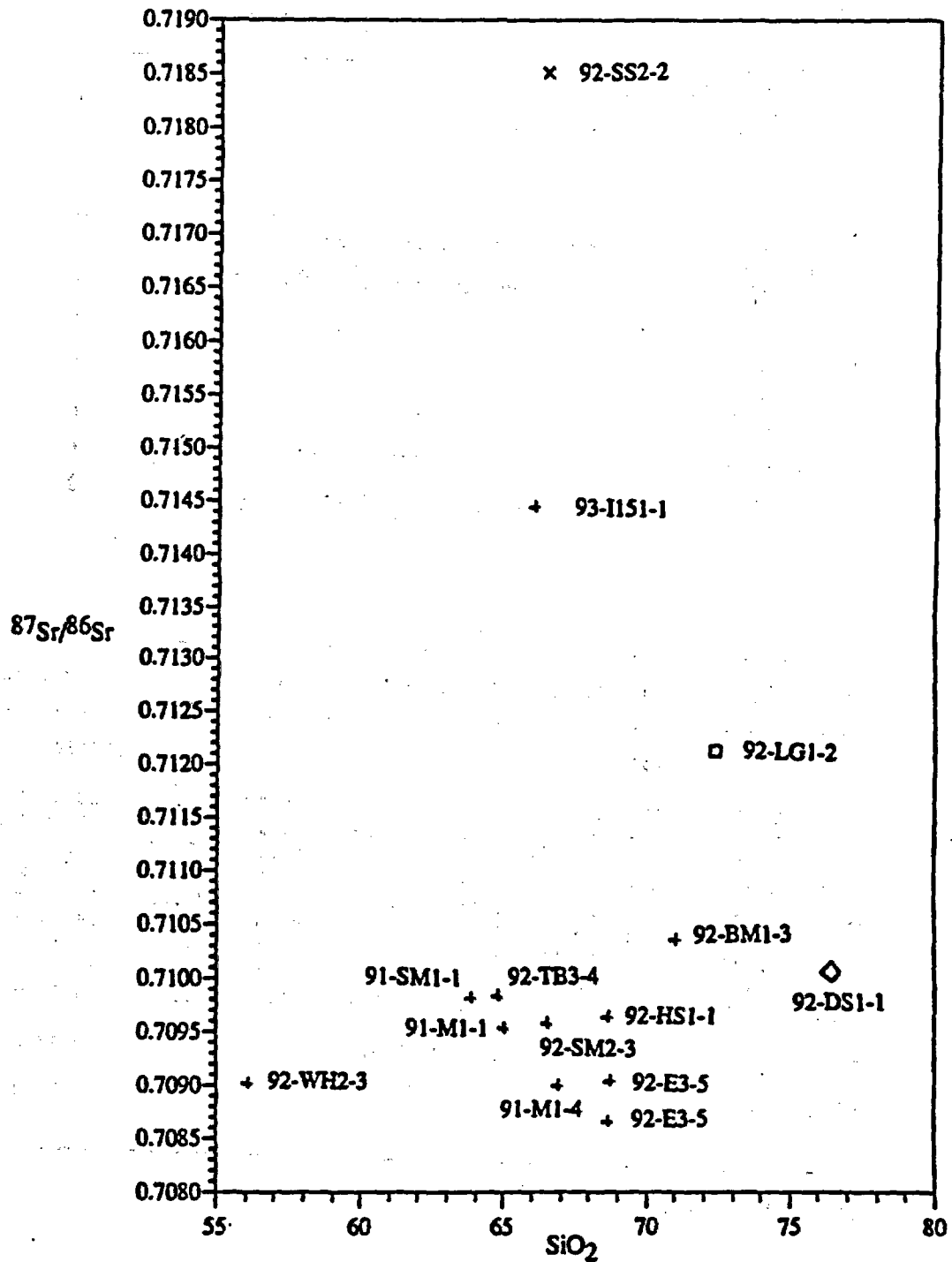
Table 6: Isotope Analyses. (* = analysis pending.)

Section	Sample Number	87Sr/86Sr	Epsilon Nd	206Pb/204Pb	207Pb/204Pb	208Pb/204Pb
McCullough Range	91-M1-1	0.709534	-9.16	18.04	15.557	38.908
	91-M1-4	0.70901	-8.07	18.177	15.58	38.89
Eldorado Mountains	92-E3-5	0.708653	-8.61	*	*	*
	Duplicate	0.709112	*	*	*	*
Highland Spring Range	92-HS1-1	0.70964	-8.34	18.176	15.571	38.958
Sheep Mountain	91-SM1-1	0.70983	-9.28	18.052	15.563	39.025
	92-SM2-3	0.70958	-10.07	14.596	15.204	38.001
Temple Bar	92-TB3-4	0.70984	-8.83	18.24	15.586	38.988
White Hills	92-WH2-3	0.70902	-8.45	18.232	15.567	38.941
Black Mountains	92-BM1-3	0.71036	-9.43	18.038	15.562	39.016
Interstate 15	93-I151-1	0.714628	-10.11	18.038	*	*
Dolan Springs	92-DS1-1	0.71007	-9.56	*	*	*



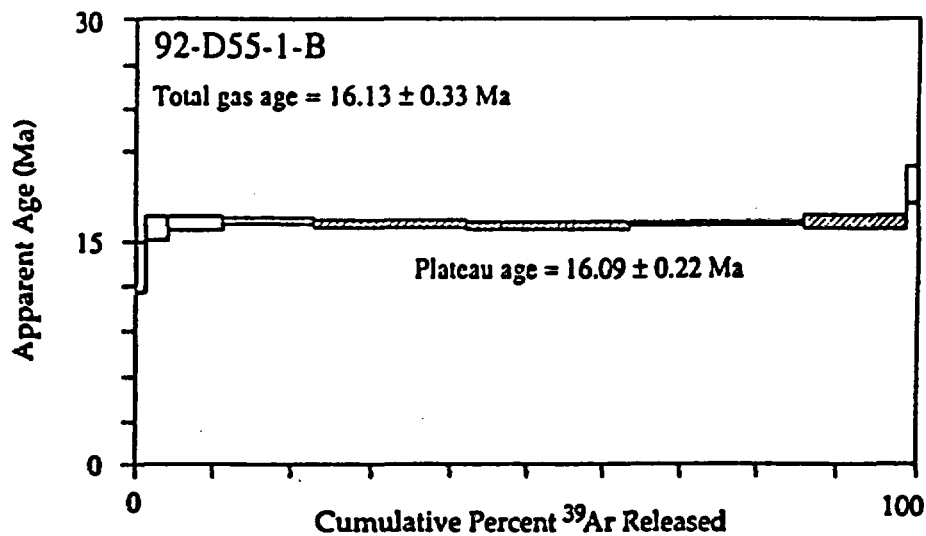
◇ Dolan Springs □ Lucy Gray Range x Salt Spring Wash + Tuff of Bridge Spring

Figure 11: Plot of ϵ_{Nd} vs. $^{87}\text{Sr}/^{86}\text{Sr}$ of the Tuff of Bridge Spring and three non-correlative tuffs. Data points labeled with sample numbers.



◇ Dolan Springs □ Lucy Gray Range x Salt Spring Wash + Tuff of Bridge Spring

Figure 12. Plot of $^{87}\text{Sr}/^{86}\text{Sr}$ vs. SiO_2 of the Tuff of Bridge Spring and three non-correlative tuffs. Data points labeled with sample numbers.



TEMP	40/39	37/39	36/39	MOLES 39	%TOTAL	% RAD	K/Ca	AGE (Ma)
92-D55-1-B				J = .016479				
500	7.058	0.116	0.0223	125.0	1.2	6.3	4.22	13.25 ± 1.70
810	1.684	0.048	0.0038	298.6	2.8	31.9	10.30	15.89 ± 0.81
915	0.967	0.018	0.0014	764.8	7.3	56.7	27.26	16.22 ± 0.43
1815	0.779	0.011	0.0007	1207.0	11.5	71.0	45.07	16.37 ± 0.22
1080	0.762	0.013	0.0007	2034.2	19.3	71.3	37.81	16.08 ± 0.28
1180	0.783	0.023	0.0008	2225.8	21.1	69.0	20.98	16.00 ± 0.25
1245	0.798	0.034	0.0008	2375.4	22.6	68.3	14.37	16.12 ± 0.15
1310	0.790	0.051	0.0008	1327.3	12.6	69.1	9.61	16.17 ± 0.44
FUSE	1.031	0.124	0.0013	170.2	1.6	61.5	3.95	18.74 ± 1.24
TOTAL				10528.3	100.0			16.13 ± 0.31
PLATEAU AGE								16.09 ± 0.22

(Moles ^{39}Ar X E-14)

Figure 13. $^{40}\text{Ar}/^{39}\text{Ar}$ incremental release age analysis (biotite) of the tuff of Dolan Springs.

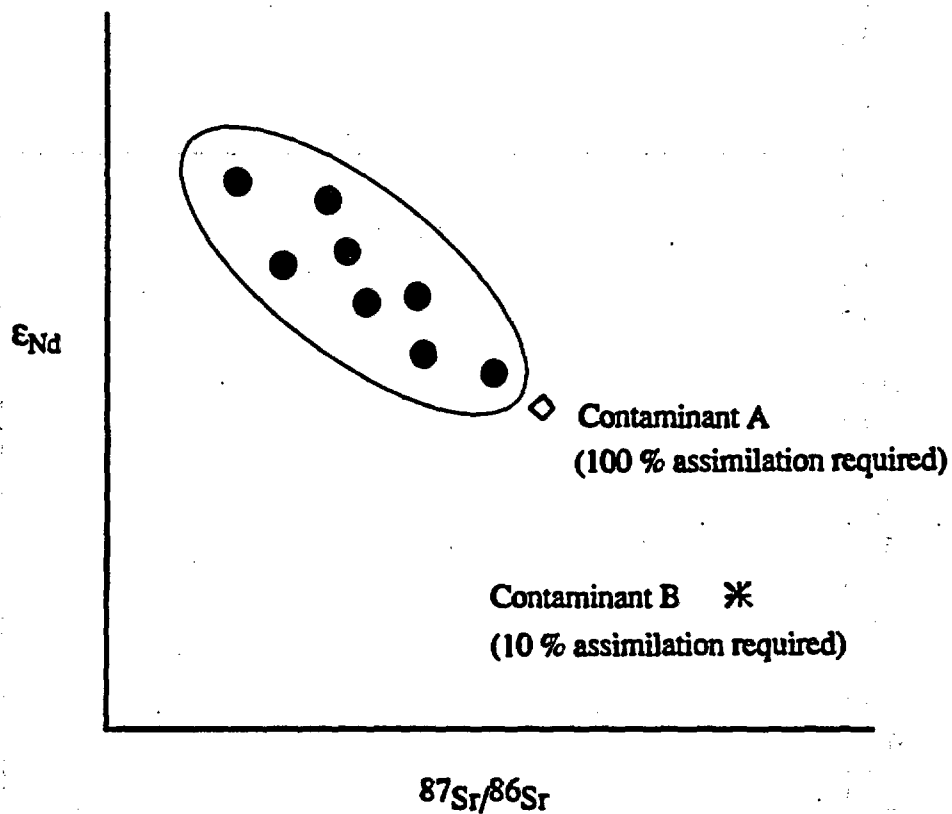
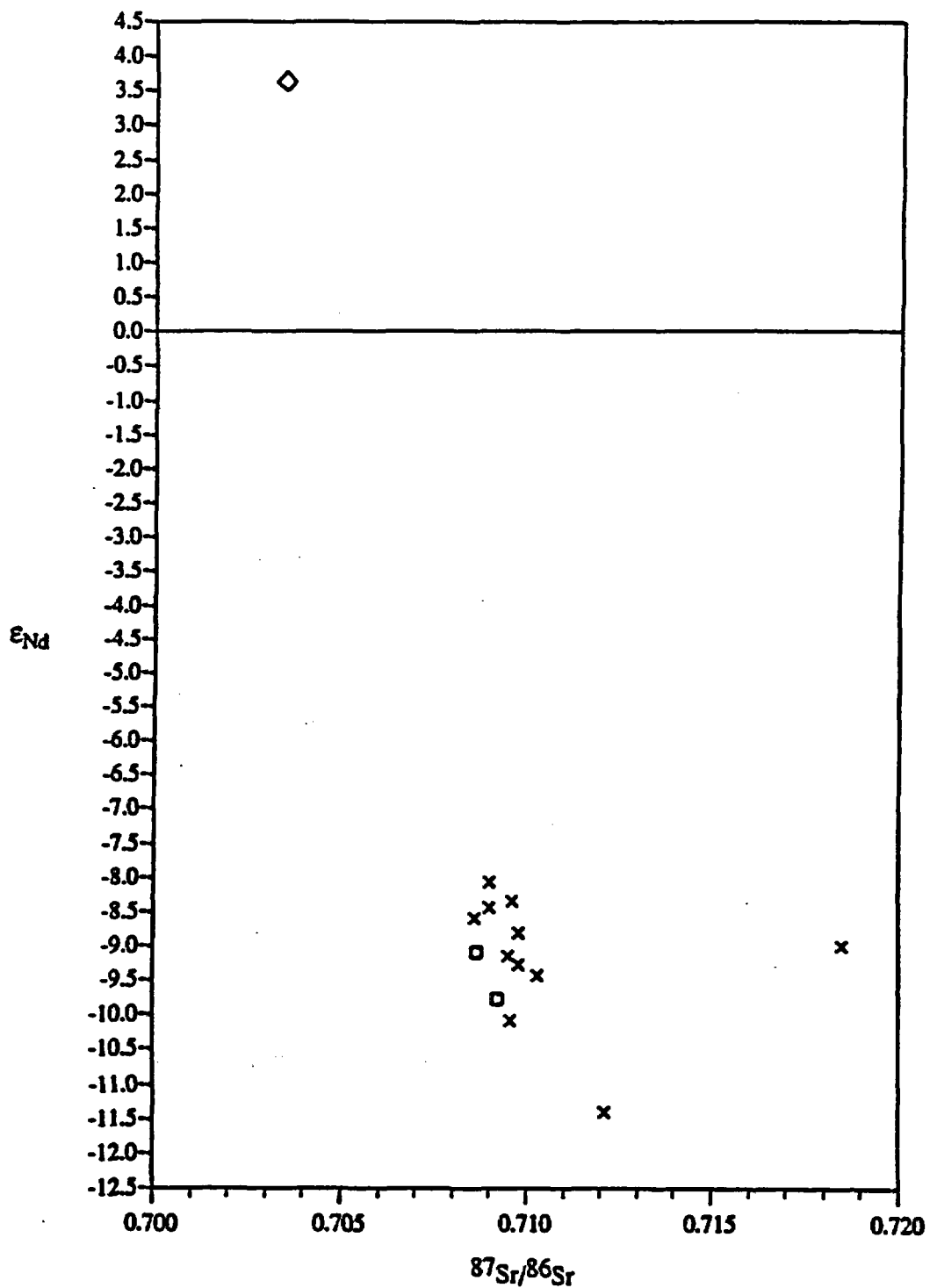


Figure 14. Generation of a hypothetical isotope array by xenolith contamination.
See text for explanation.



◇ Petroglyph Wash Basalt □ Patsy Mine Volcanics × Tuff of Bridge Spring

Figure 15. Plot of ϵ_{Nd} vs. $^{87}\text{Sr}/^{86}\text{Sr}$ for the Tuff of Bridge Spring, Patsy Mine Volcanics, and Petroglyph Wash Basalt.

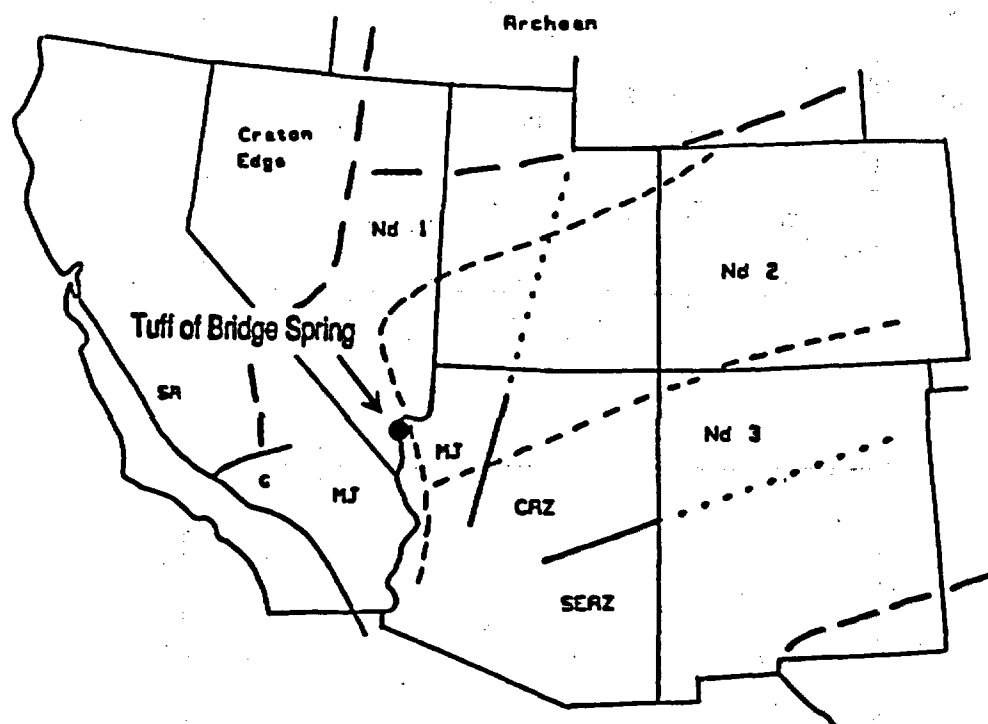


Figure 16. Approximate geographic distribution of Early Proterozoic Nd and Pb provinces in the southwestern United States shown with the distribution area of the Tuff of Bridge Spring. Pb provinces: MJ = Mojave, CAZ = central Arizona, SEAZ = southeastern Arizona. Southwestern Arizona province boundaries are uncertain because of lack of data. From Wooden and Miller (1990).

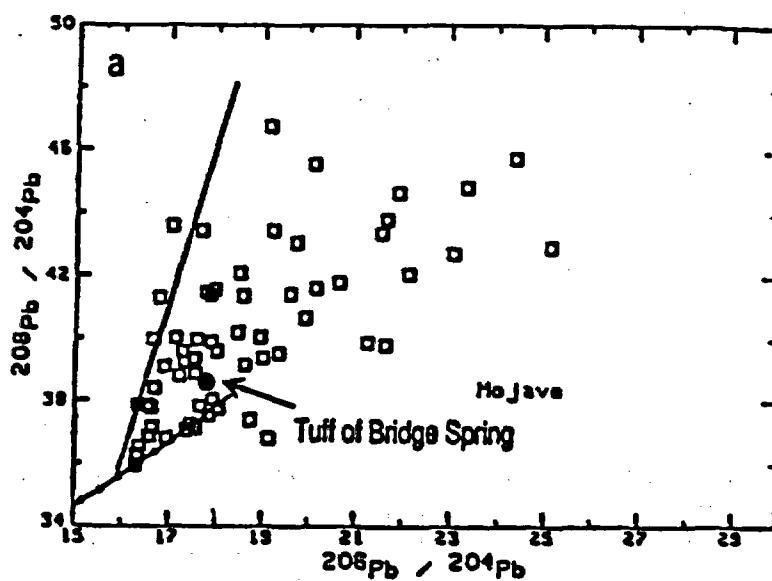
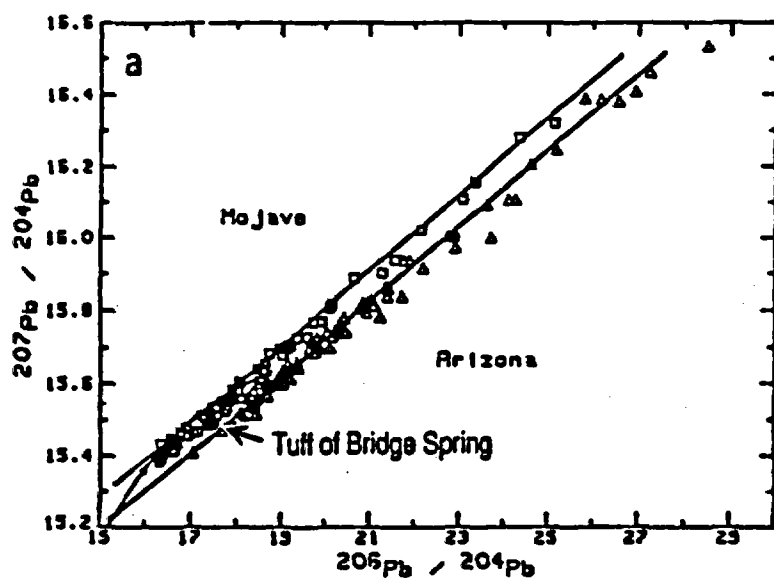


Figure 17. Pb isotope plots of a representative Tuff of Bridge Spring sample and samples of Mojave and Arizona Early Proterozoic crustal provinces rocks. Pb isotope analyses of crustal rocks from Wooden and Miller (1990).

Internal Stratigraphy

Introduction

Determination of the internal stratigraphy of an ash-flow tuff is based upon recognition of vertical and lateral variation in geochemistry, lithology, mineralogy, and isotopic and paleomagnetic signatures (Hildreth and Mahood, 1985). These variations form by primary magmatic differentiation processes and syn- and post emplacement/secondary processes which act to modify the magmatic signatures of ash-flow tuffs. Primary variations in ash-flow tuffs reflect chemical gradients present in the parent magma chamber at the instant of their eruption. For this reason, ash-flow tuffs are commonly referred to as "snapshots" of syn-eruption magmatic conditions (Hildreth, 1985). If the primary characteristics of ash-flow tuffs are not altered by secondary processes, these internal variations are useful criteria for stratigraphic correlations.

Secondary modification processes can physically fractionate or chemically alter the magmatic signature of ash-flow tuffs during or after their emplacement. These processes include (1) elutriation of fine-grained material during pyroclastic flow; (2) concentration of lithic fragments and phenocrysts by either pyroclastic flow-associated ground surges or by post-emplacement compaction; and (3) devitrification and vapor phase crystallization of flows following emplacement (Hildreth and Mahood, 1985; Fisher and Schmincke, 1984). Devitrification and vapor phase processes are associated with specific horizons of the ash-flow tuff section (Cas and Wright, 1987). Devitrification typically occurs in the middle- to upper middle parts of the section. Vapor phase crystallization, which occurs in the moderately- to poorly-welded part of the section that overlies the zone of devitrification, may locally overprint devitrified tuff. These

processes may affect the degree of welding of ash-flow tuffs and the preservation of cooling breaks. Local zones of devitrification form in response to variations in the thickness of each ash flow which in turn are controlled by variations of pre-eruption topography. Because syn- and post-eruptive modification of ash-flow tuffs is common (Hildreth and Mahood, 1985), any division of ash-flow tuff internal stratigraphy that is based upon physical features of ash-flow tuffs (cooling breaks, phenocryst modes, degree of welding, color, etc.) that can be changed by secondary processes must be considered suspect.

In this study, the recognition of regionally-extensive chemical zonations in the Tuff of Bridge Spring (described below) indicates that secondary modification processes did not significantly alter the primary chemical signatures of the Tuff of Bridge Spring. This observation suggests that these signatures are magmatic in origin.

Determination of the internal stratigraphy of the Tuff of Bridge Spring is based upon the recognition of patterns of major/trace element enrichment and depletion of each section. In many cases, patterns can be linked to a specific outcrop features (e.g., cooling breaks) which correspond to distinct changes in the eruptive cycle.

Recognition of the relationship between chemical patterns and outcrop features subsequently allows the division of each section into a series of eruptive units, which are the geochemically-defined equivalents of the conventional flow unit of Smith (1960). The presence of consistently reoccurring patterns of major and trace element variation across the distribution area of the Tuff of Bridge Spring allows division of the unit into two separate chemical members which formed in response to two different magmatic processes. Correlation of these chemical members across the distribution area of the Tuff of Bridge Spring leads to further division of the unit into three regional members. Persistence of regional chemical trends of the Tuff of Bridge Spring has important implications for understanding magma chamber processes.

Eruptive Units

Chemical Criteria

Plots of relative stratigraphic position vs. major element oxides and trace elements (Fig. 9) for the Tuff of Bridge Spring show trends of relative depletion and enrichment of each element. The pattern of these variations preserves a sequence of magmatic compositions that were present in the Tuff of Bridge Spring magma chamber immediately prior to eruption.

Plots of Tuff of Bridge Spring geochemistry on relative position vs. element concentration diagrams (Fig. 9) consists of alternating trends of elemental depletion or enrichment that are expressed as lines of changing slope. Two types of chemical breaks (interruptions) separate adjacent chemical trends on these plots (Fig. 18). The first type of chemical break is marked by a reversal in slope at an inflection point. The second, less frequently-occurring type of break is marked by the separation of two trends by a wide compositional gap between two trends of opposing slope, or between two trends with the same slope.

A certain amount of interpretation is required to locate chemical breaks in relative stratigraphic position vs. element concentration plots (see discussion below of Eldorado Mountains section). Such ambiguities can be resolved by using additional criteria for locating stratigraphic breaks in ash-flow tuffs such as cooling breaks, basal surge deposits, etc.

Although the pattern of elemental variation preserved in each section differs with each element, the relative stratigraphic position at which significant slope changes, inflection points, and/or compositional gaps occur is generally consistent in each section regardless of which element is being considered. These consistent patterns

define the chemical signatures of the Tuff of Bridge Spring and mark specific chemical horizons in the Tuff of Bridge Spring magma chamber. These signatures provide points of reference upon which division of the internal stratigraphy of the Tuff of Bridge Spring is based. Stratigraphic units defined on the basis of the chemical signature of the Tuff of Bridge Spring are referred to as "eruptive units" in this study.

An example of the division of a stratigraphic section into eruptive units is presented in Fig. 19, a compilation of relative stratigraphic position vs. normalized elemental oxide and trace element plots for the Eldorado Mountains stratigraphic section. These plots suggest that there are three major compositional trends in this section. These trends are formed by the grouping of intervals 1-3, 4-5, and 6-9. Corresponding chemical breaks occur above stratigraphic level 3, and 5. Fig. 20 summarizes the division of each Tuff of Bridge Spring stratigraphic section into successive eruptive units.

Field Evidence

The occurrence of cooling breaks are the main field evidence used to support geochemically-defined divisions of internal stratigraphy. In relatively short-lived magmatic systems, changes in magmatic chemistry do not necessarily occur isochronously with those types of chemical and physical changes in magmatic conditions that result in formation of cooling breaks.

Cooling breaks form during periods of eruptive quiescence. If the quiescent stage is of sufficient duration, the magma chamber may undergo complete re-equilibration, resulting in the formation of a normally-zoned magma chamber. In such cases, a period of quiescence is directly associated with the formation of cooling breaks, and because periods of eruptive quiescence are associated with major changes

of magma chamber chemistry, cooling breaks commonly coincide with the position of chemical breaks as well.

In some eruptive sequences, re-equilibration of a magma chamber may be interrupted by volatile saturation or by injection of mafic magma, two processes that may initiate eruption. If the re-equilibration process is interrupted by an ash-flow tuff eruption, the chemical signature of the resultant volcanic outflow will not differ significantly from older flows. In this case, formation of a chemical break that reflects an abrupt chemical gradient in the magma chamber will occur at a later time (i.e., above the most recent cooling break).

Field evidence supports the division of each Tuff of Bridge Spring stratigraphic section into a series of chemically distinctive eruptive units. Supporting field observations include (see Fig. 9 and 20, and Appendix C):

(1) **Black Mountains:** A poorly-exposed cooling break is present below stratigraphic interval 10, which correlates with chemical breaks shown by Th, Y, Ba, Cr, Rb, Sr, Mn, Mg, K, Fe, and Ti.

(2) **Eldorado Mountains:** Major chemical breaks occur below stratigraphic intervals 4 and 6, and a minor break occurs below interval 9. Placement of a chemical break below interval 4 is supported by the presence of gas-escape pipes, which are zones of concentrated lithic fragments that are typically preserved at the top of flow units (Fisher and Schmincke, 1985). A chemical break occurs between interval 5 and 6 (a massive vitrophyre and vapor phase zone, respectively), but cannot be associated with an obvious cooling break.

(3) **Highland Spring:** A sharp, laterally-continuous cooling break occurs between stratigraphic intervals 7 and 9. This cooling break correlates with a major geochemical break (Ti, Ca, K, Na, Mg, Mn, Zr, Sr, Rb, Ni, Nb, Cr, and Ba). A minor

chemical break occurring between the basal interval and interval 5 does not correlate to any specific outcrop feature.

(4) Interstate 15: Chemical breaks occur above the basal stratigraphic interval and between intervals 4 and 5. Isotope geochemistry (previously discussed) suggests that the basal interval is not cogenetic with the Tuff of Bridge Spring. The occurrence of a massive vitrophyre which may represent the base of a cooling unit at interval 6 weakly corresponds to the chemical break below interval 5.

(5) McCullough Range: A thin, pumice-rich interval of very poorly-welded crystal tuff occurs at stratigraphic interval 8, which correlates with a chemical break. Additional chemical breaks occur below the uppermost interval of the section (interval 10.5) and below the basal interval. A cooling break was not observed below the uppermost interval of the section. The basal interval of the McCullough Range section consists of a discontinuous, very-poorly welded lithic tuff which is possibly related to a pyroclastic surge deposit. This interval has a different chemical signature than the Tuff of Bridge Spring for most elements with the exception of P, Mn, Ni, Nb, and Th.

(6) Sheep Mountain: A possible cooling break occurs below a massive vitrophyre at interval 9. This cooling break correlates with a chemical break. Another chemical break separates the basal interval of the section from the units lying above it. This interval consists of a very poorly-welded, pumiceous vitrophyre that has a shard-rich matrix.

(7) Temple Bar: Chemical breaks occur between intervals 5 and 6, and 8 and 9.5, respectively. Obvious cooling breaks were not observed in the Temple Bar section.

(8) White Hills: A poorly exposed cooling break is present between stratigraphic intervals 8 and 9, which corresponds to a chemical break that is strongly established by variation of most trace elements.

Chemical Members of the Tuff of Bridge Spring

The dominant geochemical trend shown on Harker variation plots of the Tuff of Bridge Spring data involves Cr, an element which partitions into mafic mineral phases such as clinopyroxene (Fig. 21). The partitioning of Cr provides the basis of division of Tuff of Bridge Spring stratigraphic sections into two geochemically distinct members.

Assignment of sections to an appropriate geochemical member were made by examining numerous element/element and ratio/element plots. For reasons that will be discussed below, such assignments occasionally varied, depending upon the specific elements being considered in each plot. This requires that the final assignment of each stratigraphic section is based upon a consensus of many different plots that used many different combinations of elements and/or ratios. While the partitioning of Cr provides the best general criteria for division of the Tuff of Bridge Spring into two chemical members, the Eldorado Mountains section does not exhibit the same sensitivity to variation of Cr as the rest of the sections. Assignment of this section to an appropriate chemical member was based upon examination of element plots other than Cr vs. SiO₂.

The first chemical member of the Tuff of Bridge Spring generally exhibits a trend of relatively constant Cr and highly variable SiO₂, and includes the White Hills, McCullough Range, lower Eldorado Mountains (stratigraphic intervals 1-5), and upper Highland Spring Range (stratigraphic intervals 8-9), and upper Temple Bar (interval 9) stratigraphic sections. This chemical member will be referred to as the constant Cr member. The second Tuff of Bridge Spring chemical member generally exhibits a trend of highly variable Cr and moderately variable SiO₂, and includes the Black Mountain, Interstate 15, upper Eldorado Mountains (intervals 5-9), lower Highland Springs (intervals 1-7), lower Temple Bar (intervals 1-8), and Sheep Mountain sections. This group will be referred to as the variable Cr member.

As discussed above, division of the Tuff of Bridge Spring into chemical members is also shown in element /element plots (such as Cr vs. Sr and Y vs. Zr) (Fig. 22), and ratio/element plots (such as Ti/Sr vs. Fe and Zr/Ti vs. Ba) (Fig. 23 and 24, respectively). The interpretation of element/element and ratio/element diagrams relies both on the grouping of data within specific trends and the direction of the sequential path of changing chemistry within each stratigraphic section. For example, on the Zr/Ti vs. Ba diagram (Fig. 24), two groups are recognized on the basis of both trend and clustering of data. One group shows variable Zr/Ti and relatively constant Ba, and the second group shows variability of both Zr/Ti and Ba.

Although the assignment of sections to different chemical groups may vary with the specific elements and elemental ratios being considered, the majority of plots support the chemical member designations described above. Deviations from these groupings for certain elements possibly reflect the use of whole-rock samples for geochemical analysis. The presence of xenoliths and phenocrysts in analyzed samples will cause compatible element concentrations to differ from magma (glass) concentrations. Since it is the contention of this study that the consistent separation of sections into two distinct chemical groups is the product of two distinct magmatic differentiation processes, only element and element ratios not appreciably affected by phenocrysts and /or xenoliths can be used to define chemical groups. The use of elements like Zr and Y, and to a lesser extent Cr may provide a means of bypassing the chemical "static" produced by phenocrysts and xenoliths to allow an undistorted view of the magmatic chemistry of the Tuff of Bridge Spring. A prime example of the role of chemical "static" in masking magmatic signatures involves the Eldorado Mountains section. Both the Harker variation plot of Cr and the Ti/Zr vs. Ba plot of this section indicate that entire section should be grouped in the variable Cr chemical member. Such an assignment, however, is strongly contradicted by the majority of Harker,

element/element, and ratio/element plots (e.g., Cr vs. Sr, Y vs. Zr, and Ti/Sr vs. Fe) (Fig. 22 and 23), which indicate that the section actually contains both chemical members.

Examination of the constant Cr chemical member indicates that two of the sections included in this group, (upper Highland Spring Range and upper Temple Bar sections), do show variance from both the constant Cr and variable Cr members for some elements, but for the most part exhibit the same geochemical signature as the rest of the constant Cr member sections in the majority of element/element and ratio/element plots. These differences suggest that the upper Highland Spring Range and upper Temple Bar sections were produced from a hybridized batch of magma in which the constant Cr signature is dominant, but which also preserves signatures that are intermediary between the signatures of both the constant Cr and variable Cr members.

Regional Members of the Tuff of Bridge Spring

Meaningful reconciliation of chemical member assignments with regional stratigraphic relationships of each Tuff of Bridge Spring section allows the division of the Tuff of Bridge Spring into three regionally-extensive ash-flow sheets, or regional members (Fig. 25). The stratigraphically lowest regional member of the Tuff of Bridge Spring (Member I) consists of the lower Eldorado Mountains, McCullough Range, and White Hills sections and is characterized by the constant Cr trend. The stratigraphically intermediate regional member (Member II) exhibits the variable Cr trend and consists of the Interstate 15, Sheep Mountain, lower Highland Springs, upper Eldorado Mountains, Black Mountains, and lower Temple Bar sections. The stratigraphically uppermost member (Member III) has, for the most part (but with some differences),

the same chemical signature as the basal regional member (constant Cr trend) and includes the upper Highland Springs and the upper Temple Bar sections. Fig. 26 shows the areal distribution of the three regional members of the Tuff of Bridge Spring.

Fine Scale Chemical Variation

The plot of Zr/Ti vs. Ba (Fig. 26) provides a means of observing fine-scale chemical variations in the Tuff of Bridge Spring. Because these variations are preserved across the distribution area of the tuff, they probably reflect variations in the Tuff of Bridge Spring source magma chamber.

In the ratio Zr/Ti, Zr is an incompatible trace element that is partitioned only by the mineral zircon. Ti is slightly more compatible than Zr, and is partitioned into clinopyroxene and hornblende. Ba, the independent variable in this plot, is a compatible element which is fractionated by potassium feldspars and biotite. The relationship of Zr and Ti in the Tuff of Bridge Spring is unique for two reasons. First, changes in the Zr/Ti ratio seem to represent changes in magmatic compositions. Second, the direction of change of the ratio (relative increase or decrease) does not seem to be affected by the abundances of phenocrysts and/or lithic fragments in the samples.

The Zr/Ti vs. Ba plot (Fig. 24) separates the Tuff of Bridge Spring sections into two groups. The first group shows highly variable Zr/Ti in conjunction with relative invariability of Ba. Stratigraphic sections with this geochemical signature include the Eldorado Mountains, Sheep Mountain, lower Highland Spring (stratigraphic intervals 1-7), Interstate-15, and Black Mountains sections. This group of sections corresponds closely to the sections that make up the constant Cr chemical member. The second group is characterized by variability of both Zr/Ti and Ba. Sections with this signature

include the upper Highland Spring Range (intervals 8-9), McCullough Range, Temple Bar, and White Hills sections. This group of sections corresponds closely to the sections that make up the variable Cr chemical member.

Figure 27 is a compilation of the plots of each of the sections that have highly variable Zr/Ti, relatively invariable Ba plotted side by side (only the y-axis is functional in this plot; however, the magnitude of separation for Ba of the two parts of the Highland Spring section has been preserved). Numerals beside each data point denote its relative stratigraphic position in that particular section. If the pattern of enrichment and depletion of Zr/Ti within each stratigraphic section is followed from basal interval to stratigraphic top, a sequence or path of evolving chemistry can be traced. Each path consists of a series of vertical to slightly inclined segments that have alternating upward (increasing Zr/Ti) or downward (decreasing Zr/Ti) directed lines. The relative direction of each segment is controlled by the stratigraphic order of the analyzed samples. Data points in upward-directed segments have increasing Zr/Ti ratio values in the upsection direction. Data points in downward-directed segments have decreasing Zr/Ti ratio values in the upsection direction. The transition between adjacent segments is marked by inflection points where the Zr/Ti chemical path changes direction.

The sequence of increasing and decreasing Zr/Ti in the variable Zr/Ti, constant Ba trend forms similar patterns in each section. Each section may record only a part of the magmatic zoning that was present in the Tuff of Bridge Spring source chamber at the time of eruption. Complete reconstruction of the chemical profile of the chamber requires combining chemical path diagrams from different sections.

The stratigraphically uppermost inflection points of the variable Zr/Ti, constant Ba trend (i.e., interval 8 in the Eldorado Mountains, interval 7 in the Sheep Mountains, interval 8 in the Black Mountains, interval 6 in the Highland Spring Range, and interval 4 in the I-15 section) all occur at approximately the same Zr/Ti value (average = 538.2;

standard deviation = 41.4). Theoretically, this inflection point should occur at the same Zr/Ti value. Deviation from this value is expected to occur because the Zr/Ti ratio will change in response to changes in phenocryst and/or lithic fragment abundances, which will vary from section to section. This chemical inflection point is interpreted to represent a specific variable Zr/Ti, constant Ba magmatic horizon in the Tuff of Bridge Spring magma chamber that has been preserved in five sections spread over a distance of 90 km in the present day distribution area of the Tuff of Bridge Spring. This is perhaps the first report in the literature of such a widespread chemical marker horizon in ash-flow tuffs.

The variable Zr/Ti, constant Ba path of the upper interval of the Highland Spring section is separated from the lower part of the section by a significant change in Ba concentration (Fig. 24 and 27). This gap suggests that the rocks of the upper Highland Spring Range section were affected by magmatic processes that changed both Zr/Ti and Ba concentrations. Such a relationship is consistent with several other element vs. element and ratio vs. element plots of the Tuff of Bridge Spring in the Highland Spring Range (e.g., Cr vs. Sr) and indicates that this stratigraphic section preserves a major chemical transition that formed in the Tuff of Bridge Spring magma chamber.

The chemical path concept also has implications for location of the source of the Tuff of Bridge Spring (see source section).

Magma Chamber Processes

Differential retention of Cr in the two Tuff of Bridge Spring chemical members suggests that two different differentiation processes dominated the petrogenesis of the

Tuff of Bridge Spring at different points in its evolution. The trend of increasing SiO_2 and relatively constant Cr indicate that differentiation of the constant Cr chemical member occurred without the involvement of mafic minerals such as clinopyroxene. These conditions are suggestive of differentiation of the upper levels of a normally zoned felsic magma body. The trend of variable SiO_2 and Cr of the variable Cr member suggests magma differentiation by either subtraction or addition of clinopyroxene and perhaps olivine from a mafic magma. These conditions are more typical of the lower parts of a magma chamber. Coexistence of these two trends suggests that the Tuff of Bridge Spring originated from a magma chamber with a felsic top and a basal part that was injected with mafic magma which indicates that magma mixing may have been a dominant mechanism in the development of the chamber. This model is supported by both Harker variation plots and abundant lithologic evidence of magma mixing.

Harker variation plots of the Tuff of Bridge Spring show cyclical patterns of variation for several major and trace elements (Fig. 28), which suggests hybridization of a felsic-dominated magma chamber by an influx of mafic magma, and subsequent re-equilibration of the system to more felsic compositions.

Lithologic evidence that magma mixing occurred in the source chamber of the Tuff of Bridge Spring include the occurrence of (1) glomerocrysts, (2) mafic enclaves, and (3) disequilibrium textures in feldspars.

Glomerocrysts are ubiquitous in thin sections of the Tuff of Bridge Spring. The presence of crystal clusters is evidence of magma hybridization processes. These processes can include magma mixing (Davidson et al., 1990; Seaman and Ramsey, 1992).

The presence of disequilibrium textures in feldspars indicate re-equilibration in response to changes in magma composition. Such changes may be due to magma

mixing processes (Hyndman, 1985). Disequilibrium textures in Tuff of Bridge Spring feldspar phenocrysts include resorbed margins in sanidine phenocrysts, sieve textures in plagioclase and sanidine, and mantling of plagioclase phenocrysts by sanidine.

Macroscopic indicators of magma mixing in the Tuff of Bridge Spring include the occurrence of banded fiamme and mafic enclaves (see field description section). Mills (1991, 1993) interpreted the presence of banded, compositionally-mixed pumice in the Rainier Mesa and Ammonia Tanks Members of the Timber Mountain Tuff, Nevada, and mafic enclaves in the Tuff of Hoover Dam, Nevada/Arizona as the volcanic equivalent of the classic magma mixing textures described in northern Colorado River extensional corridor intrusive rocks (e.g., Naumann, 1987; Larsen, 1990; Larsen and Smith, 1990; Metcalf et al., 1992, 1993). The occurrence of banded fiamme at the Bridge Spring type locality (unpublished field observation, Smith, 1993), and several small, porphyritic mafic inclusions (< 3.0 cm wide) in the Eldorado Mountains and Temple Bar sections are interpreted here to be mafic enclaves. These inclusions have crenulate margins but lack the characteristic chilled, glassy margins and coarser-grained interiors of "typical" mafic enclaves (Koyaguchi, 1986).

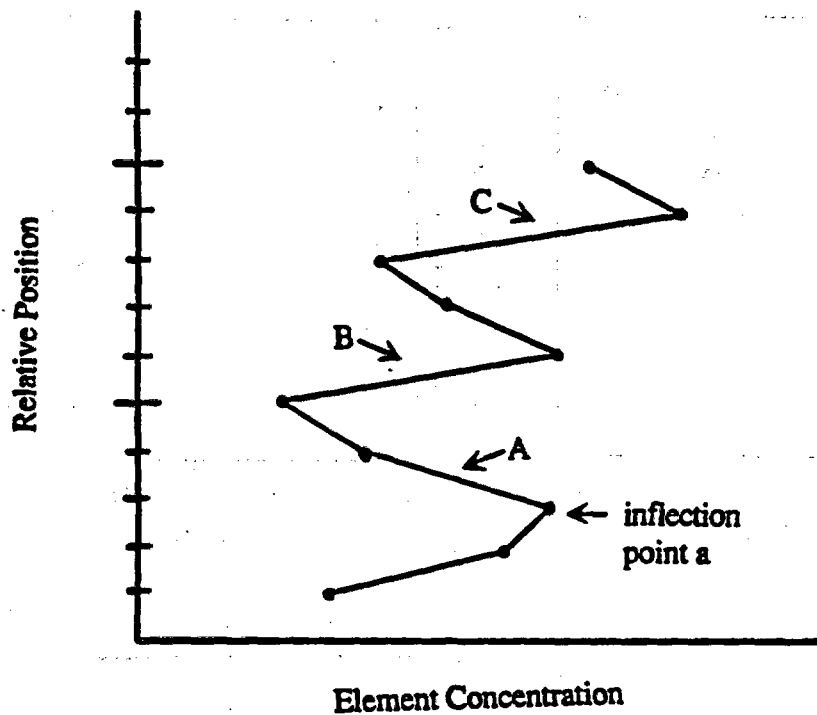


Figure 18. Diagram showing different types of chemical breaks. (A) Chemical break occurs between two trends that have opposite slopes. Reversal in slope occurs at inflection point a. (B) Chemical break occurs between two trends that have the same slope. Trends are separated by a wide chemical gap. (C) Chemical break occurs between two trends that have opposite slopes. Trends are separated by a wide chemical gap.

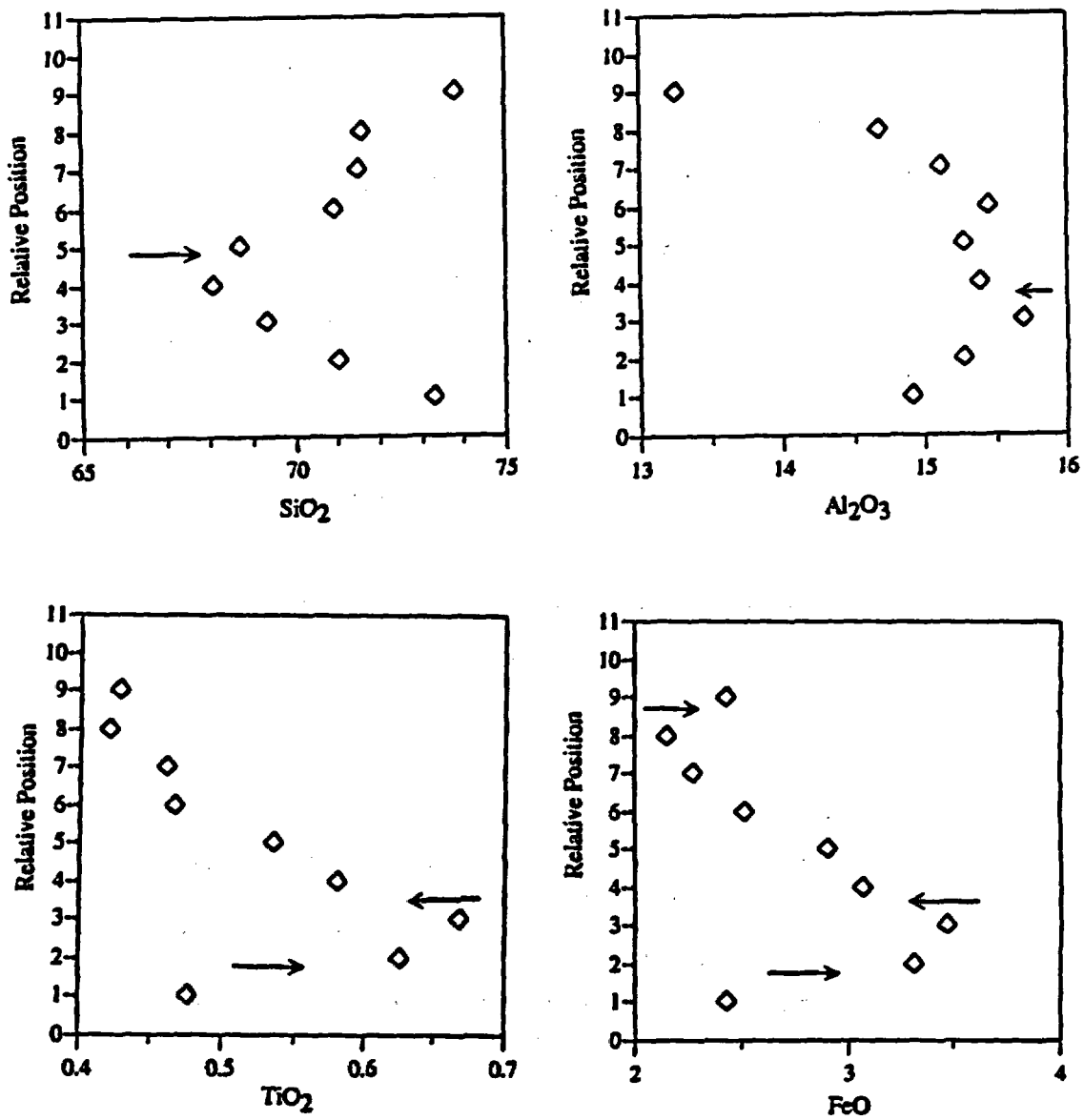


Figure 19. Plot of relative position vs. element concentration for the Eldorado Mountains section showing chemical breaks. Arrows indicate positions of chemical breaks.

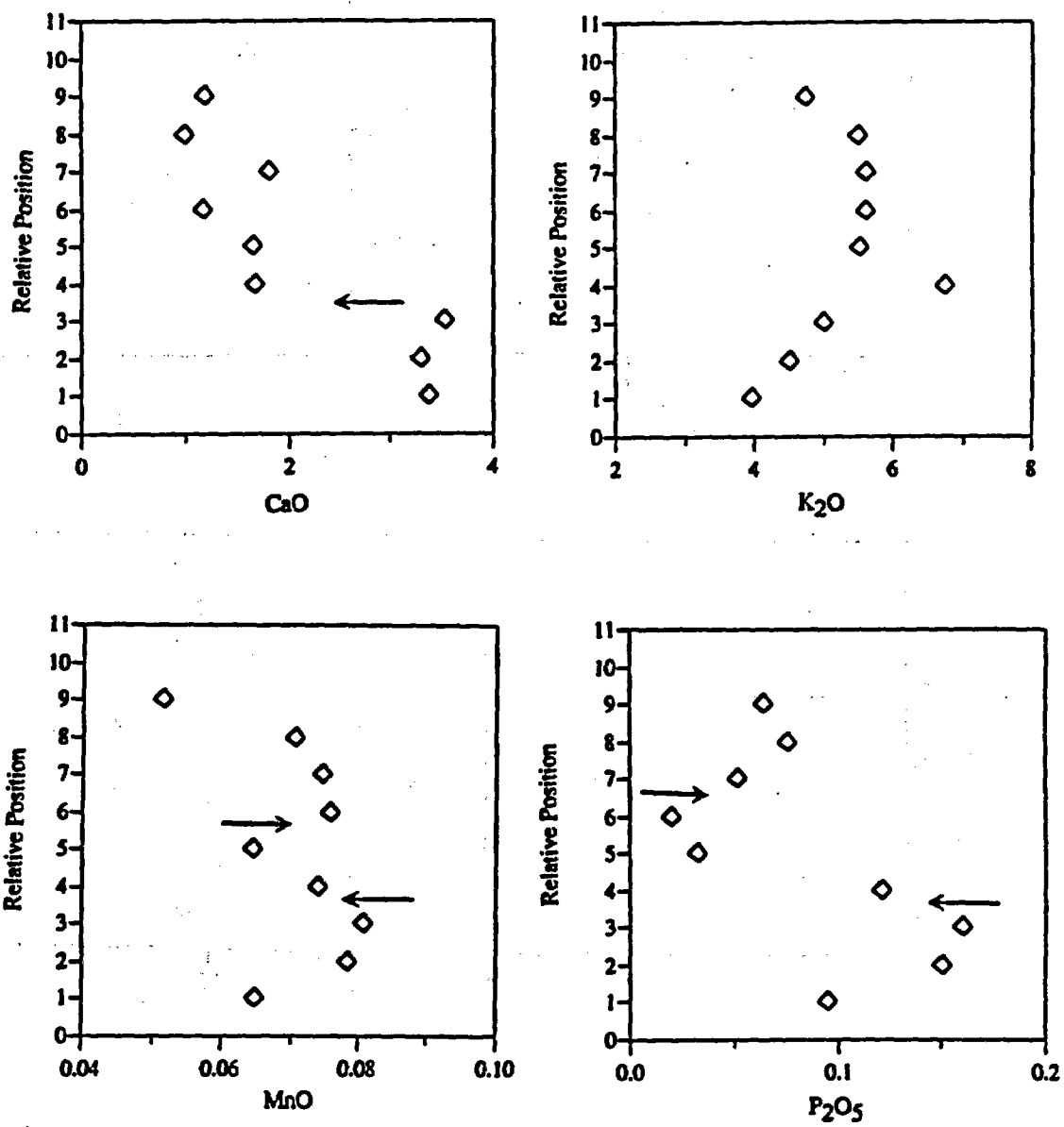


Figure 19, continued.

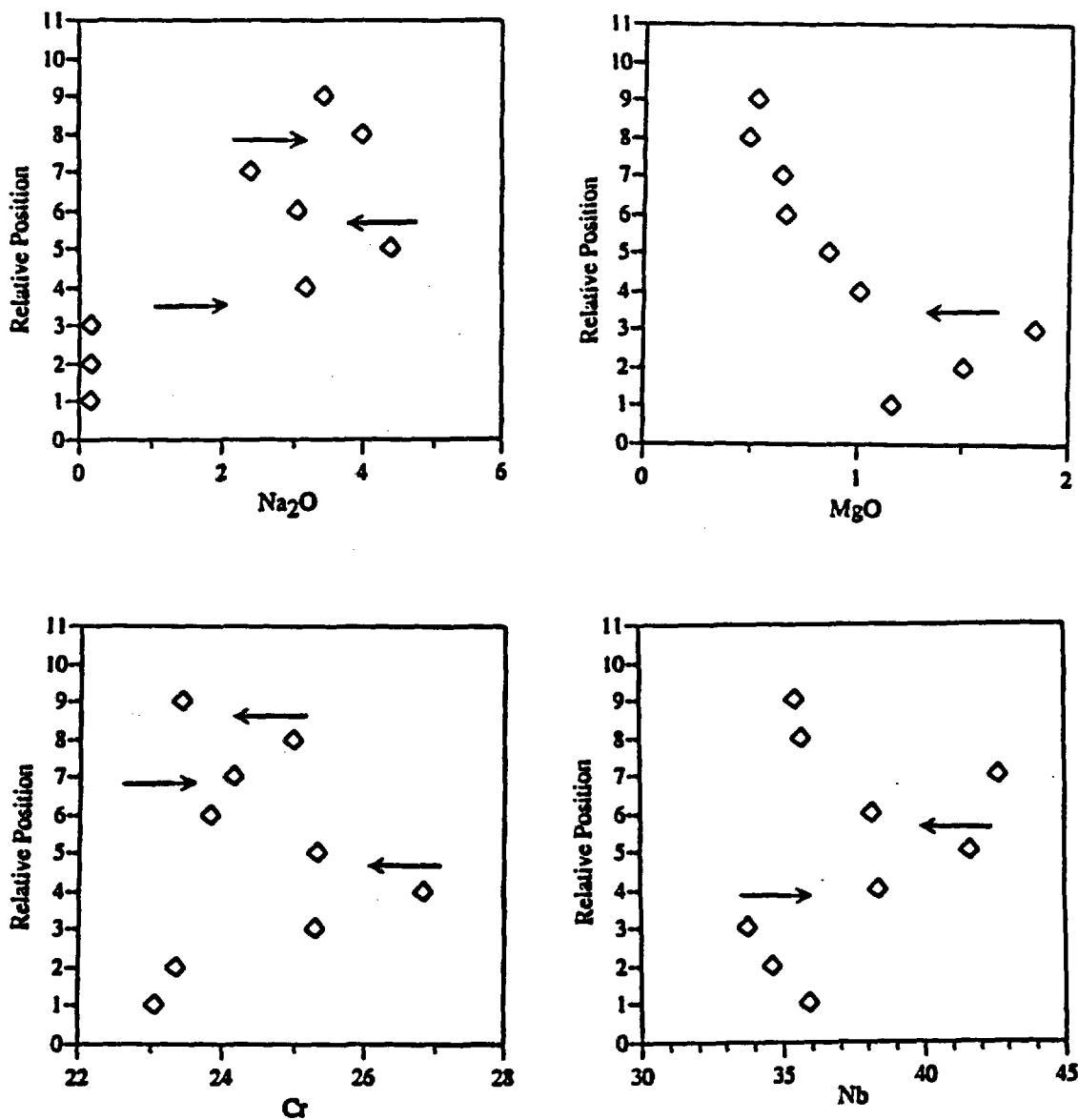


Figure 19, continued.

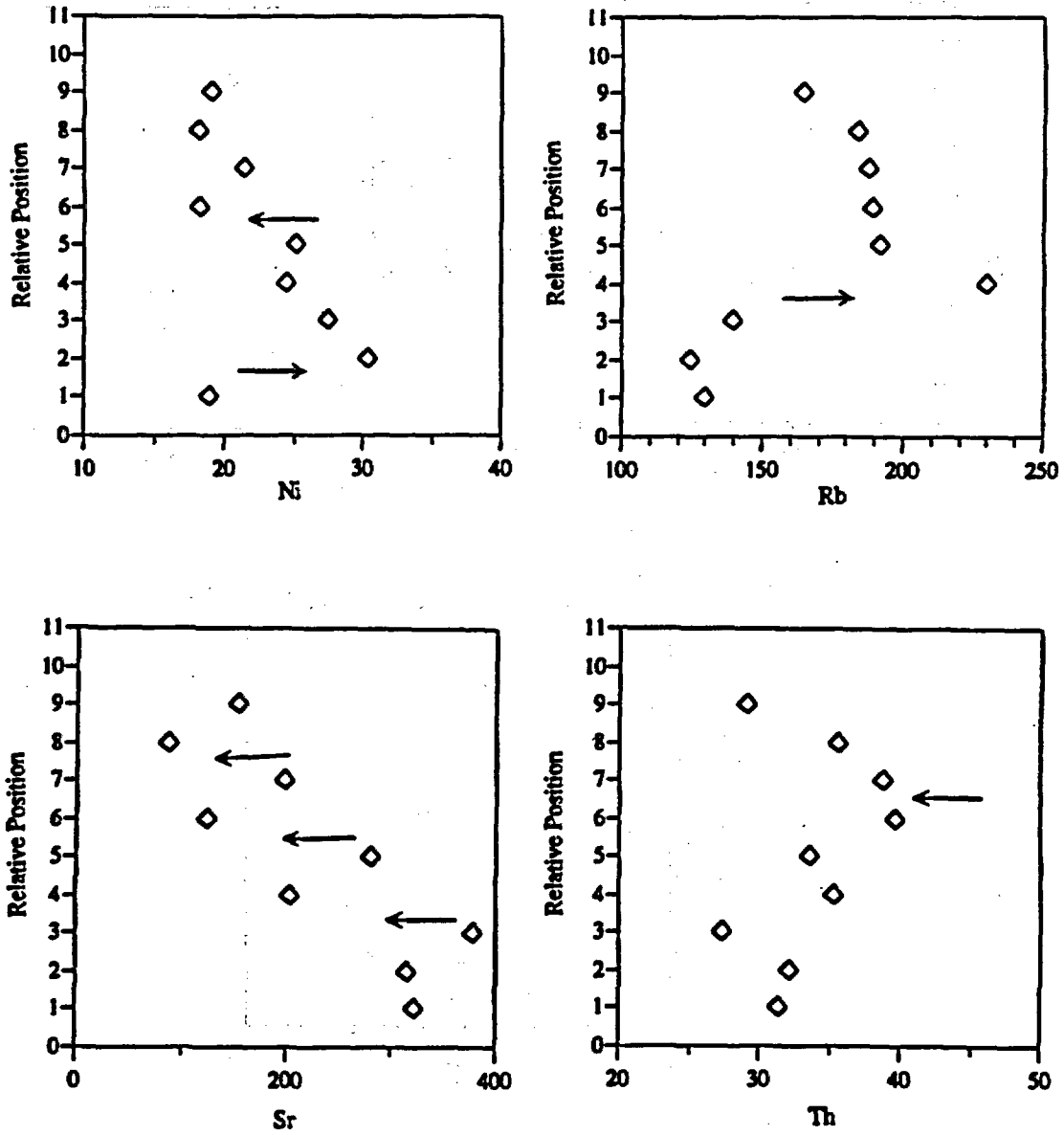


Figure 19, continued.

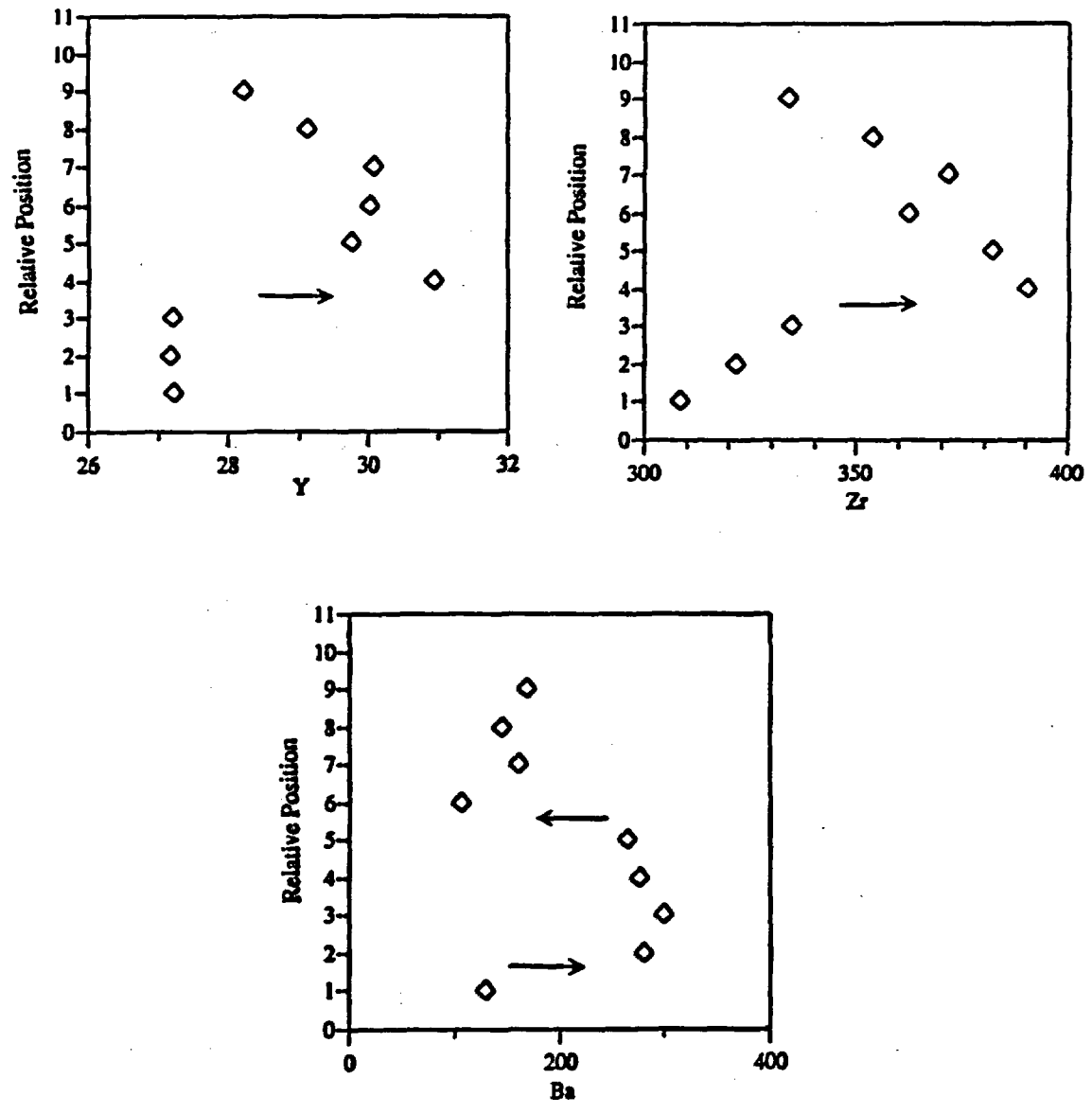


Figure 19, continued.

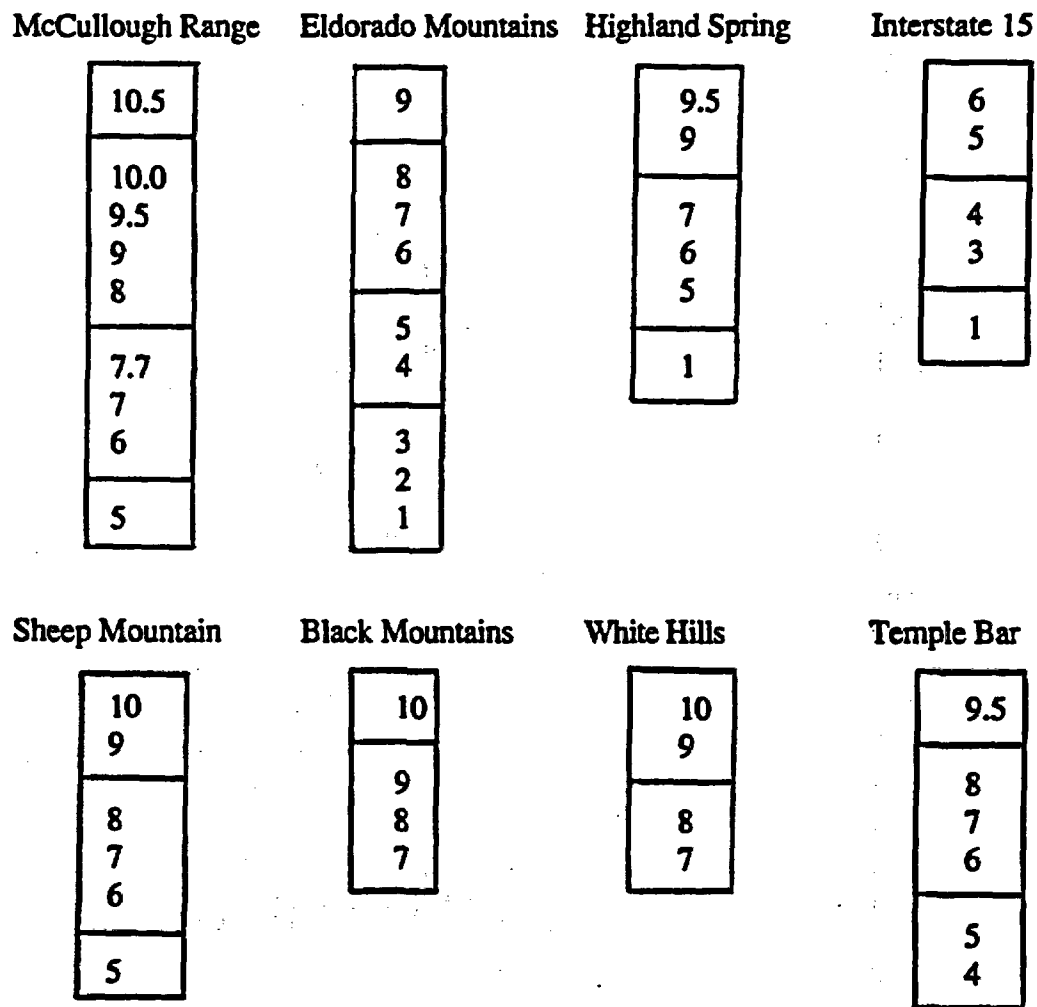


Figure 20. Division of Tuff of Bridge Spring stratigraphic sections into eruptive units. Numbers indicate relative stratigraphic position of each interval.

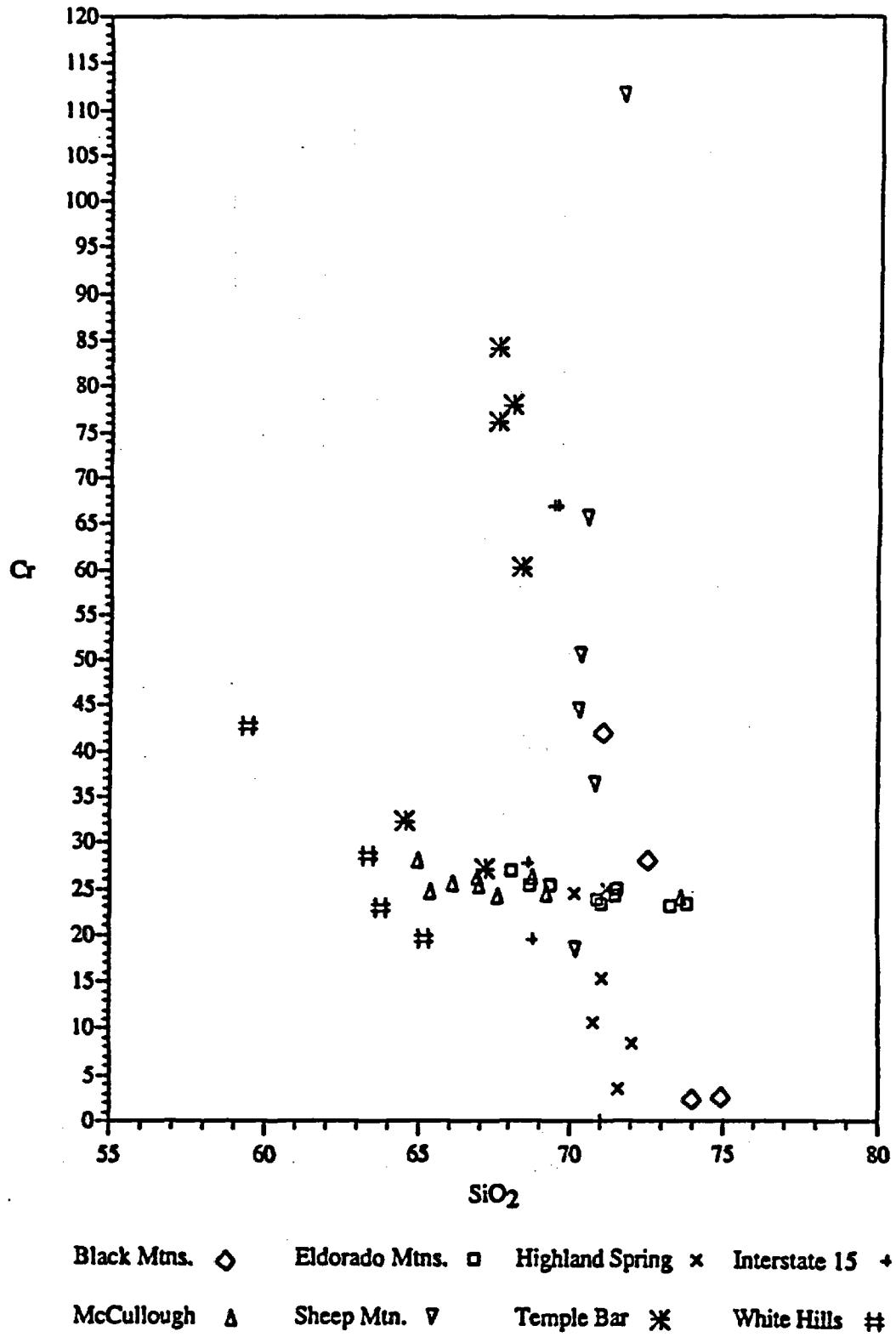


Figure 21. Plot of Cr vs. SiO_2 showing division of the Tuff of Bridge Spring into constant Cr and variable Cr members. See text for explanation.

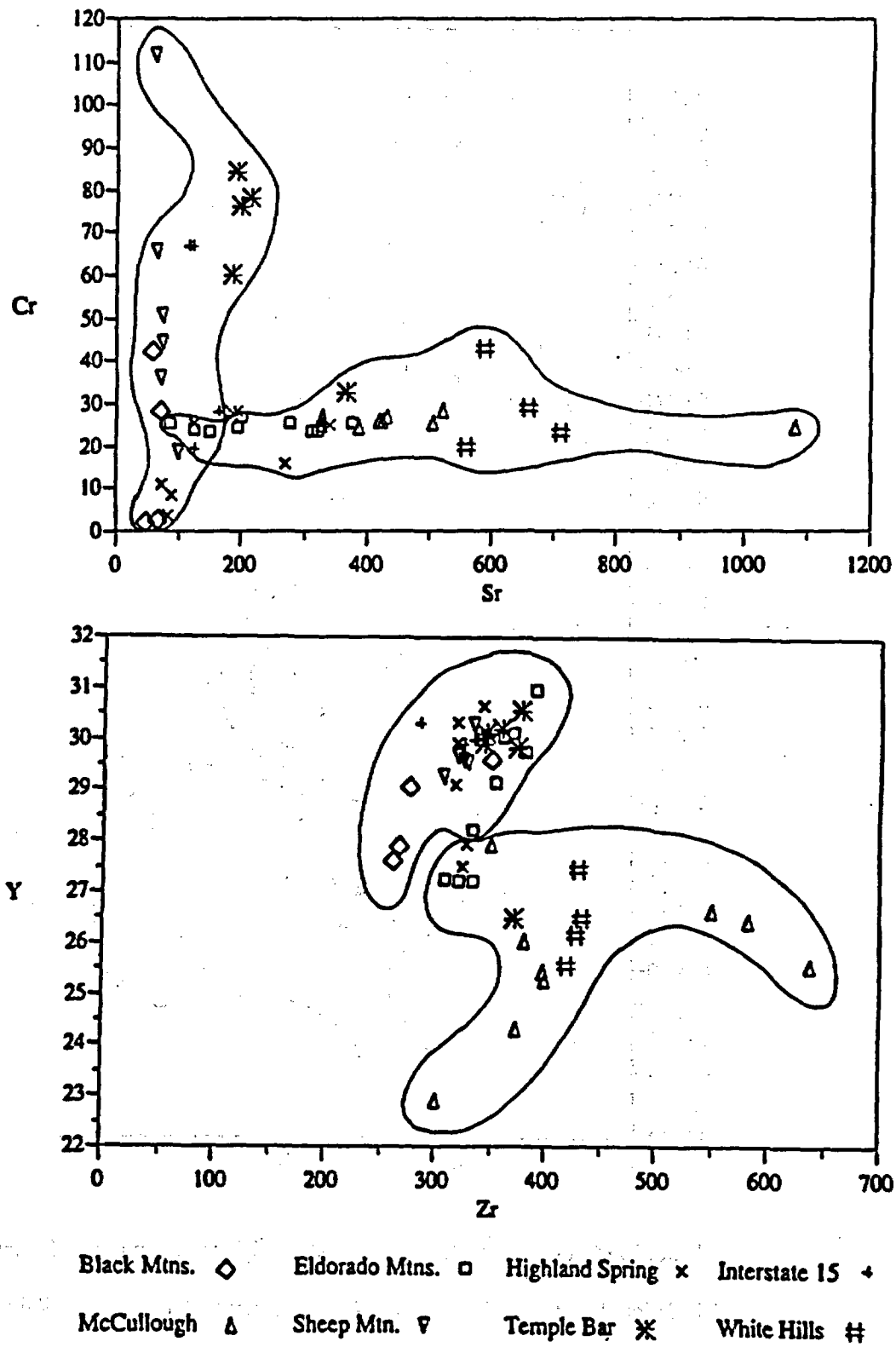


Figure 22. Plots of Cr vs. Sr and Y vs. Zr. See text for explanation.

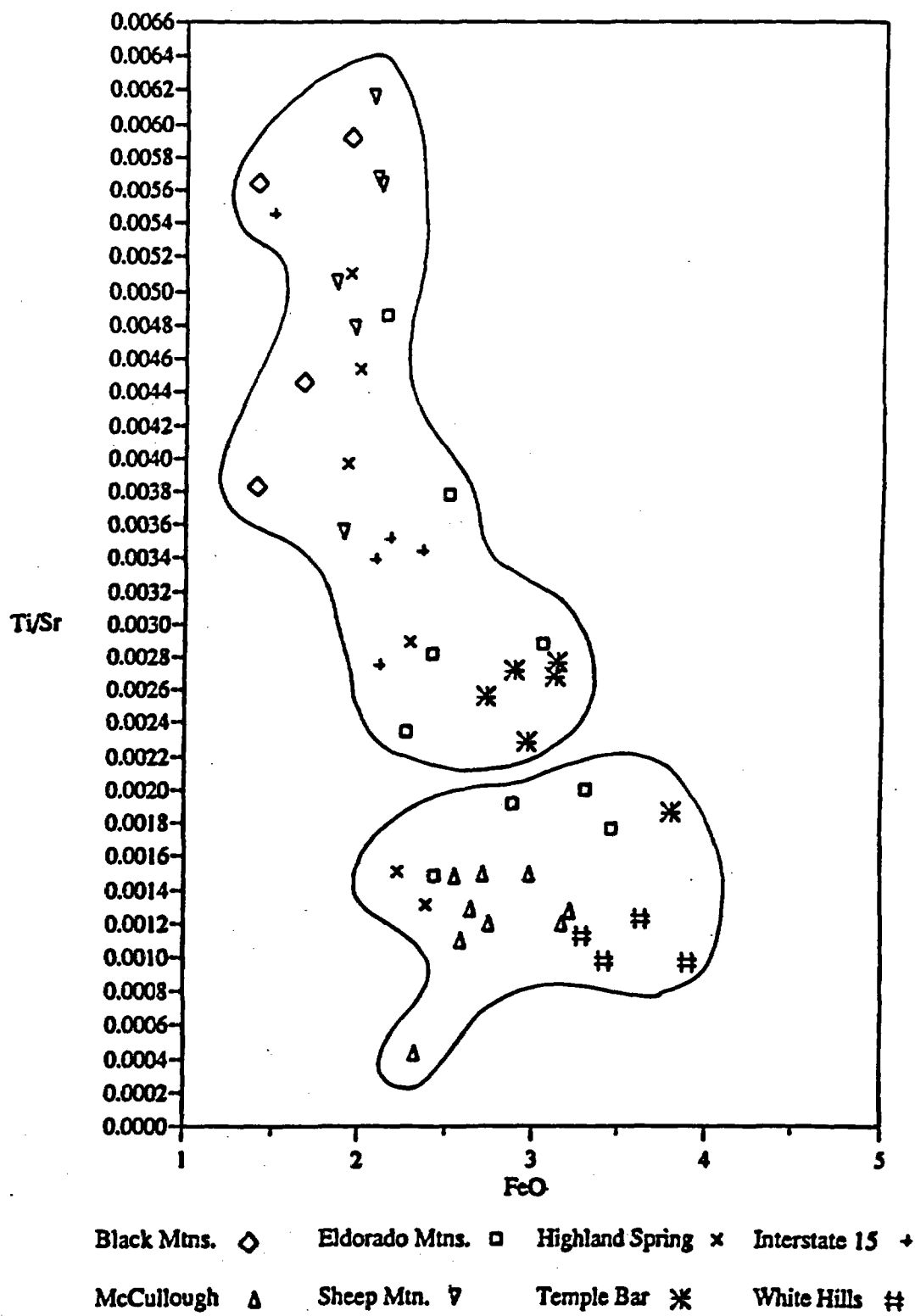


Figure 23. Plot of Ti/Sr vs FeO. See text for explanation.

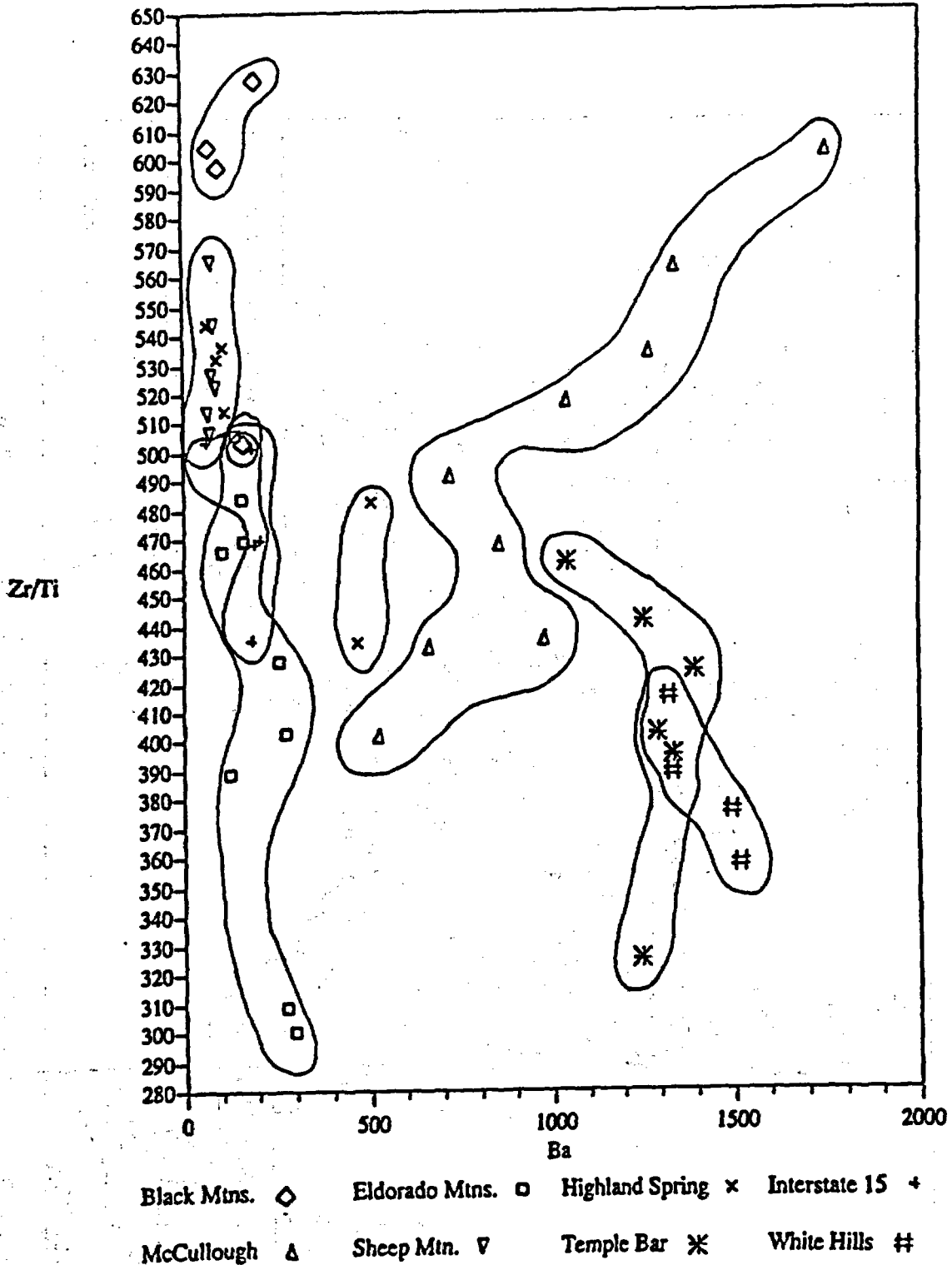


Figure 24. Plot of Zr/Ti vs. Ba showing division of the Tuff of Bridge Spring into variable Zr/Ti, constant Ba group (constant Cr member), and variable Zr/Ti, variable Ba group (variable Cr member).

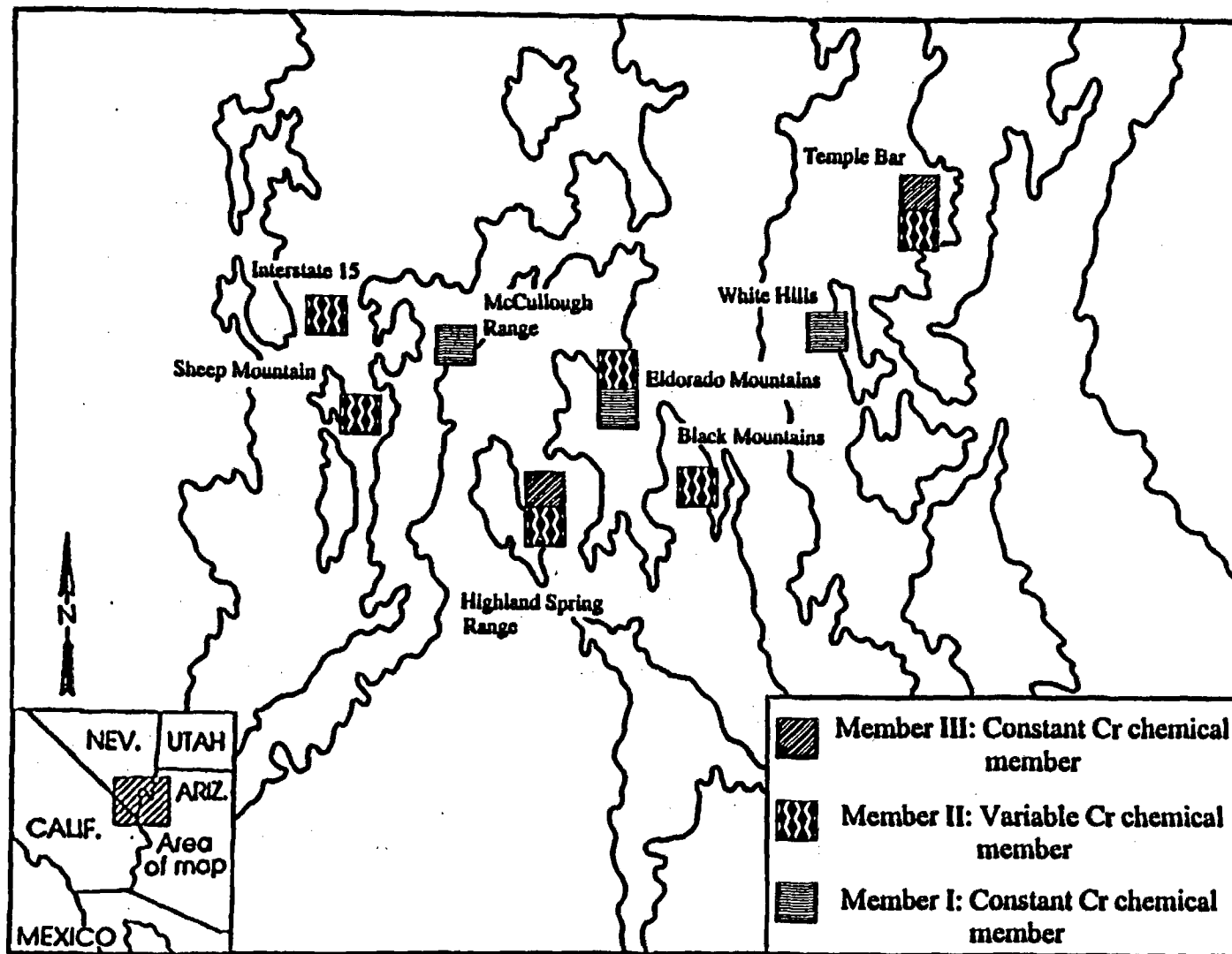


Figure 25. Regional members of the Tuff of Bridge Spring. See text for explanation.

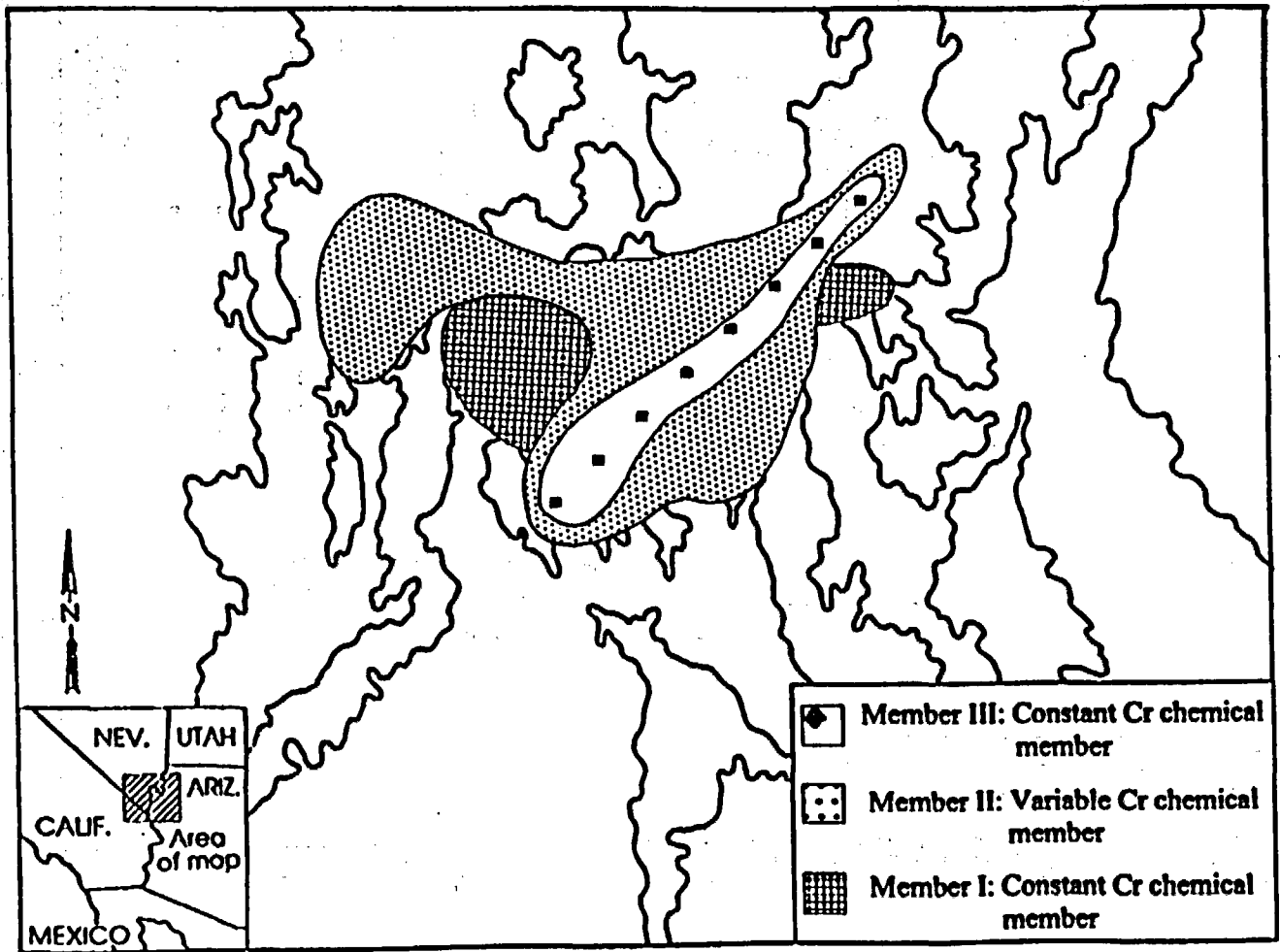


Figure 26. Distribution of the regional members of the Tuff of Bridge Spring.

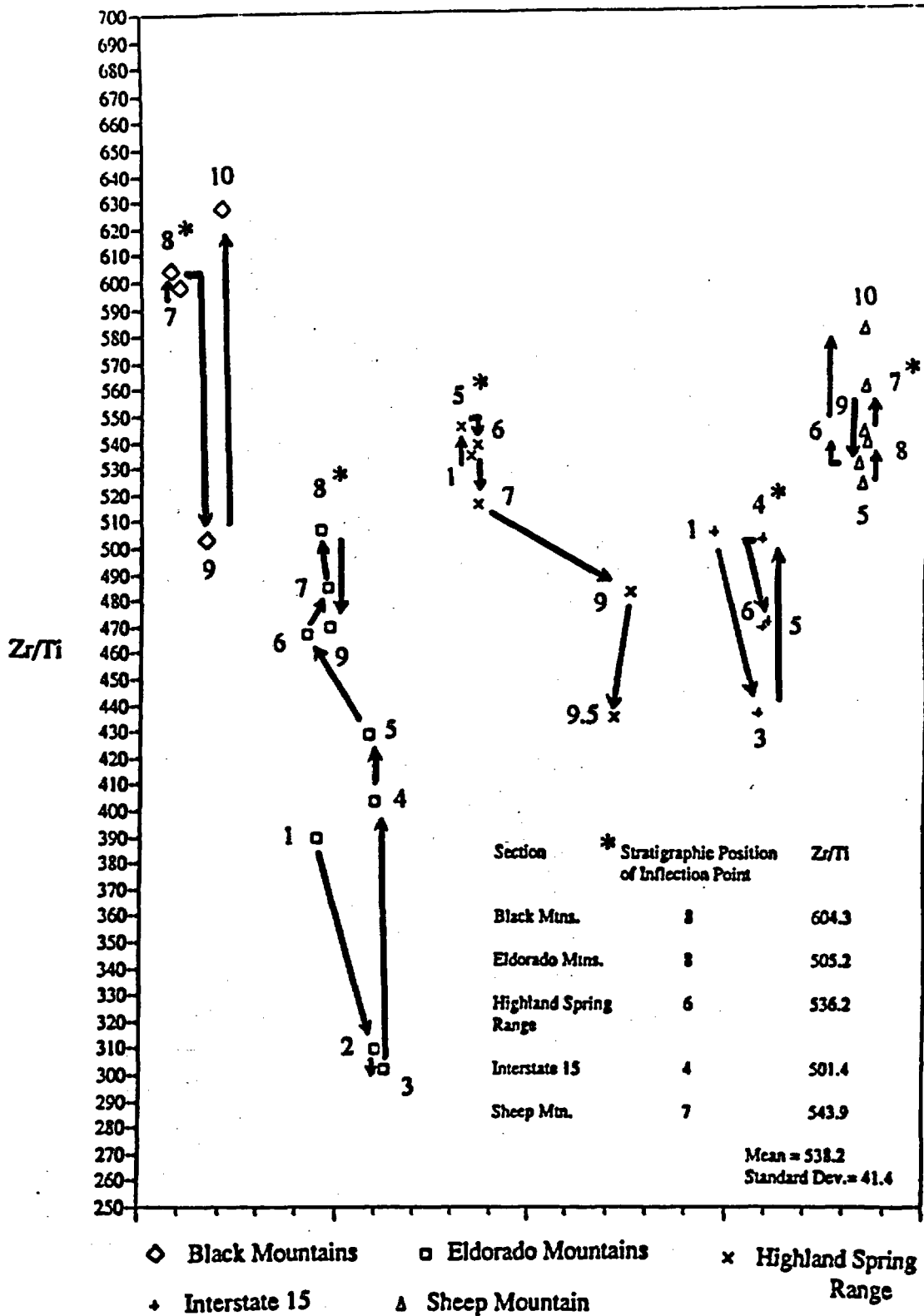


Figure 27. Compilation of plots of sections with variable Zr/Ti, constant Ba showing chemical paths and inflection points. See text for explanation.

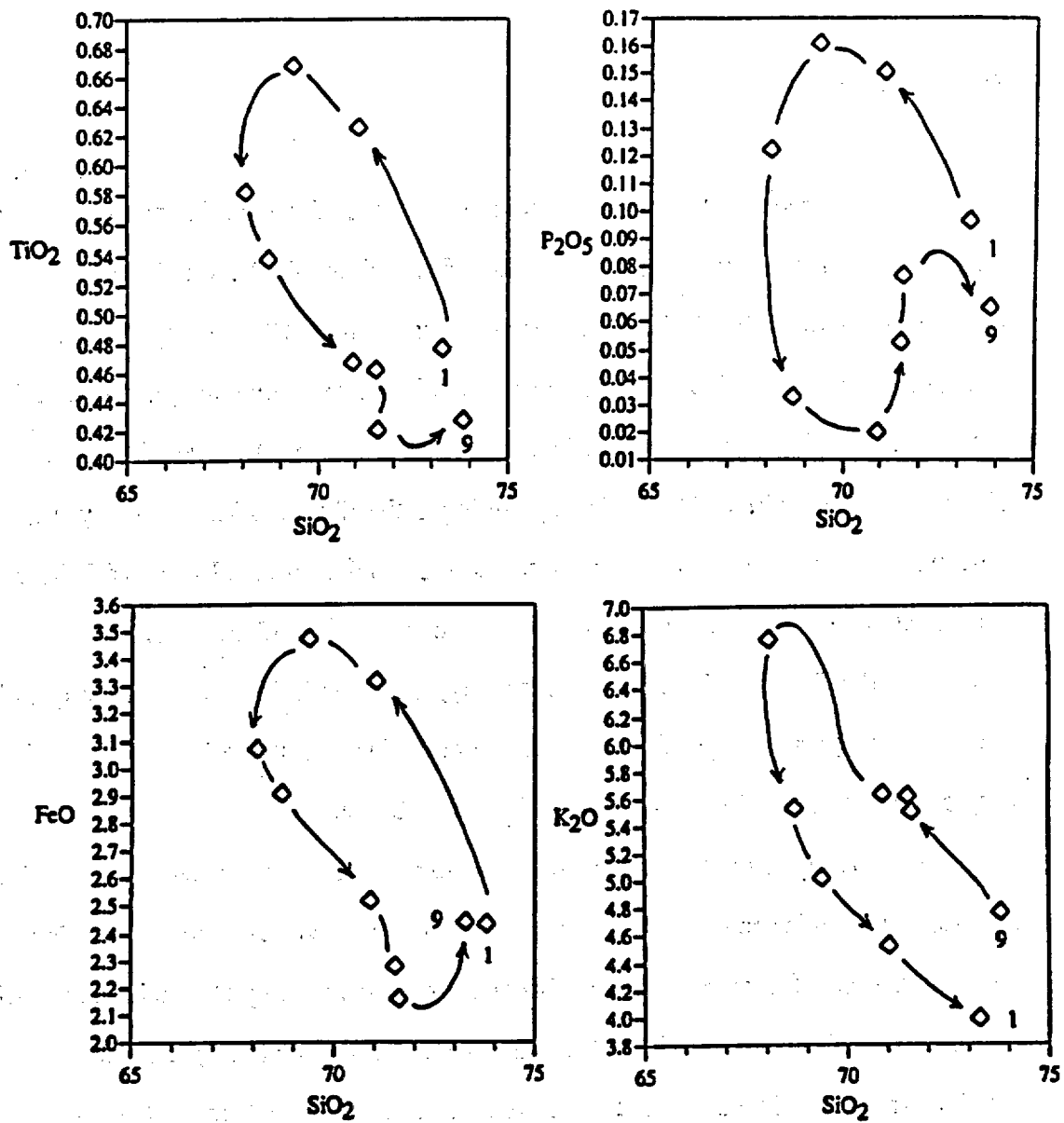


Figure 28. Harker variation plots of the Eldorado Mountains section showing cyclical variation. Numbers indicate relative stratigraphic position of each sample.

Location of Source

Introduction

Several investigators who have utilized the Tuff of Bridge Spring as a marker horizon have also inquired as to the location of its source. Anderson (1971) suggested that the source of the Tuff of Bridge Spring is located in the Chemehuevi Valley, California based on similarities of lithology and phenocryst mineralogy of these rocks to the Tuff of Bridge Spring in the Eldorado Mountains (Fig. 1). Analysis of flow direction indicators in the Tuff of Bridge Spring in the Eldorado Mountains by Brandon (1979) indicated a source to the southwest, perhaps in the Mojave Desert of California. Walker et al. (1981) speculated that the source of the Erie Tuff (the Interstate 15 member of the Tuff of Bridge Spring, this study) is the Devil Peak volcanic complex in the southern Spring Range of Nevada. Hewett (1956) suggested that the Erie Tuff erupted from a source in the western McCullough Range.

In general, correlation of ash-flow tuffs to specific source calderas is difficult in structurally-complex regions like the northern Colorado River extensional corridor. Because regions of intense structural disruption may also be subjected to high rates of erosion and sedimentation, it is probable that the characteristic topographic and lithologic features of calderas and associated intracaldera deposits (e.g., deeply-embayed topographic margins, megabreccia deposits, thick intracaldera fill deposits) may be obscured or obliterated in tectonically-active areas. In the Great Basin, over one hundred ash-flow tuffs of Oligocene to Miocene age are known compared to fewer than 70 caldera structures (Best et al., 1989). The deficit of known calderas compared to outflow sheets indicates that correlations based on "conventional" field studies in highly deformed regions are likely to be unsuccessful or inconclusive.

Because the characteristic features of calderas that crop out in structurally-disrupted regions may either be destroyed or so distorted that field-based identification of these structures is not possible, correlation of outflow sheets to their source (this may be a caldera or a pluton depending upon the degree of erosion) must be established by corroboration of several different criteria. These criteria can include: radiogenic and/or stable isotopes, geochronology, geochemistry, microscopic or macroscopic flow indicators, paleomagnetic signatures, and field relationships. The present study uses radiogenic isotopes as the primary criteria for correlation of the Tuff of Bridge Spring to possible plutonic sources of equivalent age in the extensional corridor. Geochronology (where available), major/trace element analysis, field relationships and associated petrologic studies are used to support isotope-based correlations.

Examination of the data generated during the course of this study indicates that the Aztec Wash pluton, Nevada, and the Mt. Perkins pluton, Arizona are both likely candidates for the intrusive source of the Tuff of Bridge Spring.

Although the Dolan Springs volcanic section does not correlate with the Tuff of Bridge Spring (see correlation section), it is still of considerable interest in this study because the association of the Dolan Springs ash-flow tuff with proximal-type pyroclastic deposits suggests that a caldera structure is located nearby. Also of interest is the close proximity of the Dolan Springs section to the 15.96 Ma Mt. Perkins pluton (Metcalf et al., 1992, 1993). The similarity of the isotopic signatures and ages of the Dolan Springs section and Mt. Perkins pluton and the presence of a major detachment structure (the Mockingbird Mine fault) between the two blocks has important implications for the correlation of the Mt. Perkins pluton to the Dolan Springs section (see discussion below).

Radiogenic Isotopes

Isotopic ratios are not altered by magma fractionation, eruptive, or weathering processes, which makes them excellent indicators of magmatic source (see internal stratigraphy discussion). Variation of isotopic ratios is controlled by conditions which are unique to each magma chamber. These conditions include: the isotopic signature of the contaminant, the amount of contaminant incorporated, and the isotopic signature of the host rock. Consequently, each cogenetic pluton/caldera/outflow suite should possess an unique isotopic signature which can be used as a correlation reference.

Fig. 29 shows the plot of the ϵ_{Nd} vs. $^{87}Sr/^{86}Sr$ values for the Tuff of Bridge Spring and several plutonic and volcanic suites in the northern Colorado River extensional corridor. This plot indicates that the array of the Tuff of Bridge Spring is distinct from both the River Mountains and the White Hills fields, but is coincident with the Nelson/Aztec Wash pluton and the Mt. Perkins pluton data sets. These comparisons suggest that the Tuff of Bridge Spring is cogenetic with both the Aztec Wash and Mt. Perkins plutons.

In general, Pb isotopes are more sensitive indicators of isotopic change (particularly crustal contamination) in evolving magmatic systems than are values of ϵ_{Nd} and $^{87}Sr/^{86}Sr$ (Wilson, 1989). Given this sensitivity, correlation of outflow sheets to possible plutonic equivalents using Pb is generally not attempted. However, several interesting relationships are present in the Tuff of Bridge Spring Pb system that warrant a brief description here.

The plot of $^{87}Sr/^{86}Sr$ vs. $^{206}Pb/^{204}Pb$ (Fig. 30) for the Tuff of Bridge Spring and selected northern Colorado River extensional corridor plutons/volcanic sequences shows that the Tuff of Bridge Spring is isotopically distinct from the Boulder City and Wilson Ridge plutons as well as from the general trend of rocks of the White Hills and

River Mountains. The plot also shows that the trend of the Tuff of Bridge Spring is generally parallel to, but not coincident with, the trend of the Nelson/Aztec Wash plutons. $^{87}\text{Sr}/^{86}\text{Sr}$ vs. $^{206}\text{Pb}/^{204}\text{Pb}$ values of Mt. Perkins quartz diorite and diorite fall significantly off the Tuff of Bridge Spring trend. The isotopic values of the Mt. Perkins pluton granodiorite and gabbro, however, lie at either end of the Tuff of Bridge Spring data array. This relationship suggests that magmatic compositions similar to granodiorite and gabbro of the Mt. Perkins pluton are end members of the Tuff of Bridge Spring mixing array.

Geochronology

An important criterion for correlation of outflow sheets to cogenetic intrusive rocks is radiometric dating (Hildreth and Mahood, 1985; Best et al., 1989). Due to the utility of the Tuff of Bridge Spring as a stratigraphic marker horizon, a considerable number of radiometric age analyses of the Tuff of Bridge Spring are available for comparison to ages of selected plutons. Presently, geochronology of the Tuff of Bridge Spring consists of three $^{40}\text{Ar}/^{39}\text{Ar}$ analyses (two incremental release and two laser fusion analyses) and six K/Ar analyses (Table 7). The presence of substantial discrepancies between $^{40}\text{Ar}/^{39}\text{Ar}$ and K/Ar analyses of the Tuff of Bridge Spring (discussed below) indicates that any final determination of the age of the Tuff of Bridge Spring cannot be made without obtaining additional incremental release $^{40}\text{Ar}/^{39}\text{Ar}$ data on the Tuff of Bridge Spring. In lieu of this work, however, an age of 15.23 ± 0.14 Ma (incremental release Ar/Ar, sanidine, Bridwell, 1991) will be tentatively accepted in this study as being representative of the true age of the Tuff of Bridge Spring. Comparison of this date to radiometric age analyses of the Aztec Wash and Mt. Perkins plutons will also be presented below.

Discrepancies in Tuff of Bridge Spring Geochronology

$^{40}\text{Ar}/^{39}\text{Ar}$ dates of the Tuff of Bridge Spring range from 15.12 ± 0.03 Ma to 15.24 ± 0.01 Ma, and K/Ar analyses range from 14.4 ± 0.5 to 16.6 ± 0.5 Ma (Table 7). In general, inconsistencies in dates generated by the two analytical methods are significant and can be summarized as follows: (1) K/Ar dates are generally 0.80 to 1.37 Ma older than $^{40}\text{Ar}/^{39}\text{Ar}$ values; (2) Tuff of Bridge Spring samples collected from different areas and analyzed using the same method have different dates; and (3) samples collected at different stratigraphic positions from the same section and analyzed by the same method have different dates.

Differences in radiometric dates of the Tuff of Bridge Spring may have resulted from one or more of the following factors: (1) differences in retention of Ar and K in sanidine and biotite; (2) differences due to geographic origin of the sample being analyzed; (3) differences associated with stratigraphic position of the sample; (4) differences generated by the method of analysis chosen; and (5) non-agreement of cross laboratory data (unpublished study, Morikawa, 1993). Although it is generally conceded that the small sample size requirements and high precision of the laser fusion $^{40}\text{Ar}/^{39}\text{Ar}$ method makes it the technique of choice in correlations of ash-flow tuffs (Hildreth and Mahood, 1985), the presence of substantial inconsistencies between $^{40}\text{Ar}/^{39}\text{Ar}$ and K/Ar analyses of the Tuff of Bridge Spring indicate that more information is required to evaluate the effects of these factors on the calculated age of the Tuff of Bridge Spring. Until the reason for these inconsistencies are understood, all dates of the Tuff of Bridge Spring should be regarded with suspicion.

Comparative Geochronology

A recently completed U/Pb analysis by Calvin Miller (personal communication to E.I. Smith, 1993) indicates that the Aztec Wash pluton is 15.12 ± 0.6 Ma old. Laser fusion $^{40}\text{Ar}/^{39}\text{Ar}$ analysis (sanidine) of the Mt. Perkins pluton by Faulds (personal communication to E.I. Smith, 1993) indicates a date of 15.96 ± 0.04 Ma. While the older date of the Mt. Perkins pluton appears to preclude it from consideration as the source of the Tuff of Bridge Spring, it is the contention of this study that any correlation of the Tuff of Bridge Spring to a specific pluton/caldera that is based on either K/Ar or $^{40}\text{Ar}/^{39}\text{Ar}$ geochronology should be considered inconclusive based on the arguments presented above. The U/Pb age of the Aztec Wash pluton, on the other hand, is analytically consistent within uncertainty to the 15.23 ± 0.14 Ma age of the Bridwell (1991) analysis of the Tuff of Bridge Spring. The large uncertainty of the Aztec Wash pluton analysis, however, severely limits its usefulness for correlation purposes.

In summary, correlation of the Tuff of Bridge Spring with the Mt. Perkins and Aztec Wash plutons cannot, at this time, be made on the basis of comparative geochronology due to inconsistencies between K/Ar and $^{40}\text{Ar}/^{39}\text{Ar}$ analyses of the Tuff of Bridge Spring and the large uncertainty of the Aztec Wash pluton analysis.

Geochemistry

Conventional geochemistry-based correlations of volcanic outflow to cogenetic intrusive rocks (e.g., Weber and Smith, 1987) cannot be applied in this study due to lack of available geochemistry of either the Mt. Perkins or the Aztec Wash plutons. Geochemistry-based correlation of both the Aztec Wash and Mt. Perkins plutons to the

Tuff of Bridge Spring is limited, at this time, to two empirical observations. First, the three magmatic systems are highly variable in composition. The Aztec Wash pluton ranges in composition from an olivine gabbro to an aplite ($\text{SiO}_2 = \text{ca. } 50 \text{ to } 76 \text{ wt. } \%$) (Falkner et al., 1993). The Mt. Perkins pluton ranges in SiO_2 composition from 43 to 73 wt. % (Metcalf et al., 1993). The Tuff of Bridge Spring varies from andesite to rhyolite in composition ($\text{SiO}_2 = 57.467 \text{ to } 74.912 \text{ wt. } \%$). The second observation is that the three magmatic systems generally exhibit geochemical signatures that suggest that magma mixing was important in their petrogenesis (Falkner et al., 1993; Metcalf et al., 1993).

Presented below is a more unconventional technique of geochemistry-based correlation developed for this study that uses Zr/Ti vs. Ba chemical paths (previously introduced in the internal stratigraphy section) as points of reference to determine the completeness with which a particular stratigraphic section preserves the chemical evolution of the Tuff of Bridge Spring. This information can then be used to distinguish proximal sections from distal sections, and, by inference, which sections are located closest to the Tuff of Bridge Spring caldera.

Chemical path correlation

Chemical paths, as described previously in the internal stratigraphy section, preserve a sequential chemical record of the magmatic evolution of the Tuff of Bridge Spring. In addition to their utility in regional correlation of Tuff of Bridge Spring flow units, chemical paths can also be used to roughly quantify how completely the chemical record is preserved in a given stratigraphic section. Since proximal pyroclastic deposits contain more complete accumulations of pyroclastic material than more distally located deposits, those sections which are characterized by chemical paths which preserve the

most complete magmatic histories of the Tuff of Bridge Spring, by inference, were deposited in relatively more proximal positions. Determination of the relative proximity of selected sections can then be used much in the same manner as conventional stratigraphic fence diagrams to pinpoint the location of the Tuff of Bridge Spring source.

Fig. 31 shows a plot of an idealized Zr/Ti versus Ba chemical path that preserves the entire magmatic history of a hypothetical, complete stratigraphic section. Also shown is a diagrammatic representation of an idealized, incompletely mixed magma chamber with several Zr/Ti chemical paths. Assuming that the chemical paths preserve a sequential chemical record of the magmatic evolution of the Tuff of Bridge Spring, any point on the chemical path represents a specific magmatic composition that was present in a zoned magma chamber prior to eruption of the Tuff of Bridge Spring. More distally located sections will preserve only fragments of the complete chemical path and more proximal sections will contain more complete records of the path.

The Zr/Ti versus Ba plot of the Tuff of Bridge Spring (Fig. 24) shows that of the five stratigraphic sections that comprise the constant Cr chemical member, the chemical path of the Eldorado Mountains Tuff of Bridge Spring section preserves the most complete record of magmatic evolution of the upper and intermediate levels of the Tuff of Bridge Spring source magma chamber. This implies that the Eldorado Mountains section is the most proximally located of these sections. Similarly, the chemical path of the Highland Spring section, which is the most incomplete of the constant Cr chemical member, implies that early and late occurring flows of the Tuff of Bridge Spring never reached the Highland Spring Range, which was located at the edge of the Tuff of Bridge Spring distribution area. Similarly, chemical path records of both the Sheep Mountain, Interstate 15, and Black Mountains sections preserve magmatic

variations that were present during the middle and late stages of the Tuff of Bridge Spring eruptive sequence.

A proximal deposit should preserve a complete chemical record of a magmatic sequence erupted from a zoned parent chamber. Hypothetically, the chemistry of the most proximally located section of the Tuff of Bridge Spring should have the most complete chemical path on a Zr/Ti vs. Ba plot (i.e., a plot of such a section should preserve both the variable Zr/Ti, constant Ba trend as well as the variable Zr/Ti, variable Ba trend) (Fig. 24). Paradoxically, the Eldorado Mountains section does not preserve such a chemical record. Magmatic variations that characterize the lower levels of the evacuated Tuff of Bridge Spring magma chamber are missing from the chemical path record of this section. This discrepancy may be an artifact of either incomplete sampling or incomplete preservation. The presence of large-scale flow lobes in the Tuff of Bridge Spring in the Eldorado Mountains suggest that ash-flow tuff deposition was laterally discontinuous in the Eldorado Mountains (see field criteria section). This observation suggests that the stratigraphic section chosen for geochemical sampling in the Eldorado Mountains is incomplete. Sampling of a series of sections in the Eldorado Mountains would be required to overcome the effects of laterally-discontinuous exposures.

Field and Petrologic Studies

Conventional field-based correlations of ash-flow tuffs to cogenetic intrusive rocks in tectonically-disrupted regions such as the western United States may be inconclusive or unsuccessful due to problems of preservation, exposure, and/or extreme distortion of contact relationships. However, field studies and related petrographic studies are useful adjuncts to the other correlation criteria employed in this study.

There are many distinctive field indicators that can be used to aid correlation of ash-flow tuffs to cogenetic intrusive rocks. These features include: (1) outcrop-scale field indicators of distal/proximal deposition (these include cooling breaks, coignimbrite lag breccias, differences in modal phenocryst populations, gas segregation features, stratigraphic thicknesses, lobate outcrop habit, surge/airfall deposits, and pumice-rich deposits) (Fisher and Schmincke, 1984); (2) geographical location and spatial relationships of pluton to outflow; and (3) the presence of features commonly associated with calderas including megabreccia deposits, topographic caldera rim, thick intracaldera accumulations, etc.; and (4) the occurrence of magmatic mixing textures in both intrusive and extrusive members of the same cogenetic suite.

Several lines of field evidence support the isotope-based correlation of the Tuff of Bridge Spring to the Aztec Wash pluton (Fig. 4). These include: (1) field indicators of proximal deposition; (2) geographical location of the Aztec Wash pluton with respect to the Tuff of Bridge Spring distribution area; and (3) presence of mixing textures in both the Tuff of Bridge Spring and the Aztec Wash pluton.

Field Indicators

Field indicators of proximal deposition that are present in the Tuff of Bridge Spring in the Eldorado Mountains include lobate bedforms and coignimbrite lag deposits. The presence of complex, large-scale lobate (pinch-and-swell) bedforms exposed in outcrop is one of the most striking outcrop features of the Tuff of Bridge Spring in the Eldorado Mountains. The presence of lobate bedforms indicate ash-flow tuff deposition in either very rough, incised terrain, or in near-vent depositional environments (Fisher and Schmincke, 1984).

Coignimbrite lag deposits, another indicator of near-vent deposition (Fisher and Schminke, 1984), were observed in exposures of Tuff of Bridge Spring that crop out at the Bridge Spring type locality. Tuff of Bridge Spring coignimbrite lag deposits consists of an approximately 1 m thick, laterally-discontinuous interval of lithic tuff that is composed of approximately 39 volume percent of angular to subrounded clasts (< 2 cm) of andesite and basaltic andesite in a glomerocrystic, devitrified matrix that contains phenocrysts of sanidine, plagioclase, biotite, and clinopyroxene.

Location of Pluton

The location of the Aztec Wash pluton in the center of the distribution area of the Tuff of Bridge Spring suggests it is the source of the Tuff of Bridge Spring (Fig. 2). Calderas commonly occur in the centers of radially-distributed outflow sheets in other areas of the Basin and Range (Best et al., 1989). The elongated shape of the present outcrop distribution of the Tuff of Bridge Spring probably resulted from extensional deformation of an ash flow sheet which originally had a circular distribution pattern (c.f., Best et al., 1989).

Magmatic Mixing Textures

The occurrence of magmatic mixing textures in the Tuff of Bridge Spring and in both the Aztec Wash and Mt. Perkins plutons lends support to the hypothesis that the Tuff of Bridge Spring may be related to either one of these intrusive bodies. Falkner et al. (1993) documented impressive magmatic mixing textures in the Aztec Wash pluton including mafic enclaves and the late stage occurrence of mafic and felsic dikes.

Metcalf et al. (1993) reported similar magmatic mixing textures in the Mt. Perkins pluton.

Evidence of magma mixing in the Tuff of Bridge Spring includes the occurrence of banded fiamme in outcrop near the formation's type section, and the possible occurrence of mafic enclaves in outcrop (see lithology section). Microscopic-scale indicators of magma mixing processes present in the tuff include: (1) glomerocrysts, (2) altered mafic enclaves, and (3) disequilibrium textures in plagioclase and potassium feldspar phenocrysts (see lithology section). These characteristics are interpreted here as comprising additional evidence of the occurrence of magma mixing processes in the Tuff of Bridge Spring.

The Dolan Springs Volcanic Section

Similarity of the Nd and Rb isotopic signature of the proximal volcanic deposits of the Dolan Springs section with the Mt. Perkins pluton, their similar ages, and the close proximity of the two magmatic systems (approximately 15 km) suggests they are cogenetic (see regional correlation section). An eastward dipping, low-angle detachment fault, the Mockingbird Mine fault, crops out between the Dolan Springs section and the Mt. Perkins pluton (Faulds, 1989). At the present time, the kinematics of this structure is unknown (Faulds, personal communication to Smith, 1993). Definitive correlation of the Dolan Springs section to the Mt. Perkins pluton must be deferred until the geochemistry and isotope chemistry of the Mt. Perkins pluton is determined, and the kinematics of the Mockingbird Mine fault are understood.

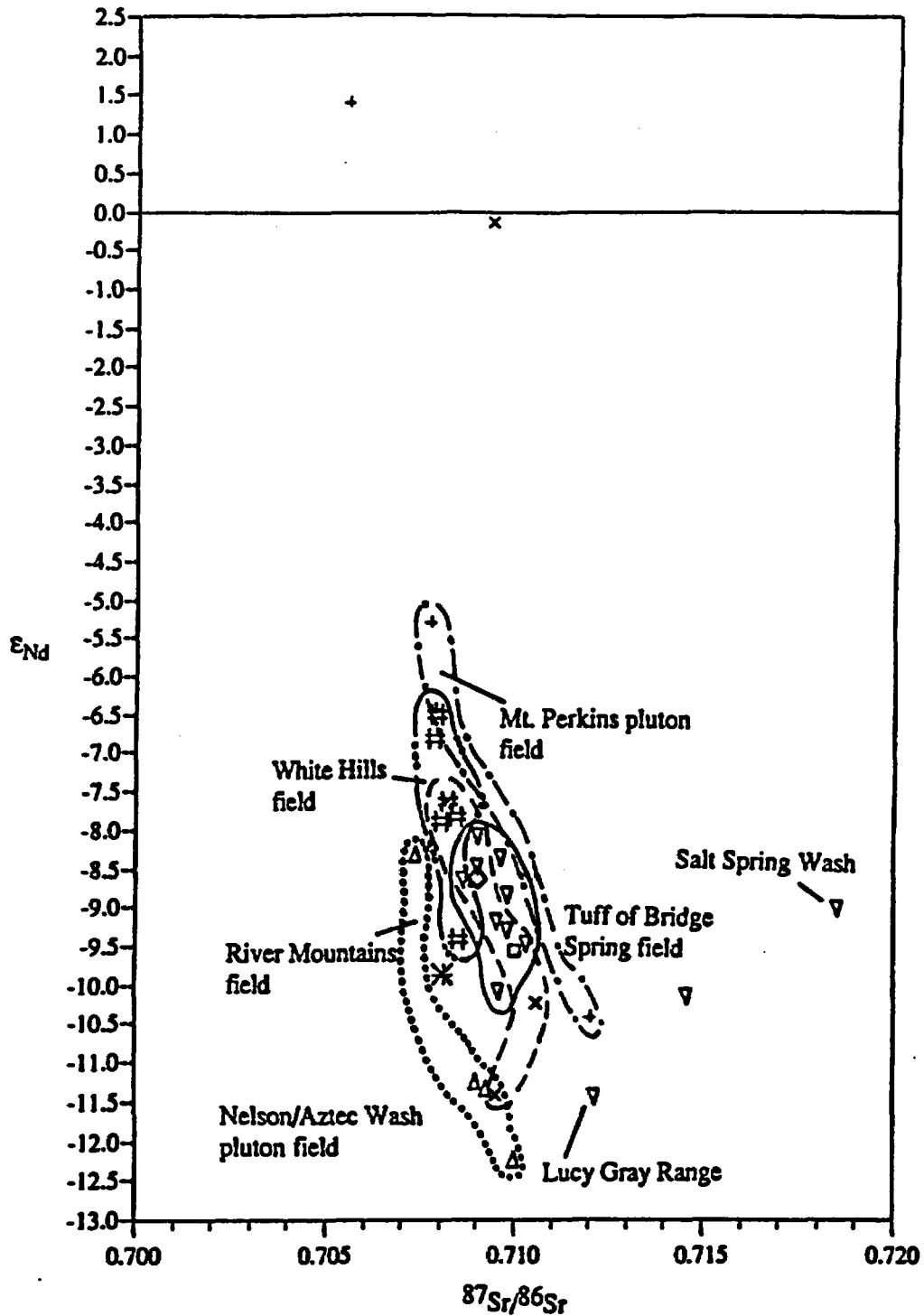
Summary and Conclusion

Correlation of the Tuff of Bridge Spring to the Aztec Wash pluton, Nevada is supported by similarities of isotopic signature, highly variable geochemistry, chemical signatures that are suggestive of magma mixing processes, the presence of magma mixing textures in outcrop, and the occurrence of lobate flow features, coignimbrite lag deposits, and several other field indicators of proximal deposition that are present in the Tuff of Bridge Spring of the Eldorado Mountains. Correlation is also supported by the location of the Aztec Wash pluton near the center of the distribution area of the Tuff of Bridge Spring.

Radiogenic dates of the Tuff of Bridge Spring and the Aztec Wash pluton overlap within uncertainty, but the large error of the Pb date analysis of the Aztec Wash pluton makes any correlation that is based upon radiometric age analyses questionable.

Correlation of the Tuff of Bridge Spring to the Mt. Perkins pluton, Arizona is supported by similarities of isotopic signature, highly variable geochemistry, chemical signatures that are suggestive of magma mixing processes, and the presence of magma mixing textures in outcrops. However, these similarities may indicate that the two entities are not cogenetic, but were derived from similar isotopic reservoirs, and formed by magmatic processes that were operating on a regionally-extensive scale in this area during the middle Miocene. Similarities between the Tuff of Bridge Spring and the Mt. Perkins pluton are also contradicted by the significant differences in age analyses of the two entities. However, correlation of the Mt. Perkins pluton to the Tuff of Bridge Spring cannot be ruled out solely on the basis of radiometric age analyses because the $^{40}\text{Ar}/^{39}\text{Ar}$ and K/Ar geochronology of the Tuff of Bridge Spring has not been satisfactorily resolved.

Final correlation of either pluton to the Tuff of Bridge Spring is dependent upon the identification of intracaldera features in the Eldorado Mountains Tuff of Bridge Spring or in the volcanic cover of the Mt. Perkins pluton.



\diamond Boulder City pluton \square Dolan Springs \times Nelson/Aztec Wash pluton $+$ Mt. Perkins pluton
 Δ River Mountains ∇ Tuff of Bridge Spring \ast Wilson Ridge $\#$ White Hills

Figure 29. Plot of ϵ_{Nd} vs. $^{87}Sr/^{86}Sr$ for the Tuff of Bridge Spring and selected plutons and volcanic suites of the northern Colorado River extensional corridor.

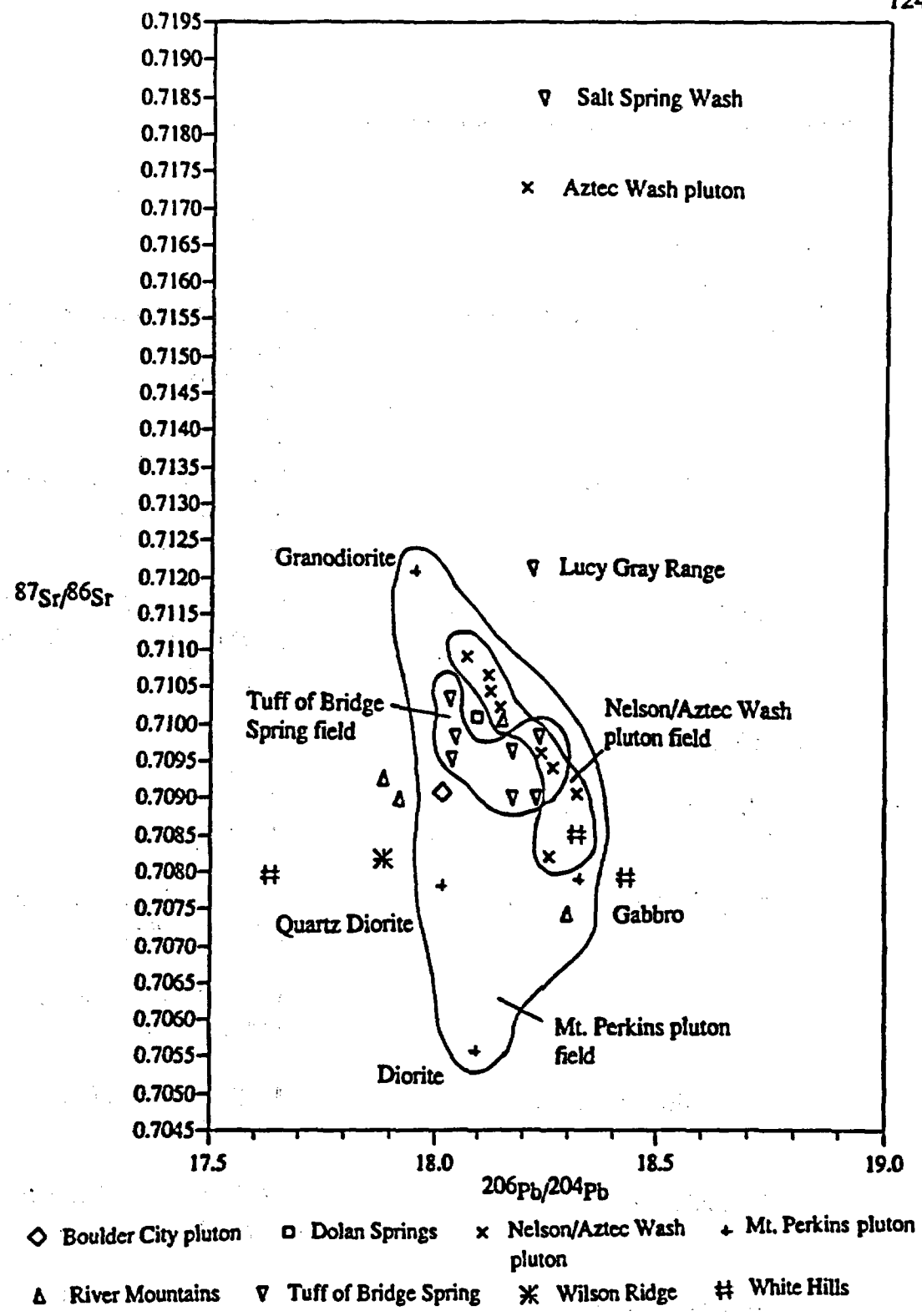


Figure 30. Plot of $^{87}\text{Sr}/^{86}\text{Sr}$ vs. $^{206}\text{Pb}/^{204}\text{Pb}$ for the Tuff of Bridge Spring and selected volcanic complexes and plutons of the northern Colorado River extensional corridor.

Table 7: $^{40}\text{Ar}/^{39}\text{Ar}$ Geochronology of the Tuff of Bridge Spring**Method: $^{40}\text{Ar}/^{39}\text{Ar}$**

Northern Eldorado Mountains, NV	15.12 ± 0.03 Ma (personal commun., (basal cooling unit) Faulds, 1993) (laser fusion-sanidine)
Black Mountains, AZ	15.24 ± 0.01 Ma (personal commun., Faulds, 1993) (laser fusion-sanidine)
McCullough Range, NV	15.23 ± 0.14 Ma (Bridwell, 1991) (incremental release-sanidine)

Method: K/Ar

Eldorado Mountains, NV	15.92 ± 0.36 Ma (Faulds et al., 1992) (biotite)
Eldorado Mountains, NV	14.5 ± 0.6 Ma (Anderson et al., 1972) (sanidine)
	14.4 ± 0.5 Ma (Anderson et al., 1972) (biotite)
Black Mountains, AZ	16.43 ± 0.36 Ma (Faulds et al., 1992) (biotite)
McCullough Range, NV	16.6 ± 0.4 Ma (Bridwell, 1991) (biotite)
White Hills, AZ	16.4 ± 0.5 Ma (Cascadden, 1991) (biotite)

Summary and Conclusion

The Tuff of Bridge Spring (15.23 ± 0.14 Ma) (Bridwell, 1991), a regionally-extensive ash-flow tuff, ranges in composition from andesite to rhyolite (59.50 to 74.91 wt. % SiO_2). The average composition of the Tuff of Bridge Spring is dacite (67 wt. % SiO_2). Phenocrysts include sanidine, plagioclase feldspar, biotite, clinopyroxene, sphene, opaque iron oxide, \pm zircon, and \pm apatite. Hornblende is rare and possibly xenocrystic. Quartz is a not primary phase in the Tuff of Bridge Spring.

Samples of the Tuff of Bridge Spring form linear data arrays on Sm, Rb, and Pb isotope diagrams. The linearity of these data arrays suggest that the Tuff of Bridge Spring is a cogenetic suite that formed as the result of magma mixing. Modelling using crustal and mantle derived contaminants that were present in this region during the Mid-Miocene (i.e., Patsy Mine Volcanics, Precambrian crystalline basement, and alkali olivine basalts) eliminates the possibility that the linear isotope arrays were produced by contamination. Based on these interpretations, and supported by geochemistry, petrology, and geochronology, the following stratigraphic sections are included within the Tuff of Bridge Spring; in Nevada, the Eldorado Mountains, Highland Spring Range, Interstate 15 (near Sloan), Sheep Mountain, and the McCullough Range, and in Arizona, the Black Mountains, Temple Bar, and White Hills. Isotope analyses of the Lucy Gray Range and Salt Spring Wash sections suggest that they are not cogenetic with the Tuff of Bridge Spring. The isotope signature of the Dolan Springs volcanic section falls within the Tuff of Bridge Spring data array, but an incremental release $^{40}\text{Ar}/^{39}\text{Ar}$ date of 16.01 ± 0.15 Ma (biotite; this study, 1993) shows that the section is significantly older than the Tuff of Bridge Spring. These relationships suggests that, although the Dolan Springs section does not correlate with the Tuff of Bridge Spring, the two rock types were derived from a common, regionally-extensive crustal/mantle

source that was present in the extensional corridor during the mid-Miocene. The overlap of ages of the Dolan Springs section with the Mt. Perkins pluton, and the presence of a low-angle detachment structure, the Mockingbird Mine Fault (Faulds, 1981) between the two bodies suggests that the Dolan Springs section may be the volcanic cover of the Mt. Perkins pluton.

The chemical variation in the Tuff of Bridge Spring is remarkably large and exists not only on the regional scale but on the scale of the stratigraphic section. Radical changes in chemical variation within each section form chemical boundaries which can be used to divide each section into a series of eruptive units which are the chemical equivalents of pyroclastic flow units (Smith, 1960). Because the formation of chemical boundaries is controlled by chemical re-equilibration of the magma chamber during periods of quiescence, chemical boundaries do not always coincide with cooling breaks. However, cooling breaks are not always preserved due to devitrification and/or vapor phase crystallization of ash-flow tuffs, which makes the use of chemical breaks and the eruptive unit concept extremely useful for determination of the internal stratigraphy in ash-flow tuffs.

The differential partitioning of elements such as Zr, Y, Cr, Sr, and Ba in the Tuff of Bridge Spring provide a means of dividing the formation into two chemically-distinct members. The constant Cr chemical member, which includes the McCullough Range, lower Eldorado Mountains, White Hills, upper Highland Spring Range, and upper Temple Bar sections, exhibits geochemical trends in which concentrations of Cr generally remain constant with respect to SiO_2 . The variable Cr chemical member exhibits trends in which both Cr and SiO_2 are variable. This chemical member includes the Black Mountain, Interstate 15, upper Eldorado Mountains, lower Highland Spring, lower Temple Bar, and Sheep Mountain sections.

The division of the Tuff of Bridge Spring into three regional-extensive stratigraphic members is based on chemical member assignments and regional stratigraphic relationships. The stratigraphically lower and upper regional members belong to the constant Cr trend and the stratigraphically-intermediate regional member is part of the variable Cr trend. The regional members of the Tuff of Bridge Spring consist of the following (listed in ascending stratigraphic order): (1) Regional Member I: lower Eldorado Mountains, McCullough Range, and White Hills sections; (2) Regional Member II: Interstate 15, Sheep Mountain, lower Highland Springs, upper Eldorado Mountains, and lower Temple Bar; (2) Regional Member III: upper Highland Springs and upper Temple Bar.

Fine-scale chemical variations in the Tuff of Bridge Spring can be used as a stratigraphic marker horizon. A single Zr/Ti vs. Ba chemical marker horizon occurs across 90 km of the tuff's distribution area. The presence of this horizon and the consistent patterns of geochemical partitioning found in the Tuff of Bridge Spring suggests that these patterns reflect chemical boundaries that were present in the Tuff of Bridge Spring magma system at the time of eruption. The presence of the Zr/Ti vs. Ba horizon also implies that, for certain elements, the chemical signatures exhibited by the Tuff of Bridge Spring are magmatic signatures that are not affected by changes in abundances of phenocrysts and/or xenoliths in whole rock samples. For these elements, and especially for Zr, Ti, and Ba, the signature imparted by the tuff's matrix is strong enough to overprint the non-magmatic signature or chemical "static" imparted from phenocrysts and xenoliths incorporated in the tuff.

The different behavior of Cr, Sr, Ba, and other elements in the Tuff of Spring suggests that petrogenesis of the tuff was controlled by two contrasting magmatic processes. The first process involved normal differentiation of a felsic magma in the top of the magma chamber. The second process involved injection of a mafic magma

into the lower part of the chamber and subsequent incomplete mixing of the two. The occurrence of these two processes are reflected in the assignments of the three regional members of the Tuff of Bridge Spring. The chemical signature of Regional Member I (constant Cr, variable SiO₂) reflects derivation from the top of a normally-zoned, felsic magma chamber. The chemistry of Regional Member II reflects derivation from a magma batch whose variable Cr, variable SiO₂ signature indicates injection and incomplete incorporation of a mafic magma into a felsic magma. The chemical signature of Regional Member III (constant Cr, variable SiO₂) indicates the return of the magma chamber to more felsic conditions. This model is supported by petrologic evidence including disequilibrium textures in feldspars and the rare presence of mafic enclaves.

Correlation of the Tuff of Bridge Spring to various plutons in the northern Colorado River extensional corridor by means of isotopic analysis suggests that both the Aztec Wash pluton, Nevada and the Mt. Perkins pluton, Arizona are likely sources for the Tuff of Bridge Spring. Isotope-based correlation of the Aztec Wash pluton to the Tuff of Bridge Spring is supported by several field indicators of proximal deposition, the presence of magma mixing textures, location near the center of the tuff's distribution center, and similarities in geochronology. Although the isotope signature of the Mt. Perkins pluton falls within the Tuff of Bridge Spring array, correlation of the Tuff of Bridge Spring to the Mt. Perkins pluton is not as well supported as the correlation with the Aztec Wash pluton. Also, dates of the two rock types are significantly different. However, the presence of consistent discrepancies between ⁴⁰Ar/³⁹Ar and K/Ar dates for the Tuff of Bridge Spring indicates that the geochronology of the tuff has not been adequately constrained. Therefore, correlation of the Mt. Perkins to the Tuff of Bridge cannot be ruled out.

Future Work

The following studies are recommended for future research in order to resolve several unanswered questions concerning the Tuff of Bridge Spring.

(1) Confirmation and refinement of the chemical member concept requires that analysis of Tuff of Bridge Spring for rare-earth elements (REE) geochemistry be completed.

(2) Microprobe analysis of tuff matrix and phenocrysts/xenoliths in whole rock tuff samples could not only be used to confirm the role of matrix in controlling the isotopic signature of the Tuff of Bridge Spring, but theoretically also could be used to numerically model/quantify the effects of chemical interferences imparted by phenocrysts/xenoliths.

(3) Resolution of the problems concerning $^{40}\text{Ar}/^{39}\text{Ar}$ and K/Ar analyses of the Tuff of Bridge Spring would require extensive dating of several sections using both incremental release and laser fusion $^{40}\text{Ar}/^{39}\text{Ar}$ techniques on both sanidine and biotite.

(4) Correlation of the Tuff of Bridge Spring to either the Mt. Perkins pluton or the Aztec Wash pluton is dependent on locating a caldera in the vicinity of either of those plutons. However, locating such a structure may not be possible. Correlation of the Tuff of Bridge Spring specifically to the Aztec Wash pluton could be strengthened by geochemical comparison.

(5) Correlation of the Dolan Springs section to the Mt. Perkins pluton requires detailed mapping of both the Mockingbird Mine fault and the Dolan Springs volcanic section.

References Cited

- Anderson, R.E., 1971, Thin skin distension in Tertiary rocks of southeastern Nevada: Geological Society of America Bulletin, v. 82, p. 43-58.
- Anderson, R.E., 1973, Large-magnitude late Tertiary strike-slip faulting north of Lake Mead, Nevada: U.S. Geological Survey Professional Paper 794, 18 p.
- Anderson, R.E., Longwell, Cr.R., Armstrong, R.L., and Marvin, R.F., 1972, Significance of K-Ar ages of Tertiary rocks from the Lake Mead region, Nevada-Arizona: Geological Society of America Bulletin, v. 83, no. 2, p. 273-288.
- Bennett, V.C., and DePaolo, D.J., 1987, Proterozoic crustal history of the western United States as determined by neodymium isotopic mapping; Geological Society of America Bulletin, v. 99, p. 674-685.
- Best, M.G., Christiansen, E.H., Deino, A.L., Gromme, C.S., McKee, E.H., and Noble, D.C., 1989a, Eocene through Miocene volcanism in the Great Basin of the western United States: New Mexico Bureau of Mines and Mineral Resources Memoir 47, p. 91-133.
- Brandon, C.F., 1979, Flow direction studies of the Tuff of Bridge Spring, Nevada: Senior Project, University of Wisconsin-Parkside (unpublished).
- Bridwell, H.L., 1991, The Sloan Sag: a mid-Miocene volcanotectonic depression, north-central McCullough Mountains, southern Nevada [M.S. thesis]: Las Vegas, Nevada, University of Nevada, 147 p.
- Carmichael, I.S.E., Turner, F.J., and Verhoogan, J., 1974, Igneous Petrology: New York, McGraw Hill Book company, 739 p.
- Cas, R.A.F., and Wright, J.V., 1987, Volcanic successions: Ancient and modern: London, United Kingdom, Allen and Unwin, 528 p.

- Cascadden, T.E., 1991, Style of volcanism and extensional tectonics in the eastern Basin and Range province: northern Mojave County, Arizona [M.S. thesis]: Las Vegas, Nevada, University of Nevada, 156 p.
- Choukroune, P., and Smith, E.I., 1985, Detachment faulting and its relationship to older structural events on Saddle Island, River Mountains, Clark County, Nevada: *Geology*, v. 13, p. 421-424.
- Cole, E.D., 1989, Petrogenesis of late Cenozoic alkalic basalt near the eastern boundary of the Basin-and-Range: Upper Grand Wash Trough, Arizona and Gold Butte, Nevada [M.S. thesis]: Las Vegas, Nevada, University of Nevada, 68 p.
- Daley, E.E., 1992, Temporal and spatial variations in compositions of young mafic volcanic rocks of the southwestern Basin and Range: Isotopic constraints on the relationship between thinning in the lithosphere and extensional deformation in the upper crust [Phd. dissertation]: Berkeley, California, University of California, 205 p.
- Darval, P., 1991, Normal faulting in the Eldorado Mountains, southeastern Nevada: *Geological Society of America Abstracts with Programs*, v. 23, no. 2, p. 17.
- Davidson, J.P., De Silva, S.L., Holden, Peter, and Halliday, A.N., 1990, Small-scale disequilibrium in a magmatic inclusion and its more silicic host: *Journal of Geophysical Research*, v. 95, p. 17661-17675.
- Davis, S.O., 1984, Structural geology of the central portion of the Highland Spring Range, Clark County, Nevada [M.S. thesis]: Los Angeles, California, University of California, 190 p.
- Duebendorfer, E.M., and Smith, E.I., 1991, Tertiary structure, magmatism, and sedimentation in the Lake Mead region, southern Nevada, *in* Seedorf, E., *Tertiary Geology and Volcanic-hosted Gold Deposits of the Southern Great Basin and Vicinity*; Geological Society of Nevada, Special Publication no.13, p. 66-86.

- Duebendorfer, E.M., and Wallin, E.T., 1991, Basin development and syntectonic sedimentation associated with kinematically-coupled strike-slip and detachment faulting, southern Nevada: *Geology*, v. 19, p. 87-90.
- Duebendorfer, E.M., Sewell, A.J., and Smith, E.I., 1990, The Saddle Island detachment; An evolving shear zone in the Lake Mead area, Nevada: *in* Wernicke, B.P., ed., Basin and Range extensional tectonics near the latitude of Las Vegas, Nevada: Geological Society of America Memoir 176, p. 77-97.
- Falkner, C.M., Miller, C.F., and Wooden, J.L., 1993, Petrology of the Aztec Wash pluton, Eldorado Mountains, southern Nevada: Geological Society of America Abstracts with Programs, v. 25, no. 5, p. 36.
- Faulds, J.E., 1989, Structural development of a major extensional accommodation zone in the Basin and Range province, northwestern Arizona and southern Nevada: Implications for kinematic models of continental extension [Ph.D. dissertation]: Albuquerque, New Mexico, University of New Mexico, 263 pgs.
- Faulds, J.E., Geissman, J.W., and Mawer, C.K., 1990, Structural development of a major extensional accommodation zone in the Basin and Range province, northwestern Arizona and southern Nevada; Implications for kinematic models of continental extension: *in* Wernicke, B.P., ed., Basin and Range extensional tectonics near the latitude of Las Vegas, Nevada: Geological Society of America Memoir 176, p. 37-76.
- Faulds, J.E., Geissman, J.W., and Shafiqullah, Muhammad, 1992, Implications of paleomagnetic data on Miocene extension near a major accommodation zone in the Basin and Range province, northwestern Arizona and southern Nevada: *Tectonics*, v. 11, no. 2, p. 204-227.
- Feuerbach, D.L., Smith, E.I., Walker, J.D., and Tangeman, J.A., 1993, The role of the mantle during crustal extension: Constraints from geochemistry of volcanic rocks in the Lake Mead area, Nevada and Arizona: Geological Society of America Bulletin (in press).

- Fisher, R.V., and Schmincke, H.-U., 1984, *Pyroclastic Rocks*: Berlin, Germany, Springer-Verlag, 472 p.
- Hewett, D.F., 1956, *Geology and mineral resources of the Ivanpah Quadrangle, California and Nevada*: U.S. Geological Survey Professional Paper 275, 172 p.
- Hildreth, W., and Mahood, G.A., 1985, *Correlation of ash-flow tuffs*: Geological Society of America Bulletin, v. 96, p. 968-974.
- Hutchison, C.S., 1974, *Laboratory Handbook of Petrographic Techniques*: New York, John Wiley and Sons, 527 p.
- Koyaguchi, T., 1986, *Textural and compositional evidence for magma mixing and its mechanism, Abu volcano group, southwestern Japan*: Contributions in Mineralogy and Petrology, v. 93, p. 33-45.
- Larsen, L.L., 1990, *Significance of mafic enclaves in the Wilson Ridge pluton, Mojave County, Arizona* [M.S. thesis]: Las Vegas, Nevada, University of Nevada, 81 p.
- Larsen, L.L., and Smith, E.I., 1990, *Mafic Enclaves in the Wilson Ridge pluton, northwestern Arizona: Implications for the generation of a calc-alkaline intermediate pluton in an extensional environment*: Journal of Geophysical Research, v. 95, no. B11, p. 17693-17716.
- Lipman, P.W., 1976, *The roots of ash flow calderas in western North America: Windows into the tops of granitic batholiths*: Journal of Geophysical Research, v. 89, p.8801-8841.
- Longwell, C.R., 1963, *Reconnaissance geology between Lake Mead and Davis Dam, Arizona-Nevada*: U.S. Geological Survey Professional Paper 374-E, p. E1-E51.
- Metcalf, R.V., Smith, E.I., Nall, K.E., and Reed, R.C., 1992, *The Mt. Perkins pluton: Shallow-level magma mixing and mingling during Miocene extension*: Geological Society of America Abstracts with Programs, v.24, no. 7, p. 87.

- Metcalf, R.V., Smith, E.I., and Martin, M.W., 1993, Isotopic evidence of source variations in commingled magma systems: Colorado River extensional corridor, Arizona and Nevada: Geological Society of America Abstracts with Programs, Nevada, v. 25, no. 5, p. 120.
- Mills, J.G., 1985, The geology and geochemistry of volcanic and plutonic rocks in the Hoover Dam 7 1/2 Quadrangle, Clark County, Nevada, and Mohave County, Arizona [M.S. thesis]: Las Vegas, Nevada, University of Nevada, 119 p.
- Mills, J.G., 1991, The Timber Mountain Tuff, southwestern Nevada volcanic field: Geochemistry, mineralogy and petrogenesis [Ph.D. dissertation]: East Lansing, Michigan, Michigan State University, 332 p.
- Mills, J.G., 1993, The production of intermediate magmas through magma mixing and commingling: Evidence from the Hoover Dam Volcanics, Mohave County, Arizona and Clark County, Nevada: Geological Society of America Abstracts with Programs, v. 25, no. 5, p. 123.
- Naumann, T.R., 1987, Geology of the central Boulder Canyon quadrangle, Clark County, Nevada [M.S. thesis]: Las Vegas, Nevada, University of Nevada, 69 p.
- Noorish, K., and Hutton, J.T., 1969, An accurate X-ray spectrographic method for the analysis of a wide range of geological samples: *Geochimica et Cosmochimica Acta*, v. 33, p. 431-453.
- Rowland, S.M., Parolini, J.R., Eschner, E., and McAllister, A.J., 1990, Sedimentologic and stratigraphic constraints on the Neogene translation and rotation of the Frenchman Mountain structural block, Clark County, Nevada, *in* Wernicke, B.P., ed., Basin and Range extensional tectonics near the latitude of Las Vegas, Nevada: Geological Society of America Memoir 176, p. 99-121.
- Schmidt, C.E., 1987, A mid-Miocene caldera in the central McCullough Mountains, Clark County, Nevada [M.S. thesis]: Las Vegas, Nevada, University of Nevada, 78 p.

- Seaman, S.J., and Ramsey, P.C., 1992, Effects of magma mingling in the granites of Mount Desert Island, Maine: *Journal of Geology*, v. 100, p. 395-409.
- Smith, E.I., 1982, Geology and geochemistry of the volcanic rocks in the River Mountains, Clark County, Nevada and comparisons with volcanic rocks in nearby areas, *in* Frost, E.G., and Martin, D.L., eds., *Mesozoic-Cenozoic tectonic evolution of the Colorado River region, California, Arizona, and Nevada*: San Diego, California, Cordilleran Publishers, p. 42-54.
- Smith, E.I., Schmidt, C.S., and Mills, J.G., 1988, Mid-Tertiary Volcanoes in the Lake Mead area of southern Nevada and northwestern Arizona, *in* Weide, D.L., and Faber, M.L., eds., *This extended land: Geological journeys in the southern Basin and Range; Geological Society of America Fieldtrip Guidebook, Cordilleran Section Meeting, Las Vegas, Nevada*: University of Nevada at Las Vegas Department of Geoscience Special Publication 2, p. 107-122.
- Smith, E.I., Feuerbach, D.L., Naumann, T.R., and Mills, J.E., 1990, Geochemistry and evolution of mid-Tertiary igneous rocks in the Lake Mead area of Nevada and Arizona, *in* Anderson, J.L., ed., *Cordilleran Magmatism: Geological Society of America Memoir 176*, p. 169-194.
- Smith, R.L., 1960, Ash flows: *Geological Society of America Bulletin*, v. 71, p. 795-842.
- Tuma-Switzer, T.E., and Smith, E.I., 1993, Geology of the Henderson Volcanic Complex, northern McCullough Mountains, Clark County, Nevada; Abstract: *Journal of the Arizona-Nevada Academy of Science; Thirty-seventh annual meeting, Las Vegas, Nevada, April 17, 1993*, p. 44-45.
- Valentine, G.A., Wohletz, K.H., and Kieffer, S.W., 1992, Effects of topography on facies and compositional zonation in caldera-related ignimbrites: *Geological Society of America Bulletin*, v. 104, p. 154-165.

Walker, J.D., Beaufait, M.S., and Zelt, F.B., 1981, Geology of the Devil Peak area, Spring Mountains, Nevada: Geological Society of America Abstracts with Programs, Cordilleran Section, v. 13, no. 2, p. 112.

Weber, M.E., and Smith, E.I., 1987, Structural and geochemical constraints on the reassembly of disrupted volcanoes in the Lake Mead-Eldorado Valley area of southern Nevada: *Geology*, v. 15, p. 553-556.

Wernicke, B.J., Axen, G.J., and Snow, J.K., 1988, Basin and Range extensional tectonics at the latitude of Las Vegas, Nevada: *Geological Society of America Bulletin*, v. 100, p. 1738-1757.

Wilson, B.M., 1989, *Igneous petrogenesis: A global tectonic approach*: London, United Kingdom, Unwin Hyman, p. 466.

Wooden, J.L., and Miller, D.M., 1990, Chronologic and isotopic framework for early Proterozoic crustal evolution in the eastern Mojave Desert region, southeastern California: *Journal of Geophysical Research*, v. 95, no. B12, pgs. 20,146-21,133.

Young, R.A., and Brennan, W.J., 1989, Peach Springs Tuff: Its bearing on structural evolution of the Colorado Plateau and development of Cenozoic drainage in Mohave County, Arizona: *Geological Society of America Bulletin*, v. 85, p. 83-90.

Appendix A: Major and Trace Element Analyses. Major element oxides in wt.% and trace elements in ppm.

Sample	92-BM1-2	92-BM1-1	92-BM1-4	92-BM1-3	93-DS7-1	93-DS7-2	93-DS7-3	92-E3-1	92-E3-2	92-E3-3
Position	7	8	9	10	10.5	10	3.5	1	2	3
SiO ₂	69.48	69.8	66.14	68.80	72.91	71.45	72.91	65.58	64.23	62.6
Al ₂ O ₃	11.84	12.55	11.41	14.00	12.5	12.61	12.60	13.34	13.81	14.16
TiO ₂	0.24	0.26	0.29	0.32	0.18	0.23	0.23	0.43	0.57	0.60
FeO	1.30	1.33	1.54	1.89	1.18	1.60	1.56	2.18	3.00	3.13
CaO	2.12	2.24	4.05	1.22	1.05	2.13	2.50	3.03	2.99	3.2
K ₂ O	5.95	6.23	5.78	6.33	5.24	4.49	5.20	3.56	4.08	4.53
MnO	0.03	0.04	0.04	0.04	0.04	0.05	0.06	0.06	0.07	0.07
P ₂ O ₅	0.005	0.03	0.08	0.02	0.06	0.08	0.12	0.09	0.14	0.14
Na ₂ O	1.57	1.57	1.57	4.02	2.79	3.15	2.85	0.14	0.14	0.14
MgO	0.21	0.31	0.24	0.14	0.51	0.745	0.46	1.05	1.36	1.66
LOI	N/A	1.90	N/A	4.30	N/A	N/A	N/A	10.57	N/A	N/A
Total	92.76	96.27	91.14	101.09	96.45	96.56	97.24	100.04	90.39	90.24
Cr	2.514	2.166	28.005	41.914	25.805	40.581	47.312	23.07	23.353	25.315
Nb	43.457	40.31	36.715	44.644	18.715	18.712	17.148	35.966	34.638	33.797
Ni	8.193	10.511	15.188	17.715	10.441	15.423	16.683	18.956	30.435	27.558
Rb	204	221	193	211	143	124	108	130	124	140
Sr	68	49	71	57	125	196	165	322	314	379
Th	37.154	39.242	34.225	29.946	15.913	14.037	13.225	31.512	32.182	27.408
Y	27.594	29.062	27.898	29.567	22.116	21.42	20.648	27.244	27.187	27.212
Zr	261	277	267	350	101	122	114	309	322	335
Ba	100	75	165	205	240	356	331	129	280	300

Appendix A, continued.

Sample	92-E3-4	92-E3-5	92-E3-6	92-E3-10	92-E3-9	92-E3-8	92-HS1-5	92-HS2-1	92-HS2-4	92-HS2-2
Position	4	5	6	7	8	9	1	5	6	7
SiO2	66.96	67.12	70.18	68.00	69.93	71.58	69.17	72.91	70.46	72.38
Al2O3	15.13	14.92	15.29	14.36	14.34	12.85	14.32	15.28	14.70	14.98
TiO2	0.57	0.52	0.46	0.44	0.41	0.41	0.35	0.39	0.35	0.38
FeO	3.02	2.84	2.49	2.16	2.11	2.36	2.24	2.01	1.89	2.03
CaO	1.66	1.62	1.17	1.72	0.97	1.15	0.84	1.06	0.91	0.92
K2O	6.65	5.40	5.57	5.34	5.37	4.62	5.57	5.71	5.44	5.66
MnO	0.07	0.06	0.08	0.07	0.07	0.05	0.07	0.07	0.07	0.07
P2O5	0.12	0.03	0.02	0.05	0.08	0.06	0.02	0.04	0	0
Na2O	3.15	4.31	3.026	2.30	3.90	3.35	4.05	5.15	3.76	4.31
MgO	1.0	0.84	0.66	0.61	0.48	0.52	0.50	0.42	0.2	0.42
LOI	1.72	N/A	N/A	N/A	N/A	N/A	0.64	N/A	N/A	N/A
Total	100.05	97.68	98.95	95.05	97.68	96.96	97.77	103.04	97.78	101.14
Cr	26.846	25.341	23.823	24.158	24.993	23.414	24.963	10.648	8.35	3.326
Nb	38.44	41.687	38.196	42.652	35.755	35.533	51.876	46.255	42.431	38.646
Ni	24.426	25.235	18.19	21.439	18.321	19.121	21.356	17.68	10.48	11.18
Rb	230	192	189	188	184	165	214	202	203	180
Sr	203	280	124	196	87	152	125	74	90	82
Th	35.418	33.658	39.683	38.783	35.602	29.093	44.631	34.12	29.254	29.744
Y	30.965	29.756	30.028	30.087	29.118	28.218	29.91	30.632	30.3	29.114
Zr	390	382	362	372	354	334	320	344	319	319
Ba	277	264	106	161	144	168	95	69	110	118

Appendix A, continued.

Sample	92-HS2-3	92-HS1-1	93-I151-1	93-I151-3	93-I151-4	93-I151-6	93-I151-5	92-LG1-1	92-LG1-2	92-M2-1
Position	9	9.5	1	3	4	5	6	8	9	5
SiO2	71.02	68.72	68.02	68.35	68.92	68.106	68.083	72.06	70.28	67.15
Al2O3	15.05	14.52	13.46	14.5	14.37	14.502	14.401	14.15	13.79	11.67
TiO2	0.41	0.44	0.32	0.45	0.41	0.422	0.407	0.28	0.29	0.41
FeO	2.23	2.34	1.44	2.11	2.17	2.079	2.316	1.77	1.7	2.12
CaO	1.68	1.43	2.85	2.66	2.31	2.741	2.288	0.86	0.69	3.3
K2O	5.44	5.29	4.82	6.01	5.66	5.747	5.696	5.24	5.73	2.39
MnO	0.07	0.07	0.07	0.08	0.08	0.074	0.082	0.06	0.06	0.06
P2O5	0.02	0.13	0.04	0.09	0.07	0.061	0.067	0.05	0.05	0.11
Na2O	3.16	4.25	4.35	4.40	4.55	4.485	3.883	4.07	4.25	2.02
MgO	0.87	0.71	0.44	0.9	0.72	0.862	0.607	0.34	0.2	1.94
LOI	N/A	1.03	N/A	1.45	N/A	N/A	0.17	0.4	0.23	N/A
Total	99.95	98.93	95.81	101	99.27	99.079	98	99.28	97.27	91.17
Cr	15.307	24.497	0	27.852	66.861	19.505	66.894	24.201	23.897	23.723
Nb	38.002	36.496	44.552	46.137	43.578	42.506	42.558	32.08	30.592	28.325
Ni	13.512	20.934	10.074	18.001	16.643	16.145	19.94	19.135	19.812	21.909
Rb	169	175	223	188	187	184	187	190	214	36
Sr	271	345	62	163	116	125	121	43	35	1083
Th	32.106	34.485	36.607	32.303	31.131	29.258	32.078	24.964	24.602	23.297
Y	27.937	27.483	30.314	29.909	29.971	30.003	29.702	30.36	30.824	22.859
Zr	329	325	285	325	342	334	325	261	258	301
Ba	511	477	63	188	185	207	192	28	102	530

Appendix A, continued.

Sample	91-M1-1	91-M1-2	92-M3-1	92-M2-2	91-M1-3	92-M3-4	91-M1-4	92-M3-5	91-SM1-1	92-SM2-1
Position	6	7	7.5	8	9	9.5	10	10.5	5	6
SiO ₂	62.55	62.84	62.16	65.17	66.39	66.56	64.94	66.076	63.84	65.69
Al ₂ O ₃	16.1	16.05	16.08	14.61	15.34	15.09	15.92	15.92	13.09	13.71
TiO ₂	0.6	0.59	0.6	0.46	0.47	0.48	0.50	0.46	0.32	0.35
FeO	3.06	2.84	3.06	2.41	2.63	2.61	2.68	2.55	1.74	1.75
CaO	2.14	2.08	2.59	1.84	1.90	2.76	2.79	2.21	3.22	1.39
K ₂ O	6.02	5.56	5.28	4.48	5.05	5.31	5.25	5.41	5.15	5.40
MnO	0.07	0.06	0.07	0.07	0.07	0.07	0.07	0.07	0.06	0.06
P ₂ O ₅	0.13	0.04	0.03	0.11	0.03	0.08	0.09	0.05	0.05	0.04
Na ₂ O	4.25	3.90	3.97	4.08	3.82	4.39	3.63	4.95	2.9	4.23
MgO	1.24	1.05	1.18	0.93	0.81	1.02	1.09	0.86	0.56	0.73
LOI	N/A	3.09	N/A	N/A	N/A	N/A	N/A	0.42	N/A	N/A
Total	96.16	98.1	95.04	94.16	96.51	98.37	96.96	98.96	90.94	93.35
Cr	27.782	25.311	24.458	24.145	26.007	23.897	26.081	25.056	18.674	50.649
Nb	23.97	29.001	24.024	35.784	35.355	33.844	30.014	33.317	43.663	45.952
Ni	15.52	24.275	16.686	21.56	21.312	16.368	22.267	9.412	10.778	13.621
Rb	143	134	139	180	129	146	132	143	199	202
Sr	524	420	506	331	330	387	434	428	100	74
Th	28.967	22.802	23.738	22.525	31.733	27.958	24.684	27.229	40.348	34.857
Y	26.381	26.579	25.49	27.881	25.397	25.98	24.26	25.242	29.284	29.633
Zr	584	552	638	352	398	381	374	401	306	326
Ba	1349	1280	1753	671	728	860	984	1048	69	89

Appendix A, continued.

Sample	92-SM3-3	92-SM3-2	92-SM3-4	92-SM2-3	92-SS2-1	92-SS2-2	92-TB3-1	92-TB3-3	92-TB2-1	92-TB3-2
Position	7	8	9	10	9	10	4	5	6	7
SiO2	67.05	66.95	67.94	66.56	71.267	66.52	65.86	65.40	64.045	66.565
Al2O3	13.86	13.86	13.89	13.94	11.17	14.38	15.53	14.96	15.179	14.489
TiO2	0.34	0.37	0.36	0.35	0.35	0.47	0.52	0.47	0.464	0.5
FeO	1.88	1.98	1.97	2.01	2.05	2.52	3.07	2.86	2.623	3.067
CaO	1.51	1.30	1.20	1.88	2.89	0.47	0.78	0.85	1.19	0.955
K2O	5.61	5.22	5.42	5.03	6.28	8.56	9.53	9.50	9.164	9.51
MnO	0.07	0.06	0.07	0.06	0.04	0.03	0.04	0.03	0.033	0.033
P2O5	0.06	0.04	0	0.03	0.11	0.02	0.06	0.05	0.059	0.072
Na2O	4.28	4.42	3.51	4.08	1.57	1.57	1.57	1.58	2.098	1.569
MgO	0.72	0.30	0.42	0.42	0.74	0.38	0.45	0.38	0.423	0.497
LOI	1.79	N/A	N/A	1.11	3.71	2.70	0.74	N/A	N/A	N/A
Total	97.16	94.50	94.77	95.46	100.16	97.62	98.14	96.06	95.278	97.257
Cr	44.718	36.464	111.62	65.748	13.505	23.022	76	77.729	27.072	60.012
Nb	43.445	44.908	45.805	44.761	23.522	32.208	32.291	27.412	27.142	27.769
Ni	14.677	14.081	25.915	17.93	12.868	14.241	24.894	25.833	17.167	23.57
Rb	200	203	184	191	130	196	314	308	295	309
Sr	74	70	61	65	112	56	200	214	191	186
Th	36.273	35.613	36.901	36.206	18.111	23.798	28.624	26.463	24.285	24.307
Y	29.707	30.298	29.561	30.068	23.178	27.605	30.544	30.178	29.839	30.117
Zr	320	334	329	346	226	340	378	360	375	345
Ba	85	76	81	78	388	392	1400	1260	1048	1298

Appendix A, continued.

Sample	92-TB3-4	92-TB3-5	92-WH2-2	92-WH2-4	92-WH2-3	92-WH2-1
Position	8	9.5	7	8	9	10
SiO2	64.809	60.571	62.059	59.204	56.115	61.821
Al2O3	14.162	14.438	15.937	15.622	16.969	15.713
TiO2	0.501	0.645	0.596	0.0604	0.68	0.665
FeO	2.796	3.574	3.14	3.202	3.436	3.786
CaO	2.016	4.103	2.48	4.127	5.127	3.42
K2O	9.435	6.132	6.232	5.823	7.45	5.519
MnO	0.029	0.062	0.07	0.065	0.073	0.093
P2O5	0.114	0.163	0.099	0.186	0.194	0.241
Na2O	1.569	2.835	3.769	3.525	3.362	3.815
MgO	0.428	1.243	0.718	1.009	0.892	1.782
LOI	1.63	N/A	N/A	N/A	3.35	1.53
Total	97.489	93.766	95.1	93.367	97.648	98.385
Cr	84.009	32.226	19.534	28.458	42.534	22.915
Nb	30.23	25.63	30.448	25.569	29.339	25.204
Ni	28.633	21.064	14.254	14.989	15.812	16.268
Rb	305	179	157	138	178	141
Sr	193	368	560	662	591	712
Th	24.174	21.921	22.101	16.726	22.154	18.154
Y	29.896	26.477	26.481	25.542	27.426	26.151
Zr	344	372	434	419	430	430
Ba	1341	1250	1330	1344	1524	1502

Appendix B: Point Counts. Part I: Whole Rock Modal Analyses. Counts normalized to 100%.

Position	7.0	8.0	9.0	10.0	6.0	1.0	2.5	4.5	4.7	5.0
Sample	92-BM1-2	92-BM1-1	92-BM1-4	92-BM1-3	92-BM1-6	92-E1-2	92-E1-3	92-E1-4	92-E1-5	92-E1-6
sanidine	5.4	5.2	7.8	17.2	6.6	5.7	6.8	7.6	8.4	9.6
plagioclase	0.8	2	1	0.4	3.4	2.6	3.2	2.2	3.6	2.8
matrix	92.2	91.8	87	80.2	61.6	83.3	68.3	82.6	65.5	71.8
pumice						2.4				
lithics			2.2	0.4	25.4	5.3	19.7	6.8	21.5	13.4
biotite	0.8	1	1.2	0.8	2	0.4	0.6	0.4	0.6	0.8
cpx					0.2		0.2			0.2
sphene					0.2	0.2	0.4	0.4	0.2	0.8
opaque	0.8		0.8	0.6	0.6				0.2	0.6
zircon				0.4						
hornblende										
hematite										
carbonate										
undiff. feldspar										
trace sphene										
trace zircon			y		y			y		y
trace apatite	y	y			y					
glass										
trace cpx									y	
secondary quartz										
trace opaque										
trace hornblende										

Appendix B: Part I, continued.

Position	6.0	7.0	8.0	9.0	10.0	5.5	7.5	3.0	2.0
Sample	92-E1-7	92-E3-10	92-E3-9	92-E3-8	92-E3-7	92-HS1-2	92-HS1-3	92-HS1-4	92-HS1-6
sanidine	8.4	9.6	9.8	9.2	5	6.6	3	9.8	7
plagioclase	4.6	4	5	5.1	8.9	88	77.8	83.6	85.6
matrix	76.4	76.8	76.4	62.4	80.7	2	4.6	2.6	2.1
pumice							6.8		
lithics	8.8	5.2	5.4	20.1	1.6	0.6	6.6	1	2.5
biotite	0.8	1.4	1.2	0.2	2.2	0.6	0.6	1.4	0.6
cpx	0.2	0.8	0.2		0.4	0.2	0.4	0.6	1
sphene	0.6	1.4	1.2	1	0.4	1.4		0.8	1
opaque	0.2	0.8	0.6	2	0.6	0.6	0.2	0.2	0.2
zircon			0.2		0.2				
hornblende									
hematite									
carbonate									
undiff. feldspar									
trace sphene									
trace zircon	y	y	y	y					
trace apatite		y	y	y					
glass									
trace cpx									
secondary quartz									
trace opaque									
trace hornblende									

Appendix B: Part I, continued.

Position	1.0	5.0	7.0	9.0	9.5	2.0	3.0	4.0	5.0
Sample	92-HS1-5	92-HS2-1	92-HS2-2	92-HS2-3	92-HS1-1	93-I151-2	93-I151-3	93-I151-4	93-I151-5
sanidine	7	9.4	4.8	4	6.7	5.3	5.8	7.8	9.9
plagioclase	5.4	3	2.6	4.6	4.6	1	4.6	6.2	4.2
matrix	81.2	84.8	89.2	85.6	82.9	82.9	81.8	80.8	80.7
pumice	0.2					3.6			
lithics	2.8		0.4	1.4	2.7	4	4.6	1	2.4
biotite	1.4	0.4	1.2	1.8	1.7	0.2	0.8	1.2	0.6
cpx	0.4	0.2		1.6	0.8	0.8	0.8	0.8	0.4
sphene	1.2	1.2	0.6			0.4	1.2	0.8	1.2
opaque	0.2	0.6	0.8	1	0.6	0.6	0.2	1.4	0.6
zircon	0.2	0.4	0.2			0.2	0.2		
hornblende									
hematite									
carbonate									
undiff. feldspar									
trace sphene									
trace zircon								y	y
trace apatite				y		y	y	y	y
glass									
trace cpx									
secondary quartz									
trace opaque									
trace hornblende									

Appendix B: Part I, continued.

Position	6.0	8.0	9.0	10.0	7.5	7.2	5.0	6.0	7.0
Sample	93-I151-6	92-LG1-1	92-LG1-2	92-LG1-3	91-M1-5	92-M2-3	92-M2-1	91-M1-1	91-M1-2
sanidine	12.6	9.8	12	9.2	14.3	10.2	6.4	17.4	14.3
plagioclase	3.6	1.8	1.6	1.2	10.2	7.2	3.7	10.2	9.4
matrix	77.6	65.4	81.6	86.4	59.7	64	79.8	47.1	55.8
pumice		0.6			10.8	13.4		13.9	6.6
lithics	2.2	20.8	1.6	1.6	1.8	2.6	7.9	8.6	8.6
biotite	1	0.8	0.4	0.2	1.8	1.4	0.2	1.2	1.6
cpx	0.4		1.2	0.6	0.6	0.4	0.6	0.4	2.2
sphene	1.4	0.6	0.8	0.6		0.4	0.6	0.2	0.8
opaque	1		0.6	0.2	0.8	0.4	0.8	0.6	0.4
zircon	0.2	0.2	0.2					0.2	
hornblende								0.2	
hematite									
carbonate									
undiff. feldspar									
trace sphene					y				
trace zircon				y	y				y
trace apatite	y								
glass									
trace cpx									
secondary quartz									
trace opaque		Y							
trace hornblende					y				

Appendix B: Part I, continued.

Position	8.0	9.0	9.5	10.0	10.5	5.0	6.0	7.0	8.0
Sample	92-M2-2	91-M1-3	92-M3-4	91-M1-4	92-M3-5	91-SM1-1	92-SM2-1	92-SM3-3	92-SM3-2
sanidine	3.8	10.4	10.5	17.5	22.2	4.2	10.2	8.4	12
plagioclase	74	13.4	8.6	12.7	9.6	0.6	3.6	2	1
matrix	74	66.5	69.3	59.7	62	80.4	78.4	80.8	71
pumice	9.8	5.4		2.1		11.2	1.2	4.4	12.2
lithics	2		4.2	2.8	0.6	1.2	4.4	1.8	1.4
biotite	1.6	2.2	3.4	2.8	2.2	0.8	0.4	0.6	0.6
cpx	0.6	1.1	2.2	1.6	1.4	0.4	0.2	0.2	0.4
sphene		0.4	0.2	0.6	0.2	0.8	0.8	0.8	0.6
opaque	6.2	0.6	1.4	0.2	1.2	0.2	0.8	1	0.6
zircon			0.2		0.6	0.2			
hornblende									
hematite									
carbonate									
undiff. feldspar									
trace sphene									
trace zircon		y	y		y		y	y	
trace apatite				y			y	y	y
glass									
trace cpx									
secondary quartz									
trace opaque									
trace hornblende									

Appendix B: Part I, continued.

Position	9.0	10.0	4.0	9.5	6.0	7.0	8.0	7.0	8.0
Sample	92-SM3-4	92-SM2-3	92-TB3-1	92-TB3-5	92-TB1-2	92-TB1-3	92-TB1-4	92-WH1-3	92-WH1-4
sanidine	7	10.4	19.8	10.4	20.7	10.3	23.1	11	11
plagioclase	2	5	0.6	12.5	1	0.6	0.6	4.6	11.2
matrix	73.8	80.4	60.4	61.9	60.2	54.7	53.7	70.6	67.4
pumice	10.4								
lithics	3.6	1.4	5.4	8.4	8	26	10.4	5	3.8
biotite	1	1.4	3	4.4	1.8	1.6	3.2	4.2	3.8
cpx	0.2	0.4						2.2	1.6
sphene	1.2	0.6					0.4	0.2	
opaque	0.6	0.4	1.2	1	0.8	1.4	0.8	1.6	0.8
zircon	0.2				0.2	0.4	0.4	0.2	
hornblende								.4	0.4
hematite			0.4						
carbonate									
undiff. feldspar			9.2	1.2	7.4	4.6	7.4		
trace sphene									
trace zircon								y	
trace apatite						y			
glass									
trace cpx									
secondary quartz				0.2	y				
trace opaque									
trace hornblende									

Appendix B: Part I, continued.

Position	9.0	10.0
Sample	92-WH1-2	92-WH1-1
sanidine	4.4	12.6
plagioclase	8	6.9
matrix	80	70
pumice		
lithics	3.8	6.3
biotite	2.6	3.2
cpx	0.6	
sphene	0.4	0.2
opaque	1	0.6
zircon		0.2
hornblende		
hematite		
carbonate		
undiff. feldspar		
trace sphene		
trace zircon		
trace apatite		
glass		
trace cpx		
secondary quartz		
trace opaque		
trace hornblende		

Appendix B: Point Counts. Part II: Phenocryst Modal Analyses. Counts normalized to 100%.

Position	7.0	8.0	9.0	10.0	6.0	1.0	2.5	4.5	4.7	5.0
Sample	92-BM1-2	92-BM1-1	92-BM1-4	92-BM1-3	92-BM1-6	92-E1-2	92-E1-3	92-E1-4	92-E1-5	92-E1-6
sanidine	69.2	63.4	72.2	88.7	50.8	64.0	60.7	71.7	64.6	64.9
plagioclase	10.3	24.4	9.3	2.1	26.2	29.2	28.6	20.8	27.7	18.9
biotite	10.3	12.2	11.1	4.1	15.4	4.5	5.4	3.8	4.6	5.4
cpx	0.0	0.0	0.0	0.0	1.5	0.0	1.8	0.0	0.0	1.4
sphene	0.0	0.0	0.0	0.0	1.5	2.2	3.6	3.8	1.5	5.4
opaque	10.3	0.0	7.4	3.1	4.6	0.0	0.0	0.0	1.5	4.1
zircon	0.0	0.0	0.0	2.1	0.0	0.0	0.0	0.0	0.0	0.0
hornblende	0.0	0.0	0.0	0.0	0.0	0.0	0.0	0.0	0.0	0.0
undiff. feldspar	0.0	0.0	0.0	0.0	0.0	0.0	0.0	0.0	0.0	0.0

Position	6.0	7.0	8.0	9.0	10.0	5.5	7.5	3.0	2.0
Sample	92-E1-7	92-E3-10	92-E3-9	92-E3-8	92-E3-7	92-HS1-2	92-HS1-3	92-HS1-4	92-HS1-6
sanidine	56.8	53.3	53.8	52.6	28.2	6.8	3.7	10.2	7.3
plagioclase	31.1	22.2	27.5	29.1	50.3	90.3	94.9	86.7	89.7
biotite	5.4	7.8	6.6	1.1	12.4	0.6	0.7	1.5	0.6
cpx	1.4	4.4	1.1	0.0	2.3	0.2	0.5	0.6	1.0
sphene	4.1	7.8	6.6	5.7	2.3	1.4	0.0	0.8	1.0
opaque	1.4	4.4	3.3	11.4	3.4	0.6	0.2	0.2	0.2
zircon	0.0	0.0	1.1	0.0	1.1	0.0	0.0	0.0	0.0
hornblende	0.0	0.0	0.0	0.0	0.0	0.0	0.0	0.0	0.0
undiff. feldspar	0.0	0.0	0.0	0.0	0.0	0.0	0.0	0.0	0.0

Appendix B: Part II, continued.

Position	1.0	5.0	7.0	9.0	9.5	2.0	3.0	4.0	5.0
Sample	92-HS1-5	92-HS2-1	92-HS2-2	92-HS2-3	92-HS1-1	93-I151-2	93-I151-3	93-I151-4	93-I151-5
sanidine	44.3	61.8	47.1	30.8	46.5	62.4	42.6	42.9	58.6
plagioclase	34.2	19.7	25.5	35.4	31.9	11.8	33.8	34.1	24.9
biotite	8.9	2.6	11.8	13.8	11.8	2.4	5.9	6.6	3.6
cpx	2.5	1.3	0.0	12.3	5.6	9.4	5.9	4.4	2.4
sphene	7.6	7.9	5.9	0.0	0.0	4.7	8.8	4.4	7.1
opaque	1.3	3.9	7.8	7.7	4.2	7.1	1.5	7.7	3.6
zircon	1.3	2.6	2.0	0.0	0.0	2.4	1.5	0.0	0.0
hornblende	0.0	0.0	0.0	0.0	0.0	0.0	0.0	0.0	0.0
undiff. feldspar	0.0	0.0	0.0	0.0	0.0	0.0	0.0	0.0	0.0

Position	6.0	8.0	9.0	10.0	7.5	7.2	5.0	6.0	7.0
Sample	93-I151-6	92-LG1-1	92-LG1-2	92-LG1-3	91-M1-5	92-M2-3	92-M2-1	91-M1-1	91-M1-2
sanidine	62.4	74.2	71.4	76.7	51.6	51.0	52.0	57.6	49.8
plagioclase	17.8	13.6	9.5	10.0	36.8	36.0	30.1	33.8	32.8
biotite	5.0	6.1	2.4	1.7	6.5	7.0	1.6	4.0	5.6
cpx	2.0	0.0	7.1	5.0	2.2	2.0	4.9	1.3	7.7
sphene	6.9	4.5	4.8	5.0	0.0	2.0	4.9	0.7	2.8
opaque	5.0	0.0	3.6	1.7	2.9	2.0	6.5	2.0	1.4
zircon	1.0	1.5	1.2	0.0	0.0	0.0	0.0	0.7	0.0
hornblende	0.0	0.0	0.0	0.0	0.0	0.0	0.0	0.0	0.0
undiff. feldspar	0.0	0.0	0.0	0.0	0.0	0.0	0.0	0.0	0.0

Appendix B: Part II, continued.

Position	8.0	9.0	9.5	10.0	10.5	5.0	6.0	7.0	8.0
Sample	92-M2-2	91-M1-3	92-M3-4	91-M1-4	92-M3-5	91-SM1-1	92-SM2-1	92-SM3-3	92-SM3-2
sanidine	4.4	37.0	39.6	49.4	59.4	58.3	63.8	64.6	78.9
plagioclase	85.8	47.7	32.5	35.9	25.7	8.3	22.5	15.4	6.6
biotite	1.9	7.8	12.8	7.9	5.9	11.1	2.5	4.6	3.9
cpx	0.7	3.9	8.3	4.5	3.7	5.6	1.3	1.5	2.6
sphene	0.0	1.4	0.8	1.7	0.5	11.1	5.0	6.2	3.9
opaque	7.2	2.1	5.3	0.6	3.2	2.8	5.0	7.7	3.9
zircon	0.0	0.0	0.8	0.0	1.6	2.8	0.0	0.0	0.0
hornblende	0.0	0.0	0.0	0.0	0.0	0.0	0.0	0.0	0.0
undiff. feldspar	0.0	0.0	0.0	0.0	0.0	0.0	0.0	0.0	0.0

Position	9.0	10.0	4.0	9.5	6.0	7.0	8.0	7.0	8.0
Sample	92-SM3-4	92-SM2-3	92-TB3-1	92-TB3-5	92-TB1-2	92-TB1-3	92-TB1-4	92-WH1-3	92-WH1-4
sanidine	57.4	57.1	58.6	35.3	64.9	54.5	64.3	45.8	38.2
plagioclase	16.4	27.5	1.8	42.4	3.1	3.2	1.7	19.2	38.9
biotite	8.2	7.7	8.9	14.9	5.6	8.5	8.9	17.5	13.2
cpx	1.6	2.2	0.0	0.0	0.0	0.0	0.0	9.2	5.6
sphene	9.8	3.3	0.0	0.0	0.0	0.0	1.1	0.8	0.0
opaque	4.9	2.2	3.6	3.4	2.5	7.4	2.2	6.7	2.8
zircon	1.6	0.0	0.0	0.0	0.6	2.1	1.1	0.8	0.0
hornblende	0.0	0.0	0.0	0.0	0.0	0.0	0.0	0.0	1.4
undiff. feldspar	0.0	0.0	27.2	4.1	23.2	24.3	20.6	0.0	0.0

Appendix B: Part II, continued.

Position	9.0	10.0
Sample	92-WH1-2	92-WH1-1
sanidine	25.9	53.2
plagioclase	47.1	29.1
biotite	15.3	13.5
cpx	3.5	0.0
sphene	2.4	0.8
opaque	5.9	2.5
zircon	0.0	0.8
hornblende	0.0	0.0
undiff. feldspar	0.0	0.0

Appendix C: Stratigraphic Section Descriptions

Sheep Mountain Section, Nevada

Location: SW 1/4, Sec. 17, T27N, R22W

top of section

Strongly welded, grayish red, devitrified crystal tuff containing sparse, mostly rounded lithophysal cavities which decrease in abundance upsection. Moderate carbonate alteration.

Pale brown, devitrified, spherulitic crystal tuff. Contains partially-flattened lithophysal cavities (to 4 cm) which decrease in abundance upsection. Moderate carbonate alteration.

Variably-welded, eutaxitic vitrophyre (eutaxia to 8 mm), consisting of a pale reddish brown, moderately-welded eutaxite that locally grades into lenses of medium dark gray, densely-welded eutaxite towards the base.

Poorly-welded, shard-rich, dark yellowish orange vitrophyre. Contains moderately flattened pumice (10%).

Poorly-welded, pale yellowish brown, pumiceous vitric tuff which contains slightly flattened, very pale orange, subrounded to subangular pumice (average size = 1 cm, to maximum = 7 cm; 17%).

Paleozoic carbonate rocks (undifferentiated)

bottom of section

Highland Spring Range Section, Nevada**Location: Sec. 26, T17N, R62E****References: Davis (1984)***top of section***Moderately-welded, grayish pink to pinkish gray crystal tuff****Poorly-welded, pinkish gray, pumiceous vitric tuff.****Lithophysal zone (lithophysal cavities to approximately 10 cm), which grades into a thick interval of devitrified, gray orange pink to light gray, eutaxitic crystal tuff which contains abundant, extremely flattened, grayish pink eutaxia (to 9 cm).****Pale red, spherulite-rich crystal tuff. Spherulites are up to 9 cm in diameter.****Moderately welded, pale brown, partially-devitrified crystal tuff. Locally underlain by lensoidal intervals of perlitically-altered, moderately welded, dark gray vitrophyre or unwelded, very light gray ash locally underlie this unit.****Upper Volcanic and Sedimentary Assemblage of Davis (1984): debris flow deposits and fine-grained, moderate red volcanoclastic sediments.***bottom of section***McCullough Range Section, Nevada****Location: NE 1/4, Sec. 27, T25S, R61E****References: Schmidt (1987)***top of section***Moderately-welded, lithic-poor, devitrified, pinkish gray crystal tuff that has undergone extensive vapor phase crystallization. Tuff is pale lavender gray in outcrop. Weathers into shallow, flat cavities (<1 m wide). Abundance and size of lithic fragments varies upsection.****Densely-welded to moderately-welded, spherulitic, pale red, lithic-poor crystal tuff. Matrix contains irregular patches of dark gray, less-altered matrix. In outcrop, this unit**

has a dark brownish gray color. Phenocrysts in this interval are larger (<4 mm) at the base. Lithics are very sparse (<5 %) but larger (<5 cm) with respect to the lower intervals.

Very poorly-welded, very pale orange, pumiceous vitrophyre.

Moderately-welded, moderate red crystal tuff with reddish brown fiamme (<1.0 cm), and sparse (<5%) lithics (<1.5 cm long).

Moderate reddish orange, eutaxitic crystal tuff. Devitrification increases upsection. Contains moderately to strongly flattened, pale reddish brown eutaxia (<1 cm long).

Medium dark gray lithic vitrophyre with strongly flattened, grayish black fiamme (<1.5 cm) and subangular lithic fragments (<1.0 cm).

Moderately-welded, eutaxitic crystal tuff with rounded to subrounded mafic lithic fragments (<1.2 cm) and strongly flattened, grayish black fiamme which vary between <1.5 cm (average) to <6.2 cm (maximum) in length. The matrix of this tuff is medium gray. Irregular, mottled patches of moderate reddish orange matrix occur about lithic fragments.

Dark gray, moderately-welded, eutaxitic lithic vitrophyre.

Poorly-welded, devitrified, pinkish gray lithic crystal tuff with subangular lithic fragments (generally <0.7 cm, maximum to 12 cm) and angular, white, fibrous pumice (<5mm). Locally contains cobbles (<13 cm) of the Eldorado Valley Volcanics incorporated within ash-flow tuff matrix. Rarely preserved: a thin interval of tuff enriched in lithic fragments and crystals (a possible pyroclastic surge or ground surge deposit).

Eldorado Valley Volcanics: volcaniclastic cobble breccia
bottom of section

White Hills Section, Arizona**Location: SW 1/4, Sec. 16, T29, R20W****Reference: Cascadden (1991)***top of section***Basaltic andesite flows (Basaltic Andesite of Squaw Peak? Cascadden, 1991).**

Grayish pink, ridge-forming crystal tuff with partially-flatted pumice (<2 cm wide) and basaltic andesite lithic clasts (average size: 5.6 to 9.6 mm). Rare hornblende phenocrysts are present. Modal percent of biotite and clinopyroxene increase upsection. Basaltic andesite lithic clasts display crenulate margins. This texture may be indicative of magmatic mixing processes.

Poorly-welded, slope-forming, grayish orange pink crystal tuff.**Tertiary megabreccia (Cascadden, 1991)***bottom of section***Interstate-15 (I-15) Section, Nevada****Location: SE 1/4 of Sec. 35, SW 1/4 of Sec. 36, T23S, R60E****Reference: Bridwell (1991)***top of section***Pumice Mine Volcanics: basalt flows (Bridwell, 1990).**

Massive, ridge-forming, densely-welded, pale red crystal tuff. Overall, phenocrysts in the I-15 section (in particular, sphene and clinopyroxene) increase in the upsection direction.

Eutaxitic crystal tuffs which become progressively less-welded and more crystal-rich upsection. Biotite phenocrysts and fiamme (<4.0 cm) increase in size noticeably upsection.

Very densely-welded, light gray, eutaxitic vitrophyre.

Very light gray vitrophyre.

Pale grayish orange, very-poorly to poorly-welded, pumiceous vitric tuff. Contains approximately 20% subrounded, fibrous pumice that varies in size from 0.3 to 6 cm wide, and < 5% predominantly subangular to subrounded, basaltic andesite clasts (0.4 cm wide). The matrix of this tuff is shard-rich.

Paleozoic carbonate rocks (undifferentiated).

bottom of section

Temple Bar Section, Arizona

Location: NW and NE 1/4, Sec.13, T22S, R20W

Reference: Cascadden (1991)

top of section

Light gray vitric tuff. Phenocrysts and pumice are smaller and less abundant in this unit in comparison to the underlying interval.

Grayish orange pink crystal tuff with pumice (15%; < 2 cm in length) and angular to subrounded lithic clasts (6%; < 1 cm). A mafic enclave displaying a distinctive crenulate margin was found in float at the top of this ridge.

Crystal tuff with lithic clasts that are slightly less abundant and larger in size than the underlying unit (< 3cm). Abundance of pumice is also decreased (<5%) in this interval.

Vuggy zone of crystal tuff with large (<1m wide) flattened to rounded cavities. Lithic clasts in this unit are smaller (<1cm) and less numerous than the basal interval.

Blocky ledges of pale red crystal tuff that contains moderately-flattened, grayish pink pumice (<5 cm in length) and subangular to subrounded basalt and basaltic andesite lithic fragments.

Basaltic Andesite of Temple Bar.

bottom of section

Eldorado Mountains Section, Nevada
Location: SW 1/4, Sec. 27, T25S, R64E
Reference: Anderson, 1971

top of section

Mount Davis Volcanics: basalts (Anderson, 1971).

Pale red vitrophyre with platy outcrop habit produced by heating by flows of Mt. Davis Volcanics basalts.

Very light gray to grayish orange pink vitric tuffs with strongly-flattened pumice (1 to 1.5 m) that increases in length upsection. Contacts between successive pyroclastic flow units are preserved in stratigraphically equivalent outcrops exposed at the Bridge Spring type section. These outcrops also contain banded pumice.

Pale red vitrophyre with flattened pumice (< 9 cm in length)

Pumice-rich, very pale red crystal tuff forming rounded to platy outcrops that contain large, elongated cavities (1 m to approximately 12 m in width) which indicate vapor phase crystallization. Lithic fragments are increased in size (< 8 cm). Vapor phase amygdules

(< 9 cm) that are lined with pumice and/or contain lithic fragments are common. Phenocrysts are slightly less abundant in this interval but are coarser in comparison to underlying units.

Pale brown, very-densely welded, cliff-forming vitrophyre. Lithic fragments (subrounded, < 5 cm in length) are less abundant than underlying unit. Phenocrysts and pumice are larger (< 2.5 mm and < 5 cm, respectively).

Grayish orange pink, pumice- and lithic-rich tuff that exhibits a hackly, sheared outcrop surface. Phenocrysts in this interval are noticeably coarser (< 2.5 mm) than in underlying units (< 0.5 mm). Pumice is flattened and increased in size (< 5 cm) and abundance. Lithic clasts (length: < 5 cm) are decreased in abundance.

Laterally-discontinuous outcrops of pinkish gray, ledge-forming, moderately-welded lithic tuffs interbedded with poorly-welded lithic tuffs that form rounded, exfoliated outcrops. Mafic inclusions with crenulate margins are found in this interval. Lithic fragments occur in slightly reduced amounts and are smaller (<3.5 cm), and pumice is slightly increased in abundance. A stratigraphically equivalent interval exposed at Bridge Spring contains a 1 m thick, laterally discontinuous ledge of pyroclastic breccia that is interpreted to be a coignimbrite lag deposit (Fisher and Schmincke, 1987). This outcrop consists of 50% angular to subangular mafic clasts (<2 cm) in a grayish orange pink crystal tuff matrix.

Grayish orange lithic tuffs with irregularly shaped, elongated zones of concentrated lithics and coarse phenocrysts that are interpreted here to be gas escape pipes (max. length: 0.3 m, max. width: 1.5 cm).

Poorly- to moderately-welded, pinkish gray, lithic tuffs with angular to subangular, basalt and basaltic andesite lithic fragments (2.5 cm to 0.5 cm), and white to pale yellowish orange, partially-flattened, angular pumice fragments (<1.5 cm). This interval becomes progressively more densely-welded and enriched in both lithics and pumice in the upsection direction. A rare exposure of fine-grained, barely welded, lithic-poor ash occurs within this interval. This discontinuous interval is approximately 13 cm wide and 1.2 m long, and displays subtle cross-bedding, which suggests it was formed by a surge-related process (i.e., ash-cloud surge, pyroclastic surge, or pyroclastic flow related ground surge).

Patsy Mine Volcanics: basaltic andesites (Anderson, 1971)

bottom of section

Black Mountains Section, Arizona**Location: SE 1/4, Sec. 22, T27N, R22W****Reference: Faulds (1990)***top of section*

Moderately welded, grayish pink devitrified tuff with fiamme (<7cm long) and lithic clasts (<1.4 cm). A cooling break lies beneath this unit.

Densely welded, pink, eutaxitic tuff.

Moderately welded, grayish orange pink, eutaxitic tuff with a shard rich matrix.

Thin discontinuous, light greenish gray, densely welded, lithic rich tuff with angular to subangular clasts of basaltic andesite (<3 cm in diameter). Contains flattened pumice in a shard rich matrix.

Pyroxene-olivine basaltic andesite.

*bottom of section***Dolan Springs Section, Arizona****Location: Sec. 19, 20, 24, T26N, R19W***top of section*

Regionally-extensive olivine basalt.

Poorly-welded to densely-welded, lithic-rich vitric tuff (lithics < 5 cm, pumice < 1.5 cm). Poorly-welded tuff is pale red and contains abundant (55 %) angular fragments of black glass and subrounded rhyolite lithic clasts (<3 cm). Densely-welded vitrophyre is light brown and eutaxitic (black eutaxia to 1.5 cm) and contains approximately 65% subrounded rhyolite clasts and black glass. This interval forms massive, ridge forming outcrops; crudely-formed columnar jointing is occasionally present.

Interbedded pyroclastic surge and ash-flow tuff. Lamination and cross-bedding in surge deposits is better developed upsection than in lower intervals. The uppermost part of the section is a very poorly-welded, grayish orange pink, pumice-rich vitric tuff with

pumice (< 1.5 to 8 cm) that decreases in abundance and is normally-graded upsection. Lithic fragments (predominantly rhyolite, < 2.5 cm) increases in abundance and is reversely-graded upsection. Pumice varies from: (1) a dense, grayish pink, chalky textured pumice; (2) a very light gray pumice that varies in texture from granular and densely compacted to fibrous to bubbly; and (3) a compacted pumice with fibrous texture that displays alternately-colored bands of very light gray and pinkish gray. This banding suggests that a mixture of magmatic compositions has occurred.

Laterally discontinuous, highly vesiculated, brownish gray olivine basalt a'a flows. Basalt flows ramps onto and pinches out on the flanks of an adjacent rhyolite dome, but thickens considerably to the northwest of Dolan Springs. The top of the flow contains numerous elongated, ballistically-shaped volcanic bombs (to 1 m in length), which indicates a proximally-located source. Angular basalt fragments (< 10 cm in length) were caught up and incorporated into the overlying ash-flow tuff.

Interbedded lithic tuffs and thinly-laminated pyroclastic surge deposits. Surge deposits are poorly-welded, pinkish gray and are frequently rich in accretionary lapilli (< 1 mm in width). Cross-bedded surge laminations vary in width from 4 mm in basal deposits to 2 mm at the top of the section. Modal percent of lithic clasts and phenocrysts in surge deposits remain generally constant throughout the section. Modal percent of pumice increases slightly in the upsection direction from 2 to 5%. Lithic clasts (approximately 12% of the whole rock) consists of < 2 mm wide, subrounded rhyolite (dominant fraction) and basaltic andesite.

Poorly-welded, hackly surfaced, pumice-rich, yellowish-gray lithic tuff which contains subrounded, white, fibrous pumice (< 1 cm) and subangular rhyolite lithic fragments (< 0.5 cm). Ash-flow tuffs exposed farther upsection are very pale orange, moderately-welded vitric tuffs with rhyolite and basaltic andesite lithic fragments. In general, the abundance and size of lithic fragments increase upsection. Lateral zones of concentrated mafic fragments occur periodically in the upper part of the section.

Rhyolite domes and associated breccia carapace aprons. Carapace deposits consist of angular to subangular clasts (< 1 m wide) of rhyolite glass and pumice in a very pale orange, sanidine and biotite-bearing, tuffaceous matrix. Rhyolite domes are massive, exhibit large-scale flow banding and ramping features.

Pyroxene-olivine basalts.

bottom of section

Salt Springs Wash Section, Arizona

Location: NE 1/4, Sec. 25, T30N, R19W

References: Cascadden (1991)

top of section

Tertiary megabreccia containing angular fragments of Precambrian crystalline basement.

Very light gray, swale-forming lithic tuff with a similar lithic content and abundance as the basal interval.

Stratified red brown sandstone.

Silicified, phenocryst-enriched, lithic fragment depleted zone of grayish pink tuff.

Ridge-forming, grayish pink lithic tuff with subangular lithic fragments of Precambrian basement (< 3 %; < 2.5 mm). Contains several vuggy zones with flattened cavities (possibly vapor phase zones).

Tertiary megabreccia containing angular fragments of Precambrian crystalline basement.

bottom of section